University of Southampton

Faculty of Medicine

Cancer Sciences

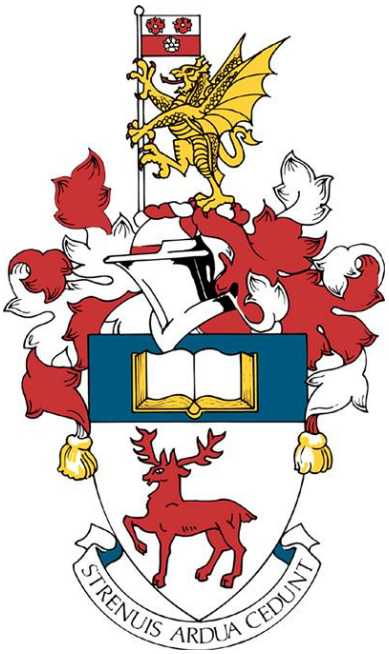

Investigation of Fc modifications and their influence on mAb function

Volume 1 of 1

by

Michael Marshall

ORCID ID 0000-0001-5410-0582

Thesis for the degree of Doctor of Philosophy

September 2018

University of Southampton

Abstract

Faculty of Medicine

Cancer Sciences

Doctor of Philosophy

Investigation of Fc modifications and their influence on mAb function

Michael Marshall

Monoclonal antibodies (mAbs) are therapeutic agents that have revolutionised the treatment of many diseases, particularly cancer. Most therapeutic mAbs rely on effector functions mediated by their Fc region. The work in this thesis focuses on the impact of alterations to this Fc region, and the consequence upon the efficacy of the antibody.

The role of different Fc regions on antibody binding and effector function was first analysed using different IgG subclass formats. Differential binding to target antigen for certain but not all specificities was clearly demonstrated, likely linked to the ability of the target to cluster in the membrane. Subsequently in effector assays of CDC, ADCC and ADCP, IgG1 and IgG3 were seen to be the most effective, with IgG2 and IgG4 being less able to engage direct depletion mechanisms.

To explore the potential consequences of lipid modifications on IgG functionality two different processes were examined- malondialdehyde and carboxyethylpyrrole. Both of these were performed on IgG1 mAbs in order to replicate potential *in vivo* processes that could occur to therapeutic mAbs. Assessment of the functional capabilities of these modified antibodies were carried out, and it was found that these lipid modified antibodies were indeed compromised in functionality.

As antibody Fc glycosylation is required for Fc effector function, and is known to vary both within health and disease as well as *in vitro* production, this modification was also explored using a series of enzymatic modifications. To probe their effects on Fc mediated effector mechanisms, anti-CD20 mAbs with distinct glycoforms were generated and tested for effector function. It was found that increasing the level of galactosylation and sialylation resulted in increased complement engagement, whilst not effecting FcγR mediated effector functions.

Finally, a novel method to assess the C1q binding property of mAbs was developed and characterised. This method, developed around a C1q affinity column, was shown to recapitulate the same hierarchies of C1q binding specificities as seen from cell based C1q recruitment and complement dependent killing assays using biologically relevant samples. As such, IgG3 showed the strongest binding to the C1q column, whereas IgG2 and IgG4 showed little specific binding. Furthermore, increasing levels of galactosylation and sialylation increased the binding to the column, and IgG mutants with altered C1q binding showed the anticipated shifts in column binding. These data suggest that the C1q column would be readily suited to high throughput screening of the binding of antibody mutants, subclasses or glycoforms to C1q.

Together, the work described in this thesis demonstrates the importance of the Fc region to antibody effector functions, their sensitivity to modifications, and ultimately to their efficacy as therapeutics.

Table of Contents

List of Figures

List of Tables

UNIVERSITY OF Southampton

Research Thesis: Declaration of Authorship

Print name:	MICHAEL MARSHALL

Title of thesis:	Investigation of Fc modifications and their influence on mAb function

I declare that this thesis and the work presented in it is my own and has been generated by me as the result of my own original research.

I confirm that:

1. This work was done wholly or mainly while in candidature for a research degree at this University;
2. Where any part of this thesis has previously been submitted for a degree or any other qualification at this University or any other institution, this has been clearly stated;
3. Where I have consulted the published work of others, this is always clearly attributed;
4. Where I have quoted from the work of others, the source is always given. With the exception of such quotations, this thesis is entirely my own work;
5. I have acknowledged all main sources of help;
6. Where the thesis is based on work done by myself jointly with others, I have made clear exactly what was done by others and what I have contributed myself;
7. Either none of this work has been published before submission, or parts of this work have been published as: [please list references below]:

Signature:		Date:	

Acknowledgements

I would like to thank my supervisors for their support: Prof. Mark Cragg, Dr. Tilman Schlothauer, Dr. Christian Klein, Prof. Steve Beers and Prof. Jessica Teeling. I would like to thank the members of the antibody and vaccine group and the lab or Dr. Schlothauer for their help in this project. I would also like to thank the BBSRC and Hoffman La Roche for funding this project.

Abbreviations

A:I	activatory:inhibitory
AB	aminobenzamide
ADCC	antibody dependent cell mediated cytoxicity
ADCP	antibody dependent cellular phagocytosis
AID	activation induced cytidine deaminase
ALG	asparagine linked glycosylation
AMD	age related macular degeneration
APC	antigen presenting cells
ATCC	American Type Culture Collection
ATP	adenosine triphosphate
BCR	B cell receptor
BSA	bovine serum albumin
C	constant
CAP	carboxyalkylpyrrole
CCR	CC chemokine receptor
CD	cluster of differentiation
CDC	complement dependent cytotoxicity
CDR	complementarity determining region
CEP	carboxyethylpyrrole
CHO	Chinese hamster ovary
CLL	chronic lymphocytic leukaemia
CMP	cytidine monophosphate
CRP	complement reactive protein
CTLA-4	cytotoxic T lymphocyte associated protein 4
D	diversity
DAMP	damage associated molecular pattern
DC	dendritic cell
DCD	direct cell death
DMEM	Dulbecco's Modified Eagle's Medium
EDTA	disodium ethylenediaminetetraacetic acid
EGFR	epidermal growth factor receptor
ELISA	enzyme linked immunosorbent assay
EPO	erythropoietin
ER	endoplasmic reticulum
Fab	fragment antigen binding
FACS	fluorescence activated cell sorting
Fc	fragment crystallisable
FcR	Fc receptor
FcRn	neonatal Fc receptor
FcRy	common gamma chain
FCS	foetal calf serum
FcyR	Fc gamma receptor

FDA	Food and Drug Administration
FITC	fluorescein isothiocyanate
Gal	galactose
gC1qR	globular C1q receptor
GDP	guanosine diphosphate
GlcNAc	N-acetylglucosamine
GnT III	β-1,4 N-acetylglucosaminyltransferase
GPI	glycophosphatidylinositol
H	heavy chain
HEPES	4-(2-hydroxyethyl)-1-piperazineethanesulfonic acid
HER2	human epidermal growth factor receptor
HPLC	high performance liquid chromatography
HRP	horse radish peroxidase
IFN	interferon
Ig	immunoglobulin
IL	interleukin
ITAM	immunoreceptor tyrosine activation motif
ITIM	immunoreceptor tyrosine based inhibitory motif
ITP	immune thrombocytopenic purpura
IVIg	intravenous immunoglobulin therapy
J	joining
KIR	killer inhibitor receptor
L	light chain
LLO	lipid linked oligosaccharide
LPS	lipopolysaccharide
Lyn	Lck/Yes novel tyrosine kinase
mAb	monoclonal antibody
MAC	membrane attack complex
MASP	MBL associated serine proteases
MBL	mannose binding lectin
M-CSF	macrophage-colony stimulating factor
MDA	malondialdehyde
MDM	monocyte derived macrophage
MES	morpholineethanesulfonic
mFcγR	mouse Fc gamma receptor
MHC	major histocompatibility complex
MQ	Milli-Q
MW	molecular weight
NANA	N-acetyl neuraminic acid
NF	nuclear factor
NFAT-RE	nuclear factor of activated T cell-response element
NK	natural killer
NSD	natural sugar donor
ODP	O-Phenylenediamine dihydrochloride

OST	oligosaccharyltransferase
PAMP	pathogen associated molecular pattern
PBMC	peripheral blood mononuclear cell
PBS	phosphate buffered saline
PD-1	programmed cell death-1
PE	phycoerythrin
PI	propidium iodide
pIgR	polymeric immunoglobulin receptor
PNGase	peptide-N-glycosidase
PRR	pattern recognition receptor
PUFA	polyunsaturated fatty acid
RNS	reactive nitrogen species
ROS	reactive oxygen species
RPMI	Roswell Park Memorial Institute
SA	sialic acid
SAXS	small angle X-ray scattering
SC	secretory component
scC1q	single chain C1q
SDS-PAGE	sodium dodecyl sulphate polyacrylamide electrophoresis
SEM	standard error mean
SH2	Src homolgy 2
sIg	surface bound immunoglobulin
sIgA	secretory IgA
sIgM	surface IgM
SLE	systemic lupus erythematosus
smFRET	single molecule Förster resonance energy transfer
SPR	surface plasmon resonance
Syk	spleen tyrosine kinase
TCA	tricarboxylic acid
TCEP	tris(2-carboxyethyl)phosphine
TCR	T cell receptor
TLR	Toll Like Receptor
TNF	tumour necrosis factor
TRAILR	TNF-related apoptosis-inducing ligand receptor
Treg	regulatory T cell
UDP	uridine diphosphate
UMP	uridine monophosphate
V	variable
VEGF	vascular endothelial growth factor
WHO	World Health Organisation

Chapter 1: Introduction

1.1 Immune System

The human body is continuously exposed to a broad host of environmental threats. These include a vast array of pathogenic organisms and particles that have the potential to induce significant harm. In addition, inappropriate or dysregulated bodily responses can themselves become the cause of disease. In order to maintain health and defend against these threats, the human body has at its disposal an equally vast armoury of tools to counteract potential causative agents of disease. These mechanisms are chiefly encapsulated within the host immune system, and broadly fit into two categories, innate and adaptive immunity.

1.1.1 Innate Immunity

The innate immune system is a network of cells and mechanisms that is present from birth, and in contrast to adaptive immunity, does not have the capacity to significantly alter its response to a given pathogen upon repeated challenge[1]. It is therefore characterised as having much broader specificity than the adaptive immune system, and is typically based upon the recognition of invariant molecules[2]. These molecules are generally expressed on pathogens or are host molecules that indicate potential damage, and are referred to collectively as pathogen or damage associated molecular patterns (P/DAMPs), which are in turn recognised by germline encoded pattern recognition receptors (PRRs) of the innate immune system[3]. These PRRs can take the form of surface expressed markers, such as Toll Like Receptors (TLRs) or soluble molecules, such as C1q (described in detail in Section 1.4.2)[4]. Innate immunity acts as an immediate interceptor to foreign pathogens, positioned *in situ* around the body[5]. In the case of infections that the innate immune system cannot clear, it acts to control the infection while the adaptive immune response develops a more specific and potentially curative response[2].

The complement system of serum proteases is one example of the innate immune system, which acts upon recognition of PAMPs, and engages a series of effector mechanisms to directly lyse the target cell/bacteria, recruit immune cells or target the molecules for engulfment by phagocytes[2,6]. Various different PRRs are compatible with the complement system, allowing it to recognise and

act upon a broad variety of targets, including bacteria, viruses, immune complexes, apoptotic cells, and opsonised targets[6,7]. This latter mechanism, facilitated by C1q mediated recognition of antibody coated targets, is an example of how adaptive immunity (Section 1.1.2) has evolved to utilise the effector mechanisms of the innate immune system, and is discussed in detail in Section 1.4.2.

There are a number of cell types involved in innate immunity, of which most are of the myeloid lineage[2]. Neutrophils are a major effector cell of the innate immune system, and are the most frequent leukocyte present in the blood acting as a first line of defence against any infections that have breached the physical barriers of the skin or mucosa[8]. Although typically short lived, on the scale of a few hours, they are able to survive longer at sites of infection[9]. They act as phagocytes to engulf foreign pathogens and particles, produce inflammatory cytokines, and can release cytotoxic granules and DNA nets to trap microbes in a process termed NETosis[9,10].

Another important cell type of the innate immune system are the monocytes. These cells emerge from precursors in the bone marrow to circulate in the blood, and have the capacity to carry out phagocytosis and release inflammatory cytokines[11]. Monocytes also have the capacity to extravasate out of the circulation into the tissues at sites of inflammation, where they can differentiate into other effector cells, such as macrophages and dendritic cells[12].

Macrophages are tissue resident cells that are specialised for phagocytosis, and are able to engulf large numbers of target cells[1]. They express a broad spectrum of PRRs, including various TLRs, complement receptors, and also receptors specific for antibodies, Fc receptors (FcRs)[13]. This expression of FcRs is another example of the interaction between the innate and adaptive immune systems. Macrophages possess a degree of plasticity, and can act in a pro- or anti-inflammatory manner, depending on their environment and type of stimulation[14]. Anti-inflammatory macrophages (sometimes called M2 macrophages and typically associated with interleukin (IL)-4/13) are involved in wound healing and angiogenesis, and can become recruited into tumours to promote growth as part of the tumour microenvironment[15]. In contrast, pro-inflammatory macrophages (sometimes called M1 macrophages and typically associated with lipopolysaccharide (LPS)/interferon (IFN) γ) are highly phagocytic, expressing high levels of activatory Fc gamma receptors (FcγRs)[16]. However, it should be noted that these states represent the two extremes and a vast array of different macrophage activation states can be evoked according to the complex milieu of stimulation they receive[17].

Dendritic cells (DCs) are another type of myeloid cell that are highly heterogeneous, consisting of various subtypes with a range of different functions[18]. A major responsibility of DCs is to take up and present antigen to activate T lymphocytes, in order to facilitate their activation (described below in Section 1.1.2.1)[19]. DCs can also produce a myriad of cytokines in order to direct the immune response as well as act in an anti-inflammatory manner to promote immune tolerance[20].

DCs, as well as macrophages, monocytes and B cells (see later) are referred to as professional antigen presenting cells (APCs)[1]. This involves the uptake up foreign particles, including bacteria and cells, often by phagocytosis, and the display of antigens on the surface of the cell, in the context of a class II major histocompatibility complex (MHC-II) protein[21]. As described below (Section 1.1.2.1), this allows presentation of the antigen to T cells, activating them.

Another cell type involved in the innate immune response are natural killer (NK) cells. These cells are lymphocytes, but unlike B and T lymphocytes (discussed below) they are not part of the adaptive immune system, and don't possess antigen specific receptors[22]. Instead, NK cells rely upon a number of PRRs expressed on their cell surface, known as killer inhibitor receptors (KIR)[23]. These receptors bind to ligands on the surface of host cells, for example MHC-I proteins, and act to prevent killing of the host cells[24]. Any non-host or infected host cell that has downregulated MHC-I, do not bind to KIRs on the NK cell surface, and are therefore targeted for death by the NK cell[25]. NK cells contain lytic granules consisting of perforins and granzymes, which upon activation are released and elicit apoptosis of the target cell[26].

The effector mechanisms of the innate immune system provide an immediate defence network against invading pathogens. However, due to the limited nature of their antigen recognition apparatus (PRRs), the system is vulnerable to the much faster rates of evolution of microbes, meaning selection for pathogens that are difficult or impossible for the innate immune system to detect and clear. Therefore, additional mechanisms are required to deal with rapidly evolving pathogens, which are provided by the adaptive immune system.

1.1.2 Adaptive Immunity

The adaptive immune system acts in a complementary manner to the innate immune system. Whereas the innate immune system is a broad acting, immediate defence network, the adaptive response takes time to develop upon initial exposure to a pathogen[27]. The adaptive response

undergoes a period of selection, to adapt to the new pathogen, and then responds through a number of mechanisms[1]. After the infection is resolved, the components of that specific response die back, but the information required to respond to that same pathogen if encountered again is retained - a process known as immunological memory[27]. Accordingly, if the same pathogen is encountered again, the adaptive response is launched far more rapidly and often with a greater magnitude to protect against the pathogen/infection (the so-called secondary response) and yet with the same exquisite specificity displayed when the pathogen was first encountered (the primary response)[28].

The cell types that mediate the adaptive immune response are lymphocytes that develop in the bone marrow and undergo further differentiation either in the bone marrow (B cells), or migrate to the thymus and differentiate into T cells[29]. Both of these cell types are characterised by their expression of a receptor on their cell surface which carries a unique specificity.

1.1.2.1 T Cells

For T cells, this antigen receptor is known as the T cell receptor (TCR), and is composed of two peptide chains, an α and a β chain, each containing a constant domain and a variable domain coupled together by a disulphide bond[30]. The αβTCR associates with a cluster of differentiation (CD) 3 complex and a homodimeric ζ chain which contributes to intracellular signalling downstream of the receptor[31].

The TCR in each cell is generated from a diverse set of gene segments that are recombined randomly to generate an enormous range of specificities[1]. These segments are classified into three groups, termed variable (V), diversity (D) and joining (J) segments, which differ in nucleotide sequence[32]. In the alpha chain, a single V and J segment are recombined and linked to the α chain constant (C) region, whereas the TCRβ chain also contains D segments, resulting in a VDJ segment combined with the β chain C region[33]. This process is highly similar to that for B cell receptor (BCR) generation, described below (Section 1.1.2.2).

After TCR generation, T cells under a process of thymic selection, where self-antigens are presented to naïve T cells on MHC molecules, and cells expressing TCRs that bind self-antigens strongly are deleted or edited through further TCR mutation, in order to prevent the release of anti-self T cells into the periphery which would could attack the host[34]. TCRs that are non-

functional are also deleted at this stage, as they make no interactions with MHC molecules, preventing them from becoming functional immune cells[35].

The T cells that leave the thymus are classified as naïve, and have not yet encountered foreign antigen[36]. Importantly, T cells only bind to antigen in the context of a peptide presented in an MHC molecule, either MHC-II on antigen presenting cells, or MHC-I, which is expressed on all cells[37,38]. However, antigen alone is insufficient to activate a naïve T cell, and a second, co-stimulatory signal is required simultaneously for initial activation- such as engagement of CD80 (B7.1), 4-1BB (CD137) or OX40 (CD134)[39-41]. Once activated, T cells require only to bind their cognate antigen in the context of MHC molecules to respond[38].

T cells are broadly split into two types, as determined by the presence of CD4 or CD8 on the T cell surface. CD4 expressing cells are termed T helper cells and consist of many subtypes each with different transcription factors [42]. These cells generally act by producing cytokines in response to antigen binding on MHC, and this can contribute to various phenomena ranging from assisting activation of CD8 T cells, assisting in maturation of other immune cell, to production of anti-inflammatory cytokines (such as IL-10) by so-called regulatory T cells (Tregs)[43,44].

CD8 cells are known as cytotoxic or killer T cells. These cells, once activated, recognise their antigen in the context of MHC-I, and kill the expressing cell through release of perforin and granzymes, similarly to NK cells, and also produce inflammatory cytokines such as IFNγ[45]. Both CD8 and CD4 T cells contain subsets that are long lived, and supply the memory capacity to the adaptive response, as they are able to rapidly proliferate upon encountering their antigen, therefore avoiding the lag period seen with the initial antigen exposure[46].

1.1.2.2 B Cells

B cells express a surface receptor, the B cell receptor that imparts upon the cell the capacity to detect a specific antigen. Each BCR is unique to that specific B cell clone and is largely generated through a complex process that takes place in the bone marrow before antigen is detected[47]. The BCR consists of two signalling chains, CD79a and CD79b, and a surface bound immunoglobulin (sIg) molecule that contains the antigen recognition regions[48]. Upon antigen binding to sIg, CD79 transduces this signal into the B cell through immunoreceptor tyrosine activation motifs (ITAMs) present in their intracellular domain[49].

As for the TCR α and β chains (Section 1.1.2.1), the BCR is composed of two chains, heavy (H) and light (L) chain, encoded by a large number of different segments, broken down into the same three classes: variable (V), diversity (D) and joining (J) segments, each present in multiple copies that differ from one another in nucleotide sequence[50]. They also differ in the number of segments in the H and L chains. For the H chain, one of each segment is joined together in a specific order (VDJ) through two recombination events, which can be used to define the progression of B cell development (Figure 1-1). Firstly, a particular D segment is joined to a particular J segment, then combining the DJ segment with a particular V segment[51]. This occurs by a process involving DNA looping utilising specific DNA repeat sequences to ensure the appropriate order of DNA cutting and joining[52].

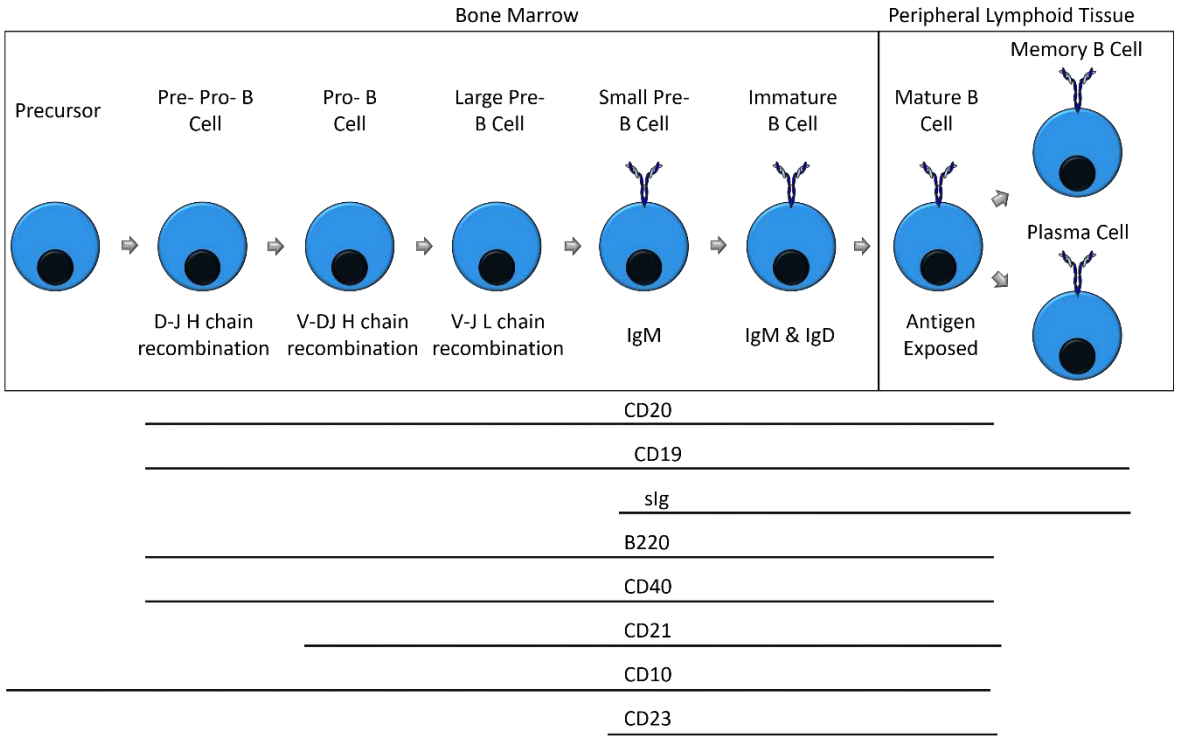

Figure 1-1 B Cell Development

B cells undergo progressive recombination events to generate a surface immunoglobulin, initially of the IgM isotype. The recombination events define various stages of B cell development, further indicated by differential expression of specific surface markers. Adapted from[27].

At the joining sites between the different segments there is also random addition or deletion of nucleotides by DNA repair mechanisms, which generates further variability[1]. The end result is a VDJ region that is unique in each B cell, and which forms the variable region of the H chain[27]. This VDJ region is located in close proximity to the constant region genes of the H chain, and is transcribed along with these gene segments to form an mRNA encoding the entire H chain[51]. The same process takes place for the L chain, with its own V and J segments, although there are no D segments[1,53]. This mature L chain is then produced as above, and two H chains associate with two L chains, through disulphide bonding further increasing the receptor diversity as two separate recombination events have occurred (one in the L chain and one in the H chain)[27]. The BCR is essentially a membrane bound form of an antibody (described further in Section 1.2).

B cells leave the bone marrow expressing their specific BCR on the cell surface, in the form of a surface bound IgM molecule (Figure 1-1)[47]. Once a B cell encounters antigen, it becomes activated and begins a period of rapid proliferation in regions of peripheral lymphoid organs known as germinal centres[54]. In the germinal centre, B cells are able to undergo affinity maturation, through a process of somatic hypermutation[55]. This is a process where further mutations are introduced randomly into the variable regions through a process of double stranded DNA breaks and error prone repair mechanisms, thought to involve the enzyme activation induced cytidine deaminase (AID)[56]. B cell clones that generate an antigen receptor with improved affinity for antigen are selected during this process, as they best compete for antigen binding and accompanying survival signals[57,58]. B cells can then differentiate into antibody secreting plasma cells, some of which reside in the bone and are long lived, contributing to the memory component of the adaptive immune response through continuous production of antibody, while others survive only during the immune response[59-61]. Alternatively, they can differentiate into long-lived memory B cells which proliferate upon rechallenge with antigen to provide the secondary response[62].

Initially this antibody will be of the IgM or IgD isotype. However, B cells can undergo a phenomenon called isotype or class switching in the germinal centre, in which irreversible genomic rearrangement results in a change in antibody isotype by relocating the VDJ region to a different constant region encoding another antibody isotype[55,56,63]. It is this process that leads to the production of antibodies of the IgG, IgA or IgE isotype. Importantly, a class switched antibody retains the same binding specificity encoded by the VDJ regions but differs only in the isotype[1]. Together, these various isotypes impart humoral immunity with the roles for each discussed below.

1.2 Antibodies

1.2.1 Antibodies

Immunoglobulins (Ig), or antibodies, are soluble glycoproteins produced by plasma cells that recognise macromolecular targets with a high degree of specificity. As detailed above, they are capable of recognising a vast number of different targets and are responsible for the humoral branch of the adaptive immune response, providing specificity and recruiting elements of the innate immune system[1]. The specific target an antibody recognises is known as an antigen, and the specific location on the antigen to which an antibody binds is referred to as its epitope. Antibodies are able to bind to these epitopes on the surface of foreign particles, microbes, viruses, parasites and non/altered self-structures such as those that can be found on diseased or cancerous cells.

Antibodies play an important role in the adaptive immune response to infections and their properties have been exploited therapeutically both through induction via vaccinations and by passive transfer from an immunologically healthy patient to an immunocompromised patient[64,65]. More recently recombinantly produced antibodies have also been used in the treatment of a number of diseases including cancer, autoimmunity, as well as anti-venom agents[66,67]. Antibodies are one of the fastest growing families of drugs and have been steadily increasing as a proportion of total biopharmaceuticals[68]. Therapeutic antibodies made up six of the top ten earning biopharmaceuticals in 2017 and have swelled in number, with 69 approved and currently in use in the USA at the time of writing[69,70]. Therapeutic antibodies have also been extremely profitable, with total sales from monoclonal antibody based products totalling almost $75 billion in 2013 and predicted to reach $125 billion by 2020[71].

A major breakthrough in antibody technology came in 1975, that earned the Nobel Prize for Physiology or Medicine in 1984. Köhler and Milstein developed a technique that enabled fusion of immunised spleen cells with myeloma cells, forming immortal hybridomas capable of producing antibody[72]. This production from a single clone of antibody producing cells is known as monoclonal antibody (mAb) technology, with the resultant mAbs all identical at the protein level and recognising the same antigenic epitope[73]. Purification of antibodies from an immunised

animal was previously used to generate antibodies that recognised the same antigen, but these were directed to different epitopes (polyclonal antibodies). As such, mAb production allows the function of antibodies to be studied much more precisely, allowing for the production of highly specific, controlled antibody preparations more suited for therapeutic and research use. Antibody production is now routinely carried out in mammalian cells, for example Chinese Hamster Ovary (CHO) cells, amenable for large scale production of glycosylated antibodies. This ability to produce large quantities of broadly homogeneous reagents is essential, as in 2013 nearly 10 tonnes of mAb products were produced[71].

1.2.2 Antibody Structure

Antibodies are a soluble form of the BCR containing the same variable regions, made up of two heavy and two light chains, each of which folds into a number of immunoglobulin domains; the heavy chain contains four or five (depending on the isotype) and the light chain contains two (Figure 1-2 and Figure 1-3)[74]. There are five different immunoglobulin isotypes, each with a unique heavy chain; IgA- α chain, IgD- δ chain, IgE- ε chain, IgG- γ chain, and IgM- μ chain (Figure 1-3). The majority of the antibody specificity is centred within three regions of high sequence variability, known as complementarity determining regions (CDRs), that form loops that can interact with the target epitope (red loops in Figure 1-2).

There are two different classes of light chain, κ and λ, which pair up with a heavy chain through formation of a disulphide bond and non-covalent interactions between the immunoglobulin domains[1]. Two of these heavy-light chain molecules then come together to form the tetrameric antibody with a stoichiometry of H2L2.

Antibodies are able to bind both to their target antigen but also to specific antibody receptors and effector molecules. This is achieved through spatial separation of the antibody binding 'Fab' region and the 'Fc' region of the antibody. These regions are so-named because cleavage of IgG with the protease papain was found to produce two functionally distinct fragments; one of which is able to bind to antigen (Fragment antigen binding- Fab) and one which was readily amenable to crystallisation (Fragment crystallisable- Fc) as shown in Figure 1-2[75]. Use of another protease, pepsin, results in a different fragment, a so called $F(ab')_2$ fragment, that retains the bivalency of the parent IgG antibody, but does not have the Fc region and thus lacks many of the interactions that full length IgG possesses[76].

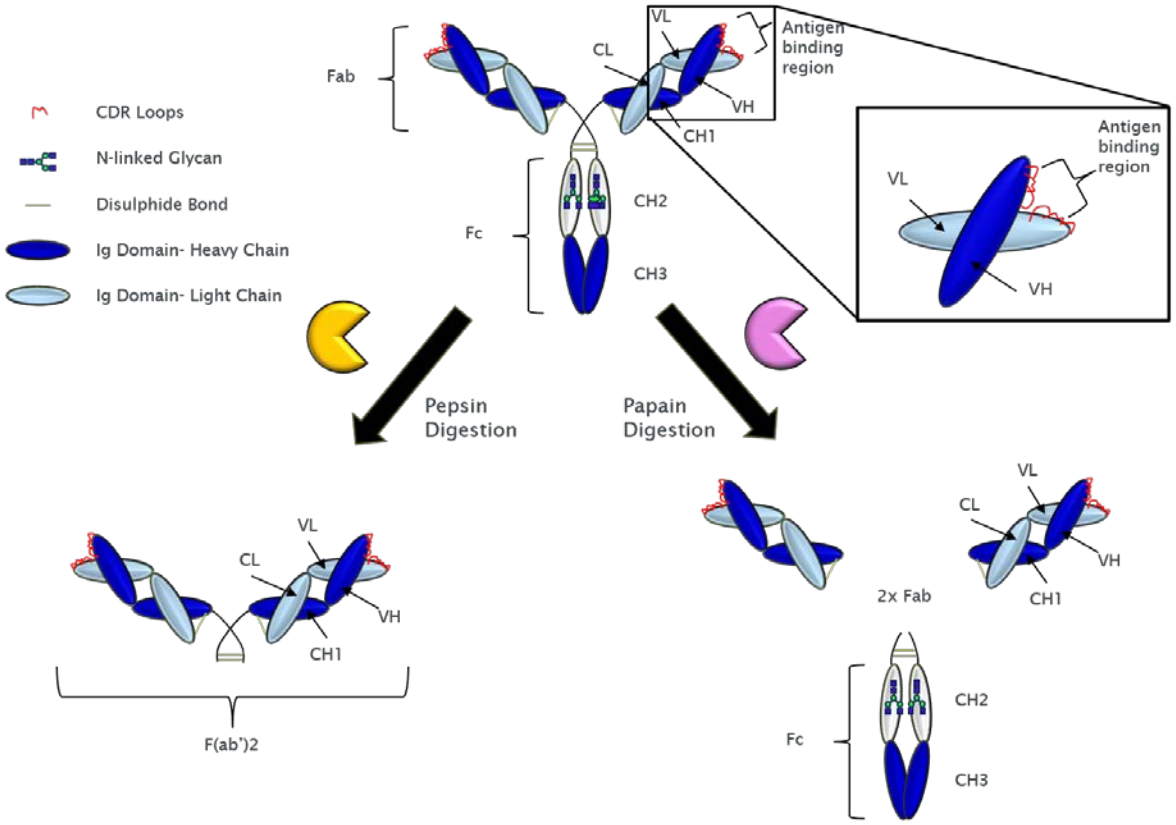

Figure 1-2 Antibody Structure (IgG1)

Schematic representation of an IgG antibody. IgG consists of two four domain heavy chains (blue) of approximately 50kDa each. Three of these domains are of a constant sequence specific to their class, while the amino terminal domain is of variable sequence. These heavy chains are each disulphide bonded to a light chain (light blue) of approximately 25kDa which consists of one constant domain and one variable domain. The variable regions of each chain combine to form the antibody binding regions, containing the hypervariable CDR loops (red). Antibodies are stabilised by disulphide bonds between the heavy chains located in the flexible hinge region (found between CH1 and CH2 as an unstructured linker) and by extensive non-covalent interactions between paired domains VH-VL, CH1-CL and CH3-CH3. In addition to amino acids, mature IgG also display sugar residues attached to asparagine 297 in their CH2 domain. CH2 domain pictured in white to show Fc glycans (blue square- N-acetylglucosamine, green circle- mannose).

1.2.3 Antibody Isotype

Antibodies fall into 5 distinct isotypes, or classes, distinguished by the identity of the heavy chain constant region: IgA (α heavy chain), IgD (δ heavy chain), IgE (ε heavy chain), IgG (γ heavy chain), and IgM (μ heavy chain), as shown in Figure 1-3[1]. The structure of these different heavy chains varies slightly, in particular with regard to the size and structure of the hinge region connecting the Fab to the Fc. In IgA, IgD, and IgG this hinge region takes the form of a flexible linker chain that contains disulphide bonds between H and L chains that differ in number between different isotypes and subclasses, whereas in IgE and IgM, there exists a fifth immunoglobulin domain

within this region that limits the flexibility of the hinge region (Figure 1-3)[77]. There are also differences in the hinge region of the antibodies IgA, IgD and IgG, for example IgG has a shorter hinge region than IgA and IgD (Figure 1-3).

Although some antibodies function as monomers, such as IgG, IgD and IgE, others are active in higher order complexes, such as secretory dimeric IgA and pentameric IgM (Figure 1-3)[77]. These polymeric structures contain an additional component, known as a joining or 'J' chain, that attaches to two of the Fc regions within the structure, and can also carry a secretory component (SC) if they have been transported by the polymeric immunoglobulin receptor (pIgR)[78].

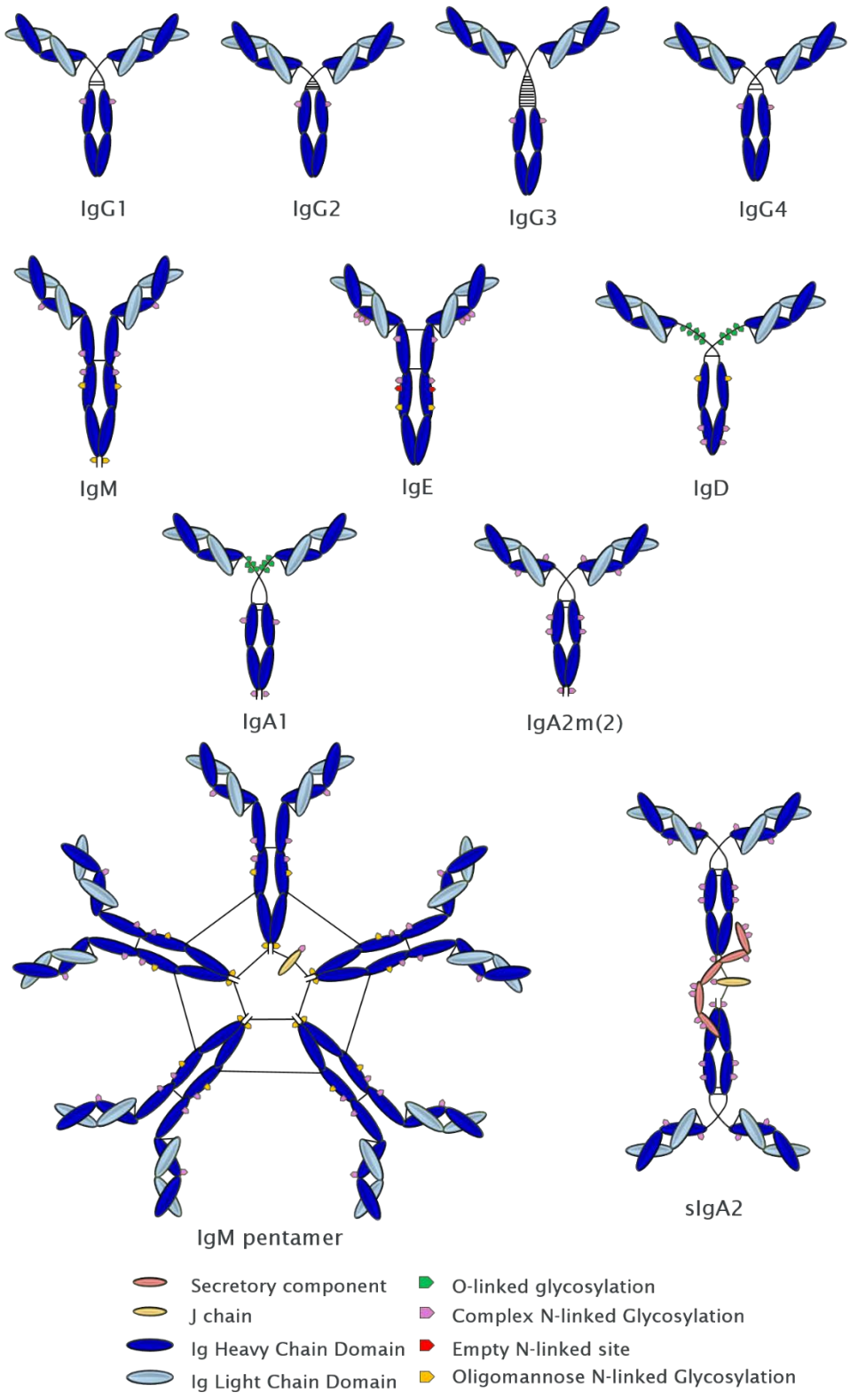

Figure 1-3 Immunoglobulin Isotypes and Subclasses

Humans possess five different isotypes of immunoglobulin, IgA, IgD, IgE, IgG, and IgM, which take a range of forms and are specialised for specific functions. Heavy and light chains are shown in dark and light blue respectively. Disulphide bridges are indicated by black lines.

1.2.4 Immunoglobulin M

IgM is active as a polymer and is commonly found as a pentamer in serum, although hexamers are also found[79]. The 5/6 IgM molecules disulphide bond to one another in their CH4 domain, while 2 of the 5 CH4 domain tails present in the IgM pentamer are also disulphide bonded to a J chain, which enables their transport across mucosal layers[79].

The different antibody classes are thought to have been selected for specific roles within the immune response. IgM for example is the first antibody class produced during an immune response and despite having a typically lower binding affinity is highly efficient at activating the complement cascade to elicit destruction and/or opsonisation of the target[79]. This is thought to be achieved through the hexameric structure of IgM enabling a high avidity interaction with the hexameric head groups of C1q, the initiator of the classical complement cascade[80]. In addition to the secreted polymeric form of IgM, monomeric surface IgM (sIgM) is also important as it functions as the first B cell receptor expressed on immature B cells to detect antigen (Section 1.1.2.2). This form of sIgM contains a short additional tailpiece necessary for integration into the membrane (provided by a transmembrane sequence) and a short KVK intracellular motif[81].

1.2.5 Immunoglobulin A

Although IgA is present in the serum at lower levels than IgG, IgA is the most abundantly produced antibody isotype[82]. This is because IgA is highly prevalent at mucosal surfaces and in bodily secretions, where it acts to defend mucosal surfaces through binding to pathogens and toxins preventing their access to the body[83]. IgA at these mucosal surfaces is dimeric, with a J chain attached via a single disulphide bond to one of the heavy chains of each IgA Fc, as shown in Figure 1-3[84].

The J chain is necessary for transport across mucosal surfaces, where the complex interacts with pIgR, during which the extracellular domain of the pIgR is cleaved off and remains attached to IgA as the secretory component, forming secretory IgA (sIgA)[85]. In contrast to dimeric IgA, serum IgA is monomeric and does not interact with the J chain or contain the amino terminal tail piece necessary for J chain binding. Serum IgA is able to bind to several surface receptors and elicit

immune effector mechanisms such as antibody dependent cell mediated cytotoxicity and phagocytosis, but does not activate the classical complement cascade[86,87-89].

There are 2 subclasses of IgA, IgA1 and IgA2. IgA1 has an extended hinge region resulting from an insertion of a 16 amino acid stretch, and this hinge contains a number of O-linked glycosylation sites[90,91]. Despite partial protection from proteases given by the glycans, IgA1 is more susceptible to degradation than IgA2, which is far more common at mucosal surfaces than IgA1[82].

1.2.6 Immunoglobulin E

IgE is present at the lowest levels of all antibody classes, but despite this is highly active[92]. This high activity is due to the high affinity IgE receptor (FcεRI), present on eosinophils, basophils, mast cells and Langerhans cells[92]. This high affinity means that these cells can be coated in IgE even in the absence of antigen, resulting in rapid degranulation when antigen is encountered [93]. IgE is thought to be primarily involved in response to parasitic infections (e.g. helminths) and allergic responses to innocuous antigens such as pollen and house dust mite faeces, through release of soluble factors such as histamine, and leukotrienes[94].

1.2.7 Immunoglobulin D

IgD is present in the serum at low levels but is not strongly associated with any particular function and so its effects remain obscure. It is able to bind to certain microbes, such as *Moraxella catarrhalis* via a specific IgD binding protein (MID)[95]. IgD is also important as a membrane bound molecule on the B cell surface, where it acts as an antigen receptor in addition to, or instead of, surface IgM[81]. Unlike the other Ig isotypes, there are no recognised IgD receptors.

1.2.8 Immunoglobulin G

IgG is the most prevalent form of antibody in the serum, and is typically the predominant form of antibody produced in an immune response after the initial IgM[1]. IgG antibodies are generally high affinity and efficient at recruiting and engaging immune effector cells, as well as activating

complement and directly causing effects through their antigen binding[74]. As a result of their importance and effectiveness in combating a range of pathogens *in vivo*, almost all current therapeutic antibodies in the clinic are of the IgG isotype[96].

IgG antibodies can be further subdivided into 4 subclasses, IgG1 – 4, based on their prevalence in serum (with IgG1 being the most common and IgG4 the least)[97]. IgG subclasses are highly homologous (over 90%) but primarily differ within the hinge region and upper CH2 domain (Figure 1-3), and in their affinities for the various FcγRs (discussed in Section 1.3) and C1q[74,98]. IgG subclasses also differ in their ability to elicit different effector functions, with IgG1 and IgG3 being the most pro-inflammatory, strongly inducing complement and FcγR mediated responses[74,99]. IgG2 antibodies are commonly directed against carbohydrate antigens but are less able to engage complement and FcγRs, as are IgG4 which are often generated in response to repeated or chronic antigens[100,101].

IgG2 and IgG4 have slightly shorter hinge regions than IgG1, which reduces their flexibility slightly[102]. The IgG2 hinge region contains more disulphide bonds (4) than IgG1 and IgG4 (2 each), which further reduces its flexibility[74]. The pattern of these disulphide bonds can shift, allowing IgG2 to exist in two different forms, termed A and B, depending on the orientation of these disulphide bonds[103]. The A and B forms of IgG2 have been reported to be functionally distinct in certain circumstances, for example in their ability to act as superagonists to, among other receptors, the costimulatory molecule CD40[104].

Due to IgG4 specific residues in the hinge region, disulphide bonds within the IgG4 hinge region are able to form intramolecularly, resulting in heterodimeric HL structures (compared to the normal H2L2)[105,106]. These HL structures can randomly combine with others of a different specificity, resulting in the formation of H2L2 IgG4 antibodies that are monovalent and bispecific in nature[107]. Mutation of the serine residue at position 229 to a proline residue (as is found at the analogous position in IgG1) prevented this Fab arm exchange[105].

In contrast, IgG3 has the largest hinge domain, which gives it greater flexibility than the other subclasses, but may also make it more susceptible to degradation by proteases, partly explaining its greatly reduced half-life (~7 days vs ~21 days) compared to the other IgG subclasses[108]. As IgG3 is the most pro-inflammatory IgG subclass, this short half-life may help to limit excess inflammation.

This long serum half-life of IgG is mediated by binding to the FcRn receptor, as described below (Section1.3.1), which is able to rescue IgG taken up into a cell from degradation and return it to the serum[109].

1.2.9 Antibodies as Glycoproteins

All antibodies are glycoproteins and as such carry covalently linked glycans which can make up a large proportion of the molecular mass of some antibodies, such as IgE and IgD[110]. The location and number of the glycans differ between isotypes and subclasses, and can be either N-linked or O-linked, present in different degrees of processing (such as complex or oligomannose)[110]. These glycans are only present on the heavy chains of the antibodies, but during somatic hypermutation it is possible that further glycosylation sites can be introduced randomly on either chain - for example, approximately 15% of IgG contain N-glycans in their Fab regions despite the lack of a germ line encoded glycosylation sites[111]. The germ line encoded glycans of the human immunoglobulins are shown in Figure 1-3.

1.3 Fc gamma Receptors (FcγR)

1.3.1 FcγR Biology

Human IgG antibodies bind antigen through their Fab regions, but many of their effects arise from the IgG Fc region binding to specific FcγRs (Figure 1-4). Humans express 6 FcγRs: FcγR I, IIa, IIb, IIc, IIIa and IIIb[112]. These receptors also have designated cluster of differentiation names; CD64, CD32a-c, and CD16a-b, respectively. These FcγRs can be grouped into those that transduce an activatory signal after IgG binding, and those that transduce an inhibitory signal[112]. FcγRIIb is the only inhibitory FcγR, with the remainder all transducing activatory signals with the possible exception of FcγRIIIb[113]. FcγRIIIb is unlike the other FcγRs in that it is linked to a glycophosphatidylinositol (GPI) anchor in the cell membrane rather than having a transmembrane region and an intracellular domain, and as such is typically referred to as a neutral receptor[114]. There are also structural differences within the FcγRs, with FcγRI being the only receptor that has three extracellular domains, the rest all having two (Figure 1-4)[115].

The activatory FcγRs transduce their intracellular signals via immunoreceptor tyrosine-based activation motifs. In the case of FcγRIIa and FcγRIIc, these ITAMs are present within the intracellular domain of the FcγR[116]. However, FcγRI and FcγRIII lack this intracellular ITAM in their cytoplasmic tail and instead rely on association with the ITAM containing common γ chain (FcRγ) for signalling[117,118]. This FcRγ chain is also required for stable production and surface expression of these FcγRs. The inhibitory FcγRIIb contains within its intracellular domain an immunoreceptor tyrosine-based inhibitory motif (ITIM) that is able to initiate inhibitory signalling downstream of IgG binding[116].

Although humans can express 6 FcγRs, these are not all expressed in all people. FcγRIIc is only expressed in a subset of people due to a specific polymorphism in the third exon of the gene encoding a stop codon which prevents transcription, with only approximately 18% of the European population expressing the gene[119,120]. Only alleles without this polymorphism are expressed. Furthermore, while FcγRI (the product of the gene *FCGR1A*) is expressed in humans the closely related genes *FCGR1B* and *FCGR1C* are not[121].

Another molecule that is capable of binding to IgG Fc is the neonatal Fc receptor (FcRn). This receptor was first discovered in neonatal rats, but it is now known to be expressed in many cell types in adult organisms and in other species, including humans[122]. It was discovered due to its role in transporting maternal IgG across the small intestine epithelium in neonatal rats, but is now known to transport antibodies from mother to foetus in humans to impart a degree of passive protection to the foetus[123,124]. Unlike the FcγRs, FcRn is structurally related to MHC-I proteins, consisting of a 45kDa α chain formed of three domains that associates with the 12kDa β_2-microglobulin for correct protein folding and IgG binding (Figure 1-4)[125,126]. FcRn binds to a distinct region at the CH2-CH3 interface of the Fc as compared to the classical FcγRs mentioned previously[127]. Furthermore, its ability to bind to IgG Fc in a pH dependent manner allows it to facilitate the recycling of endocytosed IgG back into the blood, protecting the IgG from proteasomal degradation[128]. FcRn only binds to IgG below pH 6.5, when histidine residues in the IgG Fc become protonated, for example in acidified endosomes, and releases the bound IgG extracellularly at a more neutral pH, returning it into the serum[129]. This is the mechanism responsible for the long serum half-life of IgG (~21 days), and an equivalent mechanisms is present in mice as inactivation of mouse FcRn decreases the half-life of mouse IgG by up to 80%[130-132].

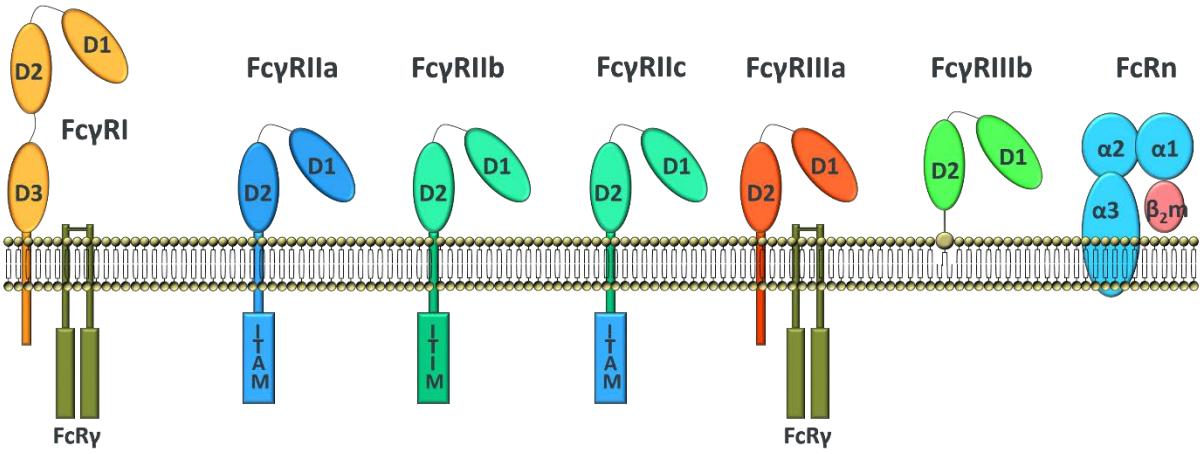

Figure 1-4 Fc Gamma Receptors (FcγR)

Human IgG bind to FcγRs through their Fc region. Humans express several FcγRs with varying structures, expression patterns and IgG affinities. All of the FcγRs consist of two or three (in the case of FcγRI) extracellular immunoglobulin domains, a transmembrane region (or a lipid anchor in the case of FcγRIIIb) and an intracellular domain. FcγRII also possesses an intracellular signalling domain, containing either an immunoreceptor tyrosine-based activation motif (ITAM) or, in the case of the inhibitory receptor FcγRIIb, an immunoreceptor tyrosine-based inhibitory motif (ITIM). FcγRI and FcγRIIIa do not have intracellular signalling domains and instead signal through the common FcRγ chain, which itself contains ITAMs. FcγRIIc is a rarely expressed Fc receptor that consists of the extracellular Fc binding domain of FcγRIIb (cyan) combined with the intracellular signalling domain of FcγRIIa (dark blue). FcRn is a non-classical FcR that is capable of binding to IgG as well as to other antibody subclasses via a unique, non-overlapping region of the antibody Fc.

1.3.2 FcγR Distribution

The different FcγRs expressed in humans described above exhibit specific patterns of cell expression, with some being highly cell-specific and others being quite widely distributed (Table 1-1). Some cells only express a single type of FcγR, for example B cells express only FcγRIIb and NK cells only express FcγRIIIa (and FcγRIIc in people with the appropriate genotype)[133]. However, many myeloid cells express multiple FcγRs, some of which can be upregulated during an immune response (Table 1-1)[134]. T cells are not thought to express any FcγRs, although some evidence for surface expression has been found in mouse T cells[135]. FcγRIIIb, the only GPI linked receptor, is found on neutrophils and has also been reported to be present on basophils[136]. FcγRs can also be expressed by non-haematopoietic cells, for example liver sinusoidal epithelial cells express FcγRIIb[137].

On many cell types, for example macrophages, both activatory and inhibitory FcγRs are expressed (Table 1-1). Furthermore, different IgG subclasses have differing affinities for FcγRs. This is well exemplified by the mouse IgG1 and IgG2a subclasses. Mouse IgG1 has a higher affinity for mFcγRII (the mouse inhibitory FcγR) than for the activating mFcγRs, whereas the opposite is true for mouse IgG2a[138]. As a result, a much greater activatory response is induced to the same antigen using a mouse IgG2a compared to a mouse IgG1 antibody[139]. This can be quantified by calculating the ratio between the affinity of an antibody subclass for activatory and inhibitory receptors, and is referred to as an activatory:inhibitory ratio (A:I ratio)[139]. This ratio can also be used to take into account the relative expression pattern of the different FcγRs - for example polarising human macrophages to increase the level of FcγRIIb expression would decrease the A:I ratio compared to a non-polarised cell[16]. Antibodies with a higher A:I ratio are predicted to be more active at inducing an FcγR dependent response than those with a low A:I ratio, and this has been found to be the case *in vivo*, for example in deleting target cells[140-143].

Cell Type	Expression Pattern					
	FcγRI	FcγRIIa	FcγRIIb	FcγRIIc	FcγRIIIa	FcγRIIIb
B cell	-	-	+	-*	-	-
T cell	-	-	-	-	-	-
Monocyte	+	+	+	-	-	-
Macrophage	+	+	+	-	+	-
Neutrophil	+	+	-	-	-	+
DC	-	+	+	-	-	-
NK cell	-	-	-	(+)	+	-

Table 1-1 Expression Pattern of FcγR on Human Immune Cells

FcγR expression patterns on a number of leukocytes is shown. FcγR expression varies between different cells, with some cells expressing multiple FcγRs (such as macrophages), others expressing just a single FcγR (for example B cells which only express FcγRIIb) and some cells express no detectable FcγRs (such as T cells, which under most circumstances express no FcγRs). (+) indicates FcγRIIc is only expressed in a subset of humans with the appropriate polymorphism, * and has also been reported on B cells[144] (table modified from[133]).

1.3.3 FcγR Affinities

As well as differing in structure, signalling mechanism and cell distribution, one of the key differences between the FcγR family members is their affinity for IgG Fc. The FcγRs can broadly be

grouped depending on their affinity for IgG, with the only high affinity member being FcγRI, although FcγRIIIa can also bind to monomeric IgG3 (Table 1-2)[98]. As FcγRI is the highest affinity receptor, and also the only receptor with three immunoglobulin domains (Figure 1-4), it is possible that the extra domain may contribute to the high affinity binding in some way, although crystallography evidence argues against a direct interaction with this third domain[56]. Other studies have suggested that a specific leucine residue from FcγRI may insert into a hydrophobic pocket on the surface of IgG, explaining the increased affinity[145,146].

Bruhns *et al.* examined the binding of monomeric and aggregated IgGs with all the FcγRs, and reported K_A values[98]. The high affinity FcγRI had a K_A of approximately 30-60nM for IgG1, IgG3 and IgG4, with IgG2 having a much reduced affinity. The next highest affinity receptor, FcγRIIIa, has affinities in the order of 100nM- 10μM, with IgG3 being the most strongly bound subclass. FcγRIIa binds all four IgG subclasses, with the highest affinity for IgG1, while FcγRIIb is the lowest affinity receptor for IgG, with affinities lower than that for FcγRIIa. FcγRIIIb is of slightly lower affinity than FcγRIIIa[98].

Receptor	IgG							
	Monomeric				Aggregated			
	IgG1	IgG2	IgG3	IgG4	IgG1	IgG2	IgG3	IgG4
FcγRI	+	-	++	++	+++	-	+++	+++
FcγRIIa $_{H131}$	-	-	-	-	+++	++	+++	++
FcγRIIa $_{R131}$	-	-	-	-	+++	+	+++	++
FcγRIIb	-	-	-	-	+	-	++	+
FcγRIIc	-	-	-	-	+	-	++	+
FcγRIIIa $_{V158}$	-	-	++	-	+++	+	+++	++
FcγRIIIa $_{F158}$	-	-	+	-	++	-	+++	-
FcγRIIIb	-	-	-	-	+++	-	+++	-

Table 1-2 FcγR Affinities for IgG Subclasses

The affinities of the FcγRs for monomeric and complexed IgG. Monomeric IgG is only bound strongly by FcγRI, and to an extent by FcγRIIIa, with the V158 polymorphism binding better than the F158 polymorphism (see below). IgG that has been multimerised with F(ab')$_2$ anti-human Fab exhibits a much broader binding pattern with binding to almost all FcγRs seen. Nonetheless subclass differences remain with IgG2 showing the lowest binding and IgG3 the highest binder to most FcγRs. Table modified from[98].

1.3.4 FcγR Polymorphisms

There are a number of polymorphisms in the human FcγR genes, some of which have been found to have functional impacts upon IgG binding and FcγR mediated functions (Table 1-2). FcγRIIa has a polymorphism at position 131, which contains either a histidine or an arginine (H131 or R131)[147]. This polymorphism has an effect on the affinity of FcγRIIa for IgG2, with the H131 polymorphism having an approximately four fold greater affinity[148,98].

FcγRIIIa also has a polymorphism that effects the IgG binding properties of the receptor, with position 158 of the receptor containing either a valine or a phenylalanine (V158 or F158)[149]. The V158 polymorphism has increased affinity for IgG1 and IgG3 over the F158 form[98]. FcγRIIIa expressing NK cells are thought to be one of the mediators of antibody mediated killing, through antibody dependent cell mediated cytotoxicity (ADCC- see Section 1.4.3), and as such it has been reported that tumour bearing patients who have V158 alleles of FcγRIIIa exhibit a greater

response to antibody therapy[150]. Associations with H131 and improved response to antibody therapy have also been reported, but are less well understood as both V158 and H131 have been associated with increased progression free survival in follicular lymphoma treated with rituximab or an anti-idiotype antibody[151,152]. Although many studies have suggested a link between FcγR polymorphisms and better response to antibody therapy, contradictory findings have also been reported[153]. Certainly, patients with the low affinity alleles can still benefit from antibody therapy.

A single nucleotide polymorphism found in FcγRIIb causes an I232T mutation in the transmembrane region[154]. This mutation reduces the ability of FcγRIIb to translocate into lipid rafts after binding to IgG and can therefore reduce the signalling induced by the ligation of this receptor[155].

FcγRIIIb is also polymorphic, with at least three different alleles being expressed in humans. These alleles, designated FCGR3B*01, 02 and 03, are quite similar with respect to their IgG binding properties, although may have some effect on FcγRIIIb mediated functions such as neutrophil phagocytosis of pathogens[156].

FcγRs can also be further regulated by the presence of copy number variation of particular receptors, which can result in increases and decreases in the number of genes for various receptors. This can have important functional implications, for example comparison of NK cells from donors with a deletion in the gene for FcγRIIIa with those from donors with 2-3 copies of the same gene revealed decreased protein expression and ADCC activity in the former donors[157]. Copy number variations have also been found to be associated with increased risk of autoimmune disorders, including systemic lupus erythematosus (SLE) in multiple different human populations[120,158].

1.4 Antibody Effector Functions

mAbs were first used as therapeutic agents in 1986, with an anti-CD3 (OKT3) antibody being approved to treat kidney transplant rejection, although issues with toxicity and anti-drug responses were apparent[159-161]. In the years that followed, many more antibodies with superior properties have been assessed with an increasing number approved for a broad range of indications from autoimmunity to oncology and macular degeneration, with several of these

molecules achieving substantial economic and therapeutic success, becoming listed on the World Health Organisation (WHO) list of essential medicines[69,70,162]. While a great deal of research has gone into delineating the effector functions of these therapeutic mAbs, in many cases the exact contributions of different mechanisms are not fully understood, and many patients undergo relapse or become resistant to therapy[163]. More recently, a new trend in mAb therapy has emerged with the development of so-called immunomodulatory antibodies that earned to 2018 Nobel Prize in Physiology or Medicine for James Allison and Tasuku Honjo[164]. These antibodies, rather than depleting target cells, act to alter the immune system in order to elicit their effect[165]. The first of these agents to be approved is the cytotoxic T lymphocyte associated protein-4 (CTLA-4), ipilimumab, for the treatment of metastatic melanoma[166,167]. This new class of antibody has shown that it can be highly effective when combined with existing chemotherapy treatments, achieving cures in previously hard to treat diseases, but there are still many patients that do not respond[168]. Further study of the mechanisms of action of these antibodies is thus of vital importance to fully optimise their evident therapeutic potential.

1.4.1 Direct Effects of Antibody Binding

When IgG antibodies bind to their cognate antigens on the surface of target cells, they can have numerous effects. Some of these effects depend on interaction with other molecules in the serum or with effector cells expressing specific FcγRs, but others are caused simply by the antibody binding to its target (Figure 1-5). In the case of binding to bacteria or viral pathogens, the binding of antibody is often able to prevent actions of the pathogen that are necessary for infection, such as cell attachment or invasion. Antibodies can also increase pathogen uptake by immune cells by forming immune complexes, binding multiple pathogens[1].

Antibodies being used to treat human disease often target cell surface receptors (e.g CD20, CD52)[70]. When binding to cell surface receptors, antibodies generally have one of two effects, being either agonistic or antagonistic. An antagonistic antibody is an antibody that prevents signalling through a particular receptor, by binding to it but not inducing signalling in the way that the natural ligand (which is blocked from binding the receptor) does. Therapeutic IgG antibodies targeted against growth factor receptors often function through this mechanism, for example the anti-human epidermal growth factor receptor (HER) 2 antibody trastuzumab (Herceptin) which has been used effectively to treat HER2+ breast cancer, and the anti-epidermal growth factor

receptor (EGFR) antibody cetuximab (Erbitux) which is used in the treatment of colorectal cancer among others engage this mechanism[169,170]. Agonistic antibodies work in the opposite way to antagonists in that they bind to the surface receptor and induce signalling, typically in the absence of ligand binding. This can transduce a strong signal to the target cells which can be utilised for therapeutic effect. One class of agonistic antibodies are directed to specific death receptors on the cell surface, and give a strong apoptotic signal to the cell (Figure 1-5)[171]. These death receptors include tumour necrosis factor (TNF)-related apoptosis-inducing ligand receptors (TRAILR), which has been targeted by the antibodies mapatumumab and lexatumumab[172].

An emerging use of agonistic and antagonistic antibodies is to try and boost immune cell function, through agonism of stimulatory receptors and antagonism of inhibitory receptors. These agents are referred to as immunomodulatory antibodies. These receptors, also known as immune checkpoints, include inhibitory molecules such as CTLA-4 and programmed cell death protein 1 (PD-1), as well as stimulatory receptors including CD27, CD40, and CD134 (OX40)[173]. Antibodies targeting these molecules have achieved success in the clinic in treating several tumours and the antibodies ipilimumab (Yervoy- anti-CTLA-4) and pembrolizumab (Keytruda- anti-PD-1) have achieved FDA approval for use in melanoma treatment[167,174].

All of these activities depend on exquisite target specificity – binding a single particular receptor/antigen. Other antibody functions require specific elements of the immune system, such as complement (discussed next).

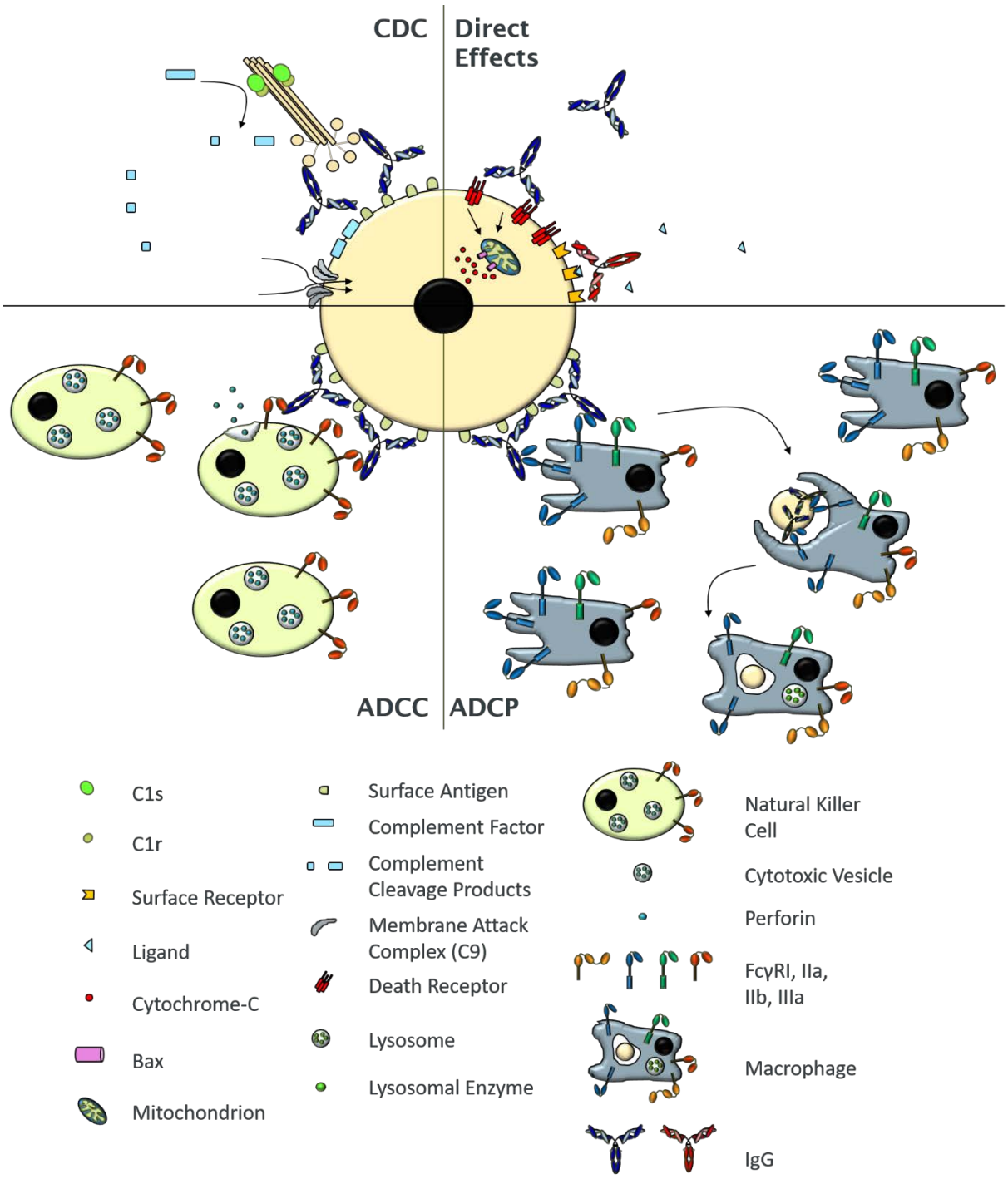

Figure 1-5 IgG Effector Functions

IgG antibodies can elicit a range of effector functions. Top left- complement dependent cytotoxicity is initiated by binding of IgG to the target cell. Top right- antibody binding to cell surface molecules can have direct effects, such as inducing death signals or blocking ligand binding. Bottom right- antibody dependent cellular phagocytosis is initiated by IgG binding to target cells and engaging FcγRs on phagocytes, such as macrophages. Bottom left- antibody dependent cellular cytotoxicity is initiated by IgG binding to target cells and engaging FcγRs on cytotoxic cells, such as NKs as shown.

1.4.2 Complement Dependent Cytotoxicity

One mechanism by which antibodies can cause target cell destruction and generate inflammatory signals is through activation of the complement cascade (Figure 1-5) - a series of serum proteins and zymogens which require cleavage for activation and then act in a feed-forward mechanism to amplify their own activation[6]. IgG and IgM antibodies predominantly activate the classical arm of the complement cascade, which can result in cell lysis, augmented phagocytosis and release of anaphylatoxins (Figure 1-6).

The first protein complex involved in the classical arm of the complement pathway is the C1 complex. This complex is responsible for recognising opsonised targets labelled by antibodies, through the C1q subunit of the C1 complex, and triggers activation of the rest of the cascade[175]. C1q is made up of 6 copies of three different polypeptide chains, C1qa, C1qb and C1qc, encoded on chromosome 1, forming an 18 polypeptide molecule with a total mass of approximately 460kDa[176]. C1q is primarily produced by macrophages, but can also be made by immature dendritic cells as well as mast cells[177].

Each subunit contains both a collagen like helical region and a globular region, at the carboxyl terminus[178]. The globular head groups of the C1q subunits form into a heterotrimeric domain, and it is these heterotrimers that binds to antibodies and other ligands, while the collagen like regions coil into a helix to bind the domains together[179]. This structure is further strengthened by a disulphide bond between a C1qa and a C1qb subunit, and these heterotrimers are then bound into dimers through an additional disulphide bond between adjacent C1qc subunits[180]. Three of these dimers made up of C1q heterotrimers assemble into a complete C1q structure containing 6 heterotrimers, often described as an ‘Eiffel Tower’ or ‘Bunch of Flowers’ structure (depending on the orientation) because of the helically coiled tail at one end and the spread head groups at the other end[181]. While the globular head groups are responsible for the broad ligand binding properties of C1q (not only limited to antibodies, but including some bacterial and viral surfaces, as well as apoptotic cells, amyloid and prion proteins), the serine proteases C1r and C1s associate with the helical region of the complex[182-186].

C1q has many important functions in the immune system beyond acting as the initiator protein for the classical arm of the complement cascade. It also acts to help label apoptotic cells for phagocytosis in the absence of antibody opsonisation, through binding to various surface ligands such as phosphatidyl serine and DNA and being recognised by surface receptors, such as the

globular C1q receptor (gC1qR) and calreticulin, expressed on macrophages[187-191]. This helps their clearance by macrophages to avoid the release of intracellular cytotoxic substances and limits inflammation[192].

C1q is also known to be important in autoimmunity. Individuals with genetically reduced C1q have a 90% chance of developing the autoimmune condition SLE, and C1q knockout mice develop a similar condition spontaneously, while SLE patients can also develop antibodies against their own C1q[193]. It is thought that this loss of C1q, whether genetic or antibody mediated, reduces the ability of C1q to help clear apoptotic cells in a non-inflammatory way, and could prevent it from carrying out other tolerogenic mechanisms[194,195].

C1q binds to antibodies, namely IgG and IgM, through their upper Fc regions, (CH2 for IgG, CH3 for IgM), with several residues known to be important for this interaction on human IgG1. It was shown with the anti-CD20 IgG1 antibody rituximab that the residues D270, K322, P329, and P331, when mutated to alanine, significantly reduced the binding to C1q, whereas the mutation of residues E318 and K320 (which are important for mouse IgG2b interaction with C1q) had no effect on the human antibody[196].

The corresponding binding site on the globular C1q head group has also been analysed, with several residues thought to be important, across all three subunits. The IgG- C1q interaction is known to be ionic in nature, and modification of charged residues on the globular head group was found to block C1q binding[197,198]. Recombinant production of the individual C1q globular subunits was achieved and allowed for the investigation of the influence of mutations on individual residues[199]. Such mutations of individual arginine and histidine residues on all three subunits were found to have an effect on C1q binding, although individual subunits were also found to have different ligand preferences[199,200].

The crystal structure of the C1q head group confirms the modular structure of the heterotrimers, and further supports the idea that residues from different subunits can co-ordinate binding to the same ligand, owing to the tightly packaged nature of the head group[201]. These results, coupled to atomic resolution modelling, all suggest that these charged residues on the C1q head group are important for the binding to IgG, and that multiple subunits can be involved in binding a single ligand, as is thought to be the case for IgG, although C1qb may be the most important and contact IgG the most[202]. Furthermore, the presence of a calcium ion at the apex of the C1q head group was reported to be required for binding to various ligands including IgG and IgM, as its removal by

EDTA decreased the ligand recognition of the head group[203]. The binding sites for IgM are less well defined, but are thought to overlap at least partially with that of IgG, based on studies using anti-C1q antibody fragments and mutated C1q[204,205].

This interaction of C1q and IgG Fc is very low affinity, in the millimolar range, so as to avoid binding of antibody to C1q in solution and inappropriate activation of the complement cascade which could cause damaging immune activation[6,206,207]. Instead, the interaction of C1q with antibody is driven through avidity, and takes place at the surface of cells or bacteria that are opsonised with antibody. In this context, a high concentration of antibody Fc regions are present, allowing for multiple interactions to occur with the 6 heterotrimeric head groups of C1q, allowing for efficient recruitment of the C1q molecule to the opsonised target surface[6].

IgM is known to recruit C1q more efficiently than IgG, most likely due it its conformation as an oligomer, containing 5 or 6 pre-arranged Fc regions[6]. In order to avoid a high avidity interaction with C1q in solution, IgM requires a conformational change that only occurs upon target binding to allow for binding to C1q[208]. Interestingly, IgG has recently been reported to form an Fc hexamer at the target cell surface to enable efficient interaction with the hexameric C1q[80].

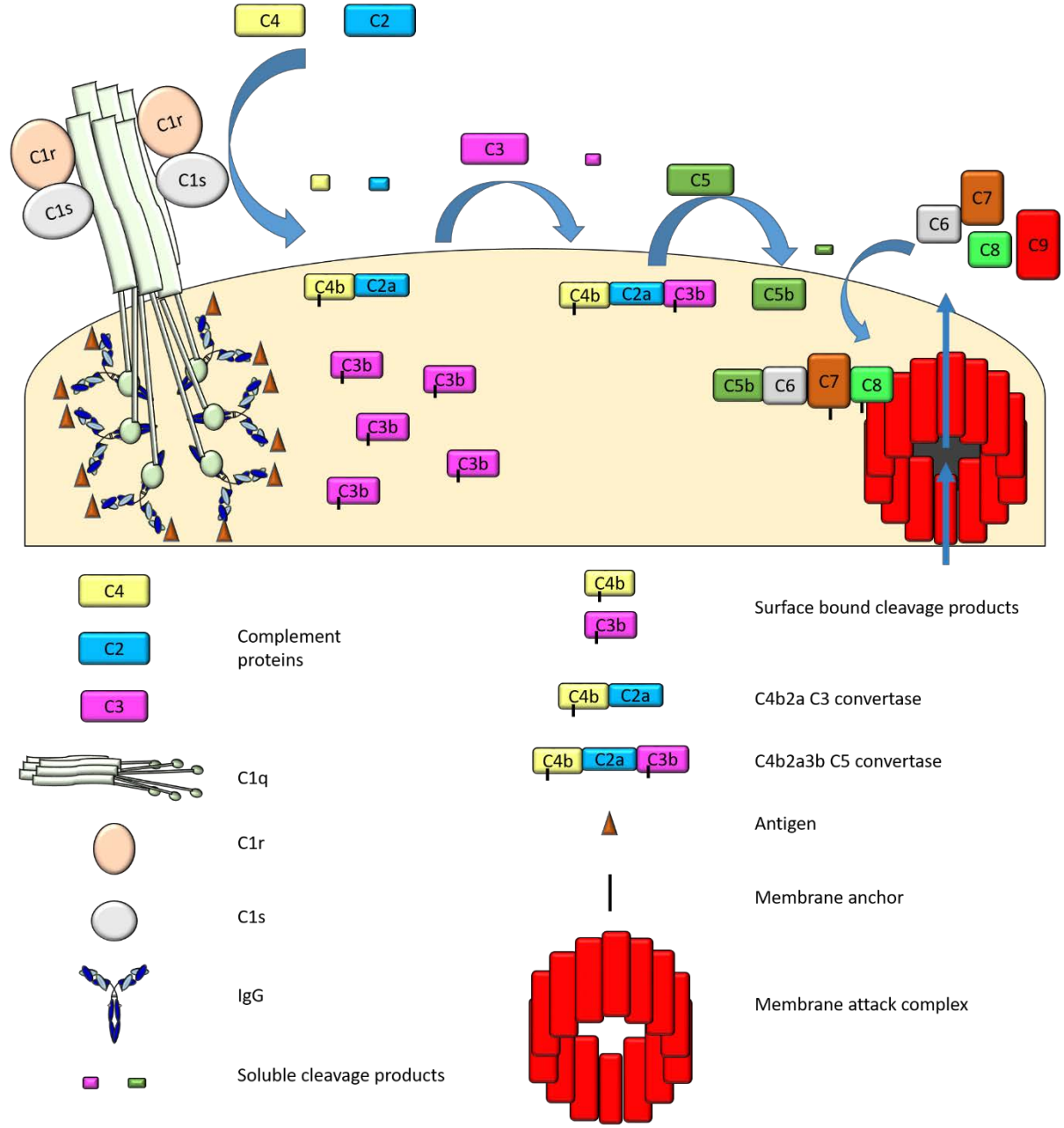

Figure 1-6 Classical Complement Cascade Activation by IgG

The classical complement cascade is initiated by binding of IgG (as shown) or IgM on a target cell surface, enabling recruitment of C1q. C1q bound proteases are then activated resulting in a sequential cascade of enzymatic steps resulting in formation of a membrane attack complex (C9 pore- red) that disrupts plasma membrane integrity. In addition, soluble fragments of several complement proteins are produced that can act as anaphylatoxins to recruit and activate immune cells such as macrophages[209]. Products of the cascade deposited on the cell surface can also act as opsonins resulting in phagocytosis of the target cell[210].

C1q is associated with 2 copies each of the serine proteases C1r and C1s, and binding of C1q to surface bound Fc results in a conformational change in C1q that enables autocatalytic cleavage of C1r to become active, followed by C1r cleaving and thereby activating C1s[211]. C1s is then able to cleave other, soluble components of the complement system. C4 (yellow- Figure 1-6) is the first molecule to be cleaved (into C4a and C4b), and the resulting C4b fragment contains a reactive thioester bond which facilitates its deposition onto the cell surface in the immediate vicinity of C1q[212]. Surface bound C4b is able to bind the next protein in the cascade, C2 (blue- Figure 1-6), which is also cleaved by C1s (into C2a and C2b)[213]. C2a, the larger fragment, is an active serine protease and forms a complex with surface bound C4b, generating the C3 convertase C4b2a[213].

The C3 convertase is able to bind to C3 (purple- Figure 1-6), another soluble complement protein, and cleave it into C3a and C3b, the latter of which anchors to the cell surface via a thioester bond[214]. The C3 convertase can cleave large numbers of C3 molecules, resulting in amplification of the cascade and generation of large numbers (up to 1000) of C3b molecules on the cell surface[1]. Soluble C3a is able to act as an anaphylatoxin, recruiting and activating immune effector cells and increasing the level of inflammation through binding to surface receptors on those cells[215]. As well as its role in formation of the C3 convertase, C3b can also act as an opsonin by binding to complement receptors on phagocytic cells such as macrophages and DCs, triggering phagocytosis of the opsonised particle[210,216].

C3b is able to bind to the C3 convertase and in doing so forms the C5 convertase C4b2a3b[217]. C3b binds the next soluble complement protein, C5 (dark green- Figure 1-6), allowing C2a to cleave C5 into C5a and C5b[218]. C5a is a highly active anaphylatoxin, whereas C5b triggers the late stages of the complement cascade[219]. C5b then binds to C6 (grey- Figure 1-6) followed by binding to C7 (dark red- Figure 1-6) and induces a structural change in C7 that allows it to insert into the cell membrane[220]. C8 (light green- Figure 1-6) binds to the complex and similarly undergoes a structural change to reveal a hydrophobic region that inserts into the membrane. Finally, C8 is able to bind to the last protein in the complement cascade, C9 (red- Figure 1-6), and cause it to polymerise and insert into the cell membrane[221]. 10-16 molecules of C9 can insert into the membrane and form an amphipathic pore approximately 100Å in diameter which disrupts membrane integrity and can lead to cell death[222].

As well as activation through antibody Fc binding, the complement cascade can also be activated by two other mechanisms, known as the lectin binding pathway and the alternative pathway (Figure 1-7). The lectin binding pathway is largely analogous to the classical Fc mediated pathway,

but instead of being initiated by C1q binding to antibody Fc it is initiated by various different activating molecules, including collectins and ficolins, that all bind to Fc and a glycan based target[223]. The best characterised of these is mannan-binding lectin (MBL), which binds to specific sugar residues found primarily on pathogens and recruits antibodies[224]. MBL is similar to C1q in that it has a collagen like structure with six head groups, each of which is capable of binding to a site on the target surface[225]. MBL complexes with MBL associated serine proteases (MASP), which are related to and functional equivalents of C1r and C1s[226 227]. These MASPs then cleave the same complement proteins in the same order, generating the same C3 convertase (C4b2a) resulting in the same downstream effects (Figure 1-7)[228].

The final complement activation pathway, the alternative pathway, is initiated in a different manner. It relies on spontaneous cleavage of the thioester bond of serum C3 by water molecules forming C3(H_2O), which then binds to another complement protein Factor B (grey- Figure 1-7)[229]. This complex is then cleaved by Factor D (blue- Figure 1-7) to generate the fluid phase C3 convertase C3(H_2O)Bb[230]. This complex can then cleave serum C3 and generate C3b which can anchor to nearby surfaces (within 60μm) before hydrolysis by water molecules[231,232]. C3b that deposits on a cell surface can then bind Factor B again, before cleavage by Factor D to generate the surface bound C3 convertase C3bBb[6]. This complex can than cleave large amounts of C3 in the same manner as the other 2 pathways. C3b binding to the C3bBb complex generates the C5 convertase of the alternative pathway, C3b_2Bb, which is able to bind C5 through C3b as for the classical pathway[233]. This complex cleaves C5 which is able to trigger formation of the membrane attack complex (MAC) as for the classical pathway.

The alternative pathway C3 convertase is also formed at the site of initiation of both the classical and lectin pathways, as C3b binds to the cell surface and can bind Factor B. In this way, the alternative pathway acts as an amplification loop, greatly increasing the amount of C3b that is generated (Figure 1-7)[214].

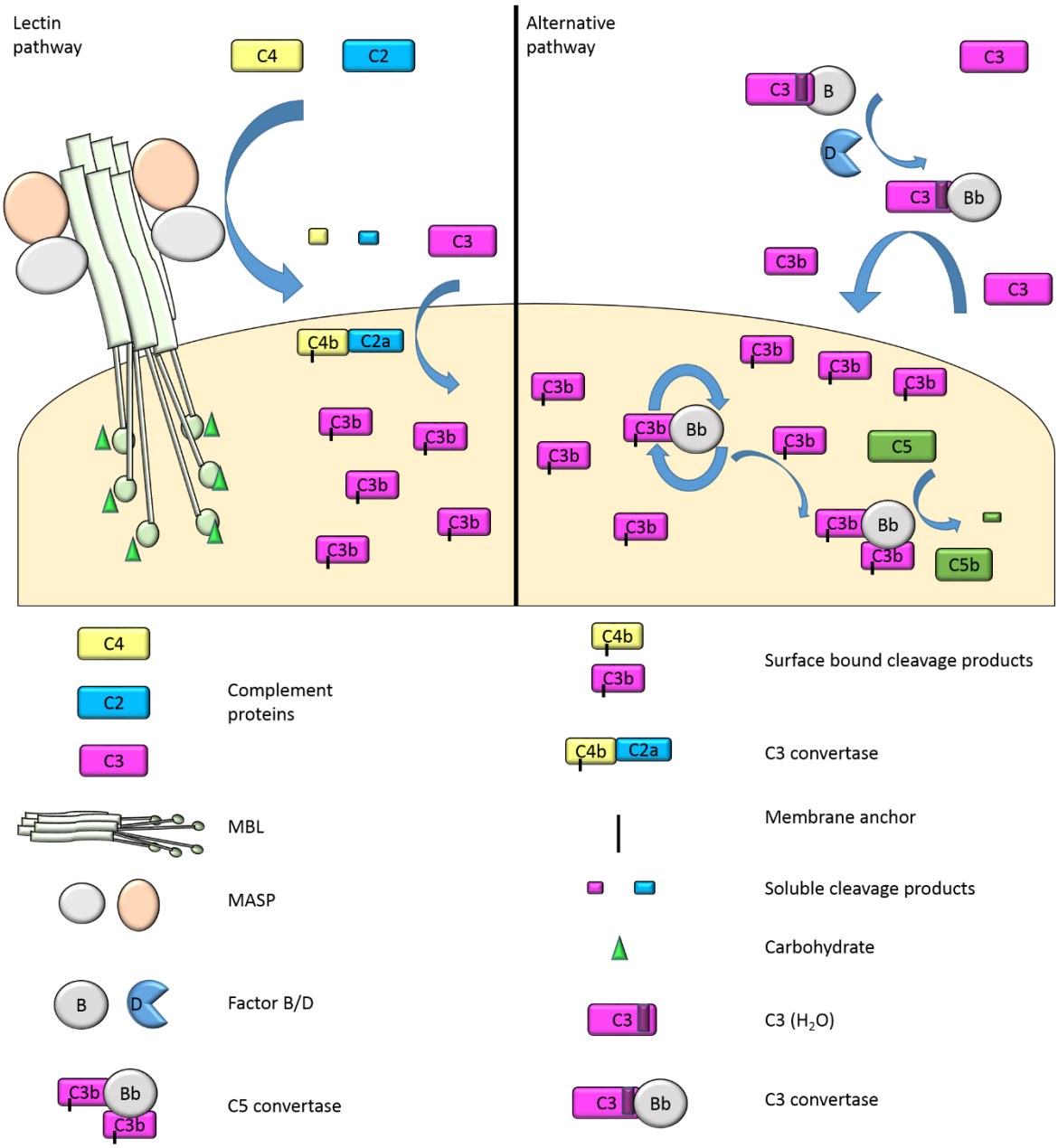

Figure 1-7 Lectin and Alternative Complement Pathways

The lectin pathway of complement activation is highly analogous to the classical pathway, albeit with a different initiator. Proteins such as MBL recognise markers of foreign cells or pathogens and associated MASPs cleave C4 and C2 as in the classical pathway, generating the same C3 convertase C4b2a. The alternative pathway is activated by spontaneous formation of C3(H_2O) and the fluid phase C3 convertase C3(H_2O)Bb. The cell bound C3bBb C3 convertase formed as part of the alternative pathway can also be formed during the classical and lectin pathways and causes amplification of the signal through generation of large amounts of C3b.

Healthy host cells need to avoid initiation of the complement cascade, for example by aberrant deposition of a C3 convertase, or by spontaneous activation of the alternative pathway in close proximity to their surface. This is achieved by a number of complement regulatory proteins, termed complement defence proteins[6]. Some of these are expressed on the cell surface and others are soluble factors. Complement defence proteins such as CD55 (decay accelerating factor) and CD59 (protectin) are commonly found on healthy cells to prevent complement mediated death of the cell[234]. CD55 is a glycophosphatidylinositol anchored membrane bound protein that acts to accelerate the decay of the C3 and C5 convertases of the classical and alternative pathways by promoting dissociation of Bb from C3bBb and C2a from C4b2a, respectively, preventing further signalling[235,236]. CD59 is another GPI anchored membrane protein, and it acts to prevent MAC formation by blocking plasma membrane insertion and polymerisation of C9, thereby maintaining cell membrane integrity[237,238]. CD55 and CD59 have been reported to be important predictors of complement sensitivity for B cell malignancies targeted with mAb on both clinical samples and cell lines, with blocking of these molecules when present restoring CDC[239].

1.4.3 Antibody Dependent Cellular Cytotoxicity

An alternative mechanism of action of mAbs is antibody dependent cellular cytotoxicity (Figure 1-5)[240]. This is direct killing of the opsonised cell by FcγR bearing immune cells, thought primarily to be NK cells, but can also be carried out by monocytes, macrophages and potentially neutrophils[241-243]. NK cells express FcγRIIIa, and in some cases FcγRIIc (Section 1.3), which can bind to the Fc region of target bound antibodies[244]. Binding of Fc to activatory FcγRs results in phosphorylation of the ITAMs in the FcRγ chain (or intracellular region of FcγRIIc) by Src family kinases such as Lck/Yes novel tyrosine kinase (Lyn)[245]. This is followed by recruitment to the FcγRs of Src homology 2 (SH2) domain containing spleen tyrosine kinase (Syk), which binds to the phosphorylated tyrosine residues and becomes active[246].

Syk is then phosphorylated causing its further activation, and this is followed by a series of Syk-mediated phosphorylations and subsequent recruitment of adaptor proteins such as LAT and Grb2[247]. This can trigger further signalling, for example through activation of phospholipase C, leading to increased calcium mobilisation and protein kinase K activation, which can trigger effects such as exocytosis of cytotoxic granules[248]. These granules contain a number of cytotoxic proteins such as perforin, multiple different types of granzymes and granulysin[26]. These proteins

then act upon the target cell, forming pores in the plasma membrane, allowing the caspase like granzymes to initiate the caspase cleavage cascade, leading to apoptosis of the cell[249].

One branch of evidence supporting NKs as effector cells of mAb therapy is the finding that patients with the V158 allele of FcγRIIIa have been reported to respond better to mAb therapy in several studies[150,241,250]. As NK cells frequently express only FcγRIIIa, an improvement in response to mAb linked to the high affinity allele of this receptor suggests that NK cells are important effectors of mAb therapy. NK cells are also present in the blood which may facilitate their activity against haematological malignancies, whereas macrophages for example are tissue resident. Furthermore, degranulation markers, such as CD107a, were found on NK cells from a whole blood assay of antibody mediated lysis which was reported to correlate with target lysis[251]. Depletion of NK cells from whole blood in this system was found to abrogate target cell lysis further supporting the key role of these cells in ADCC in the blood. However, as shown in Table 1-1, monocytes and macrophages also express FcγRIIIa, therefore conclusions about the role of NK cells based purely on FcγRIIIa binding are not entirely accurate. Furthermore, as macrophages are not present in the blood, their role in some *in vitro* blood bases effector assays is under represented. It has been shown in several models that deletion of NK cells *in vivo* does not prevent mAb mediated target depletion[252,253].

1.4.4 Antibody Dependent Cellular Phagocytosis

Another effector mechanism of IgG antibodies is antibody dependent cellular phagocytosis (ADCP- Figure 1-5), carried out largely by macrophages- although neutrophils and monocytes are also capable of inducing antibody mediated phagocytosis[254,255]. In contrast to NK cells, macrophages express several FcγRs (I, IIa, IIb and IIIa) and are able to phagocytose opsonised particles that interact with their activatory FcγRs[256]. The ratio of these receptors, in particular the ratio of activatory receptors to the inhibitory receptor (FcγRIIb) has been shown to be important for the ability of macrophages to efficiently phagocytose opsonised targets, with different macrophage phenotypes having been described to have differing A:I ratios[16].

Binding of multiple target molecules by IgG antibodies results in a large number of IgG Fc regions available for binding to FcγRs. Multiple Fc-FcγR interactions are needed to enable a stable interaction between the target cell and the macrophage[257]. Binding of these Fc regions is thought

to cluster the FcγRs on the macrophage surface, as has been found for IgE receptors[258]. This clustering is also associated with phosphorylation of the tyrosine residues within ITAMs present in the FcγR intracellular domain (FcγRIIa) or in the common FcRγ chain (FcγRI, IIIa), as described in Section 1.4.3, leading to actin remodelling and engulfment of the opsonised target[259].

Fusion of the membrane extensions around the opsonised target forms a vacuole containing the target, termed the phagosome[259]. The phagosome then matures through fusion with early and late endosomes, and eventually lysosomes, to form the phagolysosome[260]. The phagolysosome is a vesicle that becomes acidified (pH ~4.5) due to the action of the vacuolar adenosine triphosphate (ATP)ase pumping protons into the phagolysosome[261]. The phagolysosome contains numerous digestive enzymes/hydrolases (such as cathepsins and lysozyme), antimicrobial peptides (such as defensins and cationic antimicrobial peptides) and has a highly oxidative environment due to the formation of reactive oxygen and nitrogen species by NOX2 oxidase and inducible nitrous oxide synthase, respectively[262,263,264]. In addition to the engulfment and destruction of the opsonised target, macrophages also produce proinflammatory cytokines and can present antigen processed from phagocytosed cells to T cells, helping to initiate an adaptive immune response[259]. All of these components combine to kill the phagocytosed target cell that was opsonised with antibody. ADCP of opsonised B cells is thought to be the most important effector mechanism for target cell depletion using the anti-CD20 mAb rituximab (discussed below).

1.5 CD20 as a Monoclonal Antibody Target

1.5.1 CD20 Biology

One of the first targets for therapeutic antibodies was the pan B cell marker CD20[265]. CD20 is a surface protein expressed exclusively on B cells but not haematopoietic stem cells or most/all plasma cells (Figure 1-1)[266]. Furthermore, CD20 is also expressed on the surface of malignant B cells found in both lymphomas and chronic lymphocytic leukaemias[267]. This cell distribution profile makes CD20 an excellent and highly specific target for various B cell malignancies, allowing for reconstitution of the B cell population after therapy has been completed[267]. In addition, bone marrow resident plasma cells are able to survive anti-CD20 mediated depletion and continue to

produce antigen specific antibodies, maintaining a degree of humoral memory[268]. CD20 contains four membrane spanning regions with two postulated extracellular loops, one much larger than the other, where the majority of anti-CD20 antibodies bind (Figure 1-8)[269,270]. CD20 forms homo-tetramers on the B cell surface that can associate with the B cell receptor. Although CD20 function is not fully understood it is thought to be involved in the regulation of calcium flux downstream of BCR signalling[271].

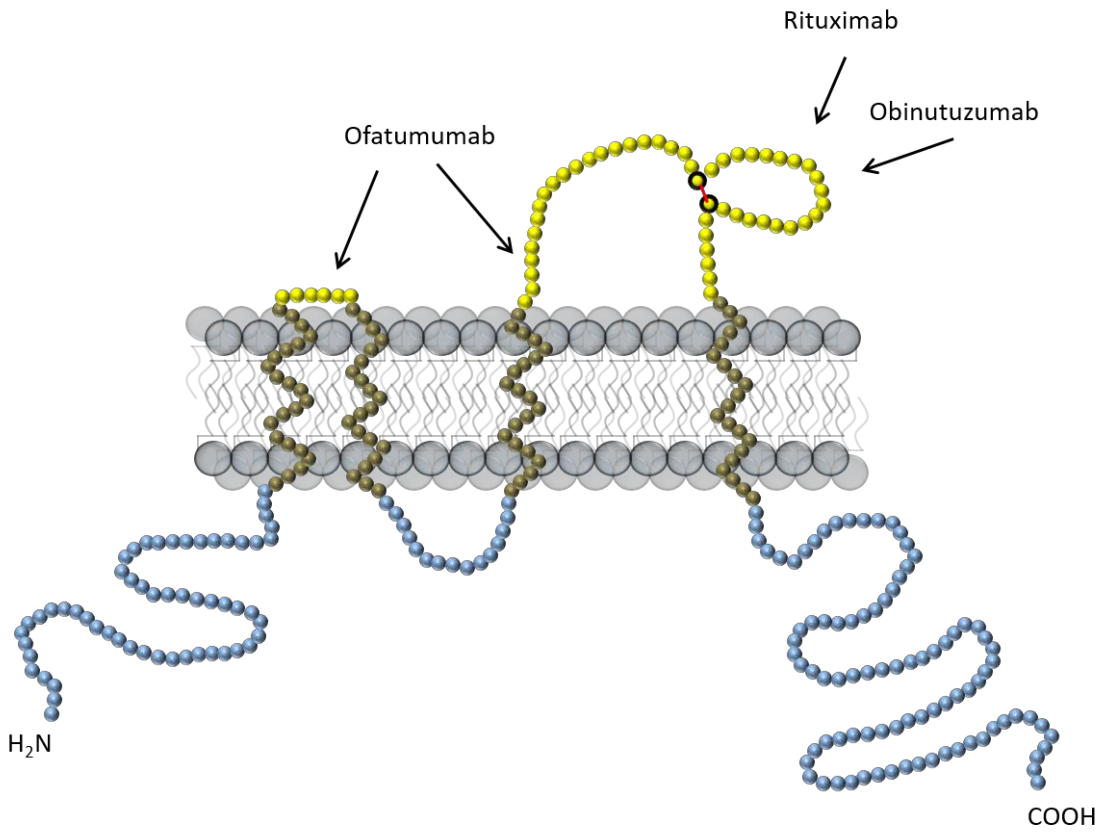

Figure 1-8 2D Schematic of CD20 Structure

Simplified diagram of CD20. Each residue is represented by a single circle. Amino and carboxyl termini are located within the cell cytoplasm and shown in blue, transmembrane helices are shown in olive and extracellular loops are shown in yellow. Approximate binding locations of the anti-CD20 antibodies ofatumumab (which makes contacts with both extracellular loops), rituximab and obinutuzumab are indicated by arrows. Disulphide bind between residues 167 and 183 is shown as a red line with the cysteine residues highlighted with a black perimeter.

1.5.2 Anti-CD20 Antibodies

Due to the specific presence of CD20 on B cells and on many B cell lymphoma and leukaemia cells, CD20 represents a good target for antibody based therapy[272]. Many antibodies recognising CD20 have been generated, and several have been granted approval for use in the clinic (Table 1-3). Although not the first anti-CD20 antibody to be used in humans, the most successful antibody thus far is the chimeric antibody rituximab, generated by cloning mouse variable regions (from the parent antibody 2B8) onto a human IgG1 backbone[273]. Rituximab has been approved for the treatment of a number of lymphomas, including follicular lymphoma and diffuse large B cell lymphoma, as well as a front line therapy in conjunction with chemotherapy for chronic lymphocytic leukaemia (CLL)[274].

Antibody	Trade Name	Format	Manufacturer	Stage of Development
Rituximab	Rituxan	Chimeric	Genentech	Approved 1997
Ofatumumab	Arzerra	Fully Human	Genmab	Approved 2009
Obinutuzumab	Gazyva	Humanised	Roche	Approved 2013
Tositumomab	Bexxar	Mouse	GlaxoSmithKline	Approved 2003*
Ocrelizumab	Ocrevus	Humanised	Genentech	Approved 2017
Veltuzumab	-	Humanised	Immunomedics	Phase II Trials

Table 1-3 Anti-CD20 Antibodies

Many therapeutic antibodies have been developed that target CD20. A selection of these are listed with their trade names (where available), format, manufacturer and current stage of development. * Tositumomab was approved for use in follicular non-Hodgkin lymphoma in a radiolabelled form (Iodine 131) but was discontinued for commercial reasons in 2014[275]. Velutuzumab is currently in clinical trials for Immune Thrombocytopenic Purpura (ITP), clinical trial NCT00547066. Trade names and stage of development refer to these antibodies in the USA. Table modified from[276].

Since the advent of rituximab, several other anti-CD20 antibodies have been developed to try and improve anti-CD20 therapy (Table 1-3). One example of this is the fully human IgG1 antibody ofatumumab, which has a different binding epitope to that of rituximab (and most other anti-CD20 antibodies) in that it appears to bind also within the smaller membrane proximal extracellular loop of CD20 (Figure 1-8)[277]. This membrane proximity has been linked to the greater complement activating potential of this antibody as compared to rituximab[278].

Another anti-CD20 antibody that has recently been approved for use in the treatment of CLL is obinutuzumab (Gazyva) [279]. Obinutuzumab is a glycoengineered antibody that is designed to have an increased affinity for FcγRIIIa to augment its ADCC inducing potential [280]. Obinutuzumab has been shown to be superior to rituximab in its ability to induce ADCC and ADCP *in vitro* (particularly in the presence of non-specific background IgG, as is the case in blood), and induces greater whole blood depletion than rituximab in healthy controls and CLL patients[280-282]. Furthermore, obinutuzumab induced greater tumour control and regression in tumour xenograft models and was shown to cause enhanced B cell depletion in the blood, spleen and lymph nodes of human CD20 transgenic mice and cynomolgus monkeys compared to rituximab[280,281,283]. As well as having enhanced binding for FcγRIIIa, obinutuzumab also has increased binding for the closely related FcγRIIIb, and has been reported to induce neutrophil activation and phagocytosis through this receptor to a greater extent than rituximab[282,284].

In clinical trials for CLL obinutuzumab combined with chlorambucil was reported to produce greater progression free survival and overall survival than rituximab combined with chlorambucil, and was subsequently approved in combination with chlorambucil for treatment of previously untreated CLL[285,286]. More recently, obinutuzumab has also been approved for the treatment of follicular lymphoma, where a significant improvement in response was observed[287].

In addition to indications in the field of oncology, anti-CD20 antibodies have also been approved for treatment of autoimmune disorders, including rheumatoid arthritis (rituximab) and relapsed-remitting multiple sclerosis (ocrelizumab), and are being investigated for several other conditions, such as SLE[288-291].

1.5.3 Type I vs. Type II Antibodies

As well as being glycoengineered, obinutuzumab differs from rituximab in its classification, being a type II anti-CD20 antibody whereas rituximab is a type I anti-CD20 antibody. Class I anti-CD20

antibodies are identified as antibodies that bind and redistribute CD20 into detergent insoluble lipid rafts in the cell membrane[292]. Class I antibodies are associated with increased levels of antibody binding per CD20 molecule as compared to class II antibodies, with twice as many class I antibodies binding to a cell as class II[293]. Comparison of type I and type II $F(ab')_2$ regions bound to a CD20 mimetope may help explain this phenomenon as they reveal a difference in binding angle, which may preclude binding of more than one type II antibody to a CD20 tetramer, whereas two type I antibodies could bind[294].

Type II antibodies have been shown to be less efficient at inducing complement mediated cell death than type I antibodies, likely due to their lack of CD20 clustering potential and reduced recruitment into lipid rafts [293]. However, type II antibodies have been found to be less prone to internalisation than type I antibodies, resulting in longer maintenance of the antibodies at the cell surface and subsequent greater engagement of FcγR dependent functions such as ADCP [281,295]. Finally, type II antibodies have been reported to induce homotypic adhesion of target cells, causing clumping and non-apoptotic cell death, more potently than type I antibodies [296,297].

As described above, obinutuzumab is a type II antibody with the characteristic binding stoichiometry and engagement of effector functions. In addition, it contains a glycoengineered Fc region with a reduced fucose content in order to increase specific effector functions (described further below). A number of studies comparing obinutuzumab to the gold standard anti-CD20 antibody rituximab have reported improved effector functions, and have resulted in approval of obinutuzumab for several indications as detailed above[286,287]. However, comparisons between rituximab and obinutuzumab are complicated due to the fact that the antibodies differ both in their classification, i.e. rituximab is a type I antibody and obinutuzumab a type II antibody, and their Fc region as obinutuzumab, but not rituximab, is glycoengineered. As such, the contribution of each factor to the overall increase in efficacy of obinutuzumab over rituximab is not always apparent. Antibody glycosylation will be considered in the following sections.

1.6 Glycosylation

Protein glycosylation, the attachment of carbohydrate glycan chains, is an essential process in all eukaryotes, and exhibits a great degree of heterogeneity. Two forms of glycosylation exist and

differ in the nature of the glycan structures attached, organelle in which attachment occurs, as well as the amino acid residues that they decorate.

1.6.1 O-linked Glycosylation

O-linked glycosylation involves the attachment of glycans to the oxygen atom of the hydroxyl group of serine and threonine residues[298]. O-linked glycans are typically short (3-4 glycans) and highly variable in the sugars they contain[299]. In contrast to the N-linked glycans (see below), O-linked glycans are added to the serine/threonine residue a single sugar at a time, with each step catalysed by a single highly specific enzyme[299]. O-linked glycosylation usually begins with addition of an N-acetylgalactosamine residue (termed mucin-type glycans) being transferred onto the serine/threonine residue, although other sugars such as fucose can also be added, after the protein is produced[298]. Further sugars can be added to this N-acetylgalactosamine residue, such as galactose and sialic acid, in the golgi. O-linked glycans are found on several antibody isotypes (Figure 1-3), but are not found on human IgG1, the subject of the work presented below, and thus are not further discussed.

1.6.2 N-linked Glycosylation

N-linked glycosylation involves the attachment of sugar residues to a nitrogen atom of asparagine residues within proteins. N-linked glycans are often large and multi-branched, and their formation and processing involves many different enzymes and is important for many functions. N-linked glycans fall into one of three categories, high (oligo) mannose, complex or hybrid (Figure 1-9). However, IgG Fc are almost exclusively populated by complex biantennary glycans. The pathway of N-linked glycan synthesis and processing is described below.

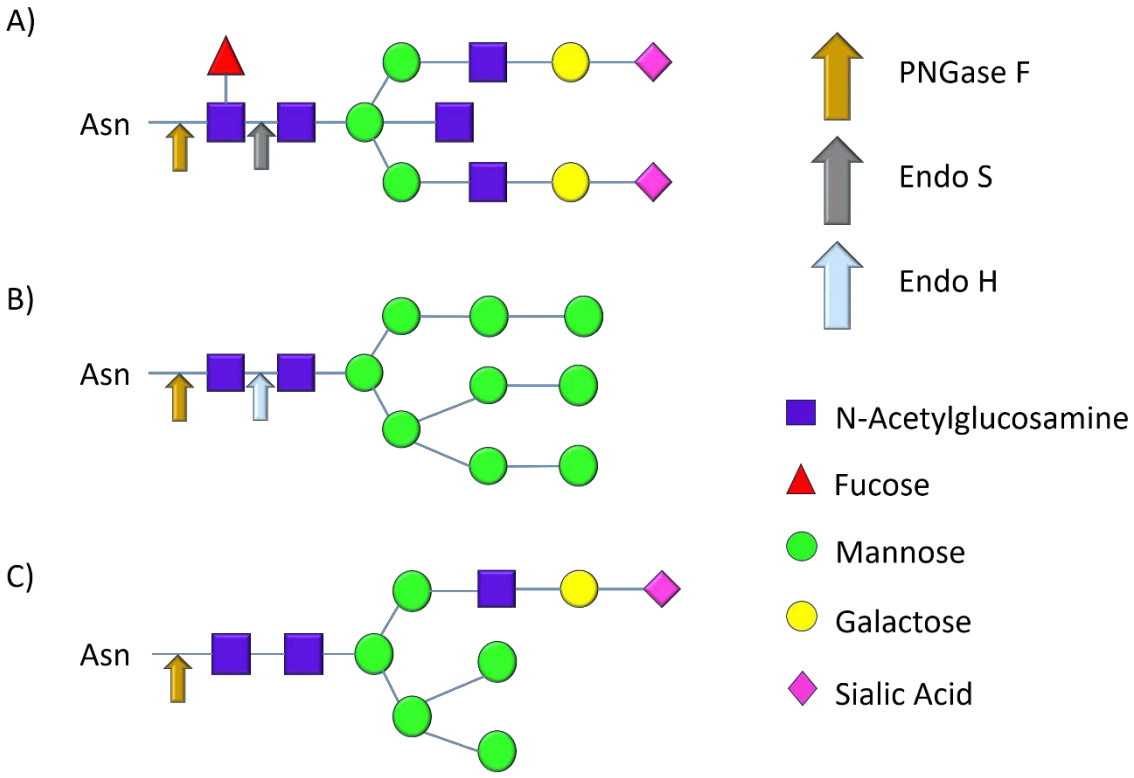

Figure 1-9 N-linked Glycosylation Structures

N-linked glycans fall into three different categories: complex (A), oligomannose (B) and hybrid (C). Complex glycans are the most highly processed, with oligomannose the least processed and most closely resembling the lipid linked oligosaccharide precursor (see text). Hybrid glycans contain elements of both complex and oligomannose glycans, with the α-1,6 arm containing the mannose residues (see below). The sites of cleavage of several de-glycosidase enzymes are also shown, with their substrate specificity differing across the glycan types.

Eukaryotic N-linked glycosylation begins in the cytoplasm with the synthesis of a lipid linked oligosaccharide (LLO) carrier (Figure 1-10). The lipid upon which this glycosylation substrate is synthesised in eukaryotes, dolichol, is an isoprenoid molecule of species specific length formed by the cis-prenyltransferase catalysed addition of 5 carbon isoprenoid groups onto a farnesylpyrophosphate molecule[300]. This dolichol lipid is first phosphorylated by dolichol kinase, making it able to accept a transferred N-acetylglucosamine (GlcNAc) residue from cytoplasmic uridine diphosphate (UDP)-GlcNAc, catalysed by the ALG7 (asparagine linked glycosylation) protein, forming dolichol pyrophosphate bonded to GlcNAc and releasing uridine monophosphate (UMP)[301,302]. A second GlcNAc is added from cytoplasmic UDP-GlcNAc via an enzyme complex consisting of ALG13 and ALG14, releasing UDP[303]. Next a mannose residue is added in a β-1,4 glycosidic bond from cytosolic guanosine diphosphate (GDP)-mannose via the ALG1 subunit of the

ALG1, 2, 11 complex[304]. The branching α-1,3 and α-1,6 chains are then formed with addition of mannose by the ALG2 subunit with the α1,3 mannose added first[305,306]. ALG11 then adds two further α-1,2 mannose residues to the α-1,3 arm[307,306].

The resulting product of these reactions is a dolichol pyrophosphate GlcNAc2 Man5 glycan present on the cytoplasmic face of the endoplasmic reticulum (ER) membrane. For further processing and transfer onto substrate proteins this molecule must be transferred to the luminal face of the membrane (Figure 1-10). This translocation reaction is believed to be carried out by the enzyme RFT1, as mutation of the corresponding gene results in loss of N-linked glycosylation and accumulation of the glycan precursor on the cytoplasmic face of the ER[308]. As well as translocation of the growing polysaccharide chain, activated dolichol phosphate linked glucose and mannose residues (produced from free nucleotide activated sugars and dolichol phosphate) are also flipped across the membrane by a protein mediated, ATP independent mechanism to act as substrates for further extensions of the glycan precursor[309,310,311].

Once inside the ER lumen, the polysaccharide chain, substrates and enzymes are all anchored to the luminal face of the ER membrane. Addition of further mannose residues is catalysed by ALG3 (forming an α-1,3 glycosidic bond) and then by ALG9 (forming an α-1,2 glycosidic bond)[312,313]. A branch is formed when a further mannose is added by ALG12 via an α-1,6 glycosidic bond, and completed by addition of another α-1,2 linked mannose by ALG9[314,313]. Once this oligomannose polysaccharide has been formed, there are further additions of glucose by ALG6, 8 and 10 resulting in an α1,2 linked glucose capping the glycan tree[315,316,317].

The entire 14 glycan unit is transferred *en bloc* from the LLO to the amide group of an asparagine residue within the N-X-S/T sequon (where X is any amino acid except proline) of the nascent polypeptide as it translocates (co-translationally) into the ER through the secretory pore, before protein folding occurs (Figure 1-10)[318]. This transfer is catalysed by the membrane bound enzyme oligosaccharyltransferase (OST), which in eukaryotes is a multisubunit complex but in certain prokaryotes exists as a single active subunit[319]. STT3 is the catalytic subunit and various other subunits are involved in complex formation and specific substrate recognition[319]. OST is able to transfer the glycan unit onto a wide variety of polypeptide substrates that contain the N-X-S/T sequon, although a preference exists for sequons containing threonine over serine[320,321]. In addition, rare sequences containing a cysteine in place of a serine or threonine can also be glycosylated[321]. The 14 unit glycan now linked to the Asn residue of the nascent protein then acts

as a substrate for a number of processing glycosylases and glycosyltransferases present within the ER and, downstream, in the golgi (Figure 1-11).

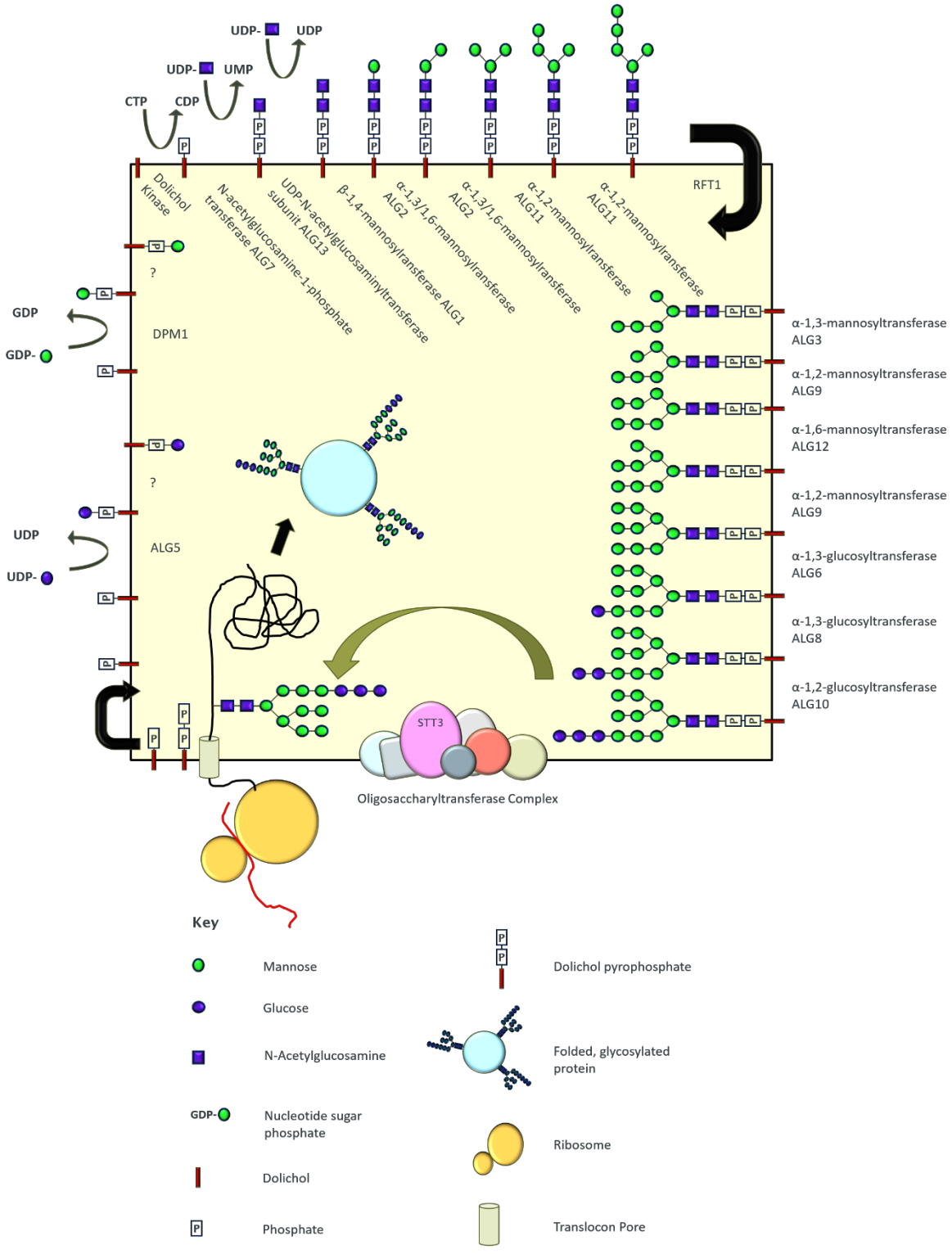

Figure 1-10 N-Glycan Synthesis

The N-glycan precursor, the lipid linked oligosaccharide, is synthesised piecemeal by a number of enzymes in the cytoplasm and endoplasmic reticulum. Synthesis of the lipid linked oligosaccharide begins on the cytoplasmic face of the endoplasmic reticulum membrane (top left) but is completed on the luminal face (right hand side). After its completion, the entire 14 unit molecule is transferred from

the membrane carrier onto an asparagine residue of the nascent protein in a co-translational manner as the polypeptide chain feeds though the translocon pore into the endoplasmic reticulum. This reaction is carried out by the multi-subunit oligosaccharyltransferase complex.

Within the ER lumen this 14 unit glycan is processed by sequential removal of the glucose residues by α glucosidase-I (removes the first α-1,2- linked glucose) and -II (removes the subsequent pair of α-1,3- linked glucose residues), and a mannose residue from the α-1,6 arm by α mannosidase-I (Figure 1-11)[322,323,324]. At this stage the heavy and light chains assemble into the complete IgG molecule. This molecule is transferred to the cis-golgi, where further mannose removal occurs, prior to the addition of a GlcNAc residue to a core mannose, catalysed by further α1-2 mannosidases and N-acetylglucosaminyltransferase-I, respectively[322,325]. This addition of a GlcNAc residue commits the glycan to either the complex or hybrid form. Next the molecule moves to the medial-golgi, the 2 remaining terminal mannose sugars are removed by α mannosidase-II and a second GlcNAc sugar is added by N-acetylglucosaminyltransferase-II to yield the core biantennary heptasaccharide GlcNAc2Man3GlcNAc2[326,327].

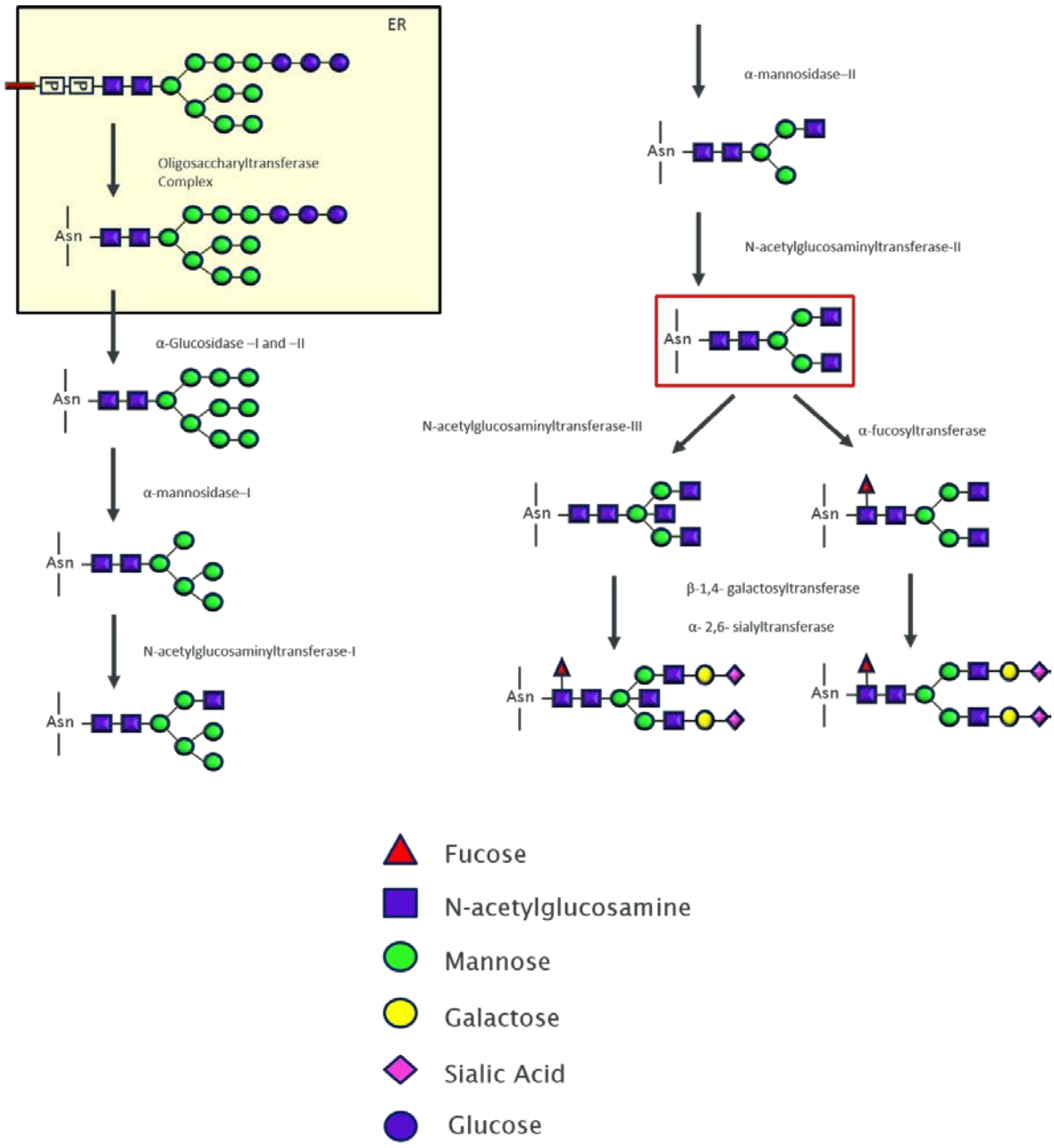

Figure 1-11 N-Glycan Processing

The N-glycan precursor (LLO) is transferred from a dolichol phosphate isoprenoid lipid carrier (red) to the Asn-297 residue of the IgG CH2 domain. This precursor is then processed down to a 7 unit core heptasaccharide (red box) prior to addition of various sugars up to and including the fully processed forms shown at the bottom of the figure. The levels of these different glycoforms vary significantly in serum IgG (see below). ER- endoplasmic reticulum.

Various further modifications can occur to this core glycan in the trans-golgi to yield a range of different glycan chains. For example, fucose can be added to the asparagine linked GlcNAc by α1,6 fucosyltransferase, a bisecting GlcNAc can be added by N-acetylglucosaminyltransferase–III, galactose and sialic acid can be added to the GlcNAc antennae by galacto/sialyltransferases, respectively (Figure 1-11)[328,329,330]. As a result of the range of different glycan chain modifications that can occur in the golgi, the glycan profile of antibody in the serum is extremely heterogeneous, with any of 32 different glycoform structures potentially present on each Asn-297[110]. However, the order of action of the different glycosyltransferases can impact the final glycoform present on a given molecule. For example, if addition of a bisecting GlcNAc residue occurs prior to the addition of fucose, then fucosylation cannot occur[331]. A schematic glycan is shown in Figure 1-12 representing all potential saccharide residues that can be added, with their most common linkages.

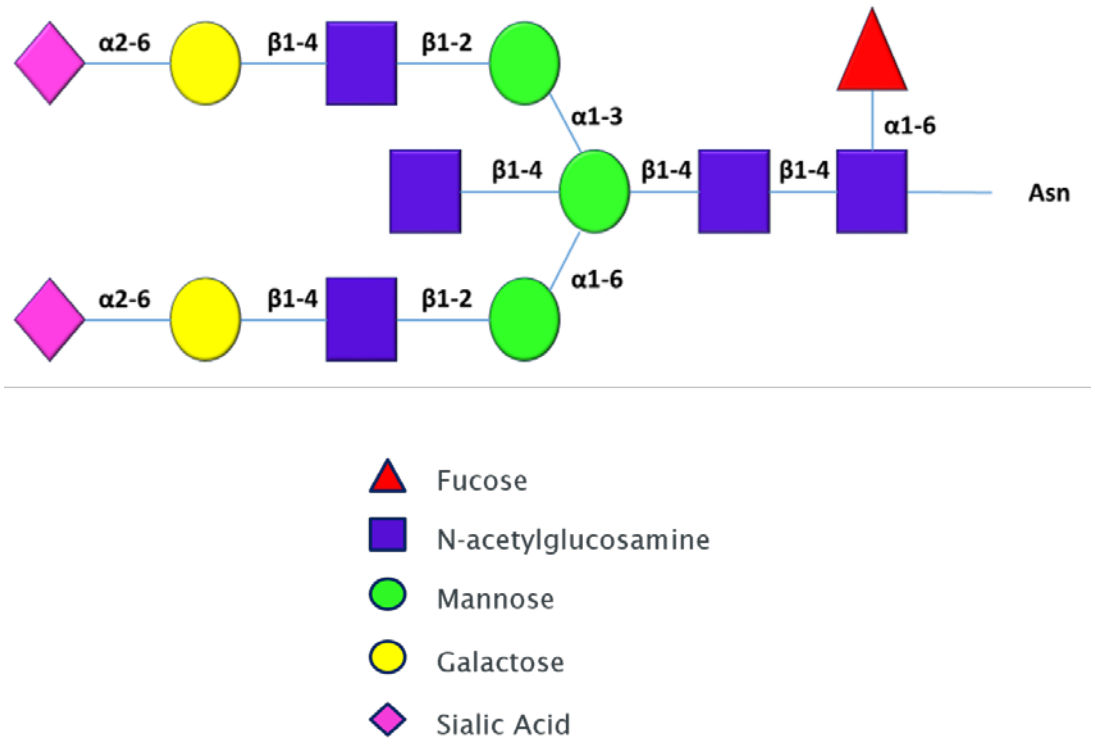

Figure 1-12 Complex N-linked Glycan Structure

Serum IgG contain a highly heterogeneous mix of glycans, with varying levels of terminal galactose and N-acetylneuraminic acid, and the presence or absence of a bisecting GlcNAc and core linked fucose. A schematic N-linked complex type glycan is shown bearing all known modifications, with the most common glycan linkages indicated (for example, in rare cases sialic acid can be linked to galactose via an α1-3 linkage). Empirically measured levels of the different glycoforms are discussed below.

1.7 IgG Glycosylation

IgG antibodies are glycoproteins that contain an asparagine linked glycan attached at residue 297, present within the CH2 domains of the Fc region. These glycans are present within the core of the Fc structure and are thus not readily exposed (Figure 1-13), which may explain the reduced level of highly processed sialylated glycans present on these glycans compared to other glycosylated molecules (see below). The role(s) of these Fc glycans are complex and not completely understood, but they are essential for certain Fc driven effector functions of IgG (discussed below). Their position between the two CH2 domains fills the intramolecular space and makes significant interactions with the protein backbone and the glycan of the opposite heavy chain (Figure 1-13). Although present in all IgG molecules, there is a great deal of heterogeneity with regard to IgG glycosylation, which is described next.

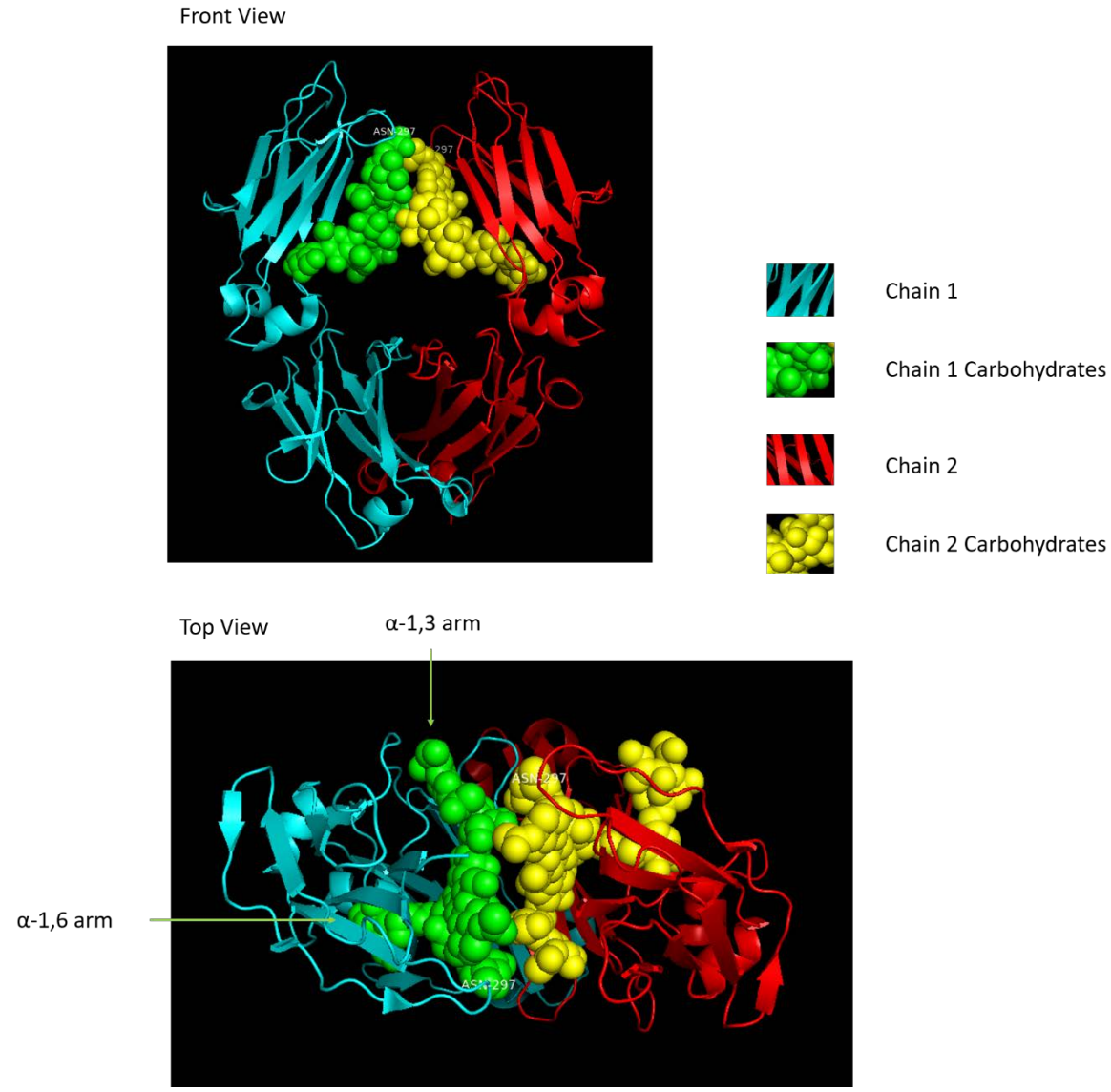

Figure 1-13 IgG Fc Glycosylation

The crystal structure of the IgG Fc region (heavy chains in cyan and red) shows the position of the Fc glycans in the interior of the Fc. Asn297 (labelled) is positioned towards the top of the CH2 domain and the glycans (shown as spheres- green and yellow) protrude downwards and along the CH2 backbone. Image generated using PyMol. Structure from Protein Data Bank: 4BYH[332].

1.7.1 IgG Glycosylation *in vivo*

Combining various forms of chromatography and mass spectrometry has allowed analysis of the entire IgG-Fc glycan pool in healthy adult humans. Although these results are complicated by the degree of heterogeneity in the IgG glycan pool, the different combinations of these glycans on the

two heavy chains (yielding over thirty distinctly glycosylated IgGs), subclass differences and changes associated with pathology and physiological changes, some consistent trends are apparent. In general, IgG Fc glycans are complex, biantennary, highly fucosylated (over 90% of IgG) molecules that have either 0, 1 or 2 galactose molecules (Table 1-4). Some reports suggest that the levels of sialic acid linked by an α- 2,6- linkage are extremely low, but more recent, large scale glycan analysis has suggested it may be present more than initially thought[333,334]. A relatively low level of bisecting GlcNAc is also found in some complex glycans (~18%). Levels of hybrid and oligomannose glycans present at the Asn-297 N glycan are very low. Interestingly, levels of these lesser processed glycans present in the homologous position of other Ig isotypes can be much higher. For example, IgE contains an oligomannose glycan that is essential for binding to its receptor, raising the prospect of targeting this glycan with specific enzymes to treat allergy[335].

Glycoform	Median
Galactose G0	37%
Galactose G1	42.6%
Galactose G2	19.17%
Fucose	95.77%
Sialic Acid (1 or 2SA)	19.71%
Bisecting GlcNAc	17.76%

Table 1-4 Serum IgG Glycan Profile

Glycosylation profiles of serum IgG from the Croatian Island of Vis (n = 915), modified from[334].

Analysis of IgG glycans is often carried out by mass spectrometry of peptide-N-glycosidase (PNGase) F treated IgG (Figure 1-9). This enzyme cleaves off the entire N-linked glycan from IgG, and these are then purified and analysed. While this allows the quantification of different glycan forms from an IgG population, any differences between IgG subclass are lost when the glycans are removed. Several groups have circumnavigated this problem by performing trypsin digests of the IgG, coupled with certain purification steps, to allow analysis of the IgG glycans present on different IgG subtypes by mass spectrometric analysis of the glycopeptides[336].

These reports indicate that there are in fact differences in glycosylation between the IgG subtypes. For example, IgG2 has been found to have an even greater degree of fucosylation than total IgG, coupled with lower levels of galactosylation[336]. IgG4 had lower levels of galactosylated molecules, and higher levels of fucose and bisecting GlcNAc. IgG1 had higher levels of galactosylation. Changes in the glycosylation present on different subclasses have also been found in hepatitis C virus induced liver cirrhosis and hepatocellular carcinoma, with increased levels of agalactosylated glycans bearing glucose across all subclasses[337]. In contrast, levels of galactose and sialic acid have been found to increase on all IgG subclasses during pregnancy[338].

1.7.2 IgG Glycan Function

Fc glycans are positioned within the Fc stem between CH2 domains (Figure 1-13) and mediate carbohydrate to carbohydrate interactions that help stabilise these domains[339]. The α1,6 arm of the Fc glycan is oriented perpendicular to, and makes extensive contacts with, the Fc protein backbone, whereas the α1,3 arm protrudes further into the cavity between CH2 domains and contacts the α1,3 arm from the other heavy chain (Figure 1-13)[340]. The stabilising effect of the glycan interactions is thought to contribute to stability in the lower region of the hinge (which contains the binding site for FcγRs and C1q) possibly enabling the transient formation of several different structures in this region[341,342]. This has been suggested to contribute to FcγR binding as these different structures could interact with differing affinities to various receptors[342].

Removal of the Fc glycan results in a shift in the conformation of the IgG CH2 region (discussed above), which reduces FcγR and C1q binding[340,343]. This highlights the structural role of the Fc glycans which sit in the space between the two CH2 domains (which unlike the other IgG domains do not extensively pair up) and mediate their interaction[344]. Furthermore, it has been suggested that removal of the Fc glycan may disrupt the tight packing of Fc regions seen in immune

complexes, the natural state in which most IgG subclasses are recognised by FcγRs (Section 1.7.5)[345].

It has been shown that antibodies bearing different glycoforms have differing activities *in vitro* and *in vivo*, and that removal of the glycan chains, for example by digestion with endoglycosidases (Figure 1-9) or site directed mutation of Asn-297 to Gln, abrogates certain antibody effector functions[346]. Aglycosylated antibodies have been shown not to bind to activating or inhibiting FcγRs, and also do not bind and activate C1q[339,344,342]. As such, efficient antibody dependent cellular cytotoxicity, antibody dependent cellular phagocytosis or complement dependent cytotoxicity are not induced in the absence of the Fc N-glycan.

It was not previously thought that the Fc glycan chains make direct contact with the protein backbone of the FcγRs; instead the glycan location, adjacent to the FcγR binding region in the lower hinge was thought to contribute to stability and proper conformation of the lower hinge to enable receptor binding[347]. The more open structure of glycosylated IgG compared to non-glycosylated IgG and the increased susceptibility to certain proteases supports this suggestion[344,346,348]. In addition, mutation of the residues that make contacts with the glycans result in a loss of activity comparable to removal of the glycan[349]. However, more recent work (as discussed below) has demonstrated that the Asn-297 glycan mediates carbohydrate to carbohydrate interactions with the N-linked glycans present on at least two FcγRs (FcγRIIIa and FcγRIIIb, Figure 1-14)[350]. This does not appear to be the case for the other receptors, where the receptor residues (protein and glycan) do not extend far enough down to interact with the Fc glycans.

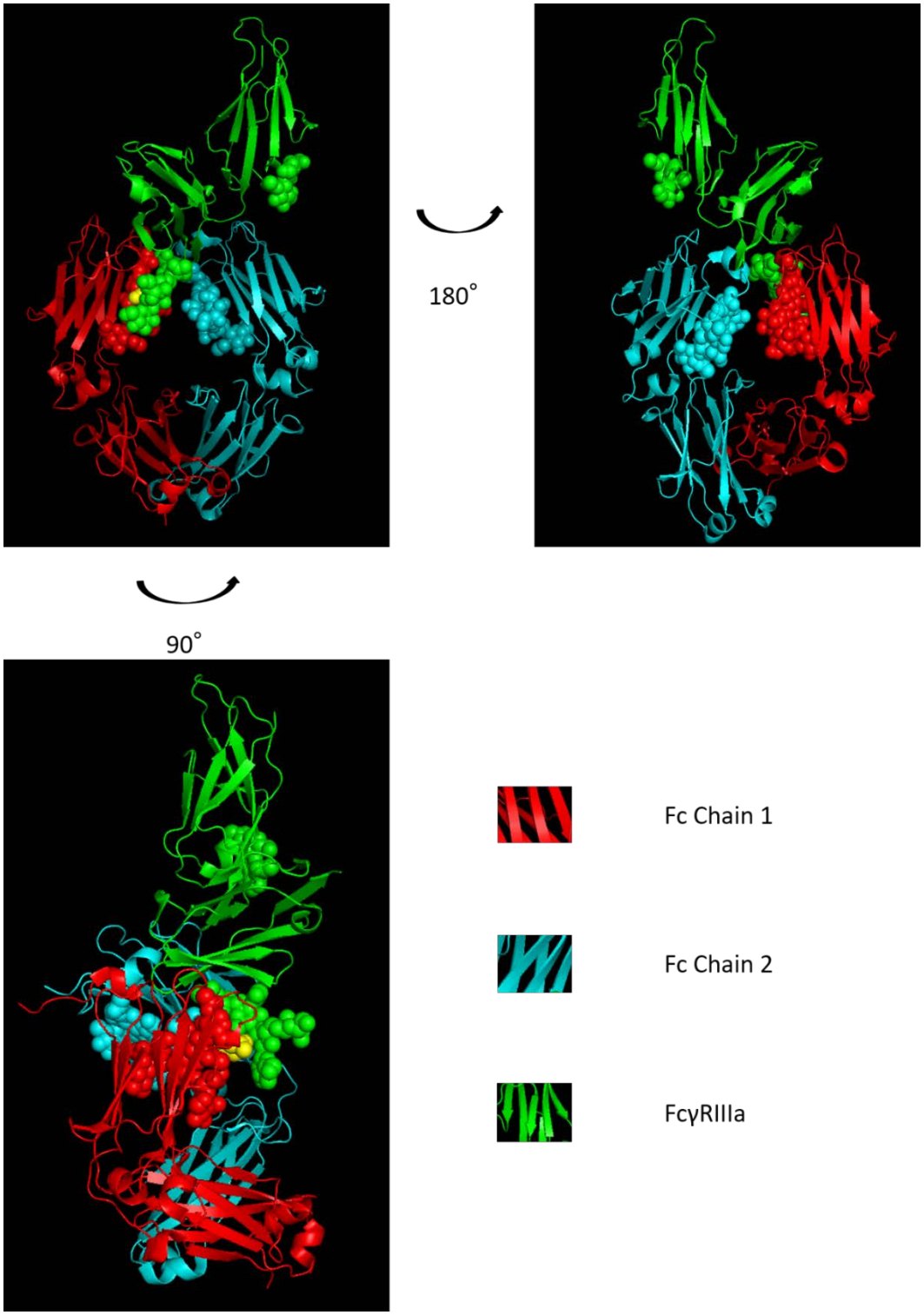

Figure 1-14 Fc-FcγRIIIa Interaction

The structure of the interaction between FcγRIIIa and IgG Fc has been solved by X-ray crystallography. IgG Fc (heavy chains in red and cyan) interacts with FcγRIIIa (green) in the hinge/upper CH2 domain. Glycan (shown as spheres) of the cyan H chain interact with glycans on the FcγRIIIa. Fucose (yellow) is in the centre of this interaction and its removal results in a shift in the proximity of the glycan residues, yielding enhanced affinity. Protein structure- PDB 3SGJ[350].

A number of studies have examined the influence of different Fc glycan structures on particular Fc effector functions. It has been shown that a lack of fucosylation of the Asn-297 linked GlcNAc increases the binding affinity of IgG1 Fc for the FcγRIIIa receptor present on NK cells, as well as monocytes and macrophages (discussed further below)[351,352]. As NK cells typically only express this receptor and are the main effector in blood, this receptor is thought to be primarily responsible for the induction of ADCC[353]. As various therapeutic antibodies targeting malignancies aim to induce ADCC, it may be anticipated that these antibodies would be afucosylated - however, in its native form, rituximab and trastuzumab are mostly fucosylated. In addition to the reported effects on obinutuzumab discussed above, glycoengineering to remove the fucose sugar from rituximab has yielded increased FcγRIIIa binding *in vitro* which is anticipated to result in increased ADCC *in vivo*[354]. Afucosylation does not seem have an effect on C1q affinity or the induction of complement dependent cytotoxicity[355].

With regards other glycans, high levels of oligomannose glycans can be a marker of incomplete glycan processing in the ER/golgi, for example in the case of N-acetylglucosaminyltransferase-I inactivation, and are therefore afucosylated (Figure 1-9). IgG bearing oligomannose glycans are reported to have 2-3x increased binding to FcγRIIIa (compared to fucosylated complex biantennary IgG) and are superior at inducing ADCC compared to complex type fucosylated antibodies, while also exhibiting reduced C1q binding[355].

Although removal of the Fc glycan chain has been shown to abrogate the interaction with activating and inhibitory FcγRs, it does not appear to affect binding of FcRn (discussed previously) or protein A/G which are known to bind to a distinct section of the Fc region at the CH2-CH3 domain interface[341,346,356].

1.7.3 Afucosylation

As discussed above, native antibodies have multiple glycosylation states. Currently used clinical mAbs are no different and some glycosylation forms are not optimal for antibody effector functions. This provides a potential opportunity for improving antibody effector functions through glycan engineering. A prime example of the potential benefits of glycoengineering on antibody function is the type II anti-CD20 antibody obinutuzumab, glycoengineered to contain reduced fucose levels in order to increase FcγRIIIa affinity and ADCC (Section1.5.2). This antibody has

recently been approved for the treatment of chronic lymphocytic leukaemia and follicular lymphoma, as discussed above[287,357]. This has been achieved by production of the antibody in CHO cells that have been engineered to overexpress the glycomodification enzymes β-1,4 N-acetylglucosaminyltransferase III (GnT III) and golgi α- mannosidase II - resulting in highly bisected, mostly afucosylated antibody[280].

Obinutuzumab is not the only antibody approved for use in humans that has been glycoengineered. The anti CC chemokine receptor 4 (CCR4) antibody mogamulizumab is a fully afucosylated IgG1 antibody approved for use in relapsed/refractory $CCR4^+$ adult T cell leukaemia-lymphoma, peripheral and cutaneous T cell lymphoma in Japan[358]. Mogamulizumab was produced in CHO cells in which the *FUT8* gene has been knocked out, meaning the level of fucosylation of antibodies produced within the system is extremely low[359]. As for obinutuzumab, the lack of fucose present in anti-CCR4 antibodies results in increased affinity for FcγRIIIa and increased ADCC[360,361]. The approval of obinutuzumab and mogamulizumab may pave the way for other glycoengineered antibodies to reach patients[358].

Recently, the anti-IL-5R mAb benralizumab, which is also glycoengineered to contain no fucose (produced in CHO cells that do not express *FUT8*), was approved by the FDA for the treatment of severe eosininophillic asthma[362,363]. Benralizumab binds to the α chain of the IL-5R on eosinophils and both blocks their activation and causes them to be depleted from the circulation (through its increased binding to FcγRIIIa) and the tissues, relieving asthma symptoms[364,365].

Finally, another anti-CD20 mAb employing glycoengineering is also is phase III clinical trials, ublituximab[366]. This antibody is produced in YB2/0 cells and contains reduced fucose, and exhibits increased ADCC and CDC compared to conventional anti-CD20 therapies (rituximab)[367,368]. Ublituximab has been found to be safe and efficacious in phase II trials in combination with standard therapy for chronic lymphocytic leukaemia[369].

1.7.4 Sialylation

Another glycan modification strongly linked to a particular function is terminal sialylation, which is linked to suppression of immune responses[370]. This can be demonstrated by considering intravenous immunoglobulin therapy (IVIg), in which pooled healthy serum IgG is given to patients with autoimmune conditions to reduce their symptoms[371]. To be effective, IVIg has to be

given at very high doses (grams per kg). However, when the pooled serum is enriched for sialylated IgG, the efficacious dose drops 10x in a mouse model of arthritis[372]. Further supporting this is the complete loss of function seen when sialylated antibody is removed from IVIg, or when terminal sialic acid moieties are removed enzymatically[372]. Sialylated Fc domains are thought to elicit this function not by interacting with FcγR (as this affinity drops), but instead with the lectin DC-SIGN on regulatory macrophages via sialic acid induced changes in the IgG structure[110]. It is thought that interleukin-33 release from DC-SIGN expressing macrophages and DCs causes basophil release of IL-4, which is known to cause an increase in the level of the ITIM containing inhibitory FcγRIIb on effector macrophages (thereby decreasing the A:I ratio- discussed above), resulting in more ITIM signalling and less activation in response to IgG binding[372,373,374,110].

However, it should be noted that these effects may be model dependent, and recent evidence has suggested that sialylation and basophils are not essential for IVIg activity, but that Fc regions are. In mouse models of rheumatoid arthritis, IVIg was effective at reducing symptoms even after depletion of basophils or enzymatic removal of sialic acids[375]. However, IVIg $F(ab')_2$ regions did not cause symptom reduction, suggesting that this is an Fc dependent phenomenon[374]. Furthermore, *in vitro* studies on human monocyte derived macrophages has suggested that sialylation has no effect on phagocytosis, as increasing the proportion of sialylated IgG did not alter the efficiency of phagocytosis[376]. This group also demonstrated that the presence of dimers within IVIg may be responsible for its therapeutic effect suggesting increased avidity may be important. The mechanism of action of IVIg in humans is still unclear. It has also been reported that the sialylation state of Fc has no impact on Fc binding to DC-SIGN, suggesting that this molecule may not be a functional receptor for sialylated Fc[377]. Interestingly, increased effector function and FcγR binding for sialylated Fc has been reported (discussed below), casting further uncertainty on the role of sialylation and its anti-inflammatory activity.

Indirect support for the anti-inflammatory role of sialic acid is the finding that sufferers of autoimmune disorders, notably rheumatoid arthritis, have decreased levels of sialylated and galactosylated antibodies[378]. In comparison, levels of sialylation and galactosylation are reported to increase during pregnancy. Interestingly, the severity of symptoms of rheumatoid arthritis decrease during this period, although some reports have questioned the role of sialic acid in this effect and suggested that galactosylation is more important[379,380]. This more anti-inflammatory glycan pool may help reduce the chances of any anti-foetal immune response, and in doing so also dampens the autoimmune response of rheumatoid arthritis.

A further glycan modification is the presence/absence of a bisecting GlcNAc sugar attached to the heptasaccharide core mannose residue by a β-1,4- glycosidic linkage (Figure 1-12). The presence of this sugar also results in a significantly increased affinity for FcγRIIIa compared to non-bisected otherwise identical glycoforms, and consequently a more potent ADCC response[381,382]. Very few reports have been published on the effect of the bisecting GlcNAc residue, although it seems to have less of an influence than the absence of fucose.

1.7.5 IgG Glycan Removal

Removal of the Fc glycans by mutation or the action of glycosidases is well known to abrogate IgG function by the loss of binding to FcγRs and C1q[346]. The prevailing theory as to how this occurs is based upon crystal structures of Fc domains with and without glycosylation. These structures suggest that the loss or truncation of the Asn297 linked glycans results in a collapse of the CH2 domains toward each other into the space previously occupied by the glycans[340]. It is proposed that this 'closure' of the Fc blocks efficient binding of the FcγRs and C1q.

However, not all Fc crystal structures exhibit this trend[383]. Some structures of non-glycosylated Fc have reported an apparently more open structure than is seen with some glycosylated Fc domains (Braden, PDB 3DNK). To try and reconcile the differences between non-glycosylated crystal structures, one group performed small angle X-ray scattering (SAXS), a technique that determines structural information about a protein in solution[384]. This group reported an increased radius of gyration for aglycosylated (*Escherichia coli* produced) IgG Fc compared to glycosylated IgG Fc, indicating an increased average size of soluble conformations and a more open structure. This indicates that loss of glycans does not definitively cause collapse of the CH2 domains.

Furthermore, another group has analysed the structure of IgG Fc with/without glycosylation using single molecule Förster resonance energy transfer (smFRET), measuring the distance between a labelled atom in each CH2 domain[385]. When comparing glycosylated and PNGase F deglycosylated Fc they reported a single non-zero peak for glycosylated Fc, but a peak representing more energy transfer after PNGase F treatment. The latter peak was also considerably broader than the former, suggesting that the deglycosylated Fc was more flexible and could take many different structures. This may help explain the contradicting crystal structures, as the single structure formed in a crystal could be just one form of many that non-glycosylated Fc can take. Interestingly

the same group also deglycosylated Fc with Endo S, an enzyme from *Staphylococcus pyogenes* that cleaves the glycan chain after the first GlcNAc residue, as opposed to PNGase F that cleaves off the entire glycan chain (Figure 1-9). The resulting antibody Fc displayed smFRET peaks characteristic of both glycosylated and PNGase F deglycosylated Fc[386]. This could be due to incomplete deglycosylation or, as the authors suggest, a stabilising effect on the structure from the remaining GlcNAc (± fucose).

1.7.6 FcγR Glycosylation

As well as IgG being glycosylated, some of its receptors are also glycosylated, and this has been shown to affect the Fc-FcγR interaction, particularly in relation to FcγRIIIa and b. FcγRIIIa contains five glycosylation sites at residues-38, 45, 74, 162 and 169. Binding studies of IgG to different glycoforms of this receptor have revealed that these glycans play a role in IgG binding, and in particular are involved in binding to non-fucosylated antibodies[387]. As mentioned above, non-fucosylated antibodies bind to FcγRIIIa with a higher affinity than fucosylated antibodies. This increase was shown to be lost if the receptor was deglycosylated, back to almost the affinity of native IgG (which increases slightly for non-glycosylated FcγRIIIa)[387]. Structurally this has been suggested to be dependent on interactions between the carbohydrates on the Fc and receptor, as well as between the carbohydrates and protein backbones (Figure 1-14). A model based on the structure of Fc in complex with FcγRIIIa has suggested that a small (2.6Å) movement of the FcγRIIIa carbohydrate due to the steric clash with Fc fucose disrupts/weakens the intermolecular interactions, causing the reduced affinity[350].

Mutation of the various N glycosylation sites within FcγRIIIa has shown that while Asn-162 is required for higher affinity interactions with non-fucosylated antibodies, the other four glycosylation sites (particularly Asn-45) are inhibitory to Fc interaction[388]. As such, the highest affinity for non-fucosylated antibodies was obtained for FcγRIIIa glycosylated only at Asn-162.

As detailed above (Section1.3.2), FcγRIIIa is expressed on both NK cells and macrophages/monocytes. Although the primary structure of these proteins is identical between the 2 cell types, a difference has been found in the affinity for IgG1 and 3 between the 2 cell types, as measured by IgG Fc engagement blocking the binding of an anti-FcγRIIIa antibody[389]. This work reported that NK cells had a greater affinity for IgG1 and IgG3 and could bind the

monomeric form of this antibody better than monocyte/macrophages. Interestingly, different glycan chains have been found on FcγRIIIa in the different cell types[389]. FcγRIIIa on NK cells is reported to have high mannose glycans with some complex type, whereas monocytes/macrophage FcγRIIIa did not contain high mannose glycans and carried predominantly complex glycans. Recent work in this area has confirmed these findings, indicating that the glycans on FcγRIIIa from NK cells contain large proportions of hybrid and oligomannose glycans, whereas recombinant FcγRIIIa contained largely complex glycans[390]. This difference in glycosylation affected the binding of IgG1, with oligomannose bearing FcγRIIIa binding IgG1 with 12 times greater affinity than FcγRIIIa with complex glycans[390]. Furthermore, FcγRIIIa bearing oligomannose glycans were shown to bind to various IgG1 glycoforms with up to 50 fold increased affinity compared to FcγRIIIa with complex glycans, and this increased affinity was entirely dependent on the glycan at position N162 of FcγRIIIa[391].

Recombinant human FcγRIIIa produced by different cells also varies in glycosylation, with the same protein expressed in HEK and CHO cells displaying altered glycans[392]. HEK produced receptor carried mostly complex biantennary glycans terminating in GalNAc with core and antennary fucose (although around a quarter were hybrid glycans), whereas CHO derived receptor carried complex bi- and triantennary glycans with core fucose, terminating in galactose or sialic acid. These differences in receptor glycosylation could potentially affect the affinity for Fc, although structural modelling of the FcγRIIIa – Fc interaction has suggested that the first 2 glycans at the Asn-162 site may be responsible for most of the interaction, and these monosaccharides do not appear to vary between HEK and CHO cells[350,392,284].

FcγRIIIb is very closely related to FcγRIIIa, having over 95% homology in its ligand binding domain[284]. It differs in the fact that it is linked to the membrane by a glycophosphatidylinositol anchor and its expression is restricted to neutrophils and basophils. FcγRIIIb displays a similar increase in affinity for non-fucosylated compared to fucosylated antibody, which is not surprising given the similarity in the ligand binding domains[284]. Interestingly, one report into FcγRIIIb binding suggested that removal of the Asn-163 glycosylation site resulted in increased affinity for IgG (greater than removing all glycosylation), suggesting that differential glycosylation may also have a role to play in the function of this FcγR too[393].

1.8 Glycan Engineered Antibodies

Building on the emerging knowledge of the importance of IgG Fc glycosylation new therapeutic antibodies have been designed that have altered glycan profiles suited to their intended function (see above)[394]. The first glycoengineered antibody to receive approval for the treatment of human disease was mogamulizumab, an anti-CCR4 antibody, in Japan 2012[358,395]. This was followed in 2013 by the approval of obinutuzumab, and in 2018 by the approval of benralizumab, by the US Food and Drug Administration (FDA)[279,357,362].

1.8.1 Glycan Engineering Methods

There are a number of methods for manipulating the glycans that are attached to an antibody, ranging from changes in cell culture conditions to the use of genetically modified cell lines for antibody production[394]. Glycan engineering is of particular importance for therapeutic mAbs because changes in the production method of therapeutic antibodies during scale up can cause changes in the glycans attached, which can consequentially have an impact upon the mAb function *in vivo*. As a result, when therapeutic antibodies are produced, a balance must be struck between maximum protein yield and the optimal level of glycan processing.

1.8.2 Culture Conditions

One method of manipulating the glycans is decreasing the culture temperature, from 36.5°C to 32°C. This caused an increase in specific productivity of therapeutic antibody, increased stability and amount of H chain mRNA and increased cell viability, but decreased cell metabolism, the level of glycosyl transferases (protein and mRNA), the level of nucleotide sugar donors (NSDs) and the proportion of glycans that are highly processed (levels of agalactosylated antibody increase)[396]. The slowdown in cell metabolism was suggested to have allowed for channelling of the cells resources toward production of the recombinant therapeutic antibody rather than toward cell growth. Furthermore, a decrease in glucose uptake and tricarboxylic acid (TCA) cycle flux was seen, possibly explaining the reduced levels of NSDs as these are derived from TCA cycle intermediates. A similar observation has been made when producing IgG in CHO cells under

varying nutrient levels, with lower levels of glutamine or glucose early on during culture being linked to an increase in highly processed glycans[397].

A number of parameters have been reported to effect N-linked glycosylation in a range of recombinantly produced proteins, including therapeutic antibodies. For example, addition of manganese to cell culture caused an increase in the level of galactosylation and sialylation of recombinantly produced erythropoietin (EPO), and also favoured biantennary glycans rather than tri or tetra-antennary[398]. Mn^{2+} is an important cofactor for several glycosyltransferases including β-1,4- galactosyltransferase and N-acetylglucosaminyltransferase-I and –II, and as a result increased Mn^{2+} may enable further glycan processing. Mn^{2+} addition has also been reported to reduce the level of high mannose IgG production by CHO cells[399]. Addition of Cu^{2+} has also been reported to increase the level of sialylation, possibly by decreasing the level of desialylation that can occur during cell culture and glycan purification[400,401].

Build-up of ammonia in culture media has been suggested to impair high level glycan processing. A high ammonia level has been demonstrated to cause a decrease in expression of β-1,4-galactosyltransferase and α-2,3- sialyltransferase in the golgi [402] and has also been found to cause a decrease in terminal sialylation and galactosylation of EPO produced in CHO cells[403]. However, the role of ammonia, and other by-products of cell metabolism such as lactate, is not fully understood and appears to vary between different cell types and proteins[404].

1.8.3 Cell Lines

The overwhelming majority of therapeutic antibodies are produced in mammalian cell lines, most often hamster or mouse derived lines or hybridomas, in order to allow for proper post translational modification[96]. The few that are produced in non-mammalian hosts are generally antibody fragments and do not require the proper processing of the N linked glycan in the Fc region. Therapeutic antibodies produced in different cell lines can display different glycosylation patterns. For example, as discussed below, mouse cell lines can incorporate different features into the N linked glycan than are found in human antibodies. Comparison of a number of marketed therapeutic mAbs produced in CHO cells or mouse myeloma cell lines has suggested that IgG produced in CHO cells has a lower level of galactosylation compared to those produced in mouse myeloma cell lines[405]. Further to this, mouse cell lines incorporate a different sialic acid to

humans, namely N-glycolylneuraminic acid (as opposed to N-acetylneuraminic acid), and can also produce a galactose α- 1,3- galactose linkage.

Neither of these moieties are found in humans and thus can be immunogenic. Although there are extremely few reports of immune responses vs antibodies attributed to these non-human modifications, they have been described. The therapeutic antibody cetuximab, when produced in NS0 (mouse) cells, has been reported to incorporate these immunogenic glycans and has caused anaphylactic shock in a small number of patients who already had circulating anti- galactose-α-1,3-galactose IgE antibodies[358]. Production of cetuximab in CHO (hamster) cells did not cause this side effect.

The recent findings that changes in glycosylation can change the affinity of IgG for FcγRs and thus effect antibody dependent functions has resulted in a desire to produce IgG with specific glycans. To this end, a number of modified cell lines have been produced that, for example, do not express particular glycosyltransferases. One example (discussed above in relation to the glycoengineered antibody mogamulizumab) is CHO cells in which the α- 1,6 fucosyltransferase (*fut8*) has been knocked out (by removal of the start codon), meaning IgG produced in this cell line are afucosylated, and therefore have a higher affinity for FcγRIIIa[359]. This technology has been developed in Japan and has been used to generate several afucosylated antibodies, the most successful of which is mogamulizumab, discussed above.

1.8.4 Enzymatic Modification

One drawback of changing the cell lines used to produce therapeutic antibodies or altering the media or growth conditions is the complexity of such changes and the effects they could have on other metabolic processes within the cell. Cell culture processes used in production of therapeutic antibodies are highly refined and optimised to give maximum yield of antibody, and by changing this process the yield could drop, increasing costs. As such an attractive alternative option that has been explored is *in vitro* glycan engineering using recombinant glycosyltransferases and substrates to achieve the desired glycan structures. This approach allows for the production of antibody to continue in its fully optimised form, while allowing for more controlled and complete manipulation of the N-linked glycans. Potential manipulation has been investigated by both

modification of existing glycans to removal of entire glycans and replacement with new pre-formed glycans[354,406].

The potential power of this technique has been demonstrated with the reengineering of existing mAbs to give vastly different functions. Cleavage of the Fc glycan of the anti-CD20 antibody rituximab achieved with EndoS was followed by transglycosylation from oxazoline-glycan donors with a mutant EndoS exhibiting minimal product hydrolysis[354]. This method was used to generate fully galactosylated, defucosylated rituximab that exhibited higher affinity for both allelic variants of FcγRIIIa, without increasing affinity for FcγRIIb, consistent with what has been reported for non-fucosylated antibodies. Furthermore, this technique was also used to fully sialylate Fc in IVIg, predicted to improve the therapeutic benefit of IVIg in mouse models of autoimmune disorders[372]. Another recent report using enzymatic modification to generate fully galactosylated and sialylated glycoforms reported increased binding to FcγRIIa and IIIa, as well as increased ADCC[406]. It is interesting to note that these reports suggest increased effector function and FcγR binding, although sialylated IgG is reported to be important for the anti-inflammatory effect of IVIg (as discussed earlier).

It has also been demonstrated that the localisation of glycomodification enzymes within the golgi can significantly affect the function of these enzymes and the final glycoform of the antibodies. This finding highlights the interacting roles of glycomodification enzymes and the order in which they act (described above). The action of certain glycomodification enzymes must occur prior to the action of others, whilst in a similar way the action of some enzymes can reduce/block the action of others (fucosylation blocked by bisecting GlcNAc). Consequently, when engineering cells to produce certain glycoforms the location of recombinant enzymes must be taken into consideration. For example, transfection of wild type GnT III enzyme into CHO cells resulted in highly bisected and mostly fucosylated Fc glycans, but transfection with a modified Gnt III (with the golgi localisation domain of α- 1,2- mannosidase II) resulted in bisected Fc glycans bearing almost no fucose[407,408]. Action of GnT III prevents the action of α- 1,6- fucosyltransferase and of α- 1,2- mannosidase II, blocking fucosylation and the trimming off of mannose residues necessary for conversion of hybrid glycans to complex glycans[408].

1.9 Fab Glycosylation

In addition to the glycosylation at Asn297 of the Fc region, the Fab domain of IgG can also be glycosylated[409]. Whereas glycosylation of the Fc is essential for IgG function and is present in all serum IgG, only about 20% of IgG are glycosylated in their Fab regions [111]. The N-linked glycosylation sequon (Asn-X-Ser/Thr) is not present in the germline Fab sequence, but it is thought that it can be introduced during somatic recombination during B cell maturation. This explains why only a proportion of antibodies have this Fab glycosylation. The function of this Fab glycosylation has received less study than that of the conserved Fc glycosylation, but there have been reports that it can contribute to the affinity of the antibody for its target epitope, as well as affecting antibody half-life and stability[111,410,411]. Unlike the Fc glycan it is not involved in binding to FcγRs or C1q.

Fab glycans have been shown to be more processed than their Fc counterparts, which has been suggested to be due to their greater availability to glycosyl transferase enzymes compared to the Fc glycan that is buried within the two CH2 domains, as Fab glycans can often be found on loops within the variable region[111]. This suggestion is supported by the finding that location of the Fab glycan can have a major effect on its processing[412]. Fab glycans are slightly less fucosylated (~70%) than Fc glycans, and also have a greater level of bisecting GlcNAc (~45%). Fab glycans are also much more highly sialylated than Fc glycans, with monosialylation (40%) and bisialylation (52%) seen at high levels.

1.10 Glycan Regulation

It has been found that in some autoimmune conditions the autoantibodies have a different glycan profile compared to the total IgG pool. This suggests that there is regulation over what type of glycans are attached to IgG in particular plasma cells. Reduced levels of galactose and sialic acid on autoantibody glycans have been found in serum and synovial fluid from rheumatoid arthritis patients, compared to total serum IgG[413,414]. Furthermore, immunization of pre-sensitized mice with sheep IgG resulted in a 50-60% reduction in the level of sialylated anti-sheep IgG antibodies, compared to only 40% in total IgG[372]. This suggests a mechanism where a steady state is

maintained with high levels of sialic acid and low inflammation, which can change in response to antigen to yield IgG with less sialic acid, facilitating a pro-inflammatory response.

Currently it is not well understood how this mechanism functions, for example the levels of glycan modifying enzymes may be regulated. However, it has been shown that certain signals can influence the glycan profiles of antibody produced by plasma cells. For example, it has been shown that IL-21 is able to increase the level of galactosylation of Fc linked glycans whereas all-trans retinoic acid causes a decrease in the levels of sialic acid and galactose, and that this response was maintained for five days[415]. IL-21 is known to induce differentiation of B cells into antibody secreting plasma cells, but this study suggests it could have an additional role in controlling the glycosylation status of the antibodies produced by a particular plasma cell[416]. Exposure to these, or other as yet unknown signals, could result in a change of the glycan profile and thus the immune response generated. It has been suggested that the microenvironment of the B cell during its activation and differentiation could play a key role in glycan profile selection, and that the type and amount of neighbouring cells will also affect this through production of different signals. This could mediate particular niches or plasma cell subsets producing IgG with different glycoforms[415].

1.11 Hypothesis and Aims

1.11.1 Hypothesis

It is known that the Fc region of an antibody is responsible for many of its functions. It is hypothesised here that modifications to that Fc region will affect the Fc mediated effector functions engaged. Although work has been carried out in this area, this thesis aims to investigate the effect of various Fc modifications in the format of a well-characterised model of antibody function, primarily using the anti-CD20 mAb rituximab. This approach will allow antibody specificity to be maintained, reducing the experimental variables, and allowing direct comparisons to be made. Primarily the work in this thesis will investigate the modification of antibody Fc through the alteration of the N-linked glycans and through addition of lipid molecules. Furthermore, the effect of different Fc regions in the context of different IgG subclasses will be

examined, and an affinity column produced for testing IgG binding to C1q, to determine the potential of various mAb forms to induce complement.

In order to test this hypothesis the following aims were set:

1) Determine the relative efficacy of all four IgG subclasses to elicit effector functions on an anti-CD20 backbone.

A- characterise the level of surface binding of anti-CD20 mAbs of different IgG subclasses.

B- determine the relative efficacy of antibody induced effector functions of anti-CD20 mAbs in assays reflecting their *in vivo* mechanism of action.

2) Assess the impact of lipid modification to IgG mAbs targeting CD20.

A- develop a protocol to modify mAbs with lipid chains based on malondialdehyde and carboxyethylpyrrole.

B- determine the functional impact of these lipid modification on the effector functions of lipid modified rituximab.

3) Analyse how Fc glycosylation modulates the Fc mediated effector functions of anti-CD20 mAbs using *in vitro* glycoengineering.

A- generate and characterise glycomodified formats of anti-CD20 mAbs.

B- analyse the effect of different glycoforms on the effector functions of anti-CD20 mAbs.

4) Produce a high performance liquid chromatography (HPLC) based method for studying the interaction between IgG Fc and C1q.

A- generate and optimise conditions for a C1q affinity column based on a single chain form of the C1q globular head group.

B- determine the specificity of the C1q affinity column for IgG and other C1q ligands.

C- validate the column findings with biologically relevant samples with known C1q binding, and confirm in cellular based assays of C1q binding and CDC.

Chapter 2: Materials and Methods

2.1 Cell Culture

2.1.1 Cell Culture Materials

Media for cell culture was prepared as follows: Complete Roswell Park Memorial Institute (cRPMI) and complete Dulbecco's Modified Eagle's Medium (cDMEM) were prepared by addition of 2mM glutamine, 1mM sodium pyruvate, 100U/ml streptomycin, 100µg/ml penicillin (all from Gibco, ThermoFisher Scientific) and 10% foetal calf serum (FCS, Sigma Aldrich). Phosphate buffered saline (PBS) was bought from Severn Biotech. Disodium ethylenediaminetetraacetic acid (EDTA) was purchased from Sigma Aldrich. Macrophage-colony stimulating factor (M-CSF) was produced in house (Protein production group, Somers, Southampton General Hospital, Dr. P. Duriez). All tissue culture plates and flasks were purchased from Corning.

2.1.2 Cell Lines

Raji (CCL-86), Ramos (CRL-1596), SUDHL4 (CRL-2957), Jurkat (TIB-152), Chinese hamster ovary (CHO)-K1 (CCL-61) and MDA-MB-453 (HTB-131) cell lines were purchased from American Type Culture Collection (ATCC).

2.1.3 Maintenance of Cell Lines

Raji, Ramos and SUDHL4 cells were cultured in cRPMI at 37°C using T25 or T75 tissue culture flasks. These cells were cultured in a humidified incubator maintained at 5% CO_2. Cells were resuspended in fresh media 3 times a week and seeded into flasks at ~$0.5x10^6$ cells per ml.

Chronic Lymphocytic Leukaemia peripheral blood mononuclear cells (CLL PBMCs) were cultured at high density ($1x10^7$ cells/ml) in cRPMI in 6 well plates after thawing (thawed as below), and incubated at 37°C, 5% CO_2 for at least 1 hour before use.

CHO-K1 cells were cultured in cRPMI at 37°C using T25 or T75 tissue culture flasks. These cells were cultured in a humidified incubator maintained at 5% CO_2. Cells were scraped, resuspended in cRPMI, and split 1 in 3 into a T25 or T75 flask, 3 times a week.

2.1.4 Cell Freezing

Cells were centrifuged at 450g for 5 minutes and resuspended in freeze media (90% FCS, 10% DMSO). Cells were aliquoted 1ml per vial at a concentration of $5x10^6$ cells/ml into cryo vials (ThermoFisher Scientific) and frozen at -80°C in a polystyrene box for at least 48 hours. Vials were then transferred to liquid nitrogen storage.

2.1.5 Cell Thawing

Cryo vials were removed from liquid nitrogen storage and thawed in a 37°C water bath. Cells were then immediately transferred into a 20ml universal tube containing warm cRPMI. This was then centrifuged at 450g for 5 minutes and the supernatant completely removed before resuspension in cRPMI. Cells were then seeded into a T25 tissue culture flask and cultured as above (Section 2.1.3).

2.1.6 PBMC Isolation

Anonymised leukocyte cones residual from leukapheresis were collected from Southampton General Hospital NHS Blood Donation Centre. The blood was drained into 50ml tubes and diluted 1 in 5 with PBS (2mM EDA, 10% FCS). The blood was then layered over lymphoprep and centrifuged at 800g for 20 minutes with the brake turned off. The buffy coat layer was harvested and washed 4 times in PBS 2mM EDTA at 400g for 5 minutes. The PBMCs were then resuspended in 10mls cRPMI, 2 drops of Zap-oglobin (Beckman Coulter) added and counted using a coulter counter (Beckman Coulter).

2.1.7 Differentiation of Monocytes into Macrophages

PBMCs were resuspended at $1x10^7$ cells/ml in RPMI supplemented with penicillin, streptomycin, glutamate, sodium pyruvate and 1% human AB serum (Sigma Aldrich). $2x10^7$ cells were aliquoted per well of a 6 well plate and incubated for 2 hours at 37°C and 5% CO_2. Cells were washed in PBS twice, 2mls of cRPMI added per well and the cells incubated overnight at 37°C and 5% CO_2. The following morning, 2µl of 100µg/ml M-CSF was added per well. Cells were fed every 2 days by removing 0.85mls of media and adding 1ml of cRPMI with 1µl of 100µg/ml M-CSF. Monocytes were considered to have differentiated into macrophages by day 7 and were used on days 7-10.

2.1.8 Serum Collection

2.1.8.1 Collection of Human Serum

Blood was collected from healthy donors directly into syringes in the absence of any anti-clotting factors. Blood was then transferred into glass centrifuge tubes and stirred with a wooden applicator. Blood was left to clot for 30-60 minutes and then centrifuged at 1000g for 20 minutes at 4°C. Serum was collected into glass storage tubes and the blood centrifuged again to allow collection of further serum. Serum was stored at -80°C until use.

2.1.8.2 Collection of Mouse Serum

Mice were warmed to 37°C and analgesia (lidocaine – Centaur Services, AmerisourceBergen) applied to the tail tip. The very tip of the tail was removed using a scalpel blade and blood was collected into 0.5ml microfuge tubes (Starlab) in the absence of any anti-clotting factors from the mouse tail. Blood was left to clot overnight at 4°C and centrifuged at 5,000g for 5 minutes to pellet out the clotted blood. Serum was removed by pipetting and stored at -20°C.

2.2 Protein Assays

2.2.1 Antibodies

All antibodies used in this work were purchased from supplier as indicated, or produced and quality controlled in house by the Antibody and Vaccine Antibody Production Group, or kindly gifted by BioInvent International AB or Hoffman La Roche.

2.2.2 Dialysis

Proteins were dialysed using Slide-A-Lyzer dialysis cassettes of appropriate volume (ThermoFisher Scientific) with a 7kDa molecular weight (MW) cut off. Protein in solution was added to these cassettes and dialysed into 1L of appropriate buffer at 4°C at a ratio of 1 part protein to 100-1000 parts diluent, with frequent exchange of diluent up to 5 times. Protein was removed using a needle and syringe of appropriate size and sterile filtered using a 0.2µm syringe filter (Merck Millipore).

2.2.3 Antibody Concentration and Buffer Exchange

Antibodies were concentrated by centrifugation in Amicon Ultra Centrifugal Filter Units with a 10kDa molecular cut off (Merck Millipore) at the manufacturer recommended speed of 4000g for 20 minutes. When using spin columns for changing antibody buffer, the antibody was concentrated down to a volume of ~100µl, and re-diluted in 10ml of the required buffer. This process was performed 3 times, to ensure complete buffer exchange.

2.2.4 Protein Concentration Assay

Protein was serially diluted 1 in 2 in Milli-Q (MQ) H_2O across Nunc MaxiSorp 96 well plates (ThermoFisher Scientific). Bovine serum albumin (BSA) was used as a standard to determine the concentration of unknown samples, at a range of approximately 2mg/ml to 1µg/ml. Protein assay

reagent (Biorad) was diluted 1 in 5 with MQ H_2O, and 250µl added to each well. Plates were read using an Epoch microplate reader (Biotek) at 570nm. The concentration of protein was determined using the linear range of the BSA standard (between 0.6mg/ml to 1µg/ml) according to the equation below, and multiplied by the appropriate dilution factor. Data were analysed on Microsoft Excel 2016 and GraphPad PRISM v7.

$X = (Y – C) /M$

Where X is the concentration of protein, Y is the mean absorbance of two measurements of the protein sample, C is the baseline absorbance and M is the gradient of a linear standard line.

2.2.5 Protein A Purification

Antibodies were purified using a 1ml HiTrap Protein A HP column (GE Healthcare) that was connected to a peristaltic pump and Unicord 280nm reader linked to a tracer. The pump and tubing were sterilised in 0.5M NaOH for 30 minutes and then washed through with Tris NaCl (20mM HCl, 2mM EDTA, 0.2M NaCl, Fisher Chemicals and 40mM Tris, Sigma Aldrich) until the pH returned to 8. 10 column volumes of Tris NaCl were pumped through the column (pump set to 1ml/minute), followed by 1 column volume of glycine pH 2.5 and then 5 column volumes of Tris NaCl buffer. This wash was repeated with another column volume of glycine pH 2.5.

Antibody samples were prepared for column purification by addition of 0.2 volumes of 5x Tris NaCl and then loaded onto the column. The sample was followed through with 5 column volumes of Tris NaCl before elution with 1 column volume of glycine pH 3.0. Eluting antibody was collected as the A280nm reading increased. The column was washed twice with alternating glycine pH2.5 and Tris NaCl as above between samples.

2.2.6 Native Gel Electrophoresis

Antibody samples were run on a native polyacrylamide gel (Sebia Hydragel (Sebia)) according to manufacturer's instructions to confirm purification of antibody from flowthrough. Antibodies were stained with Amidoschwarz Amidoblack (Sebia) at the manufacturer recommended concentration.

2.2.7 Size Exclusion Chromatography

20µl antibody samples were injected onto a Zorbax GF-250 column (Agilent) on a high performance liquid chromatography system running at 0.4ml/min and the absorbance at 280nm (A280) recorded using a Unicord 280nm reader linked to a tracer.

2.2.8 Enzyme-Linked Immunosorbent Assay (ELISA)

Enzyme-linked immunosorbent assays were performed, as described below, to detect the level of antibody present with a particular sample, or to determine the relative binding of a detection antibody to known concentrations of antibody.

2.2.8.1 Mouse Serum IgG Enzyme-Linked Immunosorbent Assay (ELISA)

Nunc MaxiSorp ELISA plates (Thermo Fisher Scientific) were coated with goat anti-human γ chain antibody (Sigma Aldrich) diluted to a final concentration of 5µg/ml in coating buffer (Na_2CO_3 15mM/L, $NaHCO_3$ 35mM, Fisher scientific) for 2 hours at 37°C or 1 hour at 37°C and then overnight at 4°C. Plates were then blocked with PBS 1% BSA for 1 hour at 37°C. Plates were then washed three times with PBS Tween (0.05%) using a Skanwasher 300 plate washer (Skatron). Standards and serum were then diluted 100 fold in PBS 1% BSA and added to the plate in a serial dilution. Standards consisted of the same antibodies that had been injected into the mice, measured in duplicate on the ELISA plates for the corresponding serum sample. Samples were incubated for 1.5 hours at 37°C, and washed five times with PBS Tween (0.05%) using a plate washer. Horseradish peroxidase (HRP) labelled goat anti-human Fc antibody (diluted 1 in 20,000 in PBS 1% BSA, Jackson Immunoresearch) was added for 1.5 hours at 37°C. Plates were washed five times with PBS Tween (0.05%) using a plate washer. A single o-Phenylenediamine dihydrochloride (OPD) tablet (Sigma Aldrich) was dissolved in 24.7mls Citrate (91mM Citric Acid Fisher Scientific) and 25.3mls phosphate (200mM Na_2HPO_4 ThermoFisher Scientific), and 50mls of distilled water. Prior to use, 40µl of 40% H_2O_2 (Merck) was added to the ELISA substrate, and 100µl added per well. ELISA plates were incubated at room temperature for 20 minutes, and after sufficient colour change had occurred, 50µl 2.5M H_2SO_4 (VWR) added. Plates were then read on an Epoch microplate reader (Biotek) at 450nm. The level of human IgG present with each sample

was determined using the linear range of the standards (between 30 and 1ng/ml) according to the equation below, and multiplied by the appropriate dilution factor. Data were analysed on Microsoft Excel and GraphPad PRISM v7.

$X = (Y – C) /M$

Where X is the concentration of antibody, Y is the mean absorbance of two measurements of the antibody sample, C is the baseline absorbance and M is the gradient of a linear standard line.

2.2.8.2 Human IgG ELISA

In order to check that the different IgG subclasses bound equally to the ELISA plate when testing the anti-kappa light chain ELISA (Section 2.2.8.3Anti-Kappa Light Chain ELISA), the goat anti-human Fc antibody (as for Section 2.2.8.1) was used to detect the level of each antibody subclass. IgG subclasses were bound directly onto the ELISA plate in a serial dilution from 1µg/ml in coating buffer for 2 hours at 37°C or 1 hour at 37°C and then overnight at 4°C. Plates were then blocked and binding detected as for Section 2.2.8.1. Data were presented as absorbance (at 280nm) against known mAb concentration.

2.2.8.3 Anti-Kappa Light Chain ELISA

2.2.8.3.1 Soluble Anti-Kappa Light Chain Antibody ELISA

Human mAbs with the kappa light chain were immobilised directly to ELISA plates, blocked and washed as in Section 2.2.8.2 at 1µg/ml. Anti-Kappa light chain antibody (MHK-49, Biolegend) was added to the plate after blocking at the indicated concentration and serially diluted across the plate, and incubated for 1.5 hours at 37°C. ELISA plates were then washed 5 times with PBS Tween (0.05%) with a plate washer. Bound anti-Kappa light chain antibody was detected through the use of an HRP conjugated Rabbit anti-mouse antibody (Jackson Immunoresearch, diluted 1 in 2,000 in PBS 1% BSA), added for 1.5 hours at 37°C. ELISA plates were washed five times with PBS Tween (0.05%) using a plate washer, and the level of bound HRP conjugated antibody detected as for Section 2.2.8.1. Data were presented as absorbance (at 280nm) against known mAb concentration.

2.2.8.3.2 Plate Bound Anti-Kappa Light Chain Antibody ELISA

Anti-Kappa light chain antibody was bound directly to the plate in coating buffer (as in Section 2.2.8.2) at a final concentration of 0.1µg/ml for 2 hours at 37°C. Plates were blocked and washed as in Section 2.2.8.1. Antibody samples were then added at a serial dilution from 1µg/ml, in PBS 1% BSA, for 90 minutes at 37°C. Bound antibody was detected using the HRP conjugated goat anti-human Fc antibody as for Section 2.2.8.1. Data were presented as absorbance (at 280nm) against known mAb concentration.

2.2.9 Surface Plasmon Resonance (SPR)

Surface plasmon resonance (SPR) was carried out using a Biacore T100 system (GE Healthcare). Recombinantly produced human FcγRs (I, IIa, IIb, IIIa, and IIIb) were purchased from R&D Systems, while buffers and reagents (Glycine pH 2.0, 10mM Acetate pH 5.0, (HBS-EP), Amine Coupling Kit, and NaOH) were purchased from GE Healthcare. Series S sensor CM5 chips (GE Healthcare) were used for ligand coupling. Approximately 2000 response units (RU) of antibody were immobilised to CM5 sensor chip flow cells via amine chemistry using the GE Healthcare Amine Coupling Kit to prepare the surface, and antibody at 200µg/ml. Fresh HBS-EP and MQ H_2O were prepared prior to kinetic analysis. FcγRs were prepared at 1-1000nM (for FcγRIIa and IIIa), 1-100nM (for FcγRI) and 200nM (FcγRIIb and IIIb) in fresh HBS-EP. Kinetic analysis was performed using a Biacore Method file according to the following parameters: sample on/off times 300 seconds at a flow rate of 30µl/min with 30 seconds regeneration with 30µl/min 10mM Glycine pH 2.0. FcγRs were flowed through all flow cells simultaneously and a blank reference flow cell subtracted from antibody containing flow cells. Kinetic analysis and steady state affinity calculation were performed using Biacore Evaluation software (GE Healthcare).

Relative binding intensity was determined as follows: response values (peak of association curve) were normalised to the amount of each antibody bound on the chip (in RU) by dividing the peak response value by the final response (from antibody immobilisation) after subtraction of the blank flow cell, e.g. galactose relative response/(final response of galactose post immobilisation – blank flow cell). The relative response (in RU) was then calculated for the maximum concentration of each FcγR tested (100nM for FcγRI and 1000nM for FcγRIIa and IIIa), and taken as a percentage of the value for native, unmodified antibody, e.g. normalised RU_{Max} galactosylated/normalised RU_{Max}

native * 100. Calculations were done in Microsoft Office Excel 2016 and graphs produced in GraphPad Prism Version 7.

2.2.10 Sodium Dodecyl Sulphate Polyacrylamide Gel Electrophoresis (SDS-PAGE)

Antibody samples were prepared in Laemmli sample buffer (Abcam) and boiled at 95°C for 5 minutes. Samples were loaded onto a 10% sodium dodecyl sulphate-polyacrylamide gel electrophoresis (SDS-PAGE, NuPAGE Bis Tris, 1.5mm, Thermo Fisher Scientific) gel and run at 110V for 2hrs. After running, gel was transferred to dH_2O and stained with Coomassie blue (Sigma Aldrich, 60mg/ml, in 10% acetic acid (v/v)) for 30 minutes. After staining, gel was de-stained with 10% ethanol/10% acetic acid (both v/v), changing periodically until the gel was no longer blue, and then imaged.

2.2.11 Glycan Analysis

Antibody glycan analysis was performed at Hoffman La Roche (Penzberg, Germany). The methods used, previously published by Roche, are briefly described below[417,418]. Samples of glycomodified antibodies were prepared in PBS and shipped at 4°C to Roche (Penzberg, Germany).

2.2.11.1 Mass Spectrometry

Samples were treated with IdeS (Fabricator, Genovis) to cleave the IgG within the hinge region[418]. Fragments were denatured and reduced using 6M Guanidine HCL and 0.11M tris(2-carboxyethyl)phosphine (TCEP), before being analysed by mass spectrometry following separation by HPLC on a Zorbax 300 Diphenyl RRHD 2.1x100mm 1.8µm column. The mass of the Fc fragment containing various glycans was calculated and peaks at the corresponding mass/charge ratios summed together to generate relative proportions of each glycan.

2.2.11.2 Instant Aminobenzamide (AB) Labelling

Samples were treated with Rapid PNGase F (NEB) to cleave the N-linked glycans off of the antibody Fc[417]. Released glycans were then labelled with Glykoprep Instant AB (prozyme) to rapidly label them, and then washed with CU cartridges. Labelled glycans were analysed by UPLC-FLR using a Waters BEH-Glycan Separations Technology column (1.7 µm, 150 × 2.1 mm). Relative glycan composition was then calculated from the resulting chromatograms.

2.3 Cell Based Assays

2.3.1 Flow Cytometry

2.3.1.1 Direct Staining

Surface staining using directly labelled antibody was carried out according to the following method. Cells were resuspended in either cRPMI or PBS at $1x10^6$ cells per ml. Antibodies were generally added at a final concentration of 10µg/ml (unless otherwise specified), according to manufacturer's instructions or diluted from manufacturer's instructions according to previous experience. Staining was typically carried out for 15 minutes at room temperature or for 30 minutes at 4°C. Cells were washed using 3mls fluorescence activated cell sorting (FACS) flow and centrifuged at 450g for 5 minutes, dragging the FACS tubes along a FACS rack to resuspend the cells in the residual buffer. Tubes containing residual volume after washing were acquired on a FACS Calibur flow cytometer, with addition of FACS flow if the volume was too low to allow for collection of sufficient events. Data were analysed using FCS Express v3 and GraphPad PRISM v7.

2.3.2 Antigen Binding

Target antigen expressing cells were resuspended in cRPMI in $1x10^6$ cells/ml. $1x10^5$ cells were transferred into FACS tubes and stained with the relevant antibody at 10µg/ml for 15 minutes at room temperature. Cells were washed twice with 3mls of FACS wash at 450g for 5 minutes. Cells were stained with 1µl/ml of secondary antibody for 30 minutes at 4°C. Cells were washed once in

FACS flow at 450g for 5 minutes, and acquired on a FACS Calibur flow cytometer. Data were analysed FCS Express V3 and GraphPad PRISM v7.

2.3.3 Antigen Blocking

Target antigen expressing cells were resuspended in cRPMI at $1x10^6$ cells/ml. $1x10^5$ cells were transferred into FACS tubes. Relevant antibody was added at 10µg/ml for 30 minutes at 4°C. Cells were washed with 3mls of FACS wash at 450g for 5 minutes. Fluorescein isothiocyanate (FITC) labelled competitor antibody directed to the same target was added for 30 minutes at 4°C. Cells were washed with 3mls FACS flow at 450g for 5 minutes and acquired on a FACS Calibur flow cytometer. Data were analysed FCS Express V3 and GraphPad PRISM v7.

2.3.3.1 Indirect Staining

When secondary staining was being carried out, cells were washed after primary staining (Section 2.3.1.1). Secondary antibody was added to the residual volume in the FACS tube (assumed to be approximately 100µl) after washing at a concentration according to manufacturer's instructions or diluted from manufacturer's instructions according to previous experience. Secondary staining was carried out at 4°C for 30 minutes, and afterwards cells were washed once in 3mls FACS flow at 450g, dragging the FACS tubes along a FACS rack to resuspend the cells. Further antibody staining was carried out in the same fashion as for secondary staining, and cells acquired as for primary stained cells. Data were analysed using FCS Express v3 and GraphPad PRISM v7.

2.3.4 C1q Binding Assay

Cells were resuspended in cRPMI at $1.1x10^6$ cells/ml and $5x10^4$ seeded into a 96 well flat bottom plate containing 50µl of 2x concentrated antibody or media, and incubated at room temperature for 15 minutes. 50µl of 24µg/ml human purified C1q (Abcam) was then added per well and incubated at 37°C for 15 minutes. The plate was then put on ice and the cells transferred to FACS tubes and washed twice with 3mls FACS wash at 450g for 5 minutes at 4°C. 10µl of 1 in 10 PBS

diluted anti-C1q-FITC antibody (Abcam) were then added to each tube, and incubated for 30 minutes at 4°C. Cells were then washed once more with 3mls FACS wash at 450g for 5 minutes at 4°C, and acquired on a FACS Calibur flow cytometer. Data were analysed using FCS Express v3 and GraphPad PRISM v7.

2.3.5 Complement Dependent Cytotoxicity (CDC) Assay

Cells were resuspended in cRPMI at $1x10^6$ cells/ml and $1x10^5$ cells seeded into a 96 well flat bottom plate containing 50µl of 2x concentrated antibody or media, and incubated at room temperature for 15 minutes. Freshly thawed human serum (Section 2.1.8.1) was added to wells to give a final concentration of 30%, and cells incubated at 37°C for 15 minutes before being placed on ice. For data gathering, cells were transferred to a FACS tube and stained with 2 drops (approximately 100µl) of 10µg/ml propidium iodide before acquisition on a FACS Calibur flow cytometer. Data were analysed using FCS Express v3 and GraphPad PRISM v7.

2.3.6 Direct Cell Death (DCD) Assay

Cells were resuspended in cRPMI at $2x10^6$ cells/ml and $1x10^5$ cells seeded into a 96 well flat bottom plate containing 50µl of 2x concentrated antibody or media. Cells were incubated for 24hrs at 37°C, 5% CO_2, in a humidified incubator. Cells were then placed on ice and transferred to FACS tubes. Tubes were stained with 2 drops (approximately 100µl) of 10µg/ml propidium iodide before acquisition on a BD FACS Calibur. Data were analysed using FCS Express v3 and GraphPad PRISM v7.

2.3.7 Antibody Dependent Cellular Cytotoxicity (ADCC) Assay

Target cells were resuspended in PBS at $1x10^7$ cells/ml and labelled with calcein AM (Life Technologies) at 10µg/ml for 30 minutes at 37°C with periodic mixing. The labelled target cells were washed 3 times in PBS containing 10% FCS at 300g and resuspended at $1.6x10^6$ cells/ml in cRPMI. $5x10^4$ labelled target cells were seeded per well of a round bottom 96 well plate

containing 50µl of 2x concentrated antibody or media for 15 minutes at room temperature. Purified PBMCs (Section 2.1.6) were adjusted to $4x10^7$ cells/ml and $4x10^6$ PBMCs, media or 4% Triton X-100 added per well. The plate was briefly pulsed and then incubated at 37°C for 4 hours. The plate was then centrifuged at 200g for 5 minutes and the supernatants transferred to a white walled plate and read on a VarioSkan plate reader (excitation at 494nm, emission at 515nm). Lysis was calculated as a percentage of maximum once background was removed according to the equation:

$$\%\ \text{of Max Lysis} = (\text{X} - \text{background})/(\text{Max Lysis} - \text{background})$$

(X= a given well, background is the mean of 3 wells containing only PBMCs and non-opsonised targets, and max lysis is the mean of 3 wells of target cells lysed with 4% Triton X-100). Data were analysed and presented using Microsoft Office Excel 2016 and GraphPad PRISM Version 7. This basic method was performed with minor adjustments for specific experiments as detailed below.

2.3.7.1 ADCC Assay with Competing IgG

To examine the effect of competing IgG, the assay was carried out as above, with addition of human polyclonal IgG added at cell opsonisation stage at a final concentration of 10mg/ml during antibody opsonisation and 5mg/ml during co-culture.

2.3.8 Antibody Dependent Cellular Phagocytosis (ADCP) Assay

MDMs were generated as detailed earlier (Section 2.1.7), washed twice with PBS and the media replaced with cold PBS for 15 minutes on ice. Macrophages were then scraped with a cell scraper and resuspended in cRPMI at $1x10^6$ cells/ml. $1x10^5$ cells were added per well of a flat bottom 96 well plate, and the plate was incubated at 37°C for 2 hours. Target cells were resuspended in PBS at $2x10^7$ cells/ml and labelled with 5µM CFSE (Life Technologies) for 15 minutes in the dark at room temperature. After labelling, 1ml of FCS was added for 1 minute, and then the cells were washed twice with cRPMI and resuspended at $2.5x10^6$ cells/ml. $2.5x10^5$ target cells were seeded per well of a round bottom 96 well plate containing 2x concentrated antibody or media for 30 minutes at 4°C. Media was removed from macrophages and replaced with 100µl fresh media.

100µl of target cells was then transferred into the macrophage plate and incubated at 37°C for 1 hour. 1µl per well of anti-CD14 (eBioscience clone 61D3) was then added and cells incubated at room temperature in the dark for 15 minutes. Media was flicked off and 200µl of cold FACS wash added to the cells, which were placed on ice for 15 minutes. Cells were scraped using a P200 pipette tip and transferred to a FACS tube for acquisition on a FACS Calibur flow cytometer. Data were analysed using FCS Express v3 and GraphPad PRISM v7. Phagocytosis was defined as macrophages (CD14 +ve) that were also positive for CFSE (target cells).

2.3.9 FcγR Binding

CHO-K1 cells transfected with FcγRI, FcγRIIa (R131), FcγRIIb, FcγRIIIa (V158), FcγRIIIa (F158) or mock transfected controls (generated by Dr. R. Oldham[419]) were incubated in PBS + 2mM EDTA for 10 minutes, scraped to remove from flasks and washed. $1x10^5$ cells were added per FACS tube and target antibody added for 30 minutes at 4°C. Cells were washed once in FACS wash at 4°C for 5 minutes at 450g. Cells were stained with 1µl tube of PE labelled polyclonal $F(ab')_2$ anti-human Fc (Jackson ImmunoResearch) for 30 minutes at 4°C. Cells were washed with FACS wash at 450g for 5 minutes and acquired on a FACS Calibur flow cytometer. Data were analysed FCS Express V3 and GraphPad PRISM v7.

2.3.10 FcγRIIb/c Reporter Assay

Jurkat T cells containing an nuclear factor of activated T cells-response element (NFAT-RE)*luc2* reporter fusion (Promega) can be used to detect nuclear factor (NF) κB signalling, for example in response to binding of surface molecules, through the use of a luciferin containing substrate (Promega). FcγRIIb and c are highly related molecules and contain identical extracellular domains[420]. As such FcγRIIc can act as a surrogate to study FcγRIIb binding in this system, and was transfected into these Jurkat reporter cells (Dr. Richard Stopforth, unpublished data). Although FcγRIIb contains an ITIM, FcγRIIc instead contains an ITAM. This ITAM can trigger activation of NFκB, resulting in transcription of the luciferase enzyme, meaning luciferase production, and therefore activity, can be used as a measure of FcγRIIc (and therefore FcγRIIb) signalling.

In order to present IgG Fc regions to the FcγRIIc expressing Jurkat cells, Raji cells were opsonised with target antibodies for 15 minutes at room temperature. Opsonised Raji cells were then washed in cRPMI prior to 6 hour incubation with FcγRIIc transfected Jurkat cells at a 1:2 (Raji to Jurkat) ratio in a white walled plate. After incubation, 75µl 2x concentration luciferin containing substrate was added to wells and luminescence measured immediately using a VarioSkan plate reader at the recommended range of wavelengths. Media containing wells were subtracted from experimental values and data were analysed using Microsoft Office Excel 2016 and GraphPad PRISM v7.

2.4 Animal Methods

2.4.1 Animals

Wild type C57BL/6 mice were bred in the Biomedical Research Facility at the University of Southampton.

2.4.2 Ethics

All animals used were maintained by the Biomedical Research Facility at the University of Southampton in accordance with Home Office Regulations. All procedures carried out were approved by the local ethics committee and performed in accordance to the Animals (Scientific Procedures) Acts 1986, as set out in the Project Licence: PB24EEE31.

2.4.3 Antibody Half-Life Experiment

25µg of sterile antibody in 200µl of PBS was injected into the tail vein of pre-warmed animals after application of analgesia (lidocaine). Mice were checked shortly after injection to confirm there were no adverse events. Blood samples were collected from the tail vein 24hrs, 48hrs and 168hrs (7 days) following antibody administration for serum isolation as outlined in Section 2.1.8.2.

2.5 C1q Column Methods

2.5.1 Column Production

2.5.1.1 C1q Production and Biotinylation

Single chain C1q (scC1q) was produced at Hoffman La Roche and kindly gifted for this project. scC1q was produced in HEK293 cells by linking of the genes for the C1q globular head groups into a single chain in the order C1qA-C1qB-C1qC. scC1q was biotinylated using the Bulk BirA: BirA biotin-protein ligase bulk reaction kit (Avidity) according to manufacturer's recommendations. Biotinylated scC1q was dialysed, as described in Section 2.2.1, into 20mM $NaH_2PO_4*H_2O$, 150mM NaCl, pH 7.5, (Merck Millipore).

2.5.1.2 Streptavidin Coupling

Streptavidin coated sepharose beads (GE Healthcare) were poured into a sintered funnel in a buchner flask and connected to a vacuum pump. Sepharose was washed with 15 funnel volumes (approximately 5mls) of MQ H_2O, followed by 10 funnel volumes of 20mM HEPES (Merck Millipore), pH 7.4. 1.1g of washed sepharose was then transferred to a 50ml Falcon tube (Eppendorf), and placed on a shaking rack. Biotinylated scC1q was added dropwise to the shaking tube from a 1ml syringe and needle. scC1q and sepharose were incubated at room temperature with periodic mixing for several hours to allow ligation.

2.5.1.3 Column Packing

Biotinylated scC1q-sepharose slurry was packed into 4.6 x 50mm chromatography columns (Tricorn 5/50, GE Healthcare) by injection from a 1ml syringe through a syringe adaptor into a water filled column. After all the biotinylated scC1q-sepharose slurry was added, the column was sealed with a filter at the top end and locked in place with a screw cap.

2.5.1.4 Blank Column

Blank columns (lacking C1q) were produced by packing mock treated sepharose into an HPLC column, using the same method as detailed above in Section 2.5.1.3.

2.5.1.5 Column Storage

Columns were stored at 4°C in 20mM 4-(2-hydroxyethyl)-1-piperazineethanesulfonic acid (HEPES).

2.5.2 C1q Column HPLC Operating Conditions

The C1q affinity column was operated on a Shimadzu 10A HPLC system with in-line degasser. Absorbance at 280nm was used for sample detection. The autosampler was maintained at 4°C and the column maintained at 25°C. Prior to injection of samples, running buffer was injected to equilibrate the column followed by two injections of 25µg of anti-HER3 human IgG1 as a standard. 25-100µg of samples were typically injected at 1mg/ml in Eluent A from Chromacol glass sample vials (ThermoFisher Scientific), with a buffer flow rate of 0.5ml/min. 100% Eluent B (20mM HEPES, 500mM NaCl, Merck Millipore, pH 7.4) was used to regenerate the column during each run, according to the gradients described in Chapter 6:. Chromatograms were generated and processed using Chromeleon v 7.2 SR4 (ThermoFisher Scientific) and Microsoft Office PowerPoint and Excel, both 2016.

Chapter 3: Influence of IgG Subclass on mAb Effector Function

3.1 Introduction

Therapeutic mAbs are approved for use in the treatment of many different conditions including cancers (such as breast cancer and chronic lymphocytic leukaemia) and autoimmune disorders (such as rheumatoid arthritis and multiple sclerosis)[421]. The majority of the targets for these antibodies are cell surface proteins (including CD20, CD52, HER2 and programmed cell death (PD)-1), whilst a smaller number target extracellular soluble components such as Factor IXa, for the treatment of haemophilia A and *Clostridium difficile* enterotoxin B for *C. difficile* infection[422-424].

Historically most therapeutic mAbs have acted in a depleting manner (also called direct targeting mAbs). Direct targeting mAbs, such as rituximab function by opsonising the targeted cell and triggering cell death/removal through cell intrinsic or immune mediated effector functions (such as CDC, ADCC and ADCP)[425]. A smaller number of mAb based agents that have also been approved carry a toxin, termed a payload, which is specifically delivered to the tumour cells through the specificity of the antibody moiety, such as trastuzumab emtansine and ozogamicin conjugates gemtuzumab and inotuzumab[426].

More recently, a major revelation in the field of immunotherapy has been the discovery of mAbs known as checkpoint blockers or immunomodulatory antibodies[427,428]. These antibodies, like direct targeting antibodies, bind to surface molecules on their target cells. However, unlike direct targeting antibodies, the cells targeted by this class of mAbs are usually immune cells, and the aim of therapy is not to deplete these cells, rather to activate their immune effector functions[164]. This can include blocking inhibitory receptors such as CTLA-4 on the surface of T cells, or activating immunostimulatory receptors such as CD40 and CD27 on various immune cells[429-431].

Targeting effector cells of the immune system rather than targeting the tumour requires a different therapeutic approach, as depletion of immune cells within a tumour is not the desired outcome. As such, the use of standard human IgG1 antibodies with their well-known pro-inflammatory functions is potentially harmful. Some IgG1 mutations that reduce antibody effector function have been produced that decrease the Fc mediated effector functions, potentially

sparing immune cells from depletion[432]. Other approaches to decrease target cell depletion could involve selecting target epitopes which induce less effective cell targeting, as both target epitope and membrane proximity of the target epitope have been shown to be important for the efficacy and mechanism of depletion[433,434].

Classically, mAbs approved for use in the clinic contain the IgG1 heavy chain. However, more recently other heavy chain IgG subclasses have been used in the clinic. Nivolumab and pembrolizumab (formerly known as lambrolizumab) are both PD-1 targeting mAbs that contain a human IgG4 heavy chain[435,436]. These show little to no Fc-mediated effector function on the targeted T cells, instead acting to release these cells from PD-1/PD-L1 induced exhaustion. Furthermore, two of the above-mentioned toxin conjugated mAbs gemtuzumab- and inotuzumab-ozogamicin are also of the IgG4 subclass, and the anti-epidermal growth factor receptor mAb panitumumab (formerly known as ABX-EGF), approved for the treatment of colorectal cancers, is of the IgG2 subclass[437,438].

Although IgG1 is the most abundant IgG subclass in human serum, IgG2, IgG3 and IgG4 are also found and are reported to have differing effector functions and characteristics[439]. IgG1 and IgG3 are generally reported to be highly active in inducing Fc-mediated effector functions, whereas IgG2 and IgG4 are thought to be less active in these capabilities[99,440].

Despite the reported characteristics of these IgG subclasses to be either highly pro-inflammatory (IgG1 and IgG3) or moderately pro-inflammatory (IgG2 and IgG4), there have been conflicting reports in the literature regarding some of these subclasses, notably IgG2, which has been reported to potentially be active in depleting target cells[441,442]. With the increasing diversity of mAbs of different human IgG subclasses entering the clinic and in clinical trials, it is of great importance to fully understand the relative activity of these different IgG subclasses. Comparisons of different IgG subclasses are sometimes based on different antibody specificities on different subclasses, making the interpretation of results difficult. In order to properly characterise the differences between IgG subclasses we used the same antibody specificity on the four IgG subclasses to remove any variables coming from different binding affinities or epitopes. We undertook a detailed investigation into the effector function of the well studied anti-CD20 mAb rituximab, produced on each of the 4 human IgG subclass backbones, as well as the more recently approved type II anti-CD20 mAb obinutuzumab (produced in-house without glycoengineering as BHH2) produced as a human IgG1 and IgG2.

3.2 Target Binding of Anti-CD20 mAb IgG Subclasses

Firstly, anti-CD20 antibodies were tested to see whether the different constant domains of the human IgG subclasses influenced the ability of the Fab domains to bind the antigen. IgG subclasses were tested by size exclusion HPLC to confirm they did not contain high degrees of aggregation (Figure 8-3). As all of the subclasses contain the same variable regions it was anticipated that the antigen binding would also be the same. To do this, Ramos cells were opsonised with 10µg/ml of the respective antibody and excess antibody washed off. Bound antibody was detected with a polyclonal anti-human Fc specific phycoerythrin (PE) conjugated $F(ab')_2$ (Figure 3-1B), and analysed by flow cytometry to compare the binding level of each antibody.

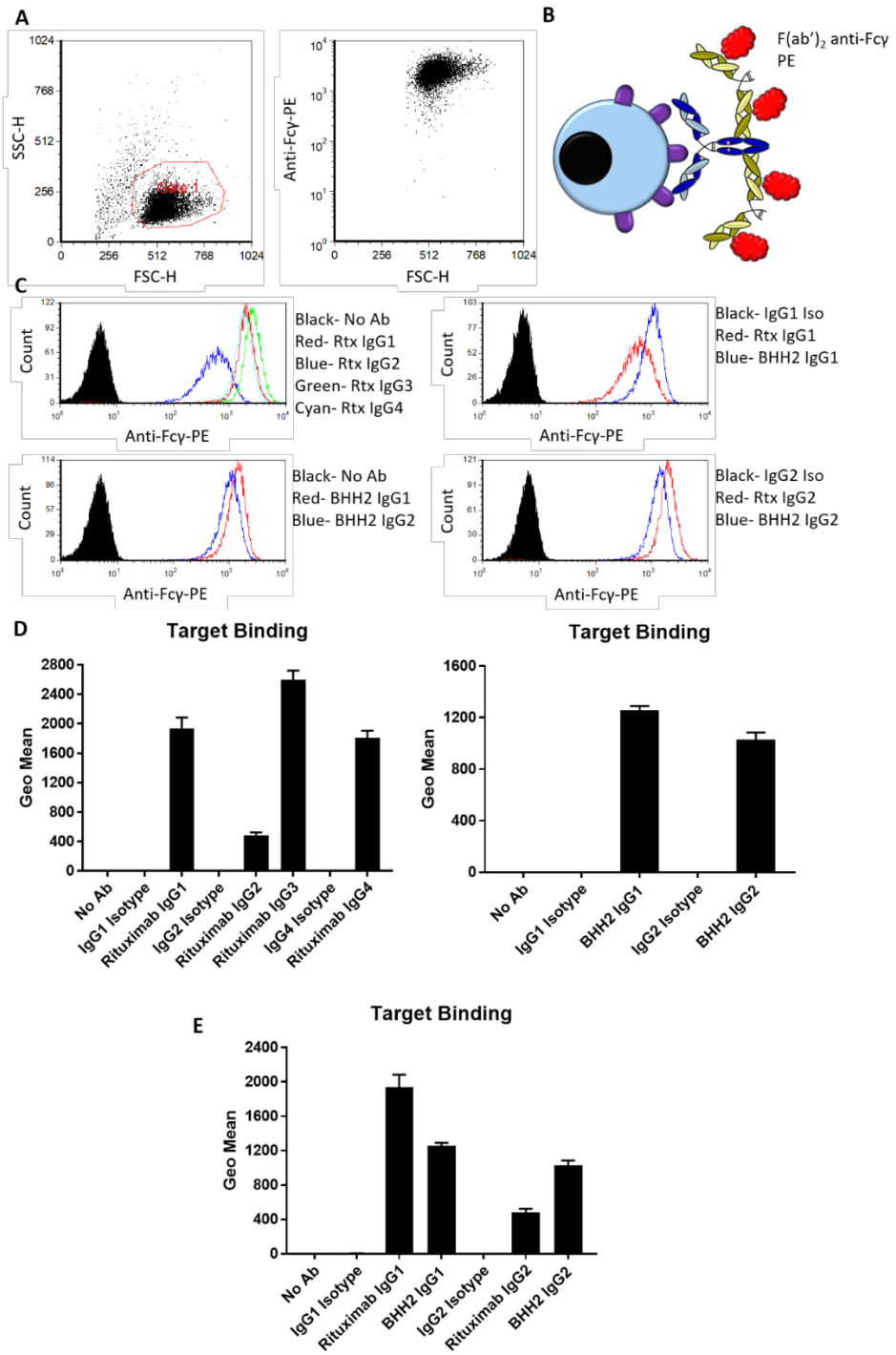

Figure 3-1 Binding of Rituximab and BHH2 IgG Subclasses to Ramos Cells

Ramos cells were opsonised with anti-CD20 antibodies at 10µg/ml. The level of surface bound antibody was detected using a polyclonal anti-Fcγ specific PE labelled F(ab')$_2$. A- gating of anti-CD20 opsonised Ramos cells, gated on viable cells and the geometric mean of the signal in the FL-2 channel taken. B- schematic diagram showing experimental setup. C- overlaid histograms of antibody subclasses binding to Ramos cells. D- geometric means of antibody subclass surface binding. Mean + range of duplicate measurements from a single experiment presented. E- direct comparison of IgG1 and IgG2 for both rituximab and BHH2.

However, testing the level of antibody on the surface of opsonised Ramos cells using a polyclonal labelled F(ab')$_2$ recognising human IgG Fc indicated differing levels of antibody subclass at the target surface (Figure 3-1). Binding of rituximab IgG2 to the Ramos cells was greatly reduced compared to the other subclasses, whilst rituximab IgG3 showed increased surface binding when compared to IgG1, and IgG4 remained similar to IgG1. BHH2 IgG2 also showed reduced binding when compared to IgG1, but the decrease was of a smaller magnitude than seen for rituximab subclasses (Figure 3-1E). Overall binding of rituximab IgG1 was greater than seen for BHH2 IgG1, as expected for a type I anti-CD20 antibody vs. a type II, respectively.

Next, to confirm that the differences in anti-CD20 binding seen for IgG1 vs. IgG2 in Figure 3-1 were independent of antibody concentration, the level of antibody at the surface of Ramos cells was titrated from 10µg/ml to 0.04µg/ml for each of the different IgG subclasses. Bound antibody was then detected using the same concentration of polyclonal labelled F(ab')$_2$ secondary which recognised human IgG Fc as performed previously.

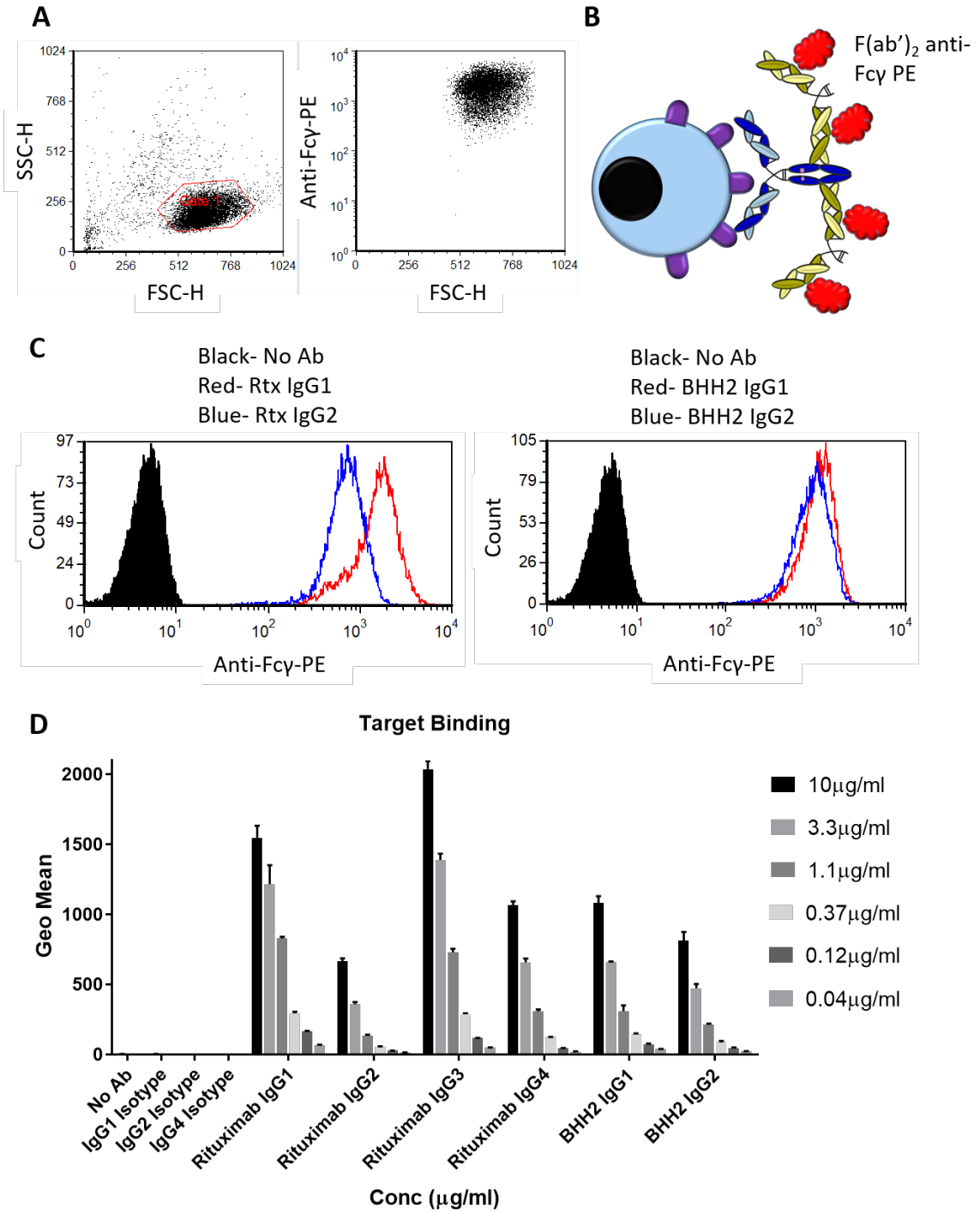

Figure 3-2 Anti-CD20 Antibody Binding Subclass Titration

Ramos cells were opsonised with anti-CD20 antibodies at a range of concentrations. The level of surface bound antibody was detected using a polyclonal anti-Fcγ specific PE labelled F(ab')$_2$. A- gating of anti-CD20 opsonised Ramos cells, gated on viable cells and the geometric mean of the signal in the FL-2 channel taken. B- schematic diagram showing experimental setup. C- overlaid histograms of antibody subclasses binding to Ramos cells at 10μg/ml. D- geometric means of antibody subclass surface binding at the indicated concentrations. Mean + range of duplicate measurements from a single experiment presented.

As seen in Figure 3-1, the level of IgG1 bound at the cell surface was greater than IgG2 both for rituximab and, to a lesser extent, for BHH2 (Figure 3-2C). This difference was maintained at all concentrations tested, from 10µg/ml to 0.04µg/ml, for both rituximab and BHH2.

The ability of the anti-CD20 mAb subclasses to block the binding of a second anti-CD20 antibody was then assessed, as another means to determine the relative level of the different subclasses at the cell surface. Ramos cells were opsonised with the different IgG subclasses of the anti-CD20 mAbs and unbound antibody washed off. A FITC labelled rituximab IgG1 antibody was then added to each sample, and the cells acquired by flow cytometry (Figure 3-3B).

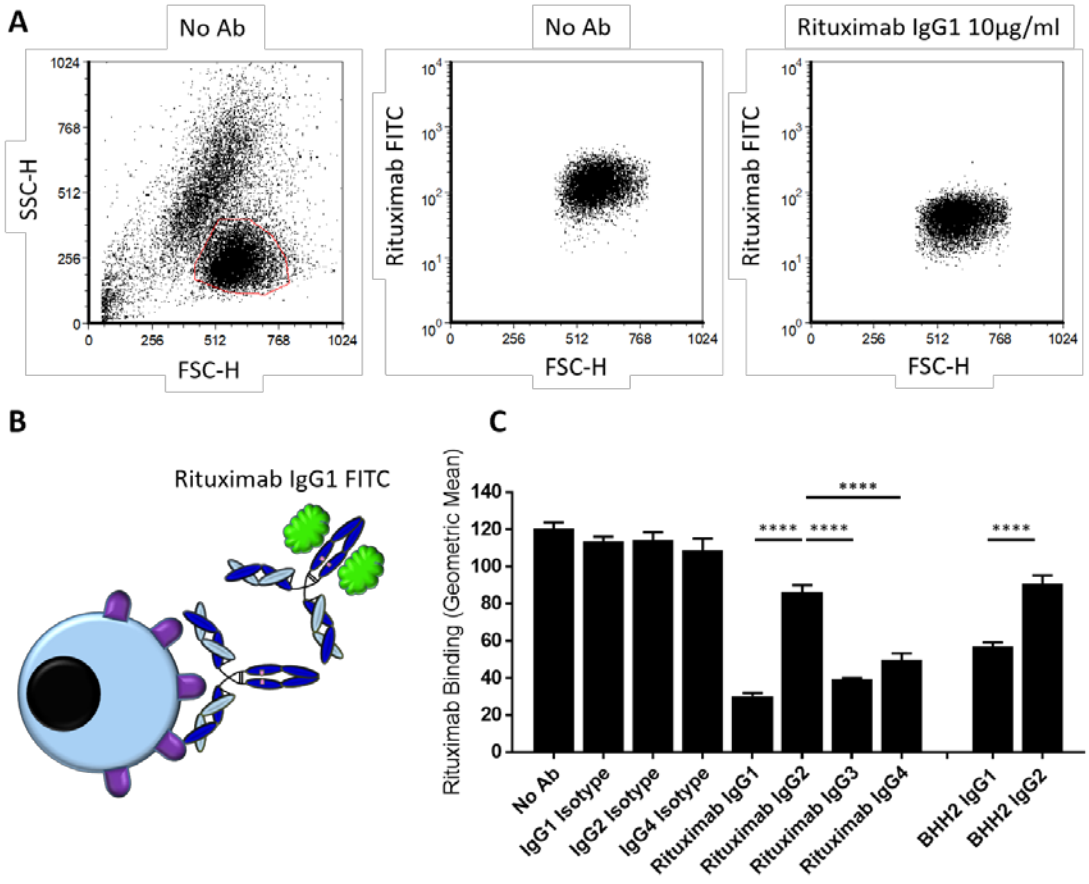

Figure 3-3 Assessment of the Ability of Anti-CD20 IgG Subclasses to Mask CD20

Ramos cells were opsonised with anti-CD20 IgG subclasses and the remaining available CD20 detected by the addition of a second anti-CD20 mAb (rituximab IgG1), directly labelled with FITC. A- live cells were gated on and the level of signal in the FL-1 channel determined. B- schematic diagram of the assay setup. C- geometric mean of the level of rituximab FITC binding detected after initial opsonisation with anti-CD20 subclasses at 10µg/ml. Data shown represent mean plus range of triplicate technical repeats of a single experiment. Statistics calculated by One Way ANOVA, **** $p<0.001$.

The binding of rituximab FITC after opsonisation of Ramos cells with anti-CD20 subclasses is an indication of the level of available CD20 and/or the ability of the rituximab IgG1 FITC to out-compete the initially bound anti-CD20 mAb. The absence of primary antibody (No Ab in Figure 3-3C) results in maximal binding of rituximab FITC. The presence of bound IgG prior to the addition of rituximab FITC reduced this binding for all subclasses tested. Rituximab IgG1 showed the biggest effect for blocking the rituximab FITC. In contrast, rituximab IgG2 shows the smallest effect. The same trend was seen for BHH2 IgG1 and IgG2, but the difference was smaller than seen for rituximab IgG1 and IgG2. Rituximab IgG3 and IgG4 showed an intermediate effect, with rituximab IgG3 blocking more rituximab FITC than rituximab IgG4.

It was next confirmed whether the trend of reduced CD20 binding for IgG2 subclasses was maintained beyond Ramos cells. Two further B cell lines, Raji and SUDHL4, were opsonised with anti-CD20 mAbs on multiple IgG subclasses, and the binding detected with the same $F(ab')_2$ anti-human Fc PE used in Figure 3-1.

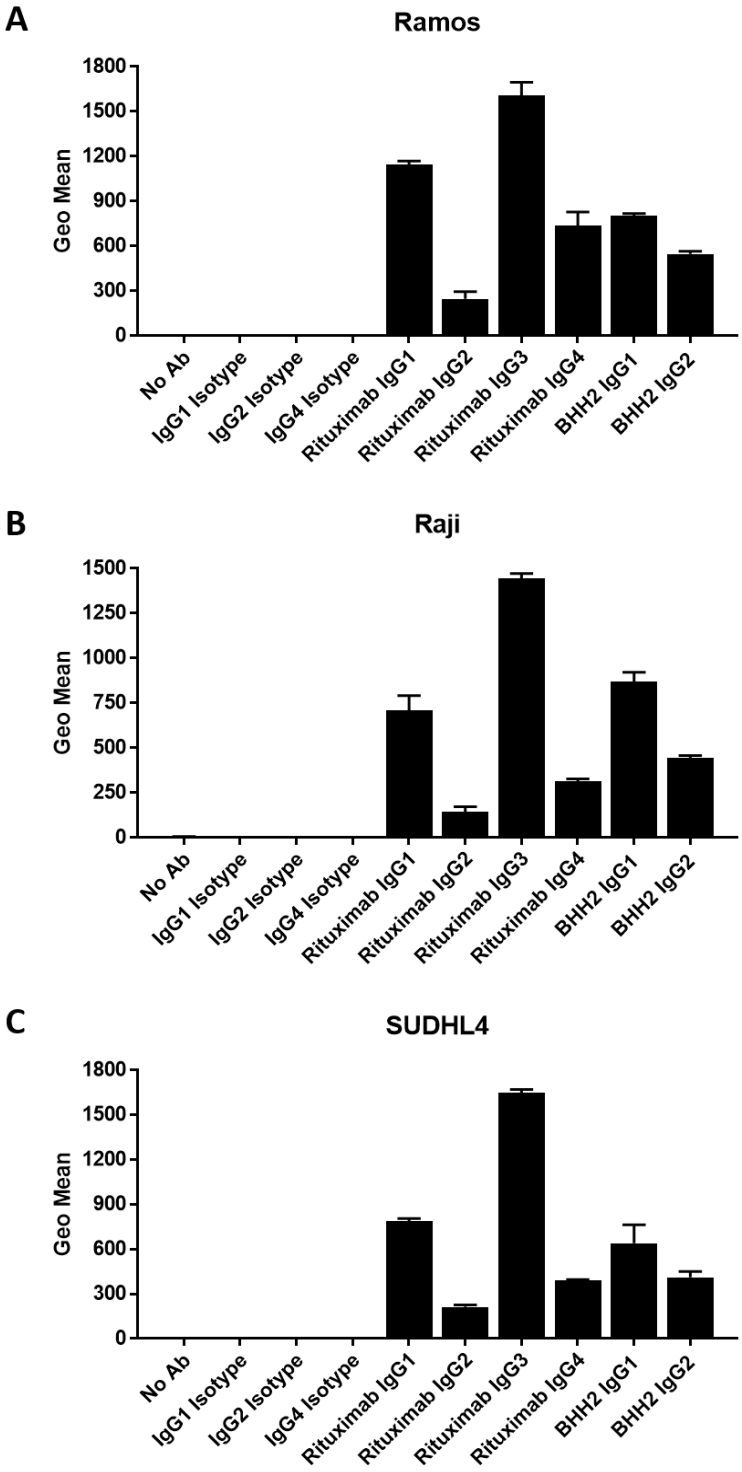

Figure 3-4 Anti-CD20 IgG Subclass Binding to CD20 Expressing Cell Lines

The binding of anti-CD20 mAbs rituximab and BHH2 on different IgG subclasses. Cells were opsonised by anti-CD20 mAbs on different human IgG subclasses at 10μg/ml, and the level of bound antibody detected with a polyclonal anti-Fcγ specific PE labelled $F(ab')_2$. Cells were gated as shown in Figure 3-1. A-C- level of IgG subclasses of rituximab and BHH2 bound to Ramos (A), Raji (B) and SUDHL4 (C) cell lines. Data shown are mean plus range of duplicate technical repeats of a single experiment.

As shown in Figure 3-1 and Figure 3-2, rituximab IgG2 demonstrated reduced binding compared to rituximab IgG1 on Ramos cells, and BHH2 IgG2 showed reduced binding compared to BHH2 IgG1, albeit with the difference less pronounced. This same trend was maintained on both Raji and SUDHL4 cells, with IgG2 showing reduced binding compared to IgG1 for both rituximab and BHH2, with a greater difference seen with rituximab (Figure 3-4).

CD20 is known to redistribute into lipid rafts upon binding with a type I anti-CD20 antibody, such as rituximab[292,293]. As the reduction in the level of binding of IgG2 was much less for BHH2 than for rituximab it was possible that differences in CD20 redistribution could be a potential factor. Therefore Ramos cells were fixed at different stages during the opsonisation and detection protocol and checked to see if the differences in the level of antibody at the cell surface was effected. By fixing the target cell with paraformaldehyde the level of CD20 redistribution in the Ramos cell membrane should be reduced. In addition, the effect of fixing opsonising antibodies before washing unbound antibodies was tested.

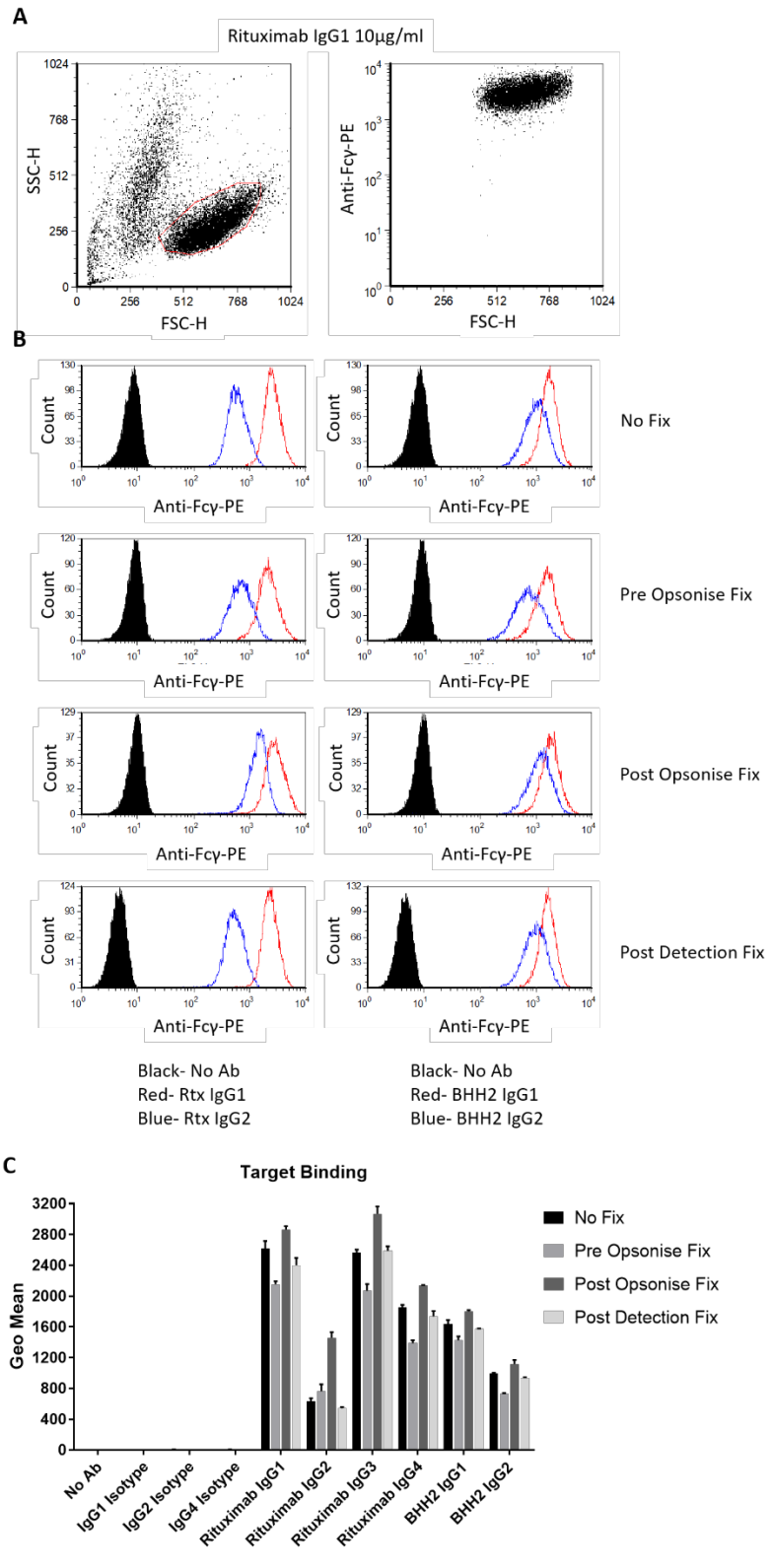

Figure 3-5 Anti-CD20 Antibody Subclass Binding After Target Fixation

Ramos cells were opsonised with anti-CD20 antibodies at 10µg/ml and fixed with paraformaldehyde at different stages during the opsonisation method. The level of surface bound antibody was detected using a polyclonal anti-Fcγ specific PE labelled F(ab')$_2$. A- gating of anti-CD20 opsonised Ramos cells,

gated on viable cells and the geometric mean of the signal in the FL-2 channel taken. B- overlaid histograms of antibody subclasses binding to Ramos cells fixed at various timepoints. C- geometric means of antibody subclass surface binding to Ramos cells fixed at various timepoints, grouped by antibody. Mean + range of duplicate measurements from a single experiment, representative of two independent experiments.

Fixation of target cells prior to opsonisation decreased the binding of all anti-CD20 antibodies except rituximab IgG2 (Figure 3-5). Fixation of Ramos cells after opsonisation caused an increase in the level of binding of all anti-CD20 antibodies, with rituximab IgG2 perhaps showing the largest increase. Fixation after staining with the polyclonal anti-Fc $F(ab')_2$ resulted in little change in the level of binding of all antibodies. BHH2 antibodies seemed less sensitive to changes in fixation than did rituximab, with pre-opsonisation fixation reducing the binding of both IgG1 and IgG2 similarly.

All of the antigen binding assays performed thus far utilised a polyclonal anti-IgG Fc secondary. Due to differences in the IgG subclass backbones it was possible that the lower levels of IgG2 detected was an artefact of the detection reagent having different affinities towards the different IgG subclass Fc backbones. In order to test this theory the opsonisation procedure was repeated on Ramos cells and the level of surface antibody detected using a FITC conjugated anti-idiotype antibody specific for the variable region of rituximab (Figure 3-6B), which was the same for all of the subclasses tested, at 10µg/ml and excess antibody was washed off prior to analysis by flow cytometry.

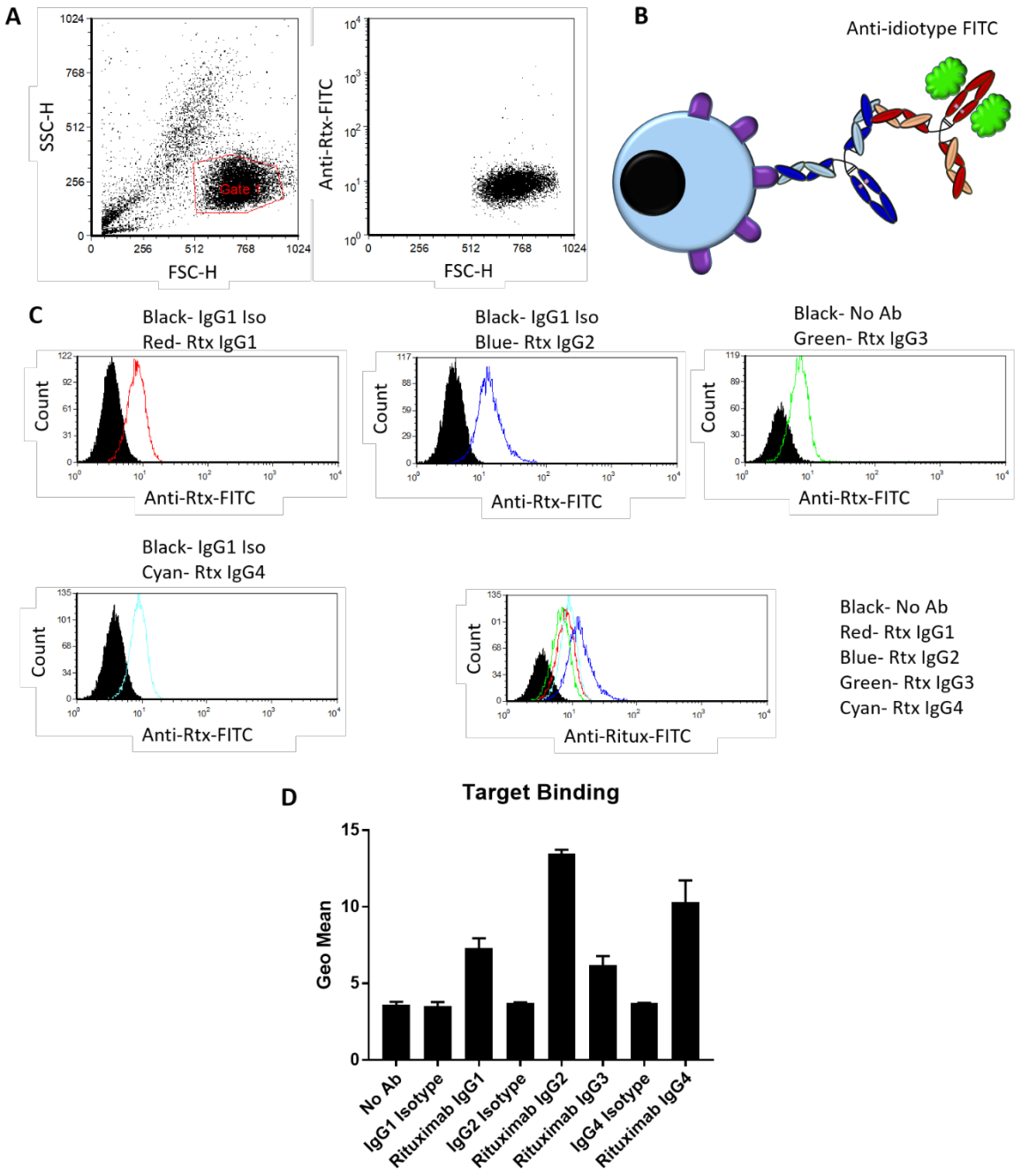

Figure 3-6 Anti-CD20 Surface Binding to Ramos Cells Detected by Anti-Idiotype

Ramos cells were opsonised with rituximab IgG subclasses at 10µg/ml. The level of surface bound rituximab was detected using a FITC labelled anti-idiotype mAb (clone MB2A4) at 10µg/ml. A- gating of rituximab subclass opsonised Ramos cells, gated on viable cells and the geometric mean of the signal in the FL-1 channel taken. B- schematic diagram showing experimental setup. C- overlaid histograms of rituximab subclasses binding to Ramos cells. D- geometric means of rituximab subclass surface binding. Mean + range of duplicate measurements from a single experiment, representative of two independent experiments.

Detection of surface binding of rituximab IgG subclasses with the anti-idiotype mAb MB2A4 reveals the highest binding of antibody subclass for rituximab IgG2 (Figure 3-6D)[443]. Rituximab IgG4 was the second highest binder, with rituximab IgG1 and IgG3 the lowest. This was in contrast with the previous measurements of surface binding, in which rituximab IgG2 had the lowest level of surface binding.

In order to clarify the discrepancy in surface binding as measured by the anti-idiotype and the anti-Fc detection methods, the level of surface binding for each of the respective IgG subclasses was tested using an anti-kappa light chain detection antibody. As each IgG subclass contained the same kappa light chain this should bind equally to all of the antibodies independently of the heavy chain constant domain. Ramos cells were opsonised with anti-CD20 antibodies at 10µg/ml and excess antibody washed off. The level of surface bound antibody was detected with 0.4µg/ml PE conjugated anti-Kappa light chain (clone MHK-49), and the level of surface bound antibody detected by flow cytometry (Figure 3-7B).

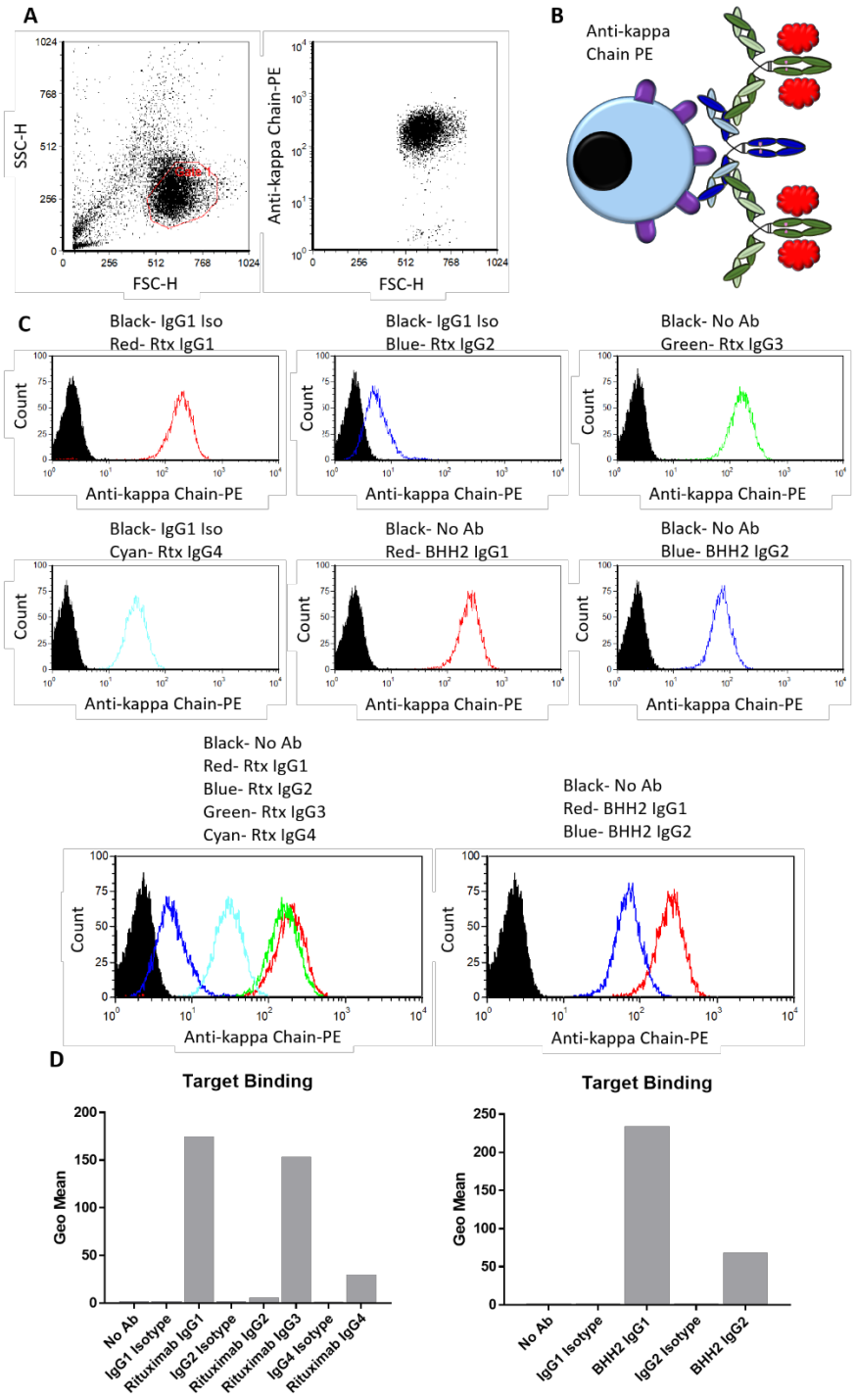

Figure 3-7 Anti-CD20 IgG Subclass Binding Detected by Anti-Kappa Light Chain Antibody

Ramos cells were opsonised with anti-CD20 IgG subclasses at 10µg/ml. The level of surface bound antibody was detected using a PE labelled anti-kappa light chain mAb (clone MHK-49). A- gating of antibody subclass opsonised Ramos cells, gated on viable cells and the geometric mean of the signal in the FL-2 channel taken. B- schematic diagram showing experimental setup. C- overlaid histograms of anti-CD20 antibody subclasses binding to Ramos cells. D- geometric means of anti-CD20 antibody subclass surface binding. Data points from a single experiment representative of two independent experiments presented.

When detecting the level of surface antibody binding on opsonised Ramos cells using an anti-kappa light chain mAb a similar trend to that seen in Figure 3-1 was observed (Figure 3-7). Rituximab IgG2 binding was only weakly detected by the anti-kappa light chain antibody, whereas a strong signal was seen for rituximab IgG1 and IgG3. Rituximab IgG4 binding was intermediate between rituximab IgG1/3 and rituximab IgG2 (Figure 3-7D). BHH2 IgG2 also showed reduced cell surface binding as compared to BHH2 IgG1, but as before (Figure 3-1) the magnitude of the difference in binding was smaller for BHH2 (~3.5 times more IgG1 than IgG2) than that between rituximab IgG1 and IgG2 (~32 times more IgG1 than IgG2).

Although all of the rituximab and BHH2 IgG subclasses used in this work contain the kappa light chain, differences in the overall conformation of the different IgG subclasses could be masking the detection epitopes recognised by the anti-kappa antibody. In order to determine whether the anti-kappa light chain antibody could recognise the different subclasses equivalently, the binding of the anti-kappa antibody to the IgG subclasses was assessed in an ELISA format, where an equal amount of each IgG subclass could be tested.

The anti-kappa light chain mAb was tested both in solution and immobilised (Figure 3-8A and B, respectively). For solution testing, rituximab IgG subclasses were coated onto maxisorb plastic 96 well plates in a serial dilution from 1µg/ml, and non-bound antibody washed off. Anti-kappa light chain mAb was then added at 0.1µg/ml in solution, and non-bound antibody washed off. Bound antibody was detected through the use of a polyclonal anti-mouse IgG1 specific antibody conjugated to HRP, and substrate added. After an appropriate period of time the reaction was quenched with 2.5M H_2SO_4, and the absorbance of the samples measured at 490nm on a plate reader.

For testing in plate bound form, anti-kappa light chain was coated directly onto maxisorb plastic 96 well plates at 0.1µg/ml, and non-bound antibody washed off (Figure 3-8B). Rituximab subclasses were then added at a serial dilution from 1µg/ml, and non-bound antibody washed off. Bound antibody was detected through the use of a polyclonal anti-human IgG Fc antibody conjugated to HRP and measured using the same substrate method described above.

As an additional control to confirm similar amounts of each IgG subclass bound to the plate, rituximab subclasses immobilised as above were detected with a polyclonal, HRP conjugated anti-human IgG Fc antibody, and the level of antibody detected using the same substrate method as above (Figure 3-8C).

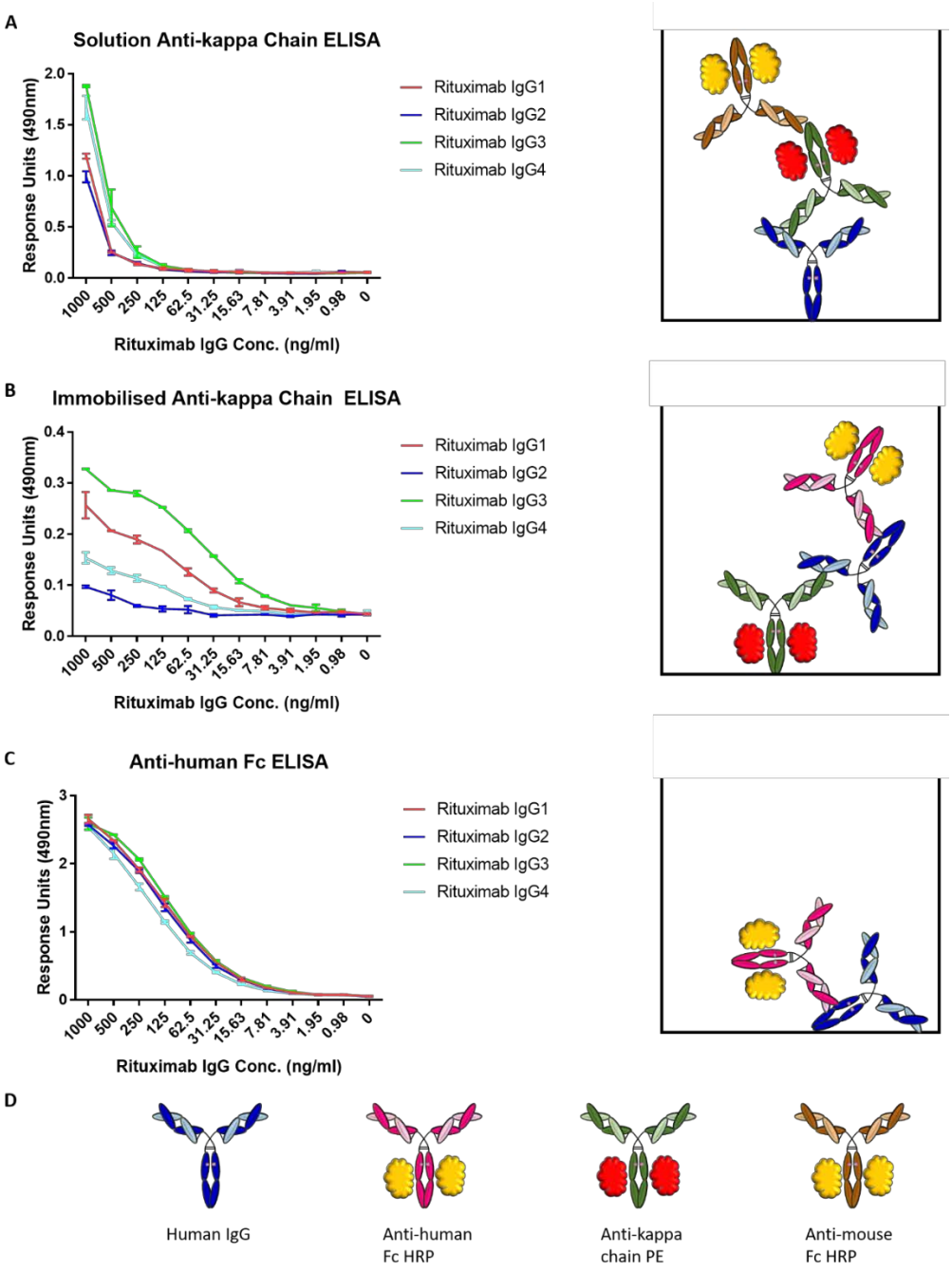

Figure 3-8 Anti-CD20 IgG Subclass ELISA

A- rituximab IgG subclasses (blue IgG) were coated onto maxisorb plastic 96 well plates at the indicated concentrations and then bound by anti-kappa light chain (green IgG) antibody at 100ng/ml. The binding of anti-kappa light chain antibody was detected by an anti-mouse Fc antibody (brown IgG) conjugated to horseradish peroxidase. OPD based peroxidase substrate was added to determine the level of anti-kappa light chain antibody. Mean of duplicate data points shown. Schematic of the assay setup shown on the right. B- 100ng/ml anti-kappa light chain antibody was coated onto maxisorb plastic 96 well plates and rituximab subclasses added onto these wells. Polyclonal anti-human Fc antibody (pink IgG) conjugated to horseradish peroxidase was added to bind the rituximab subclasses and detected by addition of OPD based peroxidase substrate. Mean of duplicate data points shown. Schematic of the assay setup shown on the right. C- rituximab IgG subclasses were coated onto maxisorb plastic 96 well

plates at the indicated concentrations and then bound by a polyclonal anti-human IgG Fc antibody conjugated to horseradish peroxidase. The binding was then detected by addition of OPD based peroxidase substrate. Mean of duplicate data points shown. Schematic of the assay setup shown on the right. D- key of antibodies used in the ELISAs.

The binding of rituximab IgG subclasses by the anti-kappa light chain antibody in the context of an ELISA indicates that the anti-kappa light chain antibody does not bind to the IgG subclasses equivalently (Figure 3-8). IgG3 was detected most strongly in both formulations of the ELISA, irrespective of whether the anti-kappa light chain antibody was added to IgG subclasses immobilised on the ELISA plate (Figure 3-8A) or if the anti-kappa light chain antibody itself was immobilised to the ELISA plate and soluble IgG subclasses were added (Figure 3-8B). Similarly, binding to IgG2 was the weakest in both ELISA formats. Binding to IgG1 and IgG4 was intermediate between that seen for IgG3 and IgG2, and the respective strength of binding appeared to be dependent on the ELISA format. When the rituximab subclasses were immobilised onto the plate, then IgG4 binding was equivalent to IgG3 binding whereas IgG1 binding was more similar to IgG2 (Figure 3-8A). However, when the anti-kappa light chain was immobilised to the plate, IgG1 binding was greater than IgG4 (Figure 3-8B).

The overall level of each IgG subclass bound to the plate was checked using a polyclonal anti-human IgG Fc specific horseradish peroxidase conjugated antibody. This antibody appeared to bind to the four IgG subclasses similarly (Figure 3-8C).

As this anti-human Fc HRP conjugated polyclonal antibody appeared to bind to all the IgG subclasses equivalently by ELISA, this antibody was tested by flow cytometry to see if it could be used to detect target cell bound IgG. As the polyclonal anti-Fc antibody is generally used for ELISAs it is conjugated with HRP, which is not detectable by flow cytometry. As such, a three-tiered staining protocol for detection of target bound cells was employed (Figure 3-9B). SUDHL4 cells were selected for these experiments because of their high expression of CD20, increasing the potential for detectable binding being maintained through the washing steps. SUDHL4 cells were opsonised with primary anti-CD20 antibody subclasses at 10µg/ml, with excess non-bound antibody washed off. Anti-Fc antibody was then added at a final dilution of 1 in 100, and excess antibody washed off. Bound antibody was then detected by the addition of a FITC labelled anti-HRP antibody at 30µg/ml and analysed by flow cytometry.

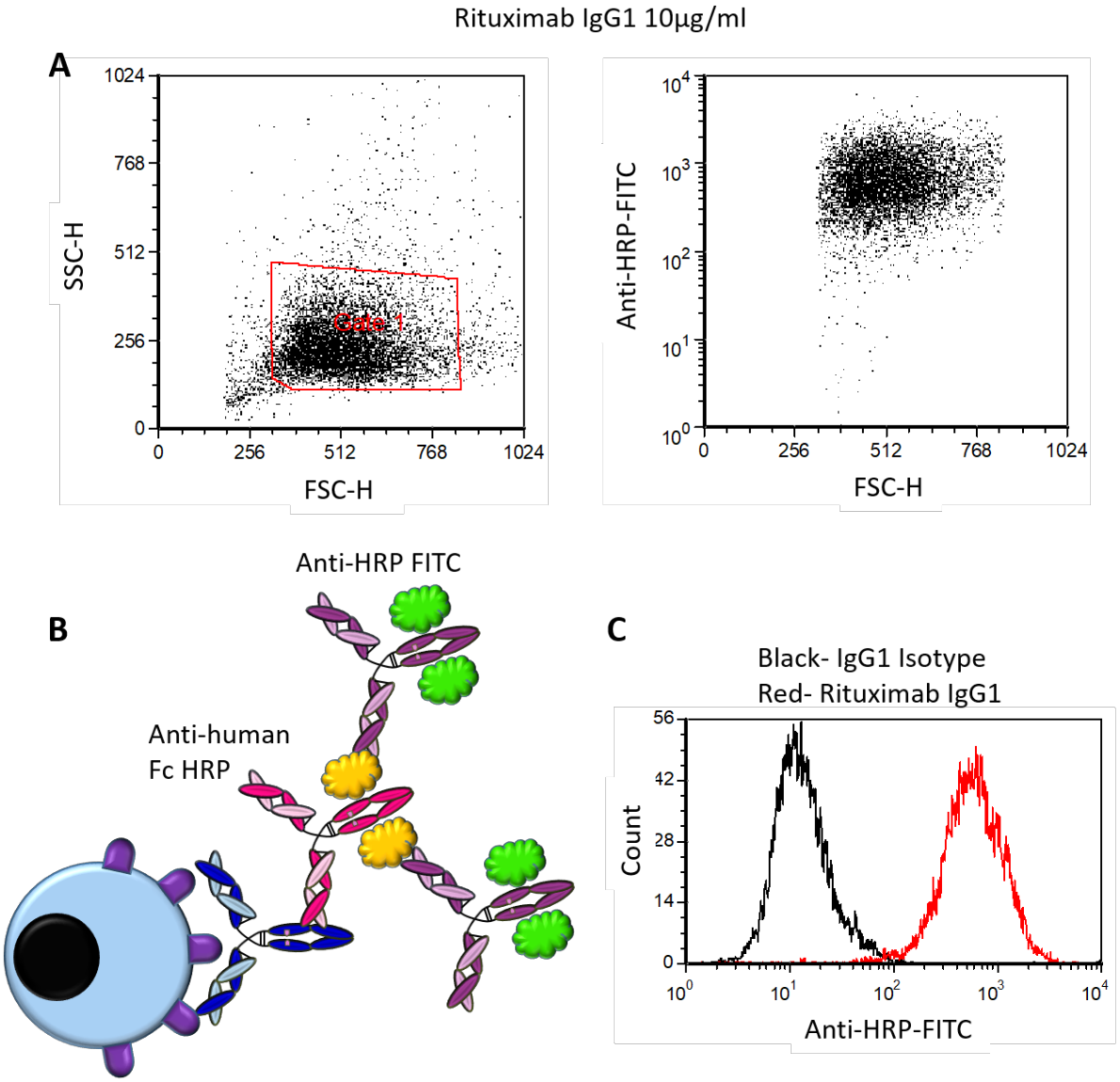

Figure 3-9 Anti-CD20 IgG Surface Binding Detection by Anti-Fc HRP

SUDHL4 cells opsonised with rituximab IgG1 or an IgG1 isotype control were probed with the polyclonal anti-human IgG Fc HRP conjugated antibody from Figure 3-8. Bound antibody was then detected by an anti-HRP FITC conjugated antibody. A- gating of rituximab/isotype IgG1 opsonised SUDHL4 cells, gated on viable cells and the geometric mean of the signal in the FL-1 channel taken. B- schematic diagram showing experimental setup. C- overlaid histograms of rituximab IgG1 (red) and an IgG1 isotype (black) binding to SUDHL4 cells.

Rituximab IgG1 binding to SUDHL4 cells could be detected using a polyclonal anti-human IgG Fc antibody that is conjugated to HRP through the use of an anti-HRP antibody labelled with FITC, as seen by the greatly increased binding of the rituximab opsonised SUDHL4 cells over the IgG1 isotype control opsonised SUDHL4 cells (Figure 3-9).

Having determined that the anti-IgG Fc HRP conjugated antibody was suitable for use in flow cytometry, the relative binding of the different IgG subclasses of the anti-CD20 antibodies was assessed using this anti-Fc antibody method on two cell lines.

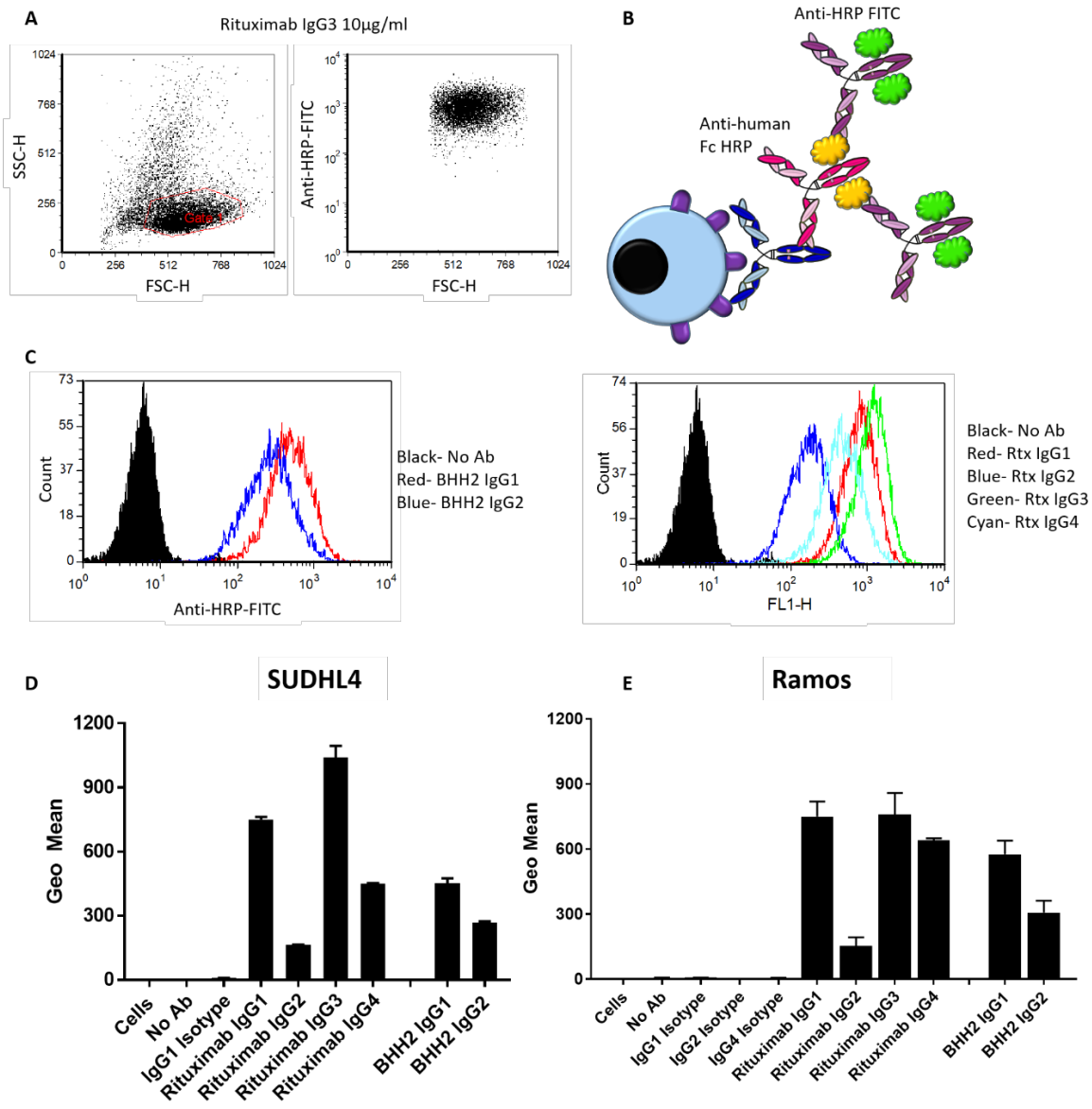

Figure 3-10 Anti-CD20 IgG Subclass Surface Binding Detected by Anti-Fc HRP Conjugate

SUDHL4 and Ramos cells opsonised with anti-CD20 IgG Subclasses were bound with the polyclonal anti-human IgG Fc HRP conjugated antibody from Figure 3-8. Bound antibody was then detected by an anti-HRP FITC conjugated antibody. A- gating of IgG subclass opsonised SUDHL4 cells, gated on viable cells and the geometric mean of the signal in the FL-1 channel taken. B- schematic diagram showing experimental setup. C- overlaid histograms of IgG subclasses binding to SUDHL4 cells. D- geometric means of anti-CD20 antibody subclass surface binding to SUDHL4 cells. Mean plus range of technical duplicate data points from a single experiment. E- geometric means of anti-CD20 antibody subclass surface binding to Ramos cells, analysed as for SUDHL4 cells. Mean plus range of triplicate technical repeats from a single experiment.

The detection of anti-CD20 IgG subclass surface binding to SUDHL4 cells with the anti-IgG Fc HRP antibody demonstrated the same trend as seen with the with the polyclonal anti-IgG Fc $F(ab')_2$ (Figure 3-1) and the anti-kappa light chain antibody (Figure 3-7). Rituximab IgG3 showed the highest surface binding (although this was similar to IgG1 on Ramos cells) with rituximab IgG2 the lowest on both cell lines (Figure 3-10). Rituximab IgG1 displayed greater surface binding than IgG4. For BHH2, greater surface binding was again seen for IgG1 than for IgG2. As seen previously, a smaller decrease in surface binding was seen between IgG1 and IgG2 for BHH2 than for rituximab on both SUDHL4 cells and Ramos cells.

3.2.1 Comparison of IgG1 and IgG2 Subclass Binding for Different Target Specificities

Having analysed the surface binding levels of rituximab and BHH2 IgG subclasses by several methods it was determined that the levels of these subclasses differ at the target cell surface for this target, CD20. Differences in the level of surface binding of different IgG subclasses targeting different antigens was therefore assessed, in order to see if this was a general property of IgG subclasses or something restricted to the anti-CD20 antibody panel. Several mAbs against T cell antigens available as multiple IgG subclasses with the same binding epitope were assessed. These reagents were tested for surface binding to target expressing cells with the different detection methods used for the anti-CD20 mAbs described above.

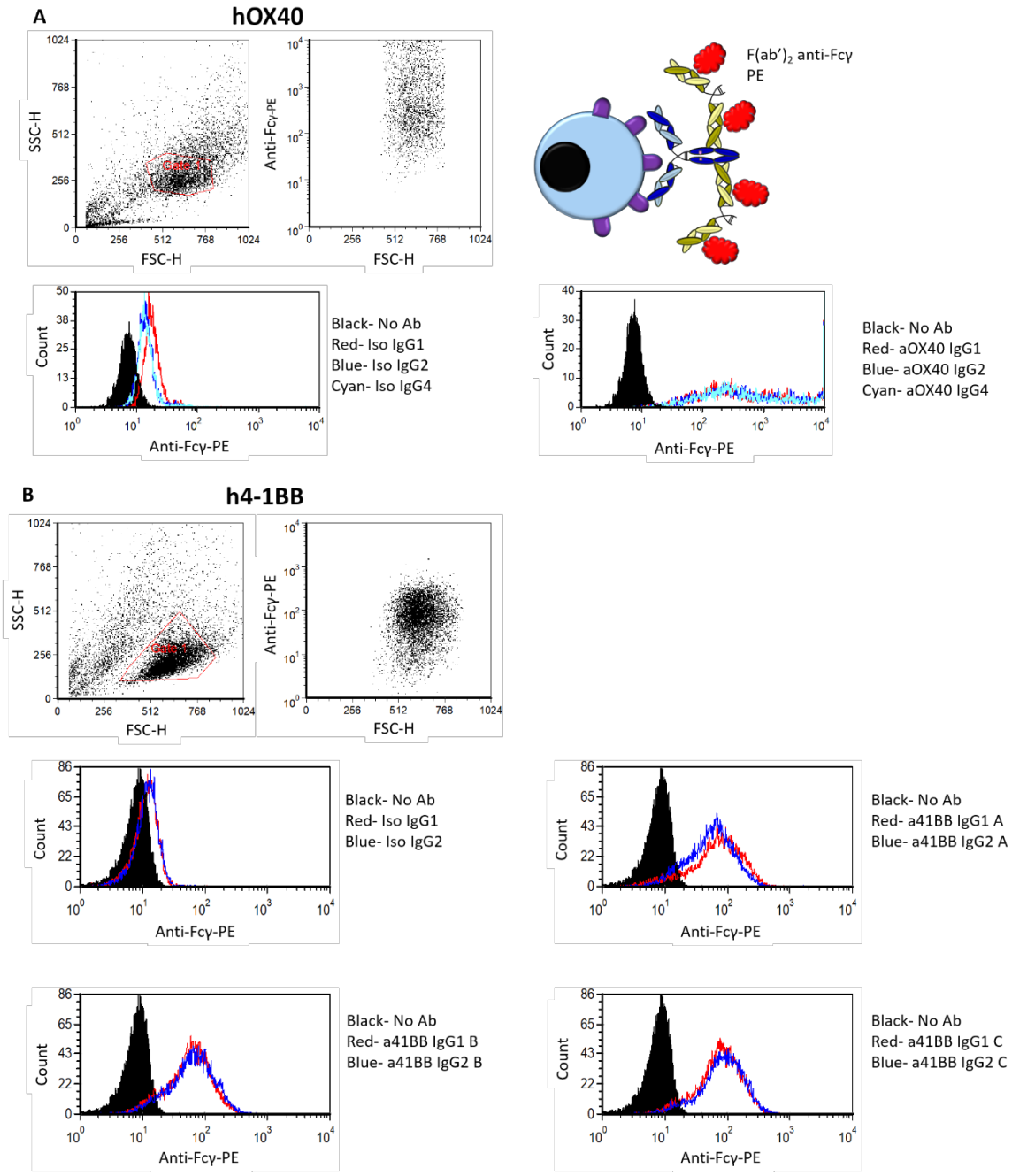

Figure 3-11 Surface Binding of IgG Subclasses to Transfected Target Cells

Surface binding of different IgG subclasses binding to TNFR superfamily targets OX40 and 4-1BB. A and B- dot plots provided show gating of viable cells based on forward vs. side scatter, followed by the binding of the detection antibody in the FL-2 channel. Overlays show the binding of no antibody (black), IgG1 (red), IgG2 (blue) and IgG4 (cyan). A- human 293F cells transfected with human OX40 stained with 10µg/ml of anti-OX40 antibodies or irrelevant isotypes on the human IgG1, IgG2 and IgG4 subclasses. The level of surface bound antibody was detected using a polyclonal anti-Fcγ specific PE labelled $F(ab')_2$, a schematic of which is shown in the top right. B- Jurkat cells transfected with human 4-1BB (CD137) stained with three different anti-4-1BB mAbs at 10µg/ml or irrelevant isotypes on the human IgG1 and IgG2 subclasses. The level of surface bound antibody was detected in the same way as for the anti-OX40 mAbs. Data shown are representative of duplicate technical repeats of a single experiment, displayed as geometric mean.

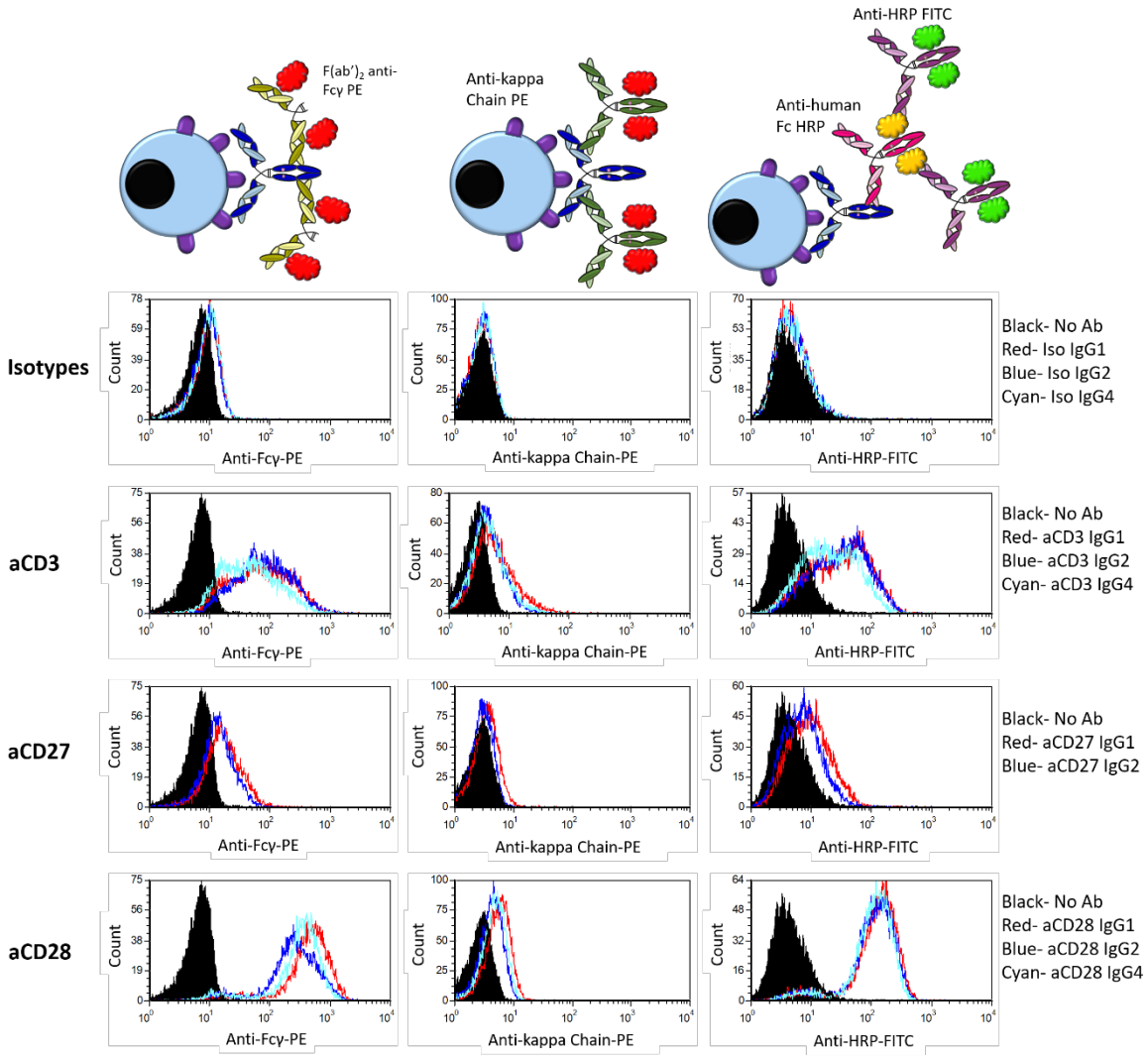

Figure 3-12 Surface Binding of IgG Subclasses Directed to T Cell Antigens on Jurkat T Cells

Jurkat T cells stained with 10µg/ml anti-CD3, anti-CD27, anti-CD28 or irrelevant subclasses, as indicated, on the human IgG1 (red), IgG2 (blue) and IgG4 (cyan, IgG1 and IgG2 only for anti-CD27) subclasses, gating as shown in Figure 3-11. The detection method used is indicated by the schematic diagram shown at the top of each column, either F(ab')$_2$ anti-human Fc PE, anti-kappa chain PE or anti-HRP FITC (left to right). Data shown are representative of duplicate technical repeats of a single experiment, displayed as geometric mean.

Several different antibody specificities were tested in multiple human IgG subclasses. Antibodies directed against OX40 were detected using the polyclonal PE labelled F(ab')$_2$ method (used for Figure 3-1) directed against human IgG Fc. These antibodies showed no differences in binding between the IgG subclasses tested (Figure 3-11A). Subsequently, three different anti-4-1BB antibodies were tested as human IgG1 and IgG2 subclasses for binding to Jurkat cells expressing

4-1BB (Figure 3-11B). Although these antibodies all target the same molecule, they have different binding epitopes. However, they all showed the same trend whereby binding of the IgG1 and IgG2 subclasses showed an equal level of binding when detected using the polyclonal PE labelled $F(ab')_2$ method (used for Figure 3-1) directed against human IgG Fc (Figure 3-11B).

Subsequently, a panel of antibodies binding human CD28 were assessed on Jurkat cells (Figure 3-12). The anti-CD28 antibody displaying the human IgG2 subclass appeared to show slightly lower binding compared to the other subclasses as detected by the polyclonal PE labelled $F(ab')_2$ directed against human IgG Fc (Figure 3-12). However, the anti-light chain antibody and the anti-human Fc-HRP antibody detection methods (used for Figure 3-9 and Figure 3-7, respectively) showed no differences in the surface binding level of the different IgG subclasses (Figure 3-11D/E). An anti-CD3 series of mAbs were assessed on Jurkat T cells. The anti-CD3 antibodies showed a trend towards slightly reduced surface binding for the IgG4 subclass when detected by the polyclonal PE labelled $F(ab')_2$ directed against human IgG Fc and the anti-human Fc-HRP antibody detection methods, but not with the anti-light chain antibody detection method (Figure 3-12). Finally, examining a series of anti-CD27 antibodies, the IgG1 subclass showed a slight trend towards greater binding as detected by all three detection methods (Figure 3-12). However, the differences seen between the IgG1 and IgG2 subclasses were not as pronounced and clear as seen for the anti-CD20 antibodies BHH2 and, particularly, rituximab.

3.3 Impact of IgG Subclass on Engagement of Effector Mechanisms by Anti-CD20 mAbs

3.3.1 Direct Cell Death

Having determined that the anti-CD20 antibodies show differences in surface binding, the relative activities of these subclasses were subsequently determined in a series of *in vitro* assays measuring antibody effector function. Firstly, the level of antibody mediated direct cell death induced by the binding of these antibodies to the target cell surface was assessed. Target cells were opsonised with antibody at the indicated concentrations and incubated at 37°C, 5% CO_2 for 24 hours. Cells were stained by the addition of propidium iodide and detected by flow cytometry.

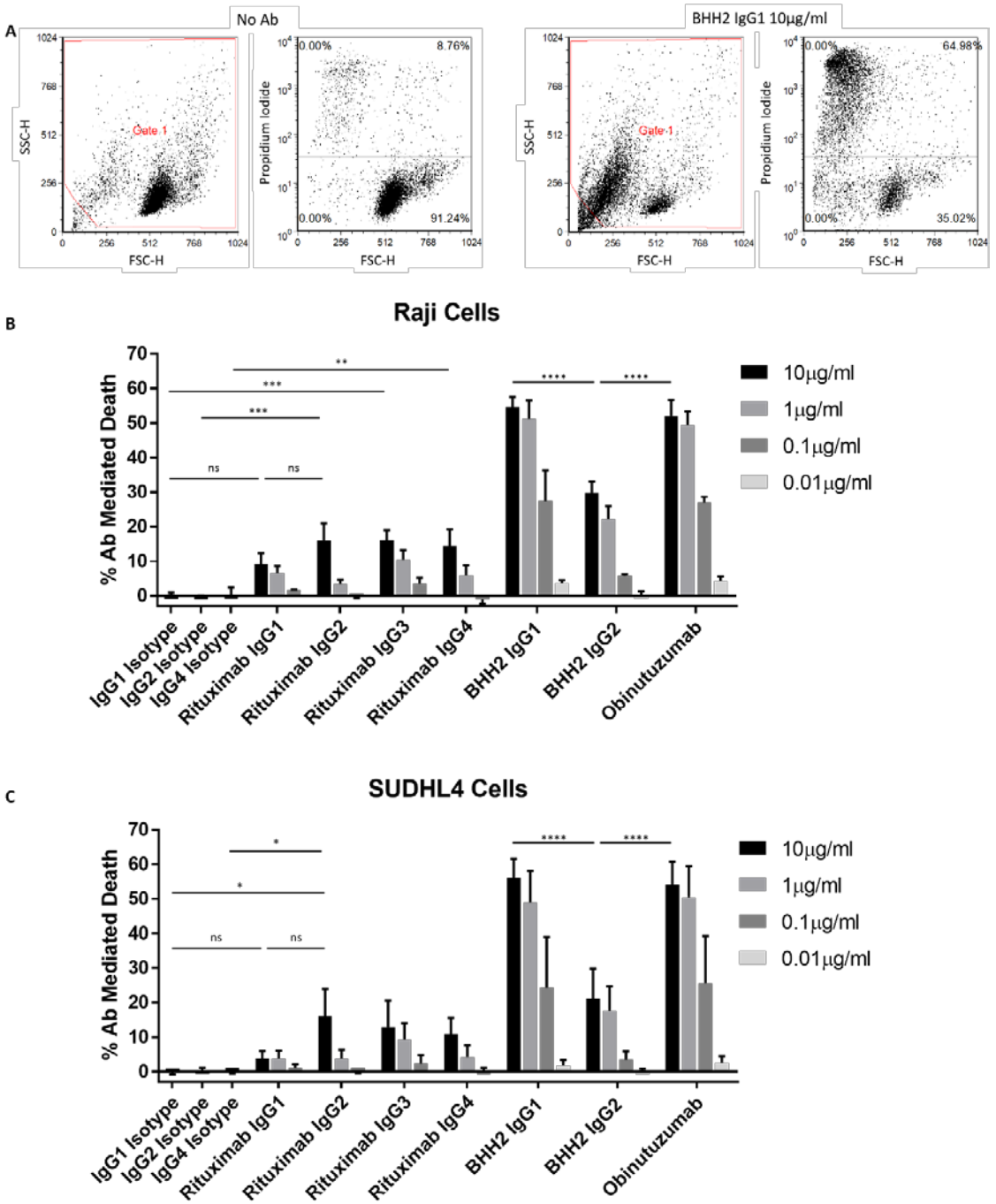

Figure 3-13 Antibody Induced Direct Cell Death of Anti-CD20 Antibodies of Varying Subclass

Target cells were opsonised with anti-CD20 or isotype control IgG subclasses at the indicated concentrations in a 96 well plate for 24 hours at 5% CO_2 and 37°C in a humidified incubator, before being stained with 10µg/ml propidium iodide for analysis by flow cytometry. A- data was analysed by gating out debris and determining the level of PI (FL-2) positive cells. The level of cell death of non-antibody treated cells (left) was subtracted from the antibody treated samples (for example, left) to give the antibody induced cell death. B and C- mAb induced cell death of Raji (B) and SUDHL4 (C) cells incubated for 24 hours with indicated antibodies. Mean + SD of three independent experiments each measured in triplicate. Statistics calculated by One Way ANOVA, * p<0.05, ** p<0.01, *** p<0.01, **** p<0.001, ns = not significant.

Type II anti-CD20 monoclonal antibodies, such as BHH2, are known to induce greater levels of direct cell death than type I antibodies, as confirmed here (Figure 3-13)[296,297]. BHH2 and obinutuzumab induce almost identical levels of DCD, indicating that DCD occurs independently of the glycans attached to the IgG Fc, as these are the only difference between these two antibodies. BHH2 IgG1 induced significantly greater DCD than did the IgG2 subclass at all concentrations tested. In contrast, for rituximab, IgG1 induced the lowest level of DCD, with IgG2, IgG3 and IgG4 all causing approximately 2-3 times as much direct cell death in both cell lines tested, although this trend did not reach statistical significance (Figure 3-13B and C). Rituximab IgG2 induced the highest level of direct cell death at 10µg/ml, although this did not reach the levels induced by the type II anti-CD20 mAbs and was concentration dependent as little DCD was seen at 1µg/ml.

Having seen differences in the level of direct cell death induced by these antibodies on cell lines, they were tested to see if they were able to induce direct cell death on primary CLL PBMCs. Frozen CLL PBMCs were thawed out and opsonised with anti-CD20 mAbs for 24hrs as for Figure 3-13.

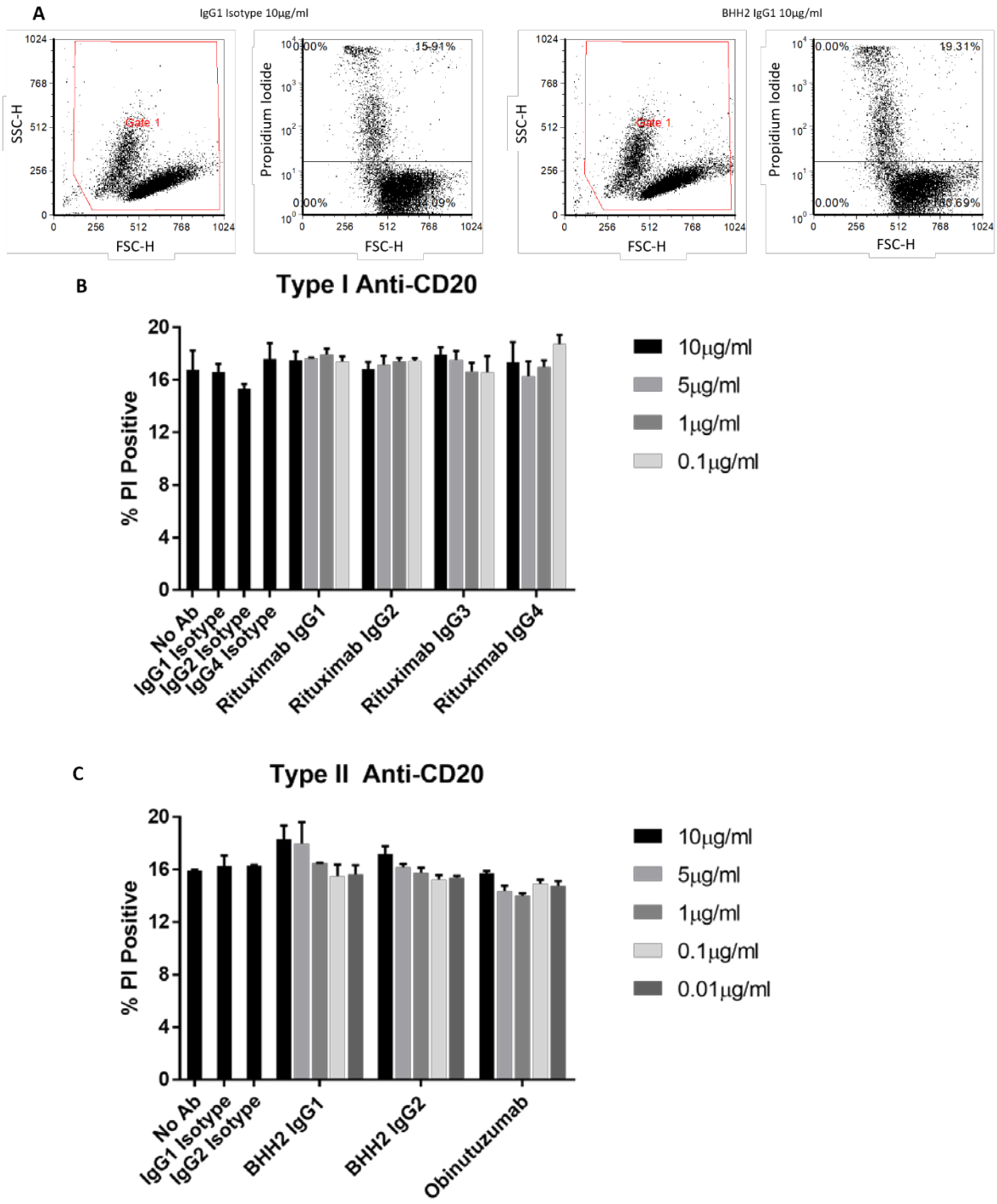

Figure 3-14 DCD of CLL PBMCs

CLL PBMCs were rapidly thawed in a 37°C water bath and rested at 37°C in a humidified incubator at 5% CO_2 for an hour. Cells were then opsonised at the indicated concentration with anti-CD20 mAbs for 24 hours, stained with propidium iodide and analysed by flow cytometry. A- data was analysed by gating out debris and determining the level of PI (FL-2) positive CLL PBMCs. B and C- mAb induced cell death of CLL PBMCs treated with type I (B) and type II (C) anti-CD20 mAbs and incubated for 24 hours. Mean + range of triplicate repeats of a single experiment, representative of two experiments.

In contrast to the effect on cell lines (Figure 3-13), with the exception of the IgG1 BHH2 mAb, neither type I or type II anti-CD20 mAbs were able to induce significant levels of direct cell death in primary CLL PBMCs (Figure 3-14).

3.3.2 Complement Dependent Cytotoxicity

Next, the Fc mediated effector functions of the anti-CD20 mAbs were assessed, looking first at the complement activating ability of the IgG subclasses. For these experiments rituximab was assessed, as type II anti-CD20 mAbs do not induce complement activation. Initially the ability of the different rituximab IgG subclasses to recruit C1q to the surface of an opsonised target cell was determined[444].

For the C1q recruitment assays Ramos cells were opsonised with titrating concentrations of the rituximab IgG subclasses. After washing, human purified C1q was added to the cells at 8µg/ml and, after washing, bound C1q was detected with a polyclonal FITC conjugated anti-C1q antibody followed by flow cytometry.

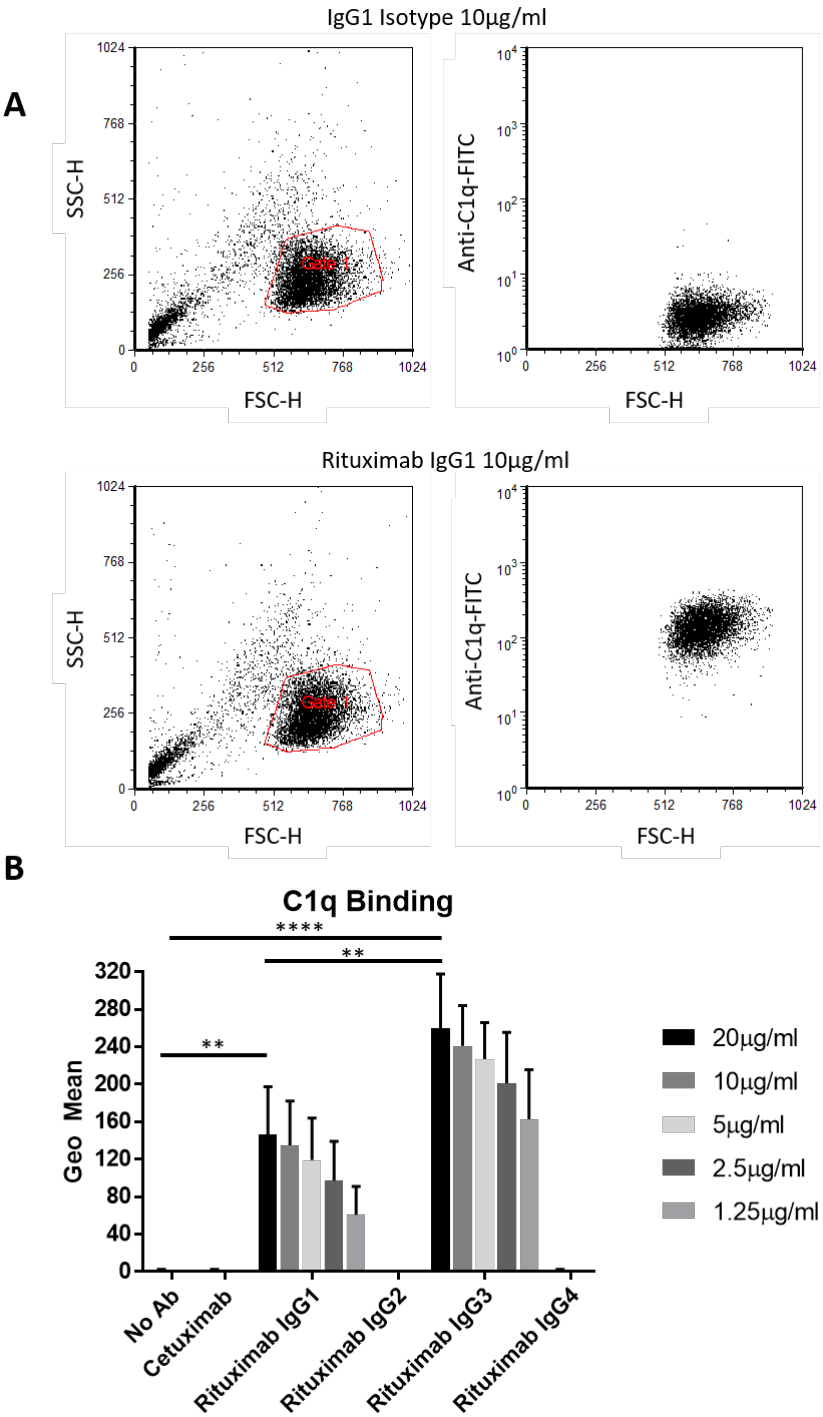

Figure 3-15 C1q Recruitment of Rituximab IgG Subclasses

Ramos cells were opsonised with rituximab IgG subclasses at the concentrations indicated. Human C1q was added to the opsonised cells and detected with a polyclonal anti-C1q FITC labelled antibody. A- gating of rituximab (bottom) and isotype control (top) IgG opsonised Ramos cells , gated on viable cells and the geometric mean of the signal in the FL-1 channel taken. B- geometric means of C1q binding to Ramos cells opsonised with the indicated antibodies. Mean + SD of three independent experiments, each measured in triplicate. Statistics calculated by one-way ANOVA with multiple comparisons correction, ** $p<0.01$, **** $p<0.0001$.

C1q binding was specific to rituximab, as no increase was seen with an irrelevant isotype control (Figure 3-15A/B). Rituximab IgG2 and IgG4 showed no recruitment of C1q to the surface of the opsonised Ramos cells. Rituximab IgG3 showed the highest level of recruitment of C1q to the target cell surface, with rituximab IgG1 also showing C1q recruitment, albeit less than that of rituximab IgG3 (Figure 3-15B). Whether the levels of C1q recruitment matched the level of complement dependent cytotoxicity (CDC) induced by these antibody subclasses was then assessed.

For the CDC assays, target cells were opsonised with the indicated concentrations of rituximab subclasses or an irrelevant IgG isotype, and non-bound antibody washed off. Healthy human serum was added to a final concentration of 30%, and cells were stained with propidium iodide to assess membrane permeabilisation through membrane attack complex formation. Data were acquired by flow cytometry. A serum alone control was included to assess the effect of potential spontaneous complement activation on non-opsonised cells in the presence of serum alone.

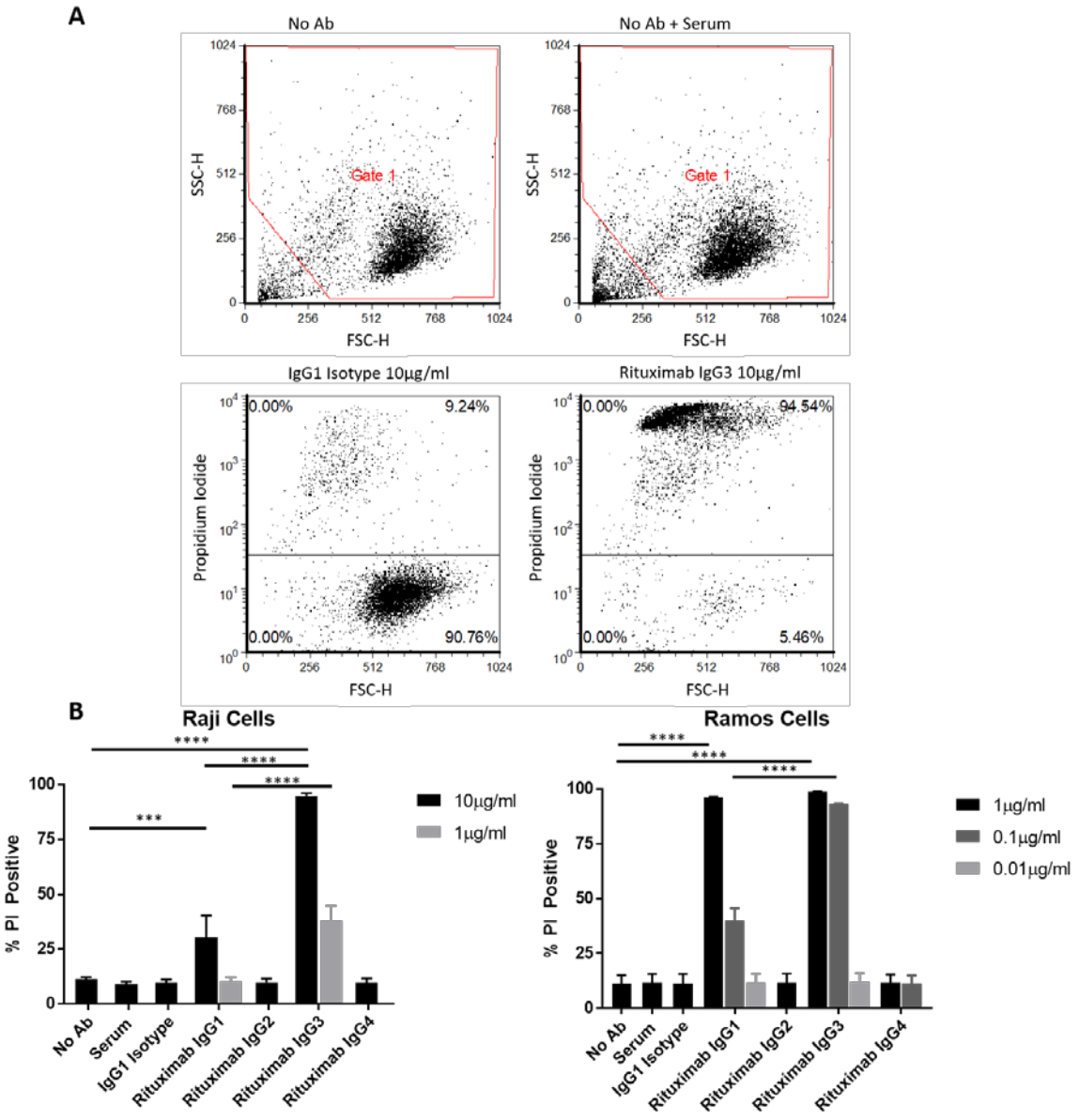

Figure 3-16 Rituximab IgG Subclass Complement Dependent Cytotoxicity

Target cells were opsonised with the indicated antibodies and incubated with 30% normal human serum. Propidium iodide staining was used to detect complement induced cell death. A- gating of target cells. Top- debris from serum (right) gated out (see Section 8.1)Figure 8-1. Bottom- propidium iodide staining of isotype (left) and rituximab IgG3 (right). B- complement induced cytotoxicity of Raji (left) and Ramos (right) cells treated with rituximab IgG subclasses. Mean + SD of three independent experiments, each measured in triplicate. Statistics calculated by one-way ANOVA with multiple comparisons correction, *** p<0.001, **** p<0.0001.

CDC induction by anti-CD20 mAbs did not appear to cause complete destruction of the cells, as no increase in debris was seen in the rituximab IgG3 treated cells compared to the isotype treated

cells (Appendix Section 8.1). The levels of CDC induced by the rituximab IgG subclasses matched the respective levels of C1q binding (shown in Figure 3-15). Rituximab IgG2 and IgG4 showed no CDC on either Raji or Ramos target cells. Rituximab IgG3 induced the highest level of complement dependent cytotoxicity on both Ramos and Raji cells, greater than rituximab IgG1. These responses were titratable, decreasing as the level of rituximab was reduced. Greater levels of CDC were observed in Ramos cells compared to Raji cells, reflecting the decreased expression of complement defence molecules found on these cells[445,446].

3.3.3 Antibody Dependent Cellular Cytotoxicity

Having determined the abilities of the IgG subclasses to induce complement activation, it was next sought to determine the ability of the IgG subclasses to mediate FcγR-dependent mechanisms of action; first testing their effectiveness in an assay of antibody dependent cell mediated cytotoxicity.

Target cells were harvested (in the case of CLL cells, thawed) and labelled with 10μg/ml calcein AM. Upon target cell permeabilisation and death, calcein will be released from the cell. After washing, target cells were opsonised with the indicated concentrations of anti-CD20 mAbs and non-bound mAbs washed. Opsonised, labelled target cells were co-cultured with PBMCs purified from healthy human donors by lymphoprep density gradient centrifugation, at a 1:50 ratio for 4 hours at 37°C in a humidified incubator at 5% CO_2. Because of the high effector to target cell ratio required, NK cells were not purified from the PBMCs, but are known to make up approximately 10% of the total cell number, giving an approximate ratio of 5 NK cells per target cell. After the co-culture, the fluorescence of the supernatant was read in a plate reader at 490nm.

In order to calculate the percentage of maximum lysis achieved for each antibody, calcein labelled target cells were lysed with 4% triton X-100 and the fluorescence measured as above. Labelled non-opsonised target cells were also incubated with PBMCs in order to determine the level of background cell death, potentially induced by cross donor anti-lymphocyte effects. The background value was subtracted from all other samples, which were then calculated as a percentage of the triton X-100 lysed cells. Both Raji cells and CLL PBMCs were tested in order to determine the effect of these mAbs on both a cell line and primary patient material from a disease that would be treated with these antibodies in the clinic.

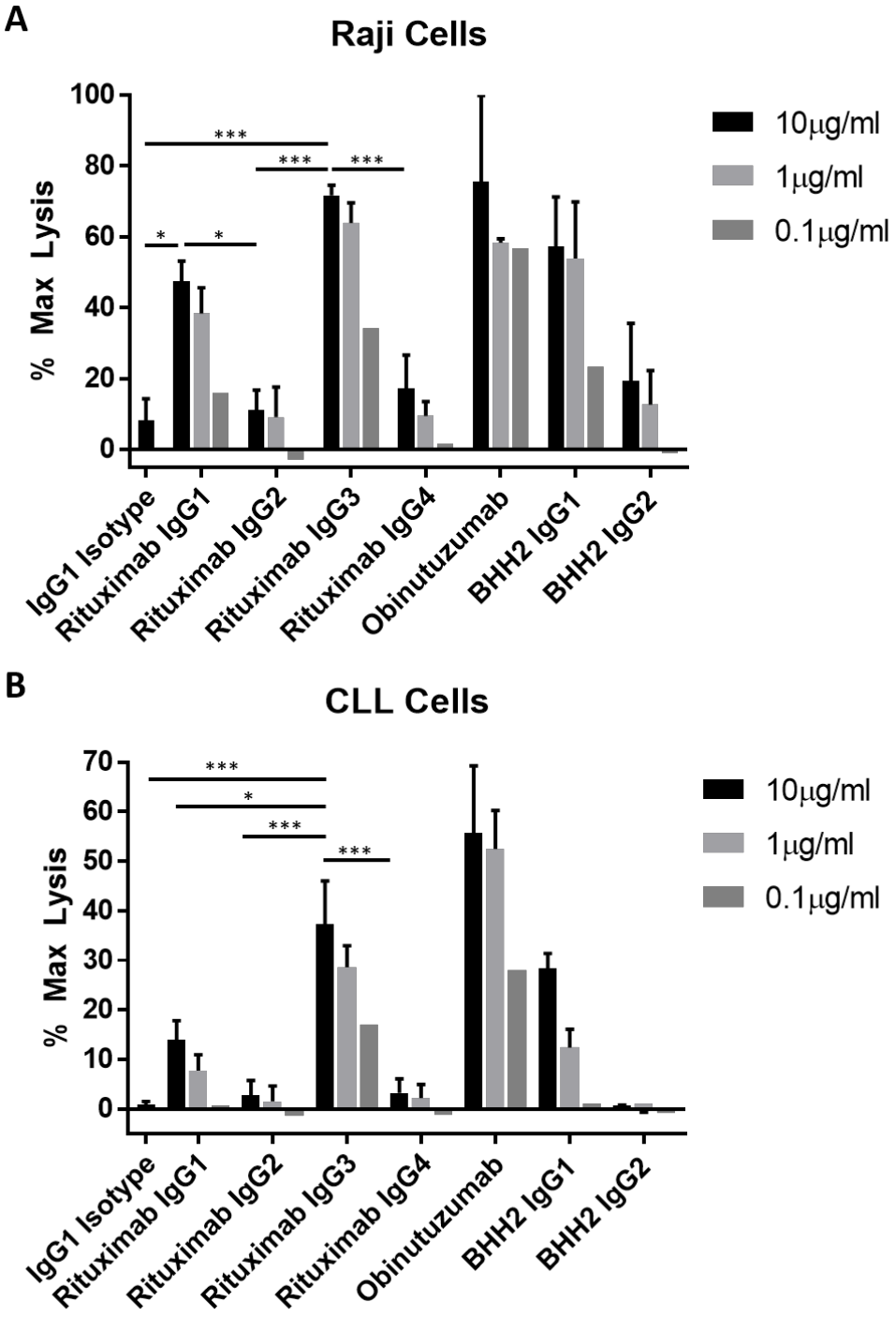

Figure 3-17 Antibody Dependent Cell Mediated Cytotoxicity of Anti-CD20 IgG Subclasses

Calcein labelled target cells were and co-cultured with effector PBMCs for 4 hours, and the supernatants measured for released calcein. Calcein release is normalised to spontaneous release and calculated as the percentage of release from total cell lysis. Antibody dependent cell mediated cytotoxicity of Raji cells (A) and CLL cells (B) treated with anti-CD20 IgG subclasses. Mean + SD of independent experiments plotted, each measured in triplicate. 10μg/ml (n=3), 1μg/ml (n=2) 0.1μg/ml (n=1). Statistics calculated for 10μg/ml using one-way ANOVA with multiple comparisons, * $p < 0.05$, *** $p < 0.001$.

Rituximab IgG2 and IgG4 were unable to induce ADCC on either cell type tested (Figure 3-17). Rituximab IgG1 induced ADCC on both Raji cells and, to a lesser extent, CLL PBMCs (approximately 50% of max lysis vs. 15%, respectively, at 10μg/ml). Rituximab IgG3 induced greater ADCC than rituximab IgG1 on both Raji cells (approximately 70% of max lysis vs. 50%, respectively, at 10μg/ml) and CLL PBMCs (approximately 35% of max lysis vs. 15%, respectively, at 10μg/ml); and mediated greater killing of Raji cells than CLL PBMCs (approximately 70% of max lysis vs. 35%, respectively, at 10μg/ml). Obinutuzumab induced greater ADCC compared to its non-glycomodified comparitor mAb, BHH2, on both target cells (75% max lysis vs 60%, respectively, on Raji cells, 55% vs. 30%, respectively, on CLL PBMCs, at 10μg/ml), thereby evidencing the importance of the IgG Fc glycan contribution to FcγRIIIa binding and ADCC[350-352].

Interestingly, rituximab IgG3 induced a similar level of maximal lysis as obinutuzumab on Raji cells (approximately 70-75% max lysis at 10μg/ml), with lower ADCC seen for rituximab IgG3 on CLL PBMCs (approximately 35% max lysis vs. 55%, respectively, at 10μg/ml). BHH2 IgG2 also failed to induce any ADCC on either target cell, whilst the IgG1 version of BHH2 did (approximately 60% of max lysis on Raji cells and 25% on CLL PBMCs, at 10μg/ml). In addition, BHH2 IgG1 induced greater ADCC on both target cells than rituximab IgG1, indicating that the type II nature of this antibody was also important for increased ADCC (approximately 60% of max lysis vs. 50%, respectively, on Raji cells, at 10μg/ml, and approximately 25% of max lysis vs. 15%, respectively, on CLL PBMCs at 10μg/ml). In summary, although Raji cells showed increased sensitivity to ADCC compared to CLL PBMCs, they displayed identical trends of response.

3.3.4 Antibody Dependent Cellular Phagocytosis

As well as ADCC, the other key mechanism for mAb induced target cell depletion is antibody dependent cell mediated phagocytosis.

To assess this, monocytes were isolated from healthy donor blood by lymphoprep density gradient centrifugation, and differentiated into macrophages with M-CSF for 7-10 days. CLL PBMCs were thawed and labelled with CFSE and opsonised with anti-CD20 mAbs at the indicated concentrations. Target cells were then co-cultured with macrophages at a 5:1 target to effector ratio for 1 hour at 37°C and assessed by flow cytometry.

Debris and target cells were gated out, and macrophages identified by $CD14^+$ staining (Figure 3-18A). The percentage of phagocytosis was defined as the percentage of macrophages that were also positive for CFSE. Background phagocytosis in the absence of antibody was determined through the co-culture of CFSE labelled, but not opsonised, CLL PBMCs with macrophages.

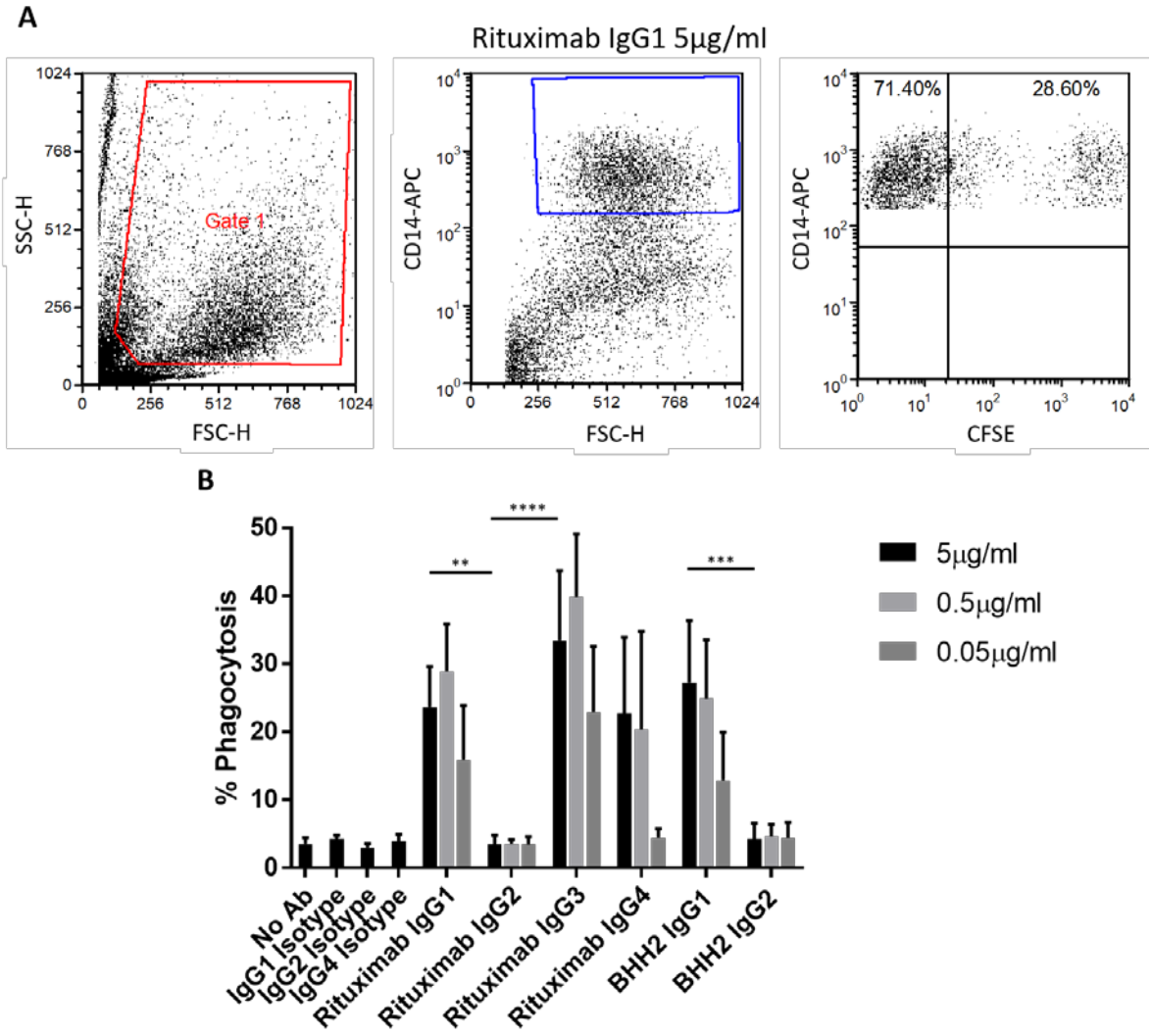

Figure 3-18 Antibody Dependent Cell Mediated Phagocytosis of CLL PBMCs with Anti-CD20 IgG Subclasses

CLL PBMCs were labelled with CFSE and opsonised with anti-CD20 IgG subclasses, and co-cultured for 1 hour with monocyte derived macrophages. A- cells were gated on forward vs side scatter (left), and then on CD14 (centre) to identify macrophages. The percent of phagocytosis was determined as the percentage of macrophages that are FL-1 (CFSE) positive (right). B- phagocytosis of CLL PBMCs of anti-CD20 IgG subclasses. Data presented as mean + SD of four independent experiments each measured in triplicate. Statistics calculated by one-way ANOVA with multiple comparisons, ** $p<0.01$, *** $p<0.001$, **** $p<0.0001$.

Rituximab IgG2 and BHH2 IgG2 showed no target cell phagocytosis (Figure 3-18B). Rituximab IgG3 showed the greatest level of ADCP (approximately 30% phagocytosis at 5µg/ml). Rituximab IgG1 and IgG4 showed intermediate levels of phagocytosis (approximately 25% phagocytosis at 5µg/ml for rituximab IgG1, and 22% phagocytosis at 5µg/ml for rituximab IgG4). Although rituximab IgG4 showed similar levels of phagocytosis to rituximab IgG1 at the top concentration tested, the level of phagocytosis for rituximab IgG4 titrated away more rapidly than for rituximab IgG1 (at 0.05µg/ml rituximab IgG1 induced 15% phagocytosis, whereas rituximab IgG4 induced no phagocytosis above the isotype control). BHH2 IgG1 induced similar levels of phagocytosis to rituximab IgG1 (approximately 28% phagocytosis vs. 25% phagocytosis at 5µg/ml,).

3.4 Discussion

Human IgG consists of four subclasses which differ in their constant regions. All four subclasses are found in human serum, with IgG1 being the most prevalent, followed by IgG2, IgG3, and with IgG4 the least prevalent[439]. Class switching that occurs within plasma cells allows for the production of the same antibody variable regions (and therefore antigen/epitope specificity) on different IgG subclass backbones[447]. This provides for a level of immune regulation based upon the different IgG subclasses having differing properties, for example in their ability to recruit immune effector mechanisms or persistence in the serum[448]. For example, the serum half-life of human IgG3 has been reported to be approximately 7 days, a third of the half-life compared to the other IgG subclasses[108].

Over the last 20 years many mAbs have been approved for the treatment of disease, with the vast majority being of the human IgG1 subclass (some chimeric, some humanised). In more recent years, and particularly with the increase in the interest in immunomodulatory therapeutic agents, there has been more attention paid to alternative IgG subclasses with different properties. In light of the increasing prevalence of these alternative IgG subclasses in the clinic, here the differences between them was assessed with regards binding and effector functions.

IgG1 and IgG3 are generally considered to be pro-inflammatory IgG subclasses, with strong binding to FcγRs and the ability to bind C1q and activate the complement cascade. In contrast, IgG2 and IgG4 subclasses are thought to be less pro-inflammatory, with lower binding to the FcγRs and little to no activation of complement[448]. Differences in the relative abilities of these

antibodies to cause direct effects following cell surface binding have been described[449]. However, these studies typically have compared these functions in the context of different V region specificity and so there is a need to study the four subclasses together in the same well-controlled system to allow for a relative comparison of their respective effector functions where subclass is the only variable.

The attractiveness of IgG2 and IgG4 subclasses for immunomodulatory agents centres around their ability to bind to the antigen, but not induce strong immune effector functions leading to deletion or death of the targeted cell. This is desired when the target cells are tumour specific cytotoxic T cells for example, as is the case with the recently approved PD-1 and CTLA-4 targeting antibodies, of which two anti-PD-1 antibodies are of the IgG4 class (pembrolizumab and nivolumab). The use of these fully human, non-mutated IgG heavy chain subclasses also gives other benefits. For example, humanisation of mouse antibodies is known to reduce, but not fully abrogate therapeutic mAb immunogenicity, and repeated administration results in a decreased half-life and increased incidence of adverse events; the use of mutated IgG to obtain specific characteristics is likely therefore to exacerbate this problem[450-452]. Furthermore, wild-type IgG subclasses retain full pH dependent binding to FcRn, the intracellular Fc receptor responsible for IgG recycling and therefore exhibit the long half-life of IgG antibodies (for IgG1, IgG2 and IgG4)[74].

Although similar, the IgG subclass backbones do differ, and this certainly effects the functions of the antibody. Due to the differences in mechanism of action of different antibodies, it is quite possible that simply swapping the variable regions of one antibody onto a different IgG subclass may not be equivalent to doing so for another antibody, considering potential differences in mechanism of action, antigen affinity and epitope characteristics.

In this chapter the relative level of each IgG subclass binding to the target cell surface was studied. As the subclasses differ in protein sequence, several different detection methods were employed in order to reach a consensus conclusion. Of the methods tested, three indicated a dramatically lower level of surface binding for rituximab IgG2 as compared to the IgG1 subclass of the same antibody. These methods included detection of both the heavy and light chains to try to account for any potential bias in affinity of the detection reagents for the different subclasses. Furthermore, rituximab IgG2 was the IgG subclass least able to block the binding of a second anti-CD20 mAb. The only method that did not show this result was the use of the rituximab anti-idiotype antibody, which recognises the variable region of the antibody (Figure 3-6).

Interestingly, this method actually indicated the highest signal for rituximab IgG2, with IgG1 and IgG3 having the lowest signal - the opposite finding to the other detection methods. A possible explanation to this finding is that the IgG2 antibody may bind to the cell surface in a different manner whereby the variable regions were more accessible for binding by the anti-idiotype than when the Fab regions were presented in the IgG1 or IgG3 backbone. The proposed mechanism of binding for the anti-idiotype is through a single Fab arm, with the remaining arm binding to the cell surface (Figure 3-6B). IgG2 has a shorter hinge region containing more inter-chain disulphide bonds than IgG1 or IgG3, which has a very elongated hinge[453]. This shorter hinge makes IgG2 the least flexible subclass, as it also contains a poly proline helix[102]. This rigidity may preclude the IgG2 antibody from binding the surface in the same conformation as the other subclasses, or possibly reduce the tendency to bind in a bivalent manner, potentially leaving an exposed Fab arm for the anti-idiotype to bind to. IgG1, and IgG3 in particular, has a longer hinge region, and this flexibility may facilitate a higher degree of bivalent binding, therefore reducing detection with the anti-idiotype but yielding higher levels of binding overall due to greater stability (due to bivalent engagement) as detected by the other methods.

As well as rituximab, BHH2, a type II anti-CD20 mAb that does not induce localisation of CD20 into lipid rafts, was also explored as an IgG1 and IgG2[281]. Using these same detection methods it was consistently found that IgG2 exhibited reduced surface binding as compared to IgG1, and displayed a reduced ability to block a second anti-CD20 mAb. However, although the same trend was seen, the magnitude of the difference was less than seen for rituximab. Due to its nature as a type II anti-CD20 mAb BHH2 does not bind as many molecules per cell, but despite this, the difference in binding of IgG1 and IgG2 was clear[293]. BHH2 contains a key mutation within its hinge region that is linked to its ability to induce direct cell death and changes the flexibility of the hinge region. It is possible that this additional impact on the hinge flexibility may reduce the impact of the difference in hinge flexibility between IgG1 and IgG2, thereby reducing the difference seen in the binding levels.

It is interesting to note that fixation of Ramos cells prior to the binding of rituximab IgG subclasses reduced the binding of all subclasses except IgG2. Fixation of the cell membrane would reduce the ability of CD20 molecules to redistribute within the plasma membrane (for example into lipid rafts). This finding, coupled with the much smaller difference in binding between IgG1 and IgG2 seen with the non-CD20 redistributing BHH2 as compared to the CD20 redistributing rituximab,

raises the possibility that the redistribution of CD20 into lipid rafts could also be contributing to the different levels of binding observed between IgG1 and IgG2 antibodies.

If rituximab IgG2 is less able to bind bivalently, this may explain the reduced clustering. IgG2 binding would not be able to cluster CD20 molecules together as they could only bind to a single molecule, whereas IgG1, binding bivalently, may be able to bring more CD20 molecules together. As discussed above, the reduced flexibility of IgG2, imparted by the disulphide bonds in the hinge region, could be responsible for the monovalency of IgG2 binding. IgG2 may be less able to flex to bind a second CD20 molecule with its free Fab arm after initial binding. Therefore, bivalent binding would require a second CD20 molecule to be present in a more restricted number of conformations, reducing the frequency of bivalent binding. This would thereby reduce the avidity of the antibody binding, making it more likely to disengage from the CD20 and be more susceptible to loss during the washing stages necessary for experimental analysis. This observation would also explain why IgG2 binding was higher following fixation, as less monovalently bound mAb would be lost during wash steps.

If IgG2 were less able to induce CD20 redistribution into lipid rafts it may be more likely to bind in a monovalent fashion due to the lack of antigen clustering, potentially coupled to limited hinge flexibility as discussed above. The latter effect could explain the difference in binding seen with BHH2 IgG1 and IgG2.

We tested several other antigens to see if this was an intrinsic property of IgG1 and IgG2 (Figure 3-11 and Figure 3-12), but found no clear evidence of significant differences between the levels of surface antibody between the different subclasses for multiple other mAb specificities. As detailed above, one of the characteristic features of CD20 is the redistribution into lipid rafts that that this molecule undergoes upon binding with certain antibodies (type I). This is not a feature common to all molecules, and it would be interesting to test antibodies to other surface antigens that undergo similar clustering. One potential target that could be tested is FcγRIIb[454]. It would be of interest to see if IgG1 and IgG2 subclasses of anti-FcγRIIb antibodies displayed the same effects as observed for rituximab. Moreover, within the laboratory there are agonistic anti-FcγRIIb mAb that cluster the receptor in the plasma membrane (E. Sutton, personal communication) and antagonistic anti-FcγRIIb mAb that do not, allowing us to test this hypothesis.

Having determined the level of surface binding of these anti-CD20 antibodies differed between IgG subclasses, it was then of interest to determine whether these differences were consequential for their effector functions.

Interestingly the IgG2 subclass of rituximab induced a higher level of antibody induced cell death, despite lower levels of surface binding detected by flow cytometry. This finding potentially supports the idea that IgG2 binds to the cell surface in a different manner to IgG1. Conversely, the IgG2 subclass of BHH2 was less active than the IgG1 subclass in terms of antibody induced cell death. It is well known that type II anti-CD20 mAbs are much more active at inducing direct cell death than type I antibodies[296,297]. Type II antibodies bind to CD20 in a different orientation compared to type I antibodies, perhaps suggesting that the differential hinge flexibility or target clustering characteristics of IgG2 have opposing effects on the functions of type I and type II subclasses in this context. Rituximab IgG3 induced a similar level of cell death to IgG2, despite the large difference in the level of surface binding of these two IgG subclasses. This may again suggest that differences in the mechanism of binding to the cell surface account for the difference in DCD.

Another characteristic of type II anti-CD20 mAbs is that they do not induce CDC, whereas type I anti-CD20 mAbs do. Complement activation by IgG antibodies is mediated through recruitment of the C1q protein complex interacting with the Fc regions of up to six target bound IgG. It has been shown that the target bound IgG form into hexameric clusters of monovalently bound IgG with the Fc regions available for interaction with the six C1q head groups[80]. This finding is unexpected, as it had previously been assumed that antibodies bind in a bivalent manner to targets to most effectively induce effector functions[74].

The induction of complement dependent cytotoxicity was tested for the four IgG subclasses of rituximab on target cells expressing CD20. In order to get a better comparison of the relative ability of the subclasses to trigger complement induced death, the antibody concentration was titrated. This aimed to identify if lower levels of IgG at the cell surface differentially affected the ability to induce CDC, perhaps linked to differences in flexibility between the subclasses. The concentration of serum was maintained at 30% across all antibody concentrations tested. This was intended to mimic the situation *in vivo* where the level of complement factors available would be expected to be fairly stable. However, depletion of complement components after administration of mAb has been reported[455]. It is possible that by decreasing the level of complement available, differences in the ability of the IgG subclasses to recruit complement

components when they are the limiting factor may be observed. This would be of interest to test for these antibody subclasses in the future.

Neither the IgG2 or IgG4 subclasses of rituximab recruited C1q to the target cell surface, and consequently induced no CDC. Rituximab IgG3 recruited the highest amount of C1q to the target cell surface and induced the most lysis. With the engagement of other molecules to drive CDC, a direct relationship to the level of antibody at the cell surface could not be determined, as the binding of the IgG subclasses to C1q may not be the same (as shown using the C1q affinity column, Figure 6-15). It is interesting to note that rituximab IgG2 induced no C1q recruitment or CDC, despite the apparent requirement for monomeric binding in order to facilitate C1q binding. However, whether or not there is enough rituximab IgG2 at the cell surface, potentially non-clustered, to efficiently bind C1q makes it hard to conclude from this whether IgG2 is binding monovalently or not. Theoretically the ability of rituximab IgG2 to bind to CD20 monovalently could be tested by SPR, using CD20 immobilised in the system, and then seeing if the addition of further, soluble CD20 further increased the mass signal bound in the system. If there was an increase in mass upon injection of soluble CD20 it would suggest there was a Fab arm available for antigen binding, indicating monovalent binding. In practice however, there is currently no accurate soluble form of CD20, due to its nature as a transmembrane, tetraspan protein.

Finally, the ability of these IgG subclasses to engage FcγR dependent effector functions was assessed. Neither rituximab IgG2 or BHH2 IgG2 were able to induce any killing through ADCC or ADCP, despite the IgG1 subclasses of these antibodies being active in both mechanisms. Once again, whether this reflected an inadequate level of antibody on the target cell membrane to efficiently trigger sufficient FcγR engagement on immune effector cells, or whether the IgG2 subclass was inherently weaker at binding to the FcγRs involved in these assays is difficult to tell. However, the fact BHH2 IgG2 also induced no ADCC or ADCP, despite there being only slightly reduced surface binding compared to the IgG1 subclass, which was very active, suggests that it is likely an inherent difference in FcγR binding of the IgG2 subclass.

This is consistent with the reported relative binding of IgG subclasses to FcγRs, as shown in Table 1-2[98]. IgG2 showed the weakest binding to the FcγRs, which matches the finding that rituximab and BHH2 IgG2 antibodies were unable to induce FcγR mediated effector functions, namely ADCC and ADCP. Furthermore, IgG4 has lower binding to FcγRs, and rituximab IgG4 also induces reduced ADCC and ADCP than rituximab IgG1 and IgG3. ADCC is largely thought to be mediated by NK cells, which only express FcγRIIIa (Section 1.3 and Section 1.4.3). Accordingly, IgG4, which does

not bind to one allele of FcγRIIIa (F158) and shows some binding to the other (V158), and IgG2 which binds only weakly to the V158 allele, induced very little ADCC. In contrast, rituximab IgG4 induced notable levels of ADCP (albeit less than rituximab IgG1 and IgG3), which is mediated by macrophages that also express FcγRI and FcγRIIa, to which IgG4 shows binding. IgG1 and IgG3 are reported to have the highest binding affinities for FcγRs of the IgG subclasses, and this is consistent with the ability of rituximab IgG1 and rituximab IgG3 to potently engage both ADCC and ADCP.

It has recently been reported by some groups that human IgG2 antibodies were similar, or even superior, in terms of target cell depletion to the equivalent IgG1[441]. In this work, CTLA-4 was the target antigen and it was shown in a co-incubation assay with human macrophages and human SupT1 T cells expressing mouse CTLA-4, that a human IgG2 was similarly effective to a human IgG1, despite it also being shown that IgG2 had reduced binding to FcγRs compared to IgG1. *In vivo* comparison of IgG1 and IgG2 in multiple tumour models also showed similar efficacy for both subclasses.

In the work presented in this thesis, the only effector function of IgG2 that is not decreased compared to IgG1 is directly induced cell death. As shown in Figure 3-14, direct killing had very little impact upon primary cells and therefore may not be a major mechanism of IgG therapeutic activity *in vivo.* Fc effector functions, which have repeatedly been shown to be essential for IgG antibody mediated target cell depletion, were essentially inert for the IgG2 subclasses of rituximab and BHH2. The reports of IgG2 being active did use different antibody targets and experimental systems to those used here; CTLA-4 and human SupT1 T cells transfected with mouse CTLA-4, compared to natively expressed CD20 on CLL cells and B cell lines. This may potentially explain why IgG2 appears to effectively deplete target cells in their systems, whereas we see no activity of the IgG2 subclass in this work.

Rituximab IgG3 induced greater ADCC and ADCP than did any of the other rituximab IgG subclasses, matching its increased level of CDC and DCD (relative to IgG1). This increased activity of the rituximab IgG3 subclass in all effector functions tested suggests that it should be explored further; for example, in animal studies to determine its relative activity compared to the well-studied rituximab IgG1. Despite the increased activity of the IgG3 subclass, there are no IgG3 based therapeutics approved for human treatments[70]. The reasons for this are largely based around the practicalities of working with IgG3. As mentioned previously, it has a significantly shorter serum half-life as compared to IgG1, and does not bind well to protein A, necessitating the

use of protein M for its purification. In spite of these issues, the increased activity of IgG3 in these effector assays raises the possibility that IgG3 could be a potentially useful therapeutic agent. Its shorter serum half-life could be of use in conditions where long-lived antibody activity is not desired, such as in the treatment of acute conditions or infections. Furthermore, antibody engineering approaches could be attempted to improve the serum half-life of IgG3. Alternatively, molecular biology approaches could be used to determine which parts of the IgG3 molecule are responsible for its enhanced effector function and short serum half-life. It may be possible to transfer portions of other IgG subclasses into an IgG3 molecule (or vice-versa) to produce a hybrid IgG with the optimum properties in terms of Fc-mediated activity and serum half-life.

A report from Natsume *et al.* details a systematic approach to identify the regions of the IgG1 and IgG3 Fc domains that are responsible for the increased functionality[456]. This group were able to generate antibodies containing the CH1 and hinge region of IgG1, with the Fc domain of IgG3 (referred to as variant 1133). This variant, among others, displayed the highest CDC of all antibodies tested, (including the IgG1 and IgG3 wild type versions of this antibody), whilst maintaining the highest level of ADCC detected in their systems. Further engineering of this construct allowed for production of an antibody variant that also had protein A binding properties similar to IgG1, whilst maintaining comparable CDC and ADCC to the 1133 variant.

Another report, from Stapleton *et al.*, demonstrated the possibility of antibody engineering to improve the serum half-life of IgG3 through mutation of the R435 residue to a histidine, matching the equivalent residue in IgG1, IgG2 and IgG4[457]. This mutation, also found in the G3m(s,t) allotype of IgG3 which has a half-life akin to IgG1, resulted in equivalent binding to FcRn even in the presence of IgG1, as well as rescuing IgG3 from lysosomal degradation. Furthermore, this IgG3 R435H mutant was more protective than IgG1 or IgG3 in protection vs. pneumococcal infection, and appeared to show similar initial clearance to the IgG1 antibody.

In another report, an antibody targeting the porin A from *Neisseria meningitides* was produced on the four IgG subclasses[440]. This group found that IgG1 and IgG3 were similar in their ability to induce complement mediated killing of the bacteria, IgG2 showed greatly reduced killing and IgG4 induced no killing at all. IgG3 was found to induce the most phagocytosis of heat-killed bacteria, whilst IgG2 and IgG4 were relatively inactive. This report supports that the trends observed in our cancer immunotherapy models are applicable to other disease models.

Human IgG subclasses clearly have different properties in terms of effector function engagement, and dependent on the antigen can also differ in the level of surface binding. It is therefore important to fully evaluate an antibody that has been class switched onto an alternative IgG subclass backbone, as many of its inherent properties and effector functions may have changed.

Chapter 4: Antibody Lipid Modification

4.1 Introduction

Antibodies are glycoproteins produced by plasma cells that are highly specific for target antigens. After somatic hypermutation and affinity maturation are complete and a particular B cell selected, all antibodies produced by that B cell and its progeny plasma cells are identical at the gene level, and consequently have identical sequences and primary structures. However, post-translational differences are found on antibody molecules that are not uniform. Glycosylation is an excellent example of this heterogeneity and up to 30 different glycoforms of an antibody can be found[348]. Therapeutic antibodies are produced *in vitro*, and differences in the glycosylation between different antibodies have been found[405]. These antibodies elicit their activity at the tumour site, mediated through FcγRs, complement, and also direct effects through target binding[458].

Although post-translational in nature, glycosylation was typically thought to be a predominantly cellular event, occurring in a sequential manner through the endoplasmic reticulum and golgi apparatus (Section 1.6). However, recently evidence of enzymatic acellular glycomodification has been reported[459]. Here, antibody sialylation is reported as occurring after antibody molecules have left the parent plasma cell. This demonstrates the possibility of antibodies being modified by enzymes once in the serum, suggesting the notion that the activity of antibodies could be modulated following their secretion from plasma cells.

The tumour microenvironment is a highly specialised region that is immunosuppressive and contains many cell types, including tumour cells, stromal cells, macrophages and tumour infiltrating lymphocytes[460]. Tumour associated macrophages, among other cell types including tumour cells themselves, produce large amounts of reactive oxygen and nitrogen species (ROS/RNS) that contribute to the highly oxidising potential of the tumour microenvironment[461]. These oxidative products can be involved in the generation of lipid adducts from polyunsaturated phospholipids. Although this is a natural phenomenon and lipid oxidation products are important in wound healing and homeostasis, very high levels of these have been found at tumour sites [462,463]. In addition to this, oxidative and lipid modifications have been found on plasma proteins at increased levels in patients with age related macular degeneration (AMD)[464] . It is possible that these lipid oxidation products, which accumulate at the tumour location, can be generated on

antibody molecules, which could be one reason why tumours do not always respond to antibody therapy despite the presence of the target antigen[462].

Given this observation that oxidative modifications can be found on plasma proteins in AMD, cancer and are increased at sites of chronic inflammation and apoptotic cells, it was decided to investigate whether such modifications on antibody molecules would impact upon their effector functions. Lipid oxidised antibodies were generated and the effect of such modifications on antibody mechanisms was investigated *in vitro*.

4.2 Generation and Characterisation of Malondialdehyde Modified Rituximab

4.2.1 MDA Modification of Rituximab

Oxygen free radicals (such as the hydroxyl radical ·OH) can react with polyunsaturated fatty acids (PUFAs) to generate lipid radicals through abstraction of an H· radical[465]. These lipid radicals can then react with oxygen to give a lipoperoxyl radical[465]. This lipoperoxyl radical can then react with another lipid to generate a further lipid radical and a lipid hydroperoxyde. Lipid hydroperoxydes are unstable and can react to generate further radicals or decompose into secondary products, such as malondialdehyde (MDA)[466]. These reactive aldehydes are sometimes referred to as secondary messengers of lipid peroxidation, due to their increased stability and ability to diffuse from their site of formation and cross cell membranes[467]. MDA can be generated from the peroxidation of PUFAs that contain 3 or more double bonds, such as arachidonic acid (20:4) or linolenic acid (18:3), following cleavage of the lipid hydroperoxydes[468].

In order to try and generate MDA modified antibodies it was necessary to first produce MDA itself (Figure 4-1). MDA is highly hygroscopic and can't be stored for long periods of time, so for use in modifying antibodies, MDA was generated by acid hydrolysis of the MDA precursor 1,1,3,3-Tetramethoxypropane (Sigma Aldrich) using 2M HCl (Figure 4-1). After acid hydrolysis the pH was adjusted back to 7.4 with 1M NaOH and the concentration of MDA adjusted to 1.07M by the addition of 0.5M sodium phosphate buffer.

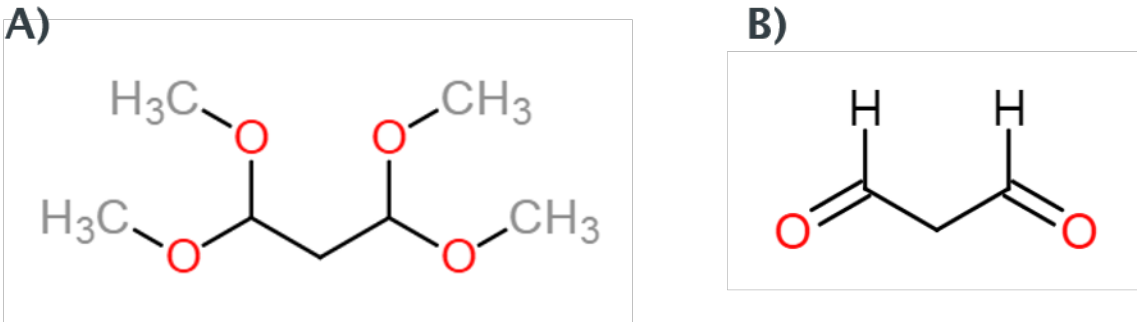

Figure 4-1 Chemical Structure of Malondialdehyde and its Precursor

Chemical structure of A) 1,1,3,3-Tetramethoxypropane and B) malondialdehyde. Structures drawn using website https://web.chemdoodle.com/demos/sketcher/

For MDA modification of the anti-CD20 antibody rituximab, the antibody was first dialysed into 0.5M phosphate buffer using Slide-A-Lyzer 10K MW cassette (ThermoFisher) at room temperature. 8.4 nanomoles of rituximab was added to 0.16 moles of MDA in a glass vial and the reaction was incubated at 37°C for 5hrs. A control reaction was set up in which rituximab was incubated alongside but without the MDA agent added. After this incubation rituximab was dialysed into PBS using Slide-A-Lyzer 10K MW cassette at 4°C. After dialysis, MDA modified antibody (but not the mock treated antibody) maintained a pale yellow colour, as has been reported previously[469]. This change in spectral properties prevented the use of light absorbance at 280nm as a means of determining antibody concentration. As such, the concentration of antibody was quantified using a colorimetric assay as described in methods (Section 2.2.4).

4.2.2 Assessment of MDA Modification of Rituximab

In order to determine whether MDA adduction had occurred, the MDA treated rituximab was run on a 10% SDS-PAGE gel along with MDA control treated, and untreated rituximab to see if any change in mass had occurred. Figure 4-2 shows that the MDA treated rituximab, compared to the MDA control treated rituximab, had a much larger apparent molecular weight with no bands present at the position that would be expected for the antibody individual heavy and light chains. This indicates that all of the molecules have been modified by the MDA treatment.

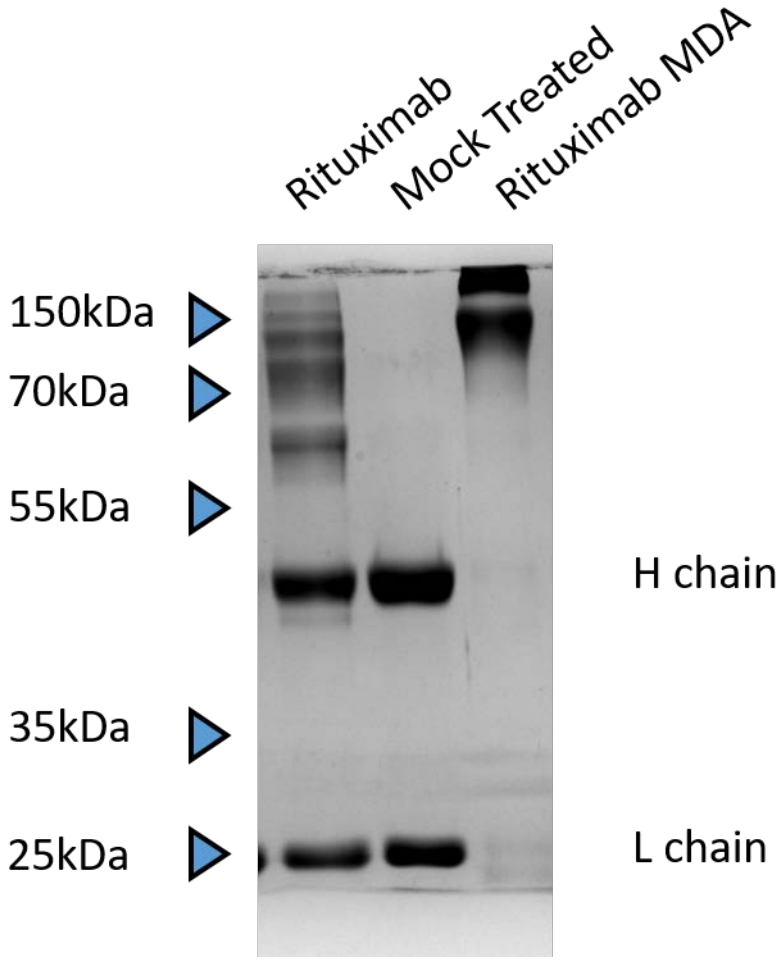

Figure 4-2 MDA Modification of Rituximab

Rituximab that was modified with MDA, mock treated or untreated was boiled in Laemmli buffer and analysed on a 10% SDS-PAGE gel for 2 hours at 110V. The gel was then fixed and stained with Coomassie Brilliant Blue prior to destaining and imaging. Heavy (H) and light (L) chains are indicated.

4.3 Functional Assessment of MDA Modified Rituximab

4.3.1 Antigen Binding

In order to see whether rituximab MDA was still functional, its ability to bind to its target antigen, CD20, was assessed using flow cytometry. Raji and Ramos cells were opsonised with rituximab MDA, mock treated rituximab, unmodified rituximab or an irrelevant isotype control, and detected with a labelled anti-IgG $F(ab')_2$. As shown in Figure 4-3, rituximab MDA showed reduced

binding to both Raji and Ramos cells, whereas mock treated rituximab maintained equivalent binding to untreated rituximab.

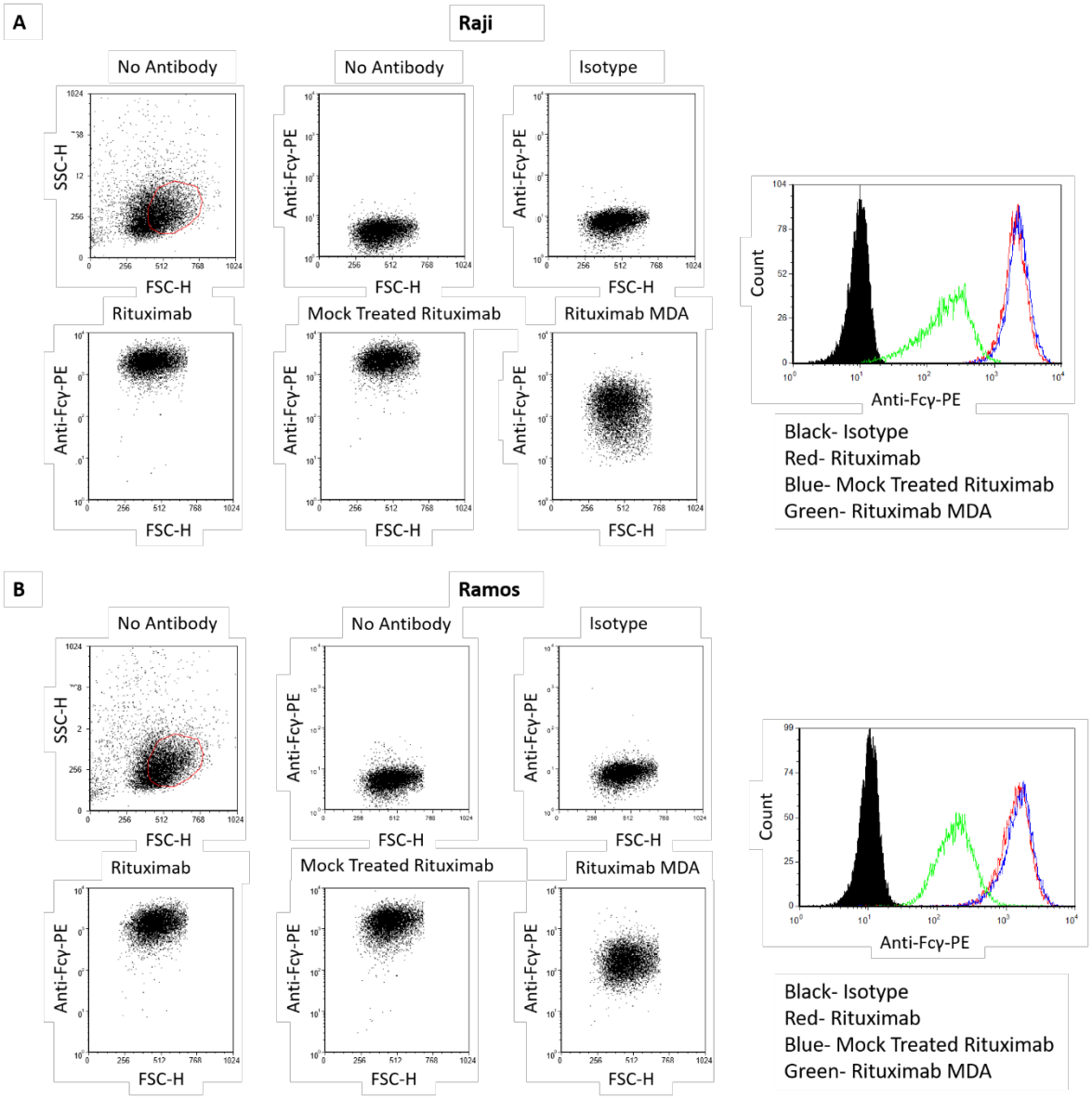

Figure 4-3 Ability of Rituximab MDA to Bind to Target Cells

Raji (A) and Ramos (B) cells were opsonised with 10µg/ml of untreated rituximab (MabThera), mock treated rituximab, rituximab MDA or an irrelevant control antibody. After washing, antibody binding was detected using a labelled polyclonal secondary $F(ab')_2$ specific for human IgG Fc. Cells were acquired by flow cytometry and gated on live cells as shown.

Next, in order to confirm that MDA modified rituximab was actually binding to CD20 on the target cell surface, MDA modified rituximab was tested to see if it was able to block binding of non-

modified rituximab to CD20 on Ramos cells. Ramos cells were opsonised with rituximab, mock treated or MDA modified rituximab, and after washing off unbound antibody, FITC labelled rituximab was added to the cells (Figure 4-4).

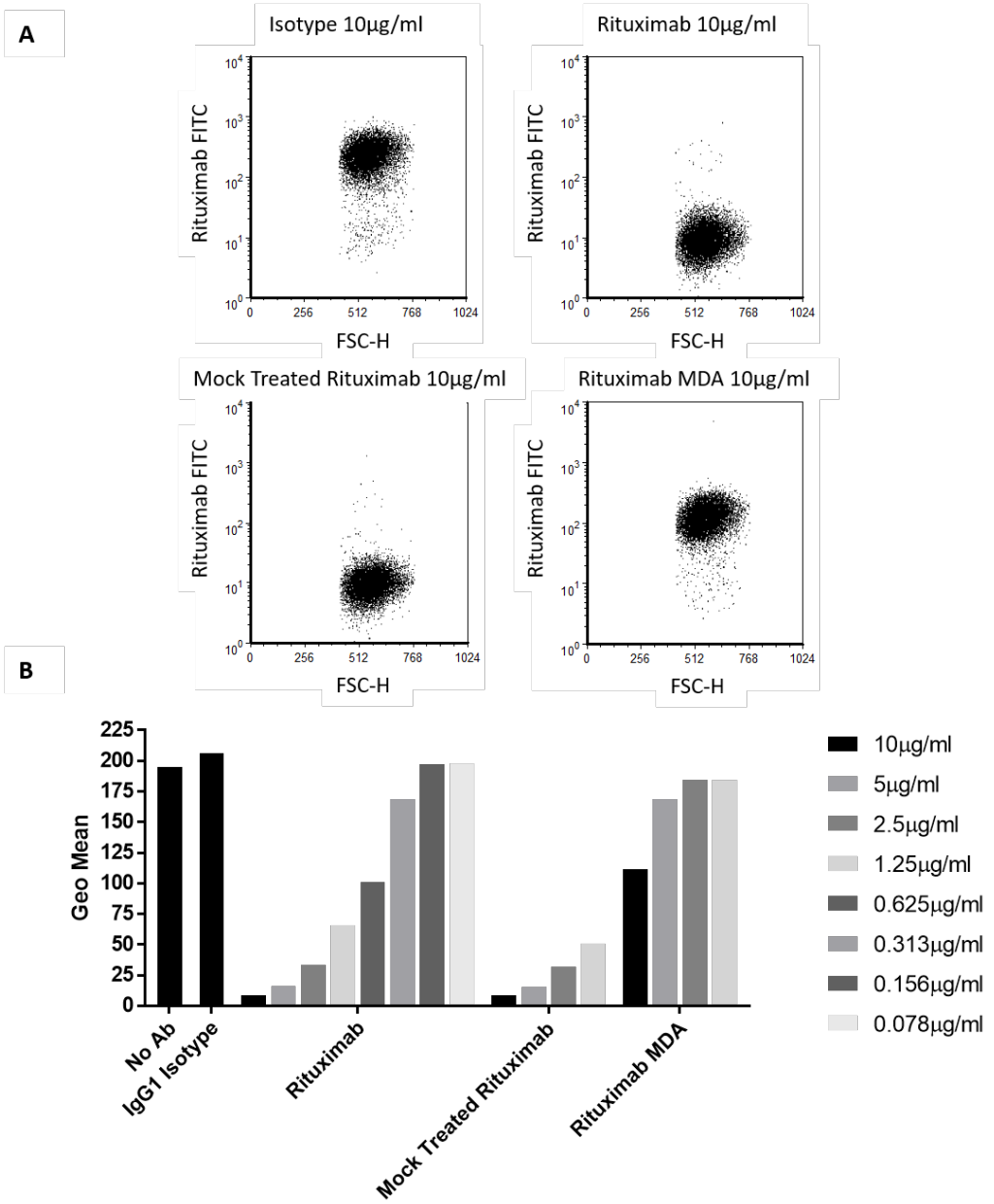

Figure 4-4 Ability of Rituximab MDA to Block Secondary Rituximab Binding

Ramos cells were opsonised with untreated rituximab, mock treated rituximab, rituximab MDA or an irrelevant control antibody (at concentrations indicated in key) and unbound antibody washed off. A FITC-labelled anti-CD20 antibody (rituximab) was then added at 10µg/ml to bind any free CD20. Excess antibody was washed off and the cells acquired by flow cytometry gated on live cells. A- example data of rituximab FITC binding to cells pre-opsonised with the indicated treatment. B- Data shown represent a single measurement of the geometric mean of rituximab FITC binding to pre-opsonised cells, representative of two independent experiments.

MDA treated rituximab bound to Ramos cells was able to partially block the binding of a labelled secondary anti-CD20 antibody (see Figure 4-4). To confirm this, and quantify how much MDA treated rituximab was functional, the level of binding of MDA treated rituximab was compared to a titration of untreated rituximab, with the level of bound antibody detected by a PE labelled anti-Fc $F(ab')^2$(Figure 4-5).

When compared to a dose titration with untreated rituximab (MabThera) as the primary antibody, the level of blocking seen with 10µg/ml MDA modified rituximab was approximately equal to that seen with 0.625µg/ml untreated rituximab (Figure 4-5). This result, coupled with the reduced CD20 binding seen in Figure 4-3 and the reduced blocking capacity seen in Figure 4-4 , suggests that only a portion of the MDA treated rituximab is still functional and capable of binding to CD20.

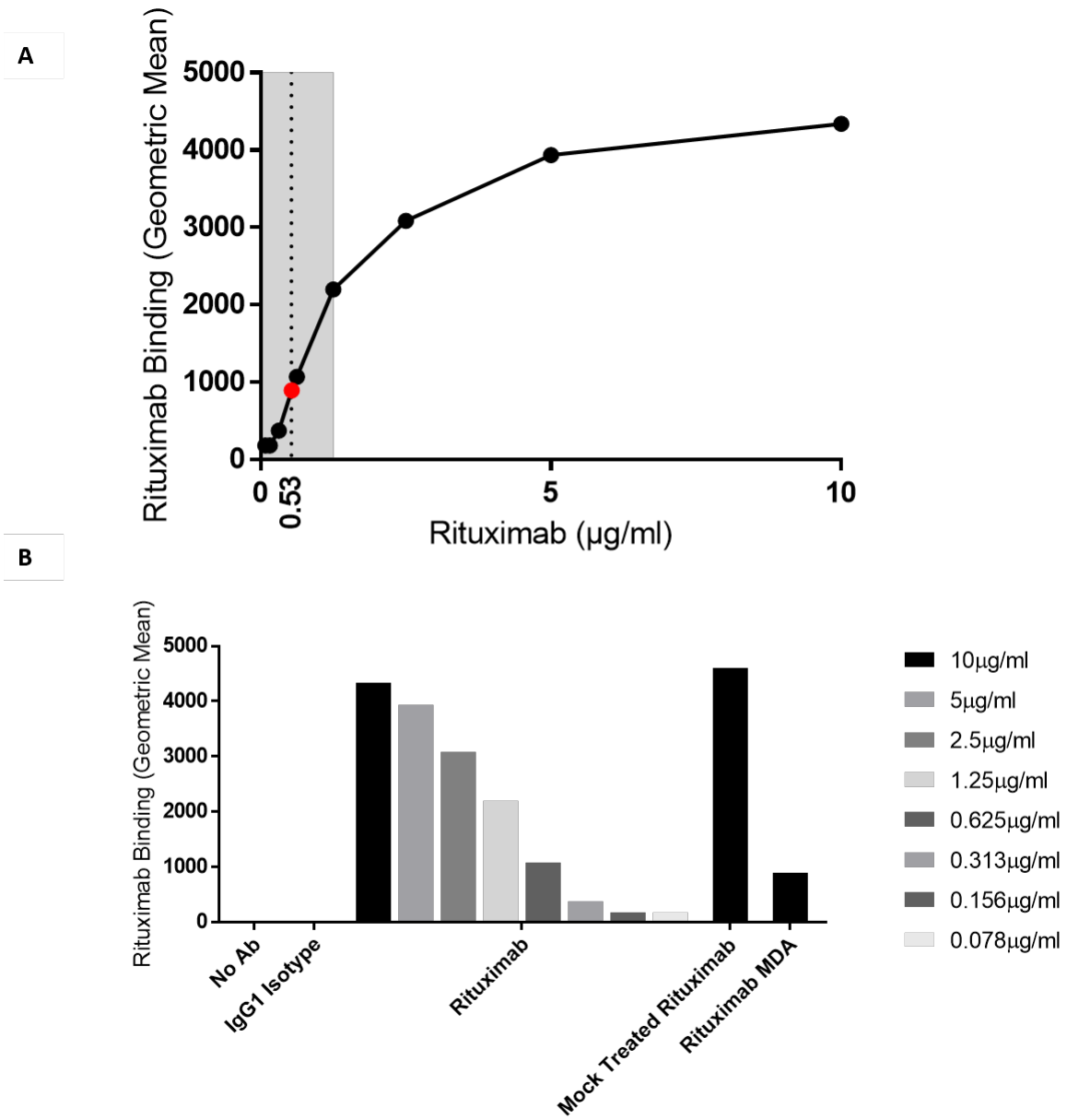

Figure 4-5 Determining Relative Concentration of Functional Antibody for Rituximab MDA Compared to Unmodified Rituximab

Ramos cells were opsonised with a 2x serial dilution of rituximab (MabThera) starting at 10µg/ml. Unbound antibody was washed off and bound antibody detected using a labelled polyclonal secondary antibody specific for human IgG Fc. Cells were acquired by flow cytometry. A- binding of rituximab MDA (10µg/ml, red dot)) compared to untreated rituximab (MabThera, black dots). The apparent concentration of rituximab MDA at 10µg/ml (0.53µg/ml) was calculated from the linear region of the standard curve (shaded region). B- binding of 10µg/ml rituximab MDA relative to a titration of untreated rituximab (10µg/ml-0.08µg/ml), from a single experiment, representative of 2 independent experiments.

4.3.2 FcγR Binding of MDA Modified Rituximab

Next, it was of interest to investigate whether MDA treatment of rituximab affected its ability to interact with FcγRs. This was performed using CHO cells transfected with various human FcγRs (personal communication- Robert Oldham). Antibodies were incubated with transfected CHO cells at 20µg/ml for 30 minutes, and after washing the bound antibody was detected using a labelled polyclonal $F(ab')_2$ recognising the human IgG Fc region.

MDA treated rituximab did not bind to untransfected CHO-K1 cells indicating no non-specific interaction was occurring due to the presence of MDA modifications (Figure 4-6B). MDA modified rituximab showed very similar binding to both untreated and mock treated rituximab for FcγRIIIa (V158 and F158). MDA treated rituximab showed reduced binding to FcγRI compared to that seen with both untreated and mock treated rituximab. The biggest difference was seen with FcγRIIa (R131) and FcγRIIb, where MDA modified rituximab showed substantially increased binding to both receptors compared to both untreated and mock treated rituximab.

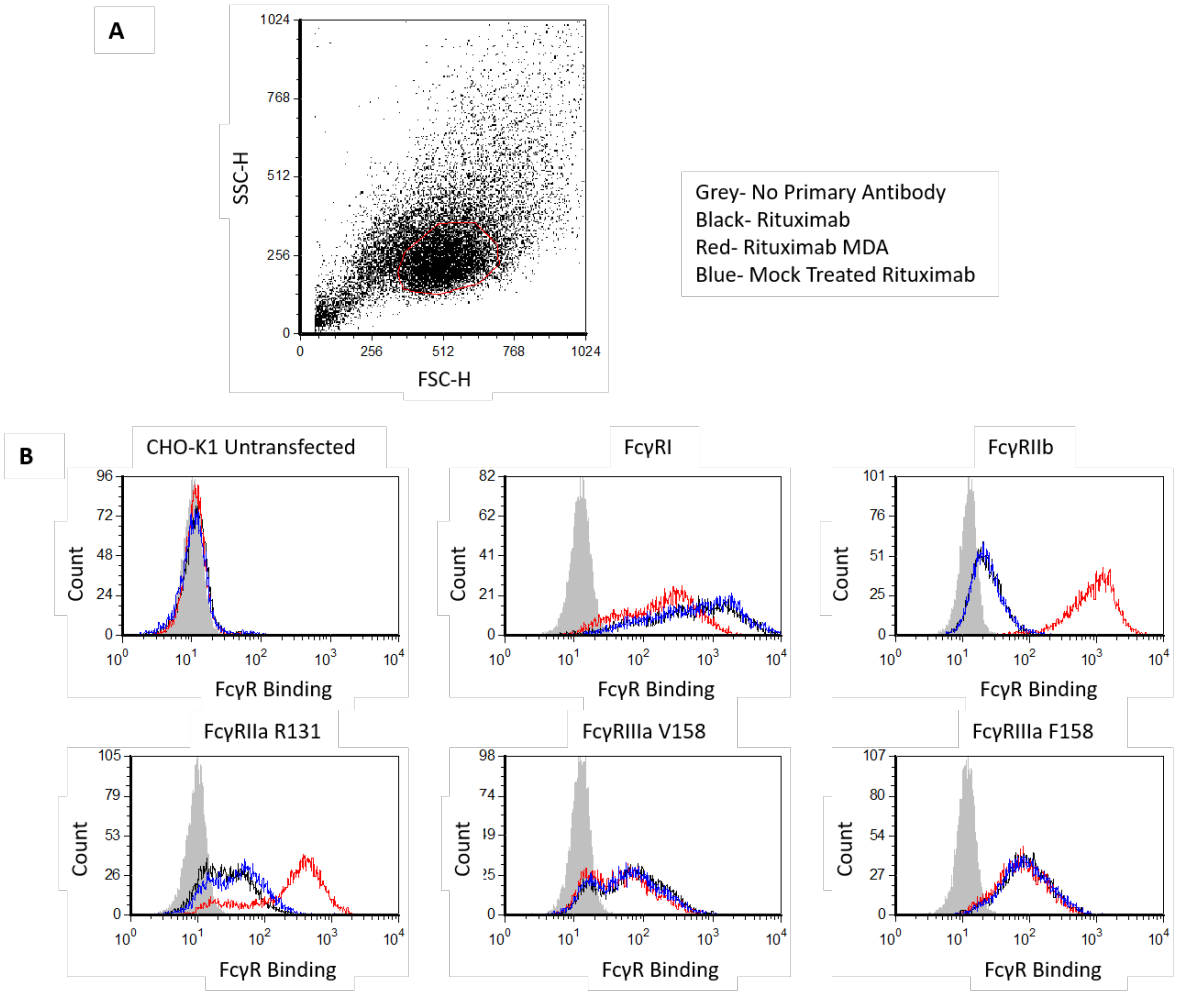

Figure 4-6 Ability of Rituximab MDA to Bind FcγRs Expressed on CHO Cells

Unlabelled rituximab MDA (red), mock treated rituximab (blue), untreated rituximab (MabThera, black) and an isotype control were applied at 20µg/ml to CHO-K1 cells stably transfected with human FcγRs I, IIa (R131 allele), IIb, and IIIa (both V158 and F158 alleles) as well as to untransfected CHO-K1s in order to assess binding. After washing bound antibodies were detected using a labelled secondary $F(ab')_2$ specific for human IgG Fc, and cells acquired by flow cytometry and gated on live cells. A- gating of live CHO-K1 cells. B- overlaid histograms of the relative binding of rituximab, mock treated rituximab and rituximab MDA to CHO-K1 cells transfected with the indicated FcγR. Data from a single experiment, representative of two independent experiments.

4.3.3 Effector Functions of MDA Modified Rituximab

Having determined that MDA treated rituximab was capable of binding to both its target antigen and also to FcγRs, albeit at different levels to that of untreated and mock treated rituximab, next we sought to investigate the effects of MDA modification on rituximab Fc mediated effector functions *in vitro*.

4.3.3.1 Complement Dependent Cytotoxicity

Firstly the effect of MDA modification on the induction of complement dependent cytotoxicity death was analysed. Raji cells, which express certain complement defence molecules such as CD55, were used and, as shown in Figure 4-7, rituximab MDA was unable to elicit complement mediated killing at any dose, whereas over 60% killing was seen with both untreated rituximab (MabThera) and MDA mock treated rituximab when applied at 10µg/ml.

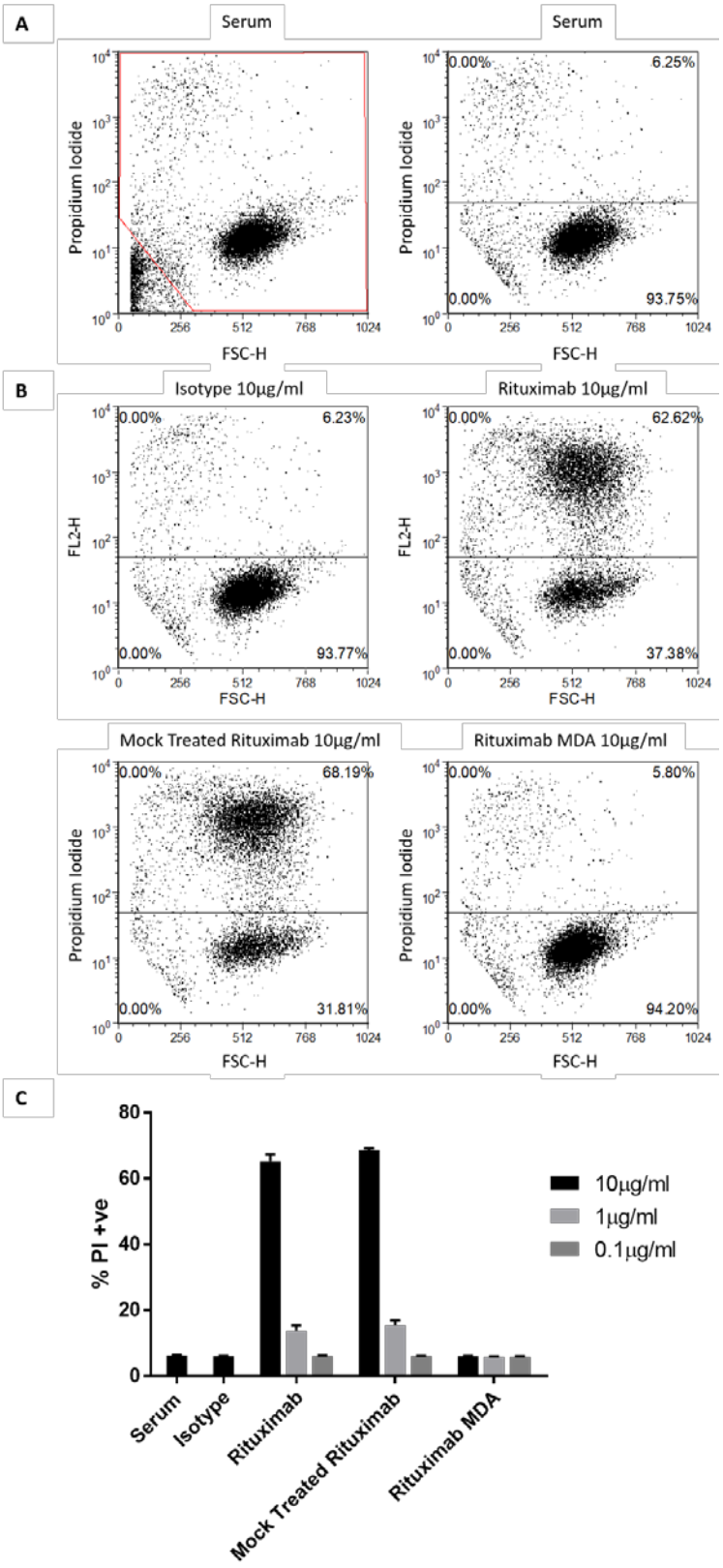

Figure 4-7 Ability of Rituximab MDA to Initiate CDC on Raji Cells

Raji cells were opsonised with various concentrations of rituximab, mock treated rituximab, rituximab MDA or an isotype control as indicated prior to a 30 minute incubation with 30% human serum.

Complement activity was detected by staining with propidium iodide followed by flow cytometry. A- debris from serum was gated out and complement dependent cytotoxicity was identified by propidium iodide (PI) staining, seen as an increase in the FL-2 signal of cells that have been permeabilised by the formation of the MAC. B- treatment of Raji cells with isotype, rituximab, mock treated rituximab or rituximab MDA. C- data shown represent the mean plus range of triplicate technical repeats of a single experiment.

The complement activation of rituximab MDA was also tested on CDC sensitive Ramos cells. A similar result was found with Ramos cells as with Raji cells, but with a greater level of killing reflecting the increased sensitivity of these cells (Figure 4-8). As such, some cell death can be seen with 10µg/ml Rituximab MDA, but this is less than the killing seen with 100x less untreated or mock treated rituximab, indicating some low level residual activity of rituximab MDA.

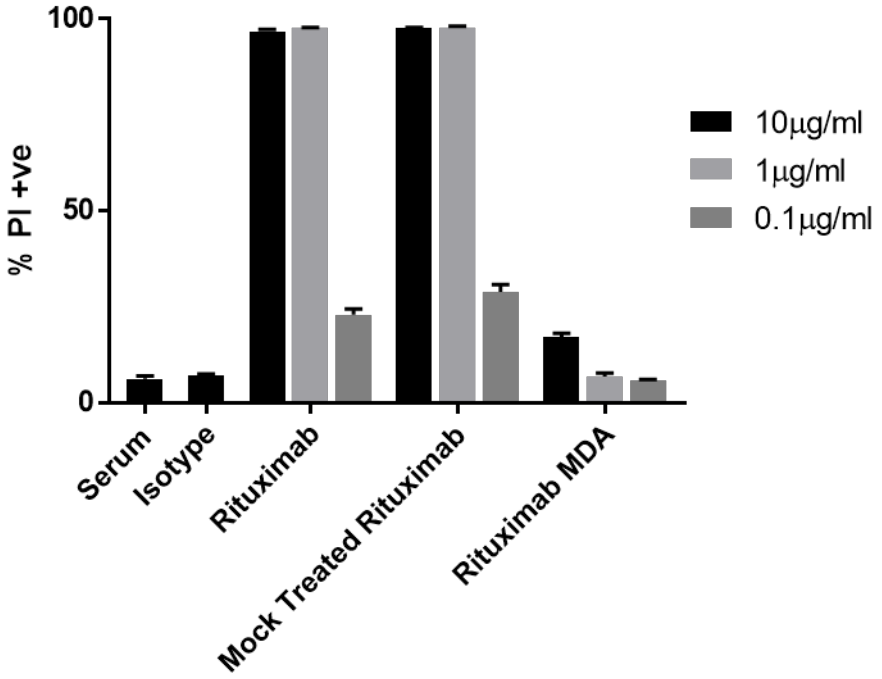

Figure 4-8 Ability of Rituximab MDA to Induce CDC on Ramos Cells

Ramos cells were opsonised with varying concentrations of rituximab MDA, mock treated rituximab, untreated rituximab or an isotype control prior to a 30 minute incubation with 30% human serum and complement dependent cytotoxicity killing was identified by PI staining. Mean plus range of triplicate repeats of a single experiment are shown.

As demonstrated in Figure 4-3, rituximab MDA showed reduced binding to target cells. It is likely therefore that the reduced CDC seen in Figure 4-7 and Figure 4-8 was due to reduced antibody

binding when compared to untreated and mock treated rituximab. In order to try and investigate whether MDA treatment reduces CDC through reduced functional antibody, or whether the functional antibodies themselves are also less able to activate the complement pathway, the dose of rituximab MDA was adjusted to give approximately the same level of functional Fc at the cell surface. This was calculated from comparison of the detectable free Fc of rituximab MDA to a titration of rituximab (see Figure 4-5). This suggested that binding of 10µg/ml of rituximab MDA was approximately equivalent to 0.5µg/ml of untreated rituximab in terms of detectable Fc regions.

Accordingly, 20µg/ml of rituximab MDA would give a concentration approximately equivalent to 1µg/ml of untreated rituximab. When Ramos cells were treated with this adjusted concentration of rituximab MDA, complement mediated death was seen (see Figure 4-9). The level of complement killing seen with this dose of MDA treated rituximab was approximately 20% lower than that seen with 1µg/ml mock treated rituximab or untreated rituximab. This suggests that either the dose correction was not entirely accurate, or that the MDA modified antibodies able to bind to CD20 may not all be able to bind to C1q as efficiently as unmodified antibody.

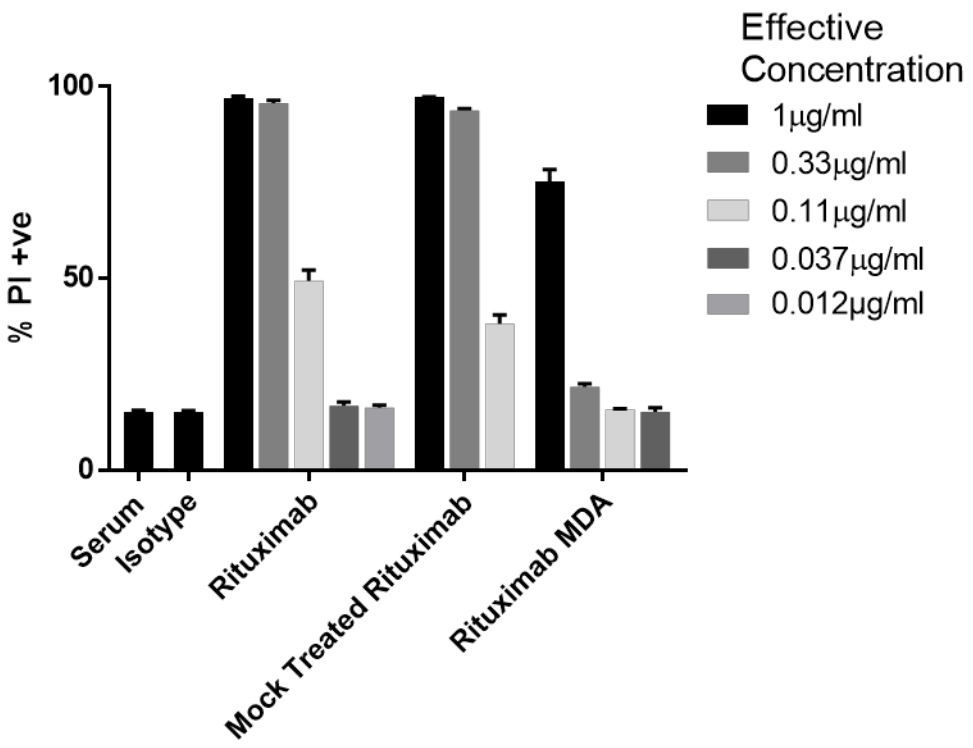

Figure 4-9 Ability of Rituximab MDA to Exhibit CDC at Equivalent Effective Binding Concentrations as Unmodified Rituximab

Ramos cells were opsonised with various concentrations of rituximab MDA, mock treated rituximab, untreated rituximab or an isotype control as indicated prior to a 30 minute incubation with 30% human serum and complement dependent cytotoxicity was identified by PI staining. Rituximab MDA doses were adjusted to correct for the 20 fold reduced target binding in order to give comparable levels of functional Fc to untreated rituximab, according to Figure 4-5 and as described in the main text. Mean plus range of triplicate repeats of a single experiment.

4.3.3.2 Antibody Dependent Cellular Cytotoxicity

Having determined that MDA modification impaired the ability of rituximab to activate CDC, its effect on FcγR mediated effector functions was investigated; namely antibody dependent cellular cytotoxicity and antibody dependent cellular phagocytosis.

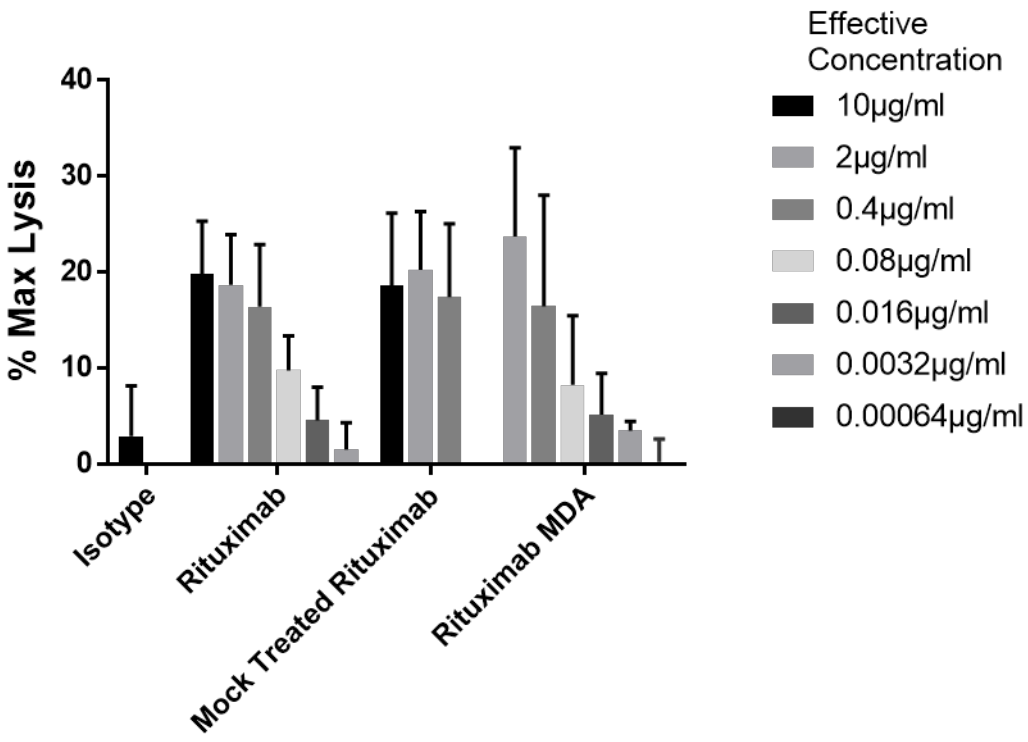

Figure 4-10 Ability of Rituximab MDA to Induce ADCC at Equivalent Effective Binding Concentrations as Unmodified Rituximab

Calcein labelled Ramos cells were opsonised with various concentrations of rituximab MDA, mock treated rituximab, untreated rituximab or an isotype control as indicated. Opsonised targets were co-cultured with freshly purified human PBMCs at a ratio of 50 PBMCs per target cell for 4 hours at 37°C, and the supernatants analysed for released calcein by measuring their emission at 515nm. Max lysis was calculated as percentage of maximum once background (non-opsonised targets and effectors) was removed according to the equation % of Max Lysis = (X – background)/(Max Lysis – background)*100. Rituximab MDA doses were adjusted to correct for the approximately 20 fold reduced target binding in order to give comparable levels of functional Fc to untreated rituximab. Data presented are the combined means + SD of 3 independent experiments using different PBMC donors.

Rituximab MDA was able to induce similar levels of ADCC as compared to untreated and mock treated rituximab when the dose correction to give approximately similar levels of antibody binding was applied; i.e. 40µg/ml rituximab MDA induced a similar level of killing as did 2µg/ml untreated rituximab which has approximately the same level of functional Fc (Figure 4-10).

4.3.3.3 Antibody Dependent Cellular Phagocytosis

Evidence from *in vivo* experiments have indicated that the primary mechanism of action of rituximab is via phagocytosis of target cells by macrophages[253,470]. Accordingly, the effect of MDA modification on rituximab induced ADCP was tested using MDMs and Ramos target cells. Rituximab MDA was able to induce phagocytosis of opsonised target cells but only to approximately two thirds of the level achieved by untreated rituximab (Figure 4-11).

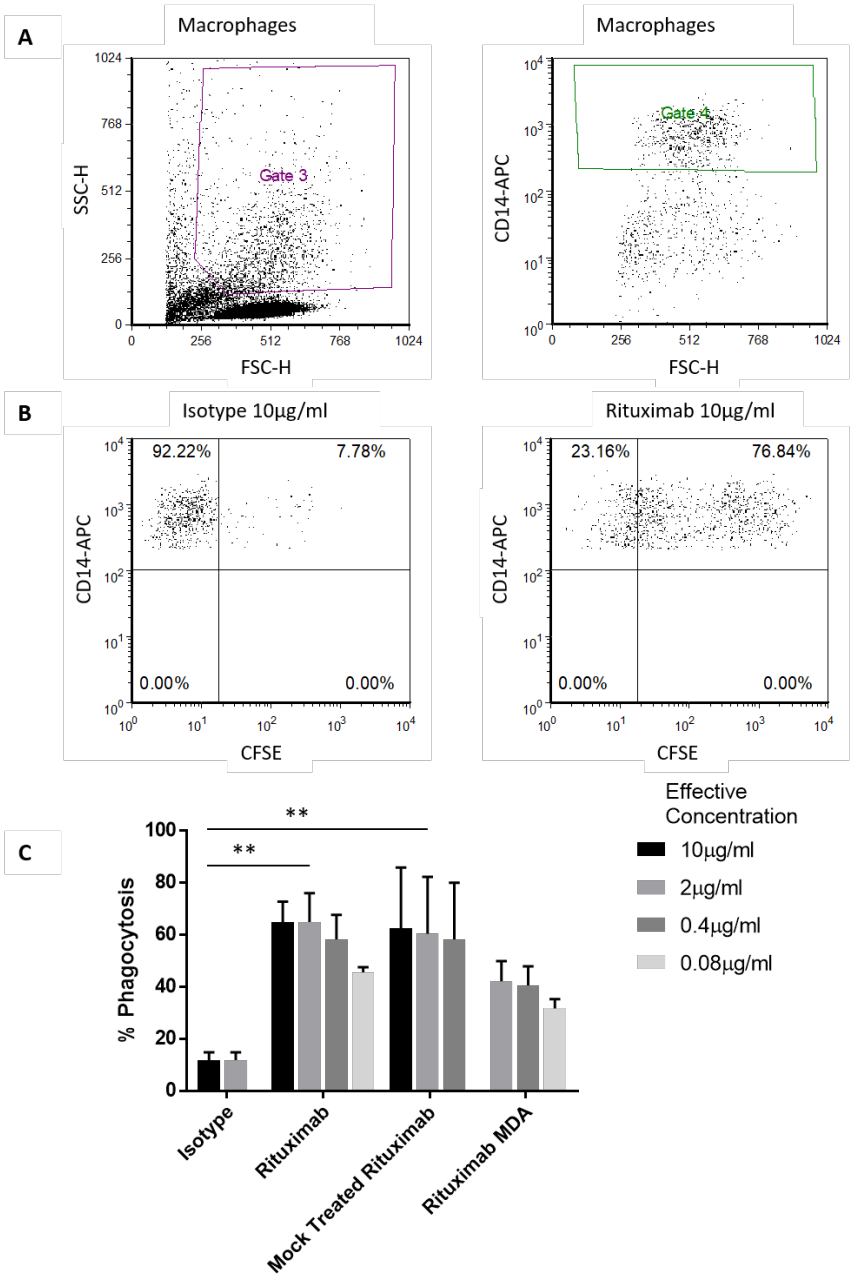

Figure 4-11 Ability of Rituximab MDA to Induce ADCP at Equivalent Effective Binding Concentrations as Unmodified Rituximab

Ramos cells were labelled with CFSE and opsonised with various concentrations of either Rituximab MDA, mock treated rituximab, untreated rituximab or an isotype control. Opsonised cells were co-cultured with MDMs for 1 hour, macrophages stained for CD14 and acquired by flow cytometry. Rituximab MDA doses were adjusted to correct for the 20 fold reduced target binding in order to give comparable levels of functional Fc to untreated rituximab. A- Representative flow cytometry plots showing gating strategy used. The percentage of macrophages that had phagocytosed a target cell was calculated as a percentage of CD14+ cells. B- example data showing phagocytosis of isotype and rituximab opsonised Ramos cells. C- Combined results showing mean + SD of three independent experiments using different MDM donors, each measured in triplicate. Statistics calculated by one-way ANOVA with multiple comparisons, ** $p<0.01$.

4.4 Optimisation of MDA Modification Method

4.4.1 Titration of MDA Modification

It was shown that rituximab MDA was still capable of binding to target cells and FcγRs, and able to induce Fc mediated effector functions, albeit to a lesser extent than unmodified antibody (Section 4.3). MDA modification of rituximab resulted in a dramatic increase in the size of the antibody when measured by SDS-PAGE (Figure 4-2). This shift in mass could be due to adduction of MDA molecules onto lysine residues within rituximab, thereby increasing its mass. However, as MDA is a dialdehyde with 2 aldehyde functional groups (Figure 4-1), it is possible for a single MDA molecule to bind to 2 different lysine residues either on the same IgG molecule, or on different IgG molecules in an intermolecular fashion. This could potentiate the formation of aggregates of antibody, which could also explain the increased size of rituximab MDA seen in Figure 4-2. Moreover, a large proportion of the MDA-modified material had evidently lost the ability to bind to the CD20 target, indicative of over-modification and destruction of the Fab binding site.

As such, it was desirable to generate antibodies that were less extensively modified in order to try and investigate the effect of MDA modification alone, separately from the effect of antibody aggregation. This would also be more likely to reflect the situation *in vivo* where such extensive modifications would not be expected[471]. In order to try and achieve this, MDA modification was repeated but with different concentrations of MDA and using different incubation periods, to see if monomeric modifications could be produced.

MDA solutions of varying concentrations were made and then mixed with antibody according to Table 4-1. In addition to varying the MDA concentration, an intermediary time point was taken after 2.5 hours to see how far the reaction had progressed by this stage. After 2.5 hours a subtle shift in colour could be seen between the highest MDA concentration (MDA 1) and the lowest MDA concentration and controls (Figure 4-12). Half of the antibody product was removed after 2.5 hours and dialysed into PBS using Amicon Ultra-4 Centrifugal Filter Units (Merck Millipore) spun at 3200g. The remaining antibody was incubated for another 2.5 hours before being dialysed into PBS in the same manner. All antibodies were filter sterilised and their concentrations assessed by a protein concentration assay as described in the methods.

Solution	MDA 1	MDA 2	MDA 3	MDA 4
Concentration (mM)	747	374	187	93
mmoles added	168	84	42	21
Ratio of MDA:IgG	$13.3x10^6$	$6.67x10^6$	$3.33x10^6$	$1.67x10^6$

Table 4-1 Rituximab MDA Modification Conditions

Various concentrations of MDA were used to give a decreasing ratio of MDA per IgG molecule.

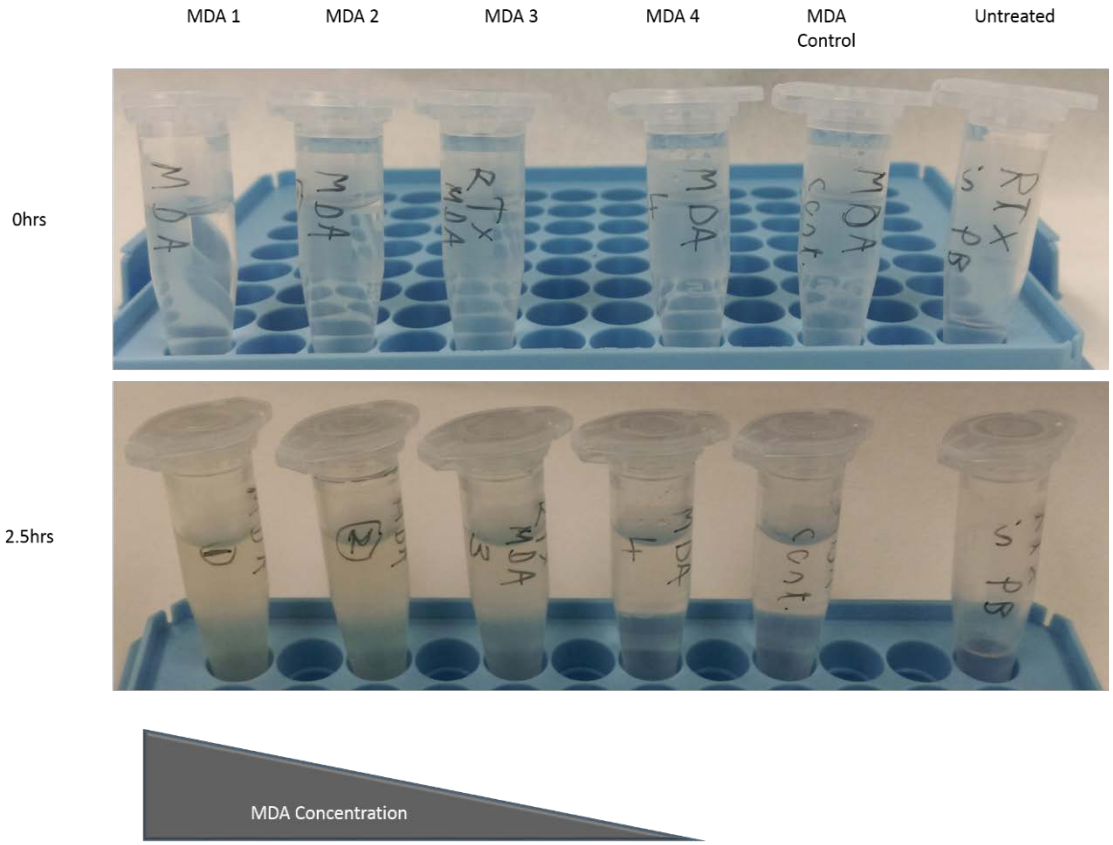

Figure 4-12 Image of MDA Samples Collected at Intermediary Time Point

Images of rituximab antibody modified with different concentrations of MDA at 0hrs (top) and 2.5hrs (bottom).

4.4.2 Assessment of MDA Modification Titration

Antibodies were analysed on a 10% SDS-PAGE gel and stained with Coomassie Brilliant Blue as previously (Figure 4-13). The majority of the staining in the MDA modified rituximab lanes was towards the top of the gel. Faint bands could be seen further down the gel, matching the H and L chain bands seen in the control lanes (9 and 10), for the lower MDA concentrations MDA 3 and MDA 4 for the 2.5hr time point.

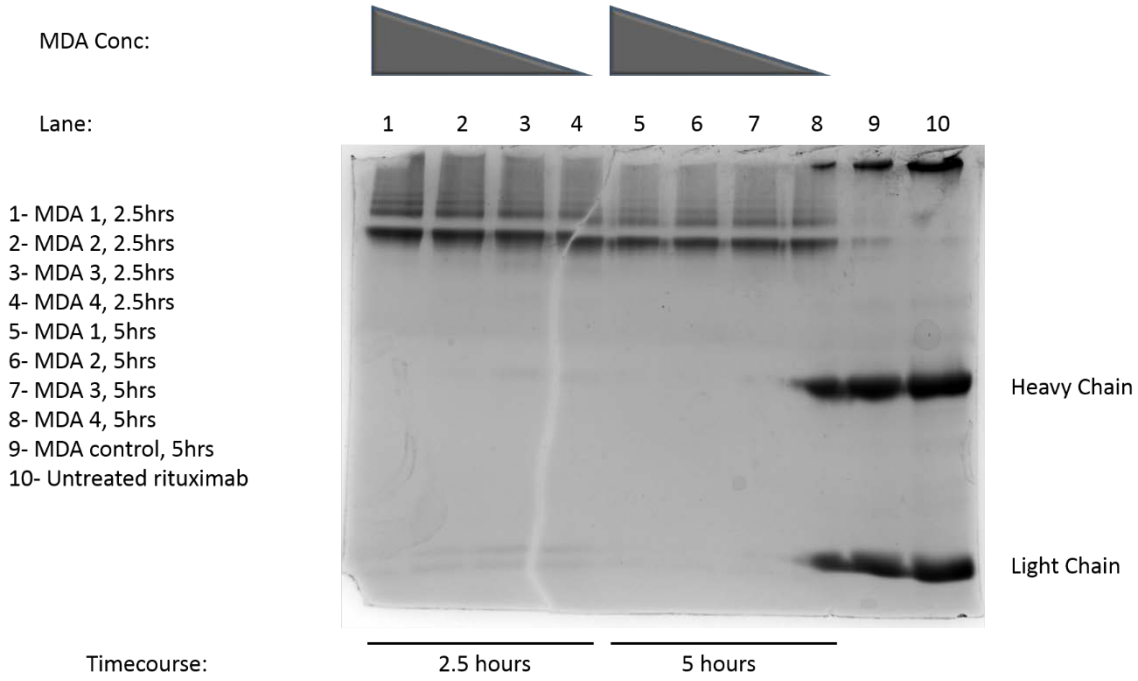

Figure 4-13 MDA Modification Time Course Assessed by SDS-PAGE

Rituximab was incubated for 2.5 or 5 hours with various concentrations of MDA (Table 4-1), and buffer transferred into PBS before analysis by SDS-PAGE on a 10% gel under reducing conditions, and imaged by Coomassie Brilliant Blue staining. Mock treated and untreated rituximab were included as controls for unmodified antibody.

4.5 Functional Characterisation of MDA Modification Titration

4.5.1 Antigen Binding

The functionality of the different MDA samples detailed above (Section 4.4) was tested by analysing the proportion of antibody that was still able to bind to target cells, as performed previously (Figure 4-3). Figure 4-14 shows that a trend can be seen whereby the lower concentrations of MDA used for rituximab modification resulted in increased levels of target binding. This trend was seen for both time points, with an overall higher level of binding seen for the 2.5hr (black) time point compared to the 5hr time point (grey). None of the MDA modified samples showed as much surface binding as mock treated rituximab (either 2.5 or 5hr samples).

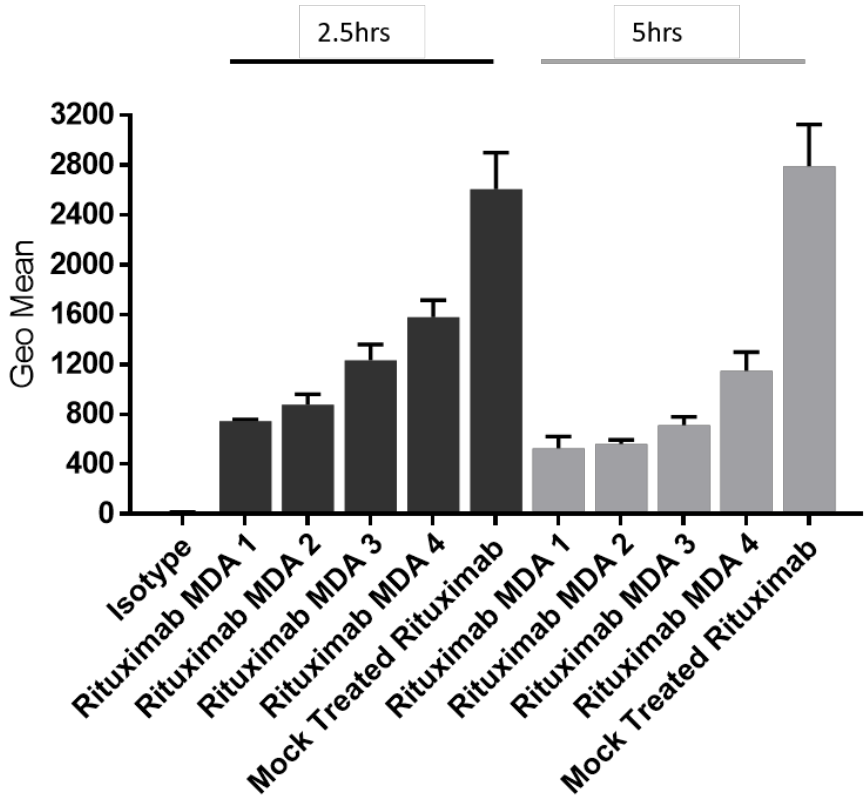

Figure 4-14 Ability of MDA-Modified Rituximab Preparations to Bind Ramos Cells

Ramos target cells were opsonised with 10µg/ml of rituximab treated with MDA, or mock treated, at different concentrations for 2.5 or 5 hours. Excess antibody was washed off and bound antibody detected using a labelled secondary $F(ab')_2$ specific for human IgG Fc, and cells acquired by flow cytometry and gated on live cells. Data presented as mean + range of two independent experiments each measured in triplicate.

4.5.2 Antibody Dependent Cellular Cytotoxicity

In order to further check the functionality of these MDA modified antibodies, they were tested in an ADCC assay as performed previously (Figure 4-10). Figure 4-15 shows the results of this assay. As in Figure 4-14, a trend was seen with decreasing MDA concentration causing an increased ADCC back to a level comparable to that seen with untreated rituximab. Again, this trend was evident at both 2.5hrs and 5hrs, and seen at both 10µg/ml and 3.33µg/ml. Compared to the mock treated rituximab at each time point, the MDA treated rituximab shows similar or even slightly superior ADCC at 10µg/ml. MDA treated rituximab samples showed a greater decrease in the level of ADCC induction upon titration to 3.3µg/ml than did the mock treated (or untreated rituximab), and the size of the decrease was greater with the samples exposed to higher concentrations of MDA.

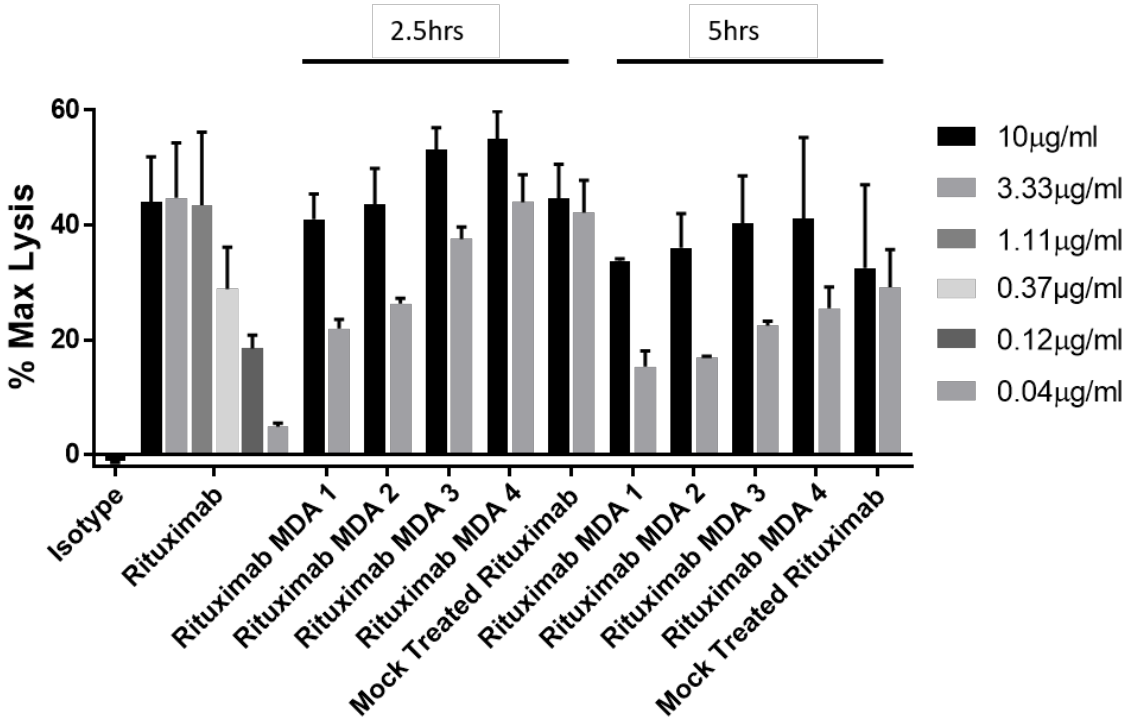

Figure 4-15 Ability of MDA-Modified Rituximab Preparations to Elicit ADCC

Calcein labelled Ramos cells were opsonised with various concentrations of differentially modified rituximab MDA, mock treated rituximab, untreated rituximab or an isotype control as indicated. Opsonised target cells were co-cultured with freshly purified human PBMCs at a ratio of 50 PBMCs per target cell for 4 hours, and the supernatants analysed for released calcein by measuring their emission at 515nm. Max lysis was calculated as percentage of maximum once background (non-opsonised targets and effectors) was removed according to the equation % of Max Lysis = (X – background)/(Max Lysis – background)*100. Data presented are the means + range of two independent experiments each measured in triplicate.

In the work described above, MDA modifications that have been reported to occur *in vivo* have been shown to modify the effector functions of rituximab. In order to expand upon this as a potential *in vivo* influence on therapeutic mAbs, we next sought to determine the effect of another lipid modification that has been found *in vivo*, carboxyalkylpyrroles, on the effector functions of mAbs.

4.6 Generation and Characterisation of Carboxyethylpyrrole Modified Rituximab

4.6.1 Carboxyethylpyrrole Background

Another by-product of lipid oxidation are the carboxyalkylpyrroles (CAPs), a group of products that are generated from the oxidation of polyunsaturated fatty acids and found in human plasma proteins[472]. These structures consist of a carboxylic acid head group, a linking alkyl chain and a pyrrole ring which can attach to available nitrogen atoms, such as those in lysine side chains (Figure 4-16). The length of the alkyl chain that links the pyrrole ring to the carboxylic acid group varies between different members of the CAP family and depends on the species of polyunsaturated fatty acid that the CAP is generated from. For example, carboxyethylpyrroles (CEPs) contain an ethyl chain (as shown in Figure 4-16) and are formed from the oxidation of docosahexaenoyl containing phospholipids[472]. Docosahexaenoyl containing phospholipids are relatively minor components of membranes and lipoproteins in most cells, but are highly abundant in cells of the brain and retina, constituting up to 80% of the phospholipids in the membranes of photoreceptors in some rod cells[473].

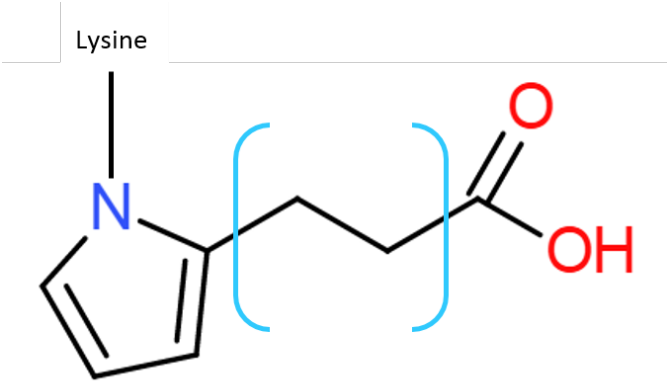

Figure 4-16 Structure of Carboxyethylpyrrole

General structure of a carboxyalkylpyrrole. Molecule consists of a pyrrole ring and a carboxylic acid functional group linked by an alkyl chain of varying length (blue brackets). The length of the chain determines the specific name of the molecule- here is shown carboxyethylpyrrole. Structure drawn using website https://web.chemdoodle.com/demos/sketcher/

CEP adducts are generated naturally in the body and a transient increase is seen at the site of injury, with the level of CEP adducts peaking 3 days after injury and then dropping down to background levels[462]. CEP adducts have been reported to play a role in angiogenesis by inducing endothelial cell migration and adhesion in a vascular endothelial growth factor (VEGF) independent manner that is thought to be driven through TLR2 signalling via MyD88 and NF-κB[462]. In this same report the authors showed that administration of CEP-adducts could promote vascularisation in a mouse hind limb ischemia model. CEP adducts and their precursors are also thought to be important in the homeostasis of rod photoreceptor cell disk membranes, acting as markers of oxidative damage and facilitating endocytosis of the outermost disk membrane sections by retinal pigmented endothelial cells[474].

High levels of CEP adducts have been found in the eyes and blood of patients with AMD compared to healthy controls, with the combination of a high abundancy of docosahexaenoyl containing phospholipids in the eye and a highly oxidising environment likely the driving factors[475,476]. Autoantibodies to CEP adducts have been found in AMD patients and CEP is capable of binding to surface receptors and may act as a DAMP[476,477]. Immunisation of mice with CEP adducts has been shown to increase the level of anti-CEP antibodies and increase the sensitivity of mice to developing dry AMD with a development of drusen under the retinal pigmented epithelium, suggesting CEP adducts could contribute to the formation of drusen in this form of AMD[478]. CEP adducts have also been shown to be capable of inducing similar levels of corneal vascularisation

after laser induced injury as VEGF, highlighting their potential role in wet AMD, caused by increased vascularisation and blood vessel leakage in the eye[479].

Increased levels of CEP adducts have been found in melanoma in both mouse and human tumours, as well as in aging tissues[462,480]. The importance on the angiogenic potential of CEP adducts as mentioned above was further demonstrated in this same work with the finding that treatment with anti-CEP antibodies reduced tumour size and vascularity in a melanoma model (B16-F10)[462].

CEP adduct clearance has recently been attributed to its binding to the scavenger receptor CD36, as well as TLR2, expressed on the surface of macrophages, as knocking out these receptors almost completely abrogated the macrophages' ability to scavenge CEP modified proteins[480]. Macrophages that fall into the M2, anti-inflammatory class were shown to be more important for CEP adduct clearance. Furthermore, CEP has been shown to contribute to inflammation by acting synergistically with low dose TLR2 ligands to increase cytokine production of TNFα and IL-12a, and contribute to M1 macrophage skewing[481]. In light of these immunomodulatory properties of CEP, we decided to generate CEP modified rituximab in order to determine the effect this had on the effector functions.

4.6.2 Generation and Assessment of CEP Modification of Rituximab

Phospholipids containing the polyunsaturated docosahexaenoyl fatty acids can be oxidised to form oxidised phospholipids with active aldehyde functional groups (Figure 4-17). These aldehyde groups can then react with the epsilon amino group of lysine residues, followed by lipolysis of the intermediate oxidised phospholipid, leaving behind the CEP adduct on the lysine amino group[473]. In order to replicate this *in vitro*, chemical intermediates that are able to generate CEP structures on proteins of interest are used. Accordingly, 3mg of CEP intermediate was dissolved in 600µl of rituximab (8.4nmol) to form a solution. This CEP-rituximab mixture was incubated at room temperature on a shaker for 14 days, and was then dialysed into PBS and filler sterilised.

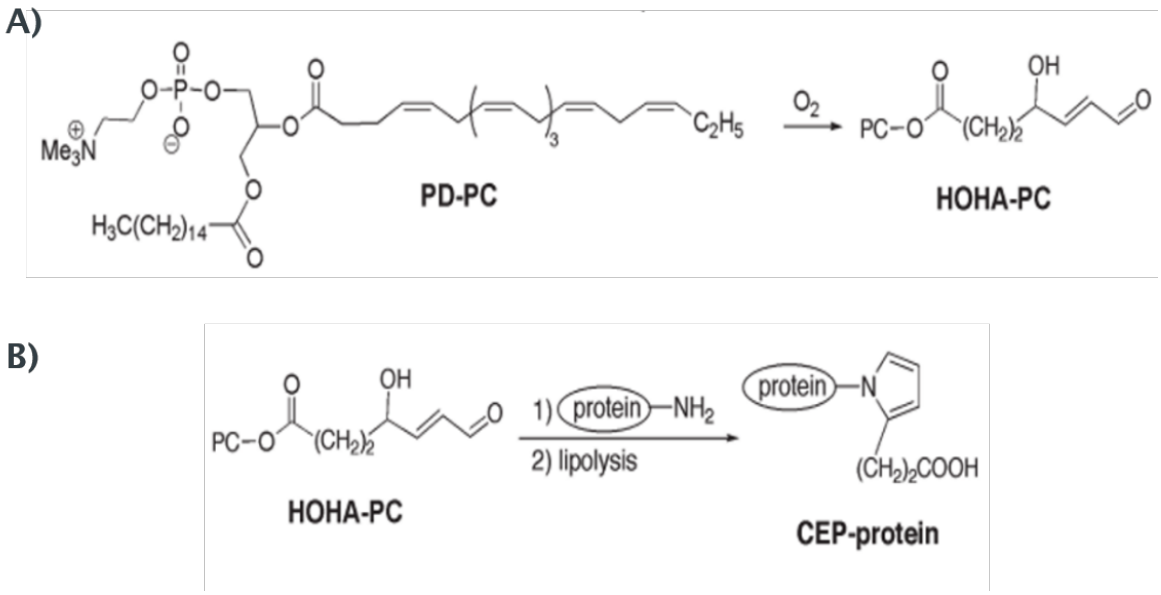

Figure 4-17 CEP Formation

CEP adducts are formed *in vivo* by oxidation of specific fatty acid chains. A- 1-palmityl-2-docosahexanoyl-sn-glycerophosphocholine (PD-PC) is a membrane phospholipid that contains a docosahexaenoyl fatty acid. Reaction of the docosahexaenoyl fatty acid with oxygen generates oxidised glycerophosphocholine containing 4-hydroxy-7-oxohept-5-enoic acid (HOHA-PC). B- reaction of this oxidised phospholipid adduct with a lysine residue and subsequent cleavage of the phospholipid forms the CEP-protein adduct. Figure modified from[476].

In order to assess the presence and degree of CEP modification that had been achieved, the rituximab sample was analysed by SDS-PAGE on a 10% gel, as for rituximab MDA. The gel was then stained with Coomassie Brilliant Blue and imaged.

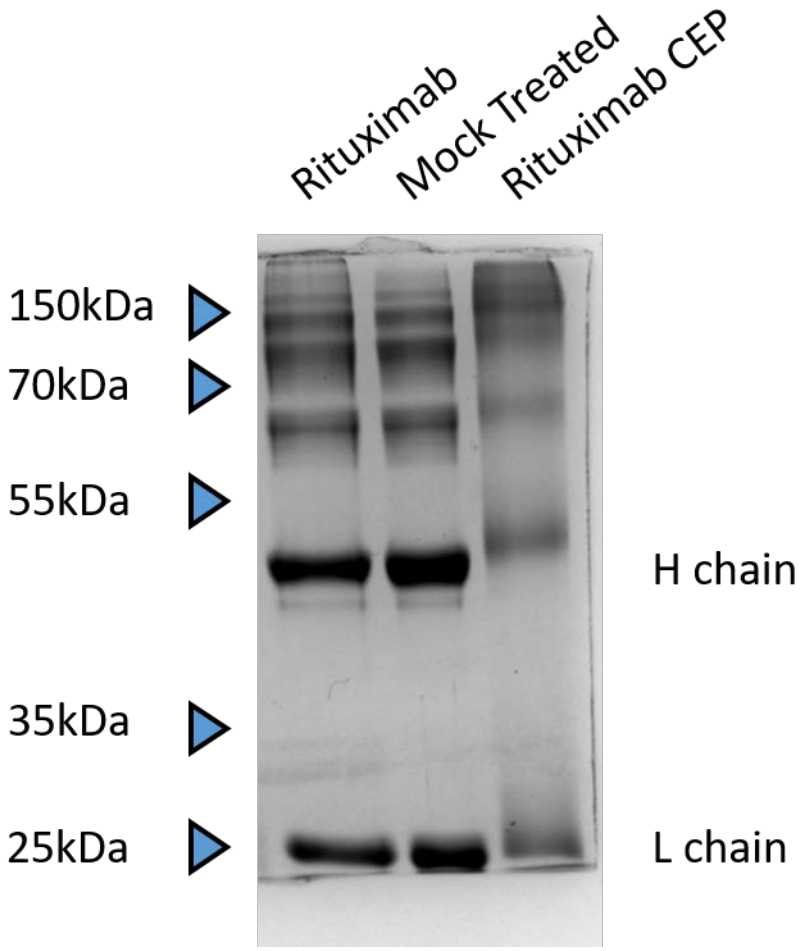

Figure 4-18 CEP Modification of Rituximab

Rituximab that was modified with CEP, mock treated or untreated was reduced in Laemmli buffer and analysed on a 10% SDS-PAGE gel for 2 hours at 110V. The gel was then fixed and stained with Coomassie Brilliant Blue prior to destaining and imaging. Heavy (H) and light (L) chains are indicated.

Figure 4-18 shows the resulting gel, and reveals that there was a small increase in mass for both the H and L chains of rituximab upon treatment with CEP compared to the mock treated sample. The top of the lane containing CEP treated rituximab appears darker than in the mock treated rituximab lane (Figure 4-18), suggesting the presence of a degree of aggregated antibody present within the sample, as was the case for rituximab MDA (shown in Figure 4-2). It appears from Figure 4-18 that all of the H chain has been modified as the entire band had shifted, as have the bands further up the gel which are most likely antibody molecules that have not been fully reduced. The L chain band appears to have also increased in size but is too close to the bottom of

the gel to be sure that the entire band has moved, or whether only a proportion of the L chain was modified.

4.7 Functional Assessment of CEP Modified Rituximab

4.7.1 Antigen Binding

To determine whether the rituximab CEP was still functional, its ability to bind to cells expressing target antigen was assessed (Figure 4-19). Rituximab CEP was able to bind to both Raji and Ramos cells, but at a lower level than was seen with mock treated rituximab or untreated rituximab.

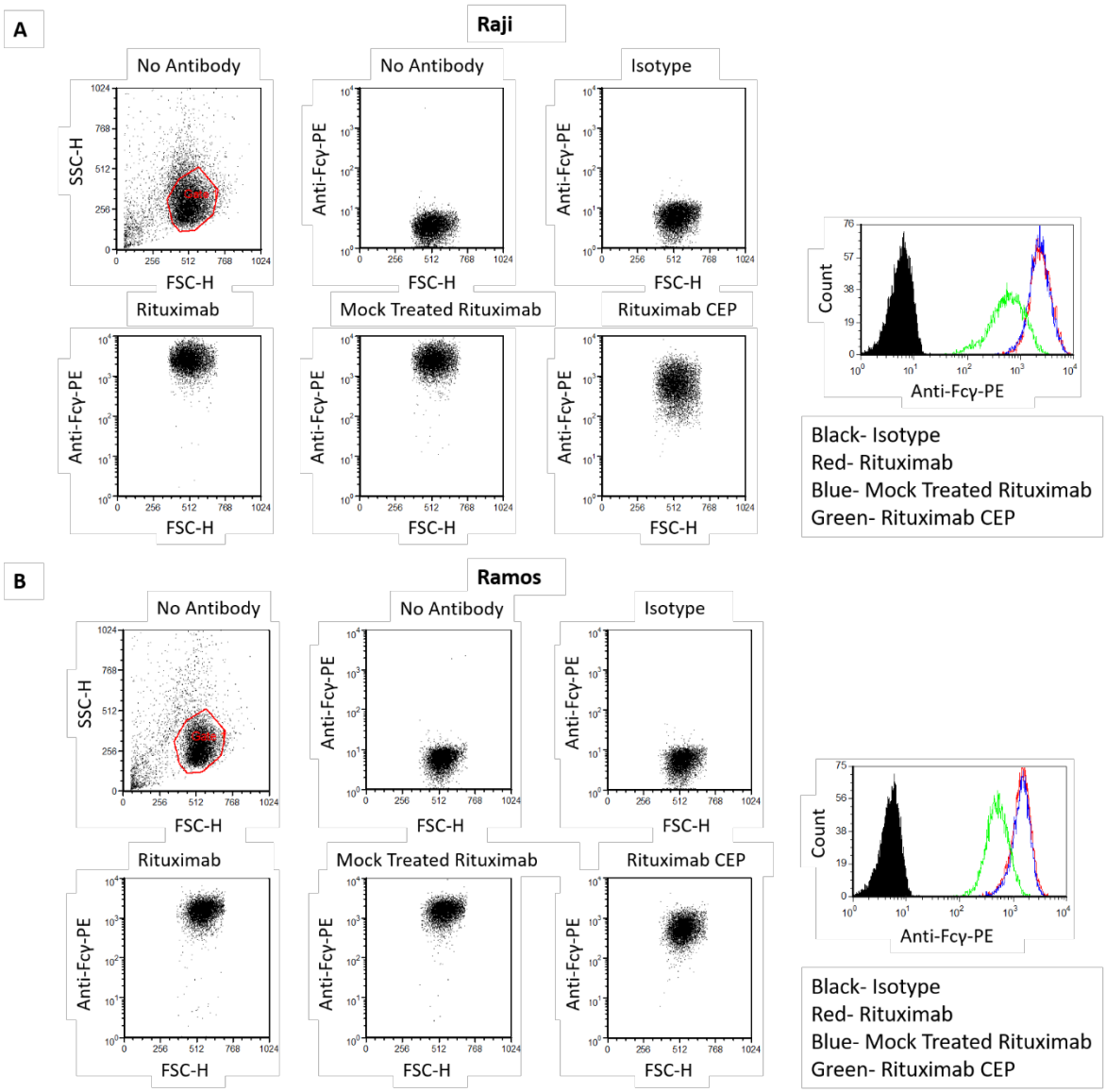

Figure 4-19 Ability of Rituximab CEP to Bind Target Cells

Raji (A) and Ramos (B) cells were opsonised with 10µg/ml of untreated rituximab, mock treated rituximab, rituximab CEP or an irrelevant control antibody. Unbound antibody was washed away and bound antibody was detected using a labelled polyclonal secondary $F(ab')_2$ specific for human IgG Fc. Cells were acquired by flow cytometry and gated on live cells as shown.

To confirm that this binding to target cells was antigen specific, the ability of rituximab CEP to block the binding of unmodified rituximab was tested, as performed for the MDA modified antibodies in Figure 4-4. Rituximab CEP was able to block the binding of FITC labelled rituximab to target antigen, but to a lesser extent than the same concentration of unmodified and mock

treated rituximab (Figure 4-20). This finding, as in Figure 4-19, implied that rituximab CEP retains specific target antigen binding, but to a lesser extent than unmodified rituximab.

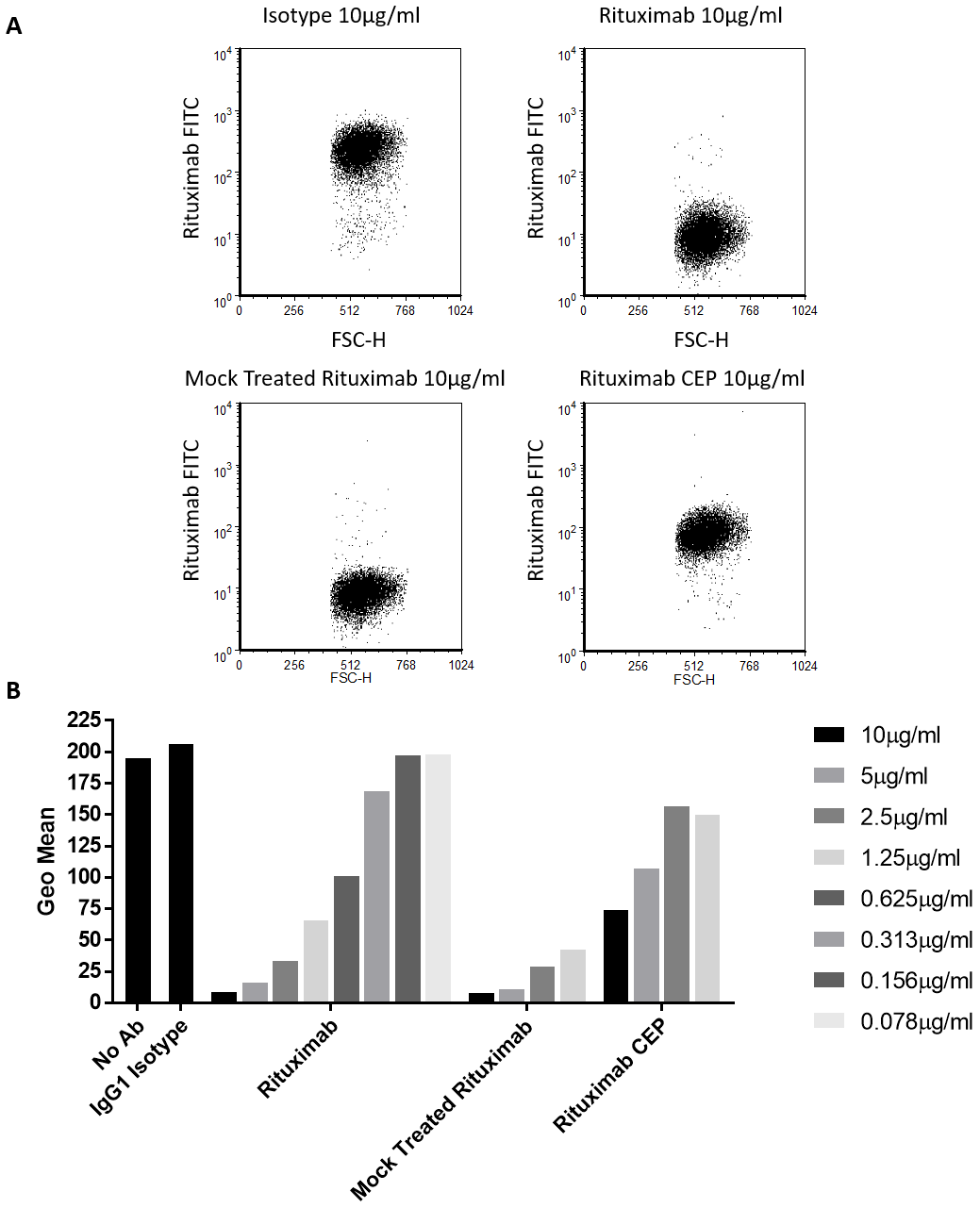

Figure 4-20 Ability of Rituximab CEP to Block Secondary Rituximab Binding

Ramos cells were opsonised with untreated rituximab, mock treated rituximab, Rituximab CEP or an irrelevant control antibody (concentrations as indicated) and unbound antibody washed off. A labelled anti-CD20 antibody (rituximab) was then applied at 10µg/ml to bind any free CD20. Excess antibody was washed off and the cells acquired by flow cytometry gated on live cells. A- example data of rituximab FITC binding to cells pre-opsonised with the indicated treatment. B- Data shown represent a single measurement of the geometric mean of rituximab FITC binding to pre-opsonised cells, representative of two independent experiments.

As for rituximab MDA shown above, given the observed reduction in binding, it was more useful to compare rituximab CEP to unmodified rituximab when an equivalent level of Fc was present at the cell surface for each antibody. As such, rituximab CEP binding was compared to a titration of unmodified rituximab. Figure 4-21 shows the titration experiment carried out with rituximab CEP, and reveals that the level of detectable Fc present following opsonisation with 10µg/ml rituximab CEP was approximately equal to that seen with 1µg/ml untreated rituximab, suggesting that rituximab CEP was binding at approximately 1/10th of the amount of untreated rituximab.

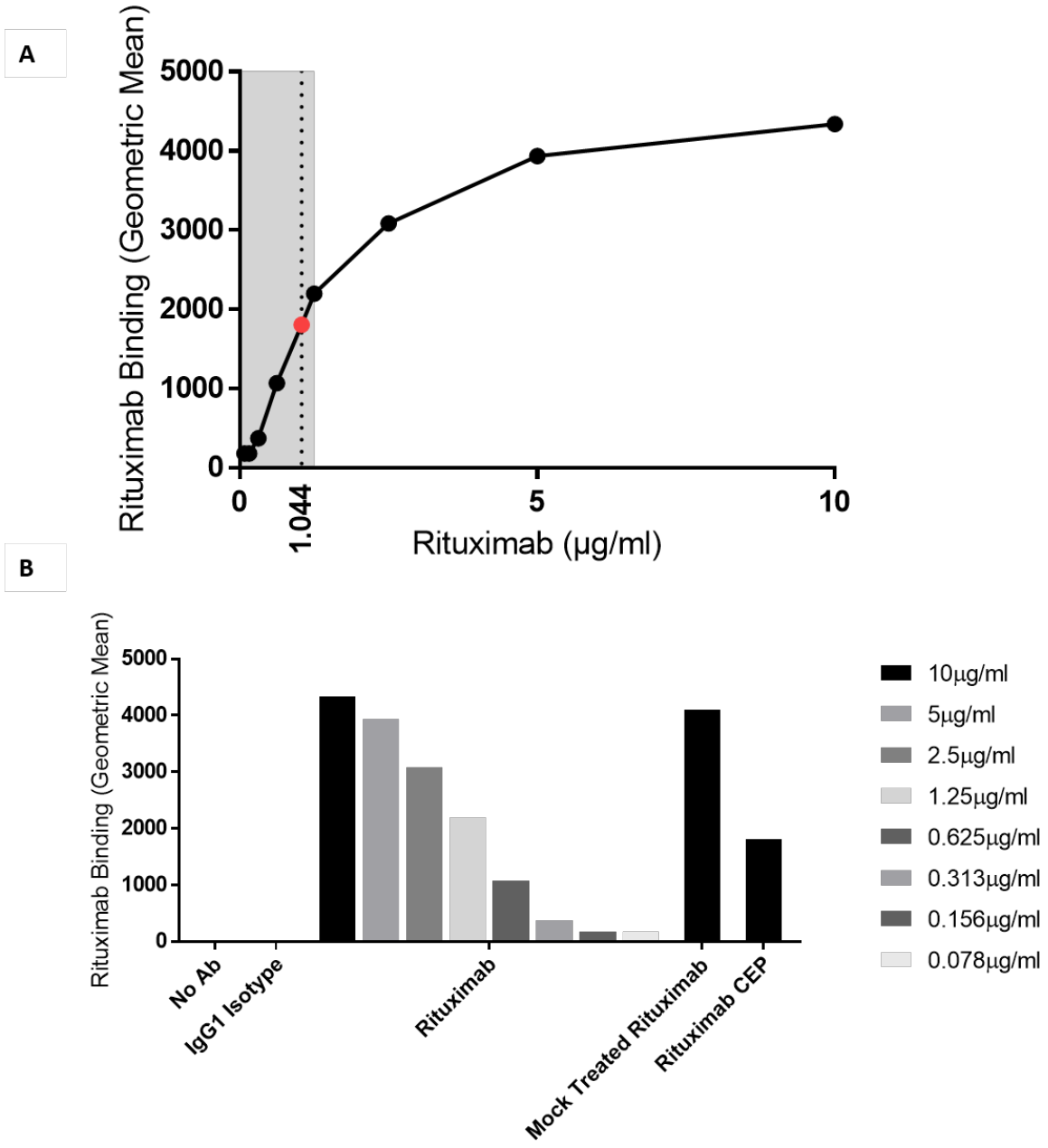

Figure 4-21 Determining Relative Concentration of Functional Antibody for Rituximab CEP Compared to Unmodified Rituximab

Ramos cells were opsonised with a serial dilution of rituximab (MabThera) starting at 10µg/ml. Unbound antibody was washed off and bound antibody detected using a labelled polyclonal $F(ab')_2$ secondary specific for human IgG Fc. Cells were acquired by flow cytometry. A- binding of Rituximab CEP (10µg/ml, red dot) compared to untreated rituximab (MabThera, black dots). The apparent concentration of rituximab CEP at 10µg/ml (1.044µg/ml) was calculated from the linear region of the standard curve (shaded region). B- binding of 10µg/ml rituximab CEP relative to a titration of untreated rituximab (10µg/ml – 0.08µg/ml) from a single experiment, representative of 2 independent experiments.

4.7.2 FcγR Binding of CEP Modified Rituximab

Next, the ability of rituximab CEP to bind to FcγRs was tested using CHO-K1 cells stably transfected with various FcγRs. As can be seen from Figure 4-22 rituximab CEP showed some non-specific binding to non-transfected CHO-K1 cells. This makes assessing the binding to FcγRs difficult to interpret, but there did appear to be an increase in the binding of rituximab CEP for several of the FcγRs, most notably FcγRI and FcγRIIb.

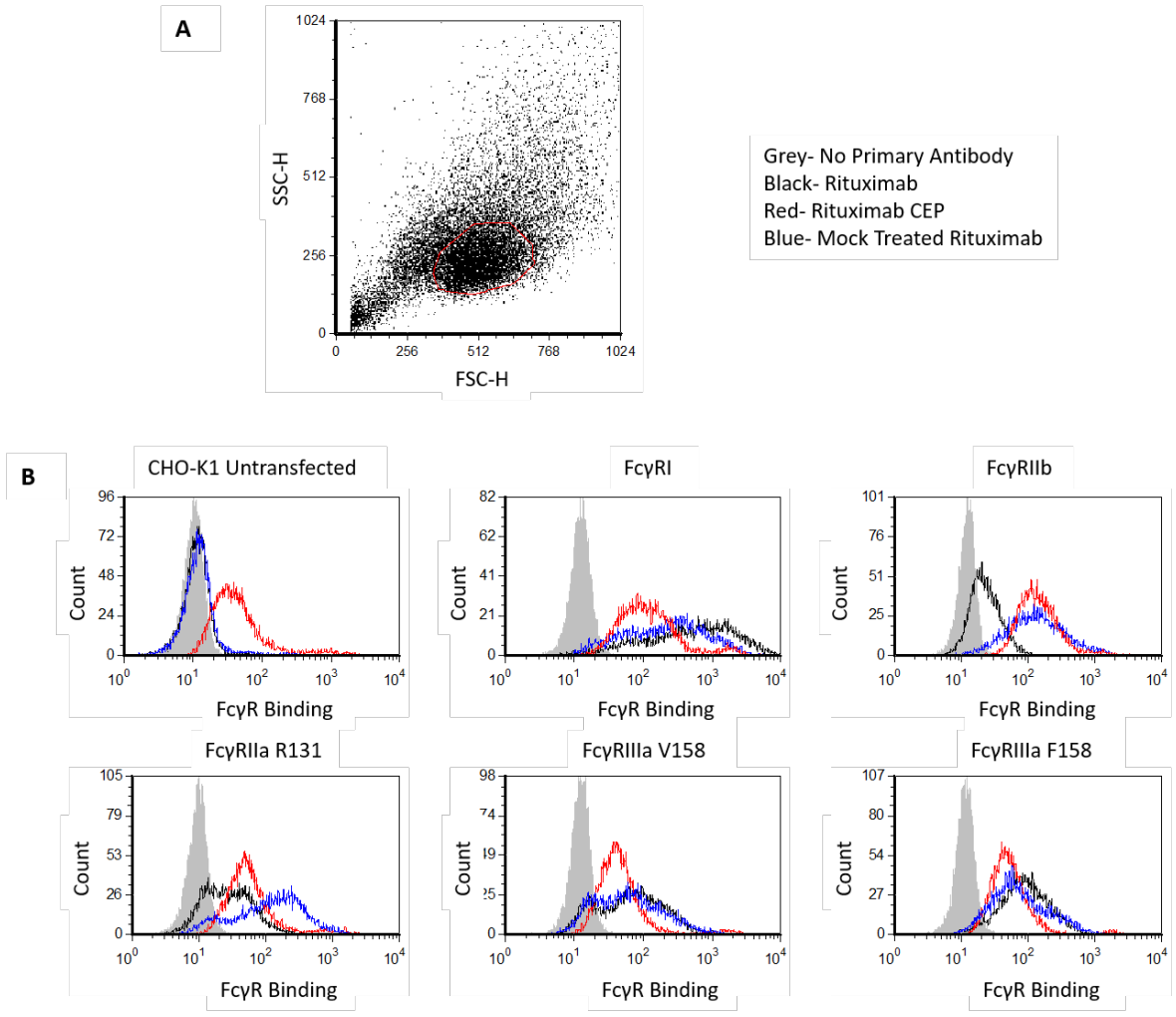

Figure 4-22 Ability of Rituximab CEP to Bind to FcγRs Expressed on CHO Cells

Rituximab CEP (red), mock treated rituximab (blue), untreated rituximab (MabThera, black) and an isotype control were applied at 20µg/ml to CHO-K1 cells stably transfected with human FcγRs I, IIa (R131 allele), IIb, or IIIa (both V158 and F158 alleles) as well as to untransfected CHO-K1s in order to assess binding. After washing away unbound antibody, bound antibodies were detected using a labelled secondary $F(ab')_2$ specific for human IgG Fc, and cells acquired by flow cytometry and gated on live cells. A- gating of live CHO-K1 cells. B- overlaid histograms of the relative binding of rituximab, mock treated rituximab and rituximab CEP to CHO-K1 cells transfected with the indicated FcγR. Data from a single experiment, representative of two independent experiments.

4.7.3 Complement Dependent Cytotoxicity

Next the effect CEP modification had on the ability of rituximab to function via its Fc domain was assessed. Firstly its CDC inducing potential was determined (Figure 4-23). Even accounting for its reduced binding (a 10x dosage compensation was applied – calculated from Figure 4-21), rituximab CEP induced very little CDC compared to untreated or mock treated rituximab.

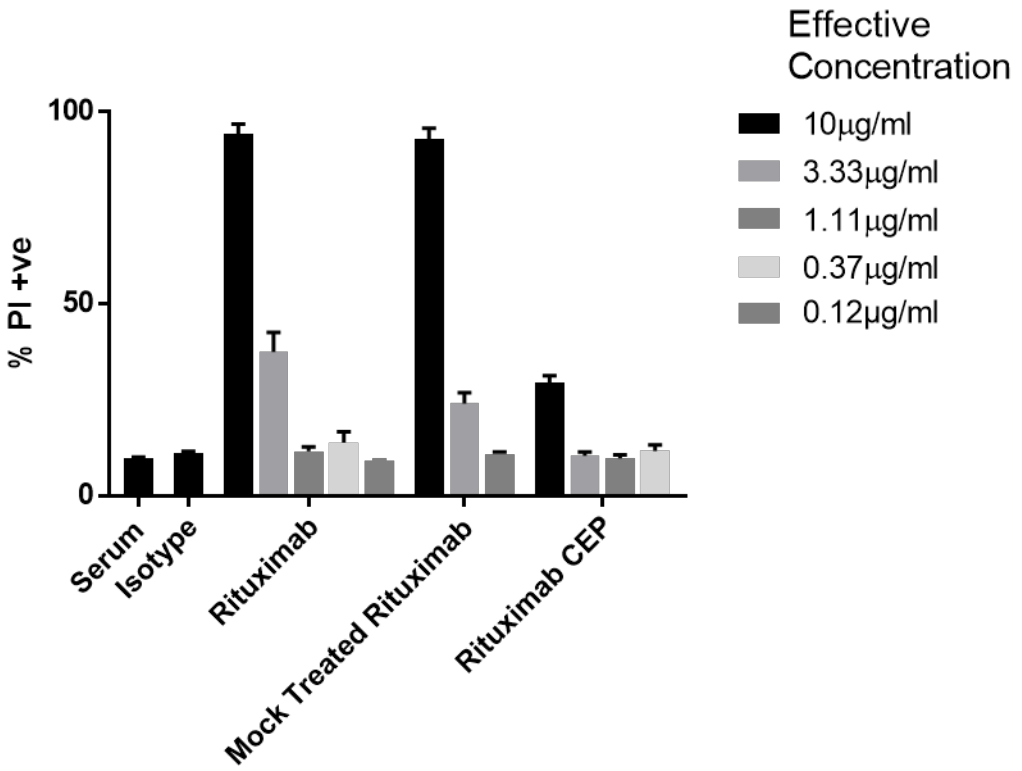

Figure 4-23 Ability of Rituximab CEP to Induce CDC at Equivalent Effective Binding Concentrations as Unmodified Rituximab

Ramos cells were opsonised with various concentrations of rituximab CEP, mock treated rituximab, untreated rituximab or an isotype control as indicated prior to a 30 minute incubation with 30% human serum and complement dependent cytotoxicity was identified by propidium iodide staining. Rituximab CEP doses were adjusted to correct for the approximately 10 fold reduced target binding in order to give comparable levels of functional Fc to untreated rituximab, according to Figure 4-21 and as described in the main text. Mean plus range of triplicate repeats of a single experiment are shown.

4.7.4 Antibody Dependent Cellular Cytotoxicity

The effect of CEP modification of the FcγR dependent effector functions ADCC and ADCP of rituximab was next assessed. Figure 4-24 shows the results for the ADCC experiments. Rituximab CEP gave a broadly similar level of ADCC to that of the dose matched level of unmodified rituximab- i.e. 20µg/ml CEP modified rituximab gave a similar level of ADCC to 2µg/ml unmodified rituximab. However, the ADCC effect of rituximab CEP titrated more sharply than that observed with unmodified or mock treated rituximab.

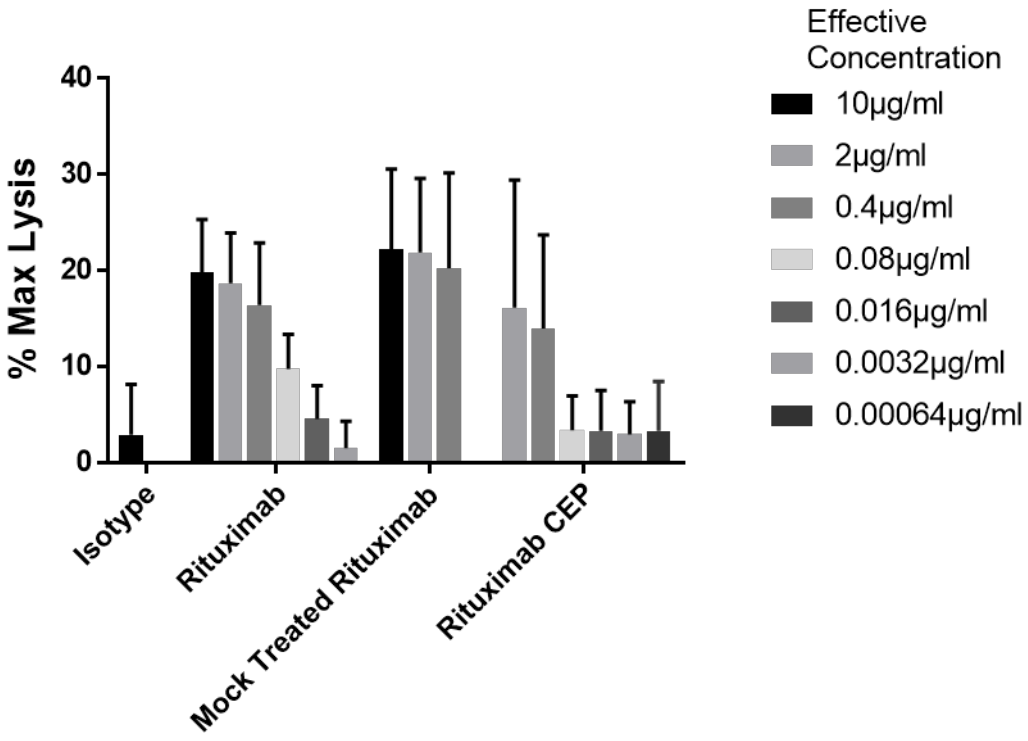

Figure 4-24 Ability of Rituximab CEP to Induce ADCC at Equivalent Effective Binding Concentrations as Unmodified Rituximab

Calcein labelled Ramos cells were opsonised with various concentrations of rituximab CEP, mock treated rituximab, untreated rituximab (MabThera) or an isotype control as indicated. Opsonised targets were co-cultured with freshly purified human PBMCs at a ratio of 50 PBMCs per target cell for 4 hours, and the supernatants analysed for released calcein by measuring their emission at 515nm. Max lysis was calculated as percentage of maximum once background (non-opsonised targets and effectors) was removed according to the equation % of Max Lysis = (X – background)/(Max Lysis – background)*100. Rituximab CEP doses were adjusted to correct for the approximately 10 fold reduced target binding in order to give comparable levels of functional Fc to untreated rituximab. Data presented are the combined means + SD of 3 independent experiments using different PBMC donors.

4.7.5 Antibody Dependent Cellular Phagocytosis

Rituximab CEP was next tested for its ADCP inducing potential, using MDMs differentiated from peripheral blood. Dose corrected CEP modified antibody exhibited reduced phagocytosis compared to unmodified and control treated rituximab, although statistical significance was not reached (Figure 4-25). ADCP with CEP modified rituximab did not titrate over the concentrations tested, but was significantly greater than that seen with the isotype control, indicating that phagocytosis was indeed occurring.

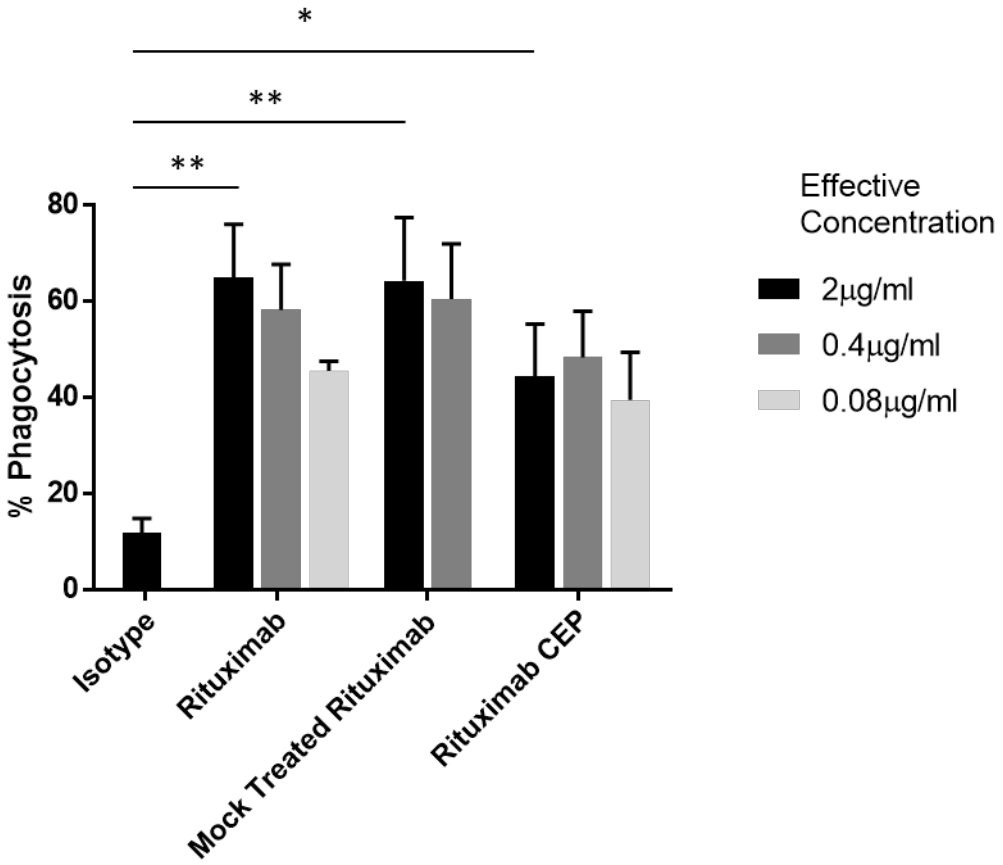

Figure 4-25 Ability of Rituximab CEP to Induce ADCP at Equivalent Effective Binding Concentrations as Unmodified Rituximab

Ramos cells were labelled with CFSE and opsonised with various concentrations of either Rituximab CEP, mock treated rituximab, untreated rituximab (MabThera) or an isotype control. Opsonised cells were co-cultured with MDMs for 1 hour, macrophages stained and acquired by flow cytometry. Rituximab CEP doses were adjusted to correct for the approximately 10 fold reduced target binding in order to give comparable levels of functional Fc to untreated rituximab. The percentage of macrophages that had phagocytosed a target cell was calculated as a percentage of CD14+ cells. Data plotted are mean + SD of three independent experiments using different MDM donors, each measured in triplicate. Statistics calculated by one-way ANOVA with multiple comparisons, * $p<0.05$, ** $p<0.01$.

4.8 Discussion

In this chapter the generation and characterisation of two separate potential chemical modifications to antibodies was assessed, namely malondialdehyde and carboxyethylpyrrole. Oxidation specific epitopes have been recognised as being important for recognition of oxidised and apoptotic cells, and can act as DAMPs in order to recruit elements of the innate immune system[482]. Natural antibodies of the IgM class that bind to these oxidation specific epitopes such as MDA have been found in both mice and humans, including those of foetal origin[483]. Apoptotic cells can have an increased level of oxidation specific epitopes on their surface that can promote phagocytosis by nearby macrophages through scavenger receptors such as CD36, as well as being a target for antibodies[477,484]. MDA modified proteins have also been found to be able to induce inflammatory responses in immune cells[485]. Moreover, MDA modifications can be found on serum proteins and at the site of tumours[462].

In this work MDA was used to modify the anti-CD20 antibody rituximab to see what impact this had on antibody functionality. Modified antibodies could indeed be generated (Figure 4-2) with an increased molecular weight compared to untreated controls. The lack of unmodified H or L chains on SDS-PAGE analysis suggests that all antibody molecules had been modified by the MDA treatment. The level of modification cannot be judged accurately from Figure 4-2, but the location of the staining at the top of the gel suggests that there may be highly crosslinked and or aggregated antibody present.

Such extensive modification is unlikely to occur *in vivo* under physiological conditions as it has been reported that the plasma concentration of MDA is in the micromolar range, compared with the millimolar levels used here[471]. Furthermore, the *in vivo* time scale for MDA modification is likely to be far longer than the 5hrs used in Figure 4-2. It was previously demonstrated that using different MDA concentrations and time courses influences the level of MDA modification that occurs[471]. Millanta *et al.* suggested that the use of millimolar MDA concentrations produces qualitatively different modifications to those generated with micromolar levels of MDA, although convincing differences were not demonstrated. Regardless, as a proof of concept that MDA modification of antibodies can alter their efficacy, the approach used in this chapter is of relevance.

It is not surprising that such a harsh treatment of antibody that causes a major change in their size had a profound effect on their ability to function. However, functional antibody molecules that

were still able to bind to their target antigen remained (Figure 4-3). Judging from Figure 4-2 it appears that all antibody molecules were modified, implying that the fraction of functional antibodies that remained were indeed modified. MDA modification preferentially targets the epsilon amino group of lysine residues, which are present throughout the primary structure of antibodies (Figure 4-26). As shown below in Figure 4-26, rituximab does not contain any lysine residues within its CDRs, but does in the framework regions of its variable domains. The lack of lysine residues present in the CDR loops does not protect rituximab's target binding properties following modification, as seen through reduced binding to CD20 compared to controls (Figure 4-3). This is potentially due to structural changes and antibody aggregation caused by MDA modification of lysine residues throughout the rest of the molecule causing secondary structural effects.

A

Antibody	Target	Isotype	H- chain	L- chain
Cetuximab	EGFR	IgG1	33	11
Trastuzumab	HER2	IgG1	32	13
Rituximab	CD20	IgG1	36	13
Alemtuzumab	CD52	IgG1	32	15
Ipilimumab	CTLA4	IgG1	31	11
Pembrolizumab	PD1	IgG4	31	12
Nivolumab	PD1	IgG4	29	11
Natalizumab	α4 integrin	IgG4	30	13
Evolocumab	PSCK9	IgG2	29	12
Denosumab	RANKL	IgG2	32	11
Panitumumab	EGFR	IgG2	29	13

B

Antibody	Target	Isotype	Framework	CDRs
Cetuximab	EGFR	IgG1	8	0
Trastuzumab	HER2	IgG1	8	1
Rituximab	CD20	IgG1	13	0
Alemtuzumab	CD52	IgG1	8	3
Pertuzumab	HER2	IgG1	9	0
Panitumumab	EGFR	IgG2	9	0

Figure 4-26 Lysine Residues of Clinically Approved IgG

Panel showing the number and position of lysine residues within the primary sequence of a number of therapeutic antibodies. A) Shows the number of lysine residues in individual heavy and light chains for a number of clinically approved IgG antibodies of different isotypes. B) Shows the number of lysine residues present in the framework and CDR regions of a number of clinically approved antibodies. EGFR- epidermal growth factor receptor, CTLA4- cytotoxic T-lymphocyte associated protein 4, PD-1- programmed death 1, RANKL- receptor activator of nuclear factor kappa-B ligand, PSCK9- proprotein convertase subtilisin/kexin type 9, HER2- human epidermal growth factor receptor 2. Figure modified from[486].

MDA modified antibody was able to bind to all FcγRs tested (Figure 4-6), with similar binding to mock treated antibody for FcγRIIIa (V158 and F158), reduced binding to FcγRI, and increased binding to both FcγRIIa (R131) and FcγRIIb. It is difficult to be sure whether or not these differences are due to the level of aggregation of the antibody and the relative differences in binding of monomeric vs. aggregated antibody for different FcγRs, or whether the MDA modifications themselves are affecting the Fc region recognised by the FcγRs. Residues 234-237 (Leu-Leu-Gly-Gly) of IgG1 are important for interactions with FcγRs[342]. However, as for the CDRs mentioned above, MDA modification to lysine residues elsewhere in the hinge/CH2 domain (of which there are several) could impact the FcγR binding region structure or flexibility. Indeed, the regions of IgG that are most important for FcγR binding, the hinge region and upper CH2 domain, are exposed to the environment to facilitate FcγR binding, thereby increasing the chance that lysine residues present will be modified[487-489].

A consequence of alterations in FcγR binding could be changes in the efficacy of the antibody to elicit Fc mediated effects. As well as FcγRs, IgG Fc also interacts with C1q, the initiator of the classical complement cascade. C1q binds to an overlapping but distinct epitope on the lower hinge region of IgG, and it is likely that if MDA modifications have altered the secondary structure around where the FcγRs bind then the binding of C1q would also be affected. Furthermore, it has been reported that several residues are important for human IgG1 binding to C1q, one of which is a lysine (Lys322), with another lysine residue present at position 320 that is important for mouse IgG2b binding to C1q, but plays no role in the binding of human IgG1[196]. Another lysine residue (Lys326) in the same region can be mutated to increase CDC, and lysine residues are also present at position 317, 334, 338 and 340[489,490]. As such, MDA modification of available lysine residues in this region may be expected to impact upon the antibodies ability to elicit CDC.

This was shown to be the case, with rituximab MDA giving no complement dependent cytotoxicity compared to an equivalent dose of mock treated rituximab that gave efficient killing (Figure 4-7 and Figure 4-8). Complement activation is thought to be based upon antibody Fc clustering on the target surface, and as such, IgM is the most efficient antibody at inducing CDC due to its high number of Fc domains[6]. It could be suggested that aggregation of IgG molecules by MDA treatment would increase the number of Fc regions present at the target surface. However, the clearly decreased level of CDC would indicate that this potential increase in the number of available Fc regions did not enhance CDC. The abundance of lysine residues in and around the C1q binding area suggests that it is highly likely some of these solvent accessible residues have been

modified, which may explain why complement mediated killing was decreased. In addition, aggregation of rituximab by MDA crosslinks may affect the orientation of the antibodies and affect their ability to form the hexameric structures necessary for C1q interaction[80].

Although reduced compared to mock treated rituximab, rituximab MDA did show specific target binding (exemplified by its ability to block rituximab binding (Figure 4-4)). Attempting to scale the dosage of rituximab MDA to get equivalent levels of functional Fc on the target cell surface allows for a more direct comparison between the ability of unmodified and MDA modified antibody to induce complement mediated killing. Figure 4-9 showed that there was a restoration of CDC when a dosage correction was applied, but it did not completely rescue CDC to the level of untreated rituximab. As discussed, a subpopulation of rituximab MDA that is able to bind to CD20 but is modified in its C1q binding domain could be responsible for this difference. Whether rituximab MDA is reduced in its capacity to bind to C1q or form hexameric structures, or at another stage in initiating the complement cascade, is not clear. In order to resolve this C1q binding to rituximab MDA and mock treated rituximab would need to be measured.

MDA has been shown to bind to complement factor H in a manner that protects MDA modified proteins from uptake by macrophages[491]. Complement factor H is a serum protein that would be present in the assays performed in this chapter when serum is added to the opsonised target cells, which could result in blockage of the C1q molecule binding to MDA modified rituximab. To determine if this is happening, C1q binding in the presence and absence of complement factor H could be measured.

Syngeneic *in vivo* mouse models using immunocompetent mice have suggested FcγRs as being essential for rituximab mediated target depletion, rather than complement[470]. Accordingly, rituximab MDA was also evaluated for its FcγR dependent effector functions. Examination of rituximab MDAs ADCC inducing potential revealed a decrease in antibody efficacy, which could be mostly restored by dosage compensation to give approximately similar levels of functional antibody Fc at the cell surface (Figure 4-10). Rituximab MDA was also evaluated for ADCP, and was found to be poorer at ADCP than mock treated rituximab even with dose compensation (Figure 4-11). This was surprising, given the finding that the binding of MDA modified rituximab to FcγRIIa was greater than that of untreated rituximab, and this receptor is expressed on macrophages. In contrast, MDA modified rituximab had equal binding to FcγRIIIa compared to untreated rituximab and performed as well in ADCC after dose compensation (Figure 4-6). ADCC is

mediated via NK cells, which express FcγRIIIa but typically no other FcγRs[492]. Therefore, it would be expected that rituximab MDA would perform as well in ADCC but better in ADCP.

A possible explanation for this discrepancy could be that the FcγR binding was done in the absence of target antigen, so the proportion of the antibody that binds to FcγRs that is also able to bind to target antigen is unknown. Rituximab MDA also displayed increased binding to the inhibitory FcγRIIb, which is also expressed on macrophages, which could explain the reduced ADCP. Furthermore, although FcγRs all bind to the same region of IgG they bind in slightly different ways- as exemplified by the finding that FcγRIIIa interaction with IgG1 involves the sugar residues present on the receptor and that the presence of fucose on the N-linked glycan of the IgG disrupts this interaction by pushing molecules further apart[350]. As such, subtle differences in the FcγR binding between FcγRIIa and FcγRIIIa could explain the relative differences in the binding of rituximab MDA compared to the functionality.

It was shown that decreasing the concentration of MDA could also reduce the level of MDA modification that occurred- as could shortening the reaction time (Figure 4-13). A dose response effect could be seen using these antibodies for both target binding (Figure 4-14) and ADCC (Figure 4-15). However, it is not possible to deduce from these results whether the less reduced functionality of these modified antibodies is due to a reduced number of MDA modifications per antibody or a population of non-modified antibody that increases with the reduced MDA concentration and shorter incubation. As such, the differences in target binding and ADCC seen in Figure 4-14 and Figure 4-15 may simply reflect the amount of unmodified antibody present in each sample. For example, similar ADCC was seen with 10µg/ml and 1.1µg/ml unmodified rituximab, so if 10% of the rituximab MDA is unmodified it could be this subgroup of the antibody that is responsible for the comparable level of ADCC to untreated rituximab. This unmodified antibody would be expected to decrease when incubated for longer or with a higher level of MDA, which could explain the decreased ADCC seen with 3.3µg/ml rituximab MDA.

In order to try and resolve this issue and generate monomeric modified antibodies, several approaches are possible. One method could be to try and purify monomeric antibodies from MDA modified rituximab using size exclusion chromatography and collecting the peak (if present) corresponding to monomeric antibody. However, MDA is a small molecule and antibody molecules carrying only a few MDA adducts will be very similar in size to unmodified molecules, which may make them very difficult to separate. This could also be complicated by the shift in absorbance caused by MDA modification which could make it difficult to identify when peaks are

coming off of the column. Purified monomeric antibodies could then be checked via SDS-PAGE to see if the H and L chains have increased in size compared to untreated rituximab H and L chains, which would suggest MDA modification. Alternatively, anti-MDA antibodies could be used to see if MDA modification has occurred. Another method could involve purifying functional antibody by using a rituximab anti-idiotype antibody affinity column[443]. This would recognise the variable region of rituximab, which would have to be relatively unmodified in order to bind to the anti-idiotype antibody and to its target antigen. This would enable the purification of only those antibodies capable of binding to the target, but they would not necessarily be monomeric or capable of binding to FcγRs. Once again, purified antibodies could be checked for modification by SDS-PAGE or with anti-MDA antibodies.

CEP modification of proteins is known to have an important physiological role in wound healing and has been reported to be present at high levels in some tumours[462]. Therefore it is feasible that therapeutic monoclonal antibodies directed against tumour antigens could be modified by the tumour microenvironment.

Work in this chapter has shown that it is possible to modify IgG antibodies with CEP adducts (Figure 4-2). As discussed above for rituximab MDA, it is likely that the conditions used to carry out this modification are more harsh and extreme than those encountered by antibody molecules *in vivo*, but represents a useful starting point to try and identify if these oxidative modifications could in principle affect antibody efficacy at what are likely supraphysiological levels.

Rituximab CEP was capable of binding to target cells, as shown in Figure 4-19, albeit at a reduced level compared to unmodified or mock treated rituximab. Furthermore, the target binding specificity of these antibodies was maintained (Figure 4-20) after CEP modification, as these modified antibodies could block the binding of other anti-CD20 antibodies. Rituximab CEP showed non-specific binding to CHO-K1 cells even in the absence of FcγRs, which made interpretation of FcγR binding difficult, although some binding to FcγRI and IIb was evident (Figure 4-22). Binding to the high affinity FcγRI is not surprising but binding to the lowest affinity receptor FcγRIIb is less expected. It is possible from looking at the SDS-PAGE gel that there was some aggregation of Rituximab CEP, and this aggregated antibody could be responsible for the increased binding to FcγRIIb (although would also be expected to increase binding to other FcγRs). As detailed above, CEP adducts have been reported to interact to several surface proteins, including TLR2 on macrophages and endothelial cells, as well as scavenger receptors including CD36 also expressed

on macrophages[462,480]. Whether CEP is binding to such a molecule on the surface of the CHO-K1 cells is unknown.

CEP modification of rituximab was analysed to see if there was an effect on Fc mediated effector functions. Firstly, the CDC inducing potential of rituximab CEP was tested. Figure 4-23 showed that even when the dose was corrected to give an equivalent level of Fc to unmodified rituximab, rituximab CEP induced less CDC. As for Rituximab MDA, this is likely due to CEP modifications within, or in the vicinity of, the C1q binding site of rituximab. There are several lysine residues within this binding site which could have been modified by CEP. In addition, the faces of rituximab that pack together to form the hexameric structure required for efficient complement binding could also be modified by CEP molecules, which may affect the tight hexameric packing[80].

FcγR dependent effector functions ADCC and ADCP were also investigated to see what effect CEP modification of rituximab had. Both of these effector functions were reduced compared to unmodified and mock treated rituximab, even after dose correction was applied (Figure 4-24 and Figure 4-25). Once again, in a similar manner to MDA modification discussed above, CEP modifications are likely present near to or within the FcγR binding site of rituximab, or are having an effect on the structure of this only partially ordered region. Figure 4-2 suggests that all H chain molecules have been modified, meaning that those molecules that still bind to target do have CEP modifications on their H chains somewhere, and that these could fall within the lower hinge and upper CH2 regions, that interact with FcγR. Furthermore, it is possible that the CEP adducts could interact with other molecules on the surface of the effector cells, for example CD36 or TLR2 on the MDMs.

In summary, lipid modification of the anti-CD20 mAb rituximab in the form of MDA adduction and CEP adduction was assessed and shown to reduce all of its principle functions: binding to its target CD20, as well as its ability to induce the effector functions of CDC, ADCC and ADCP. As mentioned, although the chemical *in vitro* approach taken here is supraphysiological, it provides the possibility that similar modification within the tumour microenvironment (or at other sites) would diminish the activity and efficacy of therapeutic mAbs. Therefore, it would be important to study these mAbs *ex vivo* to see if, and to what extent, these modifications are found and how they impact the effector functions of the mAb. This could then be used as a model system in which to assess the effectiveness of different mechanisms for protecting mAbs from such modifications.

Chapter 5: Antibody Glycosylation

5.1 Introduction

As discussed earlier (Section 1.7.2), the N-linked glycosylation site of the Fc region of IgG1, Asn297, has been shown to be essential for effective IgG function. For example, treatment of hybridoma cells with tunicamycin, which blocks formation of the N-glycan precursor, resulted in the production of aglycosylated mouse IgG that retained their ability to bind to target antigen and protein A, but showed no activation of complement, binding to macrophage FcγRs or ADCC[493,494].

Different glycoforms of human IgG1 have been linked to different functions, some pro-inflammatory and some anti-inflammatory. For example, antibodies with reduced fucose content have an increased FcγRIIIa binding affinity and induce more effective ADCC, whereas sialylated antibodies are proposed to be an important component of the anti-inflammatory properties of IVIg and have also been reported to increase during pregnancy, associated with the reduction of symptoms of rheumatoid arthritis patients observed during pregnancy[351,372,379]. The heterogeneity of IgG glycans both natively *in vivo* and of recombinantly produced IgG have complicated the analysis of the influence of these different glycoforms on antibody effector function, and leave unanswered the question of what glycoforms are most appropriate for therapeutic monoclonal antibodies. Generating antibodies of highly pure glycoforms would help to study the functional roles of these different glycans and potentially produce more effective mAb therapeutics.

There are various methods that can be employed to generate IgG with different glycan compositions. One such method is the use of genetically modified cell lines for production, as is the case for the glycomodified clinically approved antibodies mogamulizumab, benralizumab and obinutuzumab[279,362,395]. This method of production has the advantage of offering a high degree of control over the homogeneity of product glycosylation achieved- for example producing antibodies in a cell line that has had the fucosyltransferase (*FUT8*) knocked out will not contain any fucose residues[359]. However, a disadvantage of this method is that it requires the production of antibodies in the specific engineered cell lines, which may have a reduced yield or may require different media or growth conditions compared to other cell lines optimised for high efficiency antibody production.

A potential method of alleviating this problem, while maintaining a high level of homogeneity of glycosylation, is to produce the antibodies in a standard cell line, optimised for high yield production, purify them as normal and then perform *in vitro* glycoengineering. In this method, the glycans are modified using recombinantly produced glycosyltransferases in order to achieve the desired glycoforms. This method in theory allows for both high yield production of antibody, and a high degree of control over the degree of heterogeneity of glycosylation present.

In this chapter *in vitro* glycoengineering using recombinant glycosyltransferases was used to generate monoclonal antibodies with defined glycoforms, which were tested in a series of assays to determine the effect of the glycoengineering on their Fc mediated effector functions.

5.2 Generation of Glycomodified Antibodies

In order to see what effect this post-production enzymatic method of glycomodification has on the efficacy of therapeutic antibodies, the well characterised anti-CD20 antibody rituximab was selected. This antibody was subjected to glycomodification using the recombinant enzymes β- 1,4 galactosyltransferase and α- 2,6 sialyltransferase, combined with their respective activated nucleotide sugar substrates uridine 5' UDP-Gal and cytidine 5' phospho-N-acetylneuraminic acid (CMP-NANA).

The first step was to buffer exchange rituximab into the reaction buffer (10mM $MnCl_2$, 100mM morpholineethanesulfonic acid (MES) (both Sigma Aldrich), pH6.5) using centrifugal filter units. UDP-Gal was made up in the same reaction buffer. The Galactosylation reaction was performed as follows: 10.75mM UDP-Gal, 31.2µM rituximab and 658nM β- 1,4 galactosyltransferase were incubated at 37°C for 24 hours, and the reaction was stopped by freezing at -20°C. These concentrations were chosen to give an approximate ratio of 5µg of β- 1,4 galactosyltransferase per mg of rituximab. A mock treated control was incubated for the same time course with the same concentrations of substrates but no enzyme.

In order for the α- 2,6 sialyltransferase enzyme to catalyse the addition of sialic acid residues on to the N-linked glycan, it requires that the arms of the glycan bear terminal galactose residues (Figure 5-1). Consequently, the sialylation reaction is carried out on the highly galactosylated product of the previous galactosylation reaction (Figure 5-1).

The sialylation reaction was initiated as follows: 1.81mM CMP-NANA, 24µM rituximab and 1.97µM α- 2,6 sialyltransferase were incubated at 37°C for 24 hours, and the reaction was stopped by freezing at -20°C. These concentrations were chosen to give an approximate ratio of 17µg of α- 2,6 sialyltransferase per mg of rituximab.

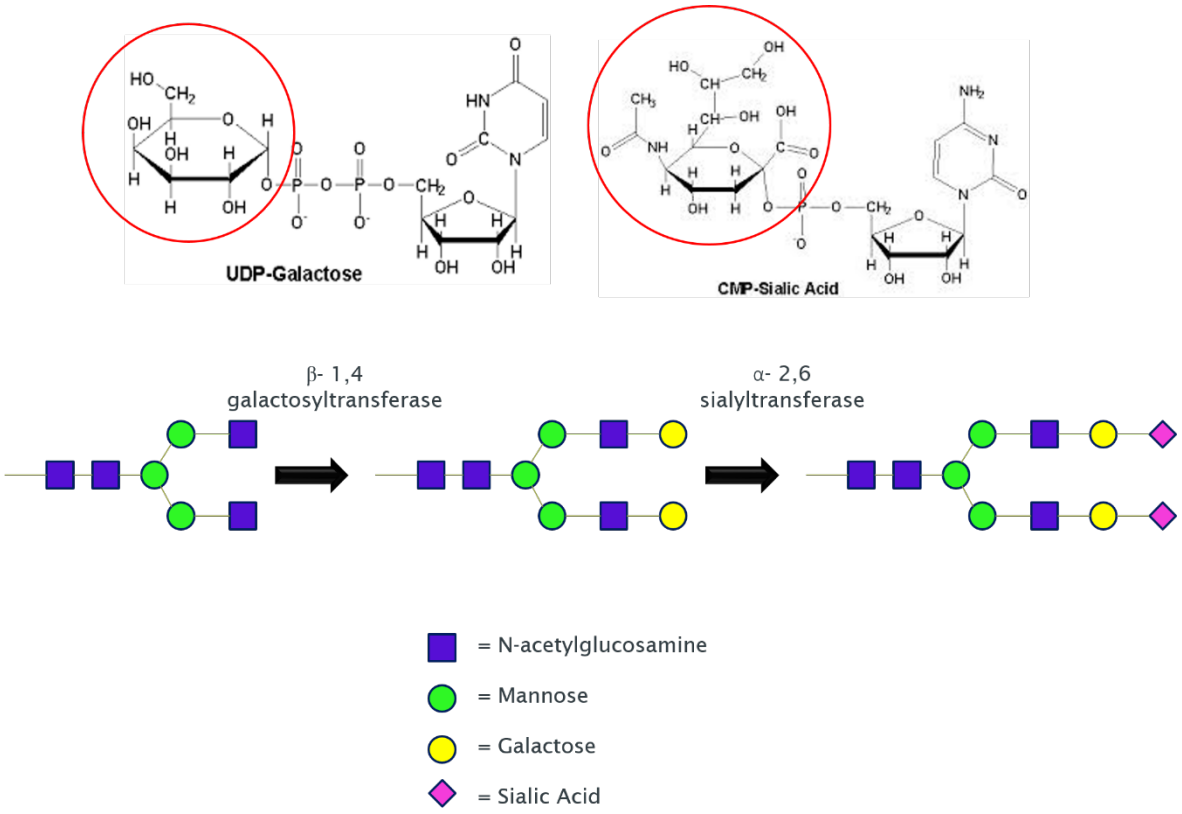

Figure 5-1 N-linked Glycosylation Modification Workflow

Schematic representation of enzymatic glycomodification workflow. Left- a typical core linked glycan consisting of the 7 conserved sugar residues. Addition of the glycosyltransferase β- 1,4 galactosyltransferase and its substrate, UDP-Galactose, catalyses the addition of galactose residues onto the GlcNAc residues of the biantennary arms. Treatment of this fully galactosylated glycan with the glycosyltransferase α- 2,6 sialyltransferase and its substrate, CMP-sialic acid, catalyses the addition of terminal sialic acid residues to the galactose residues of the biantennary arms of the glycan. The donor sugar molecule of each nucleotide sugar substrate is highlighted in a red circle.

After the glycomodification reactions, the glycomodified rituximab was purified to remove the glycosyltransferase enzymes and substrates in order to prevent any back reactions from occurring. This was achieved using protein A chromatography as described in Materials and Methods, and the capturing of maximal IgG was confirmed by performing native gel electrophoresis on the elution fraction as well as the flow through and wash fractions to confirm

all IgG had been recovered (Figure 8-2). This technique was used as it has been reported that even in the complete absence of the N-linked glycosylation it does not prevent the ability of protein A to bind to IgG. This is most likely because protein A binds to the CH2-CH3 interface region of IgG, whilst the glycan chain is buried in between the CH2 domains of the two heavy chains[493].

Antibodies were purified and dialysed into PBS and analysed by size exclusion HPLC to confirm that the modification process had not caused aggregation (Figure 8-3). Next it was necessary to determine the extent of glycomodification that had been achieved, both for the galactosylation and sialylation stages. Samples of each treatment, as well as the mock treated antibody, were sent to Hoffman La Roche, Penzberg, for analysis of the attached glycans by intact mass analysis of IdeS digested antibody.

Glycan	Control	Galactose	Sialic Acid
	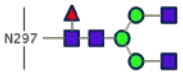	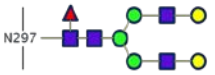	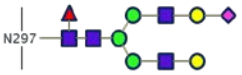
FG0	52%	-	-
FG1	40%	-	-
FG2	7%	100%	28%
FG2S1	-	-	59%
FG2S2	-	-	13%

Table 5-1 Results of Rituximab Glycomodification

The results of the glycoanalysis of enzymatically glycomodified rituximab as determined by IdeS digested intact mass spectrometry. Rituximab treated with β- 1,4 galactosyltransferase alone, β- 1,4 galactosyltransferase followed by α- 2,6 sialyltransferase, or mock treated (control) were analysed by mass spectrometry to determine the effect on glycosylation. Glycan diagrams represent the main species present within each condition. F= fucose, G= galactose= S= sialic acid.

As shown in Table 5-1 control, mock treated rituximab was completely fucosylated, as is typical for IgG produced in CHO cells, and was entirely absent of sialic acid[495]. Control, mock treated rituximab showed some heterogeneity with regard to the level of galactose present, with the majority of antibodies containing 0 (52%) or 1 (40%) galactose residue. Addition of galactose by β-1,4 galactosyltransferase was found to be highly efficient, generating a homogeneous product with 100% of antibodies containing 2 galactose residues. In contrast, addition of sialic acid showed a high degree of heterogeneity. Whilst 59% of antibodies subjected to sialylation carried a

single sialic acid, only 13% were found to contain 2 sialic acid residues, and 28% of these antibody molecules contained no sialic acid residues and were still of the FG2 glycoform.

In order to produce a greater yield of bi-sialylated antibody, changes were made to the sialylation protocol. Also, an additional antibody was included in the workflow to determine whether there were differences in the efficiency of glycomodification of different antibodies: the type II antibody obinutuzumab (which already contains a degree of glycoengineering from the cell line it is produced in). A higher ratio of α- 2,6 sialyltransferase per mg of antibody was used to achieve a higher level of sialylation- an approximate ratio of 27µg of α- 2,6 sialyltransferase per mg of antibody, compared to the 17µg of α- 2,6 sialyltransferase per mg of antibody used previously (Table 5-1). The sialylation reaction was incubated for 10 hours at 37°C as opposed to 24hrs previously used, to try and prevent any back reaction occurring which may decrease the level of sialylation (personal communication- Hoffman La Roche).

Antibodies were buffer exchanged and galactosylated as previously, and a proportion of the galactosylated antibodies were used as substrate for the second sialylation reaction. Reactions were set up as follows: 27.3µM obinutuzumab, 4.1mM CMP-NANA and 3.7µM α- 2,6 sialyltransferase. Rituximab was set up as follows: 14µM rituximab, 2.8mM CMP-NANA, 2.22µM α- 2,6 sialyltransferase. Antibodies were purified by protein A chromatography as above and samples sent to Hoffman La Roche for glycoanalysis as before using the intact mass following IdeS digestion.

Glycan	Control	Galactose	Sialic Acid
FG0	45%	-	-
FG1	44%	-	-
FG2	11%	100%	21%
FG2S1	-	-	66%
FG2S2	-	-	13%

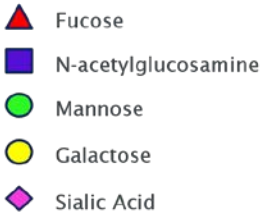

Table 5-2 Results of Rituximab Glycomodification

The results of the glycoanalysis of enzymatically glycomodified rituximab as determined by IdeS digested intact mass spectrometry. Rituximab treated with β- 1,4 galactosyltransferase alone, β- 1,4 galactosyltransferase followed by α- 2,6 sialyltransferase, or mock treated (control) were analysed by mass spectrometry to determine the effect on glycosylation. Glycan diagrams represent the main species present within each condition. F= fucose, G= galactose= S= sialic acid.

Glycan	Control	Galactose	Sialic Acid
	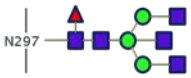	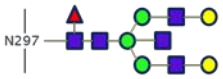	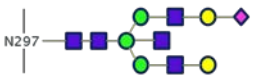
hM5B/hM4G1B	11%	6%	-
G0B	30%	-	-
G0BF	41%	-	-
G1BF	18%	-	-
G2B	-	30%	-
G2BF	-	53%	-
hM5G1B	-	11%	-
hM4G1BS1	-	-	5%
hM5G1BS1	-	-	8%
G2BS1F	-	-	29%
G2BS1	-	-	15%
G2BS2F	-	-	29%
G2BS2	-	-	15%

Abbreviation	Glycan Structure
hM5B	
hM4G1B	
G0B	
G0BF	
G1BF	
G2B	
G2BF	

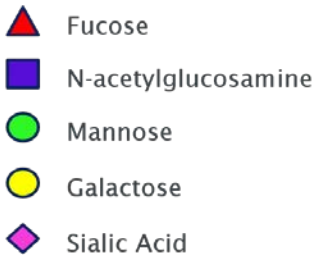

Abbreviation	Glycan Structure
hM5G1B	
hM4G1BS1	
hM5G1BS1	
G2BFS1	
G2BS1	
G2BFS2	
G2BS2	

Table 5-3 Results of Obinutuzumab Glycomodification

The results of the glycoanalysis of enzymatically glycomodified obinutuzumab as determined by IdeS digested intact mass spectrometry. Obinutuzumab treated with β- 1,4 galactosyltransferase alone, β- 1,4 galactosyltransferase followed by α- 2,6 sialyltransferase, or mock treated (control) were analysed by mass spectrometry to determine the effect on glycosylation. Glycan diagrams represent the main species present within each condition. B= bisecting GlcNAc, F= fucose, G= galactose= S= sialic acid, M= mannose.

As indicated in Table 5-2, mock treated rituximab once again consisted of completely fucosylated glycans, mostly bearing 0 or 1 galactose residues, consistent with the findings from the previous experiment (Table 5-1). Also consistent with the previous experiment was the 100% success of the galactosylation treatment for producing complete galactosylation of all glycans. In terms of sialylation, similar results were also obtained despite the increased amount of α- 2,6 sialyltransferase and shorter incubation time, with 13% bi-sialylation and 66% mono-sialylation achieved. As previously seen, 21% of non-sialylated glycans were still present.

For obinutuzumab, the results were more complex. In the mock treated starting material, although primarily of the complex type, 11% of the glycans present on obinutuzumab were of the hybrid type containing multiple mannose residues (Table 5-3). Of the complex glycans, all those detected carried a bisecting GlcNAc residue that was not seen in the rituximab glycans. Furthermore, there was a reduced level of fucosylation as compared to rituximab, with approximately 59% of total glycans (66% of complex glycans) containing fucose compared to the complete fucosylation seen with rituximab glycans. The trend of low galactosylation as seen with rituximab was also seen with obinutuzumab, with 71% of total glycans containing no galactose and 18% carrying a single galactose residue. No sialic acid containing glycans were detected within obinutuzumab, similar to that seen with rituximab (Table 5-1).

Enzymatic galactosylation was also highly successful for obinutuzumab (Table 5-3). There were no detected complex glycans that were not fully galactosylated, with the fully galactosylated species being split by the presence/absence of fucose. The appearance of the hM5G1B species and concomitant decrease of hM5B/hM4G1B suggests that there has been galactosylation of the available GlcNAc within the hM5B species.

Sialylation of obinutuzumab showed a degree of heterogeneity similar to that seen upon sialylation of rituximab. Interestingly, no non-sialylated glycan products were detected. Glycans containing 1 or 2 sialic acid residues were detected for both fucosylated and non-fucosylated glycans. For both mono and bi-sialylated species, there were more fucosylated than afucosylated glycans present. There were, however, equal amounts of mono and bi-sialylated species of both fucosylated and afucosylated glycans, suggesting that the fucose residue has no impact on the addition of sialic acid by α- 2,6 sialyltransferase.

In order to try and further increase the efficiency of the sialylation step, the CMP-NANA substrate was used at a ratio of 0.5µg per µg of IgG, and was made up in MQ H_2O instead of reaction buffer

as used previously (personal communication, Hoffman La Roche). Antibodies were buffer transferred into reaction buffer and galactosylated as before. The ratio of α- 2,6 sialyltransferase per mg of IgG was also increased, to 50µg of α- 2,6 sialyltransferase per mg of IgG. The anti-HER2 antibody trastuzumab (Herceptin), also an IgG1 antibody, was included as another target for glycomodification. Reactions were initiated as follows: 41.3µM rituximab, 4.85mM CMP-NANA, and 7.64µM α- 2,6 sialyltransferase; 29.3µM obinutuzumab, 3.44mM CMP-NANA, and 5.42µM α- 2,6 sialyltransferase; 29.3µM trastuzumab, 3.44mM CMP-NANA, 5.42µM α- 2,6 sialyltransferase. After protein A purification and dialysis into PBS, samples of antibody were sent to Hoffman La Roche for glycoanalysis.

Glycan	Control	Galactose	Sialic Acid
FG0	45%	-	-
FG1	45%	-	-
FG2	10%	100%	20%
FG2S1	-	-	61%
FG2S2	-	-	19%

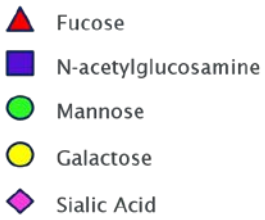

Table 5-4 Results of Rituximab Glycomodification

The results of the glycoanalysis of enzymatically glycomodified rituximab as determined by IdeS digested intact mass spectrometry. Rituximab treated with β- 1,4 galactosyltransferase alone, β- 1,4 galactosyltransferase followed by α- 2,6 sialyltransferase, or mock treated (control) were analysed by mass spectrometry to determine the effect on glycosylation. Glycan diagrams represent the main species present within each condition. F= fucose, G= galactose= S= sialic acid.

Glycan	Control	Galactose	Sialic Acid
FG0	48%	-	-
FG1	45%	-	-
FG2	7%	100%	21%
FG2S1	-	-	69%
FG2S2	-	-	10%

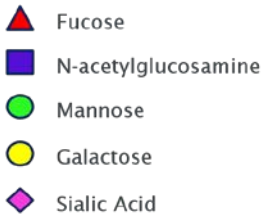

Table 5-5 Results of Trastuzumab Glycomodification

The results of the glycoanalysis of enzymatically glycomodified trastuzumab as determined by IdeS digested intact mass spectrometry. Trastuzumab treated with β- 1,4 galactosyltransferase alone, β- 1,4 galactosyltransferase followed by α- 2,6 sialyltransferase, or mock treated (control) were analysed by mass spectrometry to determine the effect on glycosylation. Glycan diagrams represent the main species present within each condition. F= fucose, G= galactose= S= sialic acid.

Glycan	Control	Galactose	Sialic Acid
	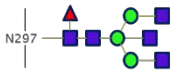	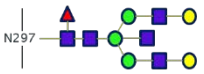	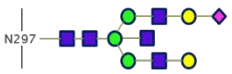
hM5B/hM4G1B	12%	7%	-
G0B	28%	-	-
G0BF	40%	-	-
G1B	-	8%	-
G1BF	20%	-	-
G2B	-	21%	-
G2BF	-	52%	10%
hM5G1B	-	12%	-
hM4G1BS1	-	-	-
hM5G1BS1	-	-	11%
G2BS1F	-	-	40%
G2BS1	-	-	21%
G2BS2F	-	-	-
G2BS2	-	-	18%

Abbreviation	Glycan Structure
hM5B	
hM4G1B	
G0B	
G0BF	
G1B	
G1BF	
G2B	
G2BF	

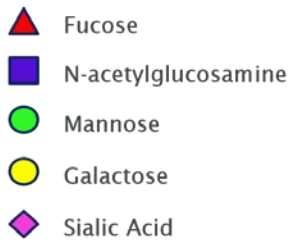

Abbreviation	Glycan Structure
hM5G1B	
hM4G1BS1	
hM5G1BS1	
G2BFS1	
G2BS1	
G2BFS2	
G2BS2	

Table 5-6 Results of Obinutuzumab Glycomodification

The results of the glycoanalysis of enzymatically glycomodified obinutuzumab as determined by IdeS digested intact mass spectrometry. Obinutuzumab treated with β- 1,4 galactosyltransferase alone, β- 1,4 galactosyltransferase followed by α- 2,6 sialyltransferase, or mock treated (control) were analysed by mass spectrometry to determine the effect on glycosylation. Glycan diagrams represent the main species present within each condition. B= bisecting GlcNAc, F= fucose, G= galactose= S= sialic acid, M= mannose.

The results of the glycoanalysis of rituximab were found to be similar to previous attempts at glycomodification, with mock treated control rituximab containing mostly G0 and G1 glycans and 100% galactosylation achieved after enzymatic addition (Table 5-4). Sialylation was again broadly similar to previous experiments, with the major population seen being mono-sialylated, with 19% bisialylated and the remaining 20% containing no sialic acid.

A similar trend was observed for trastuzumab, which is not overly surprising considering it is also a human IgG1 antibody that is produced recombinantly in CHO cells. Mock treated trastuzumab contained mostly G0 and G1 glycans, and was completely fucosylated (Table 5-5). Galactosylation of trastuzumab generated a homogenous G2 containing population, as seen with rituximab. Sialylation of trastuzumab resulted in a similar level of modification as seen with rituximab, with 21% non-sialylated, 69% mono-sialylated and 10% bi-sialylated, thereby confirming the reproducibility of this approach.

Obinutuzumab was also glycomodified under these same conditions. The mock treated control sample of obinutuzumab contained very similar glycans to the previous experiment using obinutuzumab, with G0 and G1 glycans the most prevalent and all species carrying a bisecting GlcNAc (Table 5-6). Fucose was present on approximately 60% of the glycans, and 12% of the obinutuzumab derived glycans contained hybrid species. Treatment with the β- 1,4 galactosyltransferase once again caused a dramatic shift in the glycans present, with the appearance of G2 bearing glycans in both the fucosylated and afucosylated forms. However, a small proportion (8%) of glycans carried only a single galactose, and these glycans were all afucosylated. The sialylation reaction once again generated species containing 1 or 2 sialic acid residues. However, lower levels of sialylation were seen compared to the previous experiment (Table 5-3), with no bi-sialylated glycans with fucose detected. In addition, 10% of the glycans contained no sialic acid.

Despite using identical reagents and highly similar reaction conditions to those recommended by Hoffman La Roche, high levels of sialylation could not be achieved. As compared to Roche, these reactions were done on small batches of antibody in order to reduce the total amount of enzymes and substrates required. As such, small samples of antibody were sent for analysis of the resulting glycans present. The IdeS digestion mass spectrometry method is suited for this as it requires only small amounts of starting material for detection of the major glycans present. However, the ionisation process during injection of the sample into the mass spectrometer can have an effect

on the sample and can cause in source fragmentation which could potentially result in an underestimate of the level of sialylation of a sample[496].

An alternative method for analysing glycans is to label them using a fluorescent label, such as 2-aminobenzamide (2-AB) or 2-aminobenzoic acid. This labelling boosts the spectral absorption of the glycans, enabling their detection by HPLC systems measuring at an emission wavelength of 330nm. Glycans are first cleaved off using enzymes such as PNGase F, and then labelled with 2-AB. A variation of this method that is suitable for use with small amounts of sample material uses extremely rapid cleavage and labelling steps, allowing sample preparation to take place in less than an hour and minimising the potential loss of sialic acids during acidic incubation[417]. This method of analysis, Instant AB Labelling (described in Section 2.2.11.2 and Reusch *et al.*[417]), was applied to the sialylated rituximab sample prepared in Table 5-4 to measure the level of sialylated glycans present (Table 5-7).

Glycan	Control	Sialic Acid
	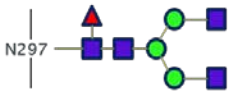	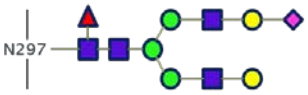
Minor	0.7%	0.2%
M5	1.4%	1.3%
G0	1.1%	-
FG0	42.4%	0.1%
G1	0.9%	-
FG1	42.5%	-
FG2	8.8%	1.2%
G2S1	-	1.2%
FG2S1	1.4%	59.9%
G2S2	-	1.2%
FG2S2	0.8%	34.9%

Abbreviation	Glycan Structure
M5	
G0	
FG0	
G1	
FG1	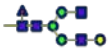

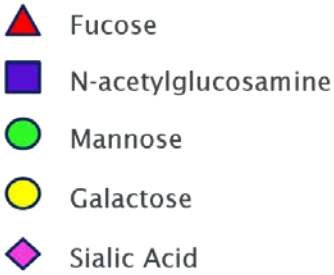

Abbreviation	Glycan Structure
FG2	
G2S1	
FG2S1	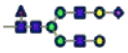
G2S2	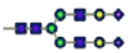
FG2S2	

Table 5-7 Results of Rituximab Glycomodification by Instant AB Labelling

Rituximab glycomodified with β- 1,4 galactosyltransferase followed by α- 2,6 sialyltransferase, or a mock treated (control) were deglycosylated and the released glycans labelled with Instant AB dye, prior to analysis by HILIC HPLC. This detection method allows for detection of low abundance glycans including afucosylated and oligomannose structures. Glycan diagrams represent the main species present within each condition. F= fucose, G= galactose, S= sialic acid, M= mannose.

Instant AB labelling followed by fluorescent detection HPLC detected a larger number of glycoforms present at low levels in the rituximab sample than could be detected using mass spectrometry following IdeS digestion. For example, trace amounts of hybrid mannose 5 glycans and afucosylated glycans were detected using this method, highlighting the heterogeneity of glycosylation present (Table 5-7). The main trends seen with this method of analysis were the same as for the mass spectrometry method, with mock treated glycans containing mostly fucosylated species with 0 or 1 galactose residues. As shown in Table 5-7, Instant AB labelling detected a higher degree of sialylated glycans compared to that detected by mass spectrometry of IdeS digested antibody (Table 5-4). The biggest difference was seen for the level of bi-sialylated structures, with 19% detected by mass spectrometry and 34.9% detected by Instant AB labelling. Perhaps more relevant, Instant AB labelling detected very low levels of glycans that contained no sialic acid (less than 3% of total glycans with no sialic acid), compared to the mass spectrometry method (20% of total glycans with no sialic acid), suggesting that in-source fragmentation may indeed be occurring and artificially increasing the level of non-sialylated glycans being detected by mass spectrometry.

After further consultation with collaborators at Hoffman La Roche, it was suggested that the presence of the β- 1,4 galactosyltransferase enzyme during the sialylation reaction may be contributing to the low levels of sialylation being achieved by competing for the galactosylated ends of the bi-antennary glycan. In order to prevent this from happening, an additional protein A purification step was included after the galactosylation reaction in order to remove the β- 1,4 galactosyltransferase enzyme. Following this the antibody was buffer exchanged into MQ H_2O prior to sialylation, as a lower buffer concentration had been suggested to increase sialylation yields (personal communication, Hoffman La Roche). The reaction was initiated under the following conditions: 24µM rituximab, 2.87mM CMP-NANA (both in MQ H_2O) and 2.96µM α- 2,6 sialyltransferase, and incubated for 4 hours at 37°C. This gave a ratio of 75µg of α- 2,6 sialyltransferase per milligram of antibody- increased from 50µg per mg of IgG used previously. Purified and PBS dialysed antibody samples were sent for glycoanalysis by both intact mass spectrometry of IdeS digested IgG and by Instant AB labelling of released glycans.

Glycan	Control	Galactose	Sialic Acid
		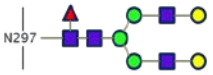	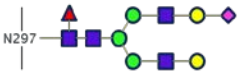
FG0	50.6%	-	-
FG1	42.2%	-	-
FG2	7.2%	100%	14.1%
FG2S1	-	-	57.7%
FG2S2	-	-	28.2%

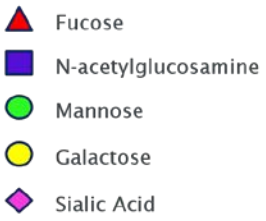

Table 5-8 Results of Rituximab Glycomodification by Intact Mass Spectrometry

The results of the glycoanalysis of enzymatically glycomodified rituximab as determined by IdeS digested intact mass spectrometry. Rituximab treated with β- 1,4 galactosyltransferase alone, β- 1,4 galactosyltransferase followed by α- 2,6 sialyltransferase, or mock treated (control) were analysed by mass spectrometry to determine the effect on glycosylation. Glycan diagrams represent the main species present within each condition. F= fucose, G= galactose= S= sialic acid.

As shown in Table 5-8, the results of the glycoanalysis reproduced the previously seen pattern of low galactosylation in the mock treated control, and the complete success of the galactosylation. Analysis of the level of sialylation by intact mass spectrometry suggested that there was a slight enhancement of the level of sialylation achieved, with 28% of the glycans now bearing 2 sialic acid residues, 57.7% being mono-sialylated and just 14% non-sialylated species.

As was seen previously (Table 5-4 and Table 5-7), Instant AB analysis of this sample suggested a higher degree of sialylation had been achieved than the mass spectrometric method, as well as revealing a number of minor species (Table 5-9). Mock treated rituximab was confirmed to be mostly containing fucosylated glycans with 0 or 1 galactose residues. Galactosylation once again proved highly efficient, with nearly 95% of glycans carrying 2 galactose residues. Sialylation using this method (75µg of α- 2,6 sialyltransferase per mg of IgG after purification of the antibody post-galactosylation) was more efficient than in previous experiments, with only trace amounts of glycans present that contained no sialic acid, and slightly more mono-sialylated than bi-sialylated glycans present.

Glycan	Control	Galactose	Sialic Acid
	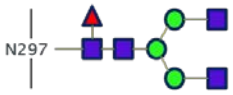	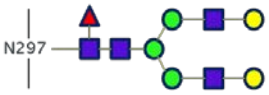	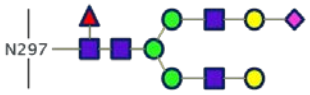
Minor	0.7%	-	-
M5	1.5%	2.2%	1.0
G0	1.3%	-	-
FG0	47.3%	-	-
FG1	40.7%	0.8%	0.5%
G2	-	2.2%	-
FG2	6.7%	94.8%	-
FG2S1	0.9%	-	53.2%
FG2S2	0.8%	-	45.3%

Abbreviation	Glycan Structure
M5	
G0	
FG0	
FG1	

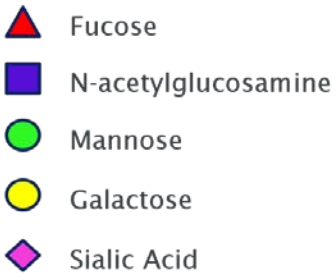

Abbreviation	Glycan Structure
G2	
FG2	
FG2S1	
FG2S2	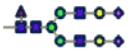

Table 5-9 Results of Rituximab Glycomodification by Instant AB Labelling

Rituximab glycomodified with β- 1,4 galactosyltransferase alone, β- 1,4 galactosyltransferase followed by α- 2,6 sialyltransferase, or mock treated (control) were deglycosylated and the released glycans labelled with Instant AB dye, before being analysed by HILIC HPLC. This detection method allows for detection of low abundance glycans including afucosylated and oligomannose structures. Glycan diagrams represent the main species present within each condition. F= fucose, G= galactose, S= sialic acid, M= mannose.

In summary, the *in vitro* glycoengineering approach was found to be suitable for consistently altering the Fc glycans of several antibodies, with both the level of galactose and sialic acid being modifiable. Two anti-CD20 mAbs with altered glycan profiles were generated using recombinant

human glycosyltransferases. Clinical grade rituximab (Mabthera) and obinutuzumab (Gazyvaro) displayed heterogeneous glycosylation with a trend towards low levels of galactosylation and an almost complete lack of sialylation. Obinutuzumab also contained a range of hybrid glycans, displayed a lower level of fucosylation than rituximab and also contained a bisecting GlcNAc. Enzymatic galactosylation using the human enzyme β- 1,4 galactosyltransferase was highly efficient, producing both rituximab and obinutuzumab with fully galactosylated glycans.

Enzymatic sialylation using the human enzyme α- 2,6 sialyltransferase was less efficient compared to the galactosylation reaction. Initial attempts at sialylation appeared to produce glycans with low levels of sialylation that still contained antibodies completely lacking in sialic acid. Modifying the reaction conditions appeared to have little effect on overall sialylation efficiency. However, when the glycans were analysed by a chromatography based method, Instant AB labelling, higher levels of sialylation were detected, suggesting that efficient sialylation may have taken place. Having generated antibodies with different glycoforms, it was of interest to determine if the antibody characteristics were effected.

5.3 Antibody Effector Functions of Glycomodified Antibodies

5.3.1 Antigen Binding

The effect of the glycomodifications performed in Section 5.2 were investigated to see if any changes in the antibody properties could be determined. Firstly, glycomodified rituximab was tested to see if its antigen binding properties had been affected by the addition of galactose or sialic acid. Raji cells were opsonised with the glycomodified antibodies at 10µg/ml and binding detected using a labelled secondary antibody specific for human IgG Fc (SB2H2). The results, shown in Figure 5-2, indicate that the incubation and purification process had not reduced the ability of rituximab to bind to CD20, as the mock treated rituximab (red) had very similar binding to that of stock rituximab (MabThera, grey). Furthermore, Figure 5-2 shows that the addition of galactose (blue) and sialic acid (green) did not impact upon the antigen binding of rituximab.

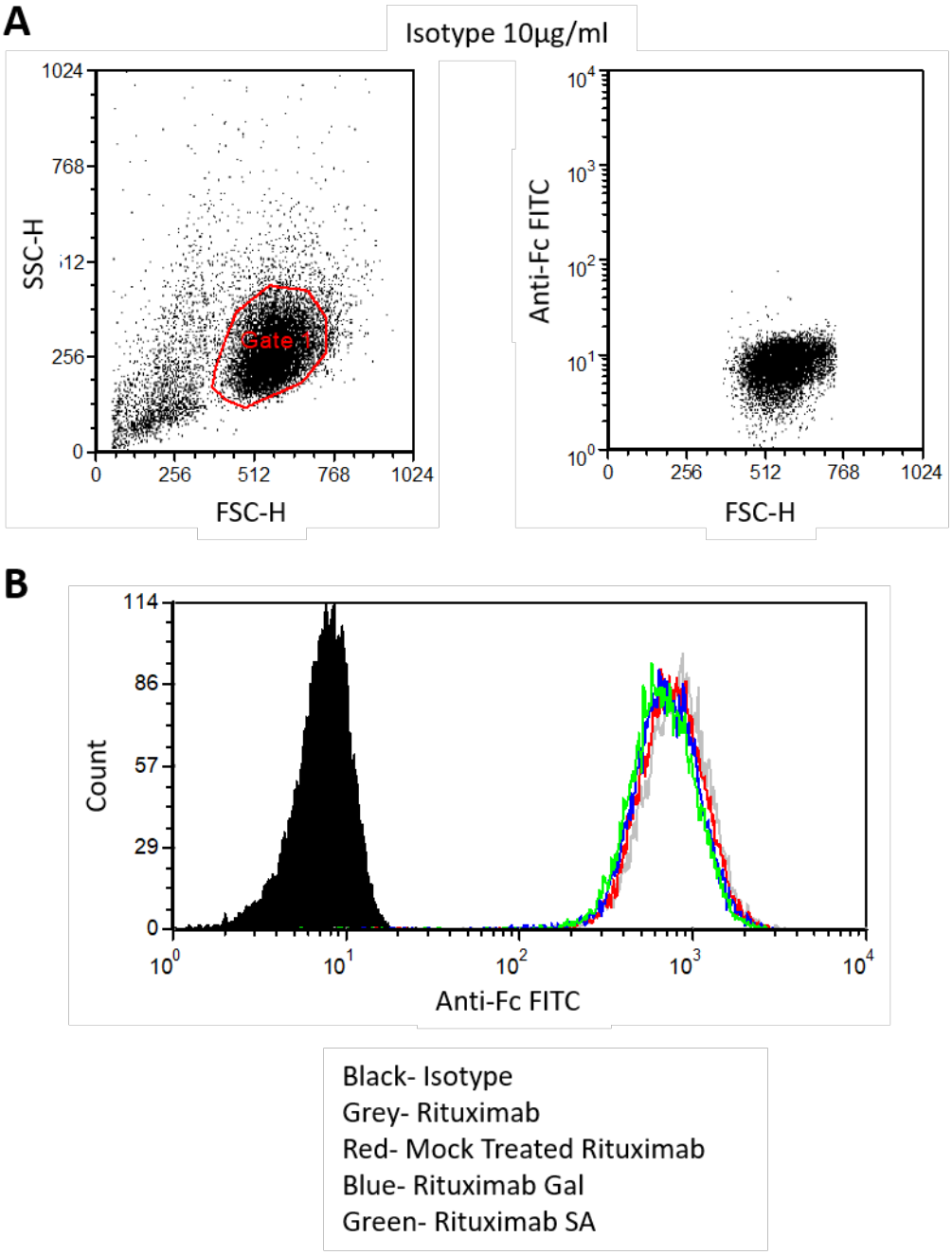

Figure 5-2 Glycomodification of Rituximab Does Not Affect Binding to CD20

Raji cells were opsonised with unmodified rituximab (MabThera, grey), mock treated rituximab (red), galactosylated (blue) or sialylated (green) rituximab, or an isotype control (black) at 10µg/ml. Unbound antibody was washed away and bound antibody detected using a FITC labelled anti-Fc antibody (SB2H2). A- live cells were gated using forward vs. side scatter. B- histogram showing relative binding of different rituximab glycoforms. Final composition of the glycomodified antibodies used is available in Table 5-4.

5.3.2 FcγR Binding of Glycomodified Rituximab

Depleting or direct targeting antibodies such as rituximab and obinutuzumab elicit most of their effects *in vivo* through activatory FcγR mediated effector functions, ADCC and ADCP. As such, it was of interest to investigate whether the addition of galactose or galactose and sialic acid to the antibodies had an effect on their ability to bind to FcγRI, FcγRIIa and FcγRIIIa.

Binding to FcγRs was measured using surface plasmon resonance (SPR) via a Biacore T100 (GE Healthcare). Mock treated, galactosylated or sialylated forms of rituximab were immobilised to one flow cell of a Series S sensor CM5 chip using amine chemistry, with a blank flow cell for reference. Recombinant soluble FcγRs were flowed over these immobilised antibodies in parallel across a range of concentrations (starting from 100nM for FcγRI and 1000nM FcγRIIa and FcγRIIIa). Representative binding curves for FcγRI, FcγRIIa and FcγRIIIa binding are shown in Figure 5-3. Sialylated rituximab showed the highest level of binding to each receptor at several concentrations tested. No major differences in binding affinity were apparent between the different glycoforms (Table 5-10). Analysis of the binding affinity of galactosylated and sialylated rituximab was determined using a 1:1 binding model and the results are shown in Table 5-10. A small increase in affinity for all FcγRs tested was seen on increasing glycosylation, with sialylated rituximab generally showing the highest affinity for each receptor, but the differences observed were only small (Table 5-10). Indications of the fitting of the data to the 1:1 modelling used is shown in Section 8.3.

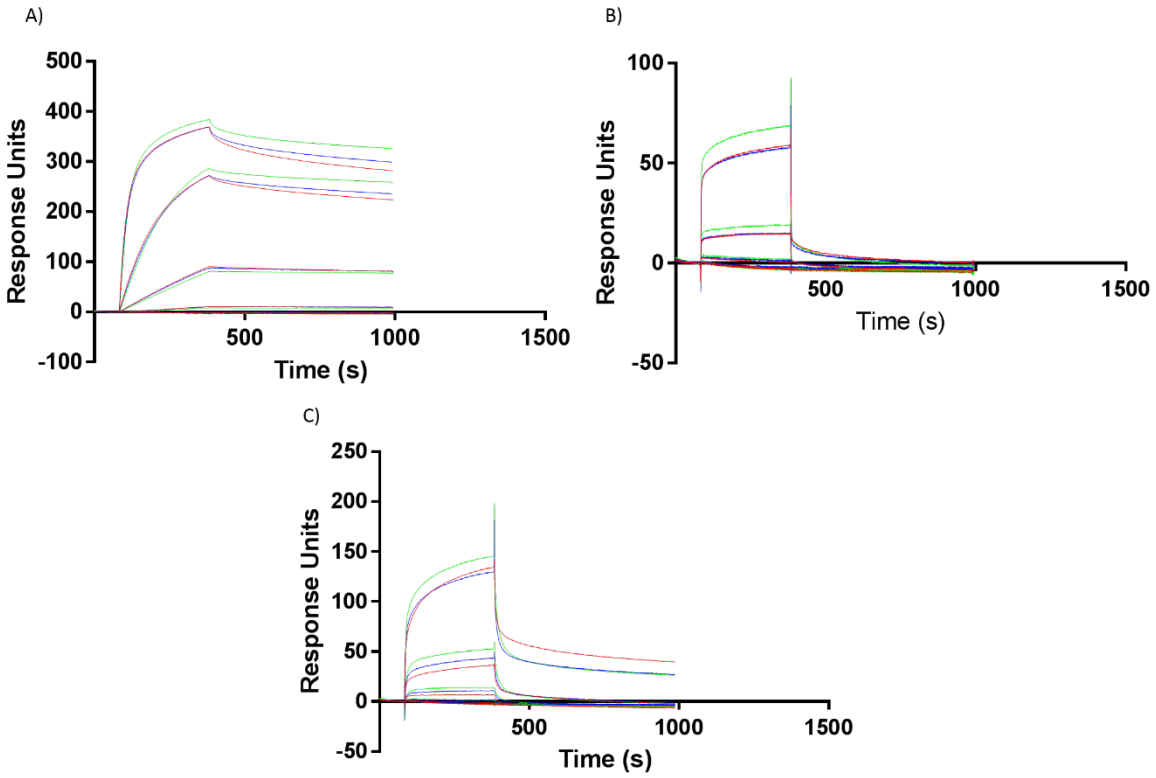

Figure 5-3 SPR analysis of Glycoengineered Rituximab Binding to FcγRs

SPR analysis of mock treated or glycomodified rituximab binding to recombinant FcγRI (A), FcγRIIa (B) and FcγRIIIa (C). The receptor was flowed over immobilised antibodies at a 1 in 5 titration from 100nM (FcγRI) or 1000nM (FcγRIIa and IIIa). Sialylated rituximab (green), galactosylated rituximab (blue), mock treated rituximab (red). Representative SPR results shown for multiple glycomodification batches.

			Preparation 1		Preparation 2
Receptor	Glycoform		KD (M^{-1})		KD (M^{-1})
FcγRI	Control		**8.49E-10**		**1.09E-09**
	Galactose		**6.66E-10**		**8.77E-10**
	Sialic Acid		**4.50E-10**		**5.39E-10**
FcγRIIa	Control		**2.01E-06**		**1.65E-06**
	Galactose		**1.88E-06**		**1.61E-06**
	Sialic Acid		**1.58E-06**		**1.31E-06**
FcγRIIIa	Control		**6.09E-07**		**3.89E-07**
	Galactose		**4.63E-07**		**3.42E-07**
	Sialic Acid		**3.83E-07**		**6.17E-07**

Table 5-10 Binding Affinities of Glycomodified Rituximab for FcγRs

Affinities of mock treated, galactosylated and sialylated rituximab were determined using SPR. Antibody was immobilised to a Biacore binding chip and recombinant FcγRs passed over at several concentrations. Affinities were determined using a 1:1 fit binding model. Preparation 1 (rituximab preparation detailed in Table 5-2) was measured twice and the average of the values obtained are presented. Preparation 2 (detailed in Table 5-4) was measured once.

Thomann *et al*. previously reported differences in the binding of glycomodified IgG1 for FcγRIIa and FcγRIIIa using a similar enzyme based method for the addition of galactose and sialic acid[406]. The data in that paper was presented as relative binding normalised to the level of binding seen with non-engineered rituximab. In order to see whether this trend was compatible with the data presented here the same method of analysis was applied. Figure 5-4 displays the results of this analysis, and shows a similar trend to that reported in the literature - that sialylated and galactosylated rituximab have a slightly increased binding to FcγRIIa and FcγRIIIa compared to non-engineered/control rituximab, and that there is no effect on FcγRI binding for either glycomodification.

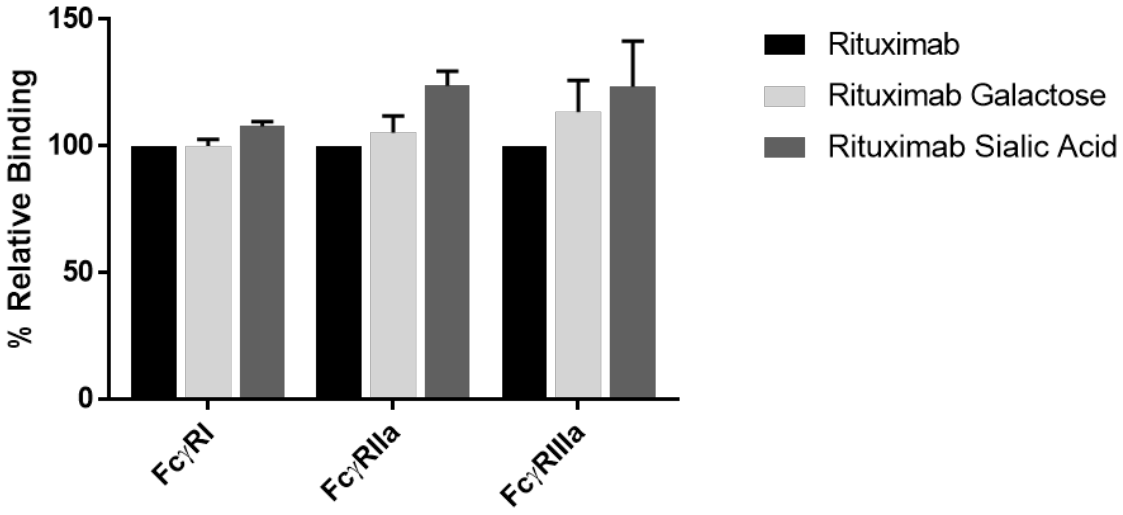

Figure 5-4 Glycoengineering of Rituximab has an Effect on FcγR Binding

SPR analysis of immobilised mock treated or glycomodified rituximab binding to recombinant FcγR. Receptor was flowed over immobilised antibodies at 100nM (FcγRI) or 1000nM (FcγRIIa and FcγRIIIa) and the maximum binding determined after normalising to the amount of each antibody bound to the chip. The binding of each glycovariant was then determined as a percentage of the mock treated rituximab for that receptor. Data shown represent mean and range of combined data from 2 separate preparations of antibody.

The affinity of glycoengineered rituximab for FcγRIIb was also tested by SPR, but only low levels of binding were seen with the concentrations used, due to the low affinity of FcγRIIb for monomeric IgG. In order to get an indication as to whether sialylation (or galactosylation) had an effect on the binding of IgG to FcγRIIb, a cell based assay system was used. Jurkat T cells transfected to expresses FcγRIIc (which shares its extracellular domain with FcγRIIb), and an NFAT-RE*luc2* reporter fusion were used to assess FcγRIIb binding. Mock treated rituximab, and rituximab bearing increased galactose and sialic acid were incubated with the transfected Jurkat T cells. Binding of Fc to FcγRIIc on the Jurkat cells results in transcription of the firefly luciferase enzyme, and addition of the luciferin substrate allows the amount of cell activation to be determined by the amount of luminescence detected (Figure 5-5).

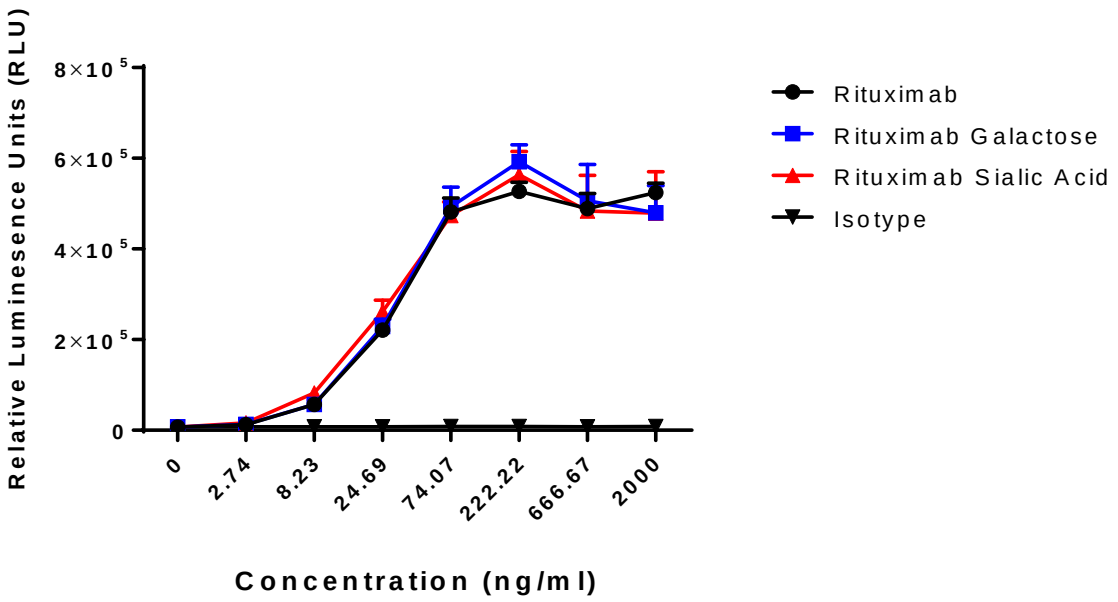

Figure 5-5 Glycomodification of Rituximab Does Not Affect FcγRIIC/B Binding

Raji cells were opsonised with various concentrations of mock treated, galactosylated or sialylated rituximab or an isotype control as indicated and co-cultured for 6 hours with Jurkat T cells transfected with FcγRIIc and an NFAT-REluc2 reporter fusion. Cells were lysed and luciferin substrate added. Relative Luminescence Units were measured using a VarioSkan plate reader as recommended by Promega. Data presented plus SD.

Figure 5-5 shows the results of the FcγRIIc binding assay. Non-modified rituximab showed Jurkat cell activation that saturated at approximately 74ng/ml of antibody used for target cell opsonisation. Both galactosylated and sialylated forms of rituximab showed almost identical levels of Jurkat cell activation to the mock treated rituximab, and saturated at the same level. This suggests that the glycomodified antibodies were equivalent in binding to FcγRIIc as was the mock treated rituximab. No Jurkat activation was seen with an irrelevant isotype control antibody.

5.3.3 FcγR Mediated Effector Function

5.3.3.1 Antibody Dependent Cellular Cytotoxicity (ADCC)

In order to investigate whether the small increases in binding to activatory FcγRIIa and FcγRIIIa were meaningful, the impact of glycomodification on FcγR mediated effector functions was

investigated. ADCC by NK cells has long been thought to be important for the clearance of tumour cells during antibody therapy. Freshly purified human PBMCs from leukocyte cones were used as effector cells, containing approximately 10% NK cells (CD56 ^{low} CD16 ^{high}), giving a final ratio of 5 NK cells per target cell. These CD56 ^{low} CD16 ^{high} NK cells are the primary cytotoxic subset of NK cells[497]. CD20 expressing B cell lines (Raji and Ramos) were used as target cells for these assays. The cells were labelled with the cytoplasmic dye calcein, and then opsonised with antibody. The cells were then co-cultured with PBMCs at a ratio of 1 target cell per 50 PMBC effectors (approximately 5 NK cells). Target cells killed during the assay release calcein, which is collected in the sample supernatants and provides a method for assessing the level of cell death induced by the PBMCs in the presence of antibody. Comparing the reading to a relevant control allows (as described in Methods) for the calculation of the maximum potential target cell lysis achieved in each condition.

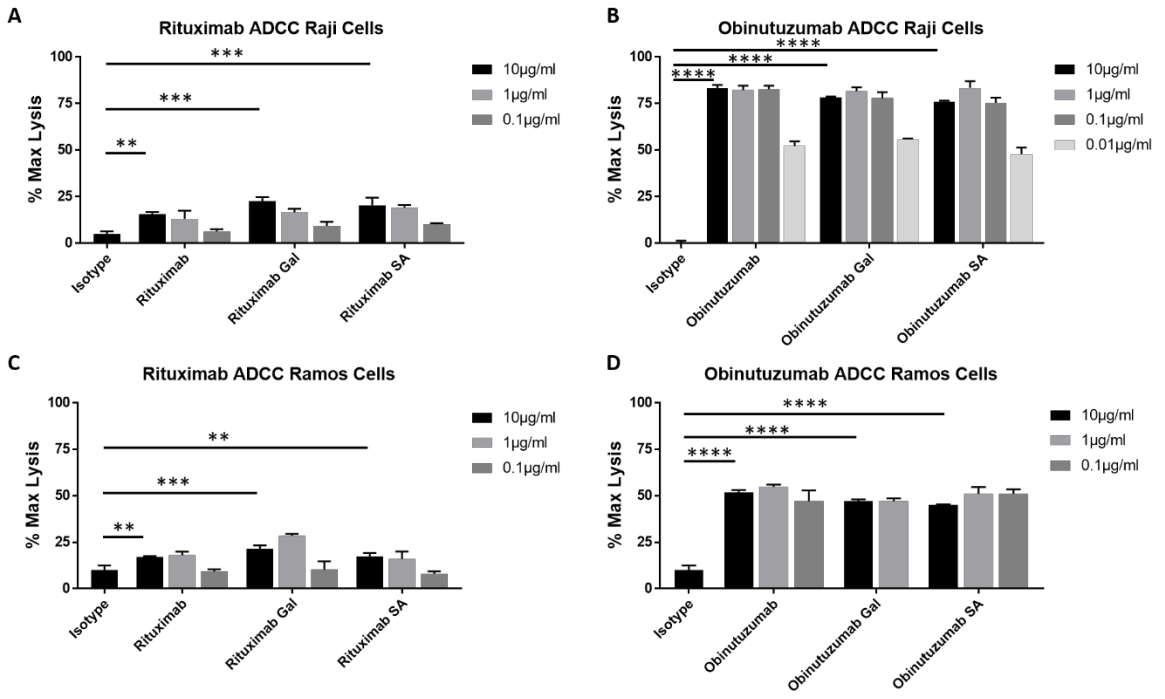

Figure 5-6 Antibody Dependent Cellular Cytotoxicity of Glycomodified Anti-CD20 Antibodies on B Cell Lines

Calcein labelled target cells (Raji or Ramos cell lines) were opsonised with various concentrations of mock treated or glycoengineered antibody, or an isotype control, as indicated. Opsonised cells were co-cultured with purified human PBMCs for 4 hours and supernatants measured for calcein release. A and C- Raji (A) and Ramos (C) cell lines treated with glycomodified rituximab from Table 5-4. B and D- Raji (B) and Ramos (D) cell lines treated with glycomodified obinutuzumab (Table 5-6Table 5-3). Data shown are means plus range of triplicate repeats of a single experiment, representative of two independent experiments using different PBMC donors. Statistics calculated by one-way ANOVA with multiple comparisons, ** $p < 0.01$, *** $p < 0.001$, **** $p < 0.0001$.

As has been reported in the literature, obinutuzumab was superior to rituximab at inducing ADCC, causing 2-3x as much killing of both Raji and Ramos cells at 10µg/ml (Figure 5-6). The increased ADCC of obinutuzumab over rituximab has been reported to be due to the reduced fucosylation of obinutuzumab, and potentially is also due to its type II nature as compared to the type I antibody rituximab. As highlighted in Figure 5-6, glycomodification of obinutuzumab or rituximab did not have an effect on the ability of these antibodies to induce ADCC, either in a positive or negative fashion, on either cell line. In order to confirm these findings on more biologically relevant target cells, ADCC experiments were carried out using CLL target cells (consisting almost entirely of tumour B cells). These cells were labelled with calcein, as was done for Raji and Ramos cells above.

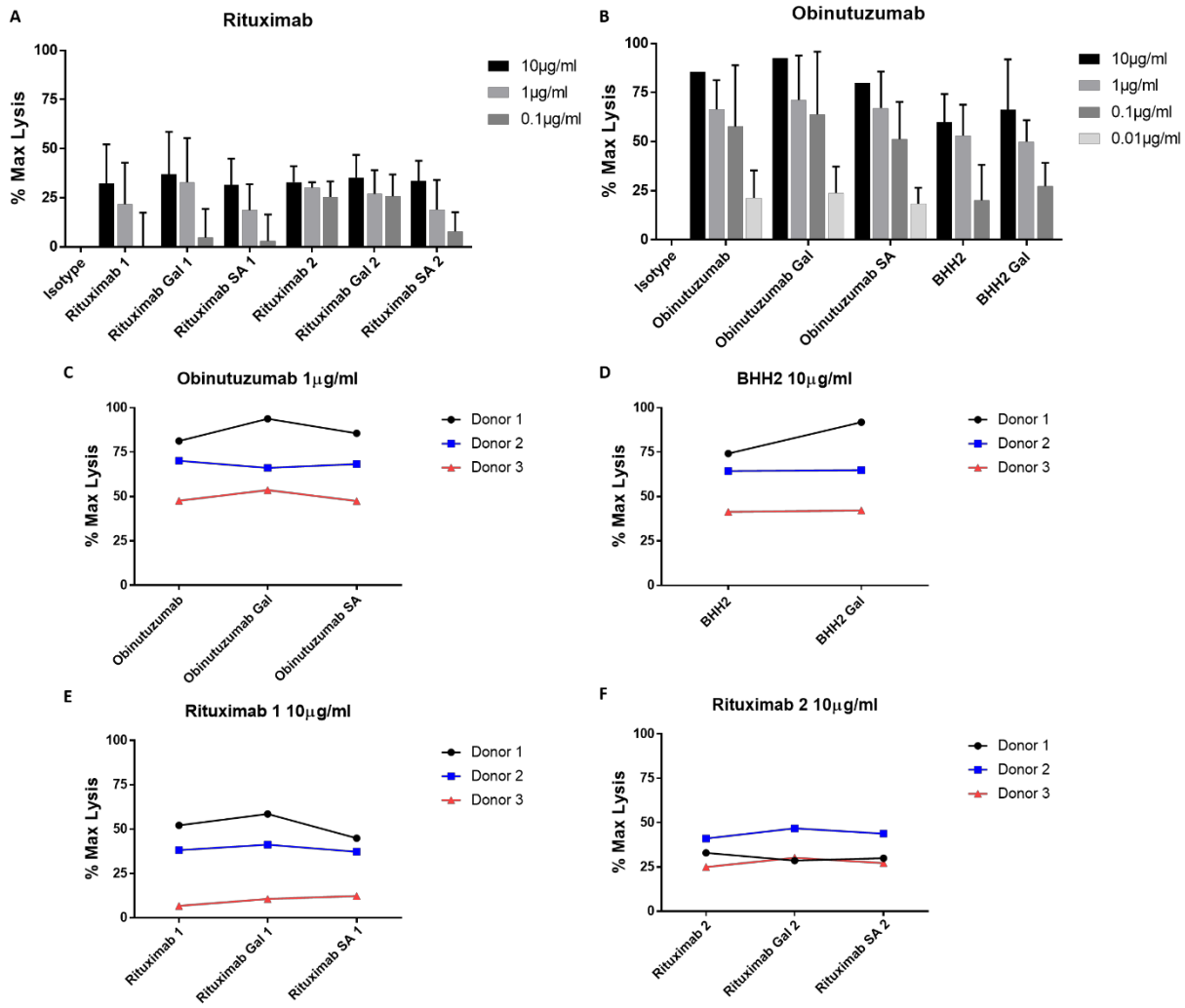

Figure 5-7 Antibody Dependent Cell Mediated Cytotoxicity with Glycomodified Anti-CD20 Antibodies of CLL Target Cells

Calcein labelled target cells (human patient CLL cells) were opsonised with various concentrations of mock treated or glycoengineered antibody, or an isotype control, as indicated. Opsonised cells were co-cultured with purified human PBMCs for 4 hours and supernatants measured for calcein release. A-glycomodified rituximab from Table 5-1 (rituximab 1) and Table 5-2 (rituximab 2). B- glycomodified obinutuzumab (Table 5-3) and BHH2. Data shown are means plus range of triplicate repeats of independent experiments (n=1 for obinutuzumab at 10µg/ml, n=2-3 for remaining antibodies) using different PBMC and CLL donors. C-F- comparison of relative ADCC of different glycoforms of anti-CD20 antibodies at the indicated concentration across independent donors of PBMC and CLL cells.

As has been reported in the literature and in Figure 5-6, obinutuzumab was superior to rituximab at inducing ADCC, causing up to twice as much killing at 10µg/ml (Figure 5-7). The increased ADCC of obinutuzumab over BHH2 is likely due to the reduced fucosylation of obinutuzumab. As highlighted in Figure 5-7C-F, glycomodification of obinutuzumab, rituximab or BHH2 did not have

an effect on the antibodies ability to induce ADCC of CLL target cells, either in a positive or negative fashion.

The previous assays were performed in the absence of human serum IgG. In order to check whether background serum IgG had any effect on the ADCC inducing potential of galactosylated or sialylated antibody, ADCC experiments using Raji cells were repeated in the presence polyclonal human IgG (pIgG; produced in-house).

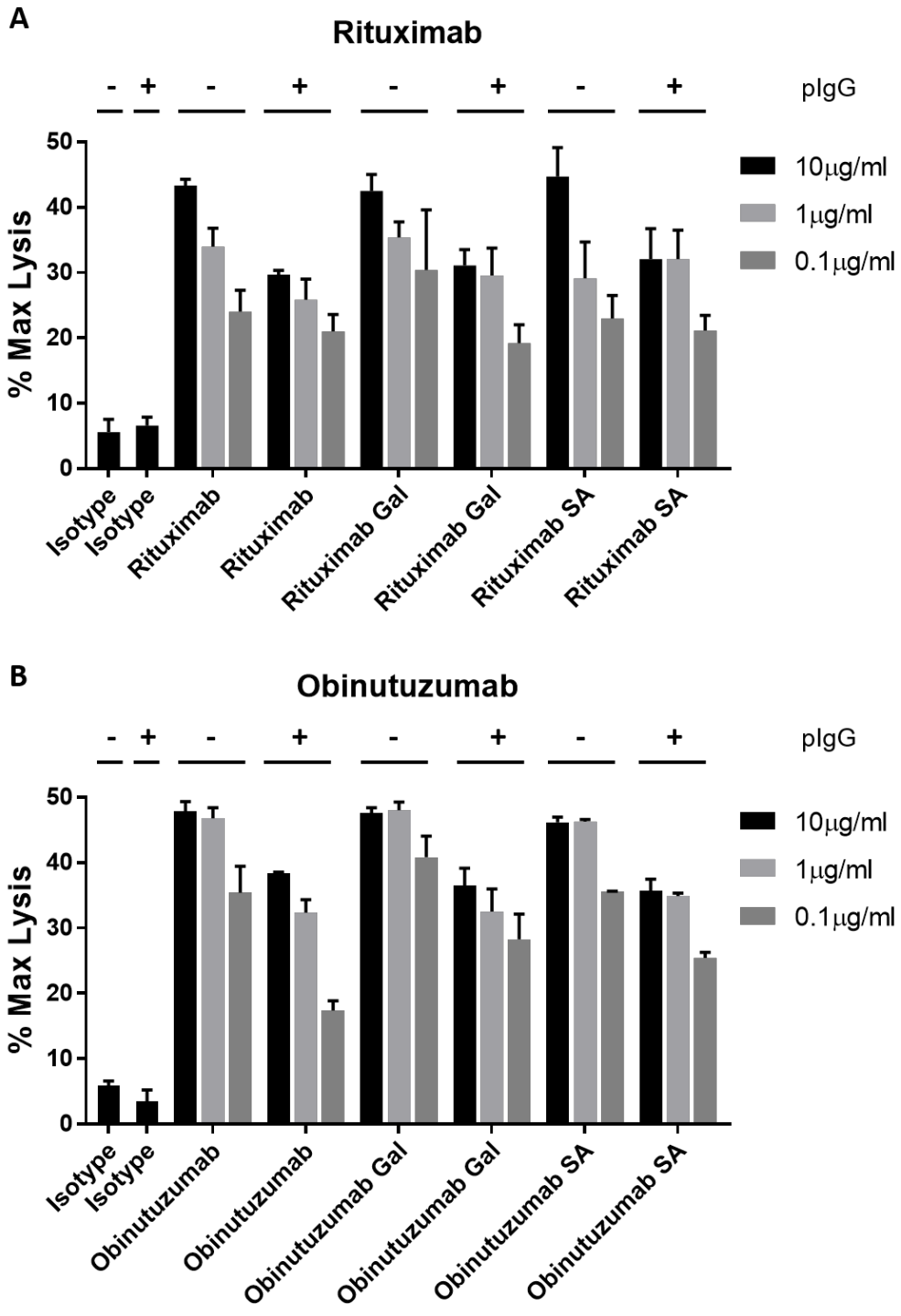

Figure 5-8 Effect of Polyclonal IgG on ADCC of Different Glycoforms of Anti-CD20 Antibodies

Calcein labelled Raji target cells were opsonised with various concentrations of mock treated rituximab (A) or obinutuzumab (B), glycomodified forms of these antibodies or an isotype control, and then incubated with freshly purified human PBMCs for 4 hours and the supernatants measured for calcein release to assess killing as above. pIgG was included from opsonisation onwards, at a final concentration of 5mg/ml during co-culture. Data shown are means of triplicate repeats of 2 independent assays using different PBMC donors, error bars indicate data range.

The effect of polyclonal IgG on ADCC is shown in Figure 5-8. The overall level of ADCC seen with both rituximab (Figure 5-8A) and obinutuzumab (Figure 5-8B) was decreased in the presence of non-specific IgG, as reported in the literature[280,284]. The affect appeared more pronounced for rituximab than for obinutuzumab. Whilst all antibodies, mock treated, galactosylated and sialylated exhibited reduced ADCC, there did not appear to be any difference in the extent of reduction for any particular glycoform.

5.3.3.2 Antibody Dependent Cellular Phagocytosis (ADCP)

In vivo cell depletion experiments have indicated macrophage mediated phagocytosis as the major effector mechanism of rituximab[295,498]. Accordingly, the effect of galactosylation and sialylation on ADCP was also investigated for both rituximab and obinutuzumab. In these assays target cells were labelled with the fluorescent dye carboxyfluorescein succinimidyl ester. They were opsonised with antibody before co-culture with macrophages for one hour, during which macrophages phagocytose opsonised target cells. Macrophages are then stained with anti-CD14 to allow for separate identification of macrophages and target cells. Cells are analysed by flow cytometry and the proportion of macrophages, identified by CD14 staining, that are also CFSE positive indicate the number of phagocytic cells

Figure 5-9 shows the results of ADCP experiments using CLL cells as targets for phagocytosis with human MDMs as effectors. As shown in Figure 5-9, obinutuzumab induced efficient phagocytosis, and neither glycomodification through galactosylation or sialylation appeared to have an effect on this process.

Similar results were found when rituximab and its glycovariants were tested in ADCP. As shown in Figure 5-10, similar levels of phagocytosis were seen for mock treated, galactosylated and sialylated rituximab across several doses tested. Two batches of glycomodified rituximab gave similar results. Direct comparison of these glycoforms indicates no consistent differences in ADCP.

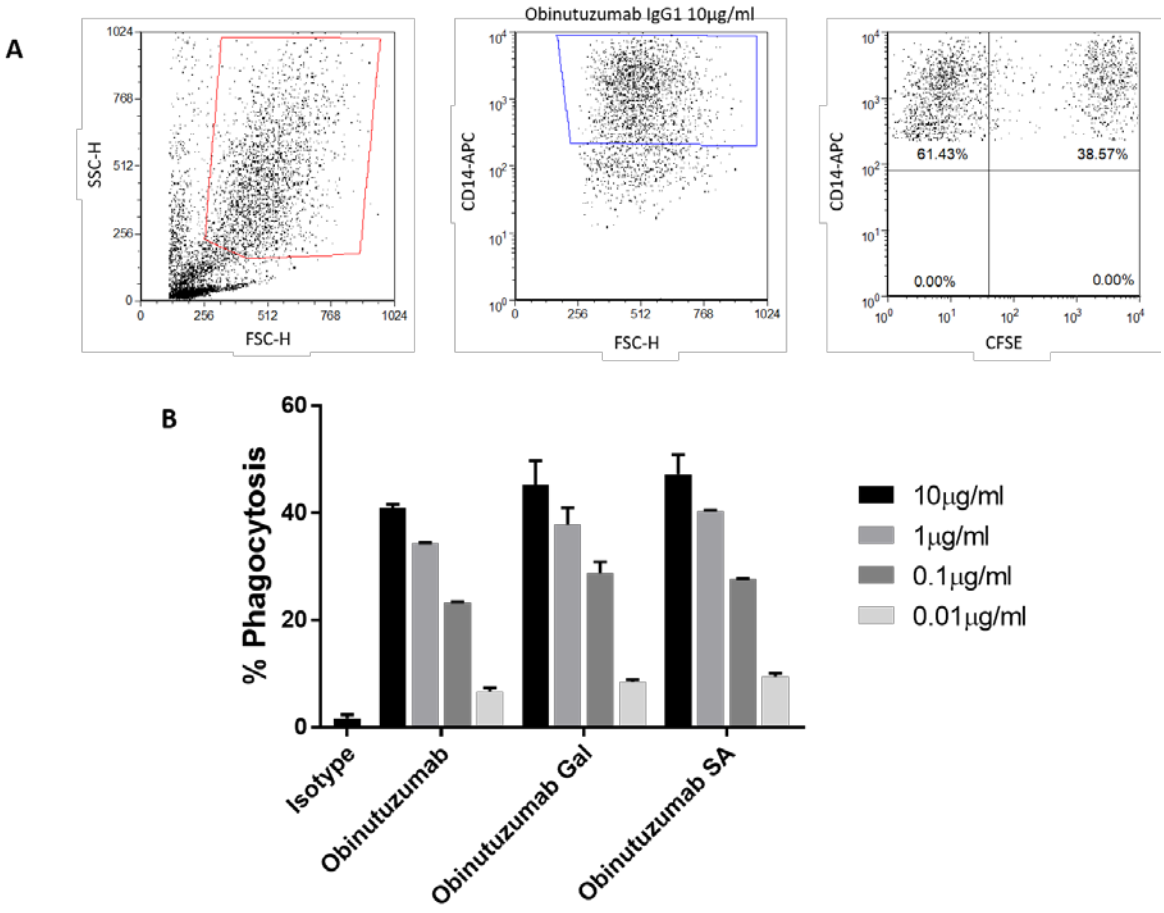

Figure 5-9 Effect of Glycomodification of Obinutuzumab on ADCP

CFSE labelled human CLL cells were opsonised with various concentrations of mock treated obinutuzumab, glycomodified obinutuzumab or an isotype control as indicated, and co-cultured with MDMs for 1 hour. A- macrophages were identified by forward vs side scatter and CD14 expression via flow cytometry on a BD FACS Calibur, and the percentage of macrophages that were CFSE positive calculated (far right). B- data shown are means of samples from triplicate wells from a single donor, error bars represent range.

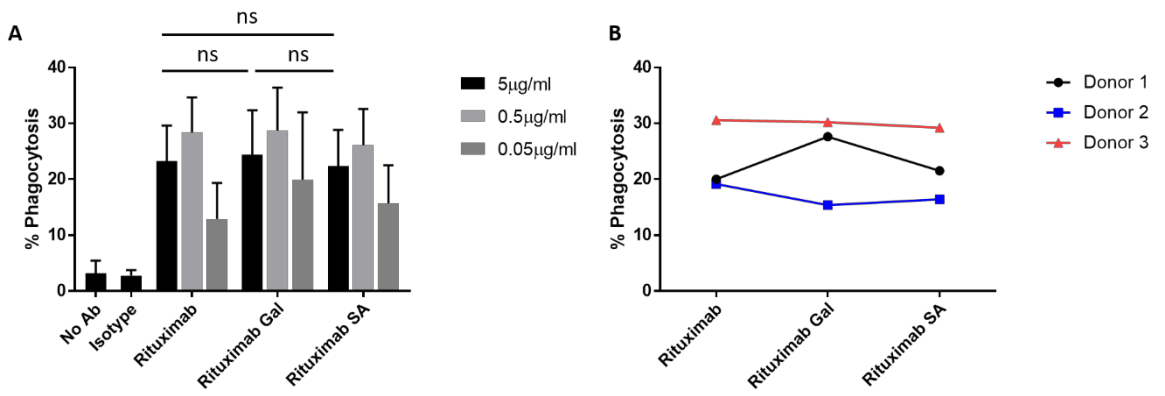

Figure 5-10 Effect of Glycomodification of Rituximab on ADCP

CFSE labelled human CLL patient cells were opsonised with various concentrations of mock treated rituximab, glycomodified rituximab or an isotype control as indicated, and co-cultured with MDMs for 1 hour. Macrophages were gated as in Figure 5-9. A- phagocytosis of CLL cells opsonised with rituximab glycoforms. Data shown are means plus SD of three independent experiments using MDMs and CLL cells from different donors, each measured in triplicate. . B- comparison of relative ADCP of different rituximab glycoforms at 5µg/ml. Statistics calculated by one-way ANOVA, ns = not significant.

5.3.4 Complement Mediated Effector Function

5.3.4.1 C1q Binding

Having determined that glycomodification may have a small influence on binding affinities to activatory FcγRs but does not appear to effect FcγR dependent effector function, the ability of these glycomodified antibodies to induce complement mediated cell lysis of tumour cells was investigated. IgG1 antibodies are strong activators of the classical complement cascade, and early work on therapeutic anti-CD20 antibodies suggested CDC as an important effector function[239,293]. The first step of the classical complement cascade that therapeutic mAbs induce is recruitment of the C1 complex to the opsonised cell surface, through binding to the C1q component. In order to test the relative ability of glycomodified rituximab to recruit C1q to the surface of the cell, Ramos cells (which lack FcγRIIb which could contribute to increased IgG at the cell surface) were opsonised with mock treated or glycomodified rituximab, or an isotype control. Unbound antibody was washed off the cells and C1q was added. Bound C1q was detected with a FITC labelled anti-C1q antibody, and the data acquired by flow cytometry.

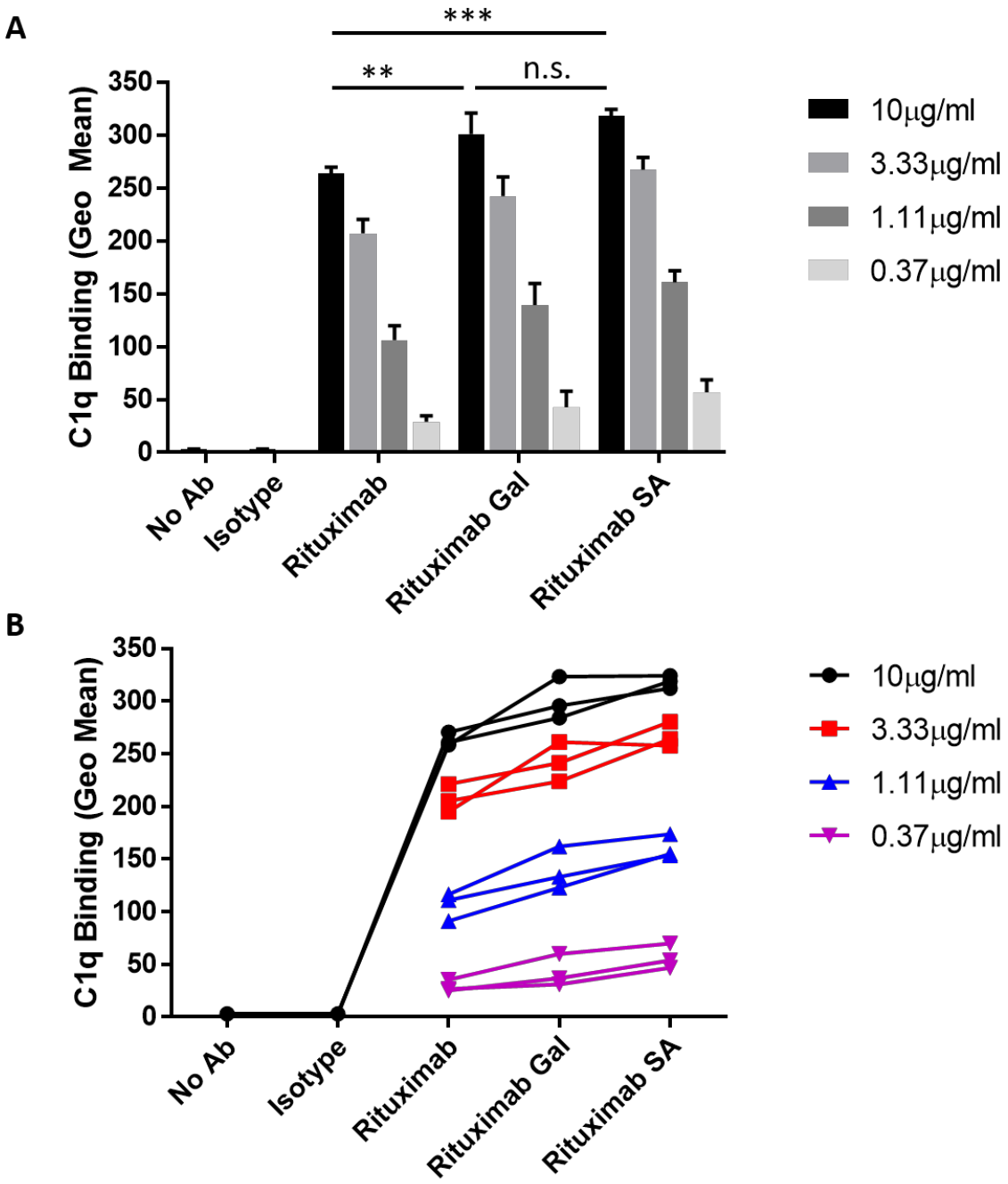

Figure 5-11 C1q Binding of Glycomodified Rituximab

Ramos cells opsonised with rituximab glycoforms at 10μg/ml were incubated with C1q, and bound C1q was detected with a FITC labelled anti-C1q antibody, and detected by flow cytometry. A- data shown represent mean plus SD of triplicate repeats of 3 independent experiments. Statistics calculated by one-way ANOVA with multiple comparisons of samples at 10μg/ml, ** p≥0.01, *** p≥ 0.001. B- data shown as individual points representing the mean of triplicate repeats of 3 independent experiments.

Rituximab displayed robust recruitment of C1q to the cell surface, whereas no signal was seen when an irrelevant, IgG1 control antibody was tested. Interestingly, galactosylated rituximab displayed significantly higher C1q recruitment than mock treated rituximab. Furthermore, sialylated rituximab recruited slightly more C1q than galactosylated rituximab. Although this trend did not reach statistical significance, it was consistent across all concentrations tested.

5.3.4.2 Complement Dependent Cytotoxicity (CDC)

We then sought to determine whether these differences in C1q recruitment translated to differences in the ability of the glycomodified antibodies to elicit CDC. In order in investigate this, target positive cell lines were opsonised with antibody and then incubated in the presence of 30% human serum in order to replicate the serum level present *in vivo*. Cells that were dead or had become permeabilised by the formation of MACs in the cell membrane were detected by PI staining.

Figure 5-12 shows the results of glycomodified rituximab (detailed in Table 5-2) in inducing CDC. Treatment of Raji cells with rituximab caused CDC in a dose dependent manner, reaching approximately 35% complement-mediated lysis at 10µg/ml. Galactosylated rituximab induced greater CDC than the mock treated rituximab at all doses tested, reaching approximately 55% killing at 10µg/ml. Sialylated rituximab shows further increased CDC compared to the galactosylated antibody, although the difference was smaller than that seen between the mock treated rituximab and the galactosylated rituximab. This increase was seen at both 10 and 5µg/ml, with over 60% killing seen at the top dose tested.

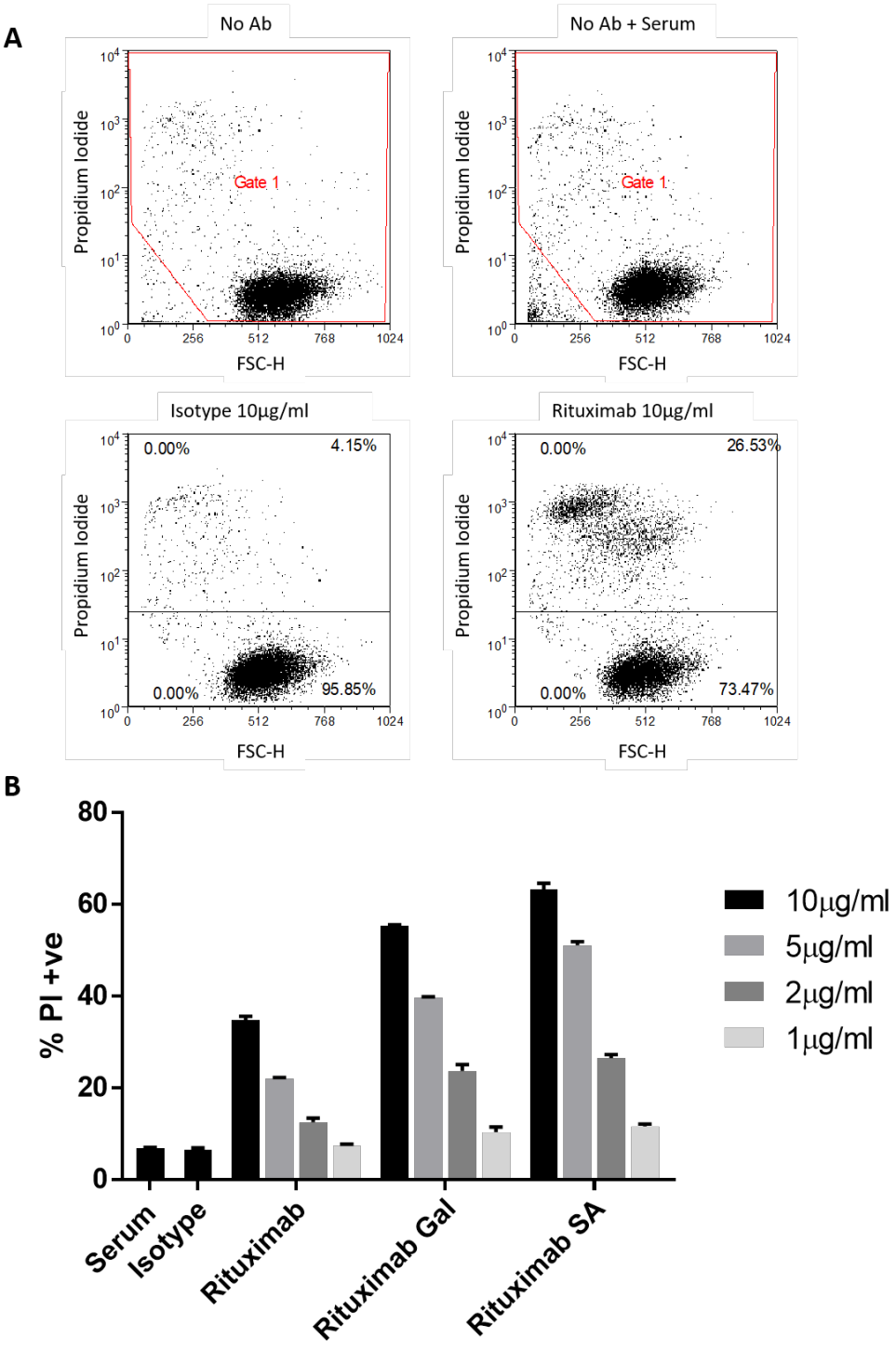

Figure 5-12 Effect of Glycomodified Rituximab on Complement Dependent Cytotoxicity

Raji cells were opsonised with various concentrations of mock treated rituximab, glycomodified rituximab, or an isotype control antibody (from Table 5-2) as indicated prior to incubation with 30% human serum for 30 minutes. Complement activation was detected as the ability of PI to enter cells, indicating activation of the MAC by the complement cascade. A- gating strategy for CDC assay, removing debris from serum and detecting cells death by propidium iodide staining. B- data plotted are mean + range of triplicate repeats of a single representative experiment.

The saturating concentration of 10µg/ml was chosen for further analysis across independent experiments. The increased killing seen with galactosylated rituximab over mock treated rituximab, and increased killing seen with sialylated rituximab over galactosylated rituximab, were found to be reproducible and statistically significant (Figure 5-13).

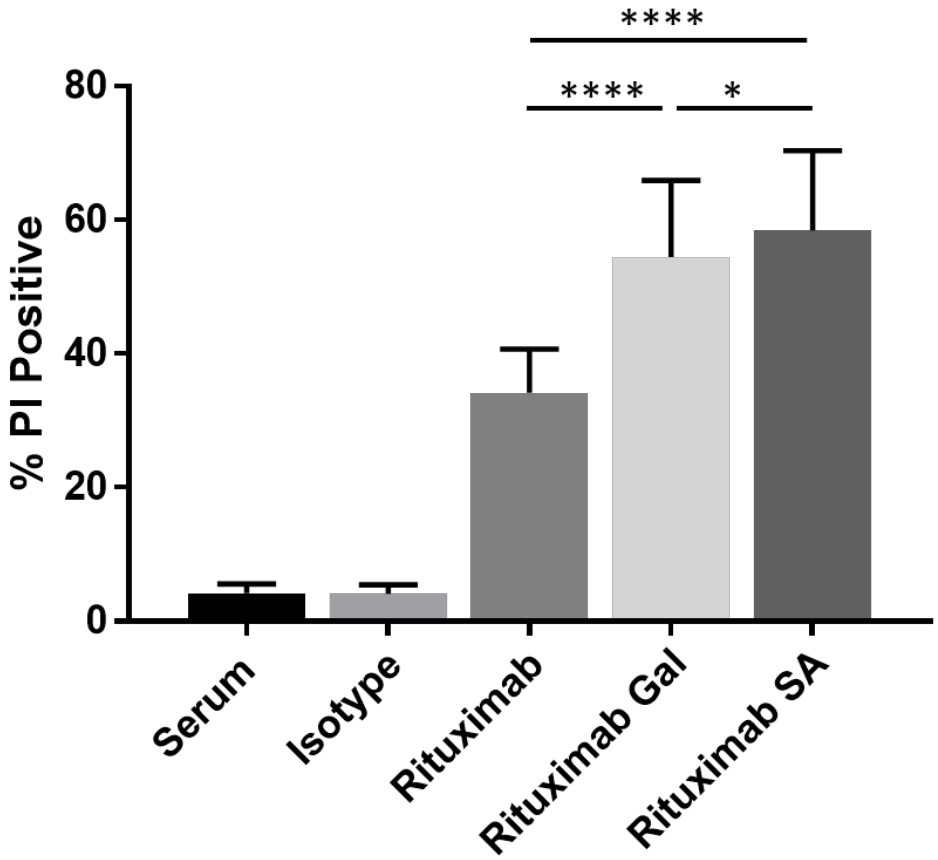

Figure 5-13 Effect of Glycomodified Rituximab on Increased Complement Dependent Cytotoxicity

Raji cells were opsonised with mock treated rituximab, glycomodified rituximab, or an isotype control antibody at 10µg/ml and incubated with 30% human serum for 30 minutes, then stained with PI to label permeabilised cells. Gating strategy as shown in Figure 5-12. Mean plus SD of nine independent experiments, each measured in triplicate. Statistics calculated by one-way ANOVA of paired data with multiple comparisons,* $P < 0.05$, **** $P < 0.0001$.

Raji cells are unusually resistant to complement mediated killing, as they retain the expression of complement defence molecules, principally CD55 and CD59, on their surface[239]. In contrast, Ramos cells lack these complement defence molecules and so are more sensitive to complement.

Therefore, Ramos cells were also tested as target cells for glycomodified rituximab induced complement mediated killing, to see if the same trends were observed.

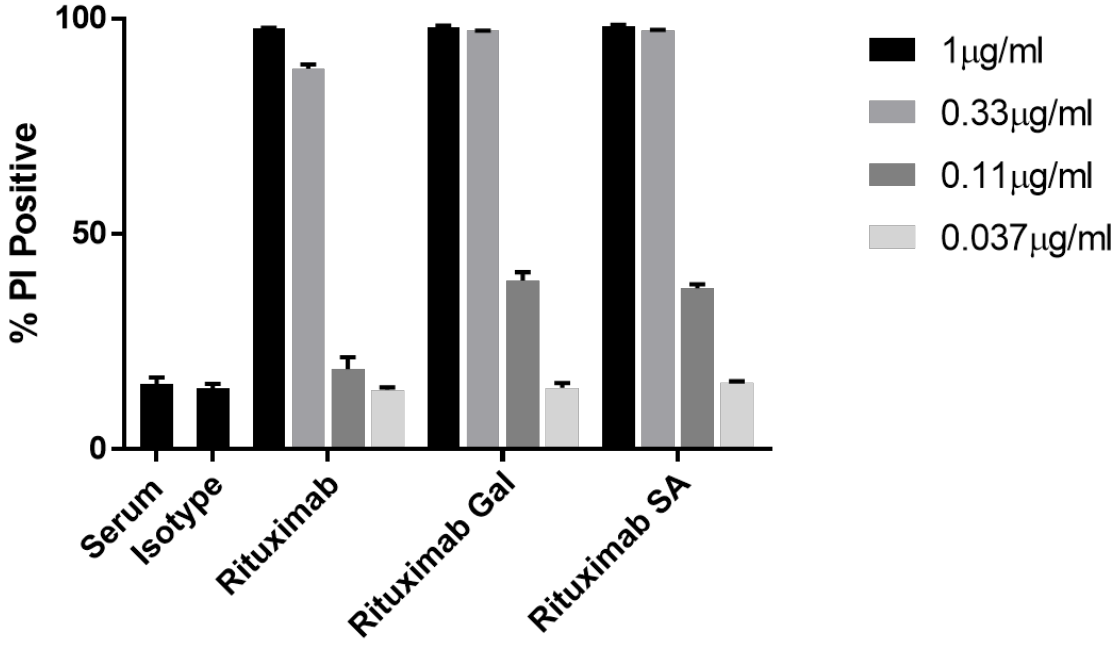

Figure 5-14 Effect of Glycomodification of Rituximab on Complement Dependent Cytotoxicity of Ramos Cells

Ramos cells were opsonised with mock treated, galactosylated or sialylated rituximab, or an isotype control, and incubated in the presence of 30% human serum for 30 minutes. Complement lysis was determined by PI staining and measured by flow cytometry. Gating strategy as shown in Figure 5-12. Data shown are means + range of triplicate repeats of a single representative experiment.

Figure 5-14 shows the increased sensitivity to complement mediated killing of Ramos cells compared to Raji cells, with 1μg/ml of mock treated, galactosylated or sialylated rituximab inducing 100% killing. The increased complement mediated killing of galactosylated and sialylated rituximab over mock treated antibody as seen for Raji cells was maintained with Ramos cells, and is evident at suboptimal doses where mock treated rituximab did not induce 100% killing (0.33 and 0.11μg/ml).

Rituximab is the prototypical type I anti-CD20 antibody in that it induces CD20 to cluster into detergent insoluble lipid rafts, and is highly efficient at binding C1q and inducing CDC[293]. Obinutuzumab and BHH2 are type II anti-CD20 antibodies, and as such do not cluster CD20 into

lipid rafts efficiently and do not induce high levels of CDC[280]. Therefore, we checked to see if glycomodification could increase the low levels of CDC seen with these type II antibodies when tested on Raji cells.

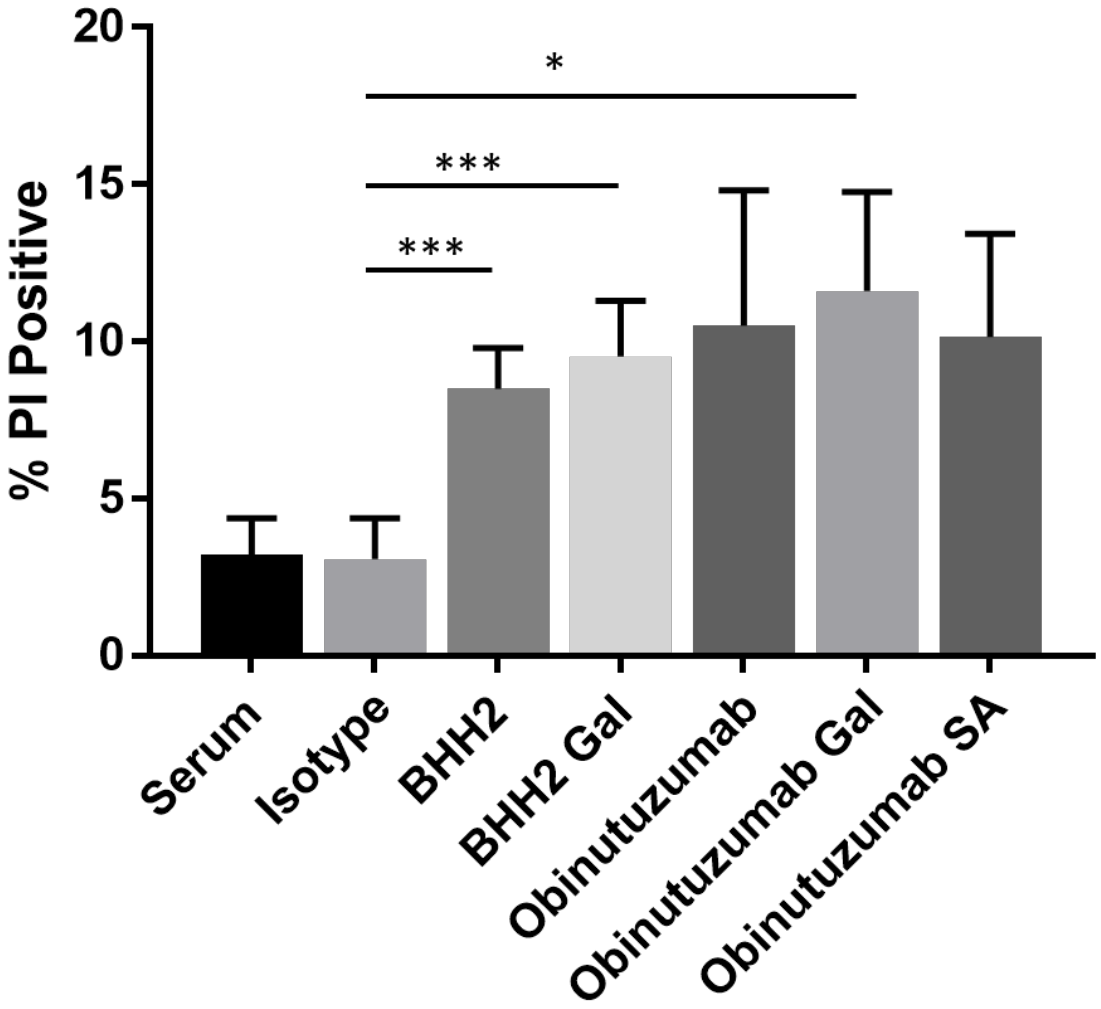

Figure 5-15 Effect of Glycomodification of Type II Antibodies on Complement Dependent Cytotoxicity

Raji cells were opsonised with 10µg/ml mock treated or glycomodified antibody, or isotype control, as indicated and incubated with 30% human serum for 30 minutes, with complement activity measured by PI penetration into cells. Gating strategy as shown in Figure 5-12. Data shown are means plus SD of 3 (Obinutuzumab) or 4 (BHH2) independent experiments, each measured in triplicate. Statistics calculated by one-way ANOVA with multiple comparisons,* $P < 0.05$, *** $P < 0.001$.

CDC assay was carried out in the same manner as for rituximab in Figure 5-12 and a low level of CDC was seen with both non-modified obinutuzumab and BHH2. However, galactosylation had no effect on the level of CDC seen with either antibody, and sialylation of obinutuzumab also had no effect (Figure 5-15). In order to see if there were any subtle effects of galactosylation or sialylation on the CDC induction of type II anti-CD20, obinutuzumab glycovariants were tested on complement sensitive Ramos cells.

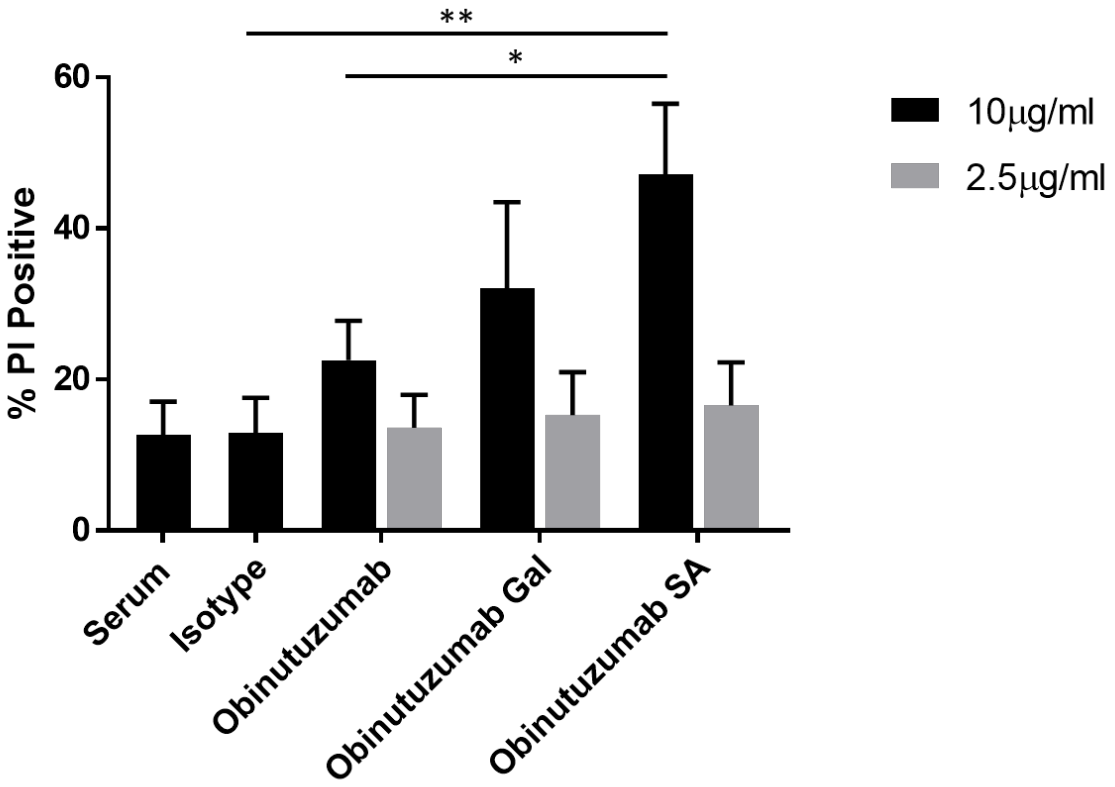

Figure 5-16 Effect of Glycomodified Obinutuzumab on Complement Dependent Cytotoxicity of Ramos Cells

Ramos cells were opsonised with mock treated, galactosylated or sialylated obinutuzumab, or an isotype control, and incubated in the presence of 30% human serum for 30 minutes. Complement activation was determined by PI staining and measured by flow cytometry. Gating strategy as shown in Figure 5-12. Data shown are means + SD of 3 independent experiments, each measured in triplicate. Statistics calculated by one-way ANOVA with multiple comparisons,* $P < 0.05$, ** $P < 0.01$.

Figure 5-16 shows that the type II antibody obinutuzumab was capable of inducing complement dependent cytotoxicity on Ramos cells, albeit to a much lower degree than the type I antibody rituximab (Figure 5-14). Whereas 1μg/ml of rituximab was sufficient to induce 100% killing of

Ramos cells (Figure 5-14), 10µg/ml of non-modified obinutuzumab only caused approximately 25% complement dependent cytotoxicity and no difference over background was seen with 2.5µg/ml. However, increased CDC was apparent with galactosylated obinutuzumab over mock treated. Furthermore, as for rituximab, sialylation of obinutuzumab appeared to induce greater CDC than did the galactosylated form, although this trend did not reach statistical significance.

Table 5-9 showed the production of a batch of glycomodified rituximab with higher levels of sialic acid. The effect of a greater amount of bi-sialylated glycans present on the Fc on complement activation was therefore tested using this material. The same trend was seen, with galactosylated rituximab showing increased CDC over mock treated rituximab and this increasing further with sialylated rituximab (Figure 5-17). Combination of galactosylated and sialylated antibody in a 1:1 ratio, giving a 5µg/ml concentration of each, gave a level of killing similar to that seen with galactosylated rituximab alone.

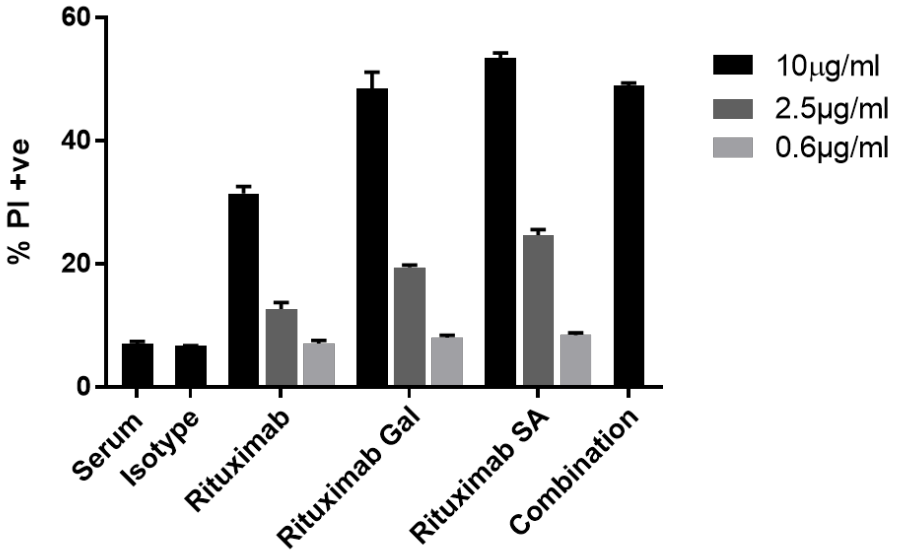

Figure 5-17 Highly Sialylated Rituximab Exhibits Increased Complement Dependent Cytotoxicity

Raji cells were opsonised with mock treated, galactosylated or sialylated rituximab (from Table 5-9), or an isotype control, and incubated in the presence of 30% human serum for 30 minutes. Complement activation was determined by PI staining and measured by flow cytometry. Gating strategy was as shown for Figure 5-12. Data shown are means + range of triplicate repeats from a single experiment.

5.3.5 Impact of Glycomodification on Antibody Half-life *in vivo*

Having established the *in vitro* production and efficacy of a range of glycomodified mAbs, next their *in vivo* persistence was examined. Prior to this, these antibodies were tested for their endotoxin level to prevent an anaphylaxis reaction (Table 8-1). All antibodies were found to have an acceptably low level of endotoxin. It has been reported that some forms of glycosylation on antibodies can affect their pharmacokinetic properties[499,500]. Accordingly, the glycomodified rituximab and obinutuzumab produced in Section 5.2 were assessed for their persistence in the serum of a wild type C57BL/6 mouse. Mice were injected intravenously with 25µg of the relevant antibody, blood samples were taken at several timepoints after injection, serum was isolated and the level of antibody present in the serum measured by an anti-human IgG ELISA.

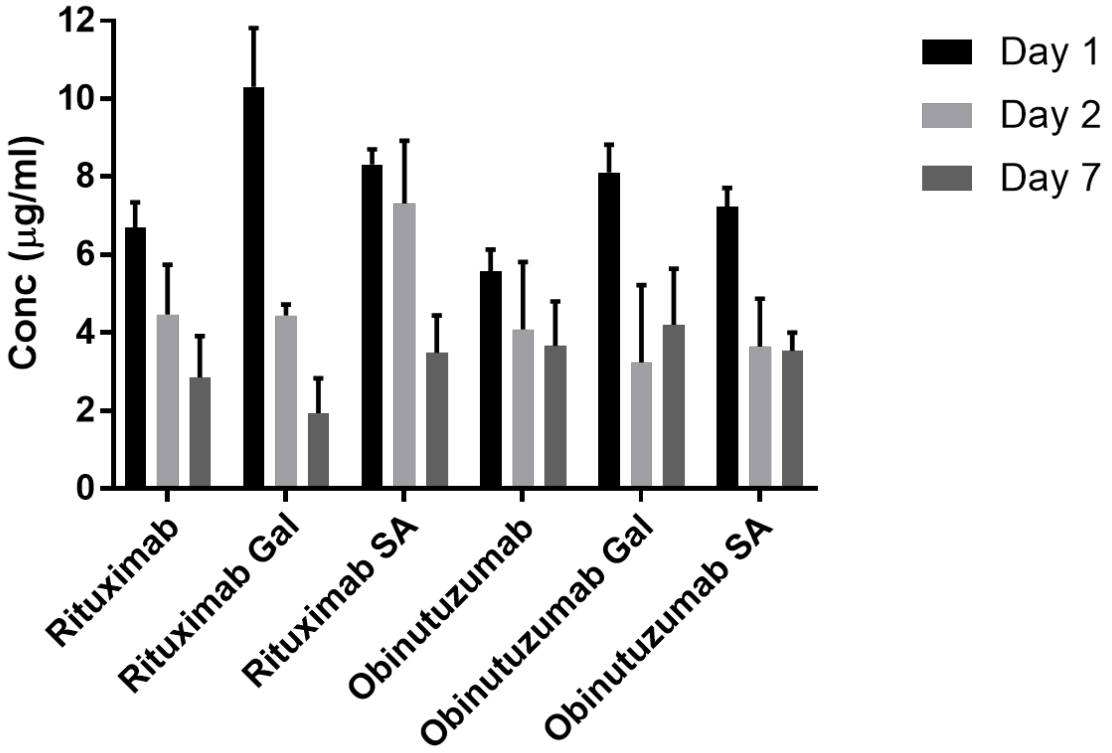

Figure 5-18 Half-Life of Glycomodified Antibodies in Wild Type Mice

25µg of mock treated or glycomodified antibodies were injected into the tail vein of wild type, immunocompetent C57BL/6 mice, and blood taken from these animals after 24hrs, 48hrs and 7 days. Serum taken from this blood was analysed by ELISA to determine the level of antibody remaining at each timepoint. Data shown represents mean plus SD antibody detected from 4 mice for each condition.

All antibodies tested were detectable in all animals for the duration of the experiment, and the concentration dropped over time as the antibodies were cleared from the circulation. For both rituximab and obinutuzumab the concentration of galactosylated antibody was higher than the level of mock treated antibody at day 1, but decreased to similar concentrations at days 2 and 7 (Figure 5-18). The sialylated antibodies also showed a slightly increased concentration at day 1 (and day 2 for rituximab), although again these became more similar to the mock treated antibodies as time progressed. Therefore the glycomodifications prolonged the short-term persistence over the first 24 hours before being cleared at a comparable level to non-glycomodified antibodies. In summary these data demonstrate that increases in galactose and sialic acid have minimal effect on the FcγR dependent effector functions of mAbs, but do increase the level of CDC induced and do not appear to influence their *in vivo* clearance.

5.4 Discussion

In this chapter the production and characterisation of a number of glycomodified antibodies was performed. Glycomodification of the Asn297 Fc linked glycan chain was achieved using purified recombinant human glycosyltransferases β- 1,4 galactosyltransferase and α- 2,6 sialyltransferase. Intact mass analysis of IdeS treated IgG revealed that complete galactosylation of starting material was achieved using 5µg of β- 1,4 galactosyltransferase per mg of IgG, in the presence of 10mM manganese chloride, 100mM MES buffer and 10mM UDP-galactose substrate. This was achieved for both rituximab and trastuzumab, which are both produced in CHO cells and contain mostly fucosylated complex glycans carrying 0 or 1 galactose residues. Following galactosylation both antibodies became fully galactosylated (G2), as shown in Table 5-1 and Table 5-5. Efficient galactosylation was also seen for obinutuzumab with its more complex set of glycans containing heterogeneity regarding fucosylation and a high degree of oligomannose (Table 5-3). Clearly, enzymatic galactosylation can be readily achieved *in vitro,* with a number of different mAbs, and to a high level of efficiency.

Sialylation of both rituximab, trastuzumab and obinutuzumab was achieved using α- 2,6 sialyltransferase and the substrate CMP-NANA at approximately 2mM. Both mono and bi-sialylated glycans were detected after sialylation, whereas these glycans were absent in both mock treated and galactosylated samples. The majority of these glycans were mono-sialylated, with only a small amount of bi-sialylated glycans detected by mass spectrometry of IdeS cleaved

antibody. Increasing the ratio of α- 2,6 sialyltransferase enzyme to IgG to 75µg per mg, increasing the substrate concentration to a 0.5:1 ratio with IgG, and decreasing the buffer concentration for the sialylation reaction increased the yield of sialylation achieved. In addition, the β- 1,4 galactosyltransferase enzyme was removed by an additional protein A purification step to prevent competition with the α- 2,6 sialyltransferase enzyme for the glycans. Analysis of the results indicated that a small increase in the level of bi-sialylation was achieved through these measures (Table 5-8), with approximately 30% of the glycans containing 2 sialic acid residues using the final protocol.

Although disappointing, communication with our collaborators at Roche led to speculation that the intact mass analysis of IdeS cleaved IgG was leading to an under-estimation of total sialylation. Consequently, glycan composition was then determined by Instant AB labelling of rapidly cleaved Fc glycans, and the resulting labelled glycan chains analysed by HILIC. This method suggested that much greater levels of sialylation had been achieved, with up to 35% of glycans containing 2 sialic acid residues (Table 5-7) using 50µg α- 2,6 sialyltransferase enzyme per mg of IgG, and 45% bi-sialylation achieved with 75µg of α- 2,6 sialyltransferase enzyme per mg of IgG (Table 5-9). Importantly, in both of these rituximab preparations there were virtually no non-sialylated glycans present, indicating that the level of sialylation was likely being underestimated by the IdeS based mass spectrometry method.

The highly complex nature of the glycosylation pattern of obinutuzumab was due to the glycoengineering strategy employed in the initial production of obinutuzumab. As discussed previously this is achieved through using CHO cells modified to overexpress the glycosyltransferase β-1,4 N-acetylglucosaminyltransferase III (Gnt III) and the glycosidase golgi α-mannosidase II enzymes (Figure 1-11)[280].

Gnt III catalyses the addition of a bisecting GlcNAc residue to the central mannose residue of the core heptasaccharide, and overexpression of this enzyme is responsible for the dramatically increased levels of bisected glycans found in obinutuzumab[407]. The presence of this bisecting GlcNAc has been reported to block the further addition of fucose, which was only present in approximately 60% of obinutuzumab glycans (Table 5-3). The absence of fucose resulted in an increased affinity for FcγRIIIa due to the absence of steric clashes between glycans, and improved ADCC [331,350]. Golgi α- mannosidase II cleaves off the final 2 mannose residues from the glycan chain during processing in the golgi apparatus [322]. This enzyme is overexpressed due to the side effect of overexpressing Gnt III, because in addition to producing a bisecting GlcNAc it also

prevents further processing by mannosidases and therefore results in an accumulation of hybrid glycans containing a bisecting GlcNAc [407]. Overexpressing golgi α- mannosidase II, as well as altering the location of the Gnt III enzyme in the golgi, pushes the glycans towards a complex type, although a significant proportion of hybrid glycans are still present (Table 5-3) [408].

11% of the glycans present on obinutuzumab were of the hybrid type, where golgi α-mannosidase II has not acted to remove both mannose residues. Of the 11% hybrid glycans, it was not possible to discern whether these glycans carried a galactose plus 4 mannose residues or 5 mannose residues, as the molecular mass of galactose and mannose are identical (180.156g/mol).

There was no difference in the level of sialylation achieved between fucosylated and afucosylated glycans (Table 5-3). This is perhaps not unexpected, since the fucose residue is at the opposite end of the glycan to the site of sialylation (Figure 1-12). The lack of detectable non-sialylated glycans on obinutuzumab suggests that this antibody could be more amenable to sialylation by α-2,6 sialyltransferase than rituximab.

The hM5B/hM4G1B signal had completely disappeared after sialylation (Table 5-3). The changes in this population allow for speculation as to the species present within the initial sample. The 11% of total glycans within this population in mock treated obinutuzumab consists of both hM5B and hM4G1B species (Table 5-3). However, after galactosylation the size of this population drops to 6% of total glycans. This likely reflects galactosylation of the hM5B species on the available GlcNAc residue (Figure 5-19). This was supported by the appearance of the hM5G1B species in the galactosylated sample (Table 5-3). After sialylation, both the hM4G1B and hM5G1B species disappear, with a concomitant appearance of the mono-sialylated forms of these species, hM4G1BS1 and hM5G1BS1. This confirms that the remaining 6% of the hM5B/hM4G1B signal was indeed hM4G1B.

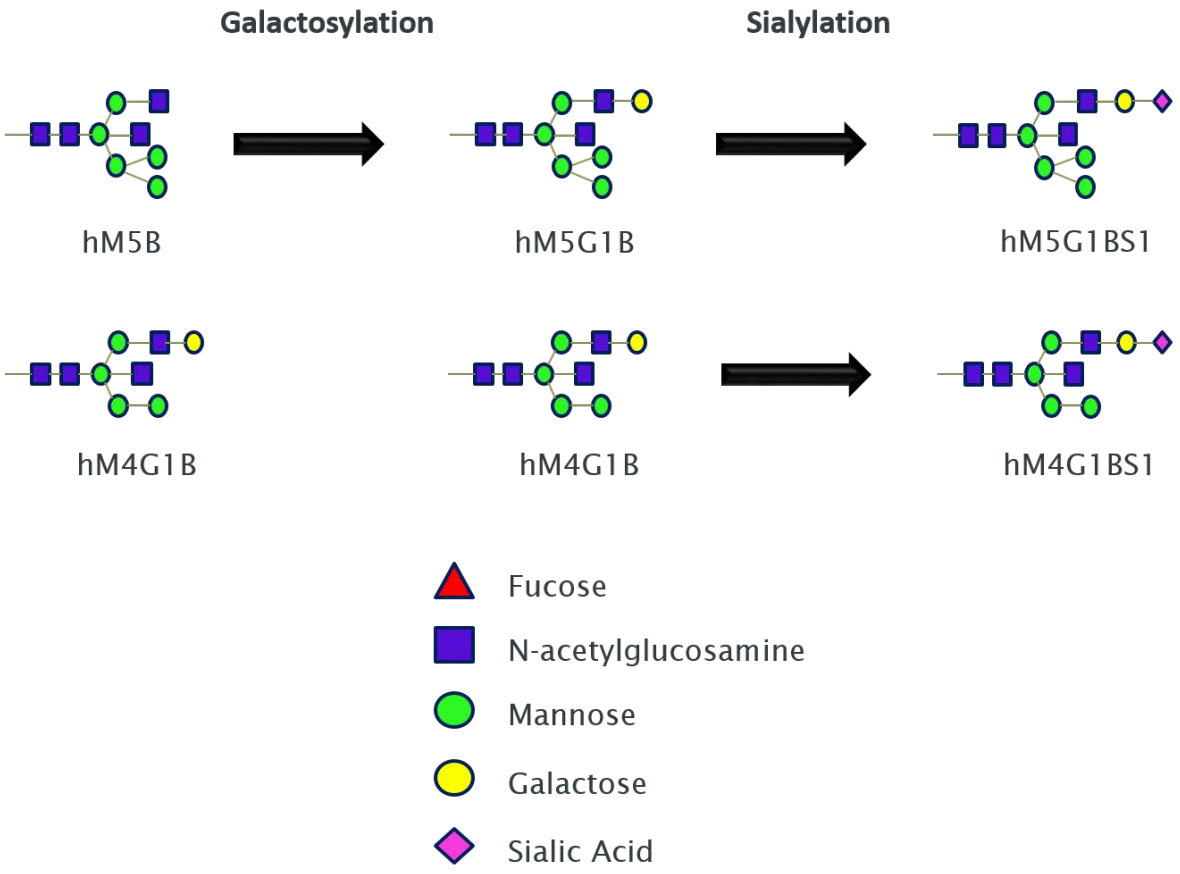

Figure 5-19 Proposed Glycomodification of Hybrid Glycans on Obinutuzumab

Obinutuzumab contains a number of hybrid glycans, containing one arm of oligomannose and one arm of complex glycans. Enzymatic glycomodification of these hybrid glycans can still result in addition of galactose and sialic acid to the complex arms of these glycans.

Addition of galactose and/or sialic acid to rituximab was demonstrated to have no effect on the antibodies ability to bind to its target antigen, CD20, as demonstrated in Figure 5-2. This is as expected, as the Fc glycans are located far away from the antigen binding regions of the Fabs. In contrast, Fab glycans, which are introduced through somatic hypermutation, have been reported to effect target antigen binding in some cases [501]. Fab glycans are also known to exhibit much higher degrees of processing than the glycans found in the antibody Fc, possibly due to increased access by glycosyltransferases.

There were also no major differences in the affinities of galactosylated and sialylated antibodies for the activatory receptors, FcγRI, FcγRIIa or FcγRIIIa, when measured by SPR (Figure 5-3 and Table 5-10). This data does not appear to match that published by Thomann *et al.* who reported

an increased binding of galactosylated and sialylated IgG1 to FcγRIIa and FcγRIIIa. However, this report did not contain the binding affinities calculated, and reported only relative binding compared to the non-glycomodified parental antibody. When the data generated here was analysed in the same manner, similar results were found (Figure 5-4), with an increased binding to FcγRIIa and FcγRIIIa seen for galactosylated and sialylated rituximab relative to the mock treated antibody.

The SPR analysis used in this work applied a 1:1 binding model to determine the affinity of glycovariants of rituximab to the FcγRs. As can be seen in Section 8.3, while some of these data appeared to fit relatively well to the 1:1 model and had a low Chi-squared value, other data deviated from the modelling to a greater extent. As such, it is therefore difficult to be entirely confident in the affinities determined here. In addition to this, there is a possible influence of mass transfer of the data. This could be the result of the amount of antibody captured to the chip (~2000RU), meaning the FcγR flowed over the chip could have been depleted, therefore altering the apparent on-rate of the antibody-FcγR interaction. To obtain a more reliable data set for this interaction it may therefore be desirable to apply a lower number of response units of IgG to the SPR chip, with the aim of maintaining enough soluble FcγR to allow for an accurate assessment of the on-rate. In turn, this may contribute to better fitting of the data to the 1:1 model, as an initial rapid binding phase that then becomes rate limited by the availability of soluble FcγR would not fit to a 1:1 binding model and would appear to be biphasic. However, given the apparent lack of differences in the calculated affinities and the maximum binding units, coupled with the broadly similar findings in the literature, it may be that these glycomodifications do indeed have little, if any, impact upon FcγR binding.

In this work, no obvious differences were found with galactosylated or sialylated forms of rituximab or obinutuzumab in the FcγR mediated mechanisms, ADCC or ADCP. Furthermore, both antibodies and their glycovariants were tested for their ability to induce ADCC in the presence of polyclonal IgG, and again no differences were apparent. This was perhaps not unexpected, as the binding data reported only a small increase in the binding to FcγRIIa and FcγRIIIa (Figure 5-3 and Figure 5-4). This is in accordance with other groups published works that suggests no impact of galactose or sialic acid upon ADCC[502].

It is indicated from studies using FcγR knockout mice that rituximab's *in vivo* effects are reliant upon FcγR dependent effector functions[253]. It is well known that absence of the Fc glycan chain leads to abrogation of these FcγR dependent effector functions[493]. It is also well established that

removal or absence of a fucose residue from the Asn297 linked complex glycan dramatically improves IgG affinity for FcγRIIIa and results in significantly improved ADCC[351].

However, regarding the influence of galactose and sialic acid upon FcγR mediated effector functions there have been conflicting reports, with some groups finding improvements and others reporting that these terminal sugars had no effect. Thomann *et al*., report an increased affinity for FcγRIIa and FcγRIIIa with highly galactosylated, as well as mono and bi-sialylated IgG1[406]. This translated into increased ADCC with the galactosylated antibody, while the mono and bi-sialylated antibody consistently showed a trend towards increased ADCC that did not reach statistical significance. The method employed in this paper was similar to the method used in this thesis, with recombinant human glycosyltransferases used to glycoengineer human IgG1 *in vitro*. Furthermore, the levels of sialylation achieved and used in Thomann *et al.'s* paper (47.7% S1 and 29.6% S2) were similar to those obtained in this work (53.2% S1 and 45.3% S2 for the highest achieved sialylation).

Quast *et al*. also report on the impact of sialylation on ADCC, using tetra-sialylated rituximab, and reported no effect of sialylation on NK mediated ADCC although there was a slight non-significant trend towards decreased killing[502]. Other groups have also reported decreases in ADCC, platelet depletion and binding to FcγRs for sialylated antibodies[372,503]. A possible reason for these discrepancies could stem from the different methods used to alter the glycosylation status of the antibodies used, and the different levels of sialylation that are achieved.

Afucosylated antibodies display a greater differential compared to fucosylated antibodies in the presence of background IgG. However, afucosylation has a large effect on the binding affinity of antibody to FcγRIIIa, increasing it by up to 50 fold[351]. This large increase is enough to allow afucosylated antibodies to effectively outcompete fucosylated antibodies present in the non-specific background IgG, whereas fucosylated forms of the same antibody cannot [280,504]. The modest increase in FcγRIIIa affinity of galactosylated and sialylated antibodies is unlikely to give these molecules enough of an advantage in competing for binding to have an impact on the total levels of cell lysis/phagocytosis seen in these assays.

The presence of the galactose and sialic acid residues distal to the fucose residue could explain the differential effect of these 2 glycans. Fucose is in contact with the glycans present on Asn162 of FcγRIIIa and FcγRIIIb, therefore removal of the fucose residue results in a closer interaction between the glycans present on the receptor and the antibody[387]. However, galactose and sialic

acid are located at the opposite end of the glycan and are present further down the CH2 domain (Figure 1-12 and Figure 5-20). This is far enough away from the FcγR binding site that there is no direct interaction with the FcγRs. Therefore, to have an effect on FcγR binding these residues would have to impact the structure of the FcγR binding site indirectly. Structural studies performed with different glycoforms of IgG have found that the sialic acid residues protrude from the IgG Fc regions, which could potentially make them available for binding to other molecules [332]. Presence or absence of these residues may thus not cause much, if any, change to the backbone conformation. This is in contrast to the structural changes seen with the CH2 backbone on removal of galactose and GlcNAc which causes the CH2 domains to collapse towards each other, hypothesised to be the cause for decreased FcγR binding to deglycosylated IgG [340].

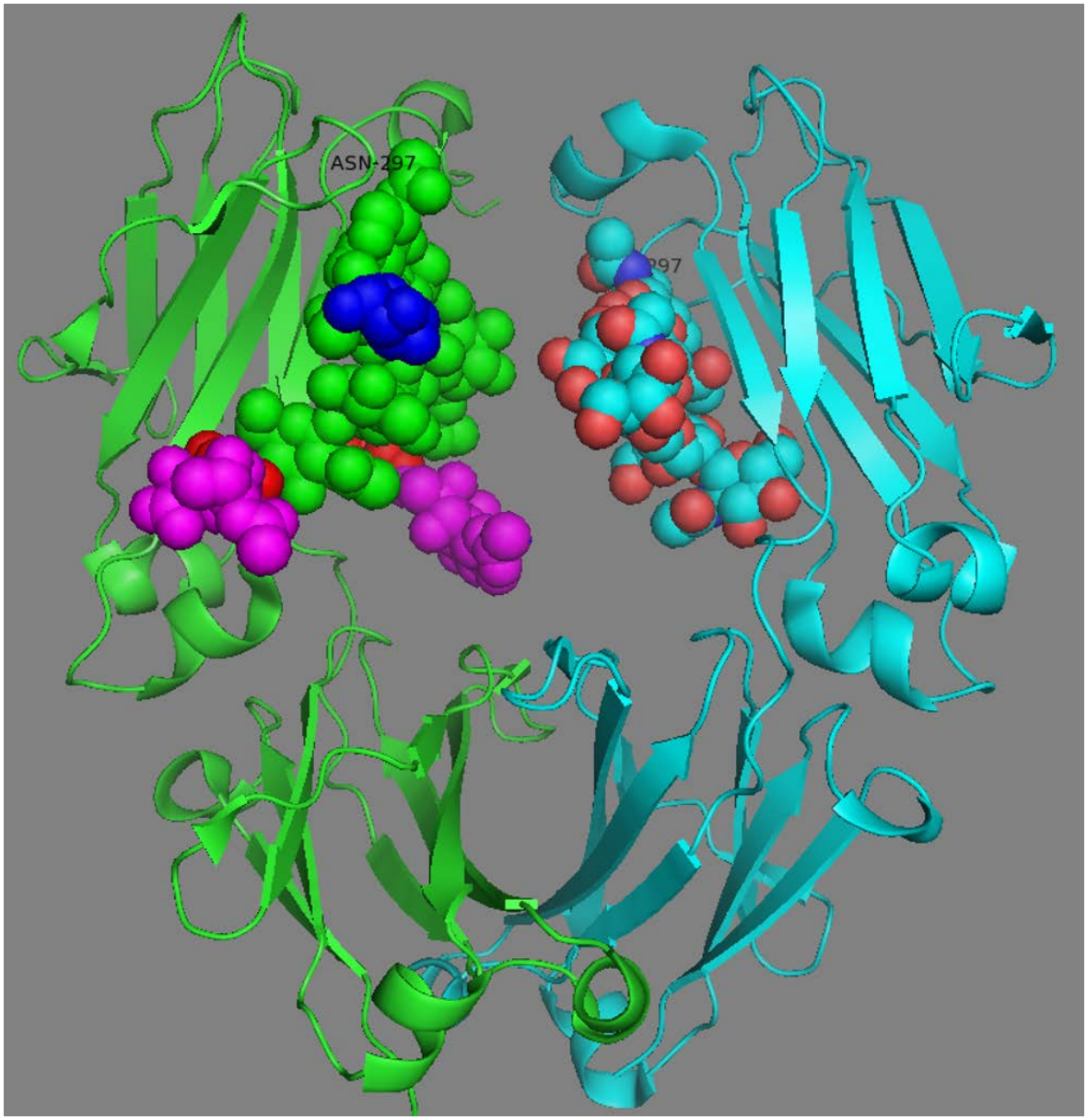

Figure 5-20 Model of Glycoengineered Fc

The position of galactose and sialic acid was modelled onto an IgG1 Fc backbone using PyMol and Coot. Dark blue- fucose, pink- sialic acid, red- galactose. IgG heavy chains are shown in ribbon form, green for one H chains and cyan for the second H chain with the glycan chains shown as spheres, coloured for the H chain they are linked to (or as described above).

It was found that galactosylation of antibodies caused an increase in the level of both C1q recruitment as well as the induction of complement dependent cytotoxicity (Figure 5-11 and Figure 5-13). This is in accordance with the literature, where highly galactosylated antibodies have been reported to induce increased CDC[505,506]. It was also found that sialylation of antibody was

able to further increase the level of CDC induced. This finding is in direct conflict with those recently reported by Quast *et al*[502]. This group found that tetra-sialylated rituximab (2 sialic acids per heavy chain glycan) induced reduced complement mediated lysis compared to control rituximab. They also reported that C1q binding of tetra-sialylated rituximab, which was increased for galactosylated rituximab, decreased to levels slightly lower than that seen for unmodified rituximab, whereas increased C1q recruitment for both glycoforms was shown here.

In Quast's paper the method used to generate tetra-sialylated rituximab differed from the approach used in this chapter. Tetra-sialylated rituximab was produced by cleaving off the Fc glycan leaving only a GlcNAc residue with fucose attached. A chemically synthesised fully sialylated glycan from a donor oxazoline was then transplanted onto this short glycan as first described by Huang *et al*[354]. As well as this chemoenzymatic glycoengineering method, Quast *et al.,* also generated galactosylated and sialylated rituximab using an enzyme based glycoengineering approach similar to that used in this work. They report that sialylated rituximab generated by this method also displays a decreased ability to induce complement mediated lysis of Raji cells, albeit exhibiting a smaller decrease than was seen for the tetra-sialylated rituximab. Furthermore, enzymatically sialylated rituximab exhibited decreased C1q binding compared to galactosylated rituximab, but increased C1q binding compared to both unmodified and tetra-sialylated rituximab.

This perhaps indicates that enzymatic sialylation was not complete (despite an enrichment step using lectin affinity chromatography), and that some terminal galactose residues were present within the sialylated rituximab- as suggested by the lectin blotting shown in the Quast paper. This matches their suggestion that sialic acid decreases complement dependent cytotoxicity, as incomplete sialylation resulted in a level of complement activation intermediate between tetra-sialylated rituximab and galactosylated rituximab. Once again this conflicts with the findings presented here, where mixing sialylated rituximab with galactosylated rituximab (Figure 5-17) - essentially reducing the concentration of sialylated rituximab - resulted in no decrease in the level of CDC seen.

Similarly, the work presented here has been done with sialylated rituximab preparations that were not homogeneous and likely contained terminal galactose residues. However, in terms of complement activation, the opposite trend was seen to that reported by Quast- addition of sialic acid residues to galactosylated rituximab caused an increase in the level of CDC seen (Figure 5-13). A possible explanation for this discrepancy could be the different methodologies used in

carrying out complement based assays. The assay in this thesis used a short incubation period with a high, physiologically relevant concentration of human serum (30%), whereas Quast *et al.*, use a longer (12 hour) incubation period with a low concentration of human serum (5%). This is important as CDC is typically rapidly initiated (within seconds to minutes) at physiological levels of serum and so the long incubation time has the possibility to involve multiple other cell death mechanisms in addition to classical CDC. In addition, different detection methods were used to highlight cell death, although both were based on accessibility of nucleic acids after complement mediated membrane damage.

Finally, the effect of glycomodification on serum half-life of both rituximab and obinutuzumab was assessed. Both galactosylation and sialylation caused a trend towards increased antibody levels in the serum 1 day after administration, although this was not maintained and by 7 days all glycoforms were at a similar concentration to the unmodified parental antibody. Sialic acid has been reported to be an important glycan on the surface of several soluble proteins for extending their half-life, likely by reducing the interaction with the asialogylcoprotein receptor by masking the surface exposed galactose residues. However, as the Fc glycans are mostly buried within the Fc of the antibody, it is possible that any terminal galactose residues are hidden. Increased galactose did not appear to increase the clearance of the antibodies compared to either the sialylated or mock treated versions. Furthermore, IgG antibodies benefit from recycling interactions with FcRn, enabling these antibodies to be rescued from lysosomal degradation. FcRn binding is not thought to be heavily affected by antibody glycoform, as shown using both SPR and a column based HPLC assay[507].

In summary, glycomodified antibodies enriched for galactose and sialic acid were generated using an *in vitro* enzymatic glycoengineering approach. Galactosylation was readily achieved producing a homogeneous product using a low enzyme to antibody ratio, in the presence of manganese. Addition of sialic acid required a greater level of enzyme per milligram of IgG and for a shorter time course. The initial method of glycoanalysis, mass spectrometry of IdeS cleaved IgG, was efficient for analysis of antibody galactosylation, but appeared to underestimate the level of sialylation. An alternative method that was still suitable for use on small amounts of sample that was more accurate for detecting sialic acid was the use of Instant AB. This method suggested that sialylation was indeed being achieved, although there was heterogeneity in the final glycan structures present within the antibody product.

Glycomodification did not alter the ability of antibody to bind to its target antigen expressed on cells, and appeared to have a modest effect on the FcγR binding affinities as measured by SPR for FcγRI, FcγRIIa and FcγRIIIa, and in a cell based assay for FcγRIIb. This minimal change in FcγR affinity translated into very little effect on FcγR mediated effector functions, with both ADCC and ADCP being unaffected by galactosylation and sialylation. Galactosylation increased the level of complement dependent cytotoxicity seen compared to mock treated antibodies. However, antibody sialylation was found to further increase the level of complement killing above that seen for purely galactosylated antibodies.

Chapter 6: C1q Column

6.1 C1q Introduction

Humoral immunity is known to be mediated by circulating antibodies consisting of five different isotypes: IgA, IgD, IgE, IgG and IgM (discussed in Section 1.2). These antibodies engage a broad range of effector functions, some specific to a particular isotype and some shared[1]. For example, all antibody isotypes have the ability to bind target antigens and form immune complexes, whereas only IgG antibodies are able to induce FcγR mediated responses, such as target phagocytosis (although other isotypes can elicit similar through alternate receptors such as IgαR)[74]. Another Fc mediated effector function is the activation and engagement of the complement system; only IgG and IgM antibody isotypes are effective at initiating this mechanism[6].

The complement system comprises a number of serum proteases that are activated in a sequential manner, resulting in a tripartite response- releasing anaphylatoxins to recruit immune effector cells, opsonising the target cell for phagocytosis and potential permeabilisation of the target cell membrane through formation of the membrane attack complex[6]. IgG and IgM antibodies activate the classical arm of the complement system, by recruiting the C1 complex to the surface of the opsonised cell (Figure 1-6). The C1 complex contains over 20 polypeptide chains, with 2 copies of the serine proteases C1r and C1s (involved in the proteolytic cascade that drives the complement cascade) mounted onto the C1q molecule[508].

As described in Section 1.4.2, C1q is a very large protein complex (450kDa), made up of 18 polypeptide chains, 6 each of C1qa, C1qb and C1qc, which form into a 'bouquet of flowers' conformation[190]. The broad ligand binding properties of C1q stem from the heterotrimeric globular head groups formed from the carboxy terminus of the peptides. For example, C1q is known to bind to IgG and IgM antibodies, but also binds to many other molecules including proteins such as C reactive protein (CRP), and certain glycan motifs commonly found on the surface of pathogenic bacteria[509].

Due to the large size of the C1q complex and its multimeric nature, it can be difficult to accurately measure its affinity for ligands. As C1q contains 6 binding head groups, it can make up to 6 interactions to ligand binding sites[190]. Some molecules, such as CRP and IgM, contain multiple

binding sites within a single molecule, allowing for efficient binding to C1q despite a generally low affinity interaction between the individual C1q head groups and their ligands[6]. However, other ligands, such as IgG, only contain a single C1q binding site, and therefore bind to C1q weakly.

Past studies have reported the binding affinity between IgG Fc and C1q to be of high millimolar affinity[207]. Various strategies have been used to study IgG-C1q interactions, however these methods largely use complexed IgG, often following immobilisation onto a solid surface or through heat or other methods of immune complex formation. This is not ideal, as each batch of complex generated will be variable in relation to ligand structure and the number of available C1q docking sites, therefore changing the overall binding avidity. Recently, the C1q globular head groups have been recombinantly produced in both wild type and various mutant forms, providing a key resource for determining the important residues required for binding of C1q ligands, such as IgG[200,510].

Building on this, a single chain form of the heterotrimeric C1q globular head group has recently been reported[510]. This construct retained comparable levels of binding to various C1q ligands compared to a wild type C1q head group liberated from the full length C1q molecule by enzymatic digestion. These findings show that a single chain form of the C1q head group is active in ligand binding and amenable for use in SPR based experimental setups. However, this same set up was unable to detect scC1q binding to monomeric IgG that had been immobilised to the experimental chip, both for recombinantly produced and serum isolated C1q head groups, whereas hexameric C1q did show IgG binding. This indicates that this method simply does not allow for enough low affinity C1q head group-IgG interactions to allow for the determination of any kinetic parameters, and another approach is required to allow for the detection of scC1q binding to monomeric IgG.

Therapeutic mAbs approved for use in humans are largely of the IgG isotype, and accordingly can activate complement *in vivo*[70]. Furthermore there is evidence of complement activation for some therapeutic mAbs (such as rituximab) *in vivo*, through the depletion of complement components[455]. Recently a number of new mAbs have entered the clinic which do not function by depleting the target cells, as earlier therapeutic mAbs such as rituximab and trastuzumab were thought to, but instead function by blocking signalling molecules that are inhibiting the immune system[164]. As these immunomodulatory mAbs bind to immune cells required for the desired therapeutic outcome, engaging depletion mechanisms such as that mediated by the complement system, is likely counterproductive. Clearly, the potential requirement for complement varies with the nature of the mAb target. Therefore a tool with which to study the consequences of

mutations and different mAb formats on C1q binding affinity would be of use for improved antibody development.

This chapter concerns the development of such a tool and sought to determine whether a single chain format of C1q globular head group trimer could be utilised in an HPLC based methodology in order to study the interaction of C1q and various ligands, including monomeric IgG. A potential benefit of this approach, in addition to being readily amenable for automation and high throughput screening, is the ability of HPLC based systems to identify and separate subpopulations from within a heterogeneous sample that would not be seen by other approaches that give an average value for the whole sample tested. For example, in the study of IgG binding to FcγRIIIa, a mixed population of antibody containing both Fcs with and without fucose would not be identifiable if studied by SPR, whereas testing these samples in an HPLC format containing immobilised FcγRIIIa shows both fucosylated and afucosylated samples[507].

In this work, a single chain version of C1q was first produced, and then a set of HPLC based conditions established that were permissive to IgG binding and reflective of biologically relevant conditions for a range of ligands.

6.2 Production and Characterisation of a Functional Single Chain C1q Molecule

6.2.1 Production of a Single Chain Form of C1q

In order to produce an HPLC column for studying C1q binding to IgG and other ligands, a single chain form of the C1q head group was produced (Section 2.5.1.1). The genes for *C1qa, C1qb* and *C1qc* were ligated together with short linker sequences and produced in HEK293 cells.

C1q was biotinylated using the BirA bulk biotinylation kit (Avidity) and dialysed into PBS. In order to confirm the activity of the single chain C1q (scC1q), the ability of this construct to bind IgG was tested in various contexts.

6.2.2 Characterisation of Single Chain C1q

The scC1q construct was biotinylated to facilitate easy coupling to sepharose for packing into HPLC columns, but also serves as a convenient tag for detecting the functional binding of this agent to cells. As such, agents that bind to biotin, including streptavidin and anti-biotin specific antibodies, could be deployed to detect scC1q binding. Using these agents flow cytometry was performed and showed that the scC1q molecule was able to bind to cells opsonised with trastuzumab mutants predicted to have an increased C1q binding, as detected with streptavidin labelled with FITC or APC, as well as with an antibody specific for biotin (Figure 6-1A).

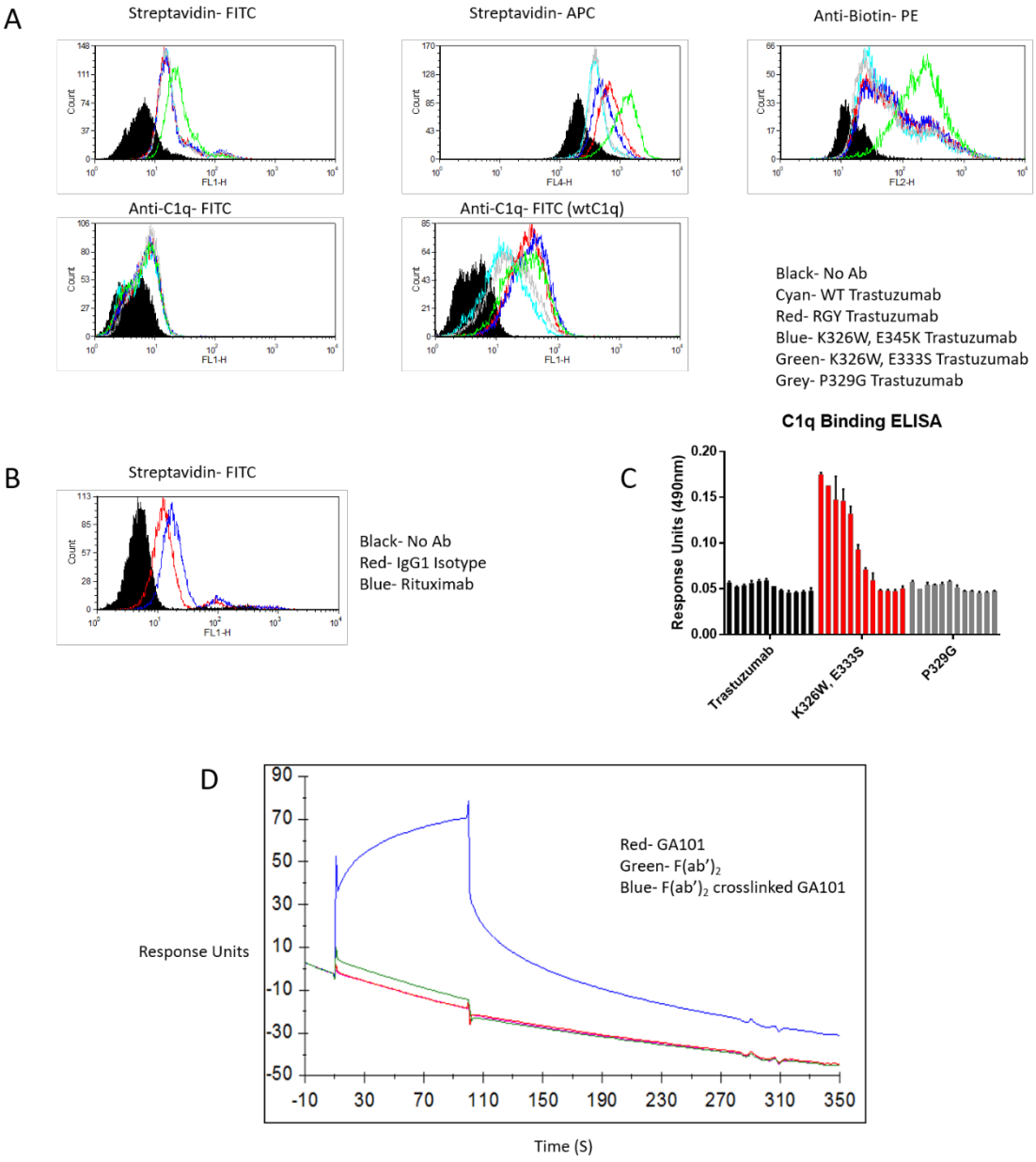

Figure 6-1 Characterisation of the scC1q Construct

Validation of the single chain C1q (scC1q) constructs binding to IgG. A- binding of scC1q to MDA-MB-453 cells opsonised with trastuzumab mutant mAbs. Top left- detection by FITC labelled streptavidin, top middle- detection by APC labelled streptavidin, top right- detection by anti-biotin antibody labelled with PE, bottom left- detection by anti-C1q antibody labelled with FITC, bottom middle- detection of full length wild type human C1q binding to trastuzumab mutants on MBA cells detected by anti-C1q antibody labelled with FITC. B- binding of scC1q to SUDHL4 cells opsonised with rituximab or an irrelevant IgG1 isotype, detected by FITC labelled streptavidin. C- scC1q was immobilised onto a maxisorb plate and incubated with trastuzumab mutants. Binding of trastuzumab mutants to plate bound scC1q was detected using an HRP conjugated anti-IgG Fc antibody. OPD based peroxidase substrate was added to determine the level of IgG bound to each well. D- biotinylated scC1q was captured on to the surface of a streptavidin coated Biacore SPR chip. Monomeric and F(ab')$_2$ crosslinked IgG was flowed over the chip to determine binding to scC1q (experiment performed by collaborators at Roche).

Of the mutations used, the RGY triple mutant contains E345R, E430G and S440Y point mutations known to cause solution state hexamerisation and dramatically increased C1q binding as tested on opsonised cells by flow cytometry, and complement activation as shown by complement mediated cell lysis[80]. The K326W E333S double mutant has been reported to significantly increase C1q binding (assayed by ELISA) and complement mediated lysis when tested on an anti-CD20 antibody backbone[490]. The K326W E345K double mutant is predicted to also display increased C1q binding through increased affinity (from the K326W mutation) and potentially increased hexamerisation (from the E345K mutation)[80,490,511]. The P329G mutant is known to abrogate IgG Fc mediated effector functions, including C1q binding (assayed by ELISA), and was thus included as a negative control[432].

Binding of a directly labelled anti-C1q antibody to the scC1q was barely detected, with no difference between positive controls that bind C1q strongly (the K326W, E333S mutant, the K326W, E345K mutant and the RGY triple mutant) and negative control that does not bind C1q (the P329G mutant). Binding of C1q to these antibody constructs was confirmed using full length C1q detected with the directly labelled anti-C1q antibody. Binding to wild type rituximab bound to SUDHL4 cells was also detected using FITC labelled streptavidin (Figure 6-1B) demonstrating the scC1q binding was not restricted to trastuzumab mutants. Binding of the K326W, E333S trastuzumab mutant to C1q was also seen when detected in an ELISA format. The P329G trastuzumab mutant was found not to bind to scC1q when opsonised onto cells or when scC1q was immobilised onto the wells of a plate (Figure 6-1C). scC1q was not able to bind to monomeric obinutuzumab (GA101) after capture onto a Biacore SPR chip, but binding was observed for obinutuzumab crosslinked by a $F(ab')_2$ targeting the IgG Fab region, highlighting the need for IgG crosslinking in order to detect IgG-C1q interactions by current methods (Figure 6-1D).

6.3 Defining and Optimising C1q Column Operating Parameters

Having determined the scC1q was functional in its capacity to bind IgG, it was coupled to streptavidin coated sepharose beads, and packed into Tricorn 1ml glass columns (4.6 x 50mm). A salt based elution gradient was selected in order to try and facilitate both the binding and release of IgG to the scC1q within the column. Starting at time zero, the column running buffer contained

0mM NaCl. NaCl was then titrated into the system from 10 minutes onwards, as summarised in Table 6-1.

Time (mins)	% Eluent A (20mM HEPES, pH 7.4)	% Eluent B (20mM HEPES, 500mM NaCl, pH 7.4)
0	100	0
10	100	0
70	60	40
80	0	100
90	0	100
93	100	0
105	100	0

Table 6-1 Standard Column Operating Conditions

6.3.1 Buffer Optimisation

Firstly, several different buffer systems were tested to see if binding and release of IgG from the column could be detected. A human IgG1 mAb directed against HER3 was used as a reference standard antibody for column testing.

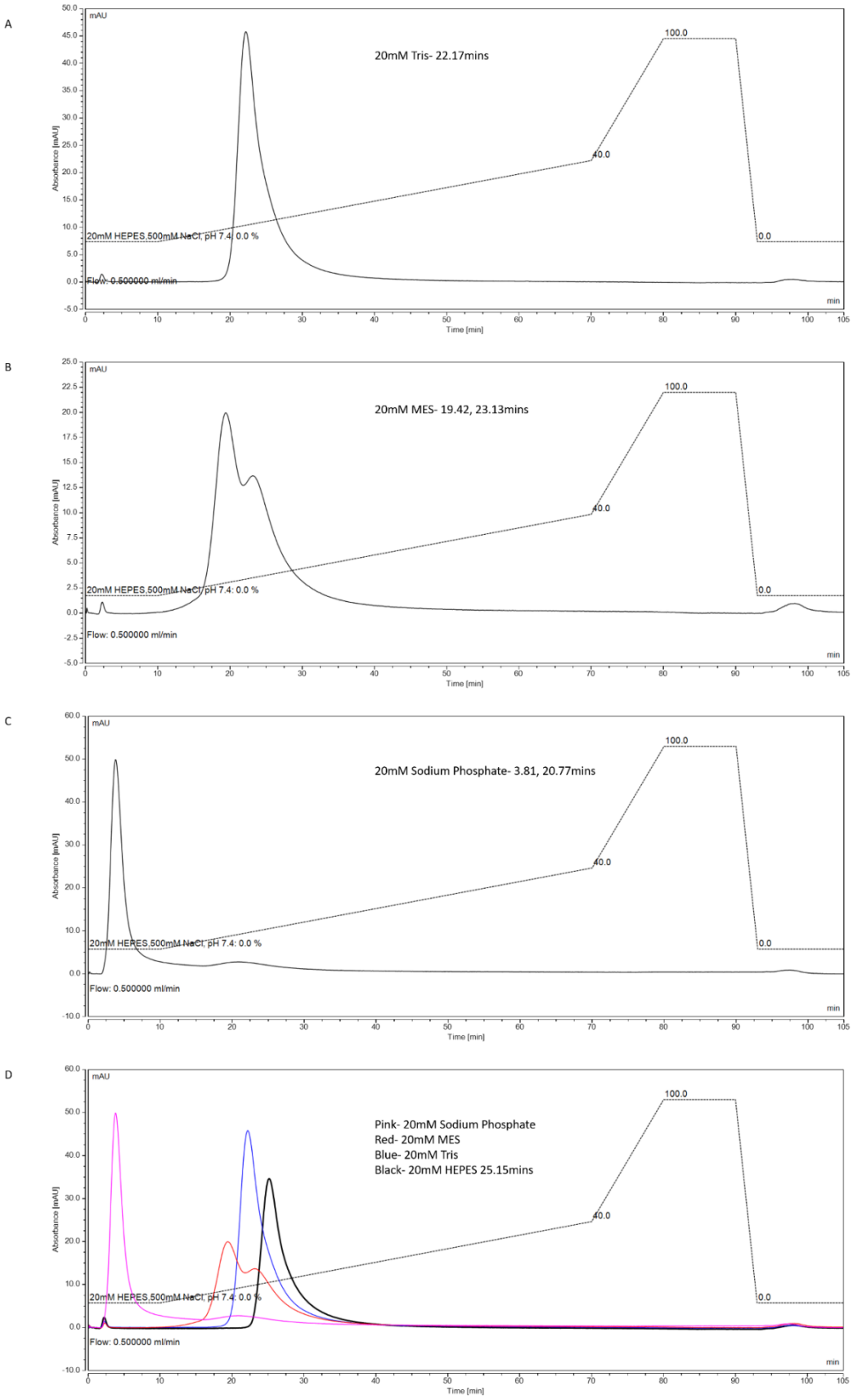

Figure 6-2 C1q Column Running Buffer Optimisation

50µg IgG1 was injected onto the column in different running buffers, tested with the same NaCl based elution gradient. A- 20mM Tris pH 7.4, B- 20mM MES pH 7.4, C- 20mM Sodium Phosphate pH 7.4, D- overlay of A-C and 20mM HEPES pH 7.4 (black).

IgG binding to the C1q column was seen in Tris, MES and HEPES buffers, but only minimal binding was seen in sodium phosphate buffer (Figure 6-2). The highest binding (defined as the latest elution time) was seen with 20mM HEPES buffer (Figure 6-2D).

6.3.2 Salt Optimisation

Having identified an optimal running buffer of 20mM HEPES, the salt used for driving antibody elution was assessed. Elution of IgG from the C1q column using KCl rather than NaCl had a slightly reduced retention time (Figure 6-3). NaCl was therefore used in all work hereafter.

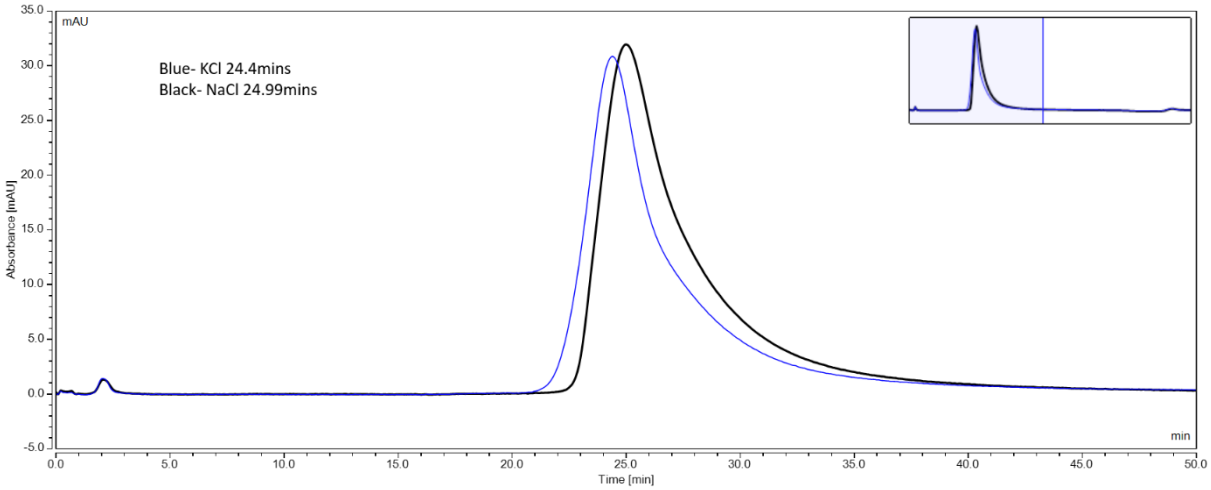

Figure 6-3 C1q Chromatography Elution Salt Optimisation

Elution of IgG1 from the C1q column with different salts. 50µg of IgG1 was injected onto the 1mg C1q column and eluted in eluent A containing 500mM of NaCl (black) or KCl (blue). Chromatogram was truncated to display the first 50 minutes for clarity, insert shows full 105 minutes.

6.3.3 IgG Subclass Specificity

Next, the column was assessed for its ability to discriminate between distinct IgG subclasses. To do this IgG1 and IgG4 (known to bind C1q more weakly than IgG1) were injected onto the column using the refined conditions previously established.

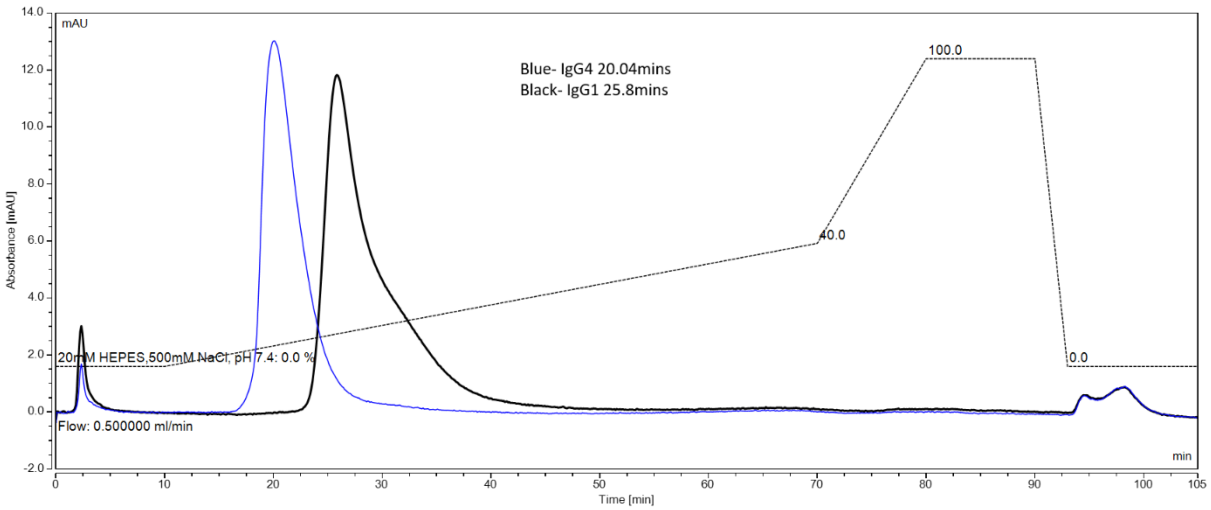

Figure 6-4 C1q Chromatography of IgG1 and IgG4

Overlaid chromatograms of 25µg of IgG1 (black) or IgG4 (blue) injected onto the C1q column in 20mM HEPES, using a 0-40-100% NaCl gradient.

Overlaying the chromatograms obtained from injecting both IgG1 and IgG4 onto the C1q column revealed the increased retention time of the IgG1 subclass, as would be expected (Figure 6-4).

6.3.4 Gradient Optimisation

In order to try and improve the resolution between IgG1 and IgG4, the change in salt gradient was explored.

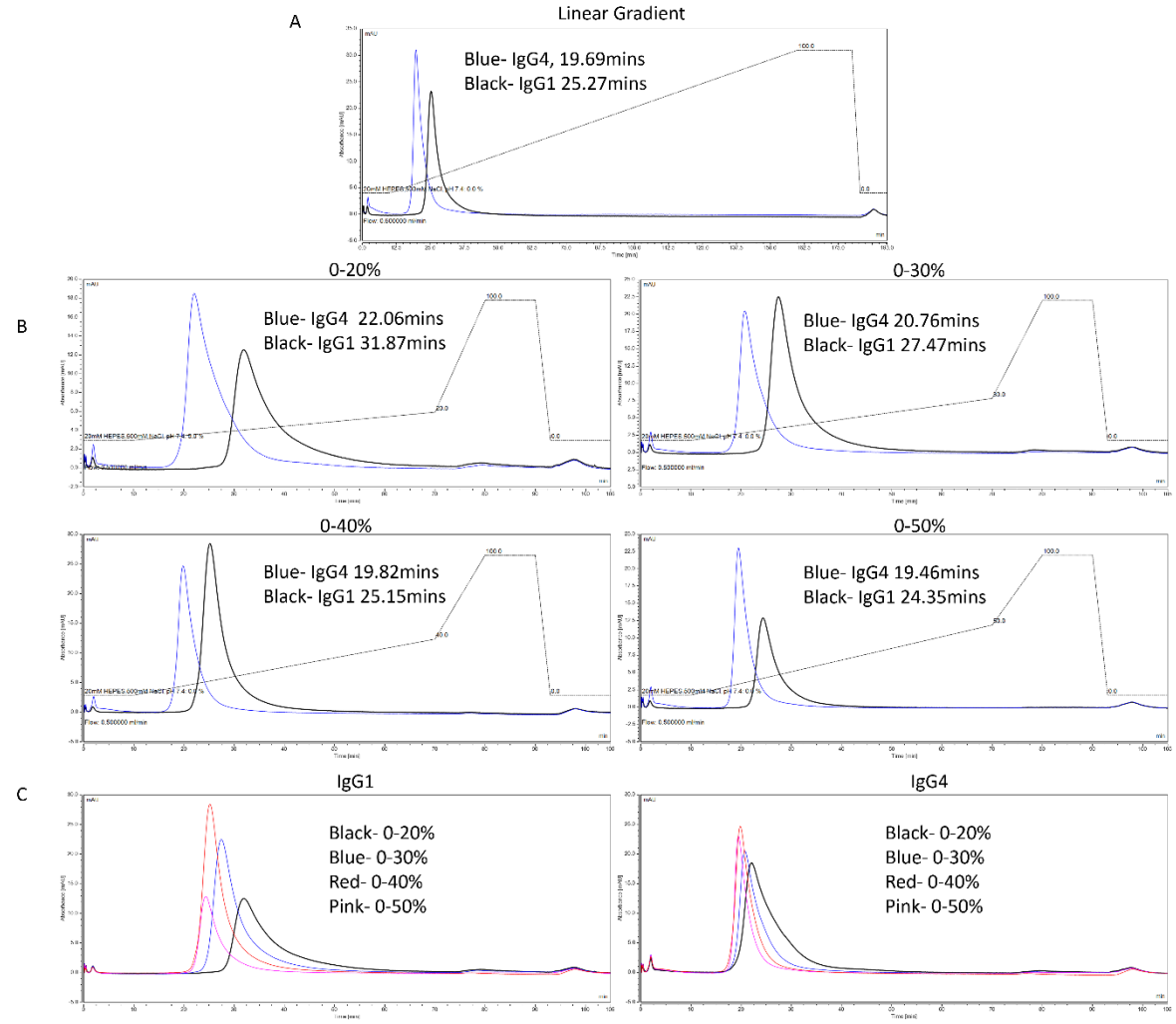

Figure 6-5 C1q Chromatography of IgG1 and IgG4 Using Different Salt Gradients

Testing of different NaCl gradients. A- comparison of IgG1 (black) and IgG4 (blue) on a linear NaCl gradient. B- comparisons of IgG1 (black) and IgG4 (blue) on various different NaCl gradients, top left- 0-20% gradient 50µg IgG, top right- 0-30% gradient 50µg IgG, bottom left- 0-40% gradient 50µg IgG, bottom right- 0-50% gradient 25µg IgG. C- overlaid chromatograms of IgG1 (left) and IgG4 (right) on the 4 NaCl gradients from B.

Altering the NaCl gradient changed the retention time of both IgG1 and IgG4. Comparing the 0-40% gradient (as used in Figure 6-2 and Figure 6-4) with a linear gradient gave very similar elution times, as expected because the linear gradient is identical to the 0-40% gradient for the first 70 minutes, and simply continues at the same gradient. Varying the gradient to achieve different salt concentrations at 70 minutes (from 20% Eluent B to 50% Eluent B) altered the elution position of IgG1 and IgG4, with the faster gradient (i.e. 0-50%) eluting earlier and the slower gradients eluting later (Figure 6-5). Although the slower gradients increased the time between the elution peaks of IgG1 and IgG4, it did not alter the overlap between the 2 samples. As such, the 0-40% NaCl gradient was selected for further use.

6.3.5 Column Density

Next the effect of varying the density of C1q packed into the column was assessed, to see if increasing the amount of C1q increased the retention time or capacity of the column.

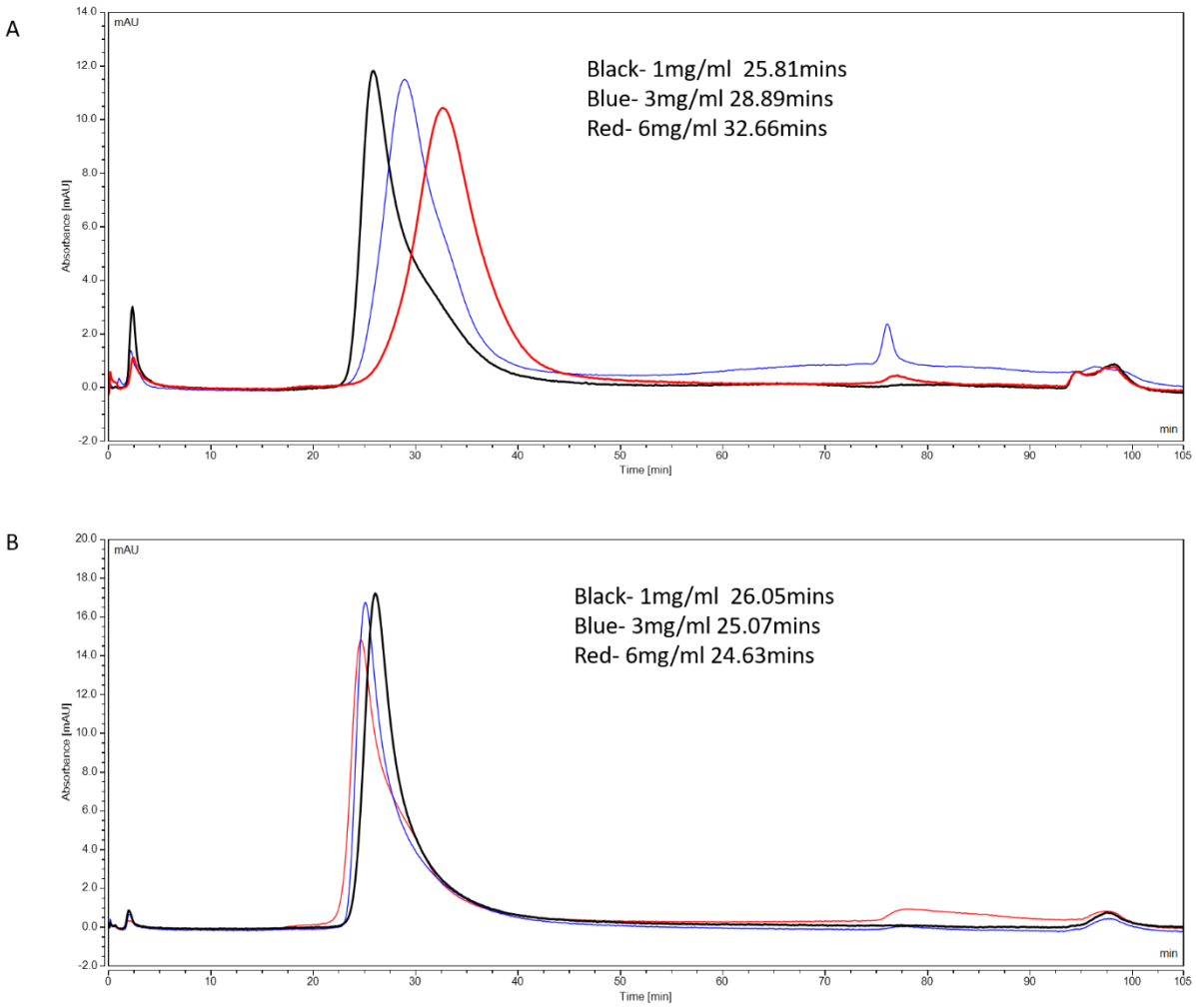

Figure 6-6 Density Optimisation of the C1q Column

25µg IgG1 injections on C1q columns containing 1mg/ml C1q (black), 3mg/ml C1q (blue) or 6mg/ml C1q (red). A- C1q columns tested immediately after production. B- C1q columns tested after storage. All columns tested under the standard operating conditions.

Initial testing of C1q columns packed at various densities suggested that increasing the amount of C1q within the column increased the retention time of IgG (Figure 6-6A). However, after storage of these columns in 20mM HEPES at 4°C for between 4-8 weeks, the retention time of the 3mg/ml and 6mg/ml columns collapsed to approximately the same as the 1mg/ml column, which remained fairly stable with storage (Figure 6-6B).

It was hypothesised that the high density columns may have lost functional C1q during storage or testing. To test the relative levels of functional C1q within each column, increasing amounts of IgG1 and IgG4 were injected onto each column density to determine the saturation point.

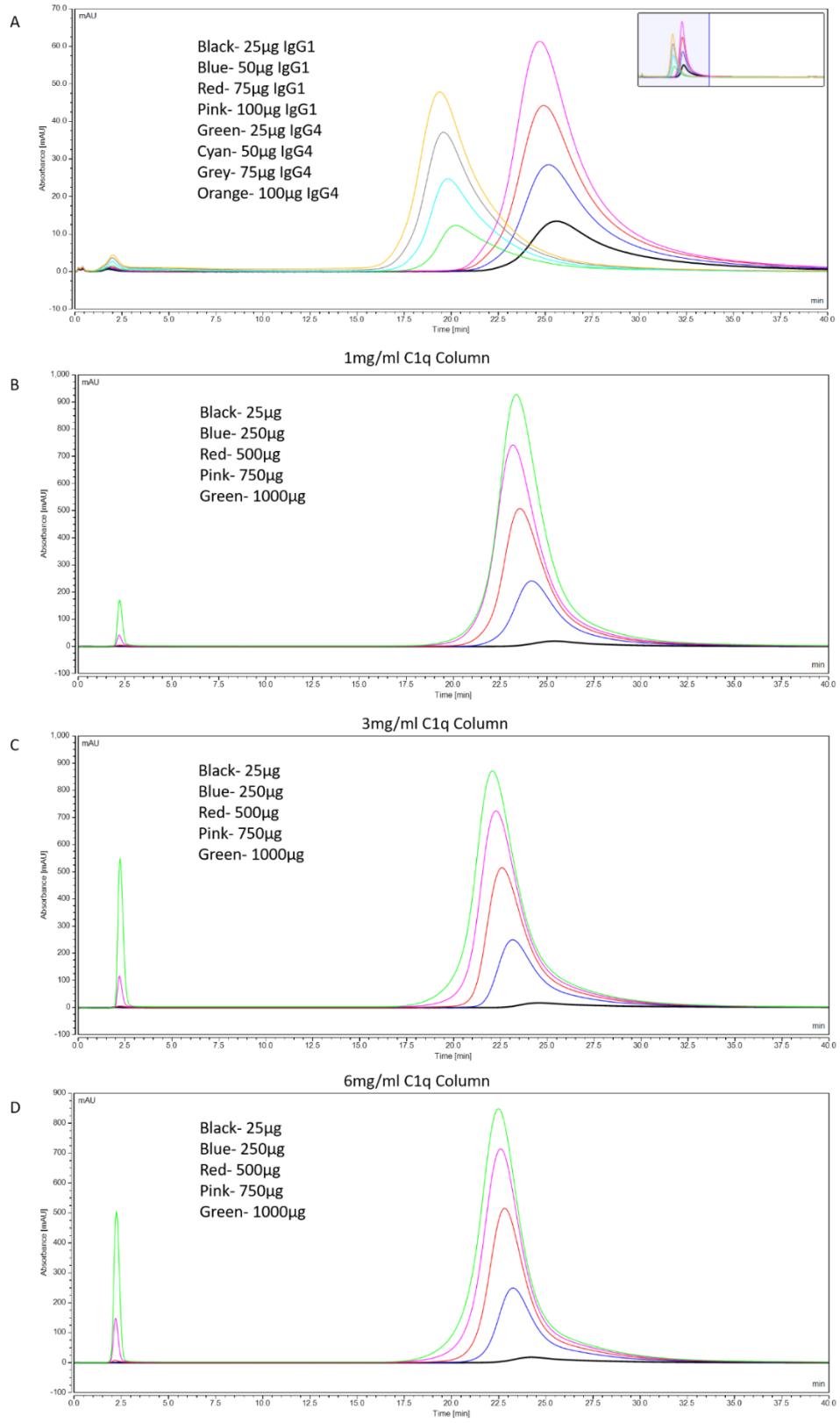

Figure 6-7 Effect of Column Density on C1q Chromatography

IgG injections onto C1q columns. A- injection of 25-100µg of IgG1 or IgG4 on the 3mg C1q column. B-D injection of IgG1 onto the 1mg (B), 3mg (C) and 6mg (D) C1q columns.

Injection of increasing amounts of IgG1 and IgG4 onto the C1q columns produced a linear increase in the response signal for both IgG1 and IgG4 (Figure 6-7A). In order to assess the total capacity of the columns, large amounts of IgG, up to 1mg, were injected onto the columns (Figure 6-7B-D). All three columns appeared to become saturated at approximately 750-1000µg of IgG, with the 1mg column displaying the highest capacity.

6.3.6 Column Specificity

Next, the specificity of the C1q columns for IgG was determined. To do this, human serum albumin was chosen as an irrelevant protein that is not a ligand of C1q, to assess whether binding to the C1q column was specifically mediated by the C1q interaction.

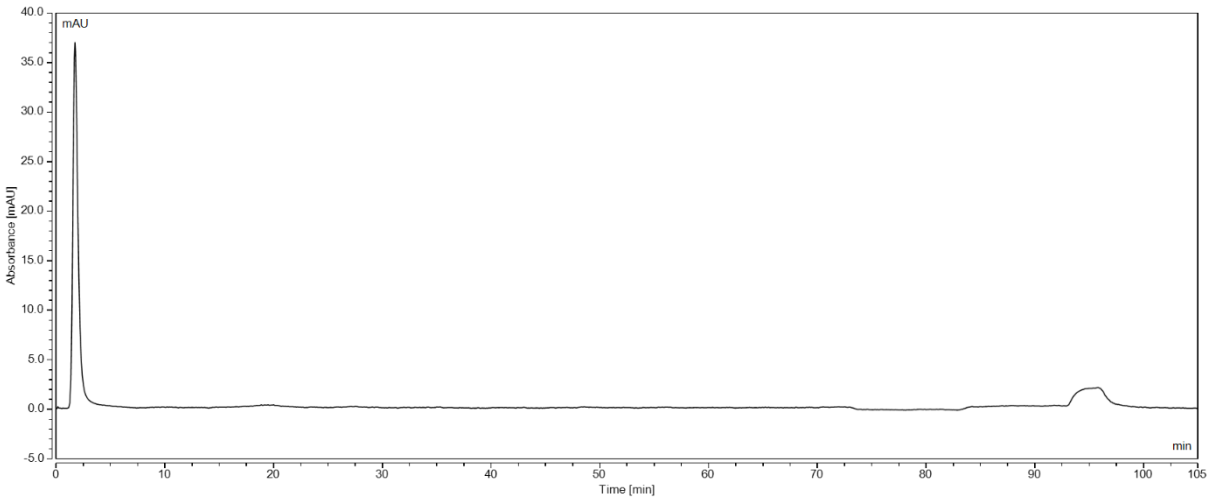

Figure 6-8 Binding of Human Serum Albumin to the C1q Column

25µg human serum albumin was tested on the 1mg C1q column under the standard operating conditions.

Human serum albumin showed no binding to the column (Figure 6-8), with all of the signal eluting off the column in the void volume peak at approximately 2 minutes.

6.3.7 Blank Column

In order to further characterise the specificity of the C1q column, a blank sepharose column was produced using the same packing method and conditions used to produce the C1q columns. IgG1 was run through the blank column to compare against the C1q column. IgG1 showed a distinct binding peak to the blank column that eluted in the region of 3-4 minutes earlier than the elution peak of IgG1 on the C1q column (Figure 6-9).

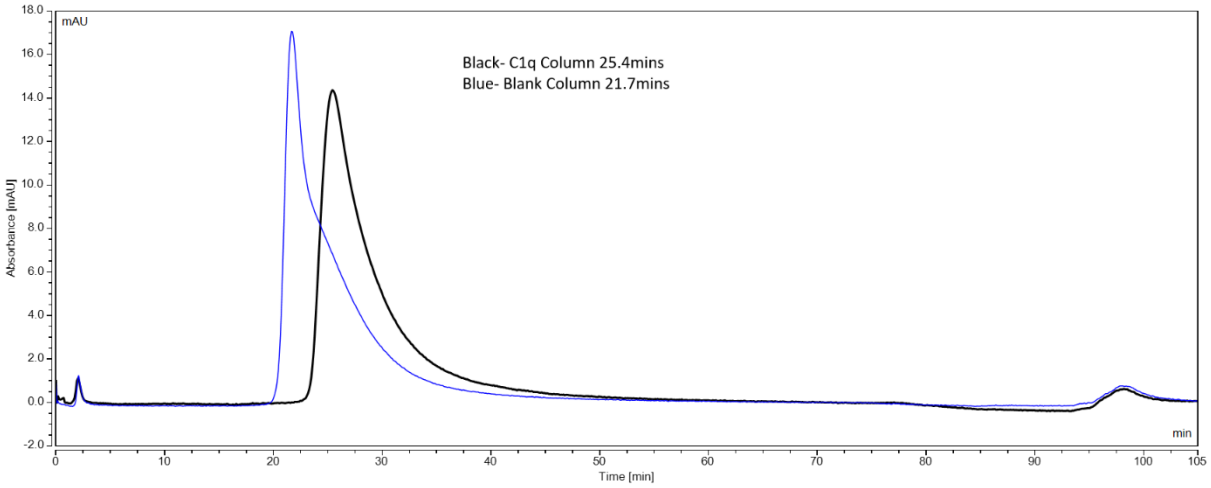

Figure 6-9 Blank Column Chromatography

25µg of IgG1 was injected onto the 1mg C1q column and the blank column, and overlaid onto the same chromatogram

6.3.8 Effect of Salt Concentration

It was hypothesised that the cause of this non-specific binding to the blank column was the lack of any salt in the system when the antibody was injected. In order to test this hypothesis, and to try and optimise the level of binding to the C1q column vs the blank column, the effect of increasing the salt concentration in the system was assessed during the antibody binding phase.

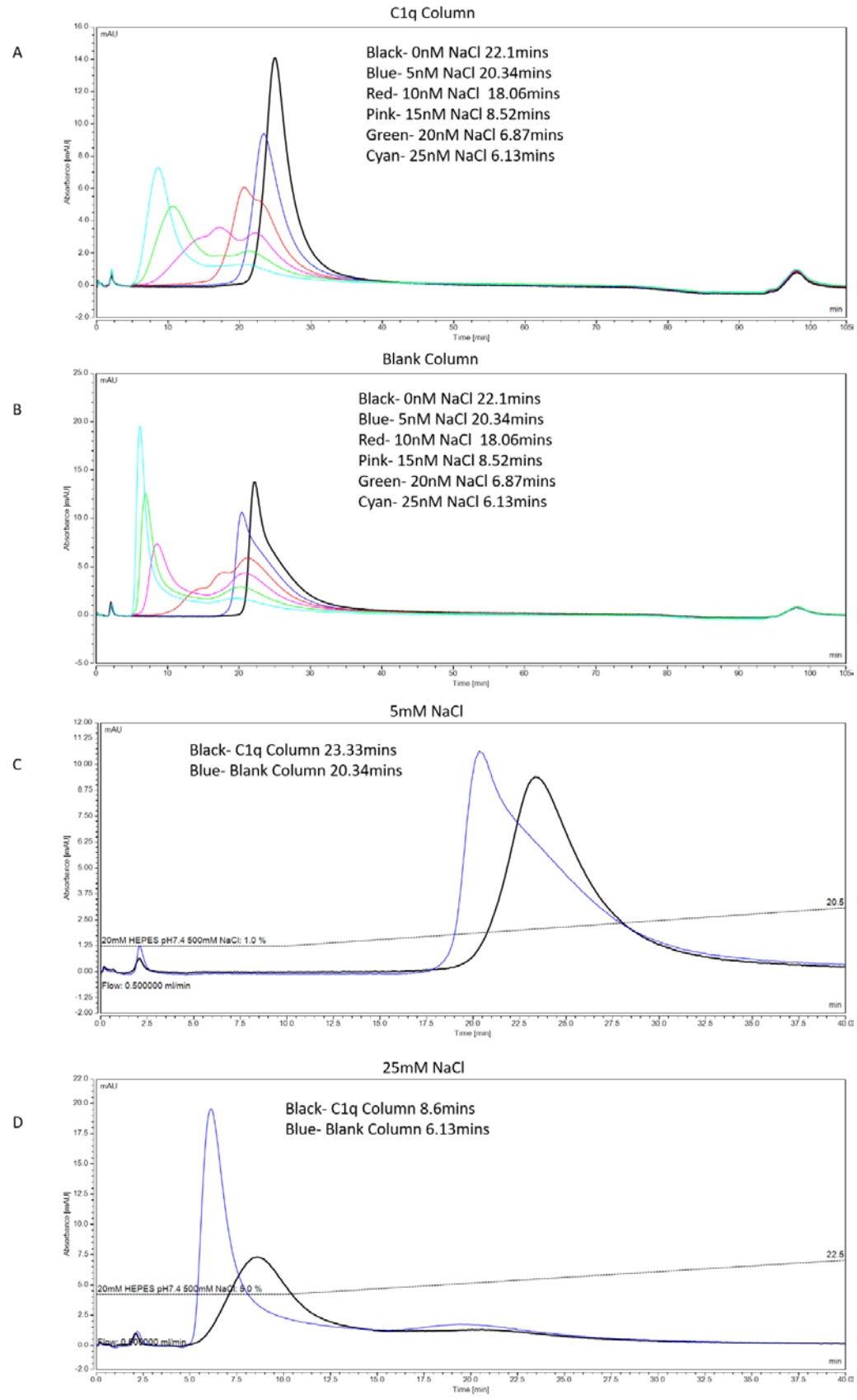

Figure 6-10 Effect of NaCl Concentration on C1q Chromatography

Testing the effect of NaCl concentration during the antibody binding phase on the 1mg C1q and blank columns. A-B- overlaid 20µg injections of IgG1 on the C1q (A) and blank (B) columns at various salt concentrations during the antibody binding phase. C-D overlaid injections of 20µg IgG1 on the blank (blue) and C1q (black) columns at a salt concentration during the antibody binding phase of 5mM NaCl (C) and 25mM NaCl (D).

Increasing the NaCl concentration present in eluent A, and thus during the antibody injection/binding phase, resulted in a progressive decrease in the retention time of IgG1 on the blank column (Figure 6-10B). However, the same effect was seen for IgG1 on the C1q column (Figure 6-10A). The increased retention time of IgG1 on the C1q column over the blank column was maintained at all C1q concentrations tested (as presented for 5mM and 25mM NaCl in Figure 6-10C and D, respectively).

6.3.9 IgG Fragments

It was further hypothesised that as a low level of salt appeared to be permissive for non-specific binding of IgG1 to the column matrix, that the C1q-Fc interaction was responsible for the increased binding seen on the C1q column. In order to test this IgG Fc and Fab regions were assessed on both the blank and C1q columns (Figure 6-11).

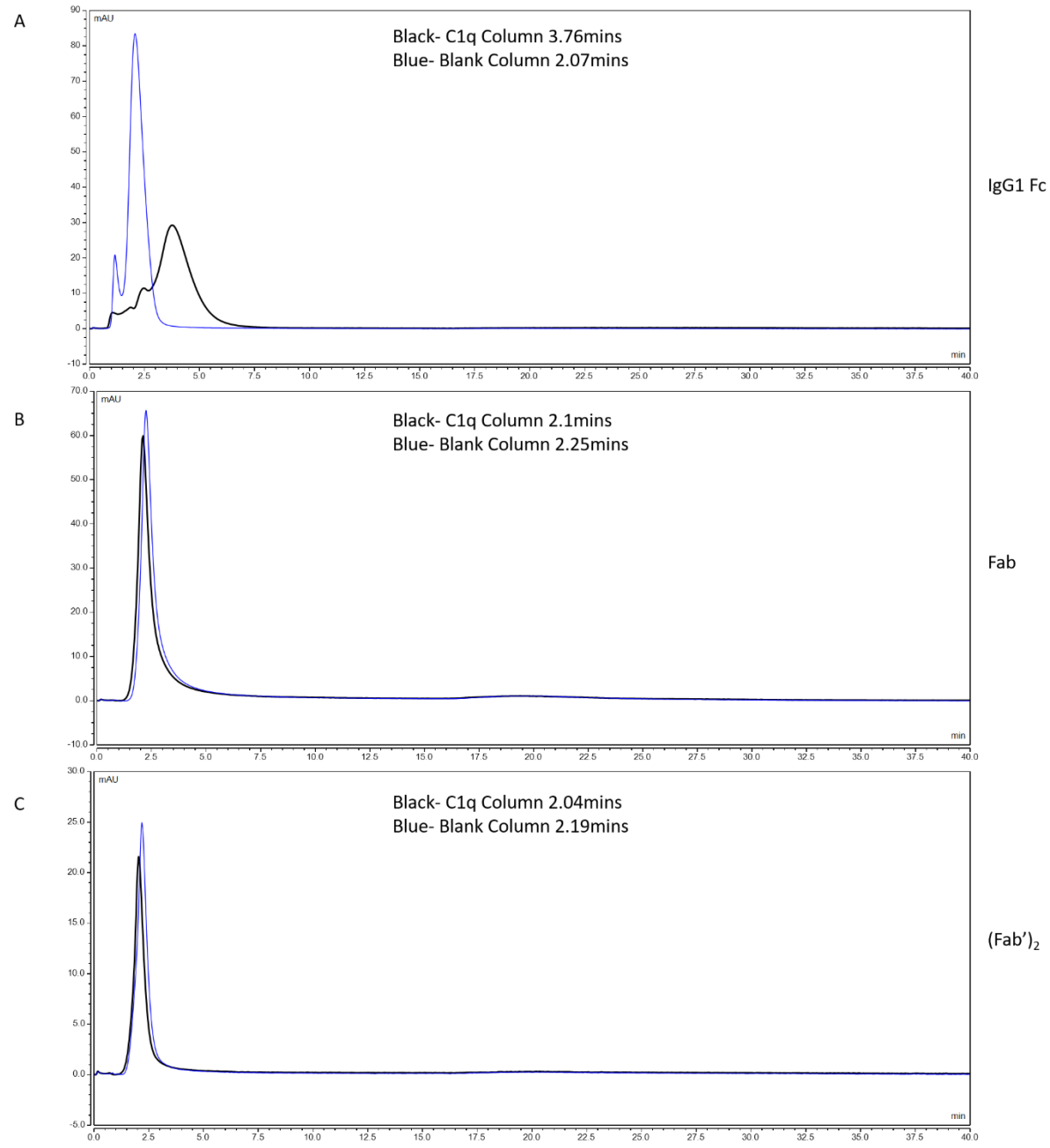

Figure 6-11 C1q Chromatography of IgG Fragments, Fab, F(ab')$_2$ and Fc

IgG fragments tested on the C1q and blank column. A-C overlaid 25µg injections of IgG Fc, Fab and F(ab')$_2$ onto the 1mg C1q (black) and blank (blue) columns.

IgG Fab and F(ab')$_2$ alone showed no binding to either C1q or blank columns, eluting entirely in the void volume at approximately 2 minutes (Figure 6-11B/C). However, the Fc fragment of IgG1 showed increased binding to the C1q column over the blank column as hypothesised (Figure 6-11A).

6.3.10 IgG Subclass Hybrids

A number of IgG hybrids with swapped Fc regions were subsequently examined to further confirm that the Fc region was responsible for the specific binding to the C1q column.

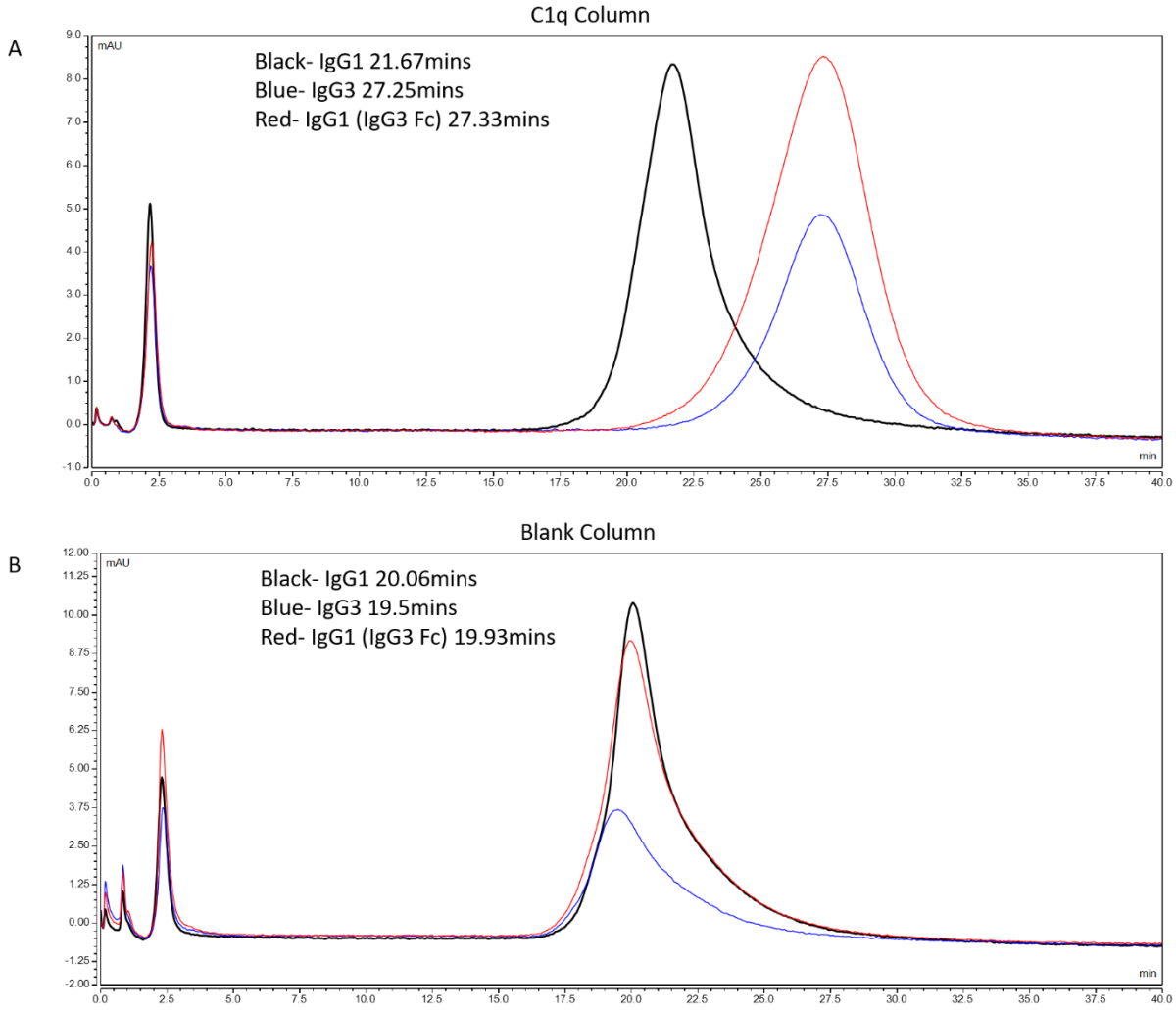

Figure 6-12 C1q Chromatography of IgG Fc Chimeras

IgG Fc chimeras were tested on the C1q (top) and blank (bottom) columns. A- overlaid chromatograms of 7.5µg injections of IgG1 (black), IgG3 (blue) and an Fc chimera of IgG1 containing the Fc region of IgG3 (red) were injected onto the C1q (A) and blank (B) columns.

IgG3 showed an increased retention time compared to IgG1 on the C1q column (Figure 6-12A), which matches the C1q binding observations made in Chapter 3:. Interestingly, the IgG3 Fc region was found to be responsible for the increased retention time, with the IgG1 backbone containing the Fc of IgG3 having the same C1q binding properties as native IgG3. This effect wasn't replicated

on the blank column where IgG1 and the IgG1-3 chimera had equal retention times on the blank column, with IgG3 having a slightly reduced retention time. These data confirm that the C1q column produced specificity above the non-specific binding to the sepharose matrix, and that this was mediated by the Fc part of the IgG.

6.3.11 IgG Testing

Other IgG1 antibodies were subsequently tested in order to determine how reproducible this effect was for different IgG1 molecules with different specificities (HER2, HER3, and IL-6R).

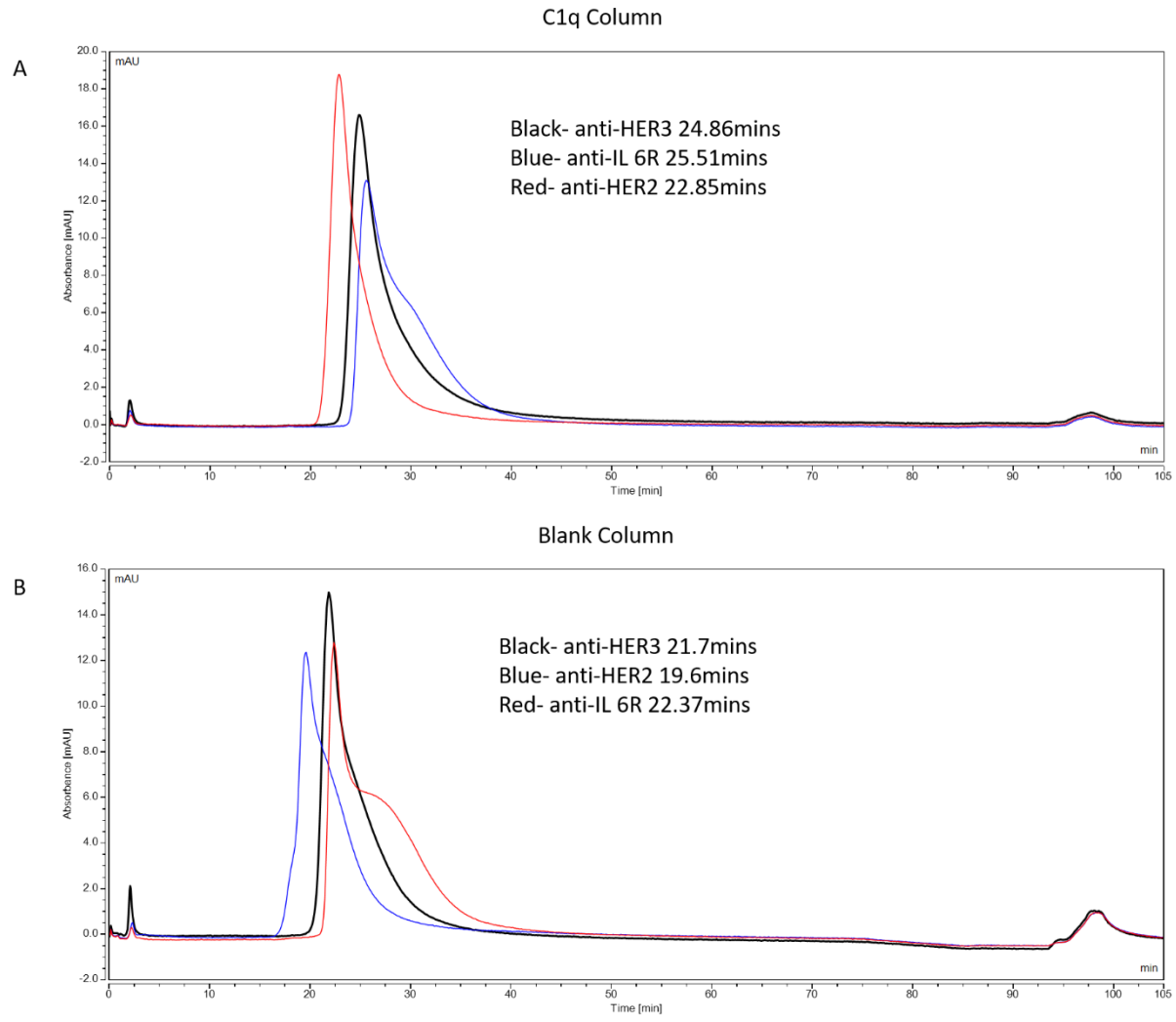

Figure 6-13 C1q Chromatography of Various IgG1 Antibodies

IgG1 mAbs on the C1q and blank columns. A-B anti-HER3, anti-IL 6R and anti-HER2 mAbs on the 3mg/ml C1q (top) and blank (bottom) column.

Each of the 3 mAbs shown in Figure 6-13 had a slightly different retention time, but for each antibody the retention time on the C1q column was greater than seen on the blank column.

6.3.12 pH Testing

Finally, the effect of varying the pH of the system on the retention time of IgG1 on the C1q and blank columns was assessed by altering the pH of both eluent A and eluent B.

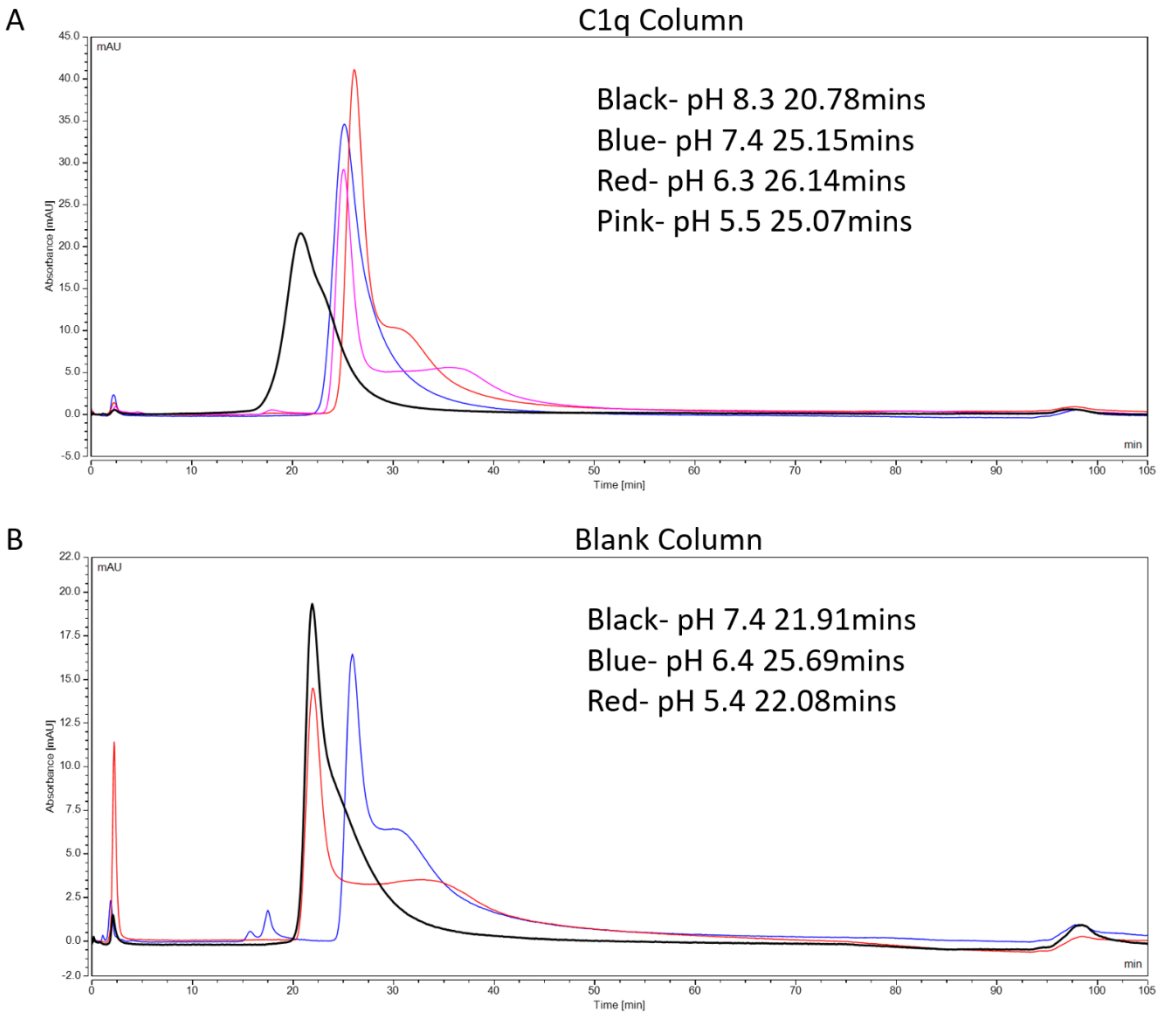

Figure 6-14 Effect of pH on C1q Chromatography

Binding of IgG1 to the C1q (top) and blank (bottom) columns at different pHs. A- 50µg IgG1 injected onto the C1q column at various pHs. B- 25µg IgG1 injected onto the blank column at various pHs.

Altering the pH of the HPLC system affected the retention time of IgG1 on both the C1q and the blank columns. Decreasing the pH of the system, towards pH 5.5, resulted in a projection off the right hand shoulder of the elution peak that became more pronounced as the pH decreased. Increasing the pH appeared to decrease the retention time for IgG1 on both the C1q and the blank column (data not shown).

Having investigated the characteristics of the C1q column and established a set of conditions that allow binding of antibodies to the C1q column with a specific shift as compared to the blank column, an optimal set of C1q column operating conditions were determined (Table 6-1). HEPES buffer and NaCl were selected as the best reagents tested for showing optimal binding to the C1q column with a salt gradient of up to 200mM (40% eluent B). pH 7.4 was selected as the optimal pH for the system as it gave a single binding peak that eluted later than for pH 8.3, and it is the most physiologically relevant pH. The 1mg C1q column was the most stable, so this column density was used for future work unless otherwise stated.

6.4 Assessing Therapeutically Relevant mAbs on the Optimised C1q Affinity Column

To validate the column findings in relation to cell based C1q recruitment and complement activation, a series of additional antibody samples were examined on the column that could be readily tested in cell based assays.

6.4.1 IgG Subclasses

First, a series of anti-CD20 antibodies displaying the rituximab variable regions produced with the four different human IgG subclasses were assessed. These results were then compared to those of C1q recruitment and CDC assays carried out and described in Section 3.3.2.

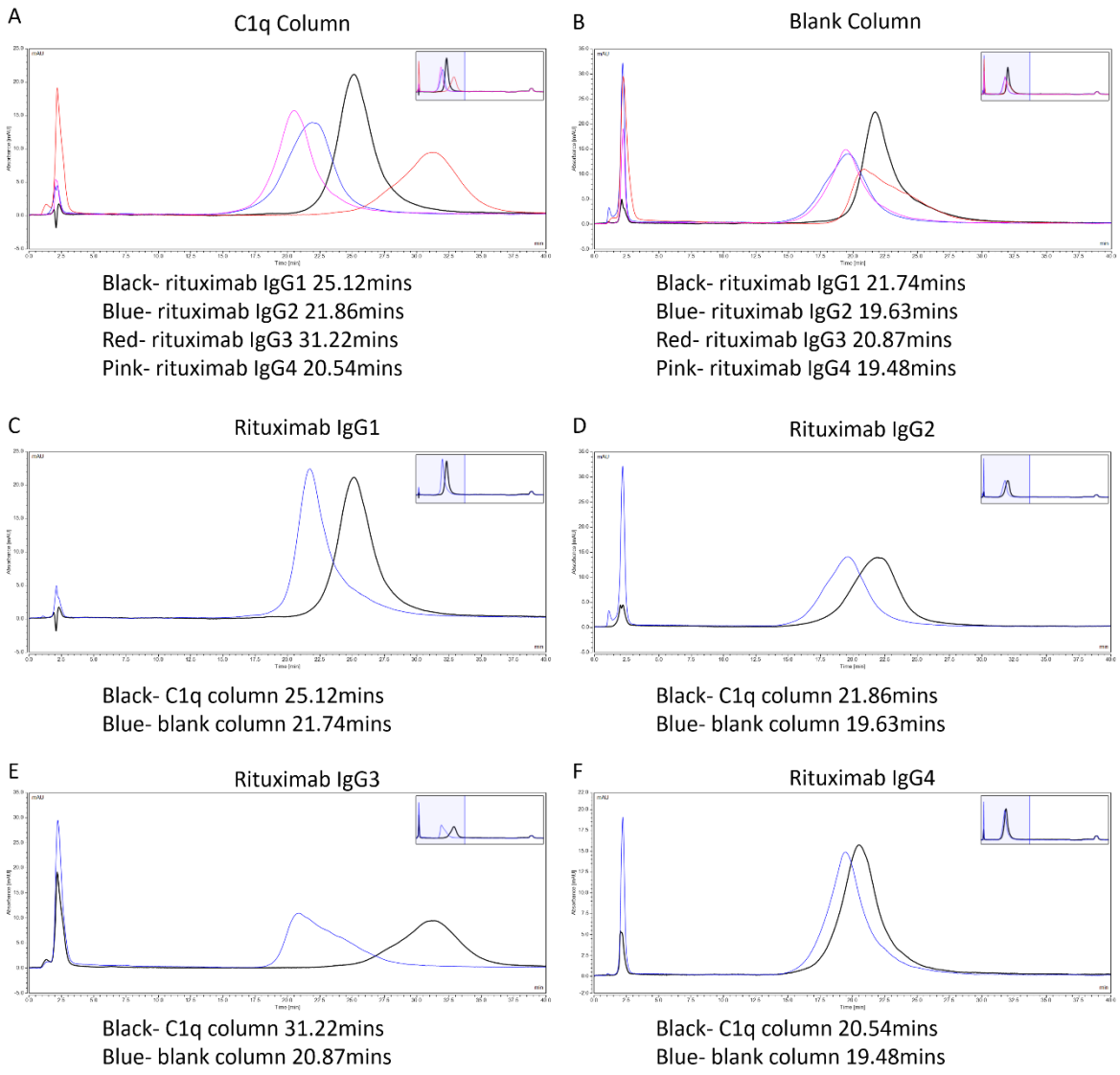

Figure 6-15 C1q Chromatography of Rituximab Subclasses

Rituximab IgG subclasses were assessed on the C1q and blank columns. A-B- overlaid 25µg injections of rituximab IgG1-4 subclasses on the C1q column (A) and the blank column (B). C- F- overlaid 25µg injections of rituximab IgG1 (C), IgG2 (D), IgG3 (E) and IgG4 (F) on the C1q column (black) and the blank column (blue). Chromatograms were truncated for clarity to show the first 40 minutes, containing the IgG elution peaks. Insert shows the complete 105 minute run.

Rituximab IgG subclasses displayed differential binding to the columns. Rituximab IgG3 had the highest binding to the C1q column and the largest shift between the retention time on the C1q column compared to the blank column (Figure 6-15E). Figure 6-15C demonstrates that rituximab IgG1 had the next highest binding to the C1q column and the second biggest shift between the retention position on the C1q column vs the blank column. Rituximab IgG2 and IgG4 had the

lowest binding to the C1q column, and the smallest shift in retention time between the C1q column and the blank column (Figure 6-15D/F). These data match the result of C1q recruitment and CDC assays, as described in Section 3.3.2, with rituximab IgG3 being the most active in all assays tested.

6.4.2 IgG Glycovariants

IgG glycosylation is known to have an influence on antibody effector functions including antibody half-life, ADCC and also complement activity. As such, we tested glycomodified antibodies (produced and characterised in Chapter 5:) on the C1q and blank columns and compared this to the results obtained in the assays measuring C1q recruitment and CDC assays using glycomodified rituximab on CD20 expressing cells (Figure 5-11 to Figure 5-17). These included antibodies with more galactose or more sialic acid.

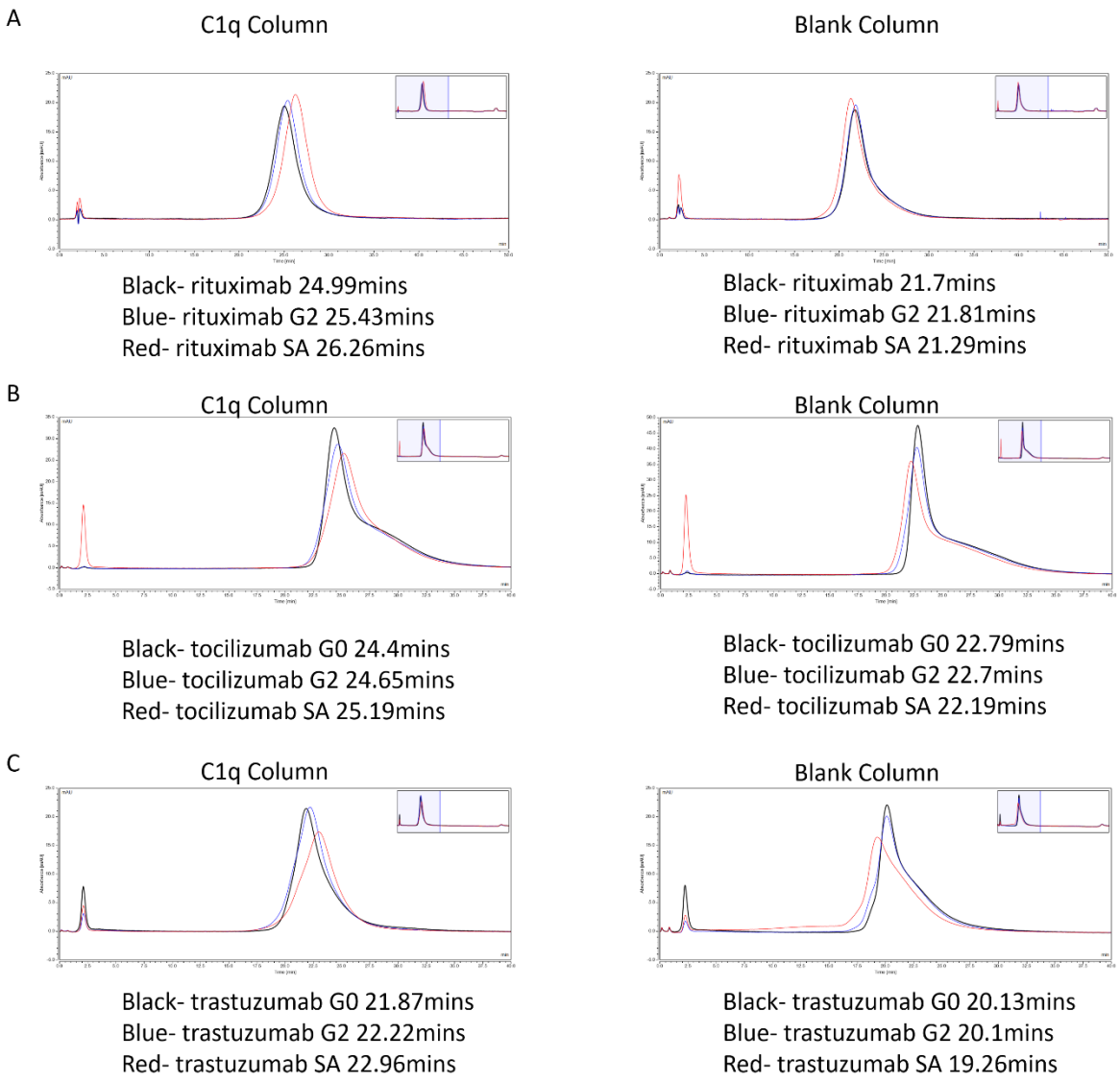

Figure 6-16 C1q Chromatography with Antibodies with Altered IgG Glycosylation

IgG1 glycovariants were injected onto the C1q column and blank columns. A- overlaid 25µg injections of rituximab glycovariants generated by *in vitro* glycoengineering, mock treated rituximab (black), fully galactosylated rituximab (blue) and enriched in sialic acid (red) on the C1q column (left) and blank column (right). Overlaid injections of tocilizumab glycovariants generated by *in vitro* glycoengineering, G0 (black), G2 (blue) and S2 (red) glycoforms on the C1q column (left- 25µg injections) and blank column (right- 50µg injections). C- overlaid 25µg injections of trastuzumab glycovariants generated by *in vitro* glycoengineering, G0 (black), G2 (blue) and S2 (red) glycoforms on the C1q column (left) and blank column (right).

IgG1 glycovariants with increased levels of galactose (G2 glycoforms) consistently showed a slightly increased retention time on the column for rituximab, tocilizumab and trastuzumab, whereas the blank column did not show this trend (Figure 6-16). More strikingly, IgG1

glycovariants with increased levels of sialic acid (SA/S2 glycoforms) showed further increases in retention time on the C1q column, for all three antibodies tested. Once again this was not observed on the blank column. These data match the results of both C1q recruitment and CDC assays as described in Chapter 5:, with sialylated rituximab being the most complement activating in all cases.

6.4.3 IgG Fc Mutants

Other modifications are known to alter the function of antibody Fc domains. We next looked at the effect of various Fc mutations known to affect C1q binding on the retention time of IgG1 molecules on the C1q column, using a similar series of mAbs used to demonstrate scC1q binding (Figure 6-1).

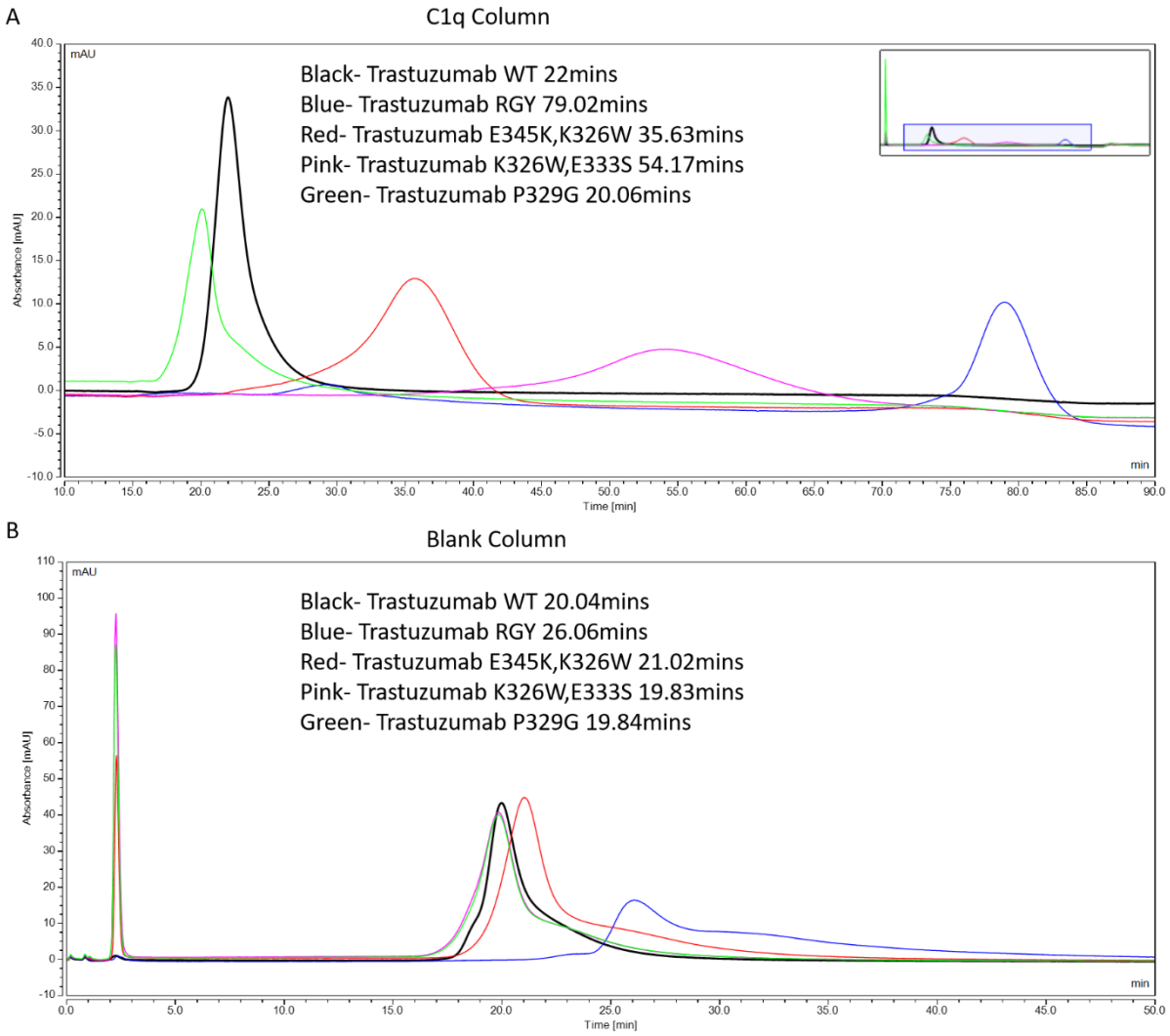

Figure 6-17 C1q Chromatography of Various IgG1 Fc Mutants

50µg IgG1 Fc mutants were injected onto the C1q (top) and blank (bottom) columns. Chromatograms were truncated to show 10-90 minutes for clarity, insert shows the complete 105 minutes.

As predicted from the literature, introduction of a P329G mutation into the Fc region of trastuzumab resulted in a clear decrease in the retention time on the C1q column, such that there

was very little difference in binding to the C1q column vs. the blank column (Figure 6-17). The EK,KW mutant (in red on the chromatogram) had an increased binding to the C1q column over the wild type antibody (in black), with only a small increase in the binding to the blank column, giving it a much bigger window of specific binding to the C1q column. The KW,ES mutant (pink) showed a dramatically increased binding to the C1q column, with no change in binding to the blank column, thereby further increasing the window of specific binding on the C1q column. The RGY triple mutant (blue) showed the highest retention time to the C1q column, only eluting off the column at the maximum salt concentration of 500mM NaCl. There was a minor elution peak present at approximately 26 minutes, representing ~20% of the total signal. This peak likely represents the monomeric fraction of the sample, as the RGY mutant is known to have a high propensity to form multimeric structures[80]. Although the RGY mutant showed a slightly increased binding to the blank column, it still had the biggest window of specific binding to the C1q column of all the samples tested.

The RGY mutant had the most dramatic retention to the C1q column out of all the antibodies tested. As it was only eluted when the run reached 500mM NaCl, it was re-tested for binding at higher salt concentrations during the binding phase to investigate the increased retention time.

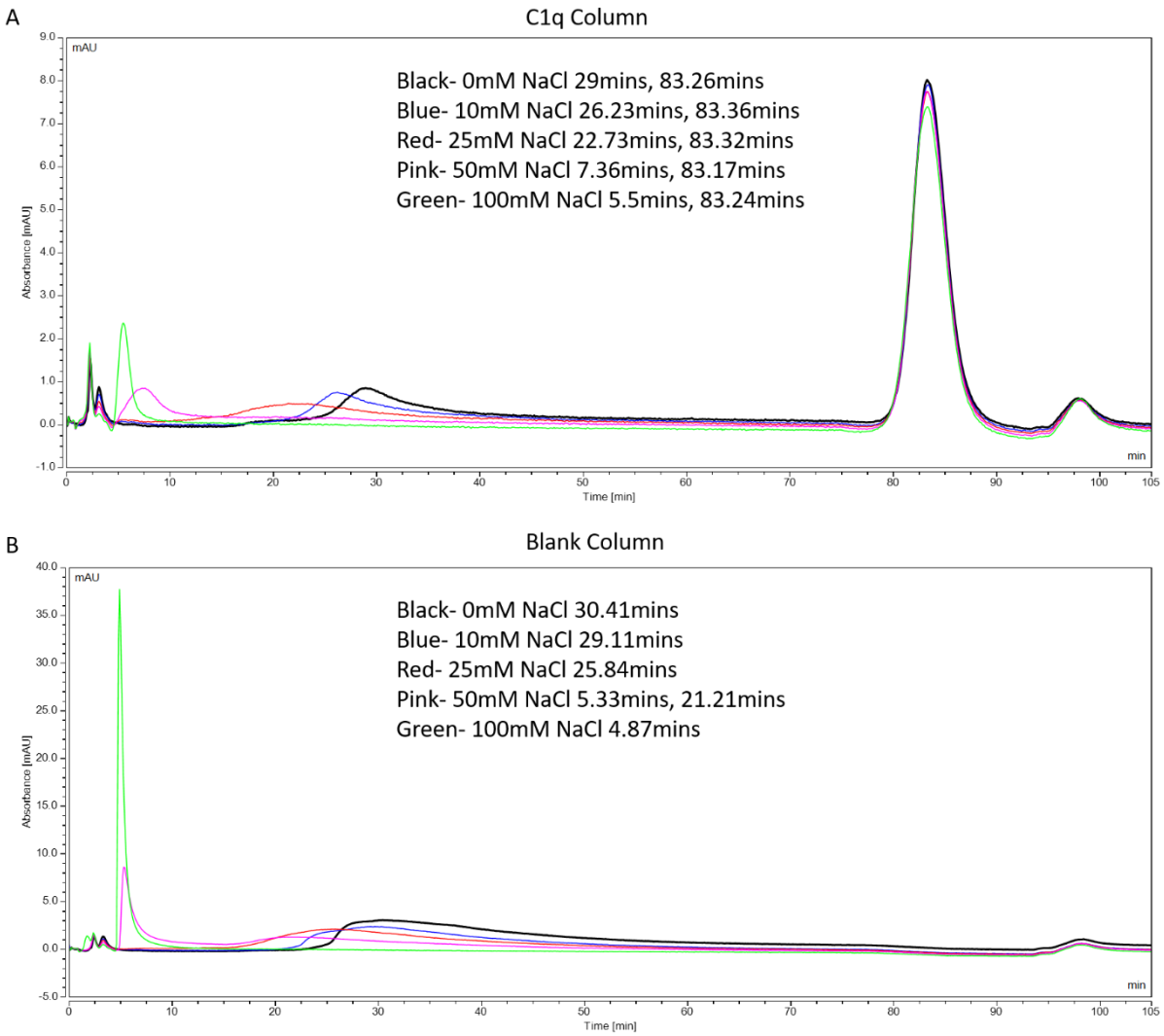

Figure 6-18 C1q Chromatography of Antibody Containing the RGY Mutation at High Salt Concentrations

Injection of 25µg IgG1 RGY mutant onto the C1q (top) and blank (bottom) columns under various salt concentrations during the antibody binding phase.

The non-specific binding peak on the blank column eluted progressively earlier as the salt concentration increased during the antibody binding phase. The first retention peak on the C1q column also eluted progressively earlier with increasing salt concentration (Figure 6-18). However, the late elution peak on the C1q column, which represented the majority of the RGY loaded onto the column, did not change in position at any salt concentration tested.

As the RGY mutation forms a solution state oligomer, a pair of trastuzumab mutants with opposing carboxyl charges, both individually and combined, were tested to examine whether the opposing charges could facilitate any increase in binding, for example by charge mediated oligomerisation.

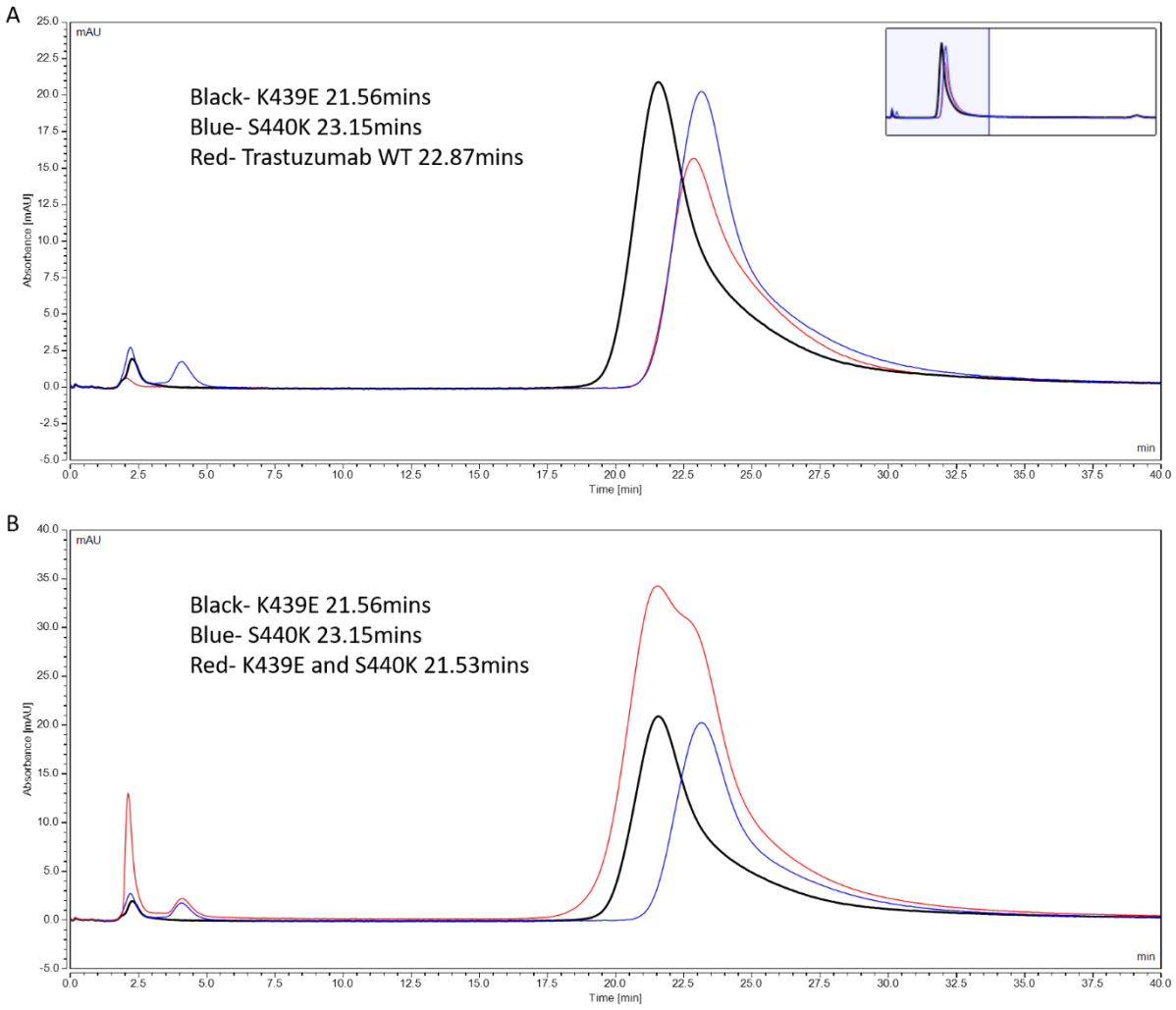

Figure 6-19 C1q Chromatography of Carboyxl Terminally Charged Trastuzumab

25µg injections of trastuzumab mutants with opposite carboxyl terminal charges on the 3mg C1q column. A- overlaid chromatograms of 25µg injections of K439E (black), S440K (blue) or wild type trastuzumab on the 3mg C1q column. B- overlaid chromatograms of K439E (black) and S440K (blue) from A, overlaid with a combined injection of 25µg of each (red) on the 3mg C1q column. Chromatograms were truncated to show between 0-40 minutes for clarity, inset shows the complete 105 minutes.

When trastuzumab had a glutamic acid inserted at the carboxyl terminus (K439E mutation), the retention time on the C1q column was reduced compared to the wild type antibody (Figure

6-19A, black and red traces, respectively). The K439E mutation had a small impact on the retention time of the antibody, eluting slightly earlier, whereas the S440K mutation had no major impact (Figure 6-19A). Combining these 2 mutants together in a 1:1 ratio resulted in a retention peak that displayed the characteristics of both mutant antibodies (Figure 6-19B). There was no clear evidence of any peaks with increased retention time.

6.4.4 RGY Fc Mutants

In addition to mutations that impact the ability of the Fc to bind C1q, there are also mutations that impact on FcγR binding. Frequently, both interactions are modulated and often multiple mutations are desired to increase or decrease either complement or FcγR binding. Therefore, as the RGY mutant demonstrated superior binding to the C1q column, it was of interest to determine the effect on C1q binding when additional mutations were combined with it. IgG1 Fc regions, without fab or hinge domains, were therefore produced containing the RGY triple mutation coupled to various attenuating mutations, and tested on the C1q and blank columns.

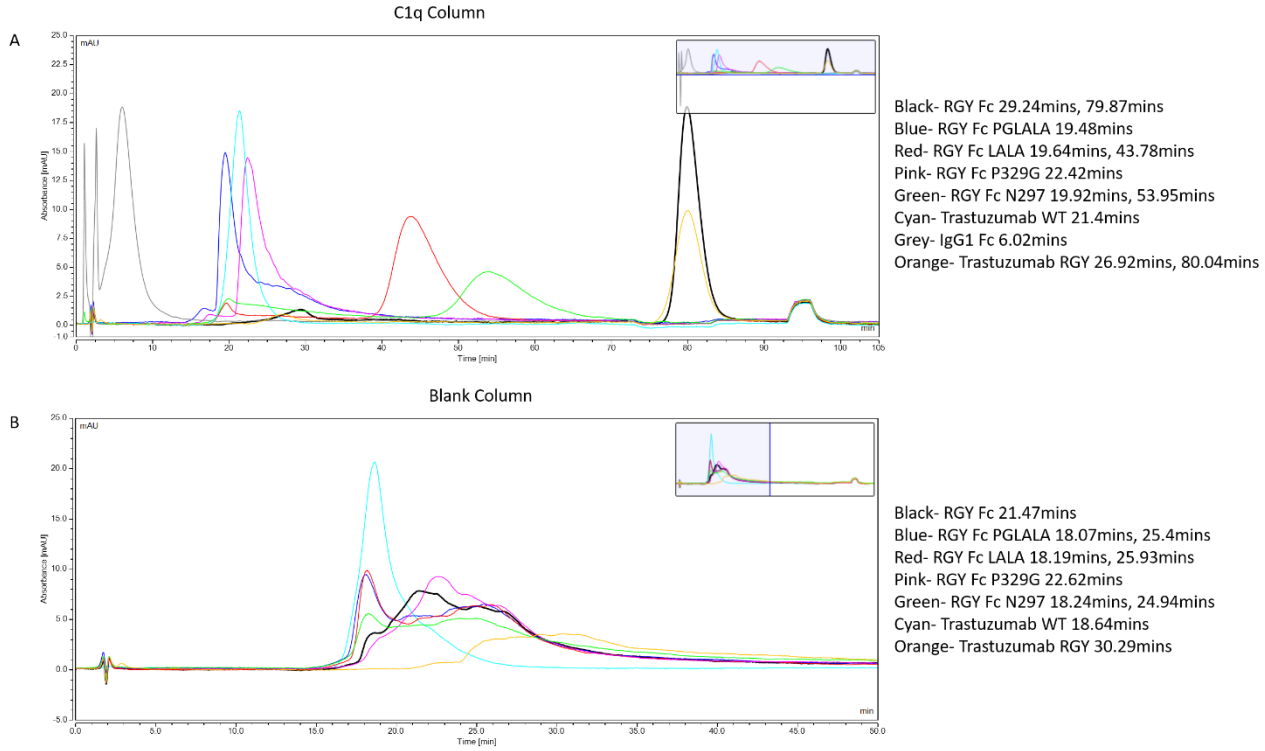

Figure 6-20 C1q Chromatography of RGY Fc Mutants

RGY Fc mutants and antibodies were tested on the C1q (top) and blank (bottom) columns. 25µg of IgG or RGY Fc was injected onto the C1q (top) and blank (bottom) column. Chromatogram for the blank column (bottom) was truncated to show 0-40 minutes for clarity, inset shows full 105 minutes.

The RGY Fc alone (black) was the only construct which had the same retention time as the full length trastuzumab RGY (orange) on the C1q column (Figure 6-20A). Various attenuating mutations all resulted in an earlier elution from the C1q column compared to the RGY Fc alone. The deglycosylated Fc (RGY Fc N297) had the smallest reduction in binding, then the LALA mutation followed by the P329G mutation which had the shortest retention time of these three mutants. Combining the LALA and P329G mutations together resulted in the earliest elution from the C1q column. All of the RGY Fc only constructs had a fairly similar broad elution profile on the blank column (Figure 6-20B), eluting earlier than the full length RGY trastuzumab (orange).

6.4.5 Non-IgG C1q Ligands

Lastly, two non-IgG molecules that should recognise C1q were assessed to see if they showed the expected behaviour towards the scC1q column. Both CRP and IgM showed binding to the C1q column. CRP showed a clear shift on the C1q column as compared to the blank column (Figure 6-21A). For IgM, there appeared to be no binding to the blank column, whereas there was a broad elution peak on the C1q column that showed binding to the column, eluting at approximately 34 minutes (Figure 6-21B).

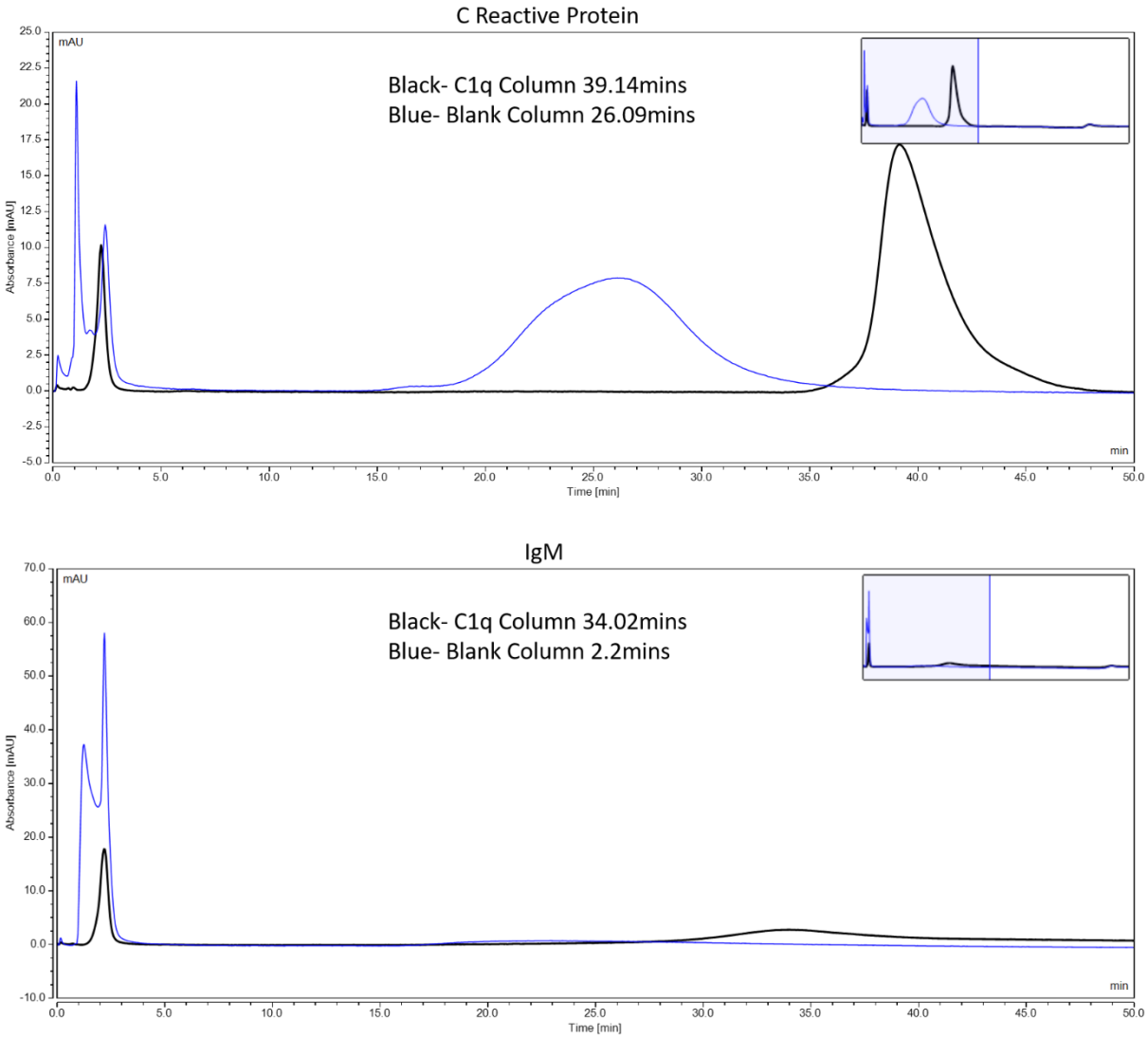

Figure 6-21 C1q Chromatography of CRP and IgM

Testing of non-IgG ligands on the C1q (black) and blank columns (blue). Overlaid chromatograms of 25µg injections of CRP (top) and IgM (bottom) on the 1mg C1q column (black) and the blank column (blue). Chromatograms presented were truncated to show 0-50 minutes for clarity, inserts show full 105 minutes.

6.5 Discussion

Having assays to measure the effector functions of therapeutic mAbs is an essential tool for predicting their *in vivo* activity. These methods should ideally be high throughput and readily amenable to automation. This facilitates testing of large numbers of antibodies directed to different epitopes of a particular target, as well as testing different mAb formats or mutants of a parental antibody screened for improved or abrogated effector functions.

Many established assays used for testing antibody effector function rely on binding the antibody of interest to its target antigen, often on the surface of a cell. This approach is relatively low-throughput and introduces additional variables into the assays. These variables can be mAb dependent, such as the affinity towards the target antigen, binding characteristics and target antigen geometry; as well as experimental and technical, with potential issues such as cell viability, antigen expression level and proper production and processing of the antigen. All of these can effect the experimental results and reproducibility of the assay and ability to screen for activity.

A different approach that is readily amenable to a first line screening program is to analyse the antibody characteristics in the absence of target antigen. This allows for highly reproducible experiments that allow for the determination of the various Fc mediated binding interactions. The lack of a requirement for target antigen allows for rapid testing of new antibody formats, mutants or glycoforms (among other variables) without the need to generate antibodies with multiple different antibody specificities.

Here, an HPLC based methodology was chosen to study C1q binding and develop a suitable assay. HPLC allows for the use of well-defined conditions and is readily amenable to semi-automation through the use of autosampler equipped devices. Furthermore, HPLC allows visualisation of the entire sample, rather than giving an average value like other methods, such as surface plasmon resonance. This is well emphasised in the case of different antibody glycoforms binding to FcγRIIIa, as detailed above (Section 6.1). This HPLC-affinity column method is even suitable for separation and purification of these 2 populations for further analysis.

The scC1q format used was similar to that generated by Moreau *et al*. in that the 3 C1q head groups were linked into a single polypeptide chain. In our work, the order of the head groups in the chain is A-B-C, whereas in the report by Moreau *et al.* the order was A-C-B. Despite the

difficulties in demonstrating the binding of scC1q to IgG because of the low affinity (particularly in the case of a monomeric head group where there is no contribution of avidity), we were able to detect binding of the scC1q to the anti-CD20 mAb rituximab when it was immobilised to SUDHL4 cells which express the highest levels of the target CD20 (Figure 6-1). In addition, trastuzumab mutants K326W, E333S and the RGY triple mutant (both known to have an increased affinity towards WT C1q binding) were also shown to bind scC1q when these antibodies were bound to a target cell (Figure 6-1). This binding of scC1q was also confirmed in a cell free ELISA based format for the K326W, E333S mutant. Moreau *et al.* were unable to demonstrate binding of the scC1q molecule to IgG by SPR, and similarly scC1q binding to IgG could not be detected here without crosslinking of the IgG (Figure 6-1D). These findings indicated that the scC1q construct was functional in its IgG binding and could be suitable for use in an HPLC based affinity system.

In order to generate an HPLC column, scC1q was biotinylated to couple it to streptavidin coated sepharose beads. These beads were then packed into 4.6 x 50mm Tricorn glass columns. C1q binding to IgG Fc is reported to be largely due to charge based interactions, and because of this a salt based gradient was used to compete with these charges. Several buffers and salts were tested with HEPES found to be the best running buffer and NaCl to be the best salt for efficient and reversible binding of antibody to the column (Figure 6-2 and Figure 6-3). Different salt gradients were also assessed with a gradient selected that allowed clear separation of IgG1 and IgG4 (known to have different levels of complement activity and WT C1q binding).

Although the salt concentration at which IgG is seen to elute is lower than that found within the body (~140mM), the interactions seen are between monomeric IgG and individual scC1q head groups, as opposed to the multiple interactions made between target bound IgG and hexameric C1q[512]. It is not thought that monomeric antibodies interact with C1q in solution in the serum. Indeed this would be counterproductive, as it would increase the chance of unwanted complement activation. Some of the trastuzumab IgG mutants do maintain C1q binding at salt concentrations above physiological levels (particularly the RGY mutant- Figure 6-17 and Figure 6-18), and as such it is possible these antibodies may bind and potentially activate C1q in the absence of target binding.

When initially generating the C1q columns, different C1q packing densities were used, ranging from 1mg of C1q per gram of sepharose to 6mg of C1q per gram of sepharose. Initial testing of these columns suggested that increasing the level of C1q within the column increased the retention time of IgG (Figure 6-6). This could be due to the increased number of C1q molecules

available for binding, meaning that IgG can make multiple interactions with C1q molecules as they pass down the column, even as the salt concentration increases. When there is less C1q available, the IgG make fewer interactions and therefore are eluted more quickly. This reasoning also provided an explanation for the slight decrease in retention time of IgG on each column observed when the amount of IgG sample injected increased (Figure 6-7). Here, the greater the number of IgG molecules in the column, the fewer free C1q molecules there will be available for binding, therefore fewer molecules of IgG can rebind to C1q as they pass through the column, giving rise to shorter retention times.

When the column reaches saturation, and all available C1q molecules are bound to IgG, then any excess IgG will pass straight through the column and elute in the void volume of the column (~2 minutes). This allows for an approximation of the capacity of the column for binding C1q. Interestingly, the capacity of the 3 different C1q column densities was quite similar, with the 1mg C1q column appearing to have the highest capacity, as a 1mg injection of IgG onto this column gave rise to a smaller void volume peak than was seen on the 3 and 6mg columns (Figure 6-7). This may provide an explanation as to the decrease in the retention time of the 3 and 6mg columns after storage. The column capacity was only measured after the columns had been stored, and the capacity of the columns was very similar. This may suggest that the 3 columns at this point in time had similar amounts of functional C1q within the column. The loss of C1q functionality, or of the C1q molecules themselves, could be caused by the higher concentrations of C1q causing aggregation or denaturation of the C1q bound to the sepharose. The 1mg column did not appear to be affected by storage, perhaps because of the lower density of the C1q within the column.

The specificity of the column for binding to IgG was assessed using human serum albumin. No binding to albumin was seen, supporting the conclusion at this stage that the column retention of IgG was mediated through specific interactions with C1q (Figure 6-8). However, IgG4, although eluting earlier from the column than IgG1, still showed binding to the column, even though this could not be demonstrated in a cell based assay (Figure 3-15). In order to further characterise the specificity of IgG binding to the C1q column a blank, sepharose only column was produced using the same method as for the C1q columns.

Interestingly, the elution peak of IgG on the blank column had a similar shape to the equivalent peak on the C1q column, but with elution several minutes earlier (Figure 6-9). This is perhaps not surprising due to the lack of salt during the antibody injection phase. Titrating salt into the system

at the antibody injection phase confirmed that the retention time of IgG on the blank column was consistently less than that of IgG on the C1q column at various salt concentrations (Figure 6-10). By testing antibody fragments, it was shown that the Fc region alone showed an increased binding to the C1q column with no binding observed to the blank column (Figure 6-11). It was hypothesised that the full IgG makes non-specific interactions with the sepharose matrix in the absence of salt, and that on the C1q column the Fc makes additional specific interactions to the scC1q, contributing to the increased retention time. In support of this, swapping the Fc domain of IgG3 onto an IgG1 molecule resulted in the same retention time as the full length IgG3, suggesting the Fc region is responsible for this specific binding (Figure 6-12). Testing of three different IgG1 antibodies showed that all three antibodies had a later retention time on the C1q column than on the blank column, regardless of the F(ab) specificity (Figure 6-13).

In order to validate the columns performance and couple it to more biologically relevant findings, four different IgG subclasses of rituximab, known to have different C1q binding properties, were assessed on the columns. The antibody chosen, the anti-CD20 mAb rituximab, is well documented to be able to activate complement efficiently on CD20+ve cell lines. The relative binding of the IgG subclasses on the C1q column, and the size of their specific shift vs the blank column, gave the same pattern of effect as C1q recruitment to the surface and CDC of rituximab opsonised cells with IgG3>1>2=4 (Figure 3-15 and Figure 3-16).

Glycosylation of IgG Fc is known to affect the effector functions of the antibody, and increased galactosylation has been reported to increase the level of C1q binding and in turn CDC (Figure 5-11 to Figure 5-17)[502,513]. Three sets of glycomodified antibodies were therefore assessed on the columns; their retention times were similar, but a consistent trend emerged. Increased galactose resulted in a slightly later retention time, and increased sialylation resulted in an even later retention time. These results tallied with the cell based assay results for glycomodified rituximab, where antibody enriched for galactose and sialic acid showed progressively increased C1q recruitment to the opsonised cell surface, and complement dependent cytotoxicity (Section 5.3)[514].

Reports in the literature have typically described sialylated Fc as an immunomodulatory agent, for example as a part of IVIg therapy, or as reducing IgG efficacy[372,503,515]. Additionally, sialylated IgG has been shown to have reduced C1q binding and CDC potential when compared to wild type parental antibody[502]. However, in the work reported in this thesis it was found that rituximab enriched for sialic acid showed an increased C1q binding, both in a cell based assay and on the

C1q column, and also increased CDC above that seen with galactosylated rituximab[514]. The reasons for this discrepancy are currently unclear.

IgG glycosylation is influenced by various factors, including the cell type producing the antibody and the culture conditions. As such, IgG glycosylation is highly heterogeneous in terms of the level of core fucose, galactose and sialic acid attached to the N297 linked glycan chain. Accordingly, to study the effect of specific glyco patterns, various methodologies are applied to try and generate purer samples. These approaches include cell line engineering, removal and replacement of the entire glycan or enzymatically remodelling the glycan in a step by step approach. The use of these different approaches, and differences in the purity of the glycoforms within a sample, could explain the differences and variation in the results reported above. However, differences in purity are perhaps unlikely to fully explain why sialylated IgG in one instance increases CDC above galactosylated IgG and in another decreases CDC below that of the parental. If sialic acid increased CDC/C1q binding then the greater the purity the greater the CDC/C1q binding. If sialic acid has no effect or decreases CDC/C1q binding, then the greater purity would be expected to decrease or have no effect on CDC/C1q binding. Another variable in studying these differences comes from differences in the methodologies used, for example different time courses, serum concentrations and sources, antibody concentrations and cell lines used for CDC assays. Further study into the effects of antibody glycosylation on complement effector functions is required to fully explain these differences.

The C1q column was tested for its suitability to test IgG mutants for their C1q binding properties, a potential use of this column in a screening capacity. Mutations were selected from the literature that were expected to show differences in C1q binding (both increased and decreased). The P329G mutation is reported to abrogate antibody effector function including complement, and this mutation appeared to eliminate all binding to the C1q column, with very similar retention times on the C1q and blank columns[432]. Two mutations, based on investigations by Idusogie *et al*. in the early 2000s, showed increases in binding to C1q without increasing the binding to the blank column[490]. Together these further corroborate the C1q-dependent specificity of the column and that the scC1q used to pack the column remained functional.

The RGY triple mutation described by Diebolder *et al.* induces CDC very efficiently, and also binds to C1q strongly[80]. A large part of this was associated with its ability to form solution state hexamers through Fc-Fc interactions. Two peaks are seen on the C1q column that reflect, in relative distribution, the two populations seen by size exclusion. The larger peak binds very

strongly to the column, with comparatively little increase in the level of binding to the blank column. Interestingly, the smaller peak also shows increased C1q binding compared to the parental IgG. This suggests that even the monomeric fraction has increased C1q binding, and therefore that the three mutations alone, in the absence of their increased tendency to hexamerise, increase C1q binding.

Two mutant IgGs were also generated with opposing carboxyl terminal charges. Such antibody pairs have been suggested to have an increased propensity to form oligomers at the target surface through complementary charge mediated interactions[80]. However, on the C1q column combining these two mutants in a 1:1 ratio did not result in any increase in binding to the column, and the peaks corresponding to the individual antibodies were discernible from the mixed sample (Figure 6-19). It is possible that the lack of a target antigen to bring the antibodies into close proximity limits the chance of carboxyl charge mediated interactions. Alternatively, it is possible that the buffer conditions within the column are not permissive for these interactions to occur.

As the C1q column interaction was shown to be dependent upon the Fc region, RGY mutant Fc domains without the hinge or fab regions were produced and examined. The wild type RGY Fc was able to bind as effectively as the full length RGY parental mAb. A number of mutations, known to reduce Fc mediated effector functions including complement activation, were then assessed on the RGY Fc backbone. All of these mutations decreased the binding of the RGY Fc to the C1q column to various extents, demonstrating their potential to act additively to produce Fc regions with the RGY mutation that bind to the column less than the wild type parental antibody. All of the RGY Fc mutants had similar binding to the blank column, indicating that the binding of these molecules to the C1q column was specific for the C1q molecule.

These findings demonstrate the potential use of this C1q column. When used in conjunction with the blank column, it is a tool for screening antibody variants for both increased and decreased C1q binding. Antibody variants and modifications that are amenable to study using the C1q column include Fc mutants, different IgG subclasses and different glycoforms.

Finally, the C1q column was used to discern binding non-IgG ligands, including both IgM and CRP. Both of these molecules are large, multi-subunit proteins that have multiple binding sites for C1q, as compared to the single binding site on IgG. Interestingly, both of these proteins only bind to C1q in certain conformations - for example IgM exists primarily in a pentameric, planar formation in the blood, and must undergo a conformational shift through antigen binding to enable the

binding of C1q. The IgM used here was serum purified and not bound to antigen, but showed binding to the C1q column. A potential explanation for this finding is that the low salt concentration employed upon binding to the column could cause an analogous conformational change in the IgM structure that permits binding to C1q. This highlights that some care must be taken when translating the findings from the column to potential *in vivo* characteristics of the molecule being studied. As such, this C1q method would make a potentially valuable first line screening tool to analyse large numbers of samples and highlight samples that potentially have enhanced or reduced C1q binding, according to the desired outcome, for further testing.

Chapter 7: General Discussion

The aim of this thesis was to test the effect of various Fc modifications on the Fc mediated effector functions of therapeutic mAbs directed against CD20. As such, assays measuring CDC, ADCC and ADCP were developed and used to compare modified mAbs. Most mAbs that have thus far been approved for clinical use in humans contain the Fc region of the IgG1 subclass[70]. In addition, these clinically approved mAbs are also mostly produced in one of a few cell lines, and are strictly controlled by regulatory guidelines in many areas including Fc glycosylation. As such, it was of interest to investigate the impact of Fc modifications upon mAb mediated effector functions, in order to determine if improvements could be made to the existing IgG1 Fc, and to understand how this might be modified *in vivo*, for example in tumour or autoimmune environments, in ways that may reduce its efficacy.

Rituximab produced on an IgG3 backbone was the most active subclass of IgG in terms of activating complement, as shown using both the C1q affinity column and cell based assays of C1q recruitment and CDC. Furthermore, as stated in Chapter 3:, it also had the highest affinities for the activating FcγRs among the IgG subclasses. This was shown to translate into the highest levels of both ADCC and ADCP among the IgG subclasses. Furthermore, IgG3 also induced more DCD than rituximab IgG1 on both cell lines tested (Figure 3-13).

Despite the high level of effector functions associated with the IgG3 subclass, there are currently no IgG3 based therapeutic mAbs approved for use in humans, whereas IgG1, IgG2 and IgG4 based mAbs are all used clinically[70]. In the context of direct targeting mAbs, that act through depletion of the target cell, the findings in this thesis with IgG3 suggest that this subclass would be highly suitable for such therapeutic antibodies. However, the main reason IgG3 has not been pursued as a therapeutic option is because it has a significantly reduced serum half-life as compared to the other IgG subclasses[108]. IgG3 does not bind to the intracellular receptor FcRn that is responsible for recycling IgG from endosomes and returning it into the extracellular space, as it is blocked from doing so by IgG1[457]. As such, IgG3 is therefore resigned to be degraded in the lysosome, meaning it is cleared from the serum more rapidly than other IgG subclasses. Furthermore, due to its elongated, highly flexible hinge region IgG3 is particularly susceptible to cleavage by proteases, a mechanism commonly employed by bacterial pathogens in order to protect themselves against host antibodies[516].

As discussed in Chapter 3:, there have been attempts to alleviate the short half-life of IgG3 by mutating the Fc region, and this has yielded IgG3 mAbs that have similar FcRn binding and *in vivo* persistence to the other IgG subclasses[457]. This report, coupled with the findings in this thesis and a recent review on the topic of antibody isotypes for tumour immunotherapy by Kretschmer *et al.*, suggest that the IgG3 subclass should be reconsidered as a potential scaffold for direct targeting antibodies and is worthy of further study[517]. Alternatively, Fc engineering approaches that aim to endow IgG1 with some of the enhanced effector functions of IgG3 have also been reported[456]. This may be an alternative mechanism with which to improve mAbs effector functions and half-life, although the Fc splicing of two different IgG subclasses could potentially lead to increased immunogenicity of the resulting IgG hybrid which may reduce its usefulness as a therapeutic agent. This would need to be assessed *in vivo* in order to assess immunogenicity, through detection of antibodies against the IgG1/3 hybrid in the serum[518].

Rituximab IgG2 and IgG4 were less active in terms of FcγR mediated effector functions than rituximab IgG1, and this matched their relative affinities for FcγRs (Table 1-2). Neither of these subclasses were able to recruit C1q to the cell surface or showed appreciable specific binding to the C1q affinity column, and accordingly neither induced any CDC on Raji cells, or the highly complement sensitive Ramos cells. Interestingly, both subclasses induced greater DCD than rituximab IgG1, although neither was able to induce any DCD on primary CLL cells. DCD is in theory a Fab mediated effect; it was therefore interesting to note that this process seems to be not just epitope specific, but also dependent on the constant regions of the antibody[296]. It is interesting to speculate that the differential capacity of these IgG subclasses to induce DCD is linked to the way in which they bind to their antigen, CD20.

For rituximab, and to a lesser extent BHH2, the IgG2 subclass was clearly binding differently compared to the other subclasses, with IgG2 binding much less than all other subclasses when examined with a range of flow cytometry methodologies (Section 3.2). IgG3 appeared to show the highest target binding and IgG4 exhibited an intermediate level of binding between that of IgG1 and IgG2. It was apparent from multiple methods of detection that the level of cell surface binding seen for the different IgG subclasses of rituximab were not equivalent, which was not expected for antibodies with the same variable regions. As these antibodies differed only in the heavy chain constant regions (they all contained the kappa light constant regions), the differences must derive from this region. Although the constant regions of the different IgG subclasses are highly homologous (90%), there are differences, particularly within the hinge region[74]. Differences

in the conformation of this hinge region and the disulphide bonds within it alter the flexibility of the subclasses, and this may explain the differences in surface binding. Interestingly, the differences in the level of target antigen bound appear to correlate with the relative sizes of the hinges and degree of flexibility. IgG3 has a highly elongated hinge region and is very flexible, whilst IgG2 and IgG4 have short hinge regions and, particularly for IgG2, high levels of inter-chain disulphide bonding[74,102].

One hypothesis proposed for the lower observed binding of the IgG2 subclass was that it was binding monovalently and as such had far lower avidity for the flow cytometry methods used for analysis (Section 3.2). With less flexible subclasses (e.g. IgG2), they man only able to bind a second CD20 molecule if it is in a specific position relative to the first bound molecule[102]. This hypothesis is supported by the increased detection of the IgG2 subclass at the cell surface using the rituximab anti-idiotype (Figure 3-6). Furthermore, the CD20 antigen is known to undergo redistribution into lipid rafts after binding of type I anti-CD20 mAbs (such as rituximab)[292,293,519]. It is possible that not all the IgG subclasses induce this to the same extent. The lower antigen density (due to decreased CD20 localisation), coupled with the reduced flexibility of IgG2 could combine to yield the low level of surface antibody detected, particularly as for all the detection methods employed the opsonised cells are washed by centrifugation several times prior to flow cytometry. This would be more likely to result in loss of surface bound antibody if it is only bound monovalently. However, how these binding effects would elicit more potent DCD (presumably through enhanced signalling) is not clear as monovalent binding is not sufficient for induction of DCD[519,520]. Rather, a dynamic binding of the IgG2, with oscillating on and off F(ab) binding (as opposed to univalent Fab) may be involved.

However, this hypothesis requires further investigation. When investigating how broadly the switching of subclass effects antigen binding for mAbs against T cell antigens this trend was not strongly replicated (Section 3.2.1). As discussed in Chapter 3:, CD20 is unique compared to the T cell antigens tested, so testing a panel of antibodies targeting antigens that localise into lipid-rafts, such as the BCR, would be interesting to see if this trend is specific to CD20. Conversely, multiple anti-CD20 mAbs exist, so testing these for each IgG subclass may also help support this observation.

Although there have been several non-IgG1 subclass mAbs approved for clinical use, these have largely (with the exception of panitumumab) been of an immunomodulatory mechanism where they act chiefly to inhibit or induce signalling rather than to deplete the target cell[70]. As such,

efficient engagement of FcγR mediated target cell clearance is not desired. Recent findings, as discussed in Chapter 3:, have suggested that in certain model systems the IgG2 subclass can be similarly active in terms of target depletion as an IgG1 version[441]. In the aforementioned study anti-CTLA-4 mAbs were examined whereas here anti-CD20 mAbs were assessed and demonstrated that hIgG1 was more active than IgG2 in all Fc mediated effector assays. The reasons for this difference are not clear, although different targets and methodologies used are possible contributing factors. In this work, IgG2 was largely inert in terms of Fc receptor engagement. The application of glycoengineering to the IgG2 subclass could be one method of attempting to increase the Fc mediated effector functions, particularly CDC, of this subclass. However, it seems unlikely that such approaches would be able to improve IgG2 to the level of IgG1 or IgG3 in terms of Fc mediated effector mechanisms, and it was shown by Peschke *et al.* that addition of galactose to rituximab IgG2 did not facilitate C1q binding or CDC of this subclass[513].

mAbs are exposed to various environments *in vivo* and therefore could become modified following administration. As such, the effect of lipid modification to therapeutic mAb was analysed. Two of these modifications, MDA and CEP, were shown to decrease the ability of these mAbs to bind to antigen and to engage all effector functions tested (Chapter 4:). Although there are currently no reports in the literature detailing these specific modifications on antibodies, they have been found on various proteins, including serum proteins, for example in drusen deposits found in patients with age related macular degeneration and at tumour sites[462,475,478]. It is also known that the tumour microenvironment is highly oxidising, and mAbs are becoming commonly used therapeutic agents for cancer therapy[70,460]. In order to be certain that these modifications do occur *in vivo*, purified *ex vivo* antibodies bearing such modifications would need to be identified and studied.

The material generated in this work were proof-of-concept studies generating extensively modified mAbs, and it has been reported that the exposure of proteins to the modifying reagents *in vivo* would result in a lesser degree of modification that is seen with *in vitro* modifications[471]. Therefore, it is of relevance to determine the level of *in vivo* modification that occurs and then generate antibodies carrying a more representative level of modification. Testing such modified antibodies in the mAb effector function assays used in this thesis would be a better model of what may be happening *in vivo*. As such, it is possible that the level of modification to antibodies that occurs *in vivo* may not have such a detrimental effect as those reported in this work.

Assuming these physiological modifications are seen to be detrimental as indicated in Chapter 4:, it should be considered how they may be overcome. The modifications are thought to target lysine residues within the mAb. As shown in Figure 4-26 mAbs contain a large number of lysine residues, so removing these residues from the protein sequence is not possible. It is possible that there may be other modifications to lysine residues which could be applied that do not alter the mAb function but could act to protect the mAb from further modification *in vivo*. Alternatively, it may be possible to try and alter the disease microenvironment to reduce the propensity of these modifications to occur, possibly through administration of antioxidants to impair the activation of lipids, thereby reducing the number of potential modifications.

It is possible that different IgG subclasses may have differing susceptibilities to modification, in which case an alternate subclass may be preferential for treatment of certain diseases where mAb modifications are occurring. However, as shown in Figure 4-26, both IgG2 and IgG4 contain similar numbers of lysine residues, although this does not necessarily mean they are equally sensitive to modification. The effect of different glycoforms could also be tested to see if they are able to provide any protection against modification of the protein backbone, or even act as a sink for such modifications. However, the glycans are relatively small compared to the size and surface area of the whole IgG molecule, so it is unlikely that they would be able to provide much protection. Furthermore, they are largely buried within the cavity between the two CH2 domains in the IgG Fc, and therefore are somewhat sequestered away from the IgG surface, where the lipid modifications would occur.

There has been a great deal of research into the effect of different glycoforms attached to the asparagine 297 linked glycan chain present within the IgG. This field has promised much, largely based on the finding that removal of fucose from the Fc glycans of an antibody significantly increases both its affinity for FcγRIIIa and the ability to induce NK-mediated ADCC[351,352]. Accordingly, a few mAbs incorporating reduced or removed fucose have been approved for use clinically (mogamulizumab, obinutuzumab and benralizumab)[279,362,394,395]. However, the influence of other glycans on antibody effector mechanisms has not been as clearly defined as that of fucose. Evidence from human serum of various healthy and disease cohorts has revealed changes in glycoforms associated with different physiological states, ranging from autoimmune disease to aging and pregnancy[334,378,379,521,522]. More recently, it has become possible to generate IgG populations with defined and relatively homogeneous glycoforms, and this has facilitated testing of these antibodies in various effector functions. However, the findings of reports from various

groups on the impact of different glycoforms have failed to reach a consensus on the effect of glycans such as galactose and sialic acid within the IgG Fc[372,377,406,502,503,514,523].

The data presented in this thesis using *in vitro* glycoengineered rituximab and obinutuzumab showed that there was not a major effect of either of these glycoforms in terms of their ability to bind to FcγRs or to induce the FcγR mediated effector functions, ADCC and ADCP. Only small increases in the binding to FcγRIIa and FcγRIIIa were found (Figure 5-3, Figure 5-4 and Table 5-10). This finding matches some of the published reports in this field. For example, Thomann *et al.* used a very similar *in vitro* glycoengineering approach to generate several different glycoforms, including fully galacostylated and highly sialylated glycoforms[406]. They reported that the affinity of samples with increased galactose and increased sialic acid were modestly higher affinity for FcγRIIa, FcγRIIb and FcγRIIIa, and this translated into slightly increased ADCC[406,507,523]. Furthermore, in a recent report by Dekkers *et al*., increased galactose and sialic acid induced similar small increases in FcγR binding, with a small effect on ADCC in the context of hypofucosylated glycans[514]. However, other reports, do not corroborate with the findings in this thesis, such as that by Scallon *et al.*, who reported that an increased sialylation of IgG reduced ADCC activity and FcγRIIIa binding, and Quast *et al.* showed no effect of hypersialylation on ADCC[502,503].

Whilst the substantial effect of fucose on FcγRIIIa binding and ADCC has led several glycomodified mAbs being approved for clinical use, the modest effects of galactose and sialic acid reported here and corroborated by Thomann *et al.* and Dekkers *et al.* suggest that these sugars have a minor impact on overall antibody efficacy[351,352,406,514]. As such, it may be that the cost of carrying out glycoengineering or modifying and optimising new antibody production methods to generate these glycoforms is not worth the small improvement to efficacy that has been demonstrated *in vitro* in these reports. Although testing of the efficacy of glycomodified mAbs *in vivo* is needed to be certain, from the evidence currently available it is unlikely these glycomodifications would make a significant clinical impact.

It is also interesting to note the although IgG1 with increased galactose and sialic acid are here reported to have slightly increased FcγR binding and Fc mediated effector functions, this appears to be in contrast to what occurs *in vivo* during pregnancy and rheumatoid arthritis patients. Rheumatoid arthritis patients have higher levels of agalactosylated IgG, and this is associated with increased disease activity[378]. Furthermore, the increase in galactosylation and sialylation of serum IgG that occurs during pregnancy is associated with an improvement in the symptoms of

rheumatoid arthritis and is presumed to reduce the inflammatory nature of IgG[379]. Post-partum, rheumatoid arthritis patients often experience a disease flare and their levels of galactosylation and sialylation also decrease. From these studies, the presence of galactose and sialic acid appear to be anti-inflammatory, and this agrees with some data suggesting that sialylated Fc is the active component of IVIg[348]. IVIg, pooled IgG from healthy donors, is given to patients with various autoimmune disorders and its mechanism of action is not fully understood. However, it has been reported that enrichment of sialylated IgG increased the efficacy of IVIg[372]. Mechanisms have been proposed to explain this finding, but it is not fully understood. The glycomodification testing in this thesis has solely used monomeric IgG. As the reports for IVIg appear contradictory, it would be interesting to see whether testing glycomodified rituximab carrying increased galactose and sialic acid has a different response when tested as an immune complex, for example generated through the use of a crosslinking $F(ab')_2$ anti-IgG.

The serum half-life of these glycomodified antibodies was also tested in immunocompetent mice. It was found that after 7 days the clearance of these glycoforms was no different to that of the mock treated control antibodies (Figure 5-18). Although there are reports in the literature that suggest that IgG glycosylation can effect half-life, for example high-mannose glycans are reported to be cleared rapidly from the serum, it is not thought that other glycoforms have a major influence on IgG half-life, as a detailed study of different glycoforms in cynomolgus monkeys demonstrated[500,524]. This may be because the Fc glycans are largely buried within the Fc of the antibody, and therefore have a limited ability to bind to surface receptors to increase or decrease antibody clearance[499]. This may also explain why antibodies with terminal galactose or GlcNAc are not cleared rapidly from the circulation by interaction with asialoglycoprotein receptors, and why sialylation doesn't appear to increase the IgG half-life[525].

The lack of a consensus on the effect of different IgG glycoforms on IgG effector function extend to their ability to activate the classical complement cascade. Increased levels of galactose are consistently reported to increase the level of complement activation, consistent with what is shown in this thesis (Section 5.3.4)[502,513,514]. However, the impact of sialic acid upon complement activation is less clear. It was found in our systems that complement engagement was increased with galactose and sialic acid. Dekkers *et al.*, report increased C1q binding, C4b deposition and CDC with galactosylated and sialylated IgG, therefore corroborating the work in Section 5.3.4[514]. However, Quast *et al.* reported increased CDC and C1q binding with galactosylation, but decreases in both upon sialylation[502]. Furthermore, Peschke *et al.* reported increased C1q binding

and CDC as a result of increased galactosylation of IgG1 and IgG3, with no effect seen on IgG2 and IgG4 subclasses[513].

One reason for these discrepancies could be that the methods and models used to demonstrate the efficacy of the different glycoforms vary between laboratories. For example, it is known that differences in target epitope characteristics can influence the engagement of effector functions, and this could contribute to differential effects of sialic acid in different systems[433]. Furthermore, it is possible that differences in the purities of the glycoforms used by different groups could contribute to these contrasting results. It is likely that the level of sialylation will have differed between the samples produced in these various reports, and therefore the extent of terminal galactose would also vary (as the sialic acid residues mask the galactose). However, this still does not explain the reported findings, where some groups report increased killing with sialic acid and others report reduced killing. If the effect on complement engagement was due to the level of exposed galactose then samples with more sialylation would be less active than those without sialic acid, but samples with sialic acid would not be able to induce more complement engagement than the fully galactosylated samples. Therefore, it appears that the effect on complement engagement is not purely regulated by the level of galactose, but that the sialic acid residues also contribute in certain experimental systems, and that it may be this contribution that differs between different laboratories.

In order to try and minimise the effect of confounding variables in studying complement engagement, a C1q affinity column was developed in order to have a system where the binding of antibodies to C1q directly could be assessed (Chapter 6:). This system offers a more direct way to compare samples generated in different laboratories; bypassing potential bias imposed by different antigens, target cells, serum sources and experimental protocols. Assessing C1q binding directly (as the first step in complement activation) may therefore help resolve some of the contrasting findings that have been reported, particularly for different IgG glycoforms.

Although assessing the various mAbs in this manner would reduce complexity, it should be noted that the binding of a monomeric C1q globular head group to a monomeric IgG molecule is not a perfect model of the ability of an antibody to engage and activate the complement cascade. Therefore, the findings from the column need to be related to cell based assays. Discrepancies between the C1q column and cell based CDC assays could be an indicator that other factors are influencing CDC beyond simple IgG-C1q binding. For example, it is known that certain IgG forms bind monovalently and then form Fc hexamers on the target cell surface in order to bind to C1q[80].

Therefore, increased or decreased tendencies to form such hexamers could increase or decrease CDC beyond the binding of IgG to C1q.

Despite the very low binding affinity of monomeric IgG to C1q, the C1q affinity column was able to detect this binding event (Chapter 6:)[207]. In order to create an environment that is permissive to the binding, the buffers used for the sample injection and binding phase contained no salt. Because of this, there was some non-specific interaction of certain protein samples with the column matrix - streptavidin coated sepharose. This necessitated the use of a blank column as a reference standard to allow the determination of the binding contribution that is specific to the C1q engagement (Figure 6-9). As shown in Section 6.4, this method was able to give biologically relevant information about the C1q engagement of various IgG samples.

Further optimisation of the column could be directed towards reducing the non-specific binding to the column or increasing the signal to noise window between the specific and non-specific binding peaks. It is possible that using an alternative column matrix could reduce the non-covalent interactions, for example using a porous sepharose matrix. Whilst it was shown that increasing the C1q density of the C1q affinity column did indeed increase the retention of IgG, this was not stable over time (Figure 6-6). The reason for this remains unclear, although there appears to be a decrease in the binding capacity of the higher density columns potentially indicating a loss of functional C1q beyond a certain point (approximately equivalent to the 1mg C1q column). However, extending the length of the column, but maintaining the same C1q density, may provide a means to enable a greater separation between specific and non-specific binding.

In spite of the non-specific binding to the column matrix, the biological validity of the C1q affinity column was demonstrated through the concordance between the relative elution profiles of IgG glycovariants and IgG subclasses tested on the column, and the performance of these samples in cell based assays (Section 6.4, Section 5.3.4 and Section 3.3.2). Three different mAbs that had undergone *in vitro* glycomodification all demonstrated a trend towards increased binding to the column with addition of galactose and sialic acid that was specific to the C1q column. One of these sets of glycovariants, based on rituximab, was also tested in cell based assays. The performance of the galactosylated and sialylated glycovariants in terms of C1q recruitment to the opsonised target cell and induction of CDC matched the trend seen on the C1q affinity column, with sialylated antibody being the most active by all methods tested (Section 3.3.2 and Section 6.4.1). Together this confirms that whilst the C1q column performs under non-physiological

conditions, it is able to measure biologically relevant differences between glycomodified antibodies.

The four different IgG subclasses are known to differ in their ability to bind to C1q and engage complement (Section 3.3.2). This finding was also recapitulated on the C1q affinity column, with the four different subclasses of IgG bearing the rituximab variable regions. IgG3 was the most active, with IgG2 and IgG4 showing little C1q-specific binding. Furthermore, the different IgG subclasses gave similar results in the cell based assays of C1q recruitment and CDC, matching both what is shown in the literature and the results from the C1q affinity column. The poor binding of rituximab IgG2 to C1q, both in the C1q affinity column and in the cell recruitment assay, further corroborates the low CDC activity of IgG2 being a consequence of the subclass, not simply the lower level of surface binding exhibited by rituximab IgG2.

In light of this concordance between the C1q affinity column findings and the results of cell based experiments, the C1q affinity column was demonstrated to be a suitable tool for studying interactions of various different IgG samples, as well as other C1q ligands, to C1q. The column has the potential to act as a tool for screening different mAbs (including subclasses, glycoforms and mutants) as well as other C1q binding proteins for their C1q binding in a high throughput manner, and could also be used to purify fractions that have increased C1q binding for further study.

Another potential use of the C1q affinity column could be in the treatment or diagnosis of autoimmune disorders that are caused by autoantibodies, such as SLE[526]. There have been reports of C1q based immunoadsorbtion to treat this autoimmune disorder, which appeared to be well tolerated and caused a reduction in circulating immune complexes seen as well as an improvement in disease symptoms[526-529]. However, this has not become a regular treatment option, possibly because these reports/trials largely used porcine C1q in their immunoadsorbant, or because the effect was limited in resolving acute symptoms. It is interesting to note that the C1q density used in those immunoadsorption columns is equal to the most stable density tested in this thesis; 1mg of C1q per ml of matrix[529]. The C1q affinity column presented here could be used to deplete the blood of these patients of IC. The physiological concentration of salts within the serum would mean that monomeric antibodies would most likely not bind to the column, but immune complexes that bind C1q strongly would be more likely to be retained and therefore reduce the potential for these complexes to initiate autoimmune damage in the patient.

In order to understand the impact of post-translational modifications on therapeutic mAbs the work in this thesis focussed on IgG1, to better reflect the majority of clinically approved mAbs, as well as use the well defined mAb model of rituximab. Therapeutic mAbs exist in a milieu of serum IgG with various glycoforms, and therefore have to compete with other IgG for ligands such as FcγRs. The serum glycan pool is known to vary in numerous physiological settings in both health and disease, which could impact upon the efficacy of therapeutic mAbs[530].

There have been reports that suggest that there are differences in the glycosylation of the different IgG subclasses *in vivo*[336]. However, it would be interesting to investigate the effects of glycomodification on the other IgG subclasses (namely IgG2, IgG3 and IgG4), to see if similar effects are seen. Towards this end, Peschke *et al.* have recently reported galactosylation of each of the IgG subclasses and that this increases the efficacy of IgG1 and IgG3 in complement activation whilst having no effect on IgG2 and IgG4[513]. It is currently unknown whether addition of sialic acid on top of galactose would further improve the CDC or C1q binding of IgG3, as it was shown to for IgG1 in this thesis. Furthermore the effect on FcγR binding and FcγR dependent effector mechanisms is currently unknown for glycomodified IgG subclasses beyond IgG1. It is possible that application of glycoengineering methods to IgG3 could further increase its capacity to induce effector functions. For example, removing fucose may increase the affinity of IgG3 for FcγRIII (as it does for IgG1) thereby increasing its ability to induce ADCC. Furthermore, testing the effect of differing levels of galactosylation and sialylation may provide a mechanism to increase the levels of C1q binding and CDC induced, and could provide small increases in FcγR binding, as has been shown for IgG1.

In this thesis the effect of glycoengineering and IgG subclass switching was examined in the context of direct targeting antibodies. However, as mentioned in Section 1.4, immunomodulatory antibodies are now beginning to exhibit success in oncology in the clinic, and these antibodies generally act to activate or suppress signalling rather than deplete the target cells[164]. It would be interesting to determine the effect that different glycoforms and IgG subclasses have on this function as they are here shown to have different mechanisms of binding, at least for anti-CD20 mAbs. It has been reported that differences in agonism are seen with different IgG subclasses, with the IgG2 subclass being shown to act as a superagonist independently of FcγRs, whereas IgG1 and IgG4 required FcγRIIb, in the context of anti-CD40 targeting[104,531]. Application of glycoengineering to IgG subclasses of an agonistic anti-CD40 antibody could therefore be carried out and tested. As increased galactose and sialic acid increased complement killing, which is

facilitated by clustered IgG binding into hexamers at the surface, it would be interesting to see whether the addition of these glycoforms enhances the activity of agonistic mAbs.

Whilst this thesis has focussed on the glycomodification of therapeutic mAbs, it is worth noting that FcγRs themselves are glycosylated. There have been recent reports that differences in the glycosylation of these FcγRs can also alter the binding affinities of IgG, particularly FcγRIII, which is known to require glycosylation at its N162 residue in order to bind to IgG[391,532]. For example, FcγRIIIa that bears oligomannose glycans displays a 50x increased affinity for IgG Fc as compared to FcγRIIIa with complex type glycans, making this receptor of a similar affinity to FcγRI[391]. Although little literature exists regarding the state of glycosylation of FcγRs *in vivo*, owing in part to the difficulty in generating sufficient material, it is not unreasonable to think that the glycoforms found on cell lines and generated *in vitro* may be different to those found *in vivo*, as is the case for recombinant mAbs produced from cell lines compared to serum IgG.

One study of FcγRIIIa glycosylation carried out in 1997 suggested that FcγRIIIa from certain cell types *in vivo* did indeed contain a large degree of oligomannose glycans, and that NK cells had a higher degree of oligomannose glycans and increased affinity for IgG than FcγRIIIa on monocytes (which had no oligomannose glycans), despite the protein cores being identical[389]. Furthermore, a very recent report from Patel *et al.* also found a significant degree of oligomannose glycans present on FcγRIIIa expressed on NK cells purified from peripheral blood, very different to the glycosylation found on recombinant FcγRIIIa, and that FcγRIIIa with oligomannose glycans once again displayed a higher affinity for IgG[390]. These studies indicate that the FcγR glycosylation can be highly important for the binding to IgG, at least for FcγRIIIa, and that this should also be taken into account when designing therapeutic mAbs. It is also possible that differences in FcγR glycosylation could be at least in part responsible for the differences in reported findings of IgG activity, particularly when comparing assays using FcγR expressing cell lines primary cells. Furthermore, the potential of trying to exploit differences in FcγR glycosylation to achieve greater specificity for a single FcγR (or even effector cell type) could also be explored through testing different glycoforms and Fc mutants or IgG subclasses on the different glycoforms of FcγRs.

In summary, the IgG Fc region is essential for many of the important functions of IgGs, including serum persistence and engagement of various effector mechanisms. Changing the Fc region can dramatically alter the properties of IgG. The IgG1 and IgG3 subclasses are highly active in inducing Fc mediated responses, whereas IgG2 and IgG4 induce these responses much more weakly. IgG2 subclass also exhibits reduced surface binding to some, but not all, targets. IgG glycosylation was

shown to be a modulator of complement engagement, with IgG1 bearing increased galactose and sialic acid more active in C1q binding and complement activation, but these glycoforms had little impact upon FcγR binding or engagement. A C1q affinity column was produced in order to facilitate direct study and screening of the binding of ligands, including IgGs, to the column. Lipid modification of IgG was shown to be detrimental to IgG properties, both Fc and Fab mediated. The importance of Fc modifications to improved or decrease mAb effector functions is clearly demonstrated, and offer potential mechanisms that could be applied in order to generate more effective therapeutics.

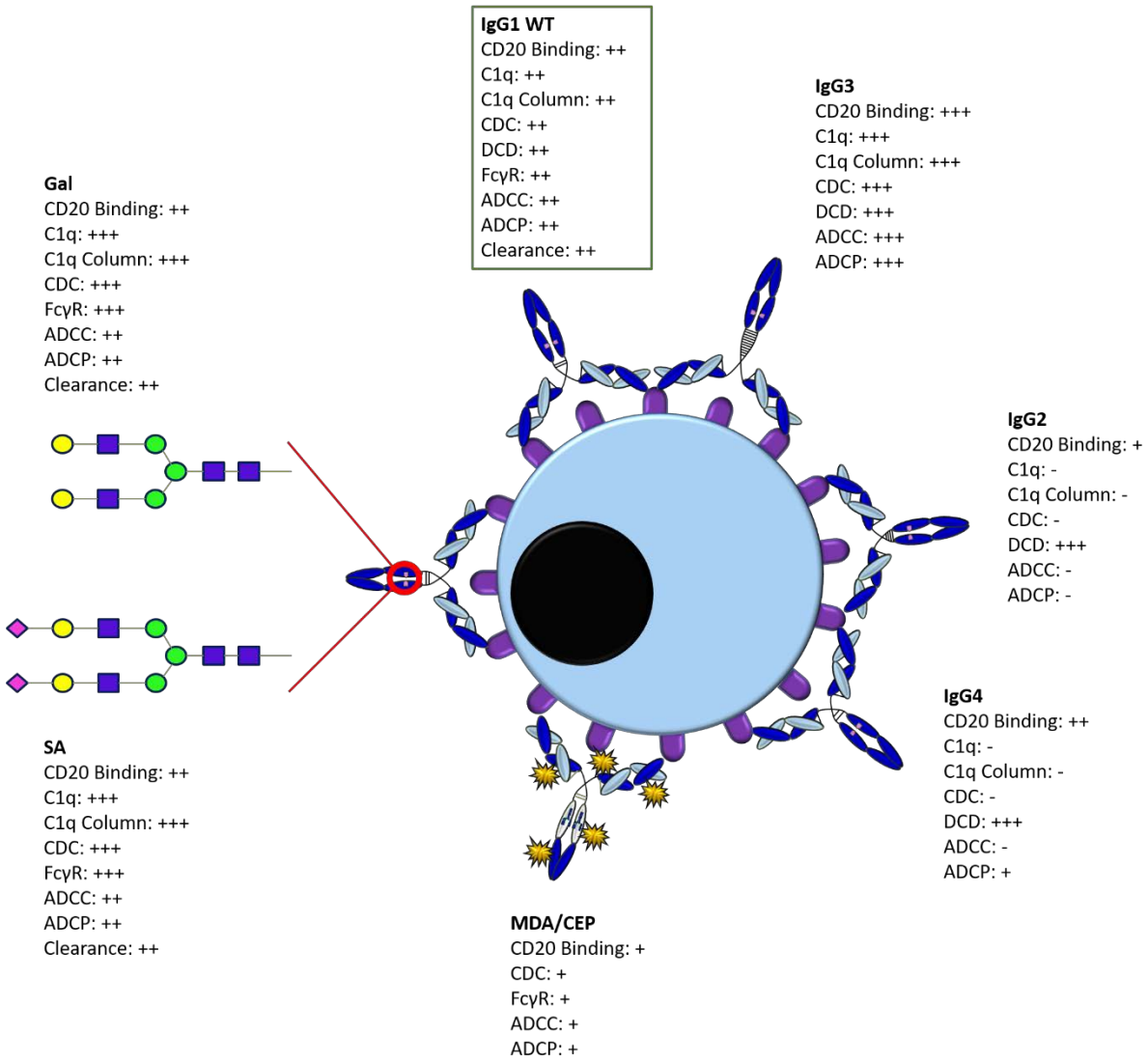

Figure 7-1 Summary of Rituximab Fc Modifications

A schematic diagram of the rituximab IgG Fc modifications discussed in this thesis. Wild type rituximab IgG1 is highlighted in green as a reference. Assays indicated: CD20 Binding- the relative level of binding to CD20, C1q- the relative level of C1q recruitment to the cell surface, C1q column- the relative binding to the C1q affinity column, CDC- the relative level of complement dependent cytotxicity induced, DCD- the relative level of direct cell death induced, FcγR- the relative level of binding to FcγRs, ADCC- the relative level of antibody dependent cellular cytotoxicity induced, ADCP- the relative level of antibody dependent cellular phagocytosis induced, and Clearance- the relative rate of clearance of antibody *in vivo*. +++ = increased above the level wild type antibody, ++ = approximate the level of wild type antibody, + = reduced below the level of wild type antibody, - = no activity detected.

Chapter 8: Appendix

8.1 Appendix A – Complement Dependent Cytotoxicity

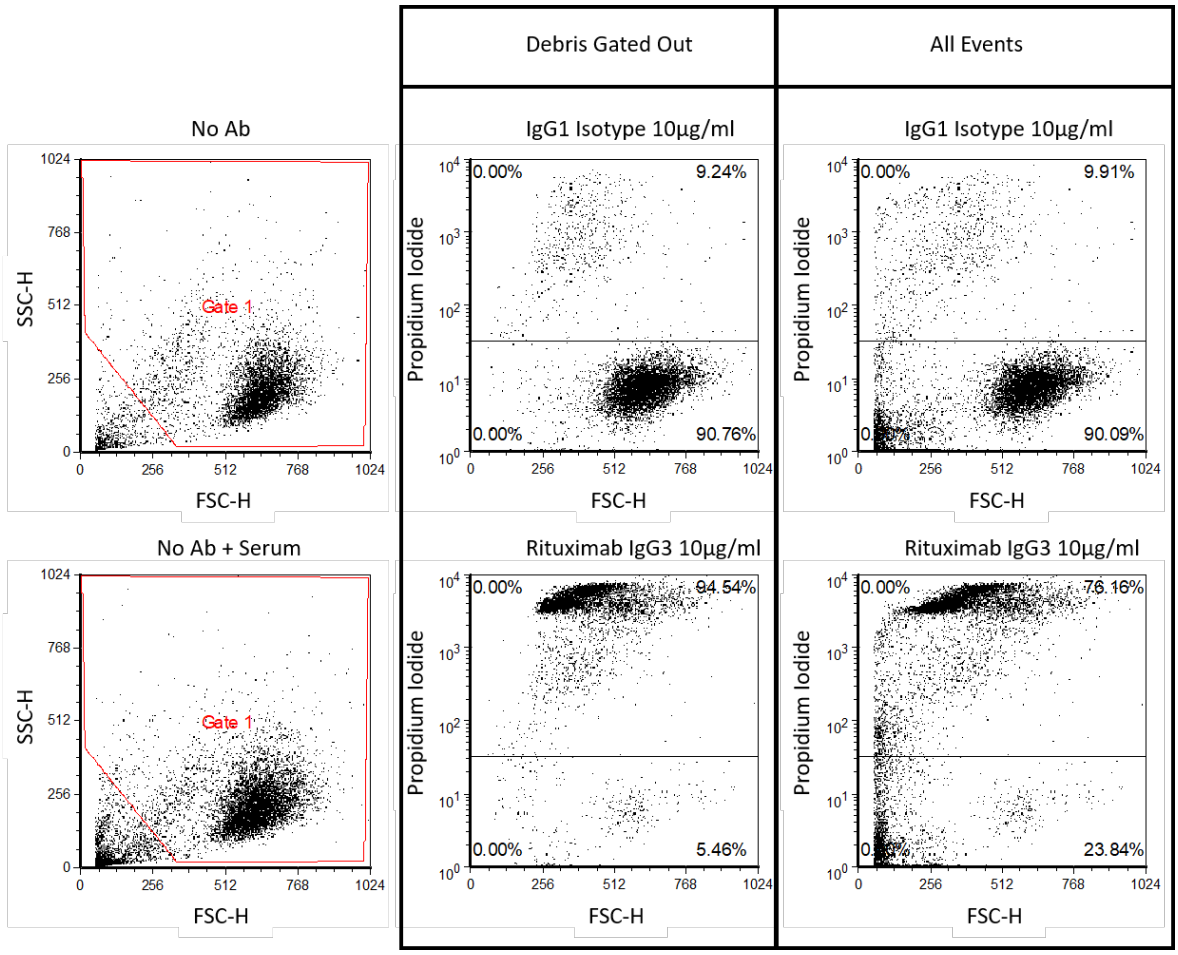

Figure 8-1 Complement Depended Cytotoxicity

Ramos cells opsonised with anti-CD20 antibody (see Figure 3-16). The CDC induced by the anti-CD20 mAbs does not result in a build-up of cell debris in the bottom left hand corner of the plot, as there is little difference between isotype treated and rituximab IgG3 treated plots.

8.2 Quality Control of IgG

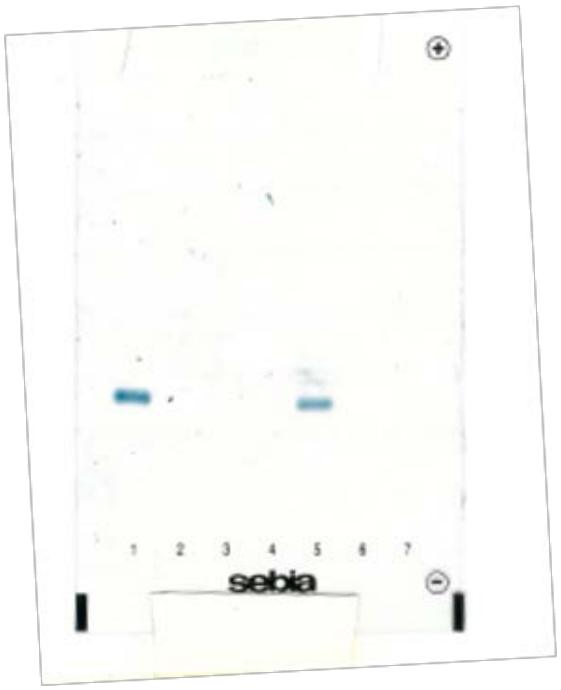

Figure 8-2 Antibody Elution

After HPLC purification, antibody samples were tested by native gel electrophoresis in order to confirm that antibody had been eluted and was not present in the column flow through or washes. Lanes 1 and 5 contain eluted antibody, lanes 2-4 and 6-7 contain washes buffer flow through samples.

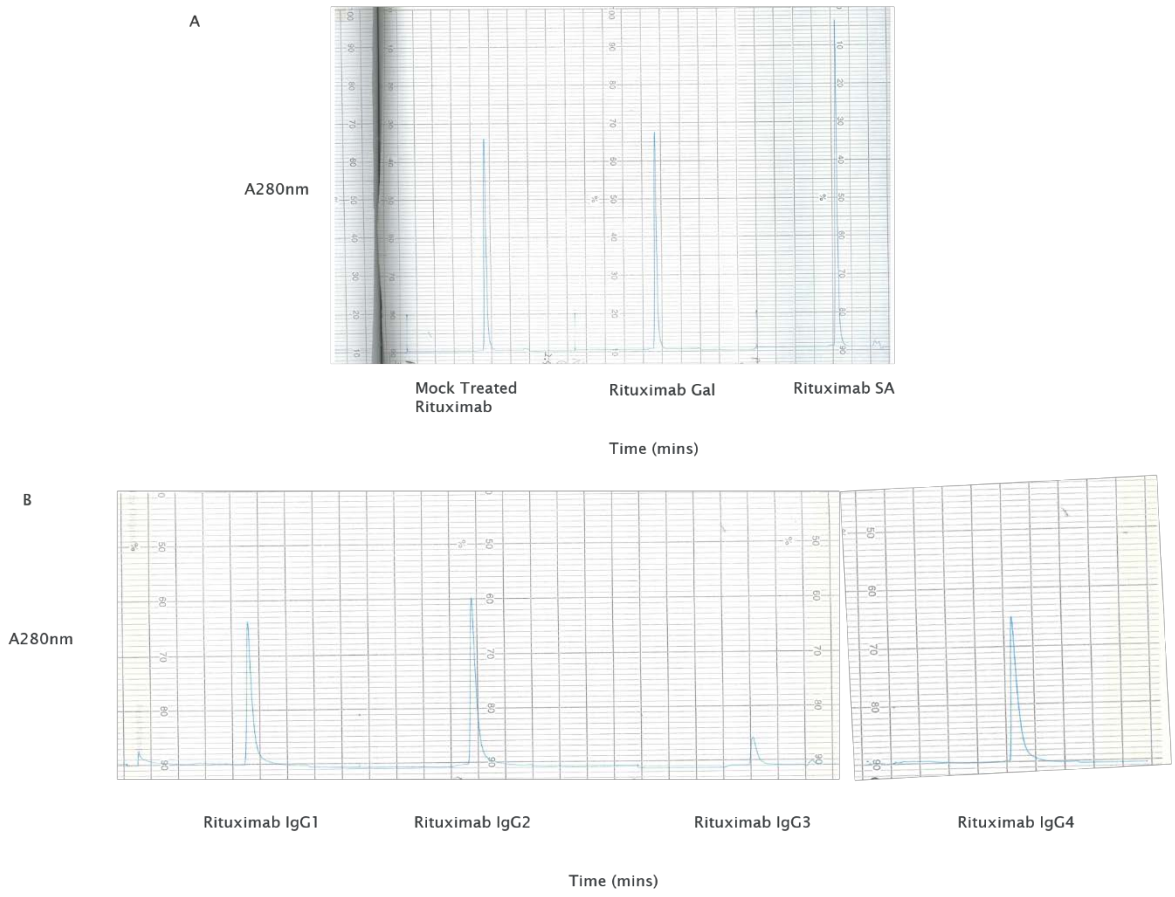

Figure 8-3 Size Exclusion HPLC of Antibody

Purified IgG were tested by size exclusion HPLC to confirm they were free of aggregation. Each sample was injected and approximately 20 minutes later the IgG peak eluted. Aggregation would be indicated by the presence of a shoulder/second peak prior to the main peak. A- glycomodified rituximab and B- rituximab subclasses were tested for aggregation.

Antibody Sample	Endotoxin (Eu/mg)
Rituximab	0.097
Rituximab Gal	0.1
Rituximab SA	0.28
Obinutuzumab	0.23
Obinutuzumab Gal	0.14
Obinutuzumab SA	0.24

Table 8-1 Antibody Endotoxin Table

Antibodies were tested for the presence of endotoxin using an Endosafe PTS endotoxin testing system according to manufacturers recommended instructions. Endotoxin levels below 0.5Eu/mg are considered to be low and safe for use *in vivo* (personal communication- Southampton Antibody and Vaccine Antibody Production Group).

8.3 Surface Plasmon Resonance Measurement of IgG-FcγR Interactions

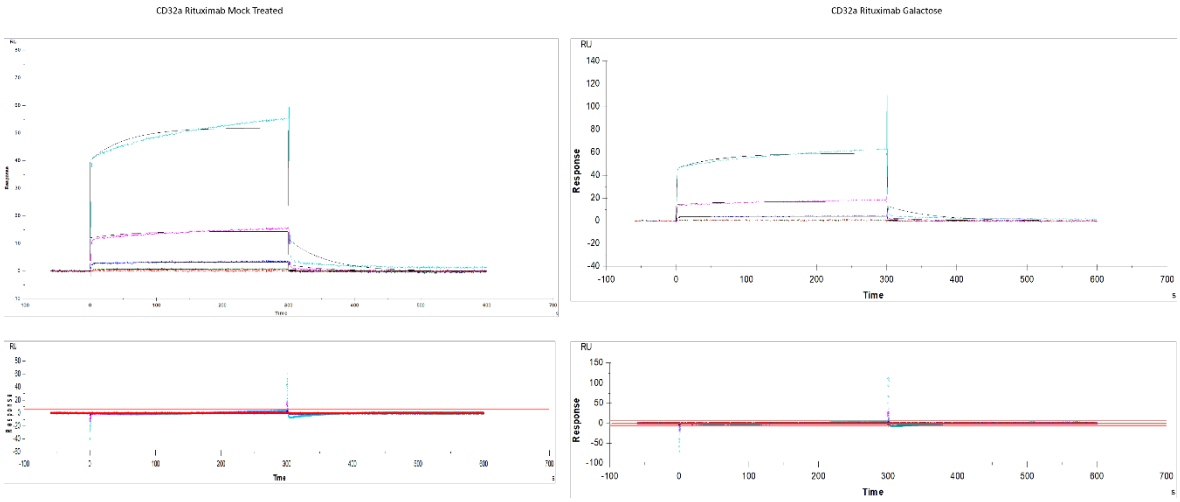

Figure 8-4 Representative SPR Plots of Apparent Good Fit of IgG Binding to FcγRIIa

Shown are two examples of SPR data obtained from the binding of rituximab IgG glycoforms to FcγRIIa. The fitting of the model (1:1 binding) is shown, and the residuals of fitting to the model are shown below the curves. These data appear to fit their modelling relatively well, as evidenced by their relatively low Chi-squared values of 1.84 (left) and 3.55 (right).

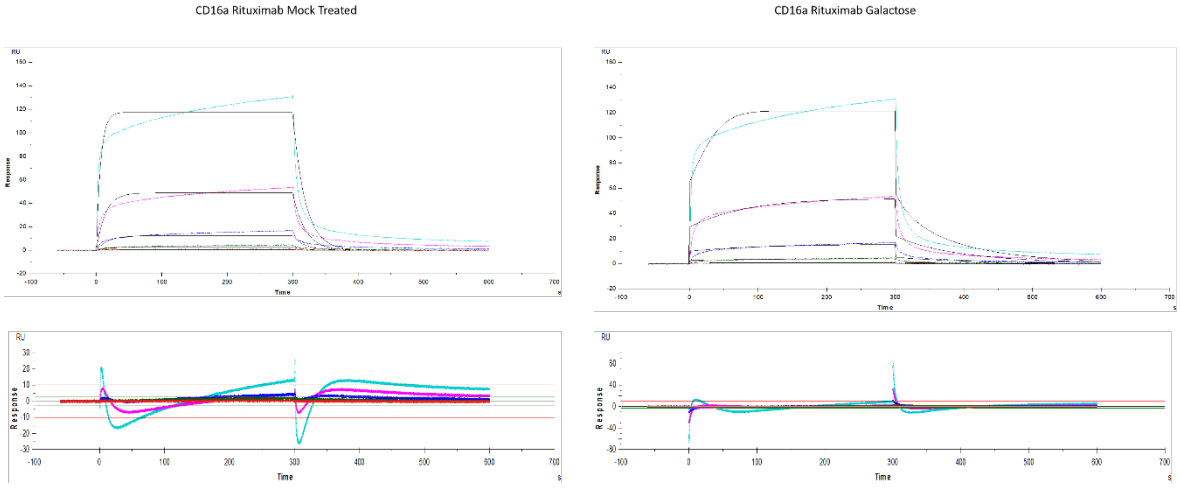

Figure 8-5 Representative SPR Plots of Apparent Bad Fit of IgG Binding to FcγRIIa

Shown are two examples of SPR data obtained from the binding of rituximab IgG glycoforms to FcγRIIa. The fitting of the model (1:1 binding) is shown, and the residuals of fitting to the model are shown below the curves. These data appear to fit their modelling relatively poorly, as evidenced by their relatively high Chi-squared values of 23.1 (left) and 25(right).

Sample	ka (1/Ms)	kd (1/s)	KD (M)	Rmax (RU)	Chi² (RU²)	Ligand	Model
hCD32a	9.72E+01	1.45E-02	1.49E-04	2271.9	4.24	Ritux NANA	1:1 Binding
hCD32a	N/A	N/A	1.36E-06	172.5	0.0219	Ritux NANA	Steady State Affinity
hCD32a	2.56E+02	1.59E-02	6.22E-05	841.5	3.55	Ritux galactose	1:1 Binding
hCD32a	N/A	N/A	1.58E-06	161.8	0.00191	Ritux galactose	Steady State Affinity
hCD64	N/A	N/A	1.34E-08	420.4	157	Ritux galactose	Steady State Affinity
hCD64	2.72E+05	1.48E-04	5.45E-10	370.1	8.75	Ritux NANA	1:1 Binding
hCD64	N/A	N/A	1.51E-08	445.8	266	Ritux NANA	Steady State Affinity
hCD64	2.22E+05	2.47E-04	1.11E-09	352.3	8.82	Ritux native	1:1 Binding
hCD64	N/A	N/A	1.33E-08	413.2	120	Ritux native	Steady State Affinity
hCD64	2.22E+05	1.89E-04	8.54E-10	356.7	8.19	Ritux galactose	1:1 Binding
hCD16a	2.93E+04	1.17E-02	4.01E-07	105.5	25	Ritux galactose	1:1 Binding
hCD16a	N/A	N/A	4.26E-07	232.1	6.16	Ritux galactose	Steady State Affinity
hCD16a	N/A	N/A	5.75E-07	202.9	2.79	Ritux native	Steady State Affinity
hCD32a	2.22E+02	1.79E-02	8.07E-05	953.5	1.84	Ritux native	1:1 Binding
hCD32a	N/A	N/A	1.79E-06	153.8	0.00164	Ritux native	Steady State Affinity
hCD16a	4.94E+04	1.42E-02	2.87E-07	132.6	29.8	Ritux NANA	1:1 Binding
hCD16a	N/A	N/A	3.55E-07	246.2	9.72	Ritux NANA	Steady State Affinity
hCD16a	9.92E+04	5.36E-02	5.41E-07	181.2	23.1	Ritux native	1:1 Binding

Table 8-2 SPR values of Binding and Model Fitting

Table of values of SPR data showing the range of fitting within the data.

References:

1 Janeway, J., Travers P, Walport M, & Shlomchik M. *Immunobiology*. Vol. 5 (Garland Publishing, 2001).

2 Beutler, B. Innate immunity: an overview. *Molecular immunology* **40**, 845-859 (2004).

3 Kumar, H., Kawai, T. & Akira, S. Pathogen recognition by the innate immune system. *Int Rev Immunol* **30**, 16-34, doi:10.3109/08830185.2010.529976 (2011).

4 Kawai, T. & Akira, S. The role of pattern-recognition receptors in innate immunity: update on Toll-like receptors. *Nat Immunol* **11**, 373-384, doi:10.1038/ni.1863 (2010).

5 Schenten, D. & Medzhitov, R. The control of adaptive immune responses by the innate immune system. *Adv Immunol* **109**, 87-124, doi:10.1016/B978-0-12-387664-5.00003-0 (2011).

6 Merle, N. S., Church, S. E., Fremeaux-Bacchi, V. & Roumenina, L. T. Complement System Part I - Molecular Mechanisms of Activation and Regulation. *Frontiers in immunology* **6**, 262, doi:10.3389/fimmu.2015.00262 (2015).

7 Noris, M. & Remuzzi, G. Overview of complement activation and regulation. *Semin Nephrol* **33**, 479-492, doi:10.1016/j.semnephrol.2013.08.001 (2013).

8 Amulic, B., Cazalet, C., Hayes, G. L., Metzler, K. D. & Zychlinsky, A. Neutrophil function: from mechanisms to disease. *Annu Rev Immunol* **30**, 459-489, doi:10.1146/annurev-immunol-020711-074942 (2012).

9 Pruchniak, M. P., Arazna, M. & Demkow, U. Life of neutrophil: from stem cell to neutrophil extracellular trap. *Respir Physiol Neurobiol* **187**, 68-73, doi:10.1016/j.resp.2013.02.023 (2013).

10 Brinkmann, V. *et al.* Neutrophil extracellular traps kill bacteria. *Science* **303**, 1532-1535, doi:10.1126/science.1092385 (2004).

11 Jakubzick, C. V., Randolph, G. J. & Henson, P. M. Monocyte differentiation and antigen-presenting functions. *Nature reviews. Immunology* **17**, 349-362, doi:10.1038/nri.2017.28 (2017).

12 Auffray, C., Sieweke, M. H. & Geissmann, F. Blood monocytes: development, heterogeneity, and relationship with dendritic cells. *Annu Rev Immunol* **27**, 669-692, doi:10.1146/annurev.immunol.021908.132557 (2009).

13 Lavin, Y., Mortha, A., Rahman, A. & Merad, M. Regulation of macrophage development and function in peripheral tissues. *Nature reviews. Immunology* **15**, 731-744, doi:10.1038/nri3920 (2015).

14 Mosser, D. M. & Edwards, J. P. Exploring the full spectrum of macrophage activation. *Nature reviews. Immunology* **8**, 958-969, doi:10.1038/nri2448 (2008).

15 Ruffell, B. & Coussens, L. M. Macrophages and therapeutic resistance in cancer. *Cancer Cell* **27**, 462-472, doi:10.1016/j.ccell.2015.02.015 (2015).

16 Dahal, L. N. *et al.* STING Activation Reverses Lymphoma-Mediated Resistance to Antibody Immunotherapy. *Cancer Res* **77**, 3619-3631, doi:10.1158/0008-5472.CAN-16-2784 (2017).

17 Murray, P. J. *et al.* Macrophage activation and polarization: nomenclature and experimental guidelines. *Immunity* **41**, 14-20, doi:10.1016/j.immuni.2014.06.008 (2014).

18 Boltjes, A. & van Wijk, F. Human dendritic cell functional specialization in steady-state and inflammation. *Frontiers in immunology* **5**, 131, doi:10.3389/fimmu.2014.00131 (2014).

19 Joffre, O. P., Segura, E., Savina, A. & Amigorena, S. Cross-presentation by dendritic cells. *Nature reviews. Immunology* **12**, 557-569, doi:10.1038/nri3254 (2012).

20 O'Keeffe, M., Mok, W. H. & Radford, K. J. Human dendritic cell subsets and function in health and disease. *Cell Mol Life Sci* **72**, 4309-4325, doi:10.1007/s00018-015-2005-0 (2015).

21 Roche, P. A. & Furuta, K. The ins and outs of MHC class II-mediated antigen processing and presentation. *Nature reviews. Immunology* **15**, 203-216, doi:10.1038/nri3818 (2015).

22 Mandal, A. & Viswanathan, C. Natural killer cells: In health and disease. *Hematol Oncol Stem Cell Ther* **8**, 47-55, doi:10.1016/j.hemonc.2014.11.006 (2015).

23 Thielens, A., Vivier, E. & Romagne, F. NK cell MHC class I specific receptors (KIR): from biology to clinical intervention. *Current opinion in immunology* **24**, 239-245, doi:10.1016/j.coi.2012.01.001 (2012).

24 Saunders, P. M. *et al.* A bird's eye view of NK cell receptor interactions with their MHC class I ligands. *Immunological reviews* **267**, 148-166, doi:10.1111/imr.12319 (2015).

25 Karre, K., Ljunggren, H. G., Piontek, G. & Kiessling, R. Selective rejection of H-2-deficient lymphoma variants suggests alternative immune defence strategy. *Nature* **319**, 675-678, doi:10.1038/319675a0 (1986).

26 Smyth, M. J. *et al.* Activation of NK cell cytotoxicity. *Molecular immunology* **42**, 501-510, doi:10.1016/j.molimm.2004.07.034 (2005).

27 Bonilla, F. A. & Oettgen, H. C. Adaptive immunity. *The Journal of allergy and clinical immunology* **125**, S33-40, doi:10.1016/j.jaci.2009.09.017 (2010).

28 Sprent, J. T and B memory cells. *Cell* **76**, 315-322 (1994).

29 Blom, B. & Spits, H. Development of human lymphoid cells. *Annu Rev Immunol* **24**, 287-320, doi:10.1146/annurev.immunol.24.021605.090612 (2006).

30 van der Merwe, P. A. & Dushek, O. Mechanisms for T cell receptor triggering. *Nature reviews. Immunology* **11**, 47-55, doi:10.1038/nri2887 (2011).

31 Weiss, A. & Littman, D. R. Signal transduction by lymphocyte antigen receptors. *Cell* **76**, 263-274 (1994).

32 Wagner, D. H., Jr. Re-shaping the T cell repertoire: TCR editing and TCR revision for good and for bad. *Clinical immunology* **123**, 1-6, doi:10.1016/j.clim.2006.08.006 (2007).

33 Attaf, M., Legut, M., Cole, D. K. & Sewell, A. K. The T cell antigen receptor: the Swiss army knife of the immune system. *Clin Exp Immunol* **181**, 1-18, doi:10.1111/cei.12622 (2015).

34 Starr, T. K., Jameson, S. C. & Hogquist, K. A. Positive and negative selection of T cells. *Annu Rev Immunol* **21**, 139-176, doi:10.1146/annurev.immunol.21.120601.141107 (2003).

35 Sebzda, E. *et al.* Selection of the T cell repertoire. *Annu Rev Immunol* **17**, 829-874, doi:10.1146/annurev.immunol.17.1.829 (1999).

36 Malissen, B. & Bongrand, P. Early T cell activation: integrating biochemical, structural, and biophysical cues. *Annu Rev Immunol* **33**, 539-561, doi:10.1146/annurev-immunol-032414-112158 (2015).

37 Rossjohn, J. *et al.* T cell antigen receptor recognition of antigen-presenting molecules. *Annu Rev Immunol* **33**, 169-200, doi:10.1146/annurev-immunol-032414-112334 (2015).

38 Clambey, E. T., Davenport, B., Kappler, J. W., Marrack, P. & Homann, D. Molecules in medicine mini review: the alphabeta T cell receptor. *J Mol Med (Berl)* **92**, 735-741, doi:10.1007/s00109-014-1145-2 (2014).

39 Sanchez-Paulete, A. R. *et al.* Deciphering CD137 (4-1BB) signaling in T-cell costimulation for translation into successful cancer immunotherapy. *Eur J Immunol* **46**, 513-522, doi:10.1002/eji.201445388 (2016).

40 Willoughby, J., Griffiths, J., Tews, I. & Cragg, M. S. OX40: Structure and function - What questions remain? *Molecular immunology* **83**, 13-22, doi:10.1016/j.molimm.2017.01.006 (2017).

41 Chen, L. & Flies, D. B. Molecular mechanisms of T cell co-stimulation and co-inhibition. *Nature reviews. Immunology* **13**, 227-242, doi:10.1038/nri3405 (2013).

42 Zhu, J., Yamane, H. & Paul, W. E. Differentiation of effector CD4 T cell populations (*). *Annu Rev Immunol* **28**, 445-489, doi:10.1146/annurev-immunol-030409-101212 (2010).

43 Yamane, H. & Paul, W. E. Early signaling events that underlie fate decisions of naive CD4(+) T cells toward distinct T-helper cell subsets. *Immunological reviews* **252**, 12-23, doi:10.1111/imr.12032 (2013).

44 Kosten, I. J. & Rustemeyer, T. Generation, subsets and functions of inducible regulatory T cells. *Antiinflamm Antiallergy Agents Med Chem* **13**, 139-153 (2015).

45 Mittrucker, H. W., Visekruna, A. & Huber, M. Heterogeneity in the differentiation and function of CD8(+) T cells. *Arch Immunol Ther Exp (Warsz)* **62**, 449-458, doi:10.1007/s00005-014-0293-y (2014).

46 Chang, J. T., Wherry, E. J. & Goldrath, A. W. Molecular regulation of effector and memory T cell differentiation. *Nat Immunol* **15**, 1104-1115, doi:10.1038/ni.3031 (2014).

47 Pieper, K., Grimbacher, B. & Eibel, H. B-cell biology and development. *The Journal of allergy and clinical immunology* **131**, 959-971, doi:10.1016/j.jaci.2013.01.046 (2013).

48 Treanor, B. B-cell receptor: from resting state to activate. *Immunology* **136**, 21-27, doi:10.1111/j.1365-2567.2012.03564.x (2012).

49 Dal Porto, J. M. *et al.* B cell antigen receptor signaling 101. *Molecular immunology* **41**, 599-613, doi:10.1016/j.molimm.2004.04.008 (2004).

50 Ghia, P., ten Boekel, E., Rolink, A. G. & Melchers, F. B-cell development: a comparison between mouse and man. *Immunology today* **19**, 480-485 (1998).

51 Jung, D., Giallourakis, C., Mostoslavsky, R. & Alt, F. W. Mechanism and control of V(D)J recombination at the immunoglobulin heavy chain locus. *Annu Rev Immunol* **24**, 541-570, doi:10.1146/annurev.immunol.23.021704.115830 (2006).

52 Bassing, C. H., Swat, W. & Alt, F. W. The mechanism and regulation of chromosomal V(D)J recombination. *Cell* **109 Suppl**, S45-55 (2002).

53 Combriato, G. & Klobeck, H. G. V lambda and J lambda-C lambda gene segments of the human immunoglobulin lambda light chain locus are separated by 14 kb and rearrange by a deletion mechanism. *Eur J Immunol* **21**, 1513-1522, doi:10.1002/eji.1830210627 (1991).

54 Liu, Y. J., Zhang, J., Lane, P. J., Chan, E. Y. & MacLennan, I. C. Sites of specific B cell activation in primary and secondary responses to T cell-dependent and T cell-independent antigens. *Eur J Immunol* **21**, 2951-2962, doi:10.1002/eji.1830211209 (1991).

55 Eibel, H., Kraus, H., Sic, H., Kienzler, A. K. & Rizzi, M. B cell biology: an overview. *Curr Allergy Asthma Rep* **14**, 434, doi:10.1007/s11882-014-0434-8 (2014).

56 Muramatsu, M. *et al.* Class switch recombination and hypermutation require activation-induced cytidine deaminase (AID), a potential RNA editing enzyme. *Cell* **102**, 553-563 (2000).

57 Chan, T. D. & Brink, R. Affinity-based selection and the germinal center response. *Immunological reviews* **247**, 11-23, doi:10.1111/j.1600-065X.2012.01118.x (2012).

58 Vinuesa, C. G., Linterman, M. A., Goodnow, C. C. & Randall, K. L. T cells and follicular dendritic cells in germinal center B-cell formation and selection. *Immunological reviews* **237**, 72-89, doi:10.1111/j.1600-065X.2010.00937.x (2010).

59 Manz, R. A. *et al.* Humoral immunity and long-lived plasma cells. *Current opinion in immunology* **14**, 517-521 (2002).

60 Gatto, D. & Brink, R. The germinal center reaction. *The Journal of allergy and clinical immunology* **126**, 898-907; quiz 908-899, doi:10.1016/j.jaci.2010.09.007 (2010).

61 Bayles, I. & Milcarek, C. Plasma cell formation, secretion, and persistence: the short and the long of it. *Crit Rev Immunol* **34**, 481-499 (2014).

62 Kurosaki, T., Kometani, K. & Ise, W. Memory B cells. *Nature reviews. Immunology* **15**, 149-159, doi:10.1038/nri3802 (2015).

63 Stavnezer, J., Guikema, J. E. & Schrader, C. E. Mechanism and regulation of class switch recombination. *Annu Rev Immunol* **26**, 261-292, doi:10.1146/annurev.immunol.26.021607.090248 (2008).

64 Irani, V. *et al.* Molecular properties of human IgG subclasses and their implications for designing therapeutic monoclonal antibodies against infectious diseases. *Molecular immunology* **67**, 171-182, doi:10.1016/j.molimm.2015.03.255 (2015).

65 Szmuness, W. *et al.* Hepatitis B vaccine: demonstration of efficacy in a controlled clinical trial in a high-risk population in the United States. *The New England journal of medicine* **303**, 833-841, doi:10.1056/NEJM198010093031501 (1980).

66 Dart, R. C. & McNally, J. Efficacy, safety, and use of snake antivenoms in the United States. *Annals of emergency medicine* **37**, 181-188, doi:10.1067/mem.2001.113372 (2001).

67 Mok, C. C. Rituximab for the treatment of rheumatoid arthritis: an update. *Drug design, development and therapy* **8**, 87-100, doi:10.2147/DDDT.S41645 (2014).

68 Walsh, G. Biopharmaceutical benchmarks 2014. *Nature biotechnology* **32**, 992-1000, doi:10.1038/nbt.3040 (2014).

69 Urquhart, L. Market watch: Top drugs and companies by sales in 2017. *Nat Rev Drug Discov* **17**, 232, doi:10.1038/nrd.2018.42 (2018).

70 Reichert, J. M. *Therapeutic monoconal antibodies approved or in review in the EU or the USA*, <https://www.antibodysociety.org/news/approved-antibodies/> (2018).

71 Ecker, D. M., Jones, S. D. & Levine, H. L. The therapeutic monoclonal antibody market. *mAbs* **7**, 9-14, doi:10.4161/19420862.2015.989042 (2015).

72 Kohler, G. & Milstein, C. Continuous cultures of fused cells secreting antibody of predefined specificity. *Nature* **256**, 495-497 (1975).

73 Barnstable, C. J. *et al.* Production of monoclonal antibodies to group A erythrocytes, HLA and other human cell surface antigens-new tools for genetic analysis. *Cell* **14**, 9-20 (1978).

74 Vidarsson, G., Dekkers, G. & Rispens, T. IgG subclasses and allotypes: from structure to effector functions. *Frontiers in immunology* **5**, 520, doi:10.3389/fimmu.2014.00520 (2014).

75 Porter, R. R. The hydrolysis of rabbit y-globulin and antibodies with crystalline papain. *Biochem J* **73**, 119-126 (1959).

76 Madsen, L. H. & Rodkey, L. S. A method for preparing IgG F(ab')2 fragments using small amounts of serum. *Journal of immunological methods* **9**, 355-361 (1976).

77 Schroeder, H. W., Jr. & Cavacini, L. Structure and function of immunoglobulins. *The Journal of allergy and clinical immunology* **125**, S41-52, doi:10.1016/j.jaci.2009.09.046 (2010).

78 Johansen, F. E., Braathen, R. & Brandtzaeg, P. Role of J chain in secretory immunoglobulin formation. *Scand J Immunol* **52**, 240-248 (2000).

79 Klimovich, V. B. IgM and its receptors: structural and functional aspects. *Biochemistry. Biokhimiia* **76**, 534-549, doi:10.1134/S0006297911050038 (2011).

80 Diebolder, C. A. *et al.* Complement is activated by IgG hexamers assembled at the cell surface. *Science* **343**, 1260-1263, doi:10.1126/science.1248943 (2014).

81 Geisberger, R., Crameri, R. & Achatz, G. Models of signal transduction through the B-cell antigen receptor. *Immunology* **110**, 401-410 (2003).

82 Kerr, M. A. The structure and function of human IgA. *Biochem J* **271**, 285-296 (1990).

83 Mestecky, J., Russell, M. W. & Elson, C. O. Intestinal IgA: novel views on its function in the defence of the largest mucosal surface. *Gut* **44**, 2-5 (1999).

84 Mestecky, J., Schrohenloher, R. E., Kulhavy, R., Wright, G. P. & Tomana, M. Site of J chain attachment to human polymeric IgA. *Proc Natl Acad Sci U S A* **71**, 544-548 (1974).

85 Brandtzaeg, P. & Prydz, H. Direct evidence for an integrated function of J chain and secretory component in epithelial transport of immunoglobulins. *Nature* **311**, 71-73 (1984).

86 van Egmond, M. *et al.* Enhancement of polymorphonuclear cell-mediated tumor cell killing on simultaneous engagement of fcgammaRI (CD64) and fcalphaRI (CD89). *Cancer Res* **61**, 4055-4060 (2001).

87 Weisbart, R. H., Kacena, A., Schuh, A. & Golde, D. W. GM-CSF induces human neutrophil IgA-mediated phagocytosis by an IgA Fc receptor activation mechanism. *Nature* **332**, 647-648, doi:10.1038/332647a0 (1988).

88 Russell, M. W., Reinholdt, J. & Kilian, M. Anti-inflammatory activity of human IgA antibodies and their Fab alpha fragments: inhibition of IgG-mediated complement activation. *Eur J Immunol* **19**, 2243-2249, doi:10.1002/eji.1830191210 (1989).

89 Russell, M. W. & Mansa, B. Complement-fixing properties of human IgA antibodies. Alternative pathway complement activation by plastic-bound, but not specific antigen-bound, IgA. *Scand J Immunol* **30**, 175-183 (1989).

90 Mattu, T. S. *et al.* The glycosylation and structure of human serum IgA1, Fab, and Fc regions and the role of N-glycosylation on Fcalpha receptor interactions. *J Biol Chem* **273**, 2260-2272 (1998).

91 Woof, J. M. & Russell, M. W. Structure and function relationships in IgA. *Mucosal immunology* **4**, 590-597, doi:10.1038/mi.2011.39 (2011).

92 Gould, H. J. *et al.* The biology of IGE and the basis of allergic disease. *Annu Rev Immunol* **21**, 579-628, doi:10.1146/annurev.immunol.21.120601.141103 (2003).

93 McDonnell, J. M. *et al.* The structure of the IgE Cepsilon2 domain and its role in stabilizing the complex with its high-affinity receptor FcepsilonRIalpha. *Nat Struct Biol* **8**, 437-441, doi:10.1038/87603 (2001).

94 Raghavan, M. & Bjorkman, P. J. Fc receptors and their interactions with immunoglobulins. *Annual review of cell and developmental biology* **12**, 181-220, doi:10.1146/annurev.cellbio.12.1.181 (1996).

95 Riesbeck, K. & Nordstrom, T. Structure and immunological action of the human pathogen Moraxella catarrhalis IgD-binding protein. *Crit Rev Immunol* **26**, 353-376 (2006).

96 Reichert, J. M. Marketed therapeutic antibodies compendium. *mAbs* **4**, 413-415, doi:10.4161/mabs.19931 (2012).

97 Pan, Q. & Hammarstrom, L. Molecular basis of IgG subclass deficiency. *Immunological reviews* **178**, 99-110 (2000).

98 Bruhns, P. *et al.* Specificity and affinity of human Fcgamma receptors and their polymorphic variants for human IgG subclasses. *Blood* **113**, 3716-3725, doi:10.1182/blood-2008-09-179754 (2009).

99 Bindon, C. I., Hale, G., Bruggemann, M. & Waldmann, H. Human monoclonal IgG isotypes differ in complement activating function at the level of C4 as well as C1q. *The Journal of experimental medicine* **168**, 127-142 (1988).

100 Siber, G. R., Schur, P. H., Aisenberg, A. C., Weitzman, S. A. & Schiffman, G. Correlation between serum IgG-2 concentrations and the antibody response to bacterial polysaccharide antigens. *The New England journal of medicine* **303**, 178-182, doi:10.1056/NEJM198007243030402 (1980).

101 Aalberse, R. C., van der Gaag, R. & van Leeuwen, J. Serologic aspects of IgG4 antibodies. I. Prolonged immunization results in an IgG4-restricted response. *Journal of immunology* **130**, 722-726 (1983).

102 Roux, K. H., Strelets, L. & Michaelsen, T. E. Flexibility of human IgG subclasses. *Journal of immunology* **159**, 3372-3382 (1997).

103 Dillon, T. M. *et al.* Structural and functional characterization of disulfide isoforms of the human IgG2 subclass. *J Biol Chem* **283**, 16206-16215, doi:10.1074/jbc.M709988200 (2008).

104 White, A. L. *et al.* Conformation of the human immunoglobulin G2 hinge imparts superagonistic properties to immunostimulatory anticancer antibodies. *Cancer Cell* **27**, 138-148, doi:10.1016/j.ccell.2014.11.001 (2015).

105 Bloom, J. W., Madanat, M. S., Marriott, D., Wong, T. & Chan, S. Y. Intrachain disulfide bond in the core hinge region of human IgG4. *Protein Sci* **6**, 407-415, doi:10.1002/pro.5560060217 (1997).

106 Aalberse, R. C., Stapel, S. O., Schuurman, J. & Rispens, T. Immunoglobulin G4: an odd antibody. *Clin Exp Allergy* **39**, 469-477, doi:10.1111/j.1365-2222.2009.03207.x (2009).

107 van der Neut Kolfschoten, M. *et al.* Anti-inflammatory activity of human IgG4 antibodies by dynamic Fab arm exchange. *Science* **317**, 1554-1557, doi:10.1126/science.1144603 (2007).

108 Morell, A., Terry, W. D. & Waldmann, T. A. Metabolic properties of IgG subclasses in man. *J Clin Invest* **49**, 673-680, doi:10.1172/JCI106279 (1970).

109 Wang, Y., Tian, Z., Thirumalai, D. & Zhang, X. Neonatal Fc receptor (FcRn): a novel target for therapeutic antibodies and antibody engineering. *J Drug Target* **22**, 269-278, doi:10.3109/1061186X.2013.875030 (2014).

110 Arnold, J. N., Wormald, M. R., Sim, R. B., Rudd, P. M. & Dwek, R. A. The impact of glycosylation on the biological function and structure of human immunoglobulins. *Annu Rev Immunol* **25**, 21-50, doi:10.1146/annurev.immunol.25.022106.141702 (2007).

111 van de Bovenkamp, F. S., Hafkenscheid, L., Rispens, T. & Rombouts, Y. The Emerging Importance of IgG Fab Glycosylation in Immunity. *Journal of immunology* **196**, 1435-1441, doi:10.4049/jimmunol.1502136 (2016).

112 Ravetch, J. V. & Bolland, S. IgG Fc receptors. *Annu Rev Immunol* **19**, 275-290, doi:10.1146/annurev.immunol.19.1.275 (2001).

113 Muta, T. *et al.* A 13-amino-acid motif in the cytoplasmic domain of Fc gamma RIIB modulates B-cell receptor signalling. *Nature* **368**, 70-73, doi:10.1038/368070a0 (1994).

114 Unkeless, J. C., Shen, Z., Lin, C. W. & DeBeus, E. Function of human Fc gamma RIIA and Fc gamma RIIIB. *Seminars in immunology* **7**, 37-44 (1995).

115 Allen, J. M. & Seed, B. Isolation and expression of functional high-affinity Fc receptor complementary DNAs. *Science* **243**, 378-381 (1989).

116 Van den Herik-Oudijk, I. E., Capel, P. J., van der Bruggen, T. & Van de Winkel, J. G. Identification of signaling motifs within human Fc gamma RIIa and Fc gamma RIIb isoforms. *Blood* **85**, 2202-2211 (1995).

117 van Vugt, M. J. *et al.* FcR gamma-chain is essential for both surface expression and function of human Fc gamma RI (CD64) in vivo. *Blood* **87**, 3593-3599 (1996).

118 Wirthmueller, U., Kurosaki, T., Murakami, M. S. & Ravetch, J. V. Signal transduction by Fc gamma RIII (CD16) is mediated through the gamma chain. *The Journal of experimental medicine* **175**, 1381-1390 (1992).

119 Metes, D. *et al.* Expression of functional CD32 molecules on human NK cells is determined by an allelic polymorphism of the FcgammaRIIC gene. *Blood* **91**, 2369-2380 (1998).

120 Hargreaves, C. E. *et al.* Fcgamma receptors: genetic variation, function, and disease. *Immunological reviews* **268**, 6-24, doi:10.1111/imr.12341 (2015).

121 Ravetch, J. V. & Kinet, J. P. Fc receptors. *Annu Rev Immunol* **9**, 457-492, doi:10.1146/annurev.iy.09.040191.002325 (1991).

122 Simister, N. E. & Rees, A. R. Isolation and characterization of an Fc receptor from neonatal rat small intestine. *Eur J Immunol* **15**, 733-738, doi:10.1002/eji.1830150718 (1985).

123 Firan, M. *et al.* The MHC class I-related receptor, FcRn, plays an essential role in the maternofetal transfer of gamma-globulin in humans. *International immunology* **13**, 993-1002 (2001).

124 Jones, E. A. & Waldmann, T. A. The mechanism of intestinal uptake and transcellular transport of IgG in the neonatal rat. *J Clin Invest* **51**, 2916-2927, doi:10.1172/JCI107116 (1972).

125 Simister, N. E. & Mostov, K. E. An Fc receptor structurally related to MHC class I antigens. *Nature* **337**, 184-187, doi:10.1038/337184a0 (1989).

126 Stapleton, N. M., Einarsdottir, H. K., Stemerding, A. M. & Vidarsson, G. The multiple facets of FcRn in immunity. *Immunological reviews* **268**, 253-268, doi:10.1111/imr.12331 (2015).

127 Kim, J. K. *et al.* Mapping the site on human IgG for binding of the MHC class I-related receptor, FcRn. *Eur J Immunol* **29**, 2819-2825, doi:10.1002/(SICI)1521-4141(199909)29:09<2819::AID-IMMU2819>3.0.CO;2-6 (1999).

128 Lencer, W. I. & Blumberg, R. S. A passionate kiss, then run: exocytosis and recycling of IgG by FcRn. *Trends Cell Biol* **15**, 5-9, doi:10.1016/j.tcb.2004.11.004 (2005).

129 Challa, D. K., Velmurugan, R., Ober, R. J. & Sally Ward, E. FcRn: from molecular interactions to regulation of IgG pharmacokinetics and functions. *Curr Top Microbiol Immunol* **382**, 249-272, doi:10.1007/978-3-319-07911-0_12 (2014).

130 Roopenian, D. C. & Akilesh, S. FcRn: the neonatal Fc receptor comes of age. *Nature reviews. Immunology* **7**, 715-725, doi:10.1038/nri2155 (2007).

131 Israel, E. J., Wilsker, D. F., Hayes, K. C., Schoenfeld, D. & Simister, N. E. Increased clearance of IgG in mice that lack beta 2-microglobulin: possible protective role of FcRn. *Immunology* **89**, 573-578 (1996).

132 Anderson, C. L. *et al.* Perspective-- FcRn transports albumin: relevance to immunology and medicine. *Trends Immunol* **27**, 343-348, doi:10.1016/j.it.2006.05.004 (2006).

133 Pincetic, A. *et al.* Type I and type II Fc receptors regulate innate and adaptive immunity. *Nat Immunol* **15**, 707-716, doi:10.1038/ni.2939 (2014).

134 Nimmerjahn, F. & Ravetch, J. V. Fcgamma receptors as regulators of immune responses. *Nature reviews. Immunology* **8**, 34-47, doi:10.1038/nri2206 (2008).

135 Stout, R. D. & Herzenberg, L. A. The Fc receptor on thymus-derived lymphocytes. I. Detection of a subpopulation of murine T lymphocytes bearing the Fc receptor. *The Journal of experimental medicine* **142**, 611-621 (1975).

136 Meknache, N., Jonsson, F., Laurent, J., Guinnepain, M. T. & Daeron, M. Human basophils express the glycosylphosphatidylinositol-anchored low-affinity IgG receptor FcgammaRIIIB (CD16B). *Journal of immunology* **182**, 2542-2550, doi:10.4049/jimmunol.0801665 (2009).

137 Ganesan, L. P. *et al.* FcgammaRIIb on liver sinusoidal endothelium clears small immune complexes. *Journal of immunology* **189**, 4981-4988, doi:10.4049/jimmunol.1202017 (2012).

138 Bruhns, P. Properties of mouse and human IgG receptors and their contribution to disease models. *Blood* **119**, 5640-5649, doi:10.1182/blood-2012-01-380121 (2012).

139 Nimmerjahn, F., Bruhns, P., Horiuchi, K. & Ravetch, J. V. FcgammaRIV: a novel FcR with distinct IgG subclass specificity. *Immunity* **23**, 41-51, doi:10.1016/j.immuni.2005.05.010 (2005).

140 Nimmerjahn, F. & Ravetch, J. V. Divergent immunoglobulin g subclass activity through selective Fc receptor binding. *Science* **310**, 1510-1512, doi:10.1126/science.1118948 (2005).

141 White, A. L. *et al.* FcgammaRIotaIotaB controls the potency of agonistic anti-TNFR mAbs. *Cancer Immunol Immunother* **62**, 941-948, doi:10.1007/s00262-013-1398-6 (2013).

142 White, A. L. *et al.* Interaction with FcgammaRIIB is critical for the agonistic activity of anti-CD40 monoclonal antibody. *Journal of immunology* **187**, 1754-1763, doi:10.4049/jimmunol.1101135 (2011).

143 Nimmerjahn, F. & Ravetch, J. V. Fcgamma receptors: old friends and new family members. *Immunity* **24**, 19-28, doi:10.1016/j.immuni.2005.11.010 (2006).

144 Li, X. *et al.* Allelic-dependent expression of an activating Fc receptor on B cells enhances humoral immune responses. *Science translational medicine* **5**, 216ra175, doi:10.1126/scitranslmed.3007097 (2013).

145 Lu, J., Ellsworth, J. L., Hamacher, N., Oak, S. W. & Sun, P. D. Crystal structure of Fcgamma receptor I and its implication in high affinity gamma-immunoglobulin binding. *J Biol Chem* **286**, 40608-40613, doi:10.1074/jbc.M111.257550 (2011).

146 Kiyoshi, M. *et al.* Structural basis for binding of human IgG1 to its high-affinity human receptor FcgammaRI. *Nature communications* **6**, 6866, doi:10.1038/ncomms7866 (2015).

147 Clark, M. R., Clarkson, S. B., Ory, P. A., Stollman, N. & Goldstein, I. M. Molecular basis for a polymorphism involving Fc receptor II on human monocytes. *Journal of immunology* **143**, 1731-1734 (1989).

148 Warmerdam, P. A., van de Winkel, J. G., Vlug, A., Westerdaal, N. A. & Capel, P. J. A single amino acid in the second Ig-like domain of the human Fc gamma receptor II is critical for human IgG2 binding. *Journal of immunology* **147**, 1338-1343 (1991).

149 Wu, J. *et al.* A novel polymorphism of FcgammaRIIIa (CD16) alters receptor function and predisposes to autoimmune disease. *J Clin Invest* **100**, 1059-1070, doi:10.1172/JCI119616 (1997).

150 Cartron, G. *et al.* Therapeutic activity of humanized anti-CD20 monoclonal antibody and polymorphism in IgG Fc receptor FcgammaRIIIa gene. *Blood* **99**, 754-758 (2002).

151 Weng, W. K. & Levy, R. Two immunoglobulin G fragment C receptor polymorphisms independently predict response to rituximab in patients with follicular lymphoma. *J Clin Oncol* **21**, 3940-3947, doi:10.1200/JCO.2003.05.013 (2003).

152 Weng, W. K., Czerwinski, D., Timmerman, J., Hsu, F. J. & Levy, R. Clinical outcome of lymphoma patients after idiotype vaccination is correlated with humoral immune response and immunoglobulin G Fc receptor genotype. *J Clin Oncol* **22**, 4717-4724, doi:10.1200/JCO.2004.06.003 (2004).

153 Mellor, J. D., Brown, M. P., Irving, H. R., Zalcberg, J. R. & Dobrovic, A. A critical review of the role of Fc gamma receptor polymorphisms in the response to monoclonal antibodies in cancer. *J Hematol Oncol* **6**, 1, doi:10.1186/1756-8722-6-1 (2013).

154 Li, X., Gibson, A. W. & Kimberly, R. P. Human FcR polymorphism and disease. *Curr Top Microbiol Immunol* **382**, 275-302, doi:10.1007/978-3-319-07911-0_13 (2014).

155 Li, X. *et al.* A novel polymorphism in the Fcgamma receptor IIB (CD32B) transmembrane region alters receptor signaling. *Arthritis and rheumatism* **48**, 3242-3252, doi:10.1002/art.11313 (2003).

156 Kobayashi, T. *et al.* Relevance of IgG receptor IIIb (CD16) polymorphism to handling of Porphyromonas gingivalis: implications for the pathogenesis of adult periodontitis. *J Periodontal Res* **35**, 65-73 (2000).

157 Breunis, W. B. *et al.* Copy number variation at the FCGR locus includes FCGR3A, FCGR2C and FCGR3B but not FCGR2A and FCGR2B. *Human mutation* **30**, E640-650, doi:10.1002/humu.20997 (2009).

158 Aitman, T. J. *et al.* Copy number polymorphism in Fcgr3 predisposes to glomerulonephritis in rats and humans. *Nature* **439**, 851-855, doi:10.1038/nature04489 (2006).

159 Vigeral, P. *et al.* Prophylactic use of OKT3 monoclonal antibody in cadaver kidney recipients. Utilization of OKT3 as the sole immunosuppressive agent. *Transplantation* **41**, 730-733 (1986).

160 Todd, P. A. & Brogden, R. N. Muromonab CD3. A review of its pharmacology and therapeutic potential. *Drugs* **37**, 871-899 (1989).

161 Hill, P., Cross, N. B., Barnett, A. N., Palmer, S. C. & Webster, A. C. Polyclonal and monoclonal antibodies for induction therapy in kidney transplant recipients. *Cochrane Database Syst Rev* **1**, CD004759, doi:10.1002/14651858.CD004759.pub2 (2017).

162 WHO. *WHO Model List of Essential Medicines*, <http://apps.who.int/iris/bitstream/handle/10665/273826/EML-20-eng.pdf?ua=1> (2017).

163 Weiner, G. J. Building better monoclonal antibody-based therapeutics. *Nat Rev Cancer* **15**, 361-370, doi:10.1038/nrc3930 (2015).

164 Lee, C. S., Cragg, M., Glennie, M. & Johnson, P. Novel antibodies targeting immune regulatory checkpoints for cancer therapy. *Br J Clin Pharmacol* **76**, 233-247, doi:10.1111/bcp.12164 (2013).

165 Suzuki, S., Ishida, T., Yoshikawa, K. & Ueda, R. Current status of immunotherapy. *Jpn J Clin Oncol* **46**, 191-203, doi:10.1093/jjco/hyv201 (2016).

166 Robert, C. *et al.* Ipilimumab plus dacarbazine for previously untreated metastatic melanoma. *The New England journal of medicine* **364**, 2517-2526, doi:10.1056/NEJMoa1104621 (2011).

167 Cameron, F., Whiteside, G. & Perry, C. Ipilimumab: first global approval. *Drugs* **71**, 1093-1104, doi:10.2165/11594010-000000000-00000 (2011).

168 Sharma, P., Hu-Lieskovan, S., Wargo, J. A. & Ribas, A. Primary, Adaptive, and Acquired Resistance to Cancer Immunotherapy. *Cell* **168**, 707-723, doi:10.1016/j.cell.2017.01.017 (2017).

169 Slamon, D. J. *et al.* Use of chemotherapy plus a monoclonal antibody against HER2 for metastatic breast cancer that overexpresses HER2. *The New England journal of medicine* **344**, 783-792, doi:10.1056/NEJM200103153441101 (2001).

170 Cunningham, D. *et al.* Cetuximab monotherapy and cetuximab plus irinotecan in irinotecan-refractory metastatic colorectal cancer. *The New England journal of medicine* **351**, 337-345, doi:10.1056/NEJMoa033025 (2004).

171 Takeda, K., Stagg, J., Yagita, H., Okumura, K. & Smyth, M. J. Targeting death-inducing receptors in cancer therapy. *Oncogene* **26**, 3745-3757, doi:10.1038/sj.onc.1210374 (2007).

172 Johnstone, R. W., Frew, A. J. & Smyth, M. J. The TRAIL apoptotic pathway in cancer onset, progression and therapy. *Nat Rev Cancer* **8**, 782-798, doi:10.1038/nrc2465 (2008).

173 Pardoll, D. M. The blockade of immune checkpoints in cancer immunotherapy. *Nat Rev Cancer* **12**, 252-264, doi:10.1038/nrc3239 (2012).

174 Poole, R. M. Pembrolizumab: first global approval. *Drugs* **74**, 1973-1981, doi:10.1007/s40265-014-0314-5 (2014).

175 Colomb, M. G., Arlaud, G. J. & Villiers, C. L. Activation of C1. *Philos Trans R Soc Lond B Biol Sci* **306**, 283-292 (1984).

176 Kishore, U. & Reid, K. B. C1q: structure, function, and receptors. *Immunopharmacology* **49**, 159-170 (2000).

177 van Schaarenburg, R. A. *et al.* The production and secretion of complement component C1q by human mast cells. *Molecular immunology* **78**, 164-170, doi:10.1016/j.molimm.2016.09.001 (2016).

178 Sellar, G. C., Blake, D. J. & Reid, K. B. Characterization and organization of the genes encoding the A-, B- and C-chains of human complement subcomponent C1q. The complete derived amino acid sequence of human C1q. *Biochem J* **274 (Pt 2)**, 481-490 (1991).

179 Ghai, R. *et al.* C1q and its growing family. *Immunobiology* **212**, 253-266, doi:10.1016/j.imbio.2006.11.001 (2007).

180 Reid, K. B. & Porter, R. R. Subunit composition and structure of subcomponent C1q of the first component of human complement. *Biochem J* **155**, 19-23 (1976).

181 Lu, J., Wiedemann, H., Timpl, R. & Reid, K. B. Similarity in structure between C1q and the collectins as judged by electron microscopy. *Behring Inst Mitt*, 6-16 (1993).

182 Tacnet-Delorme, P., Chevallier, S. & Arlaud, G. J. Beta-amyloid fibrils activate the C1 complex of complement under physiological conditions: evidence for a binding site for A beta on the C1q globular regions. *Journal of immunology* **167**, 6374-6381 (2001).

183 Korb, L. C. & Ahearn, J. M. C1q binds directly and specifically to surface blebs of apoptotic human keratinocytes: complement deficiency and systemic lupus erythematosus revisited. *Journal of immunology* **158**, 4525-4528 (1997).

184 Alberti, S. *et al.* Interaction between complement subcomponent C1q and the Klebsiella pneumoniae porin OmpK36. *Infect Immun* **64**, 4719-4725 (1996).

185 Bredt, W., Wellek, B., Brunner, H. & Loos, M. Interactions between mycoplasma pneumoniae and the first components of complement. *Infect Immun* **15**, 7-12 (1977).

186 Santoro, F., Ouaissi, M. A., Pestel, J. & Capron, A. Interaction between Schistosoma mansoni and the complement system: binding of C1q to schistosomula. *Journal of immunology* **124**, 2886-2891 (1980).

187 Paidassi, H. *et al.* C1q binds phosphatidylserine and likely acts as a multiligand-bridging molecule in apoptotic cell recognition. *Journal of immunology* **180**, 2329-2338 (2008).

188 Paidassi, H. *et al.* The lectin-like activity of human C1q and its implication in DNA and apoptotic cell recognition. *FEBS Lett* **582**, 3111-3116, doi:10.1016/j.febslet.2008.08.001 (2008).

189 Son, M., Diamond, B. & Santiago-Schwarz, F. Fundamental role of C1q in autoimmunity and inflammation. *Immunologic research* **63**, 101-106, doi:10.1007/s12026-015-8705-6 (2015).

190 Thielens, N. M., Tedesco, F., Bohlson, S. S., Gaboriaud, C. & Tenner, A. J. C1q: A fresh look upon an old molecule. *Molecular immunology* **89**, 73-83, doi:10.1016/j.molimm.2017.05.025 (2017).

191 Ogden, C. A. *et al.* C1q and mannose binding lectin engagement of cell surface calreticulin and CD91 initiates macropinocytosis and uptake of apoptotic cells. *The Journal of experimental medicine* **194**, 781-795 (2001).

192 Galvan, M. D., Greenlee-Wacker, M. C. & Bohlson, S. S. C1q and phagocytosis: the perfect complement to a good meal. *J Leukoc Biol* **92**, 489-497, doi:10.1189/jlb.0212099 (2012).

193 Walport, M. J., Davies, K. A. & Botto, M. C1q and systemic lupus erythematosus. *Immunobiology* **199**, 265-285, doi:10.1016/S0171-2985(98)80032-6 (1998).

194 Botto, M. *et al.* Homozygous C1q deficiency causes glomerulonephritis associated with multiple apoptotic bodies. *Nat Genet* **19**, 56-59, doi:10.1038/ng0598-56 (1998).

195 Leffler, J., Bengtsson, A. A. & Blom, A. M. The complement system in systemic lupus erythematosus: an update. *Annals of the rheumatic diseases* **73**, 1601-1606, doi:10.1136/annrheumdis-2014-205287 (2014).

196 Idusogie, E. E. *et al.* Mapping of the C1q binding site on rituxan, a chimeric antibody with a human IgG1 Fc. *Journal of immunology* **164**, 4178-4184 (2000).

197 Burton, D. R. *et al.* The Clq receptor site on immunoglobulin G. *Nature* **288**, 338-344 (1980).

198 Marques, G. *et al.* Arginine residues of the globular regions of human C1q involved in the interaction with immunoglobulin G. *J Biol Chem* **268**, 10393-10402 (1993).

199 Roumenina, L. T. *et al.* Interaction of C1q with IgG1, C-reactive protein and pentraxin 3: mutational studies using recombinant globular head modules of human C1q A, B, and C chains. *Biochemistry* **45**, 4093-4104, doi:10.1021/bi052646f (2006).

200 Kojouharova, M. S. *et al.* Mutational analyses of the recombinant globular regions of human C1q A, B, and C chains suggest an essential role for arginine and histidine residues in the C1q-IgG interaction. *Journal of immunology* **172**, 4351-4358 (2004).

201 Gaboriaud, C. *et al.* The crystal structure of the globular head of complement protein C1q provides a basis for its versatile recognition properties. *J Biol Chem* **278**, 46974-46982, doi:10.1074/jbc.M307764200 (2003).

202 Schneider, S. & Zacharias, M. Atomic resolution model of the antibody Fc interaction with the complement C1q component. *Molecular immunology* **51**, 66-72, doi:10.1016/j.molimm.2012.02.111 (2012).

203 Roumenina, L. T. *et al.* Role of Ca2+ in the electrostatic stability and the functional activity of the globular domain of human C1q. *Biochemistry* **44**, 14097-14109, doi:10.1021/bi051186n (2005).

204 Zlatarova, A. S. *et al.* Existence of different but overlapping IgG- and IgM-binding sites on the globular domain of human C1q. *Biochemistry* **45**, 9979-9988, doi:10.1021/bi060539v (2006).

205 Gadjeva, M. G. *et al.* Interaction of human C1q with IgG and IgM: revisited. *Biochemistry* **47**, 13093-13102, doi:10.1021/bi801131h (2008).

206 Sledge, C. R. & Bing, D. H. Binding properties of the human complement protein Clq. *J Biol Chem* **248**, 2818-2823 (1973).

207 Hughes-Jones, N. C. & Gardner, B. The reaction between the complement subcomponent C1q, IgG complexes and polyionic molecules. *Immunology* **34**, 459-463 (1978).

208 Czajkowsky, D. M. & Shao, Z. The human IgM pentamer is a mushroom-shaped molecule with a flexural bias. *Proc Natl Acad Sci U S A* **106**, 14960-14965, doi:10.1073/pnas.0903805106 (2009).

209 Bokisch, V. A., Muller-Eberhard, H. J. & Cochrane, C. G. Isolation of a fragment (C3a) of the third component of human complement containing anaphylatoxin and chemotactic activity and description of an anaphylatoxin inactivator of human serum. *The Journal of experimental medicine* **129**, 1109-1130 (1969).

210 Ehlenberger, A. G. & Nussenzweig, V. The role of membrane receptors for C3b and C3d in phagocytosis. *The Journal of experimental medicine* **145**, 357-371 (1977).

211 Arlaud, G. J. *et al.* Structural biology of the C1 complex of complement unveils the mechanisms of its activation and proteolytic activity. *Molecular immunology* **39**, 383-394 (2002).

212 Law, S. K. The covalent binding reaction of C3 and C4. *Annals of the New York Academy of Sciences* **421**, 246-258 (1983).

213 Nagasawa, S. & Stroud, R. M. Cleavage of C2 by C1s into the antigenically distinct fragments C2a and C2b: demonstration of binding of C2b to C4b. *Proc Natl Acad Sci U S A* **74**, 2998-3001 (1977).

214 Ricklin, D., Hajishengallis, G., Yang, K. & Lambris, J. D. Complement: a key system for immune surveillance and homeostasis. *Nat Immunol* **11**, 785-797, doi:10.1038/ni.1923 (2010).

215 Klos, A. *et al.* The role of the anaphylatoxins in health and disease. *Molecular immunology* **46**, 2753-2766, doi:10.1016/j.molimm.2009.04.027 (2009).

216 Merle, N. S., Noe, R., Halbwachs-Mecarelli, L., Fremeaux-Bacchi, V. & Roumenina, L. T. Complement System Part II: Role in Immunity. *Frontiers in immunology* **6**, 257, doi:10.3389/fimmu.2015.00257 (2015).

217 Kim, Y. U. *et al.* Covalent binding of C3b to C4b within the classical complement pathway C5 convertase. Determination of amino acid residues involved in ester linkage formation. *J Biol Chem* **267**, 4171-4176 (1992).

218 Vogt, W., Schmidt, G., Von Buttlar, B. & Dieminger, L. A new function of the activated third component of complement: binding to C5, an essential step for C5 activation. *Immunology* **34**, 29-40 (1978).

219 Guo, R. F. & Ward, P. A. Role of C5a in inflammatory responses. *Annu Rev Immunol* **23**, 821-852, doi:10.1146/annurev.immunol.23.021704.115835 (2005).

220 Cooper, N. R. & Muller-Eberhard, H. J. The reaction mechanism of human C5 in immune hemolysis. *The Journal of experimental medicine* **132**, 775-793 (1970).

221 Podack, E. R., Tschoop, J. & Muller-Eberhard, H. J. Molecular organization of C9 within the membrane attack complex of complement. Induction of circular C9 polymerization by the C5b-8 assembly. *The Journal of experimental medicine* **156**, 268-282 (1982).

222 Tschopp, J. Ultrastructure of the membrane attack complex of complement. Heterogeneity of the complex caused by different degree of C9 polymerization. *J Biol Chem* **259**, 7857-7863 (1984).

223 Garred, P. *et al.* A journey through the lectin pathway of complement-MBL and beyond. *Immunological reviews* **274**, 74-97, doi:10.1111/imr.12468 (2016).

224 Kawasaki, N., Kawasaki, T. & Yamashina, I. A serum lectin (mannan-binding protein) has complement-dependent bactericidal activity. *J Biochem* **106**, 483-489 (1989).

225 Weis, W. I., Drickamer, K. & Hendrickson, W. A. Structure of a C-type mannose-binding protein complexed with an oligosaccharide. *Nature* **360**, 127-134, doi:10.1038/360127a0 (1992).

226 Matsushita, M. & Fujita, T. Activation of the classical complement pathway by mannose-binding protein in association with a novel C1s-like serine protease. *The Journal of experimental medicine* **176**, 1497-1502 (1992).

227 Yongqing, T., Drentin, N., Duncan, R. C., Wijeyewickrema, L. C. & Pike, R. N. Mannose-binding lectin serine proteases and associated proteins of the lectin pathway of complement: two genes, five proteins and many functions? *Biochimica et biophysica acta* **1824**, 253-262, doi:10.1016/j.bbapap.2011.05.021 (2012).

228 Matsushita, M. & Fujita, T. Cleavage of the third component of complement (C3) by mannose-binding protein-associated serine protease (MASP) with subsequent complement activation. *Immunobiology* **194**, 443-448, doi:10.1016/S0171-2985(11)80110-5 (1995).

229 Pangburn, M. K., Schreiber, R. D. & Muller-Eberhard, H. J. Formation of the initial C3 convertase of the alternative complement pathway. Acquisition of C3b-like activities by spontaneous hydrolysis of the putative thioester in native C3. *The Journal of experimental medicine* **154**, 856-867 (1981).

230 Pangburn, M. K. & Muller-Eberhard, H. J. Relation of putative thioester bond in C3 to activation of the alternative pathway and the binding of C3b to biological targets of complement. *The Journal of experimental medicine* **152**, 1102-1114 (1980).

231 Fearon, D. T., Austen, K. F. & Ruddy, S. Formation of a hemolytically active cellular intermediate by the interaction between properdin factors B and D and the activated third component of complement. *The Journal of experimental medicine* **138**, 1305-1313 (1973).

232 Law, S. K. & Dodds, A. W. The internal thioester and the covalent binding properties of the complement proteins C3 and C4. *Protein Sci* **6**, 263-274, doi:10.1002/pro.5560060201 (1997).

233 Kinoshita, T. *et al.* C5 convertase of the alternative complement pathway: covalent linkage between two C3b molecules within the trimolecular complex enzyme. *Journal of immunology* **141**, 3895-3901 (1988).

234 Fletcher, C. M., Harrison, R. A., Lachmann, P. J. & Neuhaus, D. Structure of a soluble, glycosylated form of the human complement regulatory protein CD59. *Structure* **2**, 185-199 (1994).

235 Nicholson-Weller, A. & Wang, C. E. Structure and function of decay accelerating factor CD55. *J Lab Clin Med* **123**, 485-491 (1994).

236 Fujita, T., Inoue, T., Ogawa, K., Iida, K. & Tamura, N. The mechanism of action of decay-accelerating factor (DAF). DAF inhibits the assembly of C3 convertases by dissociating C2a and Bb. *The Journal of experimental medicine* **166**, 1221-1228 (1987).

237 Meri, S. *et al.* Human protectin (CD59), an 18,000-20,000 MW complement lysis restricting factor, inhibits C5b-8 catalysed insertion of C9 into lipid bilayers. *Immunology* **71**, 1-9 (1990).

238 Farkas, I. *et al.* CD59 blocks not only the insertion of C9 into MAC but inhibits ion channel formation by homologous C5b-8 as well as C5b-9. *J Physiol* **539**, 537-545 (2002).

239 Golay, J. *et al.* Biologic response of B lymphoma cells to anti-CD20 monoclonal antibody rituximab in vitro: CD55 and CD59 regulate complement-mediated cell lysis. *Blood* **95**, 3900-3908 (2000).

240 Alderson, K. L. & Sondel, P. M. Clinical cancer therapy by NK cells via antibody-dependent cell-mediated cytotoxicity. *J Biomed Biotechnol* **2011**, 379123, doi:10.1155/2011/379123 (2011).

241 Dall'Ozzo, S. *et al.* Rituximab-dependent cytotoxicity by natural killer cells: influence of FCGR3A polymorphism on the concentration-effect relationship. *Cancer Res* **64**, 4664-4669, doi:10.1158/0008-5472.CAN-03-2862 (2004).

242 Lefebvre, M. L., Krause, S. W., Salcedo, M. & Nardin, A. Ex vivo-activated human macrophages kill chronic lymphocytic leukemia cells in the presence of rituximab: mechanism of antibody-dependent cellular cytotoxicity and impact of human serum. *J Immunother* **29**, 388-397, doi:10.1097/01.cji.0000203081.43235.d7 (2006).

243 van der Kolk, L. E., de Haas, M., Grillo-Lopez, A. J., Baars, J. W. & van Oers, M. H. Analysis of CD20-dependent cellular cytotoxicity by G-CSF-stimulated neutrophils. *Leukemia* **16**, 693-699, doi:10.1038/sj.leu.2402424 (2002).

244 Morel, P. A., Ernst, L. K. & Metes, D. Functional CD32 molecules on human NK cells. *Leukemia & lymphoma* **35**, 47-56, doi:10.3109/10428199909145704 (1999).

245 Wang, A. V., Scholl, P. R. & Geha, R. S. Physical and functional association of the high affinity immunoglobulin G receptor (Fc gamma RI) with the kinases Hck and Lyn. *The Journal of experimental medicine* **180**, 1165-1170 (1994).

246 Ghazizadeh, S., Bolen, J. B. & Fleit, H. B. Tyrosine phosphorylation and association of Syk with Fc gamma RII in monocytic THP-1 cells. *Biochem J* **305 (Pt 2)**, 669-674 (1995).

247 Tridandapani, S. *et al.* The adapter protein LAT enhances fcgamma receptor-mediated signal transduction in myeloid cells. *J Biol Chem* **275**, 20480-20487, doi:10.1074/jbc.M909462199 (2000).

248 Getahun, A. & Cambier, J. C. Of ITIMs, ITAMs, and ITAMis: revisiting immunoglobulin Fc receptor signaling. *Immunological reviews* **268**, 66-73, doi:10.1111/imr.12336 (2015).

249 Trapani, J. A. & Smyth, M. J. Functional significance of the perforin/granzyme cell death pathway. *Nature reviews. Immunology* **2**, 735-747, doi:10.1038/nri911 (2002).

250 Musolino, A. *et al.* Immunoglobulin G fragment C receptor polymorphisms and clinical efficacy of trastuzumab-based therapy in patients with HER-2/neu-positive metastatic breast cancer. *J Clin Oncol* **26**, 1789-1796, doi:10.1200/JCO.2007.14.8957 (2008).

251 Chowdhury, F., Lode, H. N., Cragg, M. S., Glennie, M. J. & Gray, J. C. Development of immunomonitoring of antibodydependent cellular cytotoxicity against neuroblastoma cells using whole blood. *Cancer Immunol Immunother* **63**, 559-569, doi:10.1007/s00262-014-1534-y (2014).

252 Cragg, M. S. & Glennie, M. J. Antibody specificity controls in vivo effector mechanisms of anti-CD20 reagents. *Blood* **103**, 2738-2743, doi:10.1182/blood-2003-06-2031 (2004).

253 Uchida, J. *et al.* The innate mononuclear phagocyte network depletes B lymphocytes through Fc receptor-dependent mechanisms during anti-CD20 antibody immunotherapy. *The Journal of experimental medicine* **199**, 1659-1669, doi:10.1084/jem.20040119 (2004).

254 Gul, N. & van Egmond, M. Antibody-Dependent Phagocytosis of Tumor Cells by Macrophages: A Potent Effector Mechanism of Monoclonal Antibody Therapy of Cancer. *Cancer Res* **75**, 5008-5013, doi:10.1158/0008-5472.CAN-15-1330 (2015).

255 Dale, D. C., Boxer, L. & Liles, W. C. The phagocytes: neutrophils and monocytes. *Blood* **112**, 935-945, doi:10.1182/blood-2007-12-077917 (2008).

256 Nimmerjahn, F., Gordan, S. & Lux, A. FcgammaR dependent mechanisms of cytotoxic, agonistic, and neutralizing antibody activities. *Trends Immunol* **36**, 325-336, doi:10.1016/j.it.2015.04.005 (2015).

257 Jones, D. H., Nusbacher, J. & Anderson, C. L. Fc receptor-mediated binding and endocytosis by human mononuclear phagocytes: monomeric IgG is not endocytosed by U937 cells and monocytes. *J Cell Biol* **100**, 558-564 (1985).

258 Holowka, D., Sil, D., Torigoe, C. & Baird, B. Insights into immunoglobulin E receptor signaling from structurally defined ligands. *Immunological reviews* **217**, 269-279, doi:10.1111/j.1600-065X.2007.00517.x (2007).

259 Flannagan, R. S., Jaumouille, V. & Grinstein, S. The cell biology of phagocytosis. *Annu Rev Pathol* **7**, 61-98, doi:10.1146/annurev-pathol-011811-132445 (2012).

260 Desjardins, M., Huber, L. A., Parton, R. G. & Griffiths, G. Biogenesis of phagolysosomes proceeds through a sequential series of interactions with the endocytic apparatus. *J Cell Biol* **124**, 677-688 (1994).

261 Lukacs, G. L., Rotstein, O. D. & Grinstein, S. Determinants of the phagosomal pH in macrophages. In situ assessment of vacuolar H(+)-ATPase activity, counterion conductance, and H+ "leak". *J Biol Chem* **266**, 24540-24548 (1991).

262 Flannagan, R. S., Cosio, G. & Grinstein, S. Antimicrobial mechanisms of phagocytes and bacterial evasion strategies. *Nat Rev Microbiol* **7**, 355-366, doi:10.1038/nrmicro2128 (2009).

263 Lam, G. Y., Huang, J. & Brumell, J. H. The many roles of NOX2 NADPH oxidase-derived ROS in immunity. *Semin Immunopathol* **32**, 415-430, doi:10.1007/s00281-010-0221-0 (2010).

264 Aktan, F. iNOS-mediated nitric oxide production and its regulation. *Life Sci* **75**, 639-653, doi:10.1016/j.lfs.2003.10.042 (2004).

265 Stashenko, P., Nadler, L. M., Hardy, R. & Schlossman, S. F. Characterization of a human B lymphocyte-specific antigen. *Journal of immunology* **125**, 1678-1685 (1980).

266 Kehrl, J. H., Riva, A., Wilson, G. L. & Thevenin, C. Molecular mechanisms regulating CD19, CD20 and CD22 gene expression. *Immunology today* **15**, 432-436, doi:10.1016/0167-5699(94)90273-9 (1994).

267 Nadler, L. M. *et al.* A unique cell surface antigen identifying lymphoid malignancies of B cell origin. *J Clin Invest* **67**, 134-140, doi:10.1172/JCI110005 (1981).

268 DiLillo, D. J. *et al.* Maintenance of long-lived plasma cells and serological memory despite mature and memory B cell depletion during CD20 immunotherapy in mice. *Journal of immunology* **180**, 361-371 (2008).

269 Liang, Y. & Tedder, T. F. Identification of a CD20-, FcepsilonRIbeta-, and HTm4-related gene family: sixteen new MS4A family members expressed in human and mouse. *Genomics* **72**, 119-127, doi:10.1006/geno.2000.6472 (2001).

270 Oldham, R. J., Cleary, K. L. S. & Cragg, M. S. CD20 and Its Antibodies: Past, Present, and Future. **5**, 7-23, doi:10.1615/ForumImmunDisTher.2015014073 (2014).

271 LeBien, T. W. & Tedder, T. F. B lymphocytes: how they develop and function. *Blood* **112**, 1570-1580, doi:10.1182/blood-2008-02-078071 (2008).

272 Engelhard, M. Anti-CD20 antibody treatment of non-Hodgkin lymphomas. *Clinical immunology*, doi:10.1016/j.clim.2016.08.011 (2016).

273 Reff, M. E. *et al.* Depletion of B cells in vivo by a chimeric mouse human monoclonal antibody to CD20. *Blood* **83**, 435-445 (1994).

274 Casak, S. J. *et al.* U.S. Food and drug administration approval: rituximab in combination with fludarabine and cyclophosphamide for the treatment of patients with chronic lymphocytic leukemia. *Oncologist* **16**, 97-104, doi:10.1634/theoncologist.2010-0306 (2011).

275 Prasad, V. The withdrawal of drugs for commercial reasons: the incomplete story of tositumomab. *JAMA internal medicine* **174**, 1887-1888, doi:10.1001/jamainternmed.2014.5756 (2014).

276 Lim, S. H. *et al.* Anti-CD20 monoclonal antibodies: historical and future perspectives. *Haematologica* **95**, 135-143, doi:10.3324/haematol.2008.001628 (2010).

277 Du, J., Yang, H., Guo, Y. & Ding, J. Structure of the Fab fragment of therapeutic antibody Ofatumumab provides insights into the recognition mechanism with CD20. *Molecular immunology* **46**, 2419-2423, doi:10.1016/j.molimm.2009.04.009 (2009).

278 Teeling, J. L. *et al.* The biological activity of human CD20 monoclonal antibodies is linked to unique epitopes on CD20. *Journal of immunology* **177**, 362-371 (2006).

279 Cameron, F. & McCormack, P. L. Obinutuzumab: first global approval. *Drugs* **74**, 147-154, doi:10.1007/s40265-013-0167-3 (2014).

280 Mossner, E. *et al.* Increasing the efficacy of CD20 antibody therapy through the engineering of a new type II anti-CD20 antibody with enhanced direct and immune effector cell-mediated B-cell cytotoxicity. *Blood* **115**, 4393-4402, doi:10.1182/blood-2009-06-225979 (2010).

281 Herter, S. *et al.* Preclinical activity of the type II CD20 antibody GA101 (obinutuzumab) compared with rituximab and ofatumumab in vitro and in xenograft models. *Mol Cancer Ther* **12**, 2031-2042, doi:10.1158/1535-7163.MCT-12-1182 (2013).

282 Herter, S. *et al.* Glycoengineering of therapeutic antibodies enhances monocyte/macrophage-mediated phagocytosis and cytotoxicity. *Journal of immunology* **192**, 2252-2260, doi:10.4049/jimmunol.1301249 (2014).

283 Tipton, T. R. *et al.* Antigenic modulation limits the effector cell mechanisms employed by type I anti-CD20 monoclonal antibodies. *Blood* **125**, 1901-1909, doi:10.1182/blood-2014-07-588376 (2015).

284 Golay, J. *et al.* Glycoengineered CD20 antibody obinutuzumab activates neutrophils and mediates phagocytosis through CD16B more efficiently than rituximab. *Blood* **122**, 3482-3491, doi:10.1182/blood-2013-05-504043 (2013).

285 Goede, V. *et al.* Obinutuzumab plus chlorambucil in patients with CLL and coexisting conditions. *The New England journal of medicine* **370**, 1101-1110, doi:10.1056/NEJMoa1313984 (2014).

286 Rogers, K. A. & Jones, J. A. Obinutuzumab for the treatment of chronic lymphocytic leukemia. *Drugs of today* **50**, 407-419, doi:10.1358/dot.2014.50.6.2138702 (2014).

287 Edelmann, J. & Gribben, J. G. Obinutuzumab for the treatment of indolent lymphoma. *Future oncology* **12**, 1769-1781, doi:10.2217/fon-2016-0084 (2016).

288 Juanatey, A., Blanco-Garcia, L. & Tellez, N. Ocrelizumab: its efficacy and safety in multiple sclerosis. *Rev Neurol* **66**, 423-433 (2018).

289 Ocrelizumab for multiple sclerosis. *Drug Ther Bull* **56**, 80-84, doi:10.1136/dtb.2018.7.0646 (2018).

290 Casan, J., Wong, J., Northcott, M. J. & Opat, S. Anti-CD20 monoclonal antibodies: reviewing a revolution. *Hum Vaccin Immunother*, doi:10.1080/21645515.2018.1508624 (2018).

291 Marshall, M. J. E., Stopforth, R. J. & Cragg, M. S. Therapeutic Antibodies: What Have We Learnt from Targeting CD20 and Where Are We Going? *Frontiers in immunology* **8**, 1245, doi:10.3389/fimmu.2017.01245 (2017).

292 Deans, J. P., Robbins, S. M., Polyak, M. J. & Savage, J. A. Rapid redistribution of CD20 to a low density detergent-insoluble membrane compartment. *J Biol Chem* **273**, 344-348 (1998).

293 Cragg, M. S. *et al.* Complement-mediated lysis by anti-CD20 mAb correlates with segregation into lipid rafts. *Blood* **101**, 1045-1052, doi:10.1182/blood-2002-06-1761 (2003).

294 Niederfellner, G. *et al.* Epitope characterization and crystal structure of GA101 provide insights into the molecular basis for type I/II distinction of CD20 antibodies. *Blood* **118**, 358-367, doi:10.1182/blood-2010-09-305847 (2011).

295 Beers, S. A. *et al.* Antigenic modulation limits the efficacy of anti-CD20 antibodies: implications for antibody selection. *Blood* **115**, 5191-5201, doi:10.1182/blood-2010-01-263533 (2010).

296 Alduaij, W. *et al.* Novel type II anti-CD20 monoclonal antibody (GA101) evokes homotypic adhesion and actin-dependent, lysosome-mediated cell death in B-cell malignancies. *Blood* **117**, 4519-4529, doi:10.1182/blood-2010-07-296913 (2011).

297 Ivanov, A. *et al.* Monoclonal antibodies directed to CD20 and HLA-DR can elicit homotypic adhesion followed by lysosome-mediated cell death in human lymphoma and leukemia cells. *J Clin Invest* **119**, 2143-2159, doi:10.1172/JCI37884 (2009).

298 Van den Steen, P., Rudd, P. M., Dwek, R. A. & Opdenakker, G. Concepts and principles of O-linked glycosylation. *Critical reviews in biochemistry and molecular biology* **33**, 151-208, doi:10.1080/10409239891204198 (1998).

299 Harvey Lodish, D. B., Arnold Berk, S. Lawrence Zipursky, Paul Matsudaira, James Darnell. *Molecular Cell Biology*. Third Edition edn, (Scientific American Books, Inc., 1995).

300 Swiezewska, E. & Danikiewicz, W. Polyisoprenoids: structure, biosynthesis and function. *Prog Lipid Res* **44**, 235-258, doi:10.1016/j.plipres.2005.05.002 (2005).

301 Heller, L., Orlean, P. & Adair, W. L., Jr. Saccharomyces cerevisiae sec59 cells are deficient in dolichol kinase activity. *Proc Natl Acad Sci U S A* **89**, 7013-7016 (1992).

302 Lehrman, M. A., Zhu, X. Y. & Khounlo, S. Amplification and molecular cloning of the hamster tunicamycin-sensitive N-acetylglucosamine-1-phosphate transferase gene. The hamster and yeast enzymes share a common peptide sequence. *J Biol Chem* **263**, 19796-19803 (1988).

303 Bickel, T., Lehle, L., Schwarz, M., Aebi, M. & Jakob, C. A. Biosynthesis of lipid-linked oligosaccharides in Saccharomyces cerevisiae: Alg13p and Alg14p form a complex required for the formation of GlcNAc(2)-PP-dolichol. *J Biol Chem* **280**, 34500-34506, doi:10.1074/jbc.M506358200 (2005).

304 Couto, J. R., Huffaker, T. C. & Robbins, P. W. Cloning and expression in Escherichia coli of a yeast mannosyltransferase from the asparagine-linked glycosylation pathway. *J Biol Chem* **259**, 378-382 (1984).

305 Kampf, M., Absmanner, B., Schwarz, M. & Lehle, L. Biochemical characterization and membrane topology of Alg2 from Saccharomyces cerevisiae as a bifunctional alpha1,3- and 1,6-mannosyltransferase involved in lipid-linked oligosaccharide biosynthesis. *J Biol Chem* **284**, 11900-11912, doi:10.1074/jbc.M806416200 (2009).

306 O'Reilly, M. K., Zhang, G. & Imperiali, B. In vitro evidence for the dual function of Alg2 and Alg11: essential mannosyltransferases in N-linked glycoprotein biosynthesis. *Biochemistry* **45**, 9593-9603, doi:10.1021/bi060878o (2006).

307 Cipollo, J. F., Trimble, R. B., Chi, J. H., Yan, Q. & Dean, N. The yeast ALG11 gene specifies addition of the terminal alpha 1,2-Man to the Man5GlcNAc2-PP-dolichol N-glycosylation intermediate formed on the cytosolic side of the endoplasmic reticulum. *J Biol Chem* **276**, 21828-21840, doi:10.1074/jbc.M010896200 (2001).

308 Helenius, J. *et al.* Translocation of lipid-linked oligosaccharides across the ER membrane requires Rft1 protein. *Nature* **415**, 447-450, doi:10.1038/415447a (2002).

309 Heesen, S., Lehle, L., Weissmann, A. & Aebi, M. Isolation of the ALG5 locus encoding the UDP-glucose:dolichyl-phosphate glucosyltransferase from Saccharomyces cerevisiae. *Eur J Biochem* **224**, 71-79 (1994).

310 Orlean, P., Albright, C. & Robbins, P. W. Cloning and sequencing of the yeast gene for dolichol phosphate mannose synthase, an essential protein. *J Biol Chem* **263**, 17499-17507 (1988).

311 Sanyal, S. & Menon, A. K. Stereoselective transbilayer translocation of mannosyl phosphoryl dolichol by an endoplasmic reticulum flippase. *Proc Natl Acad Sci U S A* **107**, 11289-11294, doi:10.1073/pnas.1002408107 (2010).

312 Aebi, M., Gassenhuber, J., Domdey, H. & te Heesen, S. Cloning and characterization of the ALG3 gene of Saccharomyces cerevisiae. *Glycobiology* **6**, 439-444 (1996).

313 Frank, C. G. & Aebi, M. ALG9 mannosyltransferase is involved in two different steps of lipid-linked oligosaccharide biosynthesis. *Glycobiology* **15**, 1156-1163, doi:10.1093/glycob/cwj002 (2005).

314 Burda, P., Jakob, C. A., Beinhauer, J., Hegemann, J. H. & Aebi, M. Ordered assembly of the asymmetrically branched lipid-linked oligosaccharide in the endoplasmic reticulum is ensured by the substrate specificity of the individual glycosyltransferases. *Glycobiology* **9**, 617-625 (1999).

315 Reiss, G., te Heesen, S., Zimmerman, J., Robbins, P. W. & Aebi, M. Isolation of the ALG6 locus of Saccharomyces cerevisiae required for glucosylation in the N-linked glycosylation pathway. *Glycobiology* **6**, 493-498 (1996).

316 Stagljar, I., te Heesen, S. & Aebi, M. New phenotype of mutations deficient in glucosylation of the lipid-linked oligosaccharide: cloning of the ALG8 locus. *Proc Natl Acad Sci U S A* **91**, 5977-5981 (1994).

317 Burda, P. & Aebi, M. The ALG10 locus of Saccharomyces cerevisiae encodes the alpha-1,2 glucosyltransferase of the endoplasmic reticulum: the terminal glucose of the lipid-linked oligosaccharide is required for efficient N-linked glycosylation. *Glycobiology* **8**, 455-462 (1998).

318 Shrimal, S., Cherepanova, N. A. & Gilmore, R. Cotranslational and posttranslocational N-glycosylation of proteins in the endoplasmic reticulum. *Semin Cell Dev Biol* **41**, 71-78, doi:10.1016/j.semcdb.2014.11.005 (2015).

319 Mohorko, E., Glockshuber, R. & Aebi, M. Oligosaccharyltransferase: the central enzyme of N-linked protein glycosylation. *J Inherit Metab Dis* **34**, 869-878, doi:10.1007/s10545-011-9337-1 (2011).

320 Hart, G. W., Brew, K., Grant, G. A., Bradshaw, R. A. & Lennarz, W. J. Primary structural requirements for the enzymatic formation of the N-glycosidic bond in glycoproteins. Studies with natural and synthetic peptides. *J Biol Chem* **254**, 9747-9753 (1979).

321 Bause, E. & Legler, G. The role of the hydroxy amino acid in the triplet sequence Asn-Xaa-Thr(Ser) for the N-glycosylation step during glycoprotein biosynthesis. *Biochem J* **195**, 639-644 (1981).

322 Tulsiani, D. R., Hubbard, S. C., Robbins, P. W. & Touster, O. alpha-D-Mannosidases of rat liver Golgi membranes. Mannosidase II is the GlcNAcMAN5-cleaving enzyme in glycoprotein biosynthesis and mannosidases Ia and IB are the enzymes converting Man9 precursors to Man5 intermediates. *J Biol Chem* **257**, 3660-3668 (1982).

323 Bause, E., Schweden, J., Gross, A. & Orthen, B. Purification and characterization of trimming glucosidase I from pig liver. *Eur J Biochem* **183**, 661-669 (1989).

324 Hentges, A. & Bause, E. Affinity purification and characterization of glucosidase II from pig liver. *Biol Chem* **378**, 1031-1038 (1997).

325 Stanley, P., Narasimhan, S., Siminovitch, L. & Schachter, H. Chinese hamster ovary cells selected for resistance to the cytotoxicity of phytohemagglutinin are deficient in a UDP-N-acetylglucosamine--glycoprotein N-acetylglucosaminyltransferase activity. *Proc Natl Acad Sci U S A* **72**, 3323-3327 (1975).

326 Shah, N., Kuntz, D. A. & Rose, D. R. Golgi alpha-mannosidase II cleaves two sugars sequentially in the same catalytic site. *Proc Natl Acad Sci U S A* **105**, 9570-9575, doi:10.1073/pnas.0802206105 (2008).

327 D'Agostaro, G. A. *et al.* Molecular cloning and expression of cDNA encoding the rat UDP-N-acetylglucosamine:alpha-6-D-mannoside beta-1,2-N-acetylglucosaminyltransferase II. *J Biol Chem* **270**, 15211-15221 (1995).

328 Narasimhan, S. Control of glycoprotein synthesis. UDP-GlcNAc:glycopeptide beta 4-N-acetylglucosaminyltransferase III, an enzyme in hen oviduct which adds GlcNAc in beta 1-4 linkage to the beta-linked mannose of the trimannosyl core of N-glycosyl oligosaccharides. *J Biol Chem* **257**, 10235-10242 (1982).

329 Strous, G. J. Golgi and secreted galactosyltransferase. *CRC Crit Rev Biochem* **21**, 119-151 (1986).

330 Stanley, P. Golgi glycosylation. *Cold Spring Harb Perspect Biol* **3**, doi:10.1101/cshperspect.a005199 (2011).

331 Longmore, G. D. & Schachter, H. Product-identification and substrate-specificity studies of the GDP-L-fucose:2-acetamido-2-deoxy-beta-D-glucoside (FUC goes to Asn-linked GlcNAc) 6-alpha-L-fucosyltransferase in a Golgi-rich fraction from porcine liver. *Carbohydr Res* **100**, 365-392 (1982).

332 Crispin, M., Yu, X. & Bowden, T. A. Crystal structure of sialylated IgG Fc: implications for the mechanism of intravenous immunoglobulin therapy. *Proc Natl Acad Sci U S A* **110**, E3544-3546, doi:10.1073/pnas.1310657110 (2013).

333 Zauner, G. *et al.* Glycoproteomic analysis of antibodies. *Molecular & cellular proteomics : MCP* **12**, 856-865, doi:10.1074/mcp.R112.026005 (2013).

334 Pucic, M. *et al.* High throughput isolation and glycosylation analysis of IgG-variability and heritability of the IgG glycome in three isolated human populations. *Molecular & cellular proteomics : MCP* **10**, M111 010090, doi:10.1074/mcp.M111.010090 (2011).

335 Shade, K. T. *et al.* A single glycan on IgE is indispensable for initiation of anaphylaxis. *The Journal of experimental medicine* **212**, 457-467, doi:10.1084/jem.20142182 (2015).

336 Wuhrer, M. *et al.* Glycosylation profiling of immunoglobulin G (IgG) subclasses from human serum. *Proteomics* **7**, 4070-4081, doi:10.1002/pmic.200700289 (2007).

337 Yuan, W., Sanda, M., Wu, J., Koomen, J. & Goldman, R. Quantitative analysis of immunoglobulin subclasses and subclass specific glycosylation by LC-MS-MRM in liver disease. *Journal of proteomics* **116**, 24-33, doi:10.1016/j.jprot.2014.12.020 (2015).

338 Selman, M. H. *et al.* Fc specific IgG glycosylation profiling by robust nano-reverse phase HPLC-MS using a sheath-flow ESI sprayer interface. *Journal of proteomics* **75**, 1318-1329, doi:10.1016/j.jprot.2011.11.003 (2012).

339 Mimura, Y. *et al.* The influence of glycosylation on the thermal stability and effector function expression of human IgG1-Fc: properties of a series of truncated glycoforms. *Molecular immunology* **37**, 697-706 (2000).

340 Krapp, S., Mimura, Y., Jefferis, R., Huber, R. & Sondermann, P. Structural analysis of human IgG-Fc glycoforms reveals a correlation between glycosylation and structural integrity. *J Mol Biol* **325**, 979-989 (2003).

341 Jefferis, R. Isotype and glycoform selection for antibody therapeutics. *Archives of biochemistry and biophysics* **526**, 159-166, doi:10.1016/j.abb.2012.03.021 (2012).

342 Jefferis, R., Lund, J. & Pound, J. D. IgG-Fc-mediated effector functions: molecular definition of interaction sites for effector ligands and the role of glycosylation. *Immunological reviews* **163**, 59-76 (1998).

343 Feige, M. J. *et al.* Structure of the murine unglycosylated IgG1 Fc fragment. *J Mol Biol* **391**, 599-608, doi:10.1016/j.jmb.2009.06.048 (2009).

344 Mimura, Y. *et al.* Role of oligosaccharide residues of IgG1-Fc in Fc gamma RIIb binding. *J Biol Chem* **276**, 45539-45547, doi:10.1074/jbc.M107478200 (2001).

345 Nandakumar, K. S. *et al.* Dominant suppression of inflammation by glycan-hydrolyzed IgG. *Proc Natl Acad Sci U S A* **110**, 10252-10257, doi:10.1073/pnas.1301480110 (2013).

346 Tao, M. H. & Morrison, S. L. Studies of aglycosylated chimeric mouse-human IgG. Role of carbohydrate in the structure and effector functions mediated by the human IgG constant region. *Journal of immunology* **143**, 2595-2601 (1989).

347 Radaev, S., Motyka, S., Fridman, W. H., Sautes-Fridman, C. & Sun, P. D. The structure of a human type III Fcgamma receptor in complex with Fc. *J Biol Chem* **276**, 16469-16477, doi:10.1074/jbc.M100350200 (2001).

348 Anthony, R. M., Wermeling, F. & Ravetch, J. V. Novel roles for the IgG Fc glycan. *Annals of the New York Academy of Sciences* **1253**, 170-180, doi:10.1111/j.1749-6632.2011.06305.x (2012).

349 Lund, J., Takahashi, N., Pound, J. D., Goodall, M. & Jefferis, R. Multiple interactions of IgG with its core oligosaccharide can modulate recognition by complement and human Fc gamma receptor I and influence the synthesis of its oligosaccharide chains. *Journal of immunology* **157**, 4963-4969 (1996).

350 Ferrara, C. *et al.* Unique carbohydrate-carbohydrate interactions are required for high affinity binding between FcgammaRIII and antibodies lacking core fucose. *Proc Natl Acad Sci U S A* **108**, 12669-12674, doi:10.1073/pnas.1108455108 (2011).

351 Shields, R. L. *et al.* Lack of fucose on human IgG1 N-linked oligosaccharide improves binding to human Fcgamma RIII and antibody-dependent cellular toxicity. *J Biol Chem* **277**, 26733-26740, doi:10.1074/jbc.M202069200 (2002).

352 Shinkawa, T. *et al.* The absence of fucose but not the presence of galactose or bisecting N-acetylglucosamine of human IgG1 complex-type oligosaccharides shows the critical role of enhancing antibody-dependent cellular cytotoxicity. *J Biol Chem* **278**, 3466-3473, doi:10.1074/jbc.M210665200 (2003).

353 Seidel, U. J., Schlegel, P. & Lang, P. Natural killer cell mediated antibody-dependent cellular cytotoxicity in tumor immunotherapy with therapeutic antibodies. *Frontiers in immunology* **4**, 76, doi:10.3389/fimmu.2013.00076 (2013).

354 Huang, W., Giddens, J., Fan, S. Q., Toonstra, C. & Wang, L. X. Chemoenzymatic glycoengineering of intact IgG antibodies for gain of functions. *Journal of the American Chemical Society* **134**, 12308-12318, doi:10.1021/ja3051266 (2012).

355 Kanda, Y. *et al.* Comparison of biological activity among nonfucosylated therapeutic IgG1 antibodies with three different N-linked Fc oligosaccharides: the high-mannose, hybrid, and complex types. *Glycobiology* **17**, 104-118, doi:10.1093/glycob/cwl057 (2007).

356 Yamaguchi, Y. *et al.* Glycoform-dependent conformational alteration of the Fc region of human immunoglobulin G1 as revealed by NMR spectroscopy. *Biochimica et biophysica acta* **1760**, 693-700, doi:10.1016/j.bbagen.2005.10.002 (2006).

357 Lee, H. Z. *et al.* U.S. Food and drug administration approval: obinutuzumab in combination with chlorambucil for the treatment of previously untreated chronic lymphocytic leukemia. *Clinical cancer research : an official journal of the American Association for Cancer Research* **20**, 3902-3907, doi:10.1158/1078-0432.CCR-14-0516 (2014).

358 Beck, A. & Reichert, J. M. Marketing approval of mogamulizumab: a triumph for glyco-engineering. *mAbs* **4**, 419-425, doi:10.4161/mabs.20996 (2012).

359 Yamane-Ohnuki, N. *et al.* Establishment of FUT8 knockout Chinese hamster ovary cells: an ideal host cell line for producing completely defucosylated antibodies with enhanced antibody-dependent cellular cytotoxicity. *Biotechnology and bioengineering* **87**, 614-622, doi:10.1002/bit.20151 (2004).

360 Niwa, R. *et al.* Defucosylated chimeric anti-CC chemokine receptor 4 IgG1 with enhanced antibody-dependent cellular cytotoxicity shows potent therapeutic activity to T-cell leukemia and lymphoma. *Cancer Res* **64**, 2127-2133 (2004).

361 Ishii, T. *et al.* Defucosylated humanized anti-CCR4 monoclonal antibody KW-0761 as a novel immunotherapeutic agent for adult T-cell leukemia/lymphoma. *Clinical cancer research : an official journal of the American Association for Cancer Research* **16**, 1520-1531, doi:10.1158/1078-0432.CCR-09-2697 (2010).

362 Markham, A. Benralizumab: First Global Approval. *Drugs* **78**, 505-511, doi:10.1007/s40265-018-0876-8 (2018).

363 Pelaia, C. *et al.* Benralizumab: From the Basic Mechanism of Action to the Potential Use in the Biological Therapy of Severe Eosinophilic Asthma. *Biomed Res Int* **2018**, 4839230, doi:10.1155/2018/4839230 (2018).

364 Ghazi, A., Trikha, A. & Calhoun, W. J. Benralizumab--a humanized mAb to IL-5Ralpha with enhanced antibody-dependent cell-mediated cytotoxicity--a novel approach for the treatment of asthma. *Expert opinion on biological therapy* **12**, 113-118, doi:10.1517/14712598.2012.642359 (2012).

365 FitzGerald, J. M. *et al.* Benralizumab, an anti-interleukin-5 receptor alpha monoclonal antibody, as add-on treatment for patients with severe, uncontrolled, eosinophilic asthma (CALIMA): a randomised, double-blind, placebo-controlled phase 3 trial. *Lancet* **388**, 2128-2141, doi:10.1016/S0140-6736(16)31322-8 (2016).

366 Kaplon, H. & Reichert, J. M. Antibodies to watch in 2018. *mAbs* **10**, 183-203, doi:10.1080/19420862.2018.1415671 (2018).

367 Babiker, H. M., Glode, A. E., Cooke, L. S. & Mahadevan, D. Ublituximab for the treatment of CD20 positive B-cell malignancies. *Expert Opin Investig Drugs* **27**, 407-412, doi:10.1080/13543784.2018.1459560 (2018).

368 de Romeuf, C. *et al.* Chronic lymphocytic leukaemia cells are efficiently killed by an anti-CD20 monoclonal antibody selected for improved engagement of FcgammaRIIIA/CD16. *Br J Haematol* **140**, 635-643, doi:10.1111/j.1365-2141.2007.06974.x (2008).

369 Sharman, J. P. *et al.* Ublituximab (TG-1101), a novel glycoengineered anti-CD20 antibody, in combination with ibrutinib is safe and highly active in patients with relapsed and/or refractory chronic lymphocytic leukaemia: results of a phase 2 trial. *Br J Haematol* **176**, 412-420, doi:10.1111/bjh.14447 (2017).

370 Bohm, S., Schwab, I., Lux, A. & Nimmerjahn, F. The role of sialic acid as a modulator of the anti-inflammatory activity of IgG. *Semin Immunopathol* **34**, 443-453, doi:10.1007/s00281-012-0308-x (2012).

371 Looney, R. J. & Huggins, J. Use of intravenous immunoglobulin G (IVIG). *Best practice & research. Clinical haematology* **19**, 3-25, doi:10.1016/j.beha.2005.01.032 (2006).

372 Kaneko, Y., Nimmerjahn, F. & Ravetch, J. V. Anti-inflammatory activity of immunoglobulin G resulting from Fc sialylation. *Science* **313**, 670-673, doi:10.1126/science.1129594 (2006).

373 Anthony, R. M., Wermeling, F., Karlsson, M. C. & Ravetch, J. V. Identification of a receptor required for the anti-inflammatory activity of IVIG. *Proc Natl Acad Sci U S A* **105**, 19571-19578, doi:10.1073/pnas.0810163105 (2008).

374 Schwab, I. & Nimmerjahn, F. Intravenous immunoglobulin therapy: how does IgG modulate the immune system? *Nature reviews. Immunology* **13**, 176-189, doi:10.1038/nri3401 (2013).

375 Campbell, I. K. *et al.* Therapeutic effect of IVIG on inflammatory arthritis in mice is dependent on the Fc portion and independent of sialylation or basophils. *Journal of immunology* **192**, 5031-5038, doi:10.4049/jimmunol.1301611 (2014).

376 Nagelkerke, S. Q. *et al.* Inhibition of FcgammaR-mediated phagocytosis by IVIg is independent of IgG-Fc sialylation and FcgammaRIIb in human macrophages. *Blood* **124**, 3709-3718, doi:10.1182/blood-2014-05-576835 (2014).

377 Yu, X., Vasiljevic, S., Mitchell, D. A., Crispin, M. & Scanlan, C. N. Dissecting the molecular mechanism of IVIg therapy: the interaction between serum IgG and DC-SIGN is independent of antibody glycoform or Fc domain. *J Mol Biol* **425**, 1253-1258, doi:10.1016/j.jmb.2013.02.006 (2013).

378 Parekh, R. B. *et al.* Association of rheumatoid arthritis and primary osteoarthritis with changes in the glycosylation pattern of total serum IgG. *Nature* **316**, 452-457 (1985).

379 van de Geijn, F. E. *et al.* Immunoglobulin G galactosylation and sialylation are associated with pregnancy-induced improvement of rheumatoid arthritis and the postpartum flare: results from a large prospective cohort study. *Arthritis research & therapy* **11**, R193, doi:10.1186/ar2892 (2009).

380 Bondt, A. *et al.* Association between galactosylation of immunoglobulin G and improvement of rheumatoid arthritis during pregnancy is independent of sialylation. *Journal of proteome research* **12**, 4522-4531, doi:10.1021/pr400589m (2013).

381 Davies, J. *et al.* Expression of GnTIII in a recombinant anti-CD20 CHO production cell line: Expression of antibodies with altered glycoforms leads to an increase in ADCC through higher affinity for FC gamma RIII. *Biotechnology and bioengineering* **74**, 288-294 (2001).

382 Zou, G. *et al.* Chemoenzymatic synthesis and Fcgamma receptor binding of homogeneous glycoforms of antibody Fc domain. Presence of a bisecting sugar moiety enhances the affinity of Fc to FcgammaIIIa receptor. *Journal of the American Chemical Society* **133**, 18975-18991, doi:10.1021/ja208390n (2011).

383 Subedi, G. P. & Barb, A. W. The Structural Role of Antibody N-Glycosylation in Receptor Interactions. *Structure*, doi:10.1016/j.str.2015.06.015 (2015).

384 Borrok, M. J., Jung, S. T., Kang, T. H., Monzingo, A. F. & Georgiou, G. Revisiting the role of glycosylation in the structure of human IgG Fc. *ACS chemical biology* **7**, 1596-1602, doi:10.1021/cb300130k (2012).

385 Kelliher, M. T., Jacks, R. D., Piraino, M. S. & Southern, C. A. The effect of sugar removal on the structure of the Fc region of an IgG antibody as observed with single molecule Forster Resonance Energy Transfer. *Molecular immunology* **60**, 103-108, doi:10.1016/j.molimm.2014.04.005 (2014).

386 Piraino, M. S., Kelliher, M. T., Aburas, J. & Southern, C. A. Single molecule Forster resonance energy transfer studies of the effect of EndoS deglycosylation on the structure of IgG. *Immunology letters* **167**, 29-33, doi:10.1016/j.imlet.2015.06.011 (2015).

387 Ferrara, C., Stuart, F., Sondermann, P., Brunker, P. & Umana, P. The carbohydrate at FcgammaRIIIa Asn-162. An element required for high affinity binding to non-fucosylated IgG glycoforms. *J Biol Chem* **281**, 5032-5036, doi:10.1074/jbc.M510171200 (2006).

388 Shibata-Koyama, M. *et al.* The N-linked oligosaccharide at Fc gamma RIIIa Asn-45: an inhibitory element for high Fc gamma RIIIa binding affinity to IgG glycoforms lacking core fucosylation. *Glycobiology* **19**, 126-134, doi:10.1093/glycob/cwn110 (2009).

389 Edberg, J. C. & Kimberly, R. P. Cell type-specific glycoforms of Fc gamma RIIIa (CD16): differential ligand binding. *Journal of immunology* **159**, 3849-3857 (1997).

390 Patel, K. R., Roberts, J. T., Subedi, G. P. & Barb, A. W. Restricted processing of CD16a/Fc gamma receptor IIIa N-glycans from primary human NK cells impacts structure and function. *J Biol Chem* **293**, 3477-3489, doi:10.1074/jbc.RA117.001207 (2018).

391 Subedi, G. P. & Barb, A. W. CD16a with oligomannose-type N-glycans is the only "low affinity" Fc gamma receptor that binds the IgG crystallizable fragment with high affinity in vitro. *J Biol Chem*, doi:10.1074/jbc.RA118.004998 (2018).

392 Zeck, A., Pohlentz, G., Schlothauer, T., Peter-Katalinic, J. & Regula, J. T. Cell type-specific and site directed N-glycosylation pattern of FcgammaRIIIa. *Journal of proteome research* **10**, 3031-3039, doi:10.1021/pr1012653 (2011).

393 Drescher, B., Witte, T. & Schmidt, R. E. Glycosylation of FcgammaRIII in N163 as mechanism of regulating receptor affinity. *Immunology* **110**, 335-340 (2003).

394 Yu, X., Marshall, M. J. E., Cragg, M. S. & Crispin, M. Improving Antibody-Based Cancer Therapeutics Through Glycan Engineering. *BioDrugs* **31**, 151-166, doi:10.1007/s40259-017-0223-8 (2017).

395 Subramaniam, J. M., Whiteside, G., McKeage, K. & Croxtall, J. C. Mogamulizumab: first global approval. *Drugs* **72**, 1293-1298, doi:10.2165/11631090-000000000-00000 (2012).

396 Sou, S. N. *et al.* How does mild hypothermia affect monoclonal antibody glycosylation? *Biotechnology and bioengineering*, doi:10.1002/bit.25524 (2014).

397 Aghamohseni, H. *et al.* Effects of nutrient levels and average culture pH on the glycosylation pattern of camelid-humanized monoclonal antibody. *Journal of biotechnology* **186**, 98-109, doi:10.1016/j.jbiotec.2014.05.024 (2014).

398 Crowell, C. K., Grampp, G. E., Rogers, G. N., Miller, J. & Scheinman, R. I. Amino acid and manganese supplementation modulates the glycosylation state of erythropoietin in a CHO culture system. *Biotechnology and bioengineering* **96**, 538-549, doi:10.1002/bit.21141 (2007).

399 Pacis, E., Yu, M., Autsen, J., Bayer, R. & Li, F. Effects of cell culture conditions on antibody N-linked glycosylation--what affects high mannose 5 glycoform. *Biotechnology and bioengineering* **108**, 2348-2358, doi:10.1002/bit.23200 (2011).

400 Ryll, T. Mammalian cell culture process for producing glycoproteins. USA patent (2003).

401 Wei, X. F., Shimizu, Y. & Kanai, M. An Expeditious Synthesis of Sialic Acid Derivatives by Copper(I)-Catalyzed Stereodivergent Propargylation of Unprotected Aldoses. *ACS Cent Sci* **2**, 21-26, doi:10.1021/acscentsci.5b00360 (2016).

402 Chen, P. & Harcum, S. W. Effects of elevated ammonium on glycosylation gene expression in CHO cells. *Metabolic engineering* **8**, 123-132, doi:10.1016/j.ymben.2005.10.002 (2006).

403 Yang, M. & Butler, M. Effects of ammonia and glucosamine on the heterogeneity of erythropoietin glycoforms. *Biotechnology progress* **18**, 129-138, doi:10.1021/bp0101334 (2002).

404 Butler, M. Optimisation of the cellular metabolism of glycosylation for recombinant proteins produced by Mammalian cell systems. *Cytotechnology* **50**, 57-76, doi:10.1007/s10616-005-4537-x (2006).

405 Raju, T. S. & Jordan, R. E. Galactosylation variations in marketed therapeutic antibodies. *mAbs* **4**, 385-391, doi:10.4161/mabs.19868 (2012).

406 Thomann, M. *et al.* In Vitro Glycoengineering of IgG1 and Its Effect on Fc Receptor Binding and ADCC Activity. *PloS one* **10**, e0134949, doi:10.1371/journal.pone.0134949 (2015).

407 Umana, P., Jean-Mairet, J., Moudry, R., Amstutz, H. & Bailey, J. E. Engineered glycoforms of an antineuroblastoma IgG1 with optimized antibody-dependent cellular cytotoxic activity. *Nature biotechnology* **17**, 176-180, doi:10.1038/6179 (1999).

408 Ferrara, C. *et al.* Modulation of therapeutic antibody effector functions by glycosylation engineering: influence of Golgi enzyme localization domain and co-expression of heterologous beta1, 4-N-acetylglucosaminyltransferase III and Golgi alpha-mannosidase II. *Biotechnology and bioengineering* **93**, 851-861, doi:10.1002/bit.20777 (2006).

409 Taniguchi, T. *et al.* Structures of the sugar chains of rabbit immunoglobulin G: occurrence of asparagine-linked sugar chains in Fab fragment. *Biochemistry* **24**, 5551-5557 (1985).

410 Wallick, S. C., Kabat, E. A. & Morrison, S. L. Glycosylation of a VH residue of a monoclonal antibody against alpha (1----6) dextran increases its affinity for antigen. *The Journal of experimental medicine* **168**, 1099-1109 (1988).

411 Huang, L., Biolsi, S., Bales, K. R. & Kuchibhotla, U. Impact of variable domain glycosylation on antibody clearance: an LC/MS characterization. *Analytical biochemistry* **349**, 197-207, doi:10.1016/j.ab.2005.11.012 (2006).

412 Endo, T., Wright, A., Morrison, S. L. & Kobata, A. Glycosylation of the variable region of immunoglobulin G--site specific maturation of the sugar chains. *Molecular immunology* **32**, 931-940 (1995).

413 Scherer, H. U. *et al.* Immunoglobulin 1 (IgG1) Fc-glycosylation profiling of anti-citrullinated peptide antibodies from human serum. *Proteomics. Clinical applications* **3**, 106-115, doi:10.1002/prca.200800098 (2009).

414 Scherer, H. U. *et al.* Glycan profiling of anti-citrullinated protein antibodies isolated from human serum and synovial fluid. *Arthritis and rheumatism* **62**, 1620-1629, doi:10.1002/art.27414 (2010).

415 Wang, J. *et al.* Fc-glycosylation of IgG1 is modulated by B-cell stimuli. *Molecular & cellular proteomics : MCP* **10**, M110 004655, doi:10.1074/mcp.M110.004655 (2011).

416 Bryant, V. L. *et al.* Cytokine-mediated regulation of human B cell differentiation into Ig-secreting cells: predominant role of IL-21 produced by CXCR5+ T follicular helper cells. *Journal of immunology* **179**, 8180-8190 (2007).

417 Reusch, D. *et al.* Comparison of methods for the analysis of therapeutic immunoglobulin G Fc-glycosylation profiles--part 1: separation-based methods. *mAbs* **7**, 167-179, doi:10.4161/19420862.2014.986000 (2015).

418 Reusch, D. *et al.* Comparison of methods for the analysis of therapeutic immunoglobulin G Fc-glycosylation profiles-Part 2: Mass spectrometric methods. *mAbs* **7**, 732-742, doi:10.1080/19420862.2015.1045173 (2015).

419 Tutt, A. L. *et al.* Development and Characterization of Monoclonal Antibodies Specific for Mouse and Human Fcgamma Receptors. *Journal of immunology* **195**, 5503-5516, doi:10.4049/jimmunol.1402988 (2015).

420 Anania, J. C., Chenoweth, A. M., Wines, B. D. & Hogarth, P. M. The Human FcgammaRII (CD32) Family of Leukocyte FcR in Health and Disease. *Frontiers in immunology* **10**, 464, doi:10.3389/fimmu.2019.00464 (2019).

421 Jarboe, J., Gupta, A. & Saif, W. Therapeutic human monoclonal antibodies against cancer. *Methods Mol Biol* **1060**, 61-77, doi:10.1007/978-1-62703-586-6_4 (2014).

422 Geskin, L. J. Monoclonal Antibodies. *Dermatol Clin* **33**, 777-786, doi:10.1016/j.det.2015.05.015 (2015).

423 Nogami, K. Bispecific antibody mimicking factor VIII. *Thromb Res* **141 Suppl 2**, S34-35, doi:10.1016/S0049-3848(16)30361-9 (2016).

424 Markham, A. Bezlotoxumab: First Global Approval. *Drugs* **76**, 1793-1798, doi:10.1007/s40265-016-0673-1 (2016).

425 Shuptrine, C. W., Surana, R. & Weiner, L. M. Monoclonal antibodies for the treatment of cancer. *Semin Cancer Biol* **22**, 3-13, doi:10.1016/j.semcancer.2011.12.009 (2012).

426 Beck, A. & Reichert, J. M. Antibody-drug conjugates: present and future. *mAbs* **6**, 15-17, doi:10.4161/mabs.27436 (2014).

427 Honeychurch, J., Cheadle, E. J., Dovedi, S. J. & Illidge, T. M. Immuno-regulatory antibodies for the treatment of cancer. *Expert opinion on biological therapy* **15**, 787-801, doi:10.1517/14712598.2015.1036737 (2015).

428 Pico de Coana, Y., Choudhury, A. & Kiessling, R. Checkpoint blockade for cancer therapy: revitalizing a suppressed immune system. *Trends Mol Med* **21**, 482-491, doi:10.1016/j.molmed.2015.05.005 (2015).

429 Hodi, F. S. *et al.* Improved survival with ipilimumab in patients with metastatic melanoma. *The New England journal of medicine* **363**, 711-723, doi:10.1056/NEJMoa1003466 (2010).

430 Khong, A., Nelson, D. J., Nowak, A. K., Lake, R. A. & Robinson, B. W. The use of agonistic anti-CD40 therapy in treatments for cancer. *Int Rev Immunol* **31**, 246-266, doi:10.3109/08830185.2012.698338 (2012).

431 Turaj, A. H. *et al.* Antibody Tumor Targeting Is Enhanced by CD27 Agonists through Myeloid Recruitment. *Cancer Cell* **32**, 777-791 e776, doi:10.1016/j.ccell.2017.11.001 (2017).

432 Schlothauer, T. *et al.* Novel human IgG1 and IgG4 Fc-engineered antibodies with completely abolished immune effector functions. *Protein Eng Des Sel* **29**, 457-466, doi:10.1093/protein/gzw040 (2016).

433 Cleary, K. L. S., Chan, H. T. C., James, S., Glennie, M. J. & Cragg, M. S. Antibody Distance from the Cell Membrane Regulates Antibody Effector Mechanisms. *Journal of immunology* **198**, 3999-4011, doi:10.4049/jimmunol.1601473 (2017).

434 Klein, C. *et al.* Epitope interactions of monoclonal antibodies targeting CD20 and their relationship to functional properties. *mAbs* **5**, 22-33, doi:10.4161/mabs.22771 (2013).

435 Wang, C. *et al.* In vitro characterization of the anti-PD-1 antibody nivolumab, BMS-936558, and in vivo toxicology in non-human primates. *Cancer Immunol Res* **2**, 846-856, doi:10.1158/2326-6066.CIR-14-0040 (2014).

436 Hamid, O. *et al.* Safety and tumor responses with lambrolizumab (anti-PD-1) in melanoma. *The New England journal of medicine* **369**, 134-144, doi:10.1056/NEJMoa1305133 (2013).

437 Ricart, A. D. Antibody-drug conjugates of calicheamicin derivative: gemtuzumab ozogamicin and inotuzumab ozogamicin. *Clinical cancer research : an official journal of the American Association for Cancer Research* **17**, 6417-6427, doi:10.1158/1078-0432.CCR-11-0486 (2011).

438 Yang, X. D., Jia, X. C., Corvalan, J. R., Wang, P. & Davis, C. G. Development of ABX-EGF, a fully human anti-EGF receptor monoclonal antibody, for cancer therapy. *Critical reviews in oncology/hematology* **38**, 17-23 (2001).

439 Zhang, H. *et al.* Serum IgG subclasses in autoimmune diseases. *Medicine (Baltimore)* **94**, e387, doi:10.1097/MD.0000000000000387 (2015).

440 Vidarsson, G. *et al.* Activity of human IgG and IgA subclasses in immune defense against Neisseria meningitidis serogroup B. *Journal of immunology* **166**, 6250-6256 (2001).

441 Arce Vargas, F. *et al.* Fc Effector Function Contributes to the Activity of Human Anti-CTLA-4 Antibodies. *Cancer Cell* **33**, 649-663 e644, doi:10.1016/j.ccell.2018.02.010 (2018).

442 Schneider-Merck, T. *et al.* Human IgG2 antibodies against epidermal growth factor receptor effectively trigger antibody-dependent cellular cytotoxicity but, in contrast to IgG1, only by cells of myeloid lineage. *Journal of immunology* **184**, 512-520, doi:10.4049/jimmunol.0900847 (2010).

443 Cragg, M. S. *et al.* A new anti-idiotype antibody capable of binding rituximab on the surface of lymphoma cells. *Blood* **104**, 2540-2542, doi:10.1182/blood-2004-05-1733 (2004).

444 Beers, S. A. *et al.* Type II (tositumomab) anti-CD20 monoclonal antibody out performs type I (rituximab-like) reagents in B-cell depletion regardless of complement activation. *Blood* **112**, 4170-4177, doi:10.1182/blood-2008-04-149161 (2008).

445 Takei, K., Yamazaki, T., Sawada, U., Ishizuka, H. & Aizawa, S. Analysis of changes in CD20, CD55, and CD59 expression on established rituximab-resistant B-lymphoma cell lines. *Leuk Res* **30**, 625-631, doi:10.1016/j.leukres.2005.09.008 (2006).

446 Mamidi, S. *et al.* Neutralization of membrane complement regulators improves complement-dependent effector functions of therapeutic anticancer antibodies targeting leukemic cells. *Oncoimmunology* **4**, e979688, doi:10.4161/2162402X.2014.979688 (2015).

447 Stavnezer, J. & Schrader, C. E. IgH chain class switch recombination: mechanism and regulation. *Journal of immunology* **193**, 5370-5378, doi:10.4049/jimmunol.1401849 (2014).

448 Salfeld, J. G. Isotype selection in antibody engineering. *Nature biotechnology* **25**, 1369-1372, doi:10.1038/nbt1207-1369 (2007).

449 Konitzer, J. D., Sieron, A., Wacker, A. & Enenkel, B. Reformatting Rituximab into Human IgG2 and IgG4 Isotypes Dramatically Improves Apoptosis Induction In Vitro. *PloS one* **10**, e0145633, doi:10.1371/journal.pone.0145633 (2015).

450 Calabresi, P. A. *et al.* The incidence and significance of anti-natalizumab antibodies: results from AFFIRM and SENTINEL. *Neurology* **69**, 1391-1403, doi:10.1212/01.wnl.0000277457.17420.b5 (2007).

451 Ritter, G. *et al.* Serological analysis of human anti-human antibody responses in colon cancer patients treated with repeated doses of humanized monoclonal antibody A33. *Cancer Res* **61**, 6851-6859 (2001).

452 Gomez-Mantilla, J. D., Troconiz, I. F., Parra-Guillen, Z. & Garrido, M. J. Review on modeling anti-antibody responses to monoclonal antibodies. *J Pharmacokinet Pharmacodyn* **41**, 523-536, doi:10.1007/s10928-014-9367-z (2014).

453 Hamilton, R. G. Human IgG subclass measurements in the clinical laboratory. *Clin Chem* **33**, 1707-1725 (1987).

454 Roghanian, A. *et al.* Antagonistic human FcgammaRIIB (CD32B) antibodies have anti-tumor activity and overcome resistance to antibody therapy in vivo. *Cancer Cell* **27**, 473-488, doi:10.1016/j.ccell.2015.03.005 (2015).

455 Kennedy, A. D. *et al.* Rituximab infusion promotes rapid complement depletion and acute CD20 loss in chronic lymphocytic leukemia. *Journal of immunology* **172**, 3280-3288 (2004).

456 Natsume, A. *et al.* Engineered antibodies of IgG1/IgG3 mixed isotype with enhanced cytotoxic activities. *Cancer Res* **68**, 3863-3872, doi:10.1158/0008-5472.CAN-07-6297 (2008).

457 Stapleton, N. M. *et al.* Competition for FcRn-mediated transport gives rise to short half-life of human IgG3 and offers therapeutic potential. *Nature communications* **2**, 599, doi:10.1038/ncomms1608 (2011).

458 Forthal, D. N. Functions of Antibodies. *Microbiology spectrum* **2**, AID-0019-2014, doi:10.1128/microbiolspec.AID-0019-2014 (2014).

459 Jones, M. B. *et al.* B-cell-independent sialylation of IgG. *Proc Natl Acad Sci U S A* **113**, 7207-7212, doi:10.1073/pnas.1523968113 (2016).

460 Hui, L. & Chen, Y. Tumor microenvironment: Sanctuary of the devil. *Cancer letters* **368**, 7-13, doi:10.1016/j.canlet.2015.07.039 (2015).

461 Harrison, I. P. & Selemidis, S. Understanding the biology of reactive oxygen species and their link to cancer: NADPH oxidases as novel pharmacological targets. *Clinical and experimental pharmacology & physiology* **41**, 533-542, doi:10.1111/1440-1681.12238 (2014).

462 West, X. Z. *et al.* Oxidative stress induces angiogenesis by activating TLR2 with novel endogenous ligands. *Nature* **467**, 972-976, doi:10.1038/nature09421 (2010).

463 Maia, F. M., Santos, E. B. & Reis, G. E. Oxidative stress and plasma lipoproteins in cancer patients. *Einstein* **12**, 480-484, doi:10.1590/S1679-45082014RC3110 (2014).

464 Gu, J. *et al.* Assessing susceptibility to age-related macular degeneration with proteomic and genomic biomarkers. *Molecular & cellular proteomics : MCP* **8**, 1338-1349, doi:10.1074/mcp.M800453-MCP200 (2009).

465 Niki, E., Yoshida, Y., Saito, Y. & Noguchi, N. Lipid peroxidation: mechanisms, inhibition, and biological effects. *Biochemical and biophysical research communications* **338**, 668-676, doi:10.1016/j.bbrc.2005.08.072 (2005).

466 Spiteller, P., Kern, W., Reiner, J. & Spiteller, G. Aldehydic lipid peroxidation products derived from linoleic acid. *Biochimica et biophysica acta* **1531**, 188-208 (2001).

467 Esterbauer, H., Schaur, R. J. & Zollner, H. Chemistry and biochemistry of 4-hydroxynonenal, malonaldehyde and related aldehydes. *Free radical biology & medicine* **11**, 81-128 (1991).

468 Gueraud, F. *et al.* Chemistry and biochemistry of lipid peroxidation products. *Free radical research* **44**, 1098-1124, doi:10.3109/10715762.2010.498477 (2010).

469 Qiang, M. *et al.* Autofluorescence of MDA-modified proteins as an in vitro and in vivo probe in oxidative stress analysis. *Protein Cell* **5**, 484-487, doi:10.1007/s13238-014-0052-1 (2014).

470 Minard-Colin, V. *et al.* Lymphoma depletion during CD20 immunotherapy in mice is mediated by macrophage FcgammaRI, FcgammaRIII, and FcgammaRIV. *Blood* **112**, 1205-1213, doi:10.1182/blood-2008-01-135160 (2008).

471 Millanta, S. *et al.* Short exposure of albumin to high concentrations of malondialdehyde does not mimic physiological conditions. *Experimental and molecular pathology* **94**, 270-276, doi:10.1016/j.yexmp.2012.06.008 (2013).

472 Kaur, K., Salomon, R. G., O'Neil, J. & Hoff, H. F. (Carboxyalkyl)pyrroles in human plasma and oxidized low-density lipoproteins. *Chemical research in toxicology* **10**, 1387-1396, doi:10.1021/tx970112c (1997).

473 Salomon, R. G., Hong, L. & Hollyfield, J. G. Discovery of carboxyethylpyrroles (CEPs): critical insights into AMD, autism, cancer, and wound healing from basic research on the chemistry of oxidized phospholipids. *Chemical research in toxicology* **24**, 1803-1816, doi:10.1021/tx200206v (2011).

474 Sun, M. *et al.* Light-induced oxidation of photoreceptor outer segment phospholipids generates ligands for CD36-mediated phagocytosis by retinal pigment epithelium: a potential mechanism for modulating outer segment phagocytosis under oxidant stress conditions. *J Biol Chem* **281**, 4222-4230, doi:10.1074/jbc.M509769200 (2006).

475 Crabb, J. W. *et al.* Drusen proteome analysis: an approach to the etiology of age-related macular degeneration. *Proc Natl Acad Sci U S A* **99**, 14682-14687, doi:10.1073/pnas.222551899 (2002).

476 Gu, X. *et al.* Carboxyethylpyrrole protein adducts and autoantibodies, biomarkers for age-related macular degeneration. *J Biol Chem* **278**, 42027-42035, doi:10.1074/jbc.M305460200 (2003).

477 Witztum, J. L. CEP Is an Important and Ubiquitous Oxidation Specific Epitope Recognized by Innate Pattern Recognition Receptors. *Circulation research* **117**, 305-308, doi:10.1161/CIRCRESAHA.115.306928 (2015).

478 Hollyfield, J. G., Perez, V. L. & Salomon, R. G. A hapten generated from an oxidation fragment of docosahexaenoic acid is sufficient to initiate age-related macular degeneration. *Molecular neurobiology* **41**, 290-298, doi:10.1007/s12035-010-8110-z (2010).

479 Ebrahem, Q. *et al.* Carboxyethylpyrrole oxidative protein modifications stimulate neovascularization: Implications for age-related macular degeneration. *Proc Natl Acad Sci U S A* **103**, 13480-13484, doi:10.1073/pnas.0601552103 (2006).

480 Kim, Y. W. *et al.* Receptor-Mediated Mechanism Controlling Tissue Levels of Bioactive Lipid Oxidation Products. *Circulation research* **117**, 321-332, doi:10.1161/CIRCRESAHA.117.305925 (2015).

481 Saeed, A. M. *et al.* The oxidative stress product carboxyethylpyrrole potentiates TLR2/TLR1 inflammatory signaling in macrophages. *PloS one* **9**, e106421, doi:10.1371/journal.pone.0106421 (2014).

482 Miller, Y. I. *et al.* Oxidation-specific epitopes are danger-associated molecular patterns recognized by pattern recognition receptors of innate immunity. *Circulation research* **108**, 235-248, doi:10.1161/CIRCRESAHA.110.223875 (2011).

483 Chou, M. Y. *et al.* Oxidation-specific epitopes are dominant targets of innate natural antibodies in mice and humans. *J Clin Invest* **119**, 1335-1349, doi:10.1172/JCI36800 (2009).

484 Chang, M. K. *et al.* Apoptotic cells with oxidation-specific epitopes are immunogenic and proinflammatory. *The Journal of experimental medicine* **200**, 1359-1370, doi:10.1084/jem.20031763 (2004).

485 Shanmugam, N. *et al.* Proinflammatory effects of advanced lipoxidation end products in monocytes. *Diabetes* **57**, 879-888, doi:10.2337/db07-1204 (2008).

486 Magdelaine-Beuzelin, C. *et al.* Structure-function relationships of the variable domains of monoclonal antibodies approved for cancer treatment. *Critical reviews in oncology/hematology* **64**, 210-225, doi:10.1016/j.critrevonc.2007.04.011 (2007).

487 Jefferis, R. & Lund, J. Interaction sites on human IgG-Fc for FcgammaR: current models. *Immunology letters* **82**, 57-65 (2002).

488 Shields, R. L. *et al.* High resolution mapping of the binding site on human IgG1 for Fc gamma RI, Fc gamma RII, Fc gamma RIII, and FcRn and design of IgG1 variants with improved binding to the Fc gamma R. *J Biol Chem* **276**, 6591-6604, doi:10.1074/jbc.M009483200 (2001).

489 Caaveiro, J. M., Kiyoshi, M. & Tsumoto, K. Structural analysis of Fc/FcgammaR complexes: a blueprint for antibody design. *Immunological reviews* **268**, 201-221, doi:10.1111/imr.12365 (2015).

490 Idusogie, E. E. *et al.* Engineered antibodies with increased activity to recruit complement. *Journal of immunology* **166**, 2571-2575 (2001).

491 Weismann, D. *et al.* Complement factor H binds malondialdehyde epitopes and protects from oxidative stress. *Nature* **478**, 76-81, doi:10.1038/nature10449 (2011).

492 Wang, W., Erbe, A. K., Hank, J. A., Morris, Z. S. & Sondel, P. M. NK Cell-Mediated Antibody-Dependent Cellular Cytotoxicity in Cancer Immunotherapy. *Frontiers in immunology* **6**, 368, doi:10.3389/fimmu.2015.00368 (2015).

493 Nose, M. & Wigzell, H. Biological significance of carbohydrate chains on monoclonal antibodies. *Proc Natl Acad Sci U S A* **80**, 6632-6636 (1983).

494 Takatsuki, A., Kohno, K. & Tamura, G. Inhibition of Biosynthesis of Polyisoprenol Sugars in Chick-Embryo Microsomes by Tunicamycin. *Agr Biol Chem Tokyo* **39**, 2089-2091, doi:Doi 10.1080/00021369.1975.10861914 (1975).

495 Sheeley, D. M., Merrill, B. M. & Taylor, L. C. Characterization of monoclonal antibody glycosylation: comparison of expression systems and identification of terminal alpha-linked galactose. *Analytical biochemistry* **247**, 102-110, doi:10.1006/abio.1997.2036 (1997).

496 Marginean, I. *et al.* Improving N-glycan coverage using HPLC-MS with electrospray ionization at subambient pressure. *Analytical chemistry* **84**, 9208-9213, doi:10.1021/ac301961u (2012).

497 Cooper, M. A., Fehniger, T. A. & Caligiuri, M. A. The biology of human natural killer-cell subsets. *Trends Immunol* **22**, 633-640 (2001).

498 Montalvao, F. *et al.* The mechanism of anti-CD20-mediated B cell depletion revealed by intravital imaging. *J Clin Invest* **123**, 5098-5103, doi:10.1172/JCI70972 (2013).

499 Reusch, D. & Tejada, M. L. Fc glycans of therapeutic antibodies as critical quality attributes. *Glycobiology* **25**, 1325-1334, doi:10.1093/glycob/cwv065 (2015).

500 Goetze, A. M. *et al.* High-mannose glycans on the Fc region of therapeutic IgG antibodies increase serum clearance in humans. *Glycobiology* **21**, 949-959, doi:10.1093/glycob/cwr027 (2011).

501 Wright, A., Tao, M. H., Kabat, E. A. & Morrison, S. L. Antibody variable region glycosylation: position effects on antigen binding and carbohydrate structure. *EMBO J* **10**, 2717-2723 (1991).

502 Quast, I. *et al.* Sialylation of IgG Fc domain impairs complement-dependent cytotoxicity. *J Clin Invest* **125**, 4160-4170, doi:10.1172/JCI82695 (2015).

503 Scallon, B. J., Tam, S. H., McCarthy, S. G., Cai, A. N. & Raju, T. S. Higher levels of sialylated Fc glycans in immunoglobulin G molecules can adversely impact functionality. *Molecular immunology* **44**, 1524-1534, doi:10.1016/j.molimm.2006.09.005 (2007).

504 Iida, S. *et al.* Nonfucosylated therapeutic IgG1 antibody can evade the inhibitory effect of serum immunoglobulin G on antibody-dependent cellular cytotoxicity through its high binding to FcgammaRIIIa. *Clinical cancer research : an official journal of the American Association for Cancer Research* **12**, 2879-2887, doi:10.1158/1078-0432.CCR-05-2619 (2006).

505 Hodoniczky, J., Zheng, Y. Z. & James, D. C. Control of recombinant monoclonal antibody effector functions by Fc N-glycan remodeling in vitro. *Biotechnology progress* **21**, 1644-1652, doi:10.1021/bp050228w (2005).

506 Raju, T. S. Terminal sugars of Fc glycans influence antibody effector functions of IgGs. *Current opinion in immunology* **20**, 471-478, doi:10.1016/j.coi.2008.06.007 (2008).

507 Dashivets, T. *et al.* Multi-Angle Effector Function Analysis of Human Monoclonal IgG Glycovariants. *PloS one* **10**, e0143520, doi:10.1371/journal.pone.0143520 (2015).

508 Gaboriaud, C. *et al.* Structure and activation of the C1 complex of complement: unraveling the puzzle. *Trends Immunol* **25**, 368-373, doi:10.1016/j.it.2004.04.008 (2004).

509 Lu, J. H. *et al.* The classical and regulatory functions of C1q in immunity and autoimmunity. *Cell Mol Immunol* **5**, 9-21, doi:10.1038/cmi.2008.2 (2008).

510 Moreau, C. *et al.* Structural and Functional Characterization of a Single-Chain Form of the Recognition Domain of Complement Protein C1q. *Frontiers in immunology* **7**, 79, doi:10.3389/fimmu.2016.00079 (2016).

511 Wang, G. *et al.* Molecular Basis of Assembly and Activation of Complement Component C1 in Complex with Immunoglobulin G1 and Antigen. *Mol Cell* **63**, 135-145, doi:10.1016/j.molcel.2016.05.016 (2016).

512 Tisdall, B. K. a. F. F. THE DISTRIBUTION OF SODIUM, POTASSIUM, CALCIUM, AND MAGNESIUM BETWEEN THE CORPUSCLES AND SERUM OF HUMAN BLOOD. *Journal of Biological Chemistry*, 241-252 (1922).

513 Peschke, B., Keller, C. W., Weber, P., Quast, I. & Lunemann, J. D. Fc-Galactosylation of Human Immunoglobulin Gamma Isotypes Improves C1q Binding and Enhances Complement-Dependent Cytotoxicity. *Frontiers in immunology* **8**, 646, doi:10.3389/fimmu.2017.00646 (2017).

514 Dekkers, G. *et al.* Decoding the Human Immunoglobulin G-Glycan Repertoire Reveals a Spectrum of Fc-Receptor- and Complement-Mediated-Effector Activities. *Frontiers in immunology* **8**, 877, doi:10.3389/fimmu.2017.00877 (2017).

515 Li, T. *et al.* Modulating IgG effector function by Fc glycan engineering. *Proc Natl Acad Sci U S A* **114**, 3485-3490, doi:10.1073/pnas.1702173114 (2017).

516 Vincents, B. *et al.* Cleavage of IgG1 and IgG3 by gingipain K from Porphyromonas gingivalis may compromise host defense in progressive periodontitis. *FASEB J* **25**, 3741-3750, doi:10.1096/fj.11-187799 (2011).

517 Kretschmer, A., Schwanbeck, R., Valerius, T. & Rosner, T. Antibody Isotypes for Tumor Immunotherapy. *Transfus Med Hemother* **44**, 320-326, doi:10.1159/000479240 (2017).

518 Kuriakose, A., Chirmule, N. & Nair, P. Immunogenicity of Biotherapeutics: Causes and Association with Posttranslational Modifications. *J Immunol Res* **2016**, 1298473, doi:10.1155/2016/1298473 (2016).

519 Chan, H. T. *et al.* CD20-induced lymphoma cell death is independent of both caspases and its redistribution into triton X-100 insoluble membrane rafts. *Cancer Res* **63**, 5480-5489 (2003).

520 Cardarelli, P. M. *et al.* Binding to CD20 by anti-B1 antibody or F(ab')(2) is sufficient for induction of apoptosis in B-cell lines. *Cancer Immunol Immunother* **51**, 15-24, doi:10.1007/s00262-001-0247-1 (2002).

521 Huhn, C., Selman, M. H., Ruhaak, L. R., Deelder, A. M. & Wuhrer, M. IgG glycosylation analysis. *Proteomics* **9**, 882-913, doi:10.1002/pmic.200800715 (2009).

522 Parekh, R., Roitt, I., Isenberg, D., Dwek, R. & Rademacher, T. Age-related galactosylation of the N-linked oligosaccharides of human serum IgG. *The Journal of experimental medicine* **167**, 1731-1736 (1988).

523 Thomann, M., Reckermann, K., Reusch, D., Prasser, J. & Tejada, M. L. Fc-galactosylation modulates antibody-dependent cellular cytotoxicity of therapeutic antibodies. *Molecular immunology* **73**, 69-75, doi:10.1016/j.molimm.2016.03.002 (2016).

524 Leabman, M. K. *et al.* Effects of altered FcgammaR binding on antibody pharmacokinetics in cynomolgus monkeys. *mAbs* **5**, 896-903, doi:10.4161/mabs.26436 (2013).

525 Hu, J., Liu, J., Yang, D., Lu, M. & Yin, J. Physiological roles of asialoglycoprotein receptors (ASGPRs) variants and recent advances in hepatic-targeted delivery of therapeutic molecules via ASGPRs. *Protein Pept Lett* **21**, 1025-1030 (2014).

526 Hiepe, F., Schossler, W., Apostoloff, E. & Precht, K. Development of a C1q-adsorbent for the selective removal of circulating immune complexes. *Biomater Artif Cells Artif Organs* **18**, 529-534 (1990).

527 Pfueller, B., Wolbart, K., Bruns, A., Burmester, G. R. & Hiepe, F. Successful treatment of patients with systemic lupus erythematosus by immunoadsorption with a C1q column: a pilot study. *Arthritis and rheumatism* **44**, 1962-1963, doi:10.1002/1529-0131(200108)44:8<1962::AID-ART335>3.0.CO;2-R (2001).

528 Berner, B. *et al.* Rapid improvement of SLE-specific cutaneous lesions by C1q immunoadsorption. *Annals of the rheumatic diseases* **60**, 898-899 (2001).

529 Hiepe, F. *et al.* C1q: a multifunctional ligand for a new immunoadsorption treatment. *Ther Apher* **3**, 246-251 (1999).

530 Xue, J., Zhu, L. P. & Wei, Q. IgG-Fc N-glycosylation at Asn297 and IgA O-glycosylation in the hinge region in health and disease. *Glycoconjugate journal* **30**, 735-745, doi:10.1007/s10719-013-9481-y (2013).

531 Yu, X. *et al.* Complex Interplay between Epitope Specificity and Isotype Dictates the Biological Activity of Anti-human CD40 Antibodies. *Cancer Cell* **33**, 664-675 e664, doi:10.1016/j.ccell.2018.02.009 (2018).

532 Hayes, J. M. *et al.* Identification of Fc Gamma Receptor Glycoforms That Produce Differential Binding Kinetics for Rituximab. *Molecular & cellular proteomics : MCP* **16**, 1770-1788, doi:10.1074/mcp.M117.066944 (2017).